

**The evolution of southern South Africa: insights
into structural inheritance and heterogeneous
normal fault growth**



Thesis submitted as partial fulfilment of the requirements for the
degree of Doctor of Philosophy (Ph.D.) in Geology

Douglas Alan Paton
The Department of Geology and Geophysics
The University of Edinburgh

May 2002



The results of this thesis study have not been submitted for the examination of any other degree or qualification. The observations and conclusions presented in this volume are the consequence of my own studies, unless cited otherwise.

Douglas Alan Paton

17th May 2002

The evolution of southern South Africa: insights into structural inheritance and heterogeneous normal fault growth

The integration of field and seismic data from southern South Africa has provided new insights into the understanding of the role that structural inheritance has in the deformation of heterogeneous continental crust.

Southern South Africa provides an unique setting to study the extension of a pre-existing compressional belt (negative structural inversion) because of the juxtaposition of excellent levels of pre-rift exposure, enabling basement structures to be determined, and high quality 2D seismic data, allowing the detailed temporal and spatial controls on rift system evolution to be established. Through the construction of five regional transects, orientated perpendicular to the Permian-Triassic Cape Fold Belt (CFB), an intimate link between compression and the subsequent Mesozoic extension can be established. A comparison between the CFB and other orogens suggests that it is atypical and it is proposed that the north of the foldbelt is controlled by low angle listric faults, while the centre and south are dominated by high angle planar faults. These faults have been reactivated during the subsequent extension. This model is supported by depth converted seismic sections that reveal listric normal faults that detach at a shallow crustal level in the north, while the south is dominated by a limited number of large, planar crustal scale normal faults. Comparison with both contractional and extensional reactivation (structural inversion and negative inversion respectively) models and examples supports the model.

The high quality of the available 2D seismic data arrays have enabled a sequence level seismic stratigraphic framework to be established for the three offshore basins (Pletmos, Gamtoos, and Algoa). The integration of the three basins has revealed a generally uniform evolution that differs from previous studies. In particular, the formation of previously documented deformation features are re-examined in light of detailed basin modelling. The dimension and evolution of the South African system are atypical when compared to other basins. The lengths of faults are at least 150 km with approximately 12 km of throw on the basin-bounding faults, which are significantly larger than most rift settings. There is also no evidence of along trend segmentation of the faults and extreme localisation of stress occurs from an early stage in the rift history. The results provide a critical test for existing models, which adequately account for normal fault evolution in homogeneous crust, to a region with a significant pre-existing, compressional fabric.

Acknowledgements

I first heard about this project while in a tent in the Falkland Islands via a fax from John Underhill and ever since then John's enthusiasm and encouragement has been much appreciated. Despite his badgering, David Macdonald is thanked for his constant support and regional insights. This study has greatly benefited from valuable discussion with Patience Cowie, John Dixon, Roger Scrutton, Hugh Sinclair, Nancye Dawers, and Iain Bartholomew.

The project was funded by a Natural Environmental Research Council (NERC) Industrial Case Studentship with CASP as the industrial partners. CASP's financial support enabled various field seasons to be undertaken, and for much of the seismic data to be obtained (cheers James for not deleting my projects despite the insults). Petroleum Agency South Africa are thanked for allowing the data to be released; in particular David Broad, Ian McLachlan, and Eric Jungslater for their support and comments during my visit to Cape Town and Jo for coping with endless requests for data. Mark Jones and David Platt of Ranger Oil are thanked for supplying the data for the Pletmos Basin. Additional funding was attained through a Shell International postgraduate bursary. Alan Gibb and Midland Valley are thanked for the generous release of a 3 month 2D Move license.

Without the support, encouragement, and pestering, of mum, dad, Stuart and Graeme, I certainly would not have got this far, but they are thanked in particular for the many holidays hillwalking in Scotland through which my interest in Geology developed. The many other people who deserve thanks for holding compass clinos, being attentive nurses/ambulance drivers, assisting in fieldwork in the Old Bell, wearing outrageous Friday shirts, and surviving hurricane-force winds on top of mountains, include Pete, Ruth, Aliene, Jon "just one more pint", Susie, John, Matt, Theo, Rich, Lynne, Sazza, and Looney. Finally, this thesis certainly would not have been written as quickly and as easily if it had not been for the help, support and legendary chocolate banana cakes of Estelle.

*This is my country,
The land that begat me.
These windy spaces
Are surely my own.
And those who here toil
In the sweat of their faces
Are flesh of my flesh
And bone of my bone.*

*Hard is the day's task –
Scotland, stern Mother! –
Wherewith at all times
Thy sons have been faced –
Labour by day,
And scant rest in the gloaming
With want an attendant
Not lightly outpaced.*

*Yet do thy children
Honour and love thee,
Harsh is thy schooling
Yet great is the gain.
True hearts and strong limbs,
The beauty of faces
Kissed by the wind
And caressed by the rain.*

Scotland

Sir Alexander Gray (1882-1967)

TABLE OF CONTENTS – Volume 1

CHAPTER 1: Introduction

1.1 Rationale	1
1.2 Thesis objectives	3
1.3 Thesis structure	3

CHAPTER 2: Background to rationale

2.1 Introduction	5
2.2 Structural inheritance	5
2.2.1 Inversion (compression subsequent to extension)	6
2.2.2 Negative inversion (extension subsequent to compression)	7
2.3 Normal faults	8
2.3.1 Fault growth models	9
2.4 Integrating structural inheritance and fault growth	10
2.5 Southern African geological setting	11
2.5.1 Pre-Cambrian	11
2.5.2 Paleozoic	13
i) Cape Supergroup	13
ii) Karoo Supergroup	14
iii) Cape Fold Belt structural formation	16
2.5.3 Mesozoic to Present	18
i) Regional break-up of East Gondwana	19
ii) South Africa Mesozoic geology	20
2.6 Project rationale	24

CHAPTER 3 : Structural controls on the Cape Fold Belt

3.1 Introduction	25
3.2 Data sources and methodology	25
3.2.1 Methodology	26
3.2.2 Specific problems and limitations to section balancing	27
3.3 Regional transects	28
3.3.1 Transect A	28
i) Structure	28
ii) Foldbelt reconstruction and underlying structure	30
3.3.2 Transect B	31
i) Structure	31

ii) Meeringspoort Pass transect	32
iii) Foldbelt reconstruction and underlying structure	35
3.3.3 Transect C	36
i) Structure	36
ii) Foldbelt reconstruction and underlying structure	38
3.3.4 Transect D	38
i) Structure	38
ii) Foldbelt reconstruction and underlying structure	39
3.3.5 Transect E	40
i) Structure	40
ii) Foldbelt reconstruction and underlying structure	41
3.3.6 Summary of transects	41
3.4 Comparison with other compressional orogenies and discussion	43
3.5 Conclusions	45

CHAPTER 4: The role of structural inheritance on the onshore Mesozoic

4.1 Introduction	46
4.2 Exposure limitations	46
4.3 Data, methodology	46
4.4 Mesozoic and foldbelt structural trends	47
4.5 Oudtshoorn Basin	47
4.6 Gamtoos Basin	48
4.7 Cross-section geometry	49
4.8 Discussion	50
4.9 Conclusion	50

CHAPTER 5: Sub-surface data and methods

5.1 Introduction	51
5.2 Data set	51
5.2.1 Seismic data	51
i) Seismic interpretation	52
ii) 2D Move restoration	53
iii) Errors and resolution	53
5.2.2 Well data	54
i) Available data	55
ii) Time-depth conversion	55
iii) Sedimentation rate calculations	55

iv) Errors	56
5.3 Understanding fault and basin evolution	56
5.4 Conclusions	57

CHAPTER 6: Tectonic evolution of the offshore Gamtoos Basin

6.1 Introduction	58
6.2 Gamtoos data	58
6.3 Tectonic and stratigraphic framework	59
6.3.1 Basement	59
6.3.2 Pseudo-basement	60
6.3.3 Earliest Syn-Rift ?	60
6.3.4 Principal Syn-Rift	60
i) Kimmeridgian	61
ii) Early Portlandian	62
iii) Late Portlandian-Mid Berriasian	63
iv) Upper Berriasian	63
v) Early Valanginian	64
vi) Late Valanginian	64
6.3.5 Late Syn-Rift	65
6.3.6 Basin-wide unconformity	66
6.3.7 Barremian	66
6.3.8 Localised Late Syn-Rift	66
6.3.9 Post-Rift	67
6.4 Nature of Faulting	67
6.4.1 Gamtoos Fault	67
i) Geometry	67
ii) Evolution	68
iii) Gamtoos Fault : one or two faults?	69
iv) Conclusions on the development of the Gamtoos Fault	70
6.4.2 Western Basement High	70
6.4.3 Intra-basin faults	70
6.4.4 Summary of Faulting	70
6.5 Basin-fill deformational styles	72
6.5.1 Northern margin	72
i) Observed structure	72
ii) Modelling of structures	72

6.5.2 Eastern margin	73
i) Observed structures	73
ii) Modelling of structures	74
6.5.3 Central basin	75
i) Observations	75
ii) Genesis of fold structures	76
6.5.4 North-West margin	76
6.6 Timing of uplift and compression	77
6.7 Basin evolution and depositional environment interpretation	78
6.7.1 Principal Syn-Rift	78
i) Kimmeridgian	78
ii) Portlandian – Late Valanginian	79
6.7.2 Latest Valanginian-Hauterivian	80
6.7.3 Basin-wide unconformity	81
6.7.4 Barremian	82
6.7.5 Albian	82
6.7.6 Post-Rift - Recent	82
6.8 Discussion and role of structural inheritance	82
6.9 Conclusions	85

CHAPTER 7: Tectonic evolution of the Pletmos Basin

7.1 Introduction	86
7.2 Pletmos Data	86
7.3 Tectonic and stratigraphic framework	86
7.3.1 Basement	87
7.3.2 Principal Syn-Rift	88
i) Earliest Syn-Rift(?)	88
ii) Early Syn-Rift	88
iii) Portlandian	89
iv) Early Valanginian	90
v) Late Valanginian	90
7.3.3 Late Syn-Rift	91
i) Early Hauterivian and Pseudo Early Hauterivian	91
ii) Late Hauterivian	92
7.3.4 Post Rift	93
i) Early Barremian	93

ii) Late Barremian	94
iii) Early Cenomanian	94
iv) Early Turonian	94
v) Late Turonian to present	95
7.4 Faulting	95
7.4.1 Plettenberg Fault	95
i) Geometry	96
ii) Evolution	96
7.4.2 Gemsbok Fault	97
7.4.3 Pletmos Fault	97
7.4.4 Superior Fault	98
7.4.5 En-echelon nature of the Pletmos and Superior Faults	99
7.4.6 Springbok High	99
7.4.7 Intra-basin faults	99
7.4.8 Summary of faulting	100
7.5 Basin-fill deformational styles	102
7.6 Summary of basin evolution	102
7.6.1 Principal Syn-Rift	102
i) Kimmeridgian	102
ii) Portlandian – Late Valanginian	102
7.6.2 Latest Valanginian-Hauterivian	102
7.6.3 Post-Rift	102
7.7 Discussion	103
7.8 Conclusions	105

CHAPTER 8: Tectonic evolution of the Algoa Basin

8.1 Introduction	106
8.2 Algoa Basin data	106
8.3 Tectonic and stratigraphic framework	107
8.3.1 Basement	107
8.3.2 Principal Syn-Rift	108
i) Kimmeridgian	109
ii) Portlandian	109
iii) Berriasian	110
iv) Early Valanginian	110
v) Late Valanginian	111

8.3.3 Late Syn-Rift	111
8.3.4 Canyonisation and canyon fill	113
8.3.5 Top canyon / basin-wide unconformity	113
8.3.6 Principal Post-Rift	114
8.4 Faulting	114
8.4.1 Port Elizabeth Trough	115
i) Port Elizabeth Fault	115
ii) Central Port Elizabeth Trough Fault (CPETF)	116
iii) Northern Port Elizabeth Trough Fault (NPETF)	116
iv) One fault or two faults?	116
8.4.2 Uitenhage Trough	118
i) St Croix Fault	119
ii) Uitenhage Fault	120
8.4.3 Intra-basin faults	120
8.4.4 Summary of faulting	120
8.5 Basin-fill deformational styles	121
8.5.1 Folding	122
i) Port Elizabeth Trough	122
ii) Uitenhage Trough	122
8.5.2 Port Elizabeth Trough basin-wide unconformity	122
8.6 Summary of basin evolution	122
8.6.1 Principal Syn-Rift	122
i) Kimmeridgian	123
ii) Portlandian – Late Valanginian	123
8.6.2 Late Syn-Rift : Latest Valanginian-Hauterivian	123
8.6.3 Late Hauterivian-Aptian	124
8.6.4 Aptian	124
8.6.5 Post Rift : Albian - recent	125
8.7 Discussion and role of structural inheritance	125
8.8 Conclusions	127
CHAPTER 9: Regional synthesis	
9.1 Introduction	129
9.2 Onshore structures	129
9.3 Offshore Mesozoic structures and evolution	130
9.3.1 Overall structure	130

i) Representative sections	131
ii) Depth conversions and limitations	131
iii) Scale of faulting	133
iv) Implications for CFB model	133
v) Evolution of South African offshore	134
9.4 Modification of Mesozoic basins by regional events	137
i) Aghulas Falkland Fracture Zone	137
9.5 Gamtoos and Algoa Basin uplift	138
9.6 Variation in extension orientation	140
9.7 Conclusion	140

Chapter 10: Implications and conclusions

10.1 Introduction	141
10.2 Structural inheritance	141
10.3 Implications for normal fault evolution	144
10.3.1 Comparison of South African faults with fault growth models	144
10.3.2 Normal fault growth in heterogeneous crust	145
10.3.3 Scale of South African faulting	146

References

147

LIST OF FIGURES – Volume 2

CHAPTER 2 Background to rationale

2.1	Examples of positive structural inheritance	1
2.2	Examples of negative structural inheritance	2
2.3	Models of fault growth by a) radial tip propagation and b) segment linkage	3
2.4	Model of fault growth	4
2.5	Examples of displacement-length profiles of an evolved normal fault	5
2.6	Geological map of South Africa	6
2.7	Chronostratigraphy of South Africa	7
2.8	Pre-Cape geology of South Africa	8
2.9	North-south crustal transect across South Africa	8
2.10	Outcrop map of the Cape Supergroup	9
2.11	Outcrop map of the Karoo Supergroup	10
2.12	Structural geology of the Cape Fold Belt	11
2.13	Stratigraphy and structural of the Cape Fold Belt	12
2.14	Model of the evolution of the Cape Fold Belt	12
2.15	Plate reconstructions of Gondwana and the South Atlantic	13
2.16	Structural map of the Mesozoic basins	16
2.17	Compilation of seismic sections illustrating Mesozoic basins' structure	17
2.18	Sequence stratigraphy of the offshore Mesozoic basins	18

CHAPTER 3 Basement

3.1	Geological map of southern South Africa and principal offshore Mesozoic structures	20
3.2	Transect A and reconstruction	21
3.3	Sketches from the Seweespoort Pass	22
3.4	Brittle deformation in the Seweespoort Pass	23
3.5	Ambiguous fault geometries in Transect A	24
3.6	Transect B and reconstruction	25
3.7	Road cutting through the Whitehill Formation	26
3.8	Sketches from the Meeringspoort Pass	27
3.9	Summary section through the Meeringspoort Pass	28
3.10	Transect C and reconstruction	29
3.11	Ambiguous fault geometries in Transect B	30
3.12	Peninsula Formation structures in Transect C	31

3.13	a) Northward verging Peninsula Formation folds, b) Southern coast of Transect C	32
3.14	Transect D and reconstruction	33
3.15	a) Normal fault in Transect D b) Perpendicular Peninsula Formation	34
3.16	Transect E and reconstruction	35
3.17	Geometries from Transect E	36
3.18	Compilation of transects restored to pre-extensional geometry	37
3.19	Idealised summary sketch across the Cape Fold Belt and three models for the formation of the foldbelt	38
3.20	Sandbox model illustrating box fold formation with high angle controlling fault	39

CHAPTER 4 Onshore Mesozoic

4.1	Geological map of southern South Africa with principal structural trends mapped	40
4.2	Overview of the Oudtshoorn Basin geology	41
4.3	Structural map of the Gamtoos Basin	42
4.4	Overview of the Gamtoos Basin	43
4.5	Syn-rift sedimentation within the Gamtoos Basin	44
4.6	Outcrop of the Peninsula Formation, Paul Sawyer Dam	45
4.7	Compilation of transects with the location of Mesozoic extension superimposed	46
4.8	Schematic summary sketches of models of Mesozoic extension using Cape Fold Belt structures	47

CHAPTER 5 Subsurface methods

5.1	Map illustrating the distribution of seismic and well data used in this study	48
5.2	Regional tectonic framework	50
5.3	Normal fault evolution models	51

CHAPTER 6 Gamtoos Basin

6.1	Map of Gamtoos Basin illustrating the location of seismic and well data used to establish the tectono-stratigraphic evolution of the basin	52
6.2	a) Summary of wells in the southern area of the Gamtoos Basin, b) Summary of wells along the trace of the Gamtoos Fault plane	53
6.3	a) North-south section across the Gamtoos Basin, b) East-west section across the Gamtoos Basin	55
6.4	a) TWT map to top_basement, and b) 3D cartoon of basin architecture	57

6.5	North-south section showing earliest syn-rift package	58
6.6	TWT maps to the top Principal Syn-Rift sequences	59
6.7	Isochron plots for the Principal Syn-Rift sequences	62
6.8	TWT maps to the top Late Syn-Rift sequences	64
6.9	Isochron plots Late Syn-Rift sequences	65
6.10	Isochron plot of <i>basin-wide_unconformity</i> to <i>top_l-valanginian</i>	66
6.11	TWT map of <i>basin-wide_unconformity</i>	66
6.12	Section showing <i>top_e-cenomanian</i> onlapping onto <i>basin-wide_unconformity</i>	67
6.13	Sub-crop map to the <i>basin-wide_unconformity</i>	68
6.14	a) TWT map to <i>top_albian</i> reflector, b) Isochron plot of <i>top_albian</i> to <i>basin-wide_unconformity</i>	69
6.15	Sections highlighting Post-Rift deformation	70
6.16	TWT maps of the Post-Rift	71
6.17	Isochron plot of <i>basin-wide_unconformity</i> to <i>top_e-cenomanian</i>	72
6.18	Isochron plots of the Post-Rift sequences	73
6.19	Sections illustrating the Gamtoos Fault geometry	74
6.20	Isochron plots between Principal Syn-Rift reflectors and <i>top_ps-basement</i>	75
6.21	Cumulative isochron plots between Late Syn-Rift reflectors and <i>top_ps-basement</i>	77
6.22	Isochron plots between Late Syn-Rift reflectors and <i>top_l-valanginian</i>	78
6.23	Sediment accumulation – thickness profile for the Gamtoos Fault	79
6.24	Models for the evolution of the Gamtoos Fault	81
6.25	Section across the western basement high	82
6.26	Section across the western basement high flattened to <i>top_e-valanginian</i>	83
6.27	Intra-basin faults commonly form a graben structure	84
6.28	Intra-basin faults in the Principal Syn-Rift	85
6.29	North-south section across the Gamtoos Fault showing erosional truncation of the Late Syn-Rift	86
6.30	2D Move restoration of Figure 6.29	87
6.31	Three sections illustrating the short wavelength deformation of the basin fill adjacent to the Gamtoos Fault	88
6.32	East-west section, and reconstruction, illustrating the formation of basin fill deformation	91
6.33	3-D sketch to show the formation of the basin fill deformation proximal to the north-south Gamtoos Fault	92
6.34	North-south section across the eastern part of the basin demonstrating folding of Principle Syn-rift beneath the <i>basin-wide unconformity</i>	93

6.35	Section showing folding of Principle Syn-Rift package, and onlap of the Late Syn-Rift package	94
6.36	North-south sections in the centre and south of the basin that show evidence of folding	95
6.37	Reconstructed sections from Figure 6.36 plotted with approximate spatial relationships to determine 3-D geometry of Principle Syn-Rift folding in the southern part of the basin	97
6.38	Modelling of the intra-basin folding in the south of the basin using a north-south section	98
6.39	Section on the western margin containing well Ha-J1	99
6.40	Summary sketches of the evolution of the Gamtoos Basin highlighting the principal tectonic events, relative sea-level, and type of sedimentation	101

CHAPTER 7 Pletmos Basin

7.1	Map of Pletmos Basin illustrating the location of seismic and well data used to establish the tectono-stratigraphic evolution of the basin	103
7.2	North-south section across the Pletmos Basin	104
7.3	a) TWT map to <i>top_basement</i> , and b) 3D cartoon of basin architecture	105
7.4	Seismic section with intra-basement reflectors	106
7.5	TWT maps for the top of the Principal Syn-Rift sequences	107
7.6	Sequence isochron plots for the Principal Syn-Rift sequences	109
7.7	TWT maps to the top of Late Syn-Rift sequences	110
7.8	Sequence isochron plots for the Late Syn-Rift sequences	110
7.9	Section illustrating that the <i>top_l-hauterivian horizon</i> in the Pletmos Basin is conformable with the <i>basin-wide_unconformity</i> of the Gamtoos Basin	111
7.10	North-south section showing the geometries of the Principal Syn-Rift mega-sequence	112
7.11	Onlap of <i>top_e-barremian</i> onto folded <i>top_l-valanginian</i>	113
7.12	TWT maps to the top of Post-Rift sequences	114
7.13	Isochron plots of Post-Rift sequences	115
7.14	North-south section showing southward directed progradational system in the Late Barremian sequence	116
7.15	North-south section across the Springbok High	117
7.16	Series of sections across, and TWT map to the Plettenberg Fault	118
7.17	Cumulative isochron plots of the Principal Syn-Rift mega-sequence	119
7.18	Cumulative isochron plots of Late Syn-Rift	120
7.19	Throw and Sediment accumulation-Length plots along the length of the Plettenberg Fault	121
7.20	East-west section in the south-east of the Pletmos Basin showing the Plettenberg and Gembok Faults	122

7.21	North-south section across the Pletmos Fault	123
7.22	Throw-Length plots across the Pletmos and Superior Faults	124
7.23	North-south section across the Pletmos and Superior Faults	125
7.24	North-south section across the Superior Fault, 20km east of Figure 7.23	126
7.25	North-south sections across the Pletmos Fault and Superior Fault to highlight the en-echelon nature of faulting	127
7.26	North-south sections to show the structure of the Springbok High	128
7.27	Section across the Springbok High, well tied to Gb-Spk1	129
7.28	North-south section, and flattened section to illustrate timing and geometry of the antithetic structure to the Plettenberg Fault	130
7.29	North-south sections to the south of the Springbok High	131
7.30	North-south section in the north of the basin showing folding of the Late Valanginian and dissection by numerous post-Late Valanginian extensional structures	132
7.31	Sequentially restored north-south section across the Plettenberg Fault	133
7.32	Sequentially restored east-west sections across the southern area of the basin	134
7.33	West-east section at the southern extent of the data coverage illustrating the character of the top ₁ -valanginian horizon	135
7.34	Summary sketches of the evolution of the Pletmos Basin highlighting the principal tectonic events, relative sea-level, and type of sedimentation	136

CHAPTER 8-ALGOA BASIN

8.1	Map of location including onshore geology and position of offshore seismic and wells	138
8.2	Well ties and main lithologies	139
8.3	Tectono-stratigraphic framework for the Algoa Basin	141
8.4	a) TWT map of <i>top_basement</i> . b) 3D sketch viewed from the SW showing the principal features of the basin	142
8.5	Section showing the presence of intra-basement reflectors	143
8.6	Compilation of Principal Syn-Rift TWT maps	144
8.7	Thickness plots of Principal Syn-Rift sequences	146
8.8	a) TWT map of <i>top_latest-valanginian</i> b) Isochron plot of Latest Valanginian sequence	148
8.9	Section across the Uitenhage Trough canyon illustrating passive canyon infill	149
8.10	Architecture of the canyon system: a) TWT to <i>base_canyon</i> ; b) TWT to <i>base_transp</i>	150
8.11	a) Section showing the internal reflector geometry of the canyon b) The eastern margin of the Port Elizabeth Trough canyon	151

8.12	Isochron plots of the canyon fill	152
8.13	Basin-wide erosion event: a) TWT of <i>basin-wide_unconformity</i> and <i>top_canyon</i> ; b) Sub-crop to <i>basin-wide_unconformity</i> and <i>base_canyon</i>	153
8.14	Section showing the <i>basin-wide_unconformity</i> across the Port Elizabeth Trough	154
8.15	Compilation of Post-Rift TWT maps	155
8.16	Thickness plots of the Post-Rift sequences	156
8.17	Post-Rift reflector geometries	157
8.18	Southern margin of the Algoa Basin	158
8.19	TWT maps of the principal fault arrays	159
8.20	Sections across the Port Elizabeth Fault	160
8.21	Cumulative isochron plots to <i>top_basement</i>	161
8.22	Sediment accumulation vs. length plot for the Port Elizabeth Fault	163
8.23	Section showing the Northern and Central Port Elizabeth Trough Faults	164
8.24	Sections across the Northern Port Elizabeth Trough Fault	165
8.25	Sections perpendicular to the St Croix Fault	160
8.26	Sections parallel to the St Croix Fault	167
8.27	a) Sediment accumulation vs. length plot for the St Croix Fault. b) Throw of <i>top_basement</i> vs. length plot for the Uitenhage Fault	168
8.28	3-D geometry of the St Croix Fault	169
8.29	Sections perpendicular to the Uitenhage Fault	170
8.30	Sections illustrating intra-basin faults in the Port Elizabeth and Uitenhage Troughs	171
8.31	Folding in the Port Elizabeth Trough	172
8.32	Reconstruction of the Port Elizabeth Trough anticline	173
8.33	Extent of the erosion across the Port Elizabeth Trough anticline	174
8.34	Port Elizabeth Trough and Gamtoos Basin compiled section to highlight the significance of the <i>basin-wide_unconformity</i>	175
8.35	Summary of the Algoa Basin evolution	176

CHAPTER 9 Regional Synthesis

9.1	Schematic cross-section across the Cape Fold Belt with two proposed to account for sub-surface data	178
9.2	a) TWT map to <i>top_basement</i> , b) 3-D cartoon of the study area	179
9.3	Approximate depth conversion of seismic sections to illustrate the geometry of the principal offshore faults	180
9.4	Depth-time data for all wells in the study data set	181
9.5	Summary sketches of evolution of the studied basins	182

CHAPTER 10 Discussion and Implications

10.1	Sandbox model illustrating changes in hangingwall deformation with variation in ramp dip	183
10.2	Stereonet showing the similarity in trend between basement trend and Mesozoic faults	183
10.3	Regional cross section	184
10.4	TWT plots of the fault planes for the a) Plettenberg Fault, b) Gamtoos Fault, c) Port Elizabeth Fault and d) St Croix Fault	185
10.5	Sediment accumulation – Length plot for the Plettenberg Fault	186
10.6	Sediment accumulation – Length plot for the Gamtoos Fault	187
10.7	Sediment accumulation – Length plot for the Port Elizabeth Fault	189
10.8	Sediment accumulation – Length plot for the St Croix Fault	190
10.9	Proposed normal fault growth model for heterogeneous continental crust	191
10.10	Schematic Displacement – Length plot for the South African faults	192
10.11	Plot of Displacement-Length with South African and global data sets plotted	193
10.12	Plot of length versus elastic thickness and seismogenic thickness	193

LIST OF TABLES –VOLUME 2

Table 3.1	Key stratigraphic units used in the transects in Chapter 3	19
Table 5.1	List of vintages of offshore seismic data	49
Table 6.1	Sedimentation rates for Gamtoos Basin wells	100
Table 7.1	Sedimentation rates for Pletmos Basin wells	137
Table 10.1	Summary of negative structural inheritance data	183

LIST OF APPENDICES

APPENDIX A Gamtoos Basin well data

A-i	List of available data	ii
A-ii	Depth-time conversion graphs	ii-iii
A-iii	Depth (ms TWT) converted time top data	iv-v
A-iv	Compilation of available well data for individual wells (Ha-A1, Ha-B2, Ha-F1, Ha-G1, Ha-H1, Ha-I1, Ha-J1, Ha-K1, Ha-N1)	vi-xv

APPENDIX B Pletmos Basin well data

B-i	List of available data	xvi
B-ii	Depth-time conversion graphs	xvi-xix
B-iii	Depth (ms TWT) converted time top data	xx-xxiii

APPENDIX C Algoa Basin well data

C-i	List of available data	xxiv
C-ii	Depth-time conversion graphs	xxiv-xxv
C-iii	Depth (ms TWT) converted time top data	xxvi-xxvii
C-iv	Compilation of available well data for individual wells (Hb-B1, Hb-C1, Hb-D1, Hb-G1, Hb-Hart, Hb-I1, Hb-K1, Hb-P1)	xxviii-xxxv

LIST OF ENCLOSURES

Enclosure 1	Key and stratigraphic correlation for Transects
Enclosure 2	Transect A
Enclosure 3	Transect B
Enclosure 4	Meeringspoort Pass transect
Enclosure 5	Transect C
Enclosure 6	Transect D
Enclosure 7	Transect E
Enclosure 8	Seismic array of the Gamtoos Basin with location of figures highlighted
Enclosure 9	Seismic array of the Pletmos Basin with location of figures highlighted
Enclosure 10	Seismic array of the Algoa Basin with location of figures highlighted

CHAPTER 1: Introduction

1.1 Rationale

The presence of a pre-existing structural fabric is considered to be one of the first order controls on determining the locus of tectonic activity, and plays a significant part in controlling large-scale intraplate failure (e.g. Kuzsnir & Park, 1987, England & Jackson, 1989; Sandiford & Hand, 1998; Holdsworth *et al.*, 2001). If a pre-existing structure is weaker than the surrounding rock, then it will tend to reactivate when a subsequent stress is applied to the region. Reactivation of a structure with the same sense of displacement as the previous deformational phase is possible, although can often be difficult to demonstrate. More common is the reactivation of a structure with an opposite sense of displacement (Williams *et al.*, 1989; Holdsworth *et al.*, 1997), leading to either structural inversion (contractional reactivation of a former normal fault), or negative inversion (extension on a previously contractional fault). Examples of inversion and negative inversion, and the associated deformational geometries, are well documented from a variety of settings and ages of continental lithosphere (e.g. Ziegler, 1989; Cooper *et al.*, 1989; Daly *et al.*, 1989; Amato *et al.*, 1992; Buchanan & Buchanan 1995; Sandiford, 1999). The understanding of reactivation derived from field observations has been supplemented by numerous analogue and numerical modelling experiments (e.g. McClay, 1989; Buchanan & McClay, 1991; Huyghe & Mugnier, 1992; Faccenna *et al.*, 1995) and theoretical considerations (e.g. Sibson, 1985; Sibson, 1995; Ranalli, 2000). The conclusion from all these studies is that continental crust is heterogeneous, and that the resulting structural fabrics influence the subsequent evolution of the crust (Holdsworth *et al.*, 2001).

In addition to structural inheritance, another aspect of continental tectonics that is relevant to this study is that of crustal extension. It has long been recognised that normal faults play a critical role in accommodating extension in the brittle upper crust (e.g. McKenzie, 1978; Wernicke & Burchfiel, 1982; Jackson & McKenzie, 1983; Bosworth, 1985), and controlling the formation of extensional sedimentary basins (e.g. Leeder & Gawthorpe, 1987). Recently, significant advances have been made in the understanding of extensional system development, and in particular the temporal and spatial variations in normal fault evolution. These advances are a result of detailed fieldwork in areas such as the Gulf of Suez (Gupta *et al.*, 1999; Sharp *et al.*, 2000), Canyonlands, Utah (Cartwright *et al.*, 1995) and Volcanic Tablelands, California (Dawers *et al.*, 1993; Dawers & Anders, 1995), and the availability of

high quality seismic data (e.g. Gupta *et al.*, 1998; Morley, 1999; Dawers & Underhill, 2000; Contreras *et al.*, 2000; McLeod *et al.*, 2000). The integration of these studies with the results of numerical modelling (e.g. Gupta *et al.*, 1998; Cowie *et al.*, 2000) reveals that the spatial and temporal evolution of a normal fault population can be ascertained by establishing the loci of hangingwall deposition, using sediments as a proxy for accommodation generation, and determining the rate of hangingwall subsidence. Based on these observations, the proposed models suggest an initial distributed fault population that progressively undergoes strain localisation onto a few dominant structures. In this study, this model will be tested in a region with an existing strong structural fabric.

Most workers have considered either structural inheritance and basin inversion, or normal fault evolution in isolation, despite the two often being intimately linked. Some recent studies have attempted to integrate these two features of continental tectonics through field and seismic studies, and analogue modelling (e.g. Keller & McClay, 1995; Kelly *et al.*, 1999; Underhill & Paterson, 1998), but these have been restricted to structural inversion of extensional systems. The influence of pre-rift structures on the evolution of extensional systems in response to negative inversion has barely been documented (Morley, 1999; Ebinger *et al.*, 1999).

Southern South Africa provides an unique setting to study the influence of heterogeneous crust on the evolution of an extensional system. It has been well documented that southern Africa has undergone multiple phases of deformation throughout the Proterozoic and Phanerozoic (Tankard *et al.*, 1983; Dingle *et al.*, 1983; de Wit & Ransome, 1992; Hålbich, 1993). Of particular interest to this study are the Permian-Triassic Cape Foldbelt (CFB) and the subsequent Mesozoic extension associated with Gondwana break-up and South Atlantic rifting. Many workers describe this transition from compression to extension in terms of negative inversion (de Wit & Ransome, 1992, and references therein; Malan *et al.*, 1990; Hålbich, 1993; McMillan *et al.*, 1997; Thomson, 1999), but there is very little consideration of the structures at depth, discussion of the geometries in the context of other negative inversion examples, nor assessment of the influence on the extensional system evolution. Excellent exposure of the foldbelt, and high quality 2D offshore seismic data, enables the integration of CFB architecture with the large scale structural geometry of the Mesozoic faults derived from sub-surface studies.

1.2 Thesis objectives

The central question to be addressed is :

- What role has structural inheritance played in the evolution of southern South Africa?

By addressing this question, and applying the results to models of extensional system genesis and development, it is possible to address the question:

- How do heterogeneities within continental crust influence extensional sedimentary basin formation, specifically the growth of normal fault populations?

1.3 Thesis structure

The rationale for this study will be expanded in Chapter 2 with a review of previous work on structural inheritance and extensional rift evolution. The second part of Chapter 2 provides an overview of the 3.8 Ga crustal history of southern Africa, focusing on the development of the Ordovician-Devonian Cape Supergroup, the structural and sedimentological development of the Cape Orogeny and Karoo basin, and the establishment of the Mesozoic extensional systems. It will also outline why the region is a suitable setting to study the interaction between structural inheritance and rift evolution.

As the central objective of this study is to determine the role of structural inheritance in the complex evolution of the region, it is important to establish the sequential tectonic development of southern South Africa. In particular, it is imperative to constrain the structures controlling the Cape Orogeny. Five regional transects are presented in Chapter 3 to illustrate the principal features of the highly complex Cape Fold Belt (CFB), and various models are proposed to explain its genesis. Chapter 4 presents data from the onshore Mesozoic sedimentary basins and adapts the models presented in Chapter 3 to account for the observed extension.

The fundamental problem arising from the data presented in Chapters 3 & 4 is that the inferred geometries, derived from the available outcrop data, are poorly constrained at depth, and there are no suitable onshore data to assess the spatial and temporal evolution of the Mesozoic extension. To address both of these issues, seismic arrays from the offshore south coast have been analysed. The nature and distribution of data, and method of establishing a seismic stratigraphic framework to aid interpretation, are outlined in Chapter 5, along with a

discussion on how the evolution of normal faults can be ascertained through understanding temporal and spatial variations in associated syn-rift packages.

Chapter 6 presents observations from the Gamtoos Basin based on the application of the techniques and seismic stratigraphic framework outlined in Chapter 5. Additionally, the basin-scale architecture, intra-basin fault arrays and basin-fill deformation features are outlined, and their geneses are discussed. A summary of the tectonic and sedimentological evolution of the basin is presented and compared with previous studies. Observations from similar basin analysis are presented in Chapters 7 and 8 for the Pletmos and Algoa Basins respectively. The sedimentary basins discussed in Chapters 6, 7 & 8 are considered in isolation.

Chapter 9 is a regional synthesis that integrates the onshore data from chapters 3 & 4 with the offshore data of Chapters 6, 7 & 8, and is divided into two parts. In Part 1, the models for the CFB are constrained at depth using the depth conversion of key seismic sections. Part 2 is concerned primarily with the offshore data and combines the conclusions from the basins to obtain an overview of the evolution of the Mesozoic systems.

Chapter 10 summarises the findings and re-addresses the central objectives of this study. The first part synthesises evidence for structural inheritance in South Africa. The second part examines the role of structural inheritance in the growth of Mesozoic rifting, and considers the implications for fault growth models.

CHAPTER 2: Background to Rationale

2.1 Introduction

The aim of this chapter is to expand on the central rationale of this study by presenting the current understanding of structural inheritance and normal fault evolution and outlining the lack of integration between these two facets of continental tectonics. The evolution of southern Africa will then be summarised and it will be discussed why it is a suitable area to test normal fault evolution models in a region with a significant pre-existing structure.

2.2 Structural inheritance

The theoretical control on reactivation is the Mohr-Coulomb-Anderson theory, which determines the fracture orientation established when an Andersonian stress field (three orthogonal principal stresses, with one vertical and two horizontal; Anderson, 1905) is applied to a homogeneous rock volume (Buck, 1993). If the maximum principal stress (σ_1) is vertical, then normal faults are predicted to have a dip of 60° and reverse faults of 30° (Sibson, 1985), although these values are dependant upon the coefficient of friction (Forsyth, 1992; Ranalli, 2000). If the rock volume is heterogeneous, then the pre-existing structure can be re-activated if the applied stress is less than the critical stress required for the formation of a new fracture (Ranalli, 2000). Consequently, as the dip of a pre-existing normal fault gets increasingly lower compared to the theoretical 60° fracture, the required stress for reactivation increases, hence the chances of reactivation decreases. Therefore, low angle structures are less likely to be reactivated in an extensional sense compared with higher angle structures. In contrast, as reverse faults have a theoretical dip of 30° , pre-existing low angle structures are easier to reactivate in compression compared to high angle fractures. Ranalli (2000) calculates that the maximum mis-orientation angle (i.e. the angle between pre-existing fracture and idealised fracture) at which reactivation can occur is greater for steep rather than shallower structures.

Such a model of reactivation is simplistic, and numerous other factors have to be considered; the most important are pore-pressure and friction on the fault. A reduction in friction, and increase in pore pressure results in a decrease in the shear strength of a fracture, thus enabling reactivation to occur more easily (Ivins *et al.*, 1990; Sibson, 1985 & 1995). Forsyth (1992) purports that a low angle fault, with a low coefficient of friction, will be reactivated in preference to a high angle fault with a more normal friction coefficient. Huyghe &

Mugneir (1992), and Sibson (1995) also predict that the probability of fault reactivation is not uniform across a structure, and that the chances of reactivation may change with depth.

Van Wees & Beekman (2000) forward modeling of four basins in Western Europe suggest that during inversion sedimentary basins can get progressively strengthened, disagreeing with the commonly considered opinion that repeated localisation of stress results in strain weakening. They suggest that this apparent parody can be explained by deviations from standard rheological assumptions on the inverted structures.

In conclusion, the theoretical calculations indicate that low angle structures are more susceptible to be cross-cut, imply that higher angle structures are preferential for long term structural inheritance (i.e. multiples phase of reactivation and inversion). The calculations do not predict the inversion geometries associated with reactivation, although these have been well documented from field, sub-surface seismic, teleseismic and analogue modelling data (e.g. Cooper & Williams, 1989; Buchanan & Buchanan, 1995; Miller, J.A. *et al.*, 1997), and will be reviewed in the next two sections.

2.2.1 Positive structural inversion (compression subsequent to extension)

Bonini *et al.* (2000), using sand-box models, investigated internal deformation of thrust sheets controlled by a variable ramp angle of dip 15° - 30° , and a high-angle ramp (considered to be a reactivated normal fault) of 45° - 60° . During compression, inversion of the hangingwall units occurs against the bounding fault, resulting in an anticline (Figure 2.1a). Back thrusts (antithetic to the fault) develop regardless of the dip of the ramp/fault. A low angle ramp results in a long wavelength, low amplitude anticline. With increased dip of the ramp, the width of the anticline is reduced, and the amplitude increases; at a dip of 60° a definite pop-up structure develops. Sand-box model results from Buchanan and McClay (1991), McClay (1995) and Mandal & Chattopadhyay (1995) support Bonini *et al.* (2000) and predict that reactivation of a steeper structure would result in a pop-up structure with a backthrust dipping at 35° . Numerical modelling using a hybrid cellular automata by Salvini *et al.* (2001) provides further evidence that as the ramp dip increases, the anticline wavelength decreases and amplitude increases.

Similar geometries to those modelled have been observed on many sub-surface seismic studies (Figure 2.1b) including the southern North Sea (Badley *et al.*, 1989) and the Danish Central Graben (Cartwright, 1989). Reactivation of high angle extensional faults in compression has also been demonstrated by teleseismic data. Amato *et al.* (1992) calculated the 3-Dimensional velocity structure of the 1980 Irpinia, southern Italy, earthquake and

interpreted the aftershocks as the reactivation of a high angle reverse fault as a normal fault. Jackson (1980) presented data of reverse fault plane solutions from the Zagros Mountains with dips of 40° - 50° , and interpreted these to be normal faults reactivated as high angle reverse faults.

2.2.2 Negative structural inversion (extension subsequent to compression)

Faccenna *et al.* (1995) compressed a sand-box model, with a velocity discontinuity in the basal plate, to produce reverse faults, prior to extending the system to induce normal faults. Their results suggest that when the pre-existing reverse fault has a dip of less than 32° , the subsequent normal fault will ignore the underlying structure (Figure 2.2a). When the reverse fault dip is between 32° and 41° there is interaction between the normal fault and reverse fault with the normal fault branching out at the sand interface with the velocity discontinuity. For reverse faults with a dip greater than 41° then complete reactivation of the fault occurs.

Jackson & McKenzie (1983) document the similarity in trend of normal faults in Central Greece with the underlying thrusts, and suggest that they may use the same structures. Faccenna *et al.* (1995) presented data from the Italian Central Apennine chain and concluded that extensional reactivation of thrusts occurs if the pre-existing reverse fault has a dip of between 37° and 40° . They note that where the reverse faults have a shallow dip ($\sim 25^{\circ}$) there is no evidence of reactivation and the structures are cross-cut by new, steeper normal faults. These conclusions are supported by structural studies of Powell & Williams (1989) on the Lewis Thrust system, Montana which had previously been considered as a décollement surface for subsequent (post-Laramide) extension (Bally *et al.*, 1966; Constenius, 1982). Through sequential restorations of sections, Powell and Williams concluded that although negative inversion played a role, it was very localised, whilst the majority of extension was accommodated on new, steep, cross-cutting normal faults (Figure 2.2b). Ring (1994) examined the Central Malawi Rift border fault segments and concluded that steep structures are more susceptible to reactivation, and pre-existing structures will be utilised if the difference in strike between pre-existing structure and extensional strain is within 30° .

Ratcliffe *et al.* (1986) discuss evidence of low angle (25° - 35°) mylonitic thrust structures in the Newark Basin that have been reactivated in extension. There is no evidence, however, to indicate the dip at which these structures were active, and whether they were low angle normal faults (cf. Wernicke, 1981, 1995; Forsyth, 1992) or high angle normal faults that

have since been rotated to shallower dips (Proffett, 1977; Buck, 1988; Koyi & Skelton, 2001; Sharp *et al.*, 2000).

On a crustal scale, interpretation of the MOIST line imaging the deep structures of the Scottish Caledonides implies that deep crustal reactivation and inheritance can occur (Smythe *et al.*, 1982; Snyder *et al.*, 1997). The presence of crustal scale heterogeneities may play a significant role in determining both the position and architecture of subsequent passive margins (Dunbar & Sawyer, 1989a & b; McClay & White, 1995).

These studies suggest during negative inversion of a compressional system, fault reactivation of the reverse fault into extension will occur when the pre-existing fault is steep; if the pre-existing fault is shallow, then the normal fault will tend to cross-cut the reverse fault.

2.3 Normal faults

Studies of continental rift settings indicate that extension is dominantly accommodated in the brittle upper crustal through slip on normal faults. Studies of extensional settings suggest that major normal faults are typically segmented and have characteristic lengths and displacements (Jackson, 1987; de Polo *et al.*, 1991; Gawthorpe *et al.*, 1994; Roberts & Jackson, 1991).

Buck (1993) proposed a simple model of rift initiation in which the offset (or heave) of an active normal fault, with a dip of 60° , is controlled by the thickness of the lithosphere. Scholz & Contreras (1998) expanded on Buck's model, and proposed a simple model of symmetric rift initiation with two conjugate normal faults. Both faults will grow in cross-sectional aspect until one becomes dominant and the other locks-up and becomes antithetic. The principal fault will grow until it reaches the base of the seismogenic layer. They propose that the thickness of the seismogenic layer imparts a fundamental control on the along axis length of the fault, the width of the associated basin and the maximum fault displacement.

Jackson & McKenzie (1983) noted that the majority of normal fault earthquake fault plane solutions occur at depths less than 16 km, on planar structures with dips of approximately 45° , and suggested that this defined a critical size for normal faults. Jackson & White (1989), and Chen & Molnar (1983) supported this view by providing evidence that seismically active normal faults have dips in the range of 30° - 60° , and are predominately

located in the upper crust (10-15 km). They also document that fault segments in most extensional settings (including, Viking Graben, Gulf of Suez, Central Greece, Basin and Range) are commonly 20-25 km long, and basins are typically 25-40 km wide, concluding that this scaling is controlled by the thickness of the seismogenic layer. Where faults have been demonstrated to be active over much longer distances, Jackson & White suggest that they are comprised of smaller segments, and use the Wasatch Fault, Utah as an example of this. The Wasatch Fault is seismically active over its 300 km length, but is comprised of individual segments that are shorter than 60 km. The fieldwork data, therefore validates Buck, and Scholz and Contreras' models.

More recently, it has been documented that normal faults are not static features and that they evolve both spatially and temporally; this dynamic nature will be addressed in the following section.

2.3.1 Fault growth models

The growth of normal faults has been considered to be either through isolated radial growth (Figure 2.3a; Walsh & Watterson, 1988, Cowie & Scholtz, 1992; Anders & Schlische, 1994), or by segment linkage (Figure 2.3b; Dawers *et al.*, 1993; Trudgill & Cartwright, 1994; Anders & Schlische, 1994; Cartwright *et al.*, 1995; Contreras *et al.*, 2000). More recently, authors have proposed a combination of the two models, and documented a spectrum of examples between the two end members (e.g. Cartwright *et al.*, 1996; Morley & Wonganan, 2000). Current models and data demonstrate that the early stage of rifting is characterised by small, isolated fault segments which have symmetrical, displacement-length (D-L) profiles with high displacement gradients towards the segment ends (Dawers & Anders, 1995; Cartwright & Mansfield, 1998; Gupta *et al.* 1998; Cowie *et al.*, 2000). Cartwright *et al.* (1996) discuss that segments are characterised by: i) abrupt changes in strike; ii) changes in throw between segments; iii) bedding attitude changes between segments; iv) relay structures. The segmentation of faults has been documented at many scales and typically have an en-echelon distribution (Morley *et al.*, 1990; Peacock & Sanderson, 1991, 1994; Dawers & Anders, 1995; Cartwright *et al.*, 1996; Contreras *et al.*, 2000).

Gupta *et al.* (1998) propose a fault model with initial minor strength heterogeneities (Figure 2.4). As the model is subjected to an extensional stress, normal faults seed at the points of low strength, resulting in isolated fault segments with the characteristics discussed above. Associated with the segments are isolated hangingwall depocentres separated by intra-basement highs. These features are preserved in the stratigraphic record as localised, early

syn-rift sequences, which progressively onlap onto the pre-rift and have commonly been observed in both field and sub-surface studies (Schlishe, 1995; Morley, 1999; McLeod *et al.*, 2000; Young *et al.*, 2001). The intra-basement highs typically form relay structures that are frequently folded, and/or faulted, and occur in a variety of scales and settings (Figure 2.5; Morley *et al.*, 1990; Roberts & Jackson, 1991; Peacock & Sanderson, 1991, 1994; Trudgill & Cartwright, 1994).

In Gupta *et al.*'s model, as the system undergoes continued extension, fault segments begin to interact and link. Asymmetric D-L profiles and accelerated slip rates have been cited as evidence of mechanical interaction prior to physical linkage (Cartwright & Mansfield, 1998; Cowie *et al.*, 2000; McLeod *et al.*, 2000). The linkage of segments also results in the evolution of the relay-structure from a soft-linkage feature through to a hard linking structure between the two segments (Gawthorpe & Hurst, 1993; Trudgill & Cartwright, 1994). The progressive linkage of segments has a profound effect on the creation of accommodation space, resulting in often dramatic changes in the location of depocentres through time (Dawers & Underhill, 2000). As a consequence of segment linkage, Gupta *et al.*'s model predicts that the number of active faults in the system reduces with time. Various field and sub-surface studies have demonstrated how the D-L profile of a mature fault can be comprised of the cumulative effect of multiple individual segments (Figure 2.5). As the strain rate remains constant, the reduction in the fault population results in increasing strain localisation on fewer faults and consequently the development of faults with increasingly larger displacements. A further consequence is the progressive reduction in the number of intra-basin faults. This model has been validated by various field and sub-surface studies (see Cowie *et al.*, 2000).

2.4 Integrating structural inheritance and fault growth

Only a limited amount of work has integrated fault growth models with structural inheritance, and this has tended to be with respect to inversion structures. Keller & McClay (1995) undertook 3D sandbox inversion experiments by extending the system to create 60° dipping normal faults, prior to compression. They noted that relay structures established by the extension tended to remain during compression, and from this concluded that subsequent inversion structures were controlled by the extensional geometry. Structural and seismic analysis of the inverted Wessex Basin (Underhill & Paterson, 1998) supported Keller & McClay's conclusion, in particular with reference to the inherited position of relay ramps.

Similar results have been documented by Kelly *et al.* (1999) in the Mesozoic sediments of the Somerset coast.

The influence of structures on the evolution of extensional systems after negative inversion has barely been documented. Morley (1999) proposed that pre-existing structures in the Aswa Shear Zone, East African Rift, probably influenced both the position of extension and the length of fault segments; a view that is supported by Ebinger *et al.* (1999).

There is, therefore, a poor understanding of how the presence of a significant structural fabric influences normal fault evolution. The next section will summarise the geological history of Southern Africa, and establish why it is a suitable place to advance this issue.

2.5 Southern African geological setting

The geological history of southern Africa spans over 2.5 Ga and as a consequence the present day geological and tectonic framework is complex. The solid geology and chronostratigraphy of southern Africa is summarised in Figures 2.6 & 2.7. The purpose of this section is to summarise the geological events and features that are pertinent to this thesis, rather than to describe the full complexities of the region.

2.5.1 Pre-Cambrian

The Archean basement (>2.5 Ga) of southern Africa forms the Kaapval Craton (Figure 2.8) and is composed of massive and foliated granitoids, gneisses and greenstone terranes (Tankard *et al.*, 1982; Thomas *et al.*, 1993). Juxtaposed to the south and west of this craton are the high-grade metamorphic and plutonic rocks associated with the Namaqua-Natal Province (NNP) mobile belt (Figure 2.8). This mobile belt is primarily greenstone and juvenile volcanic arc sediments that were accreted onto the craton by NE directed thrusts and nappes around 1.3 Ga (Hälbich, 1993). These terranes were subsequently intruded by granites between 1.2-1.1 Ga. (Thomas *et al.*, 1993).

The southern end of the NNP is characterised by a large positive magnetic anomaly (Beattie Anomaly) that is coincident with a negative isostatic anomaly and an electrically conductive zone (Southern Cape Conductive Belt, SCCB) in the crust or upper mantle (Figure 2.8; De Beer, 1983; Pitts *et al.*, 1992). These geophysical observations have been modelled and the origin of the anomalies is inferred to be a weak zone of serpentinised basalt underlying the Karoo Basin (Figure 2.9). This feature is considered to be oceanic crust obducted during the

final closure of an ocean basin during the Namaqua-Natal Orogeny (950-900 Ma) (Tankard *et al.*, 1982; Hålbich, 1993).

Subsequent to the Namaqua-Natal Orogeny, rifting produced flexural downwarping and intra-cratonic extension (Tankard *et al.*, 1982). This extension terminated with the coalescence of Gondwana during the Pan African Orogeny, 600-450 Ma (Hålbich, 1993; Thomas *et al.*, 1993), which resulted in the formation of the Saldania, Damara and Gariep Provinces (Figures 2.6 & 8). It has been proposed that the orogeny utilised a south-dipping crustal décollement, known as the Pan African Suture (Hålbich, 1993; Tankard *et al.*, 1982). The orogeny was accompanied by the deposition of sediments in marginal and rifted basins parallel to the east-west trending suture, and the present day remnants of these basins are the three Pre-Cape inliers (Kaaimes, Kango and Gamtoos). The Kango and Gamtoos inliers, in the central and eastern Cape respectively (Figure 2.6 & 8), contain shelf and terrestrial sediments while the Kaaimes horst has sedimentation indicative of a more distal marine setting (Figure 2.8; Tankard *et al.*, 1982; Krynauw, 1983; Gresse, 1983).

The Kango sediments are comprised of carbonate shales, greywackes and turbiditic marine sandstones overlain by an eastward wedging para-conglomerate sequence (Tankard *et al.*, 1982; Le Roux & Gresse, 1983). In total over 3000m of sediments were deposited in an east-west trending basin which was open to the south-west (Toerien, 1979). The structural evolution of the basin is complicated and multiple phases of folding and uplift have punctuated sedimentary deposition (Le Roux, 1983a). The two principal compressional events were orthogonal and resulted in north-south striking folds being overprinted by east-west trending isoclinal folds and northward directed klippen. The sediments within the inlier have since been metamorphised into phyllite hornfels and schists (Tankard *et al.*, 1982).

The Pre-Cape unit in the Gamtoos inlier (Tankard *et al.*, 1982; Toerien & Hill, 1989; Shone *et al.*, 1990) is composed of shallow marine or terrestrial conglomerates, arkosic sandstones, quartzites and limestones. Although three lithological units are mappable, they are also separated by thrusts and the relationships between the thrust stacks are difficult to establish (Shone *et al.*, 1990). The stratigraphic succession is overturned to the north-east and commonly exhibits evidence of folding, thrusting and associated imbricate duplexes and ramp flat geometries. The Pre-Cape deformation in the Gamtoos inlier is evident despite overprinting by the Permo-Trias Cape Orogeny, and is dominated by NE-verging structures (Bell, 1980; Shone *et al.*, 1990). Shone *et al.* (1990) suggest that the observed Pre-Cape deformation occurred at a moderately deep crustal level.

As a result of the stratigraphic, palaeoenvironment and tectonic resemblance between the Gamtoos and Kango inliers, Tankard *et al.* (1982) infer that the inliers may have been connected and formed a single basin.

2.5.2 Paleozoic

i) Cape Supergroup

Following the Pan-African Orogeny, the south of the region underwent prolonged subsidence in the form of a passive continental margin, resulting in the deposition of the 8 km thick, Ordovician to Early Carboniferous Cape Supergroup (Figure 2.7 & 2.10). Subsidence was principally in response to isostatic effects (Lock, 1978), although two periods of accelerated subsidence have been documented (Cloetingh *et al.*, 1992). The margin's sedimentation was dominated by deltaic and shallow marine deposits sourced from the northern cratonic region (Tankard *et al.*, 1982; Thomas *et al.*, 1993).

The oldest unit in the Cape Supergroup is the Early Ordovician to earliest Devonian Table Mountain Group, which is predominantly cross bedded, super-mature, medium to coarse grained, quartz sandstones (Toerien, 1979; Bell, 1980; Toerien & Hill, 1989). The unit is approximately 4 km thick, and includes a basal conglomerate and a carbonaceous, black shale (Cedaberg Formation) that is attributed to glacial deposits (Haughton, 1963; Tankard *et al.*, 1982). The unit was deposited in an east-west trending basin by braided rivers flowing from the north and NE across a coastal plain into a shallow marine environments.

Conformably overlying the Table Mountain Group is the Bokkeveld Group that is approximately 2 km of argillaceous fine grained sandstones overlain by more massive shales and siltstones (Toerien, 1979; Toerien & Hill, 1989). Deposition was onto the margin of an epicontinental sea during the Early to Late Devonian, and variations in the deltaic sequences were in response to the interaction between tectonics and eustasy (Broquet, 1992).

During the Late Devonian to Early Carboniferous, the gradual deepening of the Bokkeveld Group depositional environment continued with the deposition of shales and subordinate sandstones of the Witteberg Group. As with the older Cape Supergroup units, sedimentation occurred from the north onto outer delta plains (Toerien, 1979; Tankard *et al.*, 1982; Toerien & Hill, 1989). Although sedimentation continued to be focused on the east-west elongated Cape Basin, the extent of the basin diminished to a third of its original size by the time the youngest sediments were being deposited. Evidence of cyclicity within the Witteberg Group has been attributed to Milankovitch eustasy cycles and led Cotter (1998) to conclude that the

basin was open to marine conditions. This is supported by marine fossils in the lower Witteberg Group, although there is an absence of them in the upper Witteberg (Tankard *et al.*, 1982). The sediments become increasingly influenced by glacial deposits with the advent of glaciers from the north during the Late Carboniferous (Tankard *et al.*, 1982; Broquet, 1992).

ii) Karoo Supergroup

The deposition of the Karoo sediments into the Karoo Basin was controlled by various tectonic and climatic factors (Turner, 1986), although the glaciation of the Late Carboniferous controlled much of the basin's early development (Tankard *et al.*, 1982; Visser, 1992; Veevers *et al.*, 1994). The principal control on the overall formation of the basin has long been considered as the progressive northward encroachment of the Cape Orogeny (Du Toit, 1937) resulting in subsidence of the weak crust associated with the Southern Cape Conductive Belt (SCCB; Cole, 1992). The position of the SCCB subsequently controlled the position of the Karoo Basin axis (Figure 2.9; Thomas *et al.*, 1993). However, recent modelling suggests loading by the Cape Orogeny can not account for all of the observed subsidence, and that there may be a significant back-arc extensional component (Visser, 1992; Turner, 1999; Trouw & de Wit, 1999).

The Cape Orogeny comprised four compressional events during the Permian and Triassic (Hälbich *et al.*, 1983), and the development of the Karoo Basin was intimately linked with these events. This section will discuss the sedimentological development of the Karoo Basin while Section 2.3.3 summarises the structural evolution of the Cape Orogeny and the resultant Cape Fold Belt.

The sediments of the Karoo Basin are sub-divided into the Dwyka, Ecca, Beaufort and Stormberg Groups (Figure 2.7) and have a total thickness of approximately 9 km (Figure 2.11; Toerien, 1979; Toerien & Hill, 1989). The Dwyka tillite sits unconformably on top of the Witteberg Group and is a diamictite that corresponds to four ice sheet advance and retreat cycles (Visser *et al.*, 1997). It contains abundant angular erratics that are dominated by granite and gneiss clasts (Veevers *et al.*, 1994) with sub-ordinate sandstones, basalts and limestones (Cole, 1992). The first paroxysm of the Cape Orogeny occurred during the lithification of this formation (Hälbich & Swart, 1983; Cole, 1992) at 278 ± 2 Ma (Hälbich *et al.*, 1983).

The Ecca Group unconformably overlies the glacial deposits and comprises carbonaceous shales and limestones with a clastic influx in response to post-glacial rebound in the north

(Cole, 1992). Unlike the Cape Supergroup, the sediments of the Karoo are derived from the south, and deposited into a northward migrating, relatively deep-water basin (Figure 2.11; Veevers *et al.*, 1994). Throughout the glacial and Lower Ecca Group there are numerous volcanic ash deposits that decreases in volume from south to north and west to east (Viljoen, 1990).

The second compressional paroxysm (258 ± 2 Ma; Hålbich *et al.*, 1983) induced rapid downwarping resulting in the deepening of the basin and an accumulation of sandy submarine fans (Cole, 1992). Abundant airborne ash is interbedded within parts of the fans with numerous rhyodacitic tuffs. The distance to the magmatic arc is debated, although its position is considered to have been between 500 and 1500 km to the south (Viljoen, 1990; Johnson, 1991; Visser, 1992). In the Late Permian, the sedimentation rate began to exceed subsidence, resulting in the gradual filling of the basin, and shallowing of the depositional environment to a fluviially dominated delta setting (Veevers *et al.*, 1994).

The Beaufort Group of the Early Triassic is dominated by mudstones and sandstones of a meandering river system that is the consequence of a large-scale regression (Dingle *et al.*, 1983). Superimposed upon the regression is the third compressional phase (247 ± 3 Ma, Hålbich *et al.*, 1983) that introduced coarse sands that were transported by braided streams from the south (Cole, 1992). A detailed study using 38,000 paleocurrents indicate a broadly centropetal basin with an east-west elongation (Cole, 1998). There is the continued presence of volcanic material, although it is uncertain whether this is recycled (Veevers *et al.*, 1994) or sourced from the magmatic arc to the south (Johnson, 1991). The Upper Beaufort Group has similar facies to the lower section, although in addition, there is evidence for the development of monoclinial structures, and syntectonic deformation associated with the fourth phase of compression at 230 ± 3 Ma (Hålbich *et al.*, 1983; Le Roux *et al.*, 1994).

Subsequent to the fourth phase of compression there is the deposition of the Stormberg Group, comprised of the proximal, fluviially dominated Molteno Formation and the distal Elliot Formation (Tankard *et al.*, 1982; Turner, 1983; Cole, 1992). The Late Triassic is typified by progressive aridification culminating in the aeolian sands of the Clarens Formation. Sedimentation is abruptly halted in the Early Jurassic with the development of the Karoo Flood Basalts (Tankard *et al.*, 1982).

iii) Cape Fold Belt structural formation

The previous section outlined the sedimentological evolution of the Karoo Basin, which is considered to be the foreland basin to the Cape Orogeny. This section will review the structural understanding of the Cape Fold Belt.

The present exposure of the Cape Fold Belt extends from the east coast at East London to Cape Town with an east-west orientation before an abrupt change in direction, called the Cape Syntaxis, to a north-south trend along the west coast to Clanwilliam (Figure 2.12; Söhnge, 1983; Dingle *et al.*, 1983). Of particular importance to this study is the development of the Central and Eastern Capes, therefore only the east-west trending portion of the fold belt will be examined. The Western Cape and Cape Syntaxis have been studied by various workers including de Beer (1990), Ransome & de Wit (1992), de Beer (1992), and Netwon (1993).

The Cape Orogeny is considered to be formed from four paroxysmic events. These events occurred over 45 Ma from the Early Permian to the Late Triassic (Hälbich *et al.* 1983; Hälbich & Swart, 1983; Gresse *et al.*, 1992). The ages of the paroxysmic events have been obtained by K/Ar, and Ar/Ar techniques (Hälbich *et al.*, 1983; Hälbich, 1992) and indicate that the orogeny youngs towards the north. The later stages of the deformation are evident as syn-tectonic deformation in the Late Triassic Beaufort Group (Le Roux *et al.*, 1994). The younging to the north is accompanied by a progressive transition in the nature of the deformation. Asymmetric folds with south-dipping axial planes are persistent throughout, although the nature of the folds change from an upright open geometry to inclined chevron fold geometry towards the north (Figure 2.13; Hälbich, 1983a; Coetzee, 1983). This has been attributed to a variation in the style of deformation through time (Dingle *et al.*, 1983; Hälbich & Swart, 1983). Although the lithologies undergoing deformation change dramatically across the fold belt they have little effect on the fold geometry, and instead control the scale of folding. The Table Mountain Group forms the major anticlines with wavelengths of up to 20 km, while the Bokkeveld folds are approximately 1 km (Coetzee, 1983). In addition to orogenic tectonic folding, disharmonic folds are present across the orogeny and have been attributed to gravity sliding detaching on less lithified units. (Hälbich, 1983a; 1992). Hälbich (1983b) and Fouché *et al.* (1992) have published a north-south transect across the foldbelt that highlights the principal tectonic features and suggest between 23-27% shortening across the area (Figure 2.13). In this transect, however, there is

little discussion of the controlling structures at depth, or of spatial continuity especially towards the east.

The tectonic fabric of the foldbelt is dominated by folds with occasional faults (Figure 2.12; Hälbich & Swart, 1983; Dingle *et al.*, 1983). Bedding plane thrusts are common throughout and in the hinge zones of the Table Mountain quartzite, folds, fractures and thrusts are common. Some thrusts have been documented but are only minor compared to the scale of the foldbelt and appear to form in response to the folding, rather than being the cause of folding (Newton, 1992; Shone & Booth, 1993; Booth, 1996).

Across the Cape region from the Cape Syntaxis in the west (Le Roux, 1983b) to Port Elizabeth in the east there is a uniform sub east-west trend of all structures from bedding planes, bedding parallel thrusts to meso- and macro-scale folds (Hälbich & Swart, 1983; Coetzee, 1983). The Cape Orogeny is also sub-parallel to the structures within the Kaaimes and Kango Pre-Cape inliers (Krynauw, 1983; Gresse, 1983; Le Roux & Gresse, 1983; Le Roux, 1983b). In the Eastern Cape there is a change in trend to a north-west to south-east orientation. Despite this change in trend, the style of deformation is identical to that observed in the Central Cape, and the Cape structures are parallel to the Pre-Cape structures (Booth & Shone, 1992a, b, & c; Shone & Booth, 1993).

Metamorphic studies broadly agree with the structural studies and show little variation along the east-west trend of the Cape Fold Belt. From north to south there is a steady increase in grade from unmetamorphosed Karoo sediments through an upper anchimetamorphic zone (T ca. 150°, P=23kb) to lowermost greenschist facies (T ca. 350°C) on the south coast (Figure 2.13; Hälbich & Cornell, 1983; Duane & Brown, 1992). This transition can be accounted for by increased burial of the southern margin compared to the north without the requirement of tectonic intervention (Hälbich & Cornell, 1983). It is important to note that there is no evidence of mid-crustal rock exhumation, or of the development of mylonites even where thrusting is observed. Therefore despite the significant folding and occasional thrusting, there is very little metamorphism, and where present it is of a low temperature and pressure origin (Booth, 1996).

a) Extent and genesis of the Gondwanide Orogeny

The Cape Fold Belt forms part of a much larger orogen known as the Gondwanian Foldbelt that includes the Sierra de la Ventana in Argentina, the South African Cape Fold Belt, the Falkland Islands, Ellsworth Mountains (Antarctica) and Pensicola Mountains portions of the Trans-Antarctic Mountains (Du Toit, 1937; Dalziel *et al.*, 2000). Du Toit (1937) recognised

the presence of the foldbelt and attributed it to a compressional origin, though did not discuss possible causal mechanisms. Newton (1973) suggests that orogenic collapse was the dominant control although this does not account for the pre-existing topography that would have to have been present to allow the collapse to occur. Other workers suggest that intra-plate compression may have resulted in the deformation (Dingle *et al.*, 1983; Hälbich, 1983b), and Johnston (1998) proposes intra-plate compression associated with a dextral shear zone as the genesis. However, the present consensus is convergence associated with paleo-pacific subduction (Hälbich, 1983b; de Wit & Ransome, 1992). The distance to the invoked subduction margin is inferred to be substantial (~1500 km) and therefore a flat plate subduction model is invoked (Lock, 1978; Dalziel *et al.*, 2000).

b) Underlying control of the Cape Fold Belt

There is very little known about the crustal structure across the area, although the crustal thickness has been calculated to be approximately a uniform 40 km across most of the fold belt (Cloetingh *et al.*, 1992; de Beer, 1983).

The Pan-African Orogeny is considered to have been the principal controlling feature, resulting in a low angle, south dipping regional décollement (Figure 2.14; Hälbich, 1993). This model is based on circumstantial data, although there is evidence in the offshore area to the south of a deep crustal structure. Most workers have therefore related the CFB to this feature (Hälbich *et al.*, 1983; Hälbich, 1993) and inferred a low angle detachment system.

2.5.3 Mesozoic to present

The Karoo Flood Basalts that cap the Karoo sediments are considered to have been emplaced in response to the initiation of a mantle plume positioned off the east coast of Southern Africa (Tankard *et al.*, 1983; White & McKenzie, 1989). The plume is proposed to be one of the principal driving forces controlling the break-up of Gondwana through regional doming (Cox, 1992; Storey & Kyle, 1997; Storey *et al.*, 1999) although other controls have been suggested, including extension associated with the western progression of the paleo-Pacific trench (Ben-Avraham *et al.*, 1993). Dalziel *et al.* (2000) suggest a causal relationship amongst the flat plate subduction genesis of the Gondwanian orogeny, plumes, subduction, and continental break-up. They propose that the downgoing paleo-Pacific was subjected to horizontal subduction as a result of the buoyancy of a plume beneath the subduction zone. Subsequently, the plume broke through the slab, resulting in the uplift of the region, the development of the Karoo igneous province, and the initiation of rifting.

This section summarises the break-up history of East Gondwana in particular focussing on the Mesozoic evolution of South Africa.

i) Regional break-up of East Gondwana

The break-up of Gondwana was a long and protracted event that initiated after the impingement of the Karoo Plume. The tectonic evolution of the region immediately prior to, and post break-up is summarised in the plate-reconstruction timeslices presented in Figure 2.15 that use a new tight fit of Gondwana (Macdonald *et al.*, 1998; Lawver *et al.*, 1998). This tight fit has been accomplished by various re-considerations of the regional geology. The most important features of the reconstruction are: South America is split into various plates, e.g. restoration of the Gastre Fault Zone in Patagonia; removal of north-south Mesozoic extension within South America; redefining the ocean-continent boundary of the South Atlantic; and closure of the Maurice Ewing Bank (MEB) and the Falkland Plateau Basin. This last feature is valid because geophysical studies of the MEB (Barker, 1999) suggest that it is the volcanic rifted margin of the Falkland Islands and it is composed of either extensively thinned continental crust, or oceanic crust. Therefore prior to break-up the MEB would have been considerably narrower. A consequence of this reconstruction is the much closer fit between South America and southern South Africa compared with previous reconstructions (e.g. Bullard *et al.*, 1965; Storey *et al.*, 1992).

Rifting initiated between Africa and Antarctica using pre-existing Proterozoic and Archaen weaknesses (Thomas *et al.*, 1993) in the Early Middle Jurassic (Figure 2.15b). Extension was accommodated by the inception of major dextral strike slip motion to the east of the Explora Escarpment, and sinistral strike slip to the west, resulting in the formation of East (South America and Africa) and West (Antarctica, Australia and India) Gondwana. In East Gondwana, dextral strike slip motion occurred along the proto-Agulhas Falkland Fracture Zone (AFFZ), which may be related to the Gastre Fault System of South America (Rapela & Pankhurst, 1992). Hälbich (1993) infers from the sedimentary age of the neighbouring basins that the full intra-continental AFFZ initiated after the beginning of rifting, and suggests an Early Cretaceous age of between 140 and 130 Ma. This is supported by the structural analysis of the AFFZ by Ben-Avraham *et al.* (1997). Macdonald *et al.* (1998) have included the 180° clockwise of the Falkland Island micro-continent's as a result of substantial sedimentological, structural and paleomagnetic work (du Toit, 1937; Adie, 1952; Mitchell *et al.*, 1986; Musset & Taylor, 1994; Marshall, 1994a & b; Curtis & Hyam, 1998; Hunter, 1998), although the rotation, and timing of rotation remains controversial (de Wit,

1992; Richards *et al.*, 1996; Thomson, 1998; Lawrence *et al.*, 1999; Johnstone, 2000). Macdonald *et al.* (1998) also include the anticlockwise rotation of the Ellsworth Mountain's anticlockwise rotation, in their Early-Middle Jurassic reconstruction (Figure 2.11b). The first oceanic crust formed in the Mozambique Basin during the Middle Jurassic (Figure 2.15c) by which time Macdonald *et al.* (1998) infer that micro-continental block rotation had ceased. Subsequently, Antarctica broke off to the south with oceanic crust being formed in the Wedell Sea at 145-122 Ma (Figure 2.15e; Martin & Hartnaday, 1981).

The complete break-up of Gondwana was concluded in the Hauterivian with the separation of South America and South Africa, associated with the M10 (130 Ma) sea floor magnetic anomaly (Figure 2.15f; Austin & Uchuppi, 1982).

ii) South Africa Mesozoic geology

The Mesozoic geology of southern South Africa is dominated by a series of sedimentary extensional basins (Figure 2.16), three of which have onshore portions. The offshore system is known collectively as the Outeniqua Basin with the 200 m isobath dividing it into northern and southern sub-basins. The Northern Outeniqua Basin is separated into the Bredasdorp, Pletmos, Gamtoos and Algoa Basin and the latter two have onshore portions. In addition to the onshore Gamtoos and Algoa Basins, there are various Mesozoic inliers, the largest of which is the Oudtshoorn Basin (Figure 2.6 & 2.16). The basins are asymmetric half grabens that downthrow towards the south and have an approximate east-west trend, except in the east where there is a swing to the south-east (Dingle *et al.*, 1983). The understanding of the offshore areas has been a result of sub-surface hydrocarbon exploration by Petroleum Agency South Africa (formerly SOEKOR).

The timing of rift initiation in South Africa is uncertain although the oldest dated sediments are Oxfordian which suggest an early Late, or possibly Middle Jurassic age (McMillan *et al.*, 1997). The oldest recorded date is 162 ± 7 Ma for the Suurberg Volcanics in the Algoa Basin (McLachlan & McMillan, 1976) and this age is supported by a partial extensional overprinting of the Cape Fold Belt at 177 Ma (determined from Ar/Ar dating technique, Gresse *et al.*, 1992).

a) Offshore

The four offshore sedimentary basins (Bredasdorp, Pletmos, Gamtoos and Algoa) have similar histories, although only the Pletmos, Gamtoos and Algoa Basins will be discussed here. The evolution of the Bredasdorp Basin is broadly similar, and is discussed by

McMillan *et al.* (1997). The overall structure is a series of half grabens (Figure 2.17), generally with the bounding faults to the east of the basins. The faults themselves are often curved in plan view and are separated by a series of basement highs and arches (Cartwright, 1989; Bate and Malan, 1992; Thomson, 1998).

The oldest syn-rift sequence to be penetrated in any of the basins is Kimmeridgian, although Late Oxfordian sediments are thought to be present in the deepest parts (Figure 2.18; Broad, 1989; Malan *et al.*, 1990; Bate, 1993; McMillan *et al.*, 1997). The earliest syn-rift sediments, which are generally fluvially dominated pebbly sandstones, onlap onto the Jurassic rift topography. During the Kimmeridgian and Berriasian, shallow marine claystones and sandstones dominated all of the basins, with localised regressions and shallowing-up sequences. The Valanginian deposits of the Gamtoos and Algoa Basin are dominated by mid-outer shelf clays (Broad, 1989). In all three basins the deposits form classic wedges into the basin-bounding fault (cf. Prosser, 1993). Bate & Malan (1992) describe three tectonostratigraphic packages within the syn-rift and attribute them to variations relative sediment supply and accommodation space. The outer shelf sandstones of the Portlandian form a divergent basal seismic package against the basin-bounding faults, and are attributed to accommodation space created by fault movement being greater than sediment supply. By the Berriasian and Early Valanginian sediment supply was equal to tectonic activity, resulting in a weakly divergent package. The depositional environment during this time was shallower than the Portlandian with mid-outer shelf deposits. By the Late Valanginian the gradual shallowing continued across the area despite being accompanied by an increase in divergence towards the fault associated with renewed fault motion.

The rift-drift transition is placed at the end of the Valanginian (Figure 2.18) and is characterised by different processes in the three basins. In the Pletmos, uplift and erosion occurred resulting in a substantial aggradational and progradational clastic package from the north (McMillan *et al.*, 1997). In the Gamtoos and Algoa Basins the section is incomplete as a result of uplift and erosion (Broad, 1989). Where present, sediments were deposited in a shelf to slope setting that was poorly oxygenated. Localised deformation, in particular folding in the Gamtoos Basin, has been attributed to compression and uplift as a consequence of strike slip motion on the on the incipient AFFZ (Thomson, 1998; Bate & Malan, 1993).

The post-rift sediments are relatively uniform across the area with very little or no tectonic deformation. Canyoning is present in the Algoa, and to a lesser extent the Gamtoos Basin, which was infilled by marine deposits (Bate & Malan, 1992). Sedimentation during the post-rift was dominated by well oxygenated slope sandstones and claystones deposition that was punctuated by unconformities associated with eustatic fluctuations (Keenan, 1990; Brink *et al.*, 1994). In the post Mid-Albian there is a decline in sedimentation rate with an increase in the width of the continental shelf followed by mild uplift and regional tilting to the south in the Late Cenomanian (McMillan *et al.*, 1997).

b) Onshore

The onshore Mesozoic outcrops are localised to the onshore portions of the Gamtoos and Algoa Basins, and various inliers, the largest of which is the Oudtshoorn Basin (Figure 2.6 & 2.12). Deposition is considered to be fault controlled (Kleywegt, 1971; Dingle *et al.*, 1983; Shone *et al.*, 1990; Viljoen, 1992). Despite the geographical distribution of these outcrops, the sedimentology is remarkably consistent, and is separated into three units: Enon Conglomerate; Kirkwood Formation; and the Sundays River Formation (Viljoen, 1992; Figure 2.7).

The Enon Conglomerate is a well sorted and rounded conglomerate containing subordinate sand and siltstones (Malan & Theron, 1987). The clasts can be up to 70 cm in diameter and depending on the location within the Cape, are either of Table Mountain Group, or Bokkeveld Group provenance. A terrestrial topographic infill, or earliest syn-rift genesis has been assigned to them, and although it is impossible to date the unit, a Middle Jurassic to Lower Cretaceous age has been attributed to it (Dingle *et al.*, 1983).

The Kirkwood Formation is a cross-bedded sandstone with channel lags interfingering with brown shales and siltstones (McLachlan & McMillan, 1976). The top of the formation is a dominantly shale unit with a large number of foraminifera specimens and a small variety of species, suggesting a brackish lacustrine depositional environment. Palaeontology of the sequence supports the lacustrine interpretation and suggests Late Valanginian and Hauterivian ages (McMillan, 1999).

The Sundays River Formation comprises grey clays, silts and sands of shallow water marine and estuarine origin, and has been dated as Late Cretaceous (McLachlan & McMillan, 1976; Dingle *et al.*, 1983; Shone, 1978).

As a result of poor exposures, especially in the Eastern Cape, the relationship between the units is poorly understood with the units either being interfingered or separated by unconformities (McLachlan & McMillan, 1976; Shone, 1978; McMillan *et al.*, 1997).

c) Reactivation of the Cape Fold Belt

Ever since Du Toit (1937) remarked on the position of the Cape's pre-existing structures being parallel to the Mesozoic normal faulting, numerous authors have documented the relationship. Dingle *et al.* (1983) observe that the south dipping normal faults typically bound the southern side of major anticlines but do not discuss whether the same faults are utilised. De Wit & Ransome (1992) attribute the extension, which resulted in the normal fault development, to the relaxation of the CFB prior to the break-up of Gondwana. de Wit (1992) discusses how the same structures are used during sequential deformation events. Onshore evidence for the relationship between extension and compression has been discussed by Hälbig (1983a, b) who addressed the presence of extensional structures within the Cape Supergroup. Le Roux (1983a & b) and Shone *et al.* (1990) document extensional deformation within the Pre-Cape units. Gresse *et al.* (1992) use $^{40}\text{Ar}/^{39}\text{Ar}$ data to produce evidence of partial overprinting of the Cape Orogeny by the rifting event. Evidence of structural inversion has been documented across the area including the west Central Cape (Newton, 1992; Viljoen, 1992), the Central Cape (Booth & Shone, 1996), and the Eastern Cape (Booth and Shone, 1992 a & b; Shone and Booth, 1993). However, a problem with many of the studies is that the age of normal faulting is very difficult to determine except where Mesozoic sediments are preserved in the hangingwalls.

Evidence from the offshore also supports the premise that there is a relationship between the Mesozoic extension and the underlying CFB. Fouché *et al.* (1992) discuss that the presence of metamorphic rocks as the basement to the extensional systems, asymmetric grabens and the arcuate nature of the extension all support the inheritance concept. Bate & Malan (1992) and Thomson (1999) invoke structural inversion of the CFB thrusts as listric normal faults. The reactivation of thrusts, intra-basement reflectors associated with basement shear zones, and the curvature of the basins have been used as further evidence by Broad (1989), Cartwright (1989), Bate (1993) and Roux (1992). Hälbig (1992) presents a regional geotranssect in which the Mesozoic extension soles out onto the inferred Pan-African décollement (Figure 2.14b).

Despite this wealth of evidence supporting the notion of structural inheritance, there is very little discussion of what the overall structure is at depth. The only model discussed is the

reactivation of the inferred Pan-African decollément in a simple shear sense. However there is very little integration of onshore and offshore data in a holistic model.

2.6 Project rationale

This chapter has outlined the styles of deformation associated with reactivation of structures during subsequent phases of deformation. It has also considered normal fault growth models, and in particular discussed the occurrence of strain localisation onto fewer structures during fault development. The previous section has considered the geological history of southern Africa and discussed the concept of structural inheritance with respect to the Cape Fold Belt and Mesozoic extension. Southern South Africa, therefore provides an ideal setting to consider the interplay between pre-existing structural fabric and extension.

CHAPTER 3 : Structural Controls on the Development of the Cape Fold Belt; Evidence from the Restoration of Regional Transects

3.1 Introduction

The role of structural inheritance on the development of an extensional system can only be assessed if the architecture of the pre-rift structure can be ascertained. It is, therefore, critical to understand the geometry of, and structural controls on, the Cape Fold Belt (CFB) prior to addressing the role of basement control on the evolution of the Mesozoic extensional system. This chapter will establish models for the formation of the CFB that will be utilised in following chapters.

Previous work (Chapter 2) and published sections across the CFB have focused on the Central Cape and specific areas within it (e.g. the Meeringspoort Pass, Transect 3). This chapter aims to consider the CFB in a regional context from the Central Cape to its eastern extent. This will be done using five regional transects across the area constructed from published maps and supplemented by field data. For each transect the observed deformation is used to discuss possible controlling structures at depth. The transects are then compared and contrasted prior to a discussion of possible mechanisms for the development of CFB.

3.2 Data sources and methodology

Five true scale transects have been constructed from published geological maps (RSA Geological Survey maps 3320, 3420, 3322, 3324) using the established stratigraphic units of the Geological Society, RSA (Table 3.1), from the Karoo Foreland Basin in the north to the south coast, perpendicular to the structural trend of the CFB at a scale of 1:125,000 (Figure 3.1). The factors considered when deciding the position of the transects were:

- Transects were positioned to maximize the use of field data especially where river gorges with high levels of exposure enabled detailed structural analyses to be undertaken. In some instances field data have been projected along strike onto the transects.
- Transects were to be as evenly spaced across the area as possible.

- To achieve an overview of the regional structures, however, some transects specifically include areas with atypical features.
- In some cases the data in the transect does not fully constrain the geometries. Therefore supplementary sections have been included and incorporated into the principal transect.

Each transect is presented in a number of ways. The enclosures include the raw map data (including supplementary sections), which are superimposed upon topography with very little interpretation. Where map data were oblique to the transect, the data were converted to apparent dip. The enclosures also include an interpreted and extrapolated section (the methods used to form this section will be discussed later). The transects are reproduced as figures in the main body of the thesis where they are accompanied by restored sections and available field data, sketches and photographs. Stereonets of structural data have been plotted for each of the transects and are shown on Figure 3.1.

3.2.1 Methodology

The transects were constructed using standard techniques (Dahlstrom 1969; Elliot & Johnson 1980; Boyer & Elliot 1982; Elliot 1983) of line length and area preservation, assuming no out of plane motion or volume change. The thickness of individual units was determined where the data were well constrained, and each transect was considered in isolation. When thicknesses were compared along transects, between transects, and with published data (Toerien 1979; Toerien & Hill 1989), the data showed near consistent thicknesses in a north-south trend, with minor variations from east to west. Therefore, for individual transects constant unit thickness was assumed, and used to extrapolate surface geometries both to the sub-surface and sub-aerially. As a further approximation, faulting was included only where mapped.

The underlying control and overall geometry of the transects were constructed using some simple assumptions regarding controlling faults and section balancing. Surface folds were assumed to result from either buckling or an underlying fault. Fold trains with regular spacing, and equal amplitudes, and wavelengths where wavelength is a function of unit thickness, tend to be associated with buckling (Morley, 1994). Folds associated with faults are often isolated and irregular. Where folds were determined to be fault controlled, the geometry, especially dip of fold limbs, and location of fold axes, was used to infer the geometry and position of the controlling fault (Boyer & Elliot, 1982; Mitra, 1990). If low-

angle detachments were either observed or inferred, they were assumed to converge onto a single décollement horizon at depth, unless evidence suggested otherwise.

Section balancing was tested using Midland Valley's 2D Move software (Version 3.1) in which a number of horizons in the transects were digitised and then sequentially restored (maintaining area) to a pre-deformed state. The first stage of the restorations was the removal of extensional faults, and the associated unrotating of the hangingwall. As there were few syn-rift data it was difficult to remove the effect of the extension, such as footwall rotation. However, the evidence below shows that an approximation of the original fold belt geometry can be achieved. The restored foldbelt geometry was then unfolded by applying 2-D Move's restoration function on four horizons (top Ripon Formation, Middle Ecca, Permian; top Witteberg Group, Middle Devonian; top Bokkeveld Group, Devonian / Silurian; and top Peninsula Formation) assuming an original layer-cake sedimentary model for the Cape Supergroup. Any resulting overlap or deficit of units was a result of an incomplete model. Although the Cape Supergroup was deposited on a passive margin and hence southward thickening away from the hinterland may be expected, the thickness data discussed above suggests that any such thickening is insignificant and therefore the layer cake model is an appropriate assumption. The exception to this is the Peninsula Formation, which is discussed below. The transects, and corresponding models produced using 2-D Move are non-unique solutions, although they are presented as the most geologically valid. In some instances, more than one geometry can explain the observed data in which case alternative models have been proposed.

3.2.2 Specific problems and limitations to section balancing

The Pre-Cape unit, which previous workers have assumed underlies the entire Cape Supergroup (Hälbich, 1983b), is only present in two inliers in the study area. Even where there is exposure, there are very few structural data, therefore the Pre-Cape unit has not been included in the transect reconstructions.

A consistent problem in all of the transects is the lack of structural data present in the Peninsula Formation outcrop. As will become evident, Peninsula Formation outcrops generally form large-scale folds with structurally well constrained limbs, but poorly constrained cores. This problem is addressed in Transects A and B as field data were used to constrain both large and small scale geometries. In the other transects the structure of the fold cores were kept as simple as possible.

The Upper Devonian sequence (cf. Da in transects) is often poorly constrained as it is relatively thin, although commonly has a very wide outcrop pattern. A subsidiary section to Transect A suggests that the Upper Devonian has a significant number of minor folds which account for the wide outcrop; this observation was used in less well defined areas in the other transects.

As a result of significant uplift and erosion the extent of the units is not always evident, and this posed some problems of how far to extrapolate the data. The Permian Karoo sequences, which are at the north of the transects, were deposited in the developing foreland basin of the CFB (cf. Chapter 2), and are therefore unlikely to have been deposited across the whole area. For this reason they have not been extrapolated significantly to the south of their present outcrop. The Devonian and older sequences crop out right across the foldbelt to the south coast in at least one transect, and therefore were extrapolated across the whole foldbelt. There is no evidence on the maps of the northern extent of these units beneath the Karoo Basin, however, published data from boreholes and geophysical data beneath the Karoo (Hälbich, 1983b) suggest that the units continue without significant thinning across this area.

A further complication is the inconsistency in naming and colour coding of units and formations between the geological maps. In each transect the mapping units have been kept as they remain on the maps (map key shows the different terms used in each map) although colour coding has been made consistent. In the text, units are referred to collectively as ages, except for the Peninsula Formation because of its importance in the region. Enclosure 1 is a table of the mapped units and a correlation between transects.

3.3 Regional transects

The position of the transects are shown in Figure 3.1, and each is discussed separately in the following sections. The data used to construct each transect have been plotted onto stereonet that are shown in Figure 3.1. Each section contains a structural summary, and a discussion on the pre-compressional restoration of the transects.

3.3.1 Transect A (Figure 3.2, Enclosure 2)

i) Structure

The northern end of the transect, formed from the Permian Karoo sediments, shows a southward transition from gentle undulations to a zone of increased folding culminating with two moderate scale folds (wavelengths 4 and 2 km, and amplitudes of approximately 2000

m). Although some beds within the folds are overturned there is no evidence of substantial deformation, however, the slight asymmetry, overturning of northern limbs and shallower southern limbs is suggestive of northward vergence.

The contact between Permian and Devonian units is undeformed and dips gently (15°) towards the north. However, unlike the other transects, the Devonian outcrop in this transect shows a significant degree of deformation with a series of moderately tight, northward verging, asymmetric folds which lie above a moderate (50°), northward dipping contact with the lower Devonian/Silurian units. The Peninsula Formation crops out towards the south.

The northern end of the Peninsula Formation outcrop is north-dipping and relatively undeformed and forms the north limb of a large scale monocline. Three sketches in Figure 3.3 illustrate deformation typical of the Peninsula Formation along the Seweespoort Pass on Transect A. The overall structure of the pass is a Z fold rotated by 90° with moderate to steep northward dipping north and south limbs, with a sub-horizontal central section. This dominantly quartzitic sandstone formation shows characteristic bedding-parallel thrusts (see Figure 3.9b in Transect B), and small scale (1-5 m wavelength) northward verging folds. Later brittle faulting cross-cutting the folds is also present in the Pass (Figure 3.4), and although the timing and nature of these faults are unknown it is suggested that they are associated with Mesozoic extension. These field observations, supported by the map data, suggest the Peninsula Formation forms either a 10 km wide anticline / syncline fold pair, or a gentle monocline depending on the dip of the core area of the fold.

To the south of the folded Peninsula Formation (Op) there is an abrupt change to the Devonian (Ds) before a northward dipping repetition of the Devonian to Peninsula sequence. There is very little evidence (in particular contact dip direction) to constrain the geometry at the faulted contact between Op and Ds. The most feasible geometries are either a northward dipping reverse fault, emplacing the Os formation on top of the Ds unit, or a southward dipping normal fault (Figure 3.5a). The second of the two models is preferred because the system is northward verging at a regional scale, therefore a southward verging thrust fault with a substantial displacement is inconsistent. Furthermore, along strike to the west the Kango normal fault is present (Figure 3.1). It is inferred that this fault is a continuation of the Kango Fault, without preservation of the Mesozoic unit in the hangingwall.

To the south of the fault, Devonian to Peninsula Formation sequences form a broad, slightly asymmetric, northward-verging anticline (wavelength 15 km, amplitude 2000 m), although it is uncertain how much of this folding is a result of rotation by the inferred normal fault to the

north. The south-dipping limb forms the northern limb of an open syncline, which itself forms the northern, steep, though not overturned, dipping limb of a large wavelength fold cored by Peninsula Formation. The deformation within the core is poorly mapped, although there are three faults which have unknown displacements and dips. The most southern of the faults down throws towards the south, and it is suggested that this has a normal attitude. The southern limb of the fold gently, and consistently, dips towards the south approximately 20 km north of Devonian outcrop. In this transect there are virtually no data in the Devonian, however, the subsidiary section, 10 km to the west, shows that the unit gently undulates.

The southern-most extent of the transect shows an abrupt change from the undeformed Devonian sequences to highly deformed, near vertical to overturned beds on the south coast. This geometry is similar to the northern limbs of anticlines present in other transects, therefore it is inferred that this forms the northern limb of a large anticline, the remains of which is currently offshore. The presence of the Da unit (Middle Devonian) at the coast appears out of place, and without data to the south is very difficult to include with certainty in the model. However it is suggested that as the contact between Da and the Peninsula Formation is faulted this may be a south dipping normal fault (Figure 3.5b).

ii) Foldbelt reconstruction and underlying structure

The folds evident in the Karoo sediments are irregular with synclines and anticlines with non-consistent amplitudes and wavelengths. As discussed in Section 3.2.1, these observations imply that the folding is unlikely to be a result of buckling, and are therefore probably controlled by underlying faults. Furthermore, the asymmetric nature of the folding, with sub-vertical to overturned northern limbs and moderately steep (50°) south dipping southern limbs, suggests a moderate, southward dipping controlling fault, as shown on the transect. As is the case throughout the transects, the key question is whether these faults continue with a steep dip, or décolle, and if so, at what level is the décollement? In the Karoo Basin, the other transects (in particular Transect B) suggest that the décollement has to be deeper than the Peninsula Formation. In this transect, therefore, the inferred faults are continued to beyond the base of the Peninsula Formation and into the Pre-Cape unit. The 2D-Move restoration of the inferred fold geometries at depth (assuming that bed thickness of units remains constant and that the faults do not décolle until at least the Pre-Cape unit) produces an incomplete model as is evident from the area deficit in the Peninsula Formation (Figure 3.2c). The model also predicts that the fold-controlling faults have an extensional throw at depth. Despite these apparent problems with the models, the transect shows the

geometries in this way as it is the simplest model. The problems with this transect are common in many of the transects and will be discussed later.

In the central and southern parts of the transects, two normal faults are evident and as these are assumed to be Mesozoic age, need to be removed to obtain the original CFB geometry. The lack of syn-rift sedimentation within the hangingwalls of the faults makes restorations difficult to achieve with any certainty, although it is assumed that the normal faults caused hangingwall rotation and subsidence, and footwall uplift. When the faults were removed, and fault blocks appropriately rotated, the result was three box folds in the main CFB area. It is suggested that these box folds are controlled by three underlying faults, the nature of which will be discussed at the end of the chapter.

3.3.2 Transect B : Merringspoort-George (Figure 3.6, Enclosure 3)

i) Structure

The Karoo sediments show gentle, symmetric undulations (wavelengths ~ 2.5 km) to the north of a zone of sub-vertical dipping sediments forming a syncline-anticline pair (wavelength and amplitudes ~ 4 km). Despite the steep dip, there is little internal deformation of the Lower Permian Whitehill Formation except for a persistent south-dipping cleavage (e.g. in the shale unit at the north of the photograph in Figure 3.7). This location forms the core of an asymmetric anticline that has an overturned, shorter, northern limb and a southern limb with a dip of approximately 60° . This pattern of tight overturned anticlinal folding is repeated again towards the south into the Devonian sequences, although the wavelength and amplitude of the folding is reduced (2 km wavelength, 1.5 km amplitude).

The majority of the Devonian sequences are sub-horizontal, with gentle undulations for approximately 8 km to the north of an abrupt increase in bedding dip towards the north, and the subsequent exposure of the Cape Supergroup, and in particular the Peninsula Formation, which forms the Swartberg Mountains. Excellent exposure allowed a sketch-montage to be compiled (see next section), which supplements the map data. Two examples of sketches detailing the complex structures present in this area are reproduced in Figure 3.8. An overturned contact at the base of the Peninsula Formation marks the change to the Pre-Cape Kango Group. The repetition of the three Kango units, all of which are overturned, implies a complex underlying structure. However, with the limited data it is impossible to include these within the transect.

The southern boundary of the Kango Group is defined by the Kango Fault that juxtaposes the Mesozoic Enon Formation against the basement. The geometry of the basement below the Mesozoic sediments is unconstrained, therefore it is assumed that it is undeformed and dips towards the fault in a similar geometry to that of Transect A. There is little control of the internal structure of the Mesozoic basin, although field observations (cf. Chapter 4) suggest a gentle dip towards the north.

The geometry of the middle Cape Supergroup directly to the south of the Mesozoic basin is difficult to determine. The southern dip of the Silurian units (Sb and Sk), especially as they are overturned, suggests that they form the northern overturned limb of an asymmetric anticline. The Peninsula Formation is folded towards the south and appears to be geometrically consistent with a short wavelength box fold (4 km). Over a short distance, the southern limb of the box fold changes to approximately 13 km of gently undulating Devonian sediments. This sequence then changes to a small (2 km wavelength) northward verging asymmetric fold, with an overturned northern limb. A further zone of relatively undeformed Devonian sediments is present before significant Peninsula Formation deformation that has an overturned lower contact with the Pre-Cape Kango Group. The Kango Group probably forms the core of an anticline towards the south.

ii) Meeringspoort Pass transect (36-40 km on Transect B, Figure 3.9 and Enclosure 4)

One of the major uncertainties with the transects is the geometry of the Peninsula Formation because of the lack of structural data. The aim of conducting this transect (see Figure 3.9 for summary section and Enclosure 4 for the full section) was to address this problem by analysing a critical exposure of the Peninsula Formation through the Meeringspoort Pass in the Swartberg Mountains (see Enclosure 3 for position). Although the outcrops along the pass have been discussed in the literature (Söhnge & Hälbig 1983 and references there in), there is not a published complete section through this part of the CFB and the purpose of this transect is to obtain an overview of the deformation. Due to the complexity and difficult access to the exposures the transect is compiled from sketch-montages supplemented by photographs, sketches, and field data. The key objectives of the section are to highlight:

1. the overall geometry of the exposed strata at Meeringspoort Pass
2. the variability of structures within it
3. some small scale structural analysis

The Pass is almost entirely composed of quartz sandstones of the Silurian, or quartzites of the Peninsula Formation without any internal marker horizons. It is therefore impossible to conduct any restoration of the transect.

a) Faulting

Throughout the transect, and the CFB as a whole, the Peninsula Formation is dominated by well cemented quartzitic sandstones, and quartzites. On a small scale, the dominant features are bedding surfaces approximately every 0.5 m, commonly with cross-bedding evident, that have been pervasively utilised by reverse faults (Figure 3.9b). Occasionally shales and siltstones are present between the quartzite beds with reverse shear indicators present. These bedding/thrusting structures are present every 0.5-1.0 m throughout the entire 8 km length of the exposure.

Evidence of large scale thrusting is present at a number of places especially at locality E (Enclosure 4) which juxtaposes Lower Silurian units upon the Peninsula Formation. This locality is further complicated by folding which has been described as being syn-depositional (Coetzee, 1983). Across the area the lack of marker horizons makes reconstruction and determination of fault throws very difficult.

As in the Seweweekspoort Pass (Transect A, Figure 3.4), larger scale brittle faults that cross cut the folded basement are evident (Figure 3.9.e). Although no shear sense indicators are present, it is suggested that these may be later stage normal faults associated with the Mesozoic extension.

b) Folding

The Meeringspoort Pass area is pervasively folded at wavelengths from 2-3 m up to the 8 km length of the exposure. Across the transect there appears to be a lower wavelength threshold value of approximately 2 m. Since bed-thickness is consistently 0.5-1 m, it is likely that this controls the wavelength threshold. The styles of folding also vary along the transect and although no detailed fold analysis has been carried out, the general features are important in determining the overall structure.

The main features are noted on the sketch section (Enclosure 4), and below only the summary points are discussed. Throughout the sections, as will be shown on the accompanying stereonet, all beds have an approximate east-west strike. This is therefore in agreement with the regional scale trends shown by the stereonet in Figure 3.1.

North

The transition from the Devonian to Silurian units is poorly exposed because both units are predominantly comprised of easily weathered sand and siltstone, although an overall northward dipping nature to the contact is observable.

The dominant feature in the north is steep north-dipping, occasionally sub-vertical to overturned beds with very little internal deformation except for bedding-parallel thrusting, and jointing perpendicular to bedding; no small-scale folding is present. These beds (Figure A, Enclosure 4) form the northern limb of a shallow, southerly dipping, large open fold (fold plane dip of 15° towards the south). The southern limb is formed from sub-horizontal beds that also show little internal deformation except for the occasional southerly plunging kink band.

Further south, deformation progressively increases from south-plunging kink bands (Figure B, Enclosure 4) to a series of stacked chevron folds that have an average axial plane dip of approximately 20° to the south (Figure C, Enclosure 4). In the mountains above the pass, there are large scale (>100 m wavelength) Z folds with horizontal long limbs and sub-vertical short limbs.

Central

Silurian units are thrust on top of the Peninsula Formation and complex geometries with frequent faults, both high angle and low angle thrust faults, are evident (Figure D, Enclosure 4). However, as has been discussed at the beginning of the section, the lack of a marker unit makes it impossible to determine either extent or displacement of these thrusts.

To the south of this complex zone, there is a substantial area where there is very limited deformation with sub-horizontal, and gently undulating beds (Figure E, Enclosure 4), similar to Figure 3.3b in the Seweweekspoort Pass, Transect A.

South

The predominantly undeformed, sub horizontal beds of the southern central area abruptly change to predominantly steep to overturned beds in the south (Figure F, Enclosure 4). Internal deformation is accommodated by tightly stacked chevron folds with wavelengths of 10's metres, and gentle (20°) southerly dipping axial surfaces. This series of stacked chevron folds then changes to less folded, sub-vertical beds with little internal deformation apart from the occasional shallow dipping southerly plunging kink band (Figure G, Enclosure 4).

The southern contact of the Peninsula Formation the Pre-Cape unit is not visible, although the southern end of the exposure shows steep northward dipping and overturned Peninsula Formation (Figure 3.9.j).

Overall structure

The transect through the Merringspoort Pass suggests that the overall structure is an overturned Z fold (Figure 3.9) which is consistent with previous workers (Coetzee 1983). Within the overall geometry, there is significant variability with a combination of open and tight isoclinal and chevron folds. The structural analysis using the stereonets on the transect (Figure 3.9) shows that all folds and kink bands throughout the transect are north verging, with an approximate east-west trend, and relatively shallow dipping axial planes.

iii) Fold Belt reconstruction and underlying structure to Transect B

The folds at the northern end are asymmetric and northward verging, implying that they are being controlled at depth by a northward verging reverse fault. Coetzee (1983) suggests that the faults controlling the Karoo folds décolle onto the Cedaberg Formation (Oc) directly above the Peninsula Formation. However, the large amplitude nature of the folding (in particular the inferred depth of the synclines) suggests that the décollement has to be deeper than the Oc level. When the units are projected at depth and the section is restored, the same problems as observed in Transect A of non-balanced section and apparent extensional faults at depth occur.

The restoration to the pre-extension state using 2D Move produces a more complicated geometry than that in Transect A, although the overall geometry is still one of large scale kink bands or box folds. The anticlinal geometry (55-60 km on Transect B) appears to be a box fold with a low-angle thrust deforming its northern limb; Hälbich (1983a) suggested that it was a broad fold that underwent subsequent thrusting.

In the model of Transect B (Figure 3.6) it is proposed that there are five principal faults controlling the deformation observed. This does not include the southern exposure of the Pre-Cape unit where the data are too limited.

3.3.3 Transect C : North-West Willomore to Plettenberg (Figure 3.10, Enclosure 5)

i) Structure

In this transect, the amount of deformation of Karoo sediments is less compared to transects A & B, with only moderate undulations, small fold amplitudes (~500 m compared to 4000 m) and occasional overturning of the northern limbs of folds. To the south, where the Dwyka tillite (Pd) outcrops, there is increased folding with sub-vertical and overturned beds across a narrow zone. This highly deformed area changes to a wide exposure of Upper Devonian (Da) with few structural constraints. In other transects, where there is better structural control, the broad outcrop pattern of the thin Da unit is explained by gentle undulations. In this transect it is therefore assumed that to maintain uniformed thickness the unit has to have minor undulations, as well as a small kink band that is evident from the data available.

As with the previous transect, the undeformed area abruptly changes to overturned Lower Devonian / Silurian sequences to the south that are likely to form the northern limb of an anticline. The core of the fold is a very narrow band of Peninsula Formation, dissected by the Kango Fault, which down throws to the south and has Mesozoic sediments preserved in the hangingwall. There is limited structural data within the Mesozoic basin, although there is a general northerly dip towards the fault and the southern boundary onlaps onto the Upper Devonian (Da).

To the south of the Mesozoic basin the geometry of the Upper Devonian outcrop is difficult to determine because of limited structural data; where there are data, there is a relatively steep northerly dip despite a wide outcrop pattern. This steep dip and wide outcrop requires sedimentological thickening, tectonic duplication, or significant folding. Sedimentological thickening is unlikely because of thickness consistency both along and between transects, and there is no evidence of tectonic duplication, therefore it is inferred that there is significant small scale folding.

The Upper Devonian sediments to the south are juxtaposed against the Silurian sediments by a southerly dipping reverse fault. Although the dip of the fault is not evident, the bed and cleavage to the south are both relatively steeply dipping (50° - 70°) suggesting a relatively steeply dipping reverse fault, especially if thrusting and folding are axial planar to cleavage.

The Silurian sequence (Sk), which the high angle reverse fault emplaces upon the Upper Devonian sediments, forms the northern limb of a southerly inclined syncline, cored by lowermost Devonian. The southern limb is overturned and forms the northern limb of the next anticline to the south, which itself is cored by the Pre-Cape sequence. Across both of these folds, the cleavage consistently dips moderately towards the south. It is useful to note that the wavelength of these folds is not substantial considering the amplitude (10 km by 10km), although the southern anticline is broader (15 km) with approximately the same amplitude. The internal geometry of the Peninsula Formation is very poorly constrained, therefore the nature of the anticline can not be determined accurately. There is no map evidence that there is a significant thrust, hence the geometry used in the transect is that of a fold with the minimum thickness of Pre-Cape unit. This assumption is supported by the low northward dip of the Pre-Cape unit. The southern extent of the Pre-Cape unit is defined by a south dipping fault with Peninsula Formation preserved to the south. The nature of the fault is unknown, although the possibilities are either a south dipping normal fault, or north dipping reverse fault (Figure 3.11). The same arguments apply as for Transect A (Figure 3.5), and therefore a south dipping normal fault is preferred.

The downthrown Peninsula Formation to the south of the fault forms the southern limb of a faulted anticline and the northern limb of a further syncline to the south. As in previous transects, the internal geometry of the Peninsula Formation is poorly constrained. The amplitude of both folds is inferred to be approximately 5 km, however, the anticline is considerably broader than the syncline (wavelength of 12 km compared to 6 km). Exposure is poor across this region, although where available the field data (Figure 3.12) imply that the styles of deformation are similar in this transect to that observed in the others. Deformation styles are also similar at many scales, with kink bands at centimetre scale, Figure 3.12a, and at 100m scale, Figure F, Enclosure 4. Evidence of later brittle faulting is also present in this transect (Figure 3.12b).

The Peninsula Formation crops out in the two belts towards the south and although the geometries are poorly constrained, these outcrops are probably cores of small anticlines. As in the other transects, the Peninsula Formation comprises bedded quartzites with bedding parallel thrusts (Figure 3.13a). This locality also shows isoclinal folds that are being cross cut by later thrusting, and both are northward verging. Towards the south coast, a fault juxtaposes two Silurian units (Sk and St) against each other. As with faults elsewhere, the dip is unknown, and therefore a south dipping normal fault is the most likely geometry.

Between the fault and the south coast there are intermittent the Mesozoic sediments lying unconformably on top of significantly eroded Peninsula Formation (Figure 3.13b).

ii) Fold Belt reconstruction and underlying structure

The folds in the Karoo sequences are asymmetric, suggesting a north-verging controlling reverse fault at the northern end of the transect. These folds are smaller than equivalent folds in previous transects, therefore when the horizons are projected to depth the problem of apparent extensional faults at depth does not occur.

When the Mesozoic extensional faults are removed, the restored fold belt has three box-folds with only minor asymmetry towards the north west, therefore it is proposed that there are three principal faults controlling the central and southern areas. The 2D modelling shows that the southern part of the transect does not have area preservation. This may be because of sub-surface geometries that have not been inferred, or differential thickening of the Peninsula Formation (e.g. Figure 3.13a) that has not been restored properly due to insufficient data.

3.3.4 Transect D (Figure 3.14, Enclosure 6)

i) Structure

The Karoo sediments at the northern end of this transect show remarkably little folding in comparison to the transects to the east, although there is a series of southward dipping faults (approximately 200-1000 m displacement on each). Two of these faults have been mapped with a reverse nature and the other two are extensional. A further normal fault is present to the south that juxtaposes Permian sediments (Pd) against a Middle Devonian sequence (Dk) with a displacement of approximately 1500 m.

As in the other transects, the exposure of Da shows very little deformation, with only small undulations, and a minor north verging kink band. To the south of this undeformed section, deformation increases, although not as significantly as in other transects. The folding here is open (inter limb-angles of 135°) with only moderately dipping southern limbs. A further fold to the south becomes increasingly steep, with an overturned southern limb, although the wavelength and amplitude is small (2 km by 3 km) in comparison to the large anticlines to the east. Furthermore, there is no surface outcrop of Peninsula Formation. The folding of the Lower Devonian sequences is truncated by a down-to-the-north fault, which is interesting for two reasons. First, it downthrows to the north, therefore, is either a south dipping reverse fault, or a north dipping normal fault. The south dipping reverse fault is preferred because

the faults observed elsewhere are all southerly dipping, and the foldbelt is northward verging, therefore a south dipping reverse fault is consistent with the regional model. Second, although the dip of the fault is unknown, the dip of the hangingwall is relatively steep (60° towards the south) and it is inferred that the fault has a similar attitude. This relatively steep hangingwall dip shallows abruptly, returning to the sub-horizontal and gently undulating outcrop of the Upper Devonian sequences, as observed in other transects.

Another south-dipping reverse fault deforms the sub-horizontal Devonian sequences and juxtaposes Peninsula Formation on top of locally deformed Devonian sediments. The Peninsula Formation outcrop is bounded to the south by a southward dipping normal fault, with Mesozoic sediments preserved in its hangingwall (Figure 3.15). The majority of the outcrop from the Mesozoic basin to the south coast is Peninsula Formation with some notable exceptions. Three of the four exceptions are outcrops of Lower Silurian deposits that core northward-verging synclines with shallow northern limbs, and steep or overturned southern limbs. The fourth exception is a small, but important, outcrop of Pre-Cape Unit. This has a faulted southern contact against Peninsula Formation, which downthrows to the south, and is therefore inferred to be a normal fault (see previous transects, e.g. Figure 3.11, for discussion). This normal fault dies out towards the east, as shown by the supplementary section in Enclosure 6. This supplementary section shows the Peninsula Formation forming a 12 km wide, and approximately 6 km high box fold. As with most of the transects, the nature of the internal structure of the Peninsula Formation is difficult to ascertain, although the available data imply that the deformation is similar to that observed in the Meeringspoort Pass (Transect B, Enclosure 4). On the southern coast, exposures in gorge cuttings show that although the Peninsula Formation is in places sub-vertically dipping, there appears to be little internal deformation except for the characteristic bedding-parallel thrusting (Figure 3.15b).

ii) Fold Belt reconstruction and underlying structure

The small reverse faults in the Karoo Basin are not accompanied by substantial folding and there is very little to suggest at which level they décolle. The two other compressional faults involve Ordovician units, consequently it is suggested that they decollé below the Peninsula Formation.

The removal of the three extensional faults to the pre-extension fold belt geometry reveals three anticlinal box folds each separated by narrow synclines that are similar to the other transects. Restoration of the horizons to the horizontal indicates that the Silurian units have

longer line lengths than the other units, although as in previous transects this may be a result of internal thickening, especially within the Peninsula Formation.

3.3.5 Transect E : Western Algoa Basin through the Algoa Basin (Figure 3.16, Enclosure 6)

i) Structure

As with the other transects, there appears to be localisation of the deformation in the Karoo sequence. The northern area gently undulates with shallow plunging, open folding, whereas towards the south there is an abrupt change with two overturned, south-dipping limbs of northern-verging anticlines (wavelengths of approximately 6 km and amplitude of 3 km).

The southern limb of the southern most anticline is folded directly north of a down-to-the south normal fault with approximately 2000 m throw. A small outcrop of the downthrown block is preserved north of the onlap of the north-western Algoa Basin Mesozoic sediments. There is no evidence of controlling faults on either side of the Mesozoic outcrop, suggesting that either there is a series of smaller faults within the basin, or the system is onlapping from the central basin (to the south-east) into a topographic low. Within the Mesozoic sediments there is very little structural data. Furthermore there is no exposure of the basement, although a transect to the west of the main transect implies that there is moderate folding of the basement (wavelengths approximately 800 m and amplitudes of 500 m).

Where the basement is exposed to the south of the Mesozoic outcrop, there is a relatively undeformed sequence of Devonian sediments that abruptly changes to highly deformed lower Devonian and Silurian sequences, which form the steep dipping northern limb of a box fold cored by Peninsula Formation sediments. Although the exposure of the Peninsula Formation is not as good as further to the west, the deformation appears to be very similar. In this area structures including bedding parallel thrusts, isoclinal folds, open folds and steep dipping, undeformed beds adjacent to the normal faults are observed (Figure 3.17). To the south, the anticlines cored by the Peninsula Formation passes into a Silurian-cored syncline with a moderately undulating and deformed core. The southern limb of this syncline is overturned and contains the contact with the Peninsula Formation, which youngs to the north and has a southern contact with the rarely outcropping Lower Ordovician (Os). A poorly exposed sequence of Pre-Cape Unit is present between the Os Formation and the Gamtoos Fault (see Chapter 4 for field data) and is steeply dipping to overturned (Figure 3.17c). Shone & Booth (1992) have suggested that the contact between the Os and Pre-Cape Units is

faulted. With the available data it is impossible to integrate the Pre-Cambrian units into the transect.

Data from the Mesozoic Gamtoos Basin are discussed in Chapter 4 although the minimum depth of the basin (2326 m; McMillan, 1999) is controlled by well (Lo1/69), and has been included in the transect.

The southern margin of the basin onlaps onto to the steeply dipping to overturned northern limb of a further Peninsula Formation cored box fold, which is the northernmost of a series of four syncline-anticline pairs. These fold pairs are all inferred to have flat-topped box fold geometry, with steep northern limbs and shallower southern limbs. The wavelengths and amplitudes of the anticlines are on the order of 10-16 km and 2 km, respectively, with the intervening synclines showing considerably shorter wavelengths (4 km), but similar amplitudes. An exception occurs in the middle of the transect where the anticlines are less defined and smaller (4 km wavelength), however, these are the lateral terminations of along strike anticlines.

ii) Fold Belt reconstruction and underlying structure

The only part of this transect that requires reconstruction is the Gamtoos Fault, however, because of the magnitude of displacement and the lack of structural data in the immediate footwall (Pre-Cape Unit), an accurate reconstruction is difficult to achieve. Therefore, in the restored section, the Cape Supergroup in the hangingwall has been restored to the elevation of the equivalent horizons in the footwall. It is impossible to project the Pre-Cape Units from the available data.

3.3.6 Summary of transects

The five transects that have been discussed are approximately 125 km long from north to south, and cover nearly 400 km from west to east. Despite this wide distribution, the field data, observations and transects show remarkable similarity in their geometries (Figure 3.18). The most consistent observations are :

- a) All of the transects appear to have very different geometric characteristics in the north and the south. This change appears to occur in approximately the same position as the southern boundary of the Southern Cape Conductive Belt (SCCB) (Figure 3.1; Beer, 1983).

- b) The north of the transects tend to have open folds with more obvious northward verging asymmetry.
- c) The central and southern areas typically show large-scale folding and deformation, generally in the form of steep limbed box folds cored with Peninsula Formation, or Pre-Cape Units, with wavelengths of the order of 10-15km. Both the northern and southern limbs tend to be steep. Internal structures within the folds are beyond the resolution of the map data, although they have been assessed in the Meeringspoort Pass, Transect B, Enclosure 4.
- d) The deformation is not uniformly distributed across the region. Some areas show very little or no deformation, and these are commonly where Upper Devonian (Da unit) outcrops, while others show significant deformation e.g. Peninsula Formation of the Meeringspoort Pass. The average width of the anticlines is of the order of 8-15 km whereas the width of the synclines is 2-4 km.
- e) The oldest units exposed in the CFB are the Pre-Cape units that are Pre-Cambrian or Cambrian in age (cf. Chapter 2).
- f) Where normal faulting occurs, it is commonly directly to the south of the northern limb of a box fold in the Peninsula Formation or Pre-Cape unit. This will be discussed further in Chapter 4.
- g) Extension is restricted to the central and southern parts of the Cape Supergroup.
- h) Similar styles of deformation, e.g. chevron folds, bedding-parallel thrusting, occur at various scales and across all of the transects.
- i) Field data and published data show approximate east-west structural trends, suggesting a north-south compression orientation with little or no oblique component (Figure 3.1)
- j) There is no evidence of large scale thrusts with features indicative of large amounts of transport, e.g. roof thrusts, allochthonous blocks. There is only one transect that shows evidence for the development of a nappe (Transect B).
- k) The percentage of shortening varies considerably along the trend of the CFB and between the north and south (summarised in Figure 3.1).

3.4 Comparison with other compressional orogenies and discussion

It is not the intention to carry out a full review of thrust tectonics here (e.g. McClay *et al.*, 1992) but it is important to assess the summary of the transects outlined in the previous section in light of other compressional orogenies. Compressional orogenies in continental settings are typically represented by fold and thrust belts. Although there are significant variations between settings, fold and thrust belts have many characteristics in common. They typically have thrust faults with developed mylonitic fabrics, klippen, low angle frontal ramps, imbrications, varying degrees of metamorphism, juxtaposition of out of sequence units (e.g. Boyer & Elliot, 1982; Butler, 1982b; Coward, 1984; Butler *et al.*, 1986; Dewey *et al.*, 1986; Le Fort, 1986; Vann *et al.*, 1986; Hossack, 1983; Mitra, 1990; Spring & Crespo-Blanc 1992; Mercier *et al.*, 1997; Philippe *et al.*, 1998). The style of deformation presented for the CFB, especially in the south, is therefore atypical of fold and thrust belts.

Three models are presented to explain the principal observations from the transects and the possible underlying control on the development of the CFB (Figure 3.19). The first two models both invoke a low angle regional décollement horizon, while the third predominantly utilises high angle reverse faults.

In models i) and ii) (Figure 3.19b) the deformation is proposed to be controlled by an underlying regional décollement. Although the depth of this horizon is unknown, the involvement of Pre-Cape units implies that it must be stratigraphically within, or below the Pre-Cape unit and therefore must have a depth of at least 10 km. In model i) the box folds are predominantly controlled by northward verging reverse faults with the southern limbs of the anticlines formed from southward verging antithetic faults, both of which assimilate onto the décollement horizon. This model is similar to Butler's (1996) pop-up model for Alpine deformation. In this model the décollement horizon splays to form the deformation at the north of the transects.

Model ii) invokes a more complex underlying structure with the box folds being controlled by duplex formation beneath the folds, with the upper Pre-Cape and Peninsula Formation units being deformed passively. The northern end of this model has a similar controlling geometry to that in model i).

The observed deformation in the south of the transects is explained in model iii) by south dipping high angle reverse faults with north dipping antithetic faults, in a similar geometry to that of the pop-up features in model i). The principal difference between model i) and iii) is

that the faults in the later model do not assimilate at depth, or at least not in the brittle upper crust (cf. Jackson & White, 1989). Such faults may be the remnants of the extensional normal faults associated with the pre-existing passive margin which were re-activated as reverse faults during the Cape Orogeny (see discussion below). In the north of the transects the deformation is accommodated by a low angle thrust fault as in the previous two models. In this model the change in tectonic nature may be explained by thin skinned compression occurring in the north and thick skinned in the south (Jackson, 1980; Boyer & Elliot, 1982; Coward, 1984).

From the available data it is difficult to determine which model is correct and it is the aim of the following chapters to constrain these models further. However it is useful to discuss additional available data. The only subsurface geophysical data come from a seismic reflection profile (discussed in Hälbig, 1993) which shows: 1. a distinct boundary at 6 s two way travel time (~16 km); 2. a reflector at 18 km that may be a décollement; and 3. the reflection moho at 9.5 s TWT (~30 km). The section is along the south coast of Transect C and it is therefore uncertain how such a horizon projects towards the north.

The data required to support model iii) would be syn-rift thickening into the inferred normal faults at depth, however, because of the lack of exposure and poor quality data available in the Pre-Cape Unit, this is not possible. Model iii) is however supported by sand box modelling of Beer (1983) in which the formation of box folds were simulated using high angle reverse fractures in the basement below the sand layers (Figure 3.20). Furthermore, the size and distribution of the box folds (approximately 15 km wide), and therefore the inferred controlling faults, is not of a dissimilar scale to that of extensional faults in a passive margin setting (Jackson & White, 1989).

A problem that is not solved in any of the models is that of the apparent extensional geometries when the sediments beneath the Karoo Basin are projected to depth. There are no data to suggest that the packages do thicken into the faults, therefore it is difficult to determine the nature of these faults at depth.

All three models suggest that the northern and southern areas have very different structural styles (Figure 3.18) and this may be a result of the underlying crustal character because the division between the two areas coincides with the southern extent of the Southern Cape Conductive Belt. Hälbig (1983b) suggests that the crust containing the SCCB is considerably weaker compared with to the southern area (cf. Chapter 2), and may play a role in determining the overlying structure. However, in all three models it would appear from

the amounts of shortening that the observed strain is greater south of the SCCB and from the transect data it appears that the SCCB may form a buttress which prevents the deformation migrating further to the north. This would contradict Hälbich's assumption of the SCCB being weaker.

3.5 Conclusions

Despite the various styles and degrees of deformation across 400 km, there is remarkable similarity at all scales, suggesting the region is responding to a single phase of deformation in a predictable way. The transects presented imply that the formation of the CFB may have been influenced by pre-existing crustal structures, and hence structural inheritance may play a role. Three models have been proposed to explain the development of the foldbelt. The first two models have deformation being accommodated by a low angle detachment fault, while the third model has high angle structures, and it has been suggested that such geometries may be controlled by the pre-existing passive margin. However, there is insufficient evidence from these observations alone to determine which of the models is most suitable. Data from the following chapter will be used to constrain the models further.

This chapter has only addressed the question of the overall structure of the CFB, and not the nature, or control of basement structures on the subsequent Mesozoic extension. The next chapter will discuss how the onshore Mesozoic geology can be used to constrain the understanding of the CFB further.

CHAPTER 4: The Role of Structural Inheritance on the Onshore Mesozoic

4.1 Introduction

The regional scale architecture of the Permo-Triassic Cape Fold Belt (CFB) has been demonstrated in the previous chapter. This chapter uses the onshore Mesozoic geology to examine the role of CFB structures in the development of the subsequent extensional system.

The interaction between the underlying foldbelt and Mesozoic extension will be ascertained by examining the structural trends of the extension, and comparing them with basement compression orientations. The structural styles and sedimentology of two of the principal onshore basins (Oudtshoorn and Gamtoos) will be integrated with results from the regional transects and used to predict the underlying structure of the CFB and geometries of the extensional systems at depth.

4.2 Exposure limitations

The original aim of the fieldwork was to conduct detailed structural and sedimentological transects perpendicular to the Mesozoic faults with a view of determining whether there are: along-strike variations in basement structures and corresponding variations in the early syn-rift sedimentation (cf. Chapter 2). Unfortunately the levels of exposure in both basement and the Mesozoic basins were very poor, therefore the original aim of the fieldwork was not attainable. The fieldwork was restricted to understanding the larger scale structures within the stratigraphic framework established by previous workers (Chapter 2).

4.3 Data, methodology

The trends of extensional features and compressional structures were compared on a regional scale using published geological maps (RSA Geological Survey maps 3320, 3420, 3322, 3324) and validated through structural fieldwork (cf. Chapter 3). The fieldwork presented in this chapter was conducted across the Central and Eastern Cape to develop a better understanding of the exposed Mesozoic basins, and the immediately adjacent Cape Fold Belt.

4.4 Mesozoic and foldbelt structural trends

The superimposition of Mesozoic basins upon the older Cape Supergroup has long been recognised (cf. Chapter 2), as has the similarity in the structural trends of the two units. These observations are evident when the trends of the principal CFB compressional features and the Mesozoic normal faults are plotted together (Figure 4.1), and when the normal faults are plotted on the stereonet of basement structures from Chapter 3 (Figure 4.1c). However, such data do not connote the nature of the interaction at depth.

To determine the interaction at depth, a better understanding of the Mesozoic sub-surface geology is required. The following two sections will assess the suitability of using the onshore Mesozoic structural and sedimentological data to infer the geometries of the Mesozoic basins at depth. The two areas studied are those with the best Mesozoic exposure; the Oudtshoorn Basin in the Central Cape and the Gamtoos Basin in the Eastern Cape.

4.5 Oudtshoorn Basin

The exposure in the Oudtshoorn Basin is very limited, although as Figure 4.2 shows, there are some important observations that can further the understanding of the area. The basin is bounded to the north by the Kango Fault, a south-dipping (40°) normal fault that juxtaposes Mesozoic conglomerates against Pre-Cape sediments. The Mesozoic sediments are poorly sorted and predominantly quartz-clast conglomerates that are bedded in packages that dip and thicken towards the Kango Fault (Figure 4.2c). It is impossible from the available field data to ascertain fault displacement.

The unfaulted southern margin of the basin consists of a substantial northward prograding conglomeratic sequence (Figure 4.2b) that lies on Devonian sediments of the Cape Supergroup. Interestingly, the clasts in this paraconglomerate are dominantly indurated laminated grey siltstone; in comparison, other Mesozoic conglomerates are dominated by a quartzite provenance (Dingle *et al.*, 1983), most likely to be from the Peninsula Formation. At this locality, however, the siltstone clasts are Bokkeveld Group, and are sourced from either outcrops directly to the south, or erosion of the Bokkeveld Group from the top of the mountains cored by Peninsula Formation that lie further to the south.

There is very little other evidence that can be used to constrain the extensional geometry at depth.

4.6 Gamtoos Basin

As in the Oudtshoorn Basin, there is limited, localised exposure in the Gamtoos Basin, making it difficult to correlate between outcrops. Where possible, structural mapping was conducted and a summary of the geology of the basin is accompanied by structural field data in Figure 4.3a. Fieldwork involved mapping the contacts between the CFB, Pre Cape and Mesozoic in the north of the onshore Gamtoos Basin. The contacts used in the south of the Gamtoos Basin, and the Algoa Basin have been taken from the published geological maps (RSA Geological Survey map 3324). The most important feature on the map is the change in regional basement structural trend from the west-east structures of the Central Cape (pole to the π -girdle of 00.2 to 096, Figure 4.3c) to the NW-SE orientation of bedding and structures in the Gamtoos Basin (pole to the π -girdle of 07 to 133°, Figure 4.3b). However, despite this significant difference, the style of deformation present in the basement is consistent between the two areas (Figure 3.17 in Chapter 3). This change in basement trend is accompanied by an identical change in orientation of the Gamtoos Fault that further supports the suggestion that there is a correlation between Mesozoic and basement structural trends.

The Gamtoos Fault is not visible anywhere in the basin, although the contact is inferred to run between the alluvial sediments of the Mesozoic and the phylitic shales of the Pre-Cape unit (Figure 4.4a). From these poor levels of exposure it is impossible either to undertake structural analysis of the fault contact, or infer sub-surface geometries using surficial syn-rift structures. It is also difficult to determine if there are internal structures within the basin, although the exposures that are visible (Figures 4.5b, 4.6a) suggest that there is very little intra-basinal deformation. These exposures also suggest that the basin was predominantly filled by fluvially dominated sandstones and flood plain mudstones with occasionally significant erosional surfaces (McLachlan & McMillan 1976; Dingle *et al.*, 1983). The poor levels of exposure do not enable correlations between outcrops or identification of classic wedge shaped syn-rift packages thickening into the fault (cf. Prosser, 1983). This prevents the determination of early syn-rift depocentres making it impossible to apply current fault growth models (cf. Chapter 2) to the onshore Gamtoos Fault.

In the north-west of the basin (Figure 4.5a), the trend of the Gamtoos Fault changes dramatically from NW-SE to NE-SW. The southern end of the NE-SW section terminates against an east-west trending, south dipping normal fault. An important consideration is whether extensional strain is localised on the Gamtoos Fault, or if it is uniformly distributed

across this part of the basin. If it is the later, then the basement to the west of the NE-SW portion would be expected to show evidence of extension (Figure 4.5a). The presence of the Komodo Dam enables a detailed structural section to be constructed to the west of the NE-SW Gamtoos Fault section (Figure 4.5b), and reveals no evidence of extension. Although this is a very limited outcrop compared with the length of the fault, it indicates that the extensional strain may be localised on the Gamtoos Fault and is not dissipated.

Also present in the north of the basin is the Enon conglomerate which is composed almost entirely of clast supported quartz pebbles, cobbles and boulders (Figure 4.5b). The stratigraphic position of the Enon is uncertain although it has been suggested that it is either the lateral equivalent to the Kirkwood Formation (Figure 4.5a), or topographic infill prior to the principal phase of Mesozoic extension (Dingle *et al.*, 1983). There is insufficient outcrop to determine whether the package thickens into the fault. Regardless of its stratigraphic position, it is important to note that it has been sourced from the Peninsula Formation. The extent of the deposit is unknown, although two exploration wells, Mk1/70 and Lo1/69 (Figure 4.3 for locations) both terminate within the Enon having drilled through 2326 and 1058m of the conglomerate respectively. These wells also show that the later syn-rift sediments are Hauterivian estuarine deposits (determined from foraminifera, McMillan, 1999).

4.7 Cross-section geometry

The previous sections have discussed the close correlation between the structural trend of the Mesozoic and the basement, however, it has not been possible to assess the correlation at depth. Therefore, the only method of examining the relationship between the extension and compression at depth is to use the transects from the previous chapter.

The foldbelt reconstructions from Figure 3.18 have been re-produced in Figure 4.7 and the positions of the extensional faults have been superimposed in order to compare the location of extension with the underlying fold belt. In all of the transects, apart from Transect D in which there is very little evidence of extension, the extensional structures consistently occur immediately to the south of the northern limbs of box folds. In Transect D the reverse fault is directly to the north of the normal fault and may be a footwall cut-off fault, although there are insufficient data to validate this.

4.8 Discussion

Four models are proposed that describe the role of basement in controlling the Mesozoic extension at depth (Figure 4.8). The first model (Figure 4.8b) proposes that there is no control at depth and that the extension cross-cuts the underlying structure (shown here as a low angle thrust system). This model, however, does not explain why the extension consistently occurs in a structurally similar setting (i.e. at the northern end of box folds). The other three models are revised from those proposed in Chapter 3 (Figure 3.19b). In both the low angle reverse fault with pop-up structure model (Figure 4.8 c i) and the high angle reverse fault model (Figure 4.8 c iii), the fault controlling the formation of the northern limb of the box fold is reactivated in extension. Both of these models require antithetic faults to account for the steep southern limb of the box fold. The third model, invoking box fold formation through underlying duplexing (Figure 4.8 c ii), requires the reactivation of thrustal flats and ramps to accommodate the extension. In this model the position of the extensional fault would therefore be determined by the specific nature of the underlying duplexes and it is unlikely that the inferred complex duplexing would result in the consistent position of extension that is observed.

4.9 Conclusions

The onshore Mesozoic geology of the Central and Eastern Cape suggests that there is a correlation between the trends of the Cape Fold Belt (CFB) and the subsequent Mesozoic extension. Furthermore, by superimposing the locations of extension onto the transects derived in the previous chapter it becomes apparent that the extension appears to utilise the northern part of the central flat of the box folds. Although the data were used to propose four models (three of which revised from Chapter 3) only two (low angle thrust with pop-up structures and high angle reverse fault) explain the observations without significant complexities.

Structural inheritance, therefore, has a significant role in the development of the Mesozoic extensional system. However, from the data discussed so far the nature of this control at depth is uncertain. This uncertainty will be addressed in the following three chapters in which data seismic data will be used to evaluate the offshore Mesozoic sedimentary basins.

CHAPTER 5: Sub-Surface Data and Methods

5.1 Introduction

The role of structural inheritance in the development of the Mesozoic extensional systems has been demonstrated, at least in plan view, in the onshore studies presented in the previous chapters. However, these onshore studies do not reveal the nature of the inheritance at depth. Offshore seismic reflection and well data have been used to evaluate this interaction in the sub-surface. Before this can be discussed it is important to have an understanding of the methods used and the limitations of the study; these are addressed in this chapter.

5.2 Data set

Sub-surface data (seismic and boreholes) from the offshore portions of three sedimentary basins in southern South Africa have been made available by the Petroleum Agency South Africa (formerly SOEKOR) for this study. The basins that will be studied are (from west to east): Pletmos, Gamtoos, and Algoa (Figure 5.1).

5.2.1 Seismic data

The seismic data are 2D seismic arrays with various vintages from four exploration tranches (Ga, Gb, Ha and Hb) covering a total aerial extent of 23,000 km² with 19,000 km of seismic section (Table 5.1); the coverage and distribution of the data for each basin will be discussed in the appropriate chapters. The 2D seismic data were obtained in digital format and interpreted using Schlumberger GeoQuest IESX Version 3.1 software at the University of Edinburgh. All seismic data have a vertical axis in milliseconds two-way-travel-time (ms TWT) with maximum recording values of either 5000 or 6000 ms. With the exception of specific sections, it was outwith the scope of this study to undertake depth-conversion. The data were processed by the Petroleum Agency South Africa, and although approximately 60% of sections were stacked and migrated, and the remaining only stacked, no significant problems were encountered in merging the data. The data were rotated to zero phase during processing, have a negative recording polarity, 60 fold geophone coverage, 25 m shotpoint interval and a range of high and low frequency recording filters that are shown in Table 5.1.

i) Seismic interpretation

The primary aim of the interpretation of the seismic data was the determination of mega-sequences using seismic stratigraphy techniques (Hubbard *et al.*, 1985a & b) through the identification of seismic reflector geometries (e.g. downlap, onlap, erosional truncation; Mitchum *et al.*, 1977), and associated unconformities and correlatable conformities. Seismic reflectors were picked on the zero phase (+/-) of the wavelet, and interpretations had to be internally consistent between sections. In all three basins, mega-sequences were attributed to the broad classification of pre-rift, syn-rift or post rift, defined by the nature of the internal reflector geometries (Prosser, 1993; Hubbard *et al.*, 1985a).

Individual mega-sequences were sub-divided into sequences to obtain a more detailed understanding of their constituent stratigraphic sequences. Sequences are conformable packages within a mega-sequence; the top of each sequence was defined by a seismic trace with an easily identifiable character (Hubbard *et al.*, 1985 a& b). The defining upper horizon of each sequence was constrained by age data from 41 boreholes (Section 5.2.2), and the appropriate age was attributed to the horizon, and underlying sequence. A regional seismic stratigraphy was established using the available age data (Figure 5.2). As a consequence of limited well data, and the presence of localised sequences, this stratigraphy was not always applicable to particular basins. Wherever possible this seismic stratigraphy was used, although in all of the basins there are variations (highlighted in Figure 5.2), with some sequences not being present, or additional sequences required to further the understanding of specific packages.

Where seismic horizons were faulted, the position of footwall and hangingwall cut-offs were marked, and the corresponding fault planes defined. For each horizon, the position of the cut-offs were plotted and correlated between sections to demarcate fault polygons. Defining such fault polygons often proved to be problematic. Where the throw on the fault is large, and line spacing is small, individual faults were easy to correlate between sections. However, where the fault throw was small, and line spacing was large, defining fault arrays was difficult. The largest faults were demarcated first, and then fault character (e.g. dip and approximate strike), was used to correlate the smaller faults. In some instances, especially where line spacing was large, it was difficult to determine whether faults either had throws beyond seismic resolution, or coalesced with neighbouring fault arrays.

Once the chosen horizons had been interpreted, various analyses were undertaken. The principal analysis was the calculation of isochrons (thickness in TWT) between specific

horizons using IESX software, allowing the thickness of mapped sequences to be obtained. Where the sequence had a para-conformable base, the isochron was calculated between the upper horizon and various lower horizons. The isochron calculation determined the vertical difference in TWT between the two horizons, therefore if the horizons were dipping the isochron value would be greater than the true sequence thickness. Across most of the region, the dips of the horizons are small, and the difference between isochron and true package thickness is considered to be minimal.

In addition to calculating sequence isochrons, cumulative sediment thickness was plotted. These plots were calculated from the *top_basement* horizon to a specific horizon to assess how cumulative sediment accumulation varies through time.

All data, whether horizon TWT, or isochrons, have been presented as contour and grid plots. The contouring and gridding was achieved using the least squares algorithm in the IESX software with the convergent/blanking option that accounts for footwall and hangingwall cut-offs and fault polygons.

ii) 2D Move restoration

To understand the temporal evolution of the geometries within the basins, specific sections were modelled using Midland Valley's 2D Move restoration programme. This programme sequentially restores horizons, from youngest to oldest, to the horizontal. A specific horizon is restored to an appropriate elevation, and the underlying horizons undergo vertical shear restoration to maintain area preservation. By this method, progressively older horizons were restored to the horizontal and the temporal evolution of observed geometries ascertained. It is, however, important to state that this restoration programme produces a non-unique solution, and there is no assessment of associated errors. Furthermore, although inclined shear can be applied, it is impossible to determine the true shear during the deformation. Vertical shear was therefore consistently used in all restorations. Despite these limitations, the programme is useful in understanding observed deformation.

iii) Errors and resolution

In general, the minimum vertical resolution of seismic data is a quarter of one seismic wavelet (Badley *et al.*, 1990; Pickering *et al.*, 1997). As the wavelength of the wavelet increases with depth, the minimum resolution correspondingly decreases, and it is estimated that the resolution varies from approximately 10-50 ms TWT depending on the depth of the reflector and the acquisition frequency (Table 5.1). Such an error, even at depth, is generally

negligible compared to the scale of the sequences that are of interest. Where the error is significant with respect to the observed feature (e.g. small-scale faults), the implications will be discussed. The horizontal resolution of the seismic pick, defined by the Fresnel zone, is deemed to be insignificant compared to line spacing, and can be ignored.

Some parts of the basins have been faulted significantly and with limited well control, the position of a particular horizon could be uncertain. In such cases, cross correlating-between sections from well-controlled positions, using the most reasonable geological interpretation, was undertaken.

Direct comparisons between sequence isochron thicknesses have to be considered carefully. As a consequence of both lithological and compaction variations with depth, if two sequences have the same isochron thickness, the lower sequence will tend to have a greater true depth in metres (assuming the lower sequence is more sand-rich, which the data in subsequent chapters will show as being valid). Such errors are difficult to quantify, and can only be excluded by depth conversion of the entire seismic data set, which is beyond the scope of this study. Therefore, these errors will be discussed where appropriate.

Although complete depth conversions will not be conducted, for specific sections it is essential to carry out approximate depth conversions; the method and associated errors will be discussed in Chapter 9. In preceding chapters approximate depth conversions will use data from McMillan *et al.* (1997).

5.2.2 Well data

The two primary applications for the well data were: to ascribe age data to seismic horizons both to date seismic packages, and to constrain seismic correlations across the basin; and integrate seismic observations with other data, including sedimentology and depositional environment.

In total 41 wells were used in the study, although the types of data available vary for individual wells. A summary of these data types are listed below, and each chapter contains the details for individual wells. It should be noted that no analytical work has been conducted on these well-logs as part of this study and that the data presented, including environmental interpretations, have been obtained from Petroleum Agency South Africa. In this study the principal work undertaken was to calculate time-depth conversions, and to extract and compile the well data relevant to the study.

i) Available data

Composite Logs: These logs contain standard down-hole recordings including gamma, caliper, and lithological descriptions of basket/side-wall cuttings. Of particular importance are gamma readings that were used to determine lithological variations, including coarsening/fining upward sequences.

Time-tops: This database (McMillan, 1999) gives the depth to the top of age units. Data are presented only in depth (metres) and therefore have been converted to time, see (ii) below.

Check-shots and synthetic seismograms: These data provide information on the time-depth relationship for individual wells.

Lithofacies: Contained in these logs are: lithological descriptions; dip-meter readings (some of which have had structural dip removed), and interpreted paleo-environments.

Palynology: These contain paleo-environment interpretation from palaeontology studies.

ii) Time-depth conversion

The depth to each available age datum is presented in the time-tops database (McMillan, 1999) in depth (metres) and requires conversion to depth (TWT). Each well contains discrete points at which depth-time conversion is known from the synthetic-seismograms and check-shots, although the majority of required time-top points are between the discrete values. Table Curve 3.0 graph package was used to calculate the best least squares fit correlation equation for each well using the available time-depth data. The resultant equation was then used to calculate the depth (in TWT, ms) to the top of each time period for individual wells. Graphs corresponding to the depth-conversions for individual wells are included in the appendix for the appropriate chapters.

iii) Sedimentation rate calculations

To understand the evolution of particular sequences within the syn-rift packages, sedimentation rates were estimated using well data and the time-top. Rates were calculated in metres per year. These rates are subjected to significant errors and have to be used with caution. The primary error is that of the age constraints, and this will be discussed in the next section. The other significant error is in determining sequence thickness as a consequence of erosion and differential compaction. These errors will be discussed for individual examples.

iv) Errors

The principal problem with the available data is that as a study of the raw data, especially palaeontology and age data, has been out with the scope of this project, it is difficult to assess the reliability of the data. However, in most cases this is not considered to be significant because the integration of seismic data with well data allows for consistency between data sets to be ascertained. Furthermore, as all the age data have been interpreted using the same technique by Petroleum Agency South Africa, it is assumed that the data is consistent between basins.

Tying of data to regional events is also problematical, especially ascribing specific ages to the defined periods. Petroleum Agency South Africa have tied palaeontological data to recognised time periods using the Haq *et al.* (1988) timescale for specific ages. This timescale has not been used in this study because it has been superseded by more recent studies, and there are problems tying the timescale to specific regional events. An example of the latter problem is that of the opening of the South Atlantic, which has been attributed to the sea floor magnetic anomaly M10 (Hauterivian, 130 Ma) by Nürnberg & Müller (1991), and Austin & Uchupi (1982). Haq *et al.* (1988) places M10 and the Hauterivian at 121 Ma, while Gradstein *et al.* (1995) dates it at 130 Ma and Harland *et al.* (1990) at 130 Ma. As Gradstein *et al.* (1995) is the most recent it has been used for this study, although this creates a problem because it uses the Rhyzianian stage, whereas the available data uses the Portlandian. This is important for sedimentation rate calculations and will be discussed where appropriate.

5.3 Understanding fault and basin evolution

To understand the evolution of the faults and basins within this study, it is important to recognise that the creation and evolution of accommodation space in the hangingwall of a normal fault is intimately associated with the growth of that fault (cf. Chapter 2; Leeder & Gawthorpe, 1987; Prosser, 1993; Gawthorpe *et al.*, 1994; Anders & Schlische, 1994; Contreras *et al.*, 1997; Gawthorpe & Leeder, 2000). As discussed, faults have been demonstrated to grow by isolated radial growth and segment linkage (Figure 5.3; Walsh & Watterson, 1987; Cowie & Scholtz, 1992a, b; Cartwright *et al.*, 1995), although many examples illustrate that faults may grow by a combination of the two (e.g. Cartwright & Mansfield, 1998; Morley & Wonganan, 2000). In 5.3a, an isolated normal fault is illustrated with displacement at a maximum at its centre and decreasing along strike resulting in onlap

onto the basin margins. The fault grows by radial propagation, and through time the fault propagates laterally whilst increasing displacement. In Figure 5.3b, four small isolated segments, and associated depocentres are present at the beginning, and grow by radial propagation in a similar mechanism to Figure 5.3a. Through time the segments interact and become mechanically linked resulting in a single fault comprised of the four segments. Correspondingly, the depocentres grow and progressively interact. In both models, the characteristic hangingwall cross-section and displacement-length profile are illustrated. Using well-tied seismic stratigraphy the determination of hangingwall cross-sections and displacement-length profiles for a particular fault system can be used to establish the spatial and temporal evolution of sedimentary basin and infer the evolution of the fault system (e.g. Gupta *et al.*, 1998; Morley, 1999; Contreras *et al.*, 2000; McLeod *et al.*, 2000; Young *et al.*, 2001) and this method is used in this study. Although accommodation space can be created by both tectonic subsidence and eustatic variations (Leeder & Gawthorpe, 1987) in this study sequences are typically between 500 and 1250 ms TWT thick (equivalent to 500 – 1500 m), therefore eustatic variations are considered as secondary. A further consideration is whether sediment accumulation can be used as a proxy for accommodation space. Although well data is available, there is insufficient data to address the question of sediment supply, therefore observed sequence thicknesses will be a minimum value for the available accommodation space. Redistribution of sediments will tend to be remobilised to the deepest areas of the basin and will therefore preferentially record local depocentres (McLeod *et al.*, 2002)

5.4 Conclusions

This Chapter has outlined the methods that will be used in the following three chapters to evaluate the evolution of the offshore Mesozoic basins using sub-surface data. The methodologies for both interpretation of the seismic data and subsequent modelling have been described, as have some of the limitations and inherent errors in the methods.

CHAPTER 6: Tectonic Evolution of the Offshore Gamtoos Basin

6.1 Introduction

The premise that structural inheritance played a role in the development of both the Cape Fold Belt (CFB) and the onshore Mesozoic extension has been explored in Chapters 3 & 4. Although previous studies have discussed this (cf. Chapter 2), the nature of the sub-surface interaction between the CFB and the extensional system is still uncertain. Likewise, the role of structural inheritance on the subsequent evolution of the extensional system has not been addressed.

The aims of this, and the following two chapters are to use sub-surface, offshore data to constrain the nature of the interaction between the CFB and extension at depth, and assess whether structural inheritance has influenced the evolution of the Mesozoic basins. This chapter will focus on the Gamtoos Basin, which has the best tectono-stratigraphic control of the three basins, while the following two chapters will examine the Pletmos and Algoa Basins.

To understand the role of structural inheritance in the formation and subsequent evolution of the basin, it is important to understand its overall tectonic framework. This framework will be established by defining tectono-stratigraphic mega-sequences, as outlined in Chapter 5. The distribution and nature of both basin-bounding faults and intra-basin faults will then be determined prior to an evaluation of structural styles within the sedimentary basin fill. The results from these three sections will be integrated with paleo-environment data from Petroleum Agency South Africa to establish the overall basin evolution. Only then is it possible to address the nature of the interaction between basement and the Mesozoic basin, and the role of structural inheritance in the development of the Gamtoos Basin.

6.2 Gamtoos data

This study has utilised 4,272 km of 1976, 1982, 1983, 1985 and 1987 vintage 2-D multi-channel seismic data (Figure 6.1) with maximum recording times of either 5000, or 6000 ms two-way time (TWT). Approximately half of the data have been migrated while the half have been stacked, although there are no discernable problems in correlating between the two data sets. The seismic data have been tied to 10 boreholes (Appendix A), which are

summarised in Figure 6.2 and reproduced in Appendix 1.C. Throughout the chapter, seismic sections will be reproduced and the positions of the lines are plotted on Enclosure 8.

6.3 Tectonic and stratigraphic framework

The determination and characterisation of sequences and mega-sequences, integrated with available well data, are used in this section to develop a tectonic and stratigraphic framework of the Gamtoos Basin. This framework comprises four mega-sequences, namely: Basement; Principal Syn-Rift; Late Syn-Rift; and Post-Rift. The Principal Syn-Rift mega-sequence is divided into six sequences, and these are evident in the two regional sections (Figure 6.3a & b). The seismic character, areal extent and thickness in TWT of each mega-sequence and sequence will be discussed. Although the primary aim is to understand the tectonic evolution of the basin, the sedimentology of each of the sequences is assessed briefly (summary of wells in Figure 6.2 with complete well logs in Appendix 1.C).

6.3.1 Basement

The *top_basement* is a strong seismic reflector (commonly a doublet) onto which the overlying syn-rift sequences onlap. Across much of the basin, the strength of the reflector results in significant lateral continuity allowing the horizon to be traced with confidence. However, as seismic resolution decreases as a function of depth, in the centre of the basin, where the reflector is deepest, the confidence of the pick is reduced. This error is increased because the reflector is occasionally deeper than the longest recording depth of 5s TWT in some of the sections. To alleviate this problem, the TWT map of *top_basement* (Figure 6.4a) has the locations at which the reflector crosses 5s TWT marked.

From the TWT map and 3D sketch (Figure 6.4a and b), it is evident that the dominant offshore basement feature is the Gamtoos Fault, which down-throws towards the south and south-east, defining an arcuate-shaped half graben. In the NW the fault is a direct continuation of the onshore Gamtoos Fault (Chapter 3) and has a NW-SE trend, while in the east there is an abrupt change in orientation to a north-south orientation. The geometry of the fault will be discussed in a later section (6.4.1).

The basement high, which forms the footwall to the Pletmos extensional basin to the west, is predominantly composed of milky-white to grey quartzite interbedded with slates and other meta-sediments (wells Ha-H1 and Ha-J1). This is consistent with the Cape Fold Belt (CFB) observed in the onshore portion of the Gamtoos Basin (Chapters 3 & 4). The only other well

to penetrate basement was drilled through the Gamtoos Fault in the NE (well Ha-K1) and as in the other two wells, indicates that basement is sedimentologically identical to the CFB.

Smaller faults are present within the basin (*top_basement* TWT map, Figure 6.4a), especially on the basement high in the west, where there are complex fault geometries (Section 6.4.2). These faults are traceable in plan view and have an arcuate trace similar to the Gamtoos Fault. In the centre of the basin, low seismic resolution makes it difficult to map faults, although a zone of deformation is observable.

6.3.2 Pseudo-basement

Although the overall basin geometry can be determined from TWT maps even where *top_basement* is deeper than 5 seconds TWT, calculating accurate isochron plots between Principal Syn-Rift horizons and *top_basement* is more problematic. Where basement is deeper than 5 seconds, the resultant isochron is artificially thin, which creates difficulties when sediment thickness is used to infer fault evolution (Section 6.4.1). To reduce this error, a pseudo *top_basement* horizon (called *top_ps.basement*) has been identified that is the lowest reflector that is fully correlatable across the whole basin and therefore enables accurate isochron maps to be plotted. Although this results in a package between *top_basement* and *top_ps.basement* being excluded from the syn-rift isochron plots it enables isochron plots to be compared.

6.3.3 Earliest Syn-Rift ?

In the west of the basin there is evidence of a wedge-shaped seismic package beneath the picked *top_basement* horizon. This is most evident in a north-south orientation (Figure 6.5) where it appears to thicken towards the north and may be truncated against a fault. However this package is not imaged well enough in perpendicular sections to be able to determine either its extent or geometry. It has also not been penetrated by any of the wells, and therefore has not been included in the overall tectonic framework.

6.3.4 Principal Syn-Rift (Middle? Jurassic-Late Valanginian)

This mega-sequence is bounded at the base by onlap onto the *top_basement* (Figure 6.2b), and at the top either by erosional truncation below a basin-wide unconformity, or a paraconformity and associated correlative conformity with the Late Syn-Rift mega-sequence in the NE of the basin. As this mega-sequence accounts for over 75% of the basin fill, it has been divided into six sequences to develop a better understanding of its evolution. These sequences were originally defined using seismic character, although it transpires that the

division of the sequences closely matches the age boundaries determined from well control. In some wells there is a mis-correlation between well data and seismic data and in these instances, because the basin architecture is of more importance than detailed age correlations, seismic continuity and reflector ties are preferential to well mis-ties. Furthermore, such mis-ties may be a result of the seismic reflectors not being true chrono-stratigraphic markers. For each sequence the following data are presented:

1. ages from published Soekor Time-Top database (McMillan, 1999),
2. grided and contoured TWT maps with associated fault polygons to evaluate the overall basin geometry,
3. inter-horizon isochron plots to determine the evolution of the sequence,
4. sedimentology from Soekor well logs and reports are summarised (complete wells are included in Appendix A).

The sequences are named after the defining top horizon and are referred to by the age of that horizon.

i) Kimmeridgian

Although the deepest sediments in the basin have not been penetrated, the oldest dated sediments are Kimmeridgian and are found on the western basement high. This sequence, which is defined as the oldest syn-rift package above *top_ps.basement*, is a relatively transparent package with occasional strong, bifurcating reflectors. The *top_kimmeridgian* horizon is defined by a very strong triple reflector that is traceable across much of the basin with the middle trace taken as the sequence top.

The two wells that penetrate this sequence (Ha-J1 and Ha-H1) are both on the western high. They demonstrate that the sequence contains a combination of coarsening and fining up sediment packages between red grit, occasionally pebbly quartzitic sandstone, and red-green siltstones. Although the wells in the centre of the basin do not penetrate to a suitable depth to encounter this sequence, the thickening nature of the seismic package (which will be discussed later), and areal extent of the *top_kimmeridgian* reflector (Figure 6.6a), suggests that this sequence underlies the entire syn-rift package. The TWT map (Figure 6.6a) shows that in addition to the Gamtoos Fault and the faults in the western basement high, there are a limited number of intra-basin faults in the south-east.

Sedimentation occurred across the entire basin, as is evident from the isochron plot of *top_ps.basement* to *top_kimmeridgian* (Figure 6.7a) with the thickest sediment accumulation occurring against the north-south trending portion of the Gamtoos Fault. There is no significant accumulation in the adjacent hangingwall of the east-west trending Gamtoos Fault, nor is there evidence of differential accumulation across the intra-basinal faults.

ii) Early Portlandian

Across much of the basin, the Early Portlandian sequence (defined by *top_e-portlandian*) is conformable with the Kimmeridgian, although towards the east there is evidence of downlap at the base of the Early Portlandian sequence onto the *top_kimmeridgian*. However, because of the poor resolution at this depth (4 seconds TWT) it is difficult to determine the specific geometry and the lateral extent of the unconformity. As the majority of the basin has a conformable contact, this complexity will be ignored.

The Early Portlandian package is characterised by strong, commonly closely spaced reflectors, and towards the top of the sequence the reflectors become increasingly well defined with a series of six very fine traces. Overlying these six traces there is a transparent package prior to a strong negative trace, and this strong trace defines the top of the sequence.

At the base of the Portlandian in the west, the coarse grained sandstones of the Kimmeridgian fine-up to a silt, before abruptly becoming a grey claystone. The Portlandian sequence is the deepest that is penetrated by the wells in the centre of the basin where it is predominantly grey silt and claystone with black shales identified at the base of Ha-B2. There are however pulses of very fine to fine, occasionally coarse grained sands, often with sharp top and bottom contacts intermittently through the section.

The TWT map of the *top_e-portlandian* (Figure 6.6b) has a similar geometry and fault distribution to the *top_kimmeridgian* map (Figure 6.6a), except that there is a greater number of intra-basin faults. The Early Portlandian sequence thickens towards the Gamtoos Fault (Figure 6.7b, isochron plot of *top_kimmeridgian* to *top_e-portlandian*) with the locus of maximum sediment thickness occurring at the apex of the Gamtoos Fault curve rather than against the north-south section of the fault as in the previous sequence. Unexpectedly, the locus of maximum sediment thickness is not immediately adjacent to the fault, instead there is an axis of lower sediment accumulation against the fault. Such a distribution may be expected to be controlled by a SW-NE trending fault however there is no evidence to support this in the seismic data. Possible causes of this unusual distribution will be discussed later.

iii) Late Portlandian-Mid Berriasian

The defining upper horizon in this package does not correspond as closely to a specific age as the other syn-rift sequences, although it is in the Late Portlandian to Mid Berriasian, and is named *top_m-berriasian*. The seismic character is a more transparent sequence than the underlying packages with finer, higher resolution reflectors capped by a series of three strong double reflectors. The first negative trace of the lowermost of the three double reflectors defines the top of this sequence and is traceable across the basin.

The dominant clay lithology of the previous sequence continues in the Late Portlandian across the whole basin. The number of sand bodies increases in this section, although unlike the sharp beds in the lower sequence, these tend to be in coarsening-up packages with sharp tops.

As is evident from the seismic section (Figure 6.3b) and the TWT map (Figure 6.6c), there are more intra-basin faults compared to the underlying sequences. Sediment accumulation continues to be focused at the apex of the Gamtoos Fault curve (isochron plot of *top_e-portlandian* to *top_m-berriasian*, Figure 6.7c), although in this plot the locus of maximum accumulation is now adjacent to the fault.

iv) Upper Berriasian

This sequence sits conformably above the Middle Berriasian package and is formed from the series of three double reflectors of which the lowest one is *top_m-berriasian*. The top of the package, *top_u-berriasian*, is the uppermost reflector in the series.

In the west of the basin the amount of clastic material in the dominantly clay and silt sediments is reduced compared to the Portlandian and Lower Berriasian, although where present it is very similar petrologically with a mixture of lithics and quartz clasts. In the centre and east there is an influx of shelly and lignitic material compared to the dominant clay lithology in the west.

The Gamtoos Fault and the basement high faults observed in the previous sequence are mappable in this sequence (TWT in Figure 6.6d), as are an increased number of intra-basin faults in the south and east that show no evidence of differential sedimentation across them. This increase is accompanied by the development of observable deformation near to the apex of the Gamtoos Fault curve, the architecture and genesis of which will be discussed in Section 6.5.2.

The locus of accumulation for this sequence (*top_m-berriasian* to *top_u-berriasian* isochron, Figure 6.7d) migrates further to the north and west compared to the lower sequences, with increased accumulation proximal to the west-east section of the Gamtoos Fault, although deposition is not necessarily greatest adjacent to the fault.

v) Early Valanginian

The Early Valanginian sequence, defined by *top_e-valanginian*, is very similar in seismic character to that of the Upper Berriasian package with three double reflectors correlatable across the basin.

Sedimentologically, the western area continues to be almost entirely dominated by claystone, with occasional siltstones and limestones. In the north, well Ha-D1 has an influx of medium to coarse grained, well sorted quartzitic sandstone, and this may have been derived from the fault scarp. The sandstones in well Ha-A1 are, however, quite different as they are fine to medium grained light grey sands with wood fragments and coaly horizons. Throughout the rest of the basin there is a significant reduction in the sand content with the sediments being almost completely dominated by claystone with occasional siltstones.

The increased intra-basin faulting and deformation observed in the Upper Berriasian (Figure 6.6d) is even more evident in the *top_e-valanginian* (TWT map in Figure 6.6e) and again there is no evidence of differential growth across the intra-basin faults (*top_u-berriasian* to *top_e-valanginian*, Figure 6.7e). This package has a uniform sediment thickness across the basin with the exception of the apex of the Gamtoos Fault and the western basement high, where minor thickening and thinning occurs respectively.

vi) Late Valanginian

The *top_l-valanginian* horizon is the uppermost horizon of the Principal Syn-Rift and is either eroded by the *basin-wide_unconformity* or NW unconformities, or is overlapped by the Late Syn-Rift mega-sequence (Figure 6.3a & b). It is cut by very few intra-basin faults (Figure 6.6f). A consequence of the partial erosion of the Late Valanginian sequence is that the *top_e-valanginian* to *top_l-valanginian* isochron plot (Figure 6.7g) does not produce the true thickness of the sequence. Despite this, it is evident from the plot that there is renewed sedimentation accumulation against the Gamtoos Fault, although it is focussed against the east-west section portion rather than at the apex of the curve.

Across the whole basin there is very little clastic input with the sequence being dominated by claystone, with occasional siltstone and limestones.

6.3.5 Late Syn-Rift

This mega-sequence, which is sub-divided into four sequences, lies conformably above the Late Valanginian proximal to the east-west trending Gamtoos Fault in the northern part of the basin and is also present to the west of the basement high block. The mega-sequence is bounded at the base by the *top_l-valanginian*, at the top by the *basin-wide_unconformity*, and internally divided into four sequences by three horizons (Late Syn-Rift (LSR) I, II, and III). These horizons are defined by strong, continuous reflectors that are easily traceable across the extent of the deposit, and have been mapped to develop a better understanding of the unit.

In comparison to the Principal Syn-Rift, the extent of this mega-sequence is restricted to the hangingwall of the east-west portion of the Gamtoos Fault in the north and east and onlaps onto the *top_l-valanginian* horizon in the south (Figure 6.8). LSR I is the most restricted (Figure 6.8a) and is contained entirely in the hangingwall of the east-west Gamtoos Fault. LSR II has a greater areal extent (Figure 6.8b) while the full extent of LSR III (Figure 6.8c) is unknown because of erosional truncation in the north and west. Only the lower most unit is cut by the intra-basin faults that are present in the Principal Syn-Rift package. Although the three LSR horizons dip towards the south (Figure 6.8), the LSR I sequence dramatically thickens towards the east-west trending Gamtoos Fault (isochron plot of *top_l-valanginian* to *top_LSR-I*, Figure 6.9a). This is in contrast to the Late Valanginian package that exhibits sedimentation across the whole basin with only moderate thickening into the fault (Figure 6.7e). Unlike the LSR I package, there is no evidence of LSR II (Figure 6.9b) thickening into the Gamtoos Fault except in the western most margin, although thickening is resumed during the LSR III package (Figure 6.9c). A result of the basin-wide unconformity (Section 6.4.6) is the significant erosion of the Late Syn-Rift mega-sequence above LSR III, although as is evident from the seismic section (Figure 6.3b) some sedimentation is preserved against the Gamtoos Fault. Late Syn-Rift sedimentation is also preserved to the west of the basement high and is inferred to be above LSR III because the *top_LSR-III* horizon onlaps onto *top_l-valanginian* further to the east. However, when the isochron between *top_l-valanginian* and *basin-wide_unconformity*, i.e. the preserved thickness of the Late Syn-Rift mega-sequence, is plotted (Figure 6.10) there is very little sedimentation in the west. Even accounting for erosion during the formation of the basin wide unconformity, sedimentation is still focussed upon the Gamtoos Fault.

The change in areal extent of deposition between the Late Valanginian and the Latest Valanginian is accompanied by a change in sedimentology. The Late Valanginian, which was dominated by grey claystones changes to a dark, commonly anoxic, claystone throughout this mega-sequence. Proximal to the Gamtoos Fault there are occasional, thin interbeds of predominantly medium-coarse grained, occasionally pebbly quartzitic sandstones.

6.3.6 Basin-wide unconformity

Directly above the Late Syn-rift package there is an unconformity (*basin-wide_unconformity*) which is traceable as a single horizon across the whole basin that shallowly dips towards the south (Figure 6.11), although is itself truncated by a subsequent unconformity in the north-west (Figure 6.12). As discussed in the previous sections, there is a significant amount of erosional truncation of both Late Valanginian and LSR sediments directly below this horizon (Figures 6.3 a & b). Furthermore, as the sub-crop map highlights (Figure 6.13), the unconformity has resulted in the erosion of a significant amount of material, and on the basement high has a sub-crop of quartzitic basement.

6.3.7 Barremian

Directly above *basin-wide_unconformity* is a small package of Barremian sediments that occur on the western margin. This sequence is present only in well Ha-J1 and is sedimentologically identical to the Late Syn-Rift massive grey claystones and occasional beds of medium-coarse, red-brown, sorted and rounded quartzitic sandstone. This sequence extends into the Pletmos Basin towards the west.

6.3.8 Localised Late Syn-Rift

The *basin-wide_unconformity* dips towards the south, forming a planar horizon (Figure 6.11). The exception to this is in the south-east of the basin where there is a very localised Albian package (see eastern part of section, Figure 6.2a, and Figure 6.14a). This package thickens towards the Gamtoos Fault (isochron plot of *basin-wide_unconformity* to *top_albian*, Figure 6.14b), and divergent nature of the internal reflector geometries (Figure 6.14c) suggest that this is a syn-rift sequence. This package extends beyond the southern extent of the data coverage.

6.3.9 Post-Rift

Overlying *basin-wide_unconformity* and conformably on top of the Barremian in the west and Albian syn-rift in the east is the Post Rift mega-sequence. Although the mega-sequence contains various internal unconformities, these tend to be small scale (Figure 6.15a) and are commonly accompanied by significant progradational packages without any evidence of faulting. Furthermore the mega-sequence lies directly across the Gamtoos Fault (Figure 6.3a & b) with only minor horizon disruption that is attributed to differential compaction between the underlying sedimentary fill and basement. Therefore, there is no tectonic signature evident and the unconformities that are present are attributed to eustatic fluctuations.

As there is limited tectonic influence this mega-sequence has not been extensively studied. However, to understand the basin scale development of the post-rift, and to be able to compare it with the other basins, three horizons have been picked. The horizons (*top_e-cenomanian*, *top_e-e-turonian*, and *top_e-turonian*) have been tied to various wells, and when mapped out across the basin form similar south dipping, planar surfaces (Figure 6.16). The isochron plots of the horizons do however show differences. There is very little differential sediment accumulation across the basin except in the west against the Gamtoos Fault during the Cenomanian (isochron plot of *basin-wide_unconformity* to *top_e-cenomanian*, Figure 6.17) which is possibly a result of differential compaction. There is also little differential sedimentation in the middle and late Turonian packages (Figure 6.18a & b), although these packages thin and onlap onto the basin-wide unconformity in the north (Figure 6.12). The package from the Turonian to sea floor shows significant thickening towards the south, except above the basement high (Figure 6.18c) where there is only minor thickening. Localised canyoning occurs above the Turonian (Figure 6.15c).

6.4 Nature of faulting

The previous section set out the tectonic and stratigraphic framework for the Gamtoos Basin. This section will build upon this framework by examining the faulting across the basin and where appropriate evaluate the spatial and temporal evolution of the fault systems.

6.4.1 Gamtoos Fault

i) Geometry

The mapping of the *top_basement* horizon defined the geometry of the Gamtoos Fault, and the subsequent tectonic framework suggests that it controlled most of the basin's

sedimentation. Figure 6.19 is a compilation of seismic sections perpendicular to the trend of the Gamtoos Fault, and demonstrates that the cross-sectional geometry is similar regardless of orientation. The only exception is Figure 6.19f in which fault scarp degradation has played a role. The fault appears as a discrete single surface, although in the north-west the principal fault splays into two faults that may be an offshore equivalent to the bounding faults of the onshore Pre-Cape block (Figure 6.1) discussed by Shone *et al.* (1990).

The nature of the fault is important for various reasons, some of which will be discussed later:

- There is no evidence in the seismic data of any cross-cutting faults or other strong reflectors within the Gamtoos Fault footwall (cf. (iii) of this section).
- When the sections are integrated with depth-time data the fault is imaged to at least 12 km (McMillan *et al.* 1997).
- The fault in all sections is a planar structure to at least 5.0s TWT (and in some sections to 5.5s TWT) . This is important in Chapter 9 to constrain the models developed in Chapter 4.

ii) Evolution

Using spatial and temporal variations in sediment accumulation it is possible to unravel the evolution of sedimentary basins (cf. Chapter 2 & 5). The isochron plots (Figures 6.7 & 6.9) for each of the syn-rift sequences suggest that the accumulation of sediment varied both spatial and temporally. However, the evolution of the Gamtoos Fault is not readily apparent from these plots. To understand the evolution of the fault, cumulative sediment accumulation has been plotted by determining sediment thickness (in TWT) from *top_ps-basement* to the top of sequential horizons (Figures 6.20 & 6.21). In these plots the sediment thickness from the Gamtoos Fault plane to the horizon under consideration has also been included.

The locus of maximum sediment accumulation in the Kimmeridgian and Portlandian (Figure 6.20a & b) is focused on the north-south portion of the Gamtoos Fault with significantly less accumulation against the east-west portion. During the Berriasian and Valanginian (Figure 6.20c & d) the locus of maximum sediment accumulation migrates towards the north-east with the east-west fault portion receiving increased accumulation. This results in the locus being focused at the apex of the fault curve by the Early Valanginian (Figure 6.20e). During the Late Valanginian (Figure 6.20f), the east-west Gamtoos Fault portion becomes the locus

of accumulation (Figure 6.7f) resulting in maximum accumulation migrating towards the west.

Using the assumptions discussed in Chapter 5, sediment accumulation in the Kimmeridgian (Figure 6.20a) suggests that in the early syn-rift phase the north-south fault portion was the active structure with only minor extension occurring on the east-west portion. During the Portlandian to Middle Berriasian the position of maximum extension migrates towards the apex of the curve suggesting that the direction of extension also changes from east-west to NE-SW, relative to the current position. In the Upper Berriasian the amount of extension increases on the east-west fault portion (Figures 6.7d & 6.20d), while there is very little extension by the Early Valanginian (Figures 6.7e & 6.20e). The amount of extension then increases again in the Latest Valanginian, focusing on the east-west fault portion, although with sedimentation across the whole basin (Figure 6.7f & 6.20f). In the LSR (Latest Valanginian and Hauterivian) extension is still focused on the east-west fault portion suggesting a north-south extension orientation (Figure 6.21). The areal extent of the LSR is much reduced compared to the Principal Syn-Rift although the position of maximum accumulation is static five kilometres east of the middle of the mapped fault segment (Figure 6.22). Figure 6.23 is a plot of sediment accumulation versus length along the fault. It illustrates that although there is some variation in sequence thickness there are no points at which accumulation is reduced to zero, not even in the lowest mappable units. The implications for this will be discussed in Chapter 10. This plot also shows the dramatic change in sediment accumulation between the Principal and Late Syn-Rift megasequences.

iii) Gamtoos Fault : one or two faults?

From the previous section it becomes apparent that the Gamtoos Fault appeared to behave almost as though it consisted of two discrete fault segments, the older being north-south trending and the younger east-west. This would explain the dramatic switching of the two extension directions between the Early Valanginian and Latest Valanginian. Such a model would suggest that the younger fault cross-cuts the older fault, hence the hangingwall package of the older fault would be expected to be preserved in the footwall of the younger fault (Figure 6.24). Furthermore, assuming a characteristic normal fault depocentre geometry (Chapters 2 & 5), the depocentre of the second fault may be expected to continue further to the east, and neither of these predictions are supported by the data. The footwall of the east-west fault is composed of quartzite basement (well Ha-11), therefore the hangingwall sedimentation of the north-south fault would require at least 12 km of uplift to account for its

removal from the footwall of the east-west fault. In addition to this, the Late Valanginian isochron (Figure 6.7f) suggests that there was a transition between extension being focussed on the north-south and east-west faults. It is therefore proposed that the Gamtoos Fault has behaved as one discrete fault, and that the active section has migrated through time. This conclusion is supported by the seismic data that show a coherent fault plane, with no evidence of cross-cutting of fault (Section 6.5.1 (i), Figure 6.19).

iv) Conclusions on the development of the Gamtoos Fault

By using sediment accumulation as a proxy for the fault activity, it is proposed that the Gamtoos Fault has undergone complex temporal and spatial changes. It appears that although the fault has behaved as a single structure throughout the evolution of the Mesozoic basin, it has been able to alter the most active portion in response to changes in the inferred extension direction. The scale of the syn-rift packages thickening in towards the fault are substantial and although eustatic changes may have some influence on the mega-sequence evolution, the scale of the packages suggest a dominant tectonic control. The eustatic effects are considered, therefore, to be small and have subsequently been ignored in this study.

6.4.2 Western basement high

The TWT maps of the *top_basement* (Figure 6.4a) and the sequences within the Principal Syn-Rift mega-sequence (Figures 6.6 a-e) reveal the presence of a number of faults on the western basement high that have an arcuate trend that parallels that of the Gamtoos Fault (Section 6.4.1). The majority of the faults are extensional (Figure 6.25) and two of the principal arrays delimit a small graben structure (approximately 5 km wide). The most westerly fault array is more interesting as there is evidence along the length of the fault that it is a west-dipping high angle reverse fault juxtaposing basement on top of the Principal Syn-Rift mega-sequence. In the south, the fault has a throw of approximately 0.5 seconds TWT, although this decreases towards the north. None of the faulting, neither reverse nor normal, cross-cut the *basin_wide-unconformity*. When the reverse faulting is removed, and the section is restored to a flattened Late Valanginian reflector (Figure 6.26), classic on-lap onto a basement high is observed suggesting that the margin was subjected to a single phase of compression resulting in reverse faulting.

6.4.3 Intra-basin faults

Across much of the eastern area there are abundant fault arrays within the Principal Syn-Rift mega-sequence that have approximate NW-SE trends (cf. TWT maps in Figure 6.6). The

upper sequences (Upper Berriasian and Valanginian) are pervasively cut by south-dipping faults with occasional antithetic north-dipping faults that result in graben structures (Figure 6.27). Fault throws are very variable, ranging from the resolution of seismic data (~30 ms TWT) up to 200 ms TWT. The faults tend to either die out, or assimilate at depth resulting in localised faulting in the Berriasian sequences. This localisation of faulting continues with only a limited number of faults cutting the Portlandian and Kimmeridgian sequences. The reduction in the number of faults with depth is accompanied by the reduction of observed throw on the faults. Therefore, not only is the *top_kimmeridgian* horizon not commonly faulted, the throw on the faults are insignificant (~50 ms). In Figure 6.28 the same characteristics are observed, although in this section many of the faults appear to décolle onto a horizon directly under *top_portlandian*. Furthermore, the lower Mid Berriasian reflectors are folded in an architecture not dissimilar to hangingwall rollover deformation associated with listric faulting (McClay & Hartnaday, 1986).

The dramatic decrease in fault throw with depth suggests that the reduction in both the number of faults, and observed throw is unlikely to be a result of resolution decrease with depth. If all the packages were undergoing uniform strain, then a decrease in the number of faults would be expected to be associated with an increase in the throw on the individual faults, and faults with throws of this magnitude would be expected to be resolved. This is not the case with these faults. Therefore it is suggested that the packages are not undergoing uniform strain and possible reasons for this will be discussed in Section 6.5.3.

The isochron plots of the Principal Syn-Rift sequences (Figure 6.7) do not show differential growth across the intra-basin faults, therefore they are post lithification, and hence post Late Valanginian. Furthermore, the majority of the faults terminate at *top_l-valanginian* and the LSR reflectors onlap onto faulted and rotated Late Valanginian reflectors (Figure 6.27). The timing of the intra-basin faults is therefore between the Late Valanginian and the Latest Valanginian/ Early Hauterivian.

The position of the faults is important in understanding the development of the basin. They are restricted to the east, and are generally south of the deposition of the LSR. It is therefore suggested that between the Late Valanginian and Latest Valanginian extension increasingly focussed on east-west fault and was taken up by that part of the Gamtoos Fault. In the eastern part close to the north-south Gamtoos Fault, extension could not be accommodated by the basin-bounding fault because it was in the wrong orientation, therefore the extension

was taken up by intra-basin normal faults with the basement to the north acting as an undeformable buttress.

6.4.4 Summary of faulting

Although the basin is dominated by the Gamtoos Fault and to a lesser extent the basement high, faulting occurs across the basin. Of the three fault systems examined only the Gamtoos fault has suitable stratigraphic control to allow the determination of its spatial and temporal evolution, although the timing of the faults in the other arrays can be determined. The effect of the faults on the basin fill has been discussed in this section, especially with respect to controlling the deposition of sediments. The next section will examine the basin-fill and discuss deformation within it.

6.5 Basin-fill deformational styles

By determining the tectonic framework and associated faulting, it becomes apparent that the basin-fill has undergone various styles and degrees of deformation. This section will discuss these observations and seismic sections will highlight the variation in both the styles and amounts of deformation across the basin. Each area will be discussed separately and where possible the observed deformation will be modeled using 2D Move and horizon restoration to determine the genesis of the structures.

6.5.1 Northern margin

i) Observed structure

Proximal to the east-west trending section of the Gamtoos Fault, the LSR packages below the *basin-wide_unconformity* dip basin-ward, away from the bounding fault and have little internal deformation (Figure 6.29). The uppermost package (between *top_LSR-III* and *basin-wide_unconformity*) comprises moderate southward dipping reflectors with significant amounts of erosional truncation directly below the *basin-wide_unconformity*. When the uppermost of these packages is restored to the horizontal, the underlying packages, which are Hauterivian in age, thicken into the fault and are therefore defined as a syn-rift sequence (Figure 6.29). This is substantiated by the isochron plots (Figure 6.8).

ii) Modelling of structures

There are two possible mechanisms to explain the observed deformation, and they both require uplift and erosion after the deposition of the Principal and Late Syn-Rift mega-

sequences (Figure 6.30 a-c). The first mechanism has differential uplift of the northern portion and subsidence in the south after the deposition of the Late Syn Rift packages (Figure 6.30 d-e i). If a relative base level fall occurred (either eustatic or tectonic) then the north, being higher, would preferentially erode, thereby resulting in an unconformity and erosional truncation. Modelling, using Midland Valley's 2D Move programme, produces truncation of the LSR reflectors but does not produce either the observed geometries, nor truncation of both ends of some of the higher reflectors.

An alternative mechanism invokes reactivation of the basin-bounding fault in a reverse sense, thereby structurally inverting the LSR sedimentary package (cf. Chapter 2). The thickening of the Post-Rift package above the *basin-wide unconformity* suggests a subsequent regional southerly tilt. If inversion was localised against the fault, modelling suggests that the observed reflector geometries can be achieved (Figure 6.30 d-e ii). There is very little internal deformation of the LSR package, therefore if structural inversion had occurred then the maximum compressive stress orientation (σ_{hmax}) would have been perpendicular to the bounding fault. If σ_{hmax} had been oblique to the fault, a component of strike-slip is likely to have resulted and the package would be expected to show oblique trending folds and faults. In the absence of such folds and faults, a major wrench component has been discounted.

6.5.2 Eastern margin

i) Observed structures

Unlike the northern margin (which has very little along-strike variability), the area proximal to the bend of the Gamtoos Fault and along its N-S shows significant variation of deformational styles on a short wavelength (Figure 6.31a-c). Of particular importance is that the geometry of the basin-bounding fault remains constant between the sections.

The most northerly section of the three (Figure 6.31a) is located at the bend in the Gamtoos Fault and shows that the upper Principal Syn-Rift package forms a box fold with an amplitude of up to 0.5 seconds TWT and a width of 8 km directly above the Gamtoos Fault plane. The apex of the box fold, containing the upper-most Principal Syn-Rift package, is formed from a complex array of small scale anticlines and synclines, with wavelengths of approximately 1 km. The middle and lower Principal Syn-Rift packages show less deformation, forming a small monocline against the fault. The reflectors in this region are subjected to minor extensional faulting (throws of up to 50 ms). Towards the west, the

deformation of all horizons dies out very abruptly and the reflectors become sub-horizontal. The Principal Syn-Rift package shows minor amounts of erosion at the top of the fold and the progressive onlap of the LSR package in the west. There is significant erosional truncation of the LSR beneath the *basin-wide_unconformity*.

In the middle section (Figure 6.31b), where the Gamtoos Fault is trending N-S, the wide box fold is replaced by a monoclinial structure involving middle and upper Principal Syn-Rift packages. The limb of the monocline is sub-parallel to the Gamtoos Fault, and is approximately 4.5 km wide and at least 1.7 seconds TWT high, although the absolute height is unknown because it is truncated by the *basin-wide_unconformity*. As in the northern section, deformation dies out abruptly away from the fault, with sub-horizontal packages to the west. Onlapping onto the monocline and diverging away from it is the LSR package which shows evidence of erosional truncation directly below the *basin-wide_unconformity*. In this seismic section the spatially restricted Albian syn-rift package is evident between the *basin-wide_unconformity* and the Gamtoos Fault.

In the southern section (Figure 6.30c) the amount of deformation of the Principal Syn-Rift is significantly reduced compared to the other two sections, and there is no evidence of the LSR package. There is also an increase in the width and thickness of the Albian Syn-Rift package.

ii) Modelling of structures

Any explanation for the deformation has to account for the large along-trend variation as well as the onlapping nature of the LSR package onto the structures. There are various mechanisms, both compressional and extensional, that may be invoked.

The principal method using compression would be compression oblique to the bounding fault where the basement (i.e. Gamtoos Fault footwall) remains undeformed and the sediment fill accommodates the strain. One major problem is that that the divergence of the Late Syn-rift package indicates extension, therefore the basin would have to be simultaneously in extension and compression. It has been suggested (Cole, 1992), that the NW-SE orientated extension on the east-west portion of the fault could result in compression. However, what this does not explain is the decrease in deformation away from the fold.

Modelling was undertaken using 2D Move to determine if the deformation could be explained entirely by extension. The section chosen for restoration was an east-west section

containing both the monocline and the LSR mega-sequence (Figure 6.32a-c). The section was restored to a horizontal Late Valanginian geometry (Figure 6.32d) and then the LSR packages were sequentially added in order that the temporal change in the basin-fill geometry could be observed (Figure 6.32e-h). This model suggests that simply by having extension on, and deposition of the LSR against the east-west fault, the Principal Syn-Rift package will deform as though it is a pre-rift to the E-W fault. Figure 6.33 is a reconstruction of the deformation associated with the deposition of the LSR packages. As the LSR is deposited it results in the Principal Syn-Rift being folded towards the east-west Gamtoos Fault. With increased deposition the areal extent of both the LSR and deformation increases as would be predicted in the standard fault growth models (cf. Chapter 2 & 5). However, the basement to the east does not deform, therefore the basin-fill adjacent to the north-south portion of the Gamtoos Fault accommodates this by forming a monocline. Through time, and increased extension, the extent and size of the monocline increases. However, in the north-east the presence of the basement prevents the immediately adjacent Principal Syn-Rift being deformed as much, hence generating box folds. The model (Figure 6.32), however, is not quite accurate because area is not preserved during the restoration. This may be a result of out of plane motion on the east-west fault; this can only be resolved by three dimensional modelling and assessing volume preservation which is not possible with the available software.

6.5.3 Central basin

i) Observations

In north-south trending sections across the central and southern basin, a series of anticlines within the Principal Syn-Rift package are evident (Figures 6.34 and 35) and although they are dissected by intra-basin faults the position of the hinge points are obvious. However, as a result of a number of factors, including horizons being dissected by faults, the spacing between sections relative to the scale of folding and the location of the sections, the axial surface traces of the folds are not always evident (Figure 6.36a(i)-k(i)) and are therefore difficult to map. To overcome this, in each section the non-faulted geometry of the *top_valanginian* reflector is restored, using 2D Move, by removal of the displacement on the intra-basin faults (Figure 6.36a(ii)-k(ii)). In many of the sections the hinge point is evident despite the southern limbs of the anticlines often being inferred beyond the southern limit of the data. There are, however, some exceptions where the hinge point is less obvious, in particular at the eastern extent of the sections (e.g. Figure 6.36a) there is very little folding

with only a gentle dip towards the north. In the central sections (Figure 6.36 g and h) a much broader and flatter anticlinal feature is evident in comparison to the tighter folds both to the east and west. To understand these folds in three dimensions the restored sections of Figure 6.36 ii have been plotted in space (Figure 6.37). A consequence of removing the extension in the faults is that the sections are reduced in length, therefore their position with respect to the other sections is only approximate. From this figure it becomes evident that the hinge points are traceable between sections and that there are two folds with an en-echelon geometry and an approximate east-west trend (i.e. parallel to the east-west Gamtoos Fault). The northern anticline (approximately 16 km wide and has an amplitude of 600 ms) dies out towards the west while the southern has a periclinal geometry (13 km wide and has an amplitude of 500 ms). Both of these folds have onlap of the Late Syn-Rift package onto *top_l-valanginian* reflector (Figure 6.34 & 6.35) suggesting that they were formed prior to deposition of the LSR.

ii) Genesis of fold structures

The onlapping geometry of the LSR package onto the folded *top_l-valanginian* reflector suggests that this folding is synchronous with the development of folding in the eastern margin (Section 6.5.2). These geometries are proposed to be the equivalent of monoclinial features frequently associated with normal fault evolution. In order to obtain the anticlinal geometry rather than simply a monocline a further fault to the south of the data set is required to form the southern limbs (Figure 6.38). Such a model explains the east-west trend of the anticlines as this is parallel to the active east-west Gamtoos Fault portion. It is proposed that the basin fill is deformed through flexure. This would result in the outer arc being in more extension than lower packages, and therefore would explain the greater number of faults in the upper sequences and the reduction in observed extension with depth (cf. Section 6.4.3).

6.5.4 North-West margin

Although much of the seismic detail in the near sea floor area is obscured by sea-bed multiples two important features are evident (Figure 6.12).

The *top-e-cenomanian* and *top_turonian* horizons, and adjacent reflectors, progressively onlap onto the *basin-wide_unconformity* towards the north-west. Such an onlap may be in response to either a eustatic base level rise or differential tilting with uplift in the north and subsidence in the south. Although it is difficult to determine which model is more applicable

without examining the other basins, the latter is preferred because of substantial thickening of sediments towards the south observed between the Turonian and sea floor (Figure 6.18c) is greater than expected from eustatic variations.

Directly beneath the sea floor reflector, both in the north-west and in the north-east, there is substantial erosional truncation involving the Post-Rift, *basin-wide unconformity*, Late and Principal Syn-Rifts, and basement (Figure 6.12). Although present in the east, it is more significant in the west and accounts for the erosion observed in the TWT maps (Figure 6.6) and the sub-crop of basement at the sea floor in the north-west. The scale of uplift suggests that it has a tectonic genesis and as it is present at the sea floor further implies that the uplift may be currently active.

6.6 Timing of uplift and compression

It has been demonstrated in the previous three sections that although the basin has predominantly undergone extension there is evidence of phases of uplift and compression at the end of the LSR, one phase of uplift in the post-rift, and one possibly occurring today. To fully understand the evolution of the basin it is imperative to determine the timing of these events.

Uplift and possible structural inversion of the Gamtoos Fault in the north of the basin occurred between the deposition of the LSR sequence (Hauterivian) beneath the basin-wide unconformity and the Albian package that overlies the unconformity in the east of the basin (Figure 6.3b). Similar arguments, with the same conclusions, are valid across much of the north and east of the basin (e.g. Figures 6.31 a-c), however in these localities the timing can not be constrained further.

At the basin's western margin the timing can be better constrained. Well Ha-J1 (Figure 6.39) penetrates to basement directly to the west of the high angle reverse faulting (Section 6.4.2) and from the well data it is evident that conformably on top of the Late Valanginian sequence is the Latest Valanginian and early Hauterivian package (analogous to the Late Syn-Rift). This package is separated from the overlying Barremian sequence by an erosional unconformity identified in the well. There is then a non-depositional, but not erosional, unconformity between the Barremian and the Albian, which is the first Post-Rift sequence to be deposited across the entire basin.

The presence of an erosional unconformity between the Hauterivian and the Barremian is substantiated in the seismic data as the highest Hauterivian reflectors are erosionally truncated against an unconformity, and when mapped out to the north and east, it is equivalent to the *basin-wide unconformity*. Furthermore, the high angle reverse fault (Figure 6.39) deforms the Principal Syn-Rift and Hauterivian sequences but terminates at the unconformity and does not deform the Barremian. From these arguments therefore the *basin-wide unconformity*, which is associated with the uplift and compression in the north-east, is equivalent to the unconformity that occurred at the end of the high angle reverse faulting and is identified in the well as being between the Hauterivian and the Barremian. It would appear that the basin under-went compression and uplift resulting in the formation of the *basin-wide unconformity* in the Late Hauterivian.

The post-rift uplift phase can be constrained from well data that indicate there is erosion, and unconformity between the Turonian and Santonian, which agrees with the seismic observations in Section 6.5.4.

6.7 Basin evolution and depositional environment interpretation

It has been demonstrated in the previous section that there are various complexities across the basin. The purpose of this section is to integrate these complexities with the tectonic and stratigraphic framework established in Section 6.3, and depositional environments to establish a spatial and temporal understanding of the basin's evolution. Throughout this section depositional environments have been taken from Soekor interpreted lithofacies and palaeontological logs (presented in the logs in Appendix 1.C).

6.7.1 Principal Syn-Rift

i) Kimmeridgian

Although the age of rifting initiation is unknown, the seismic data suggest that at least towards the end of the Kimmeridgian sedimentation occurred across the whole basin and that its distribution was being controlled by a very similar basement geometry as observed today (Figure 6.40a). The sediment accumulation plots (Figure 6.20a) suggest that the controlling fault was the Gamtoos Fault with the locus of maximum sediment accumulation at the southern end of the north-south trending section. With the exception of the minor faults on the western high, there is no evidence of significant intra-basin growth faults.

The only Kimmeridgian sediments that are penetrated by a well are on the basement high. These are a proximal marine depositional environment with switching from a continental setting to shallow-marine, river dominated system.

ii) Portlandian – Late Valanginian

Throughout the majority of the Principal Syn-Rift the basin appears to change gradually both structurally and sedimentologically (Figure 6.40b). Sedimentation continued across the whole offshore portion of the basin with thickening against the Gamtoos Fault, and no evidence of intra-basin fault growth. Throughout this period there is a gradual migration of the locus of maximum sediment accumulation from the north-south section towards the apex of the fault curve. At the beginning of this period the north-south portion of the fault was the main control on sedimentation, although the package also thickened into the east-west portion to a lesser degree. The minor faulting on the western high had abated. Towards the middle and top of this period the locus of maximum accumulation migrated to the north-east and progressively became focussed at the apex of the fault curve. The relative orientation of maximum extension is therefore inferred to have rotated from east-west during the Kimmeridgian to NW-SE. During the Late Valanginian, the east-west Gamtoos Fault portion dominates suggesting that the extension directions becomes north-south.

Overlying the fluviially dominated Kimmeridgian, the Portlandian siltstones and claystones of the western high have been interpreted to be shelf deposits (Ha-J1), therefore implying an overall base level rise from the Kimmeridgian. Black shales in well Ha-B2, radiolaria fauna in Ha-A1, and the absence of significant amounts of clastic input suggest that the central and eastern basin is significantly deeper in the Portlandian than the western margin, and may be as deep as anoxic plain.

Towards the middle and upper Portlandian, although the background sedimentation remains similar to that of the lower Portlandian, there is a significant increase in the amount of clastic input. The composite logs (Appendix A) indicate that the petrography and colour of the sands are very varied. It is important to note that there is not the dominance of quartzitic sandstones that is observed in later sections. The increasing frequency of the sand packages towards the top of the Portlandian has been inferred to indicate a gradual shallowing of the system (Appendix 1.C) and this is supported by the general shallowing trend from abyssal plain to upper slope in the palaeontological data (palaeontological logs, Appendix 1.C).

This gradual shallowing in the Portlandian continues during the Berriasian with an increase in clastic input, and paleontology data indicating a gradual change from upper slope to outer

shelf across most of the basin. The lithofacies logs suggest that the clastics have been transported and deposited in submarine channels and fans.

This base-level fall, evident from the paleontology logs, continues throughout the Early and Late Valanginian with the majority of wells recording a change from outer to middle shelf. An interesting observations in this period is that despite this observed shallowing, there is a significant reduction in the amount of clastic input.

Therefore, during the accumulation of middle and upper Principal Syn-Rift, the Gamtoos Fault remains active although the depositional environment becomes shallower. Such a shallowing could be a result of a number of reasons including reduction of tectonic activity, lowering of eustatic sea-level, or increase in sediment supply. Despite the problems with accurately calculating sedimentation rates (cf. Chapter 5), approximate rates have been obtained for the Principal Syn-Rift sequences and for the LSR mega-sequence (Table 6.1). Although these rates must be considered with caution, any errors should be applicable to all of the units and therefore comparisons between age units in the same wells are valid. These data imply that there is no significant difference in sedimentation rates between the Early and Late Valanginian even accounting for the Late Valanginian rates being minimum estimates because of erosion, hence sediment supply can not account for the shallowing of the depositional environment. The gradual change over approximately 15 million years with an overall magnitude on the order of 200 m from slope to upper shelf would tend to rule out eustatic changes, especially as sea level was more likely to have been rising rather than falling (Haq *et al.*, 1988). Therefore the change in depositional environment is most likely to be a response to a gradual reduction in tectonic activity on the Gamtoos Fault.

The lack of quartzitic sandstones, and the dominance of lithic sandstones is interesting because the current source of sandstones to the basin is the quartzitic sandstones from the eroding Cape Fold Belt (Chapters 2, 3 & 4). This absence of quartzitic sandstone during the Principal Syn-Rift, and Late Syn-Rift periods suggests that the provenance of the syn-rift material was not the quartzitic Cape Super Group.

6.7.2 Latest Valanginian-Hauterivian (135-130 Ma)

The gradual shallowing during the Valanginian comes to an abrupt halt in the Latest Valanginian with a switch from the middle shelf to a lower slope setting (Figure 3.40d). This setting is characterised by the change from light to dark grey claystones that are occasionally anoxic (McMillan *et al.*, 1997). The presence of the quartzitic sands proximal

6.7.4 Barremian

The clay dominated Barremian sequence is only preserved to the west of the high angle reverse faults and is overlain by a basin-wide hiatus.

6.7.5 Albian

There is only limited deposition of this package in a localised syn-rift package against the north-south Gamtoos Fault section and it is unclear what the cause of this extension is.

6.7.6 Post-Rift - recent

There are various packages of clastic shelf sediments, often forming the progradational features with occasional canyons. The scale of these features is significantly smaller than those associated with the basin's tectonically active phase and as there is no evidence of active tectonics during this period, these younger features are probably controlled by eustatic fluctuations. The sandstones are dominated by quartz and are therefore likely to be sourced from quartzitic basement and hence are much closer to the present onshore geology compared to the mixed petrography of the earlier units. There is, however, the presence of background clay and siltstones similar to that of the principal and late syn-rift packages.

Although many of the internal geometries are probably eustatically controlled, there is evidence of uplift and erosion in the north-west occurring today.

6.8 Discussion and role of structural inheritance

The aim of this chapter has been two-fold: firstly to attempt to constrain the sub-surface relationship between the CFB and the Mesozoic extension; secondly to understand the role of structural inheritance and in particular the control of pre-existing structures on the evolution of the extensional system.

The basement is poorly imaged by the seismic data, with no visible internal structures. The only constraint on the subsurface interaction between the extension and the CFB is the Gamtoos Fault with its 12 km of Mesozoic syn-rift sedimentation. However, as there is only one main fault present it is difficult to draw conclusions from this alone. Therefore, the models of Mesozoic superimposition upon basement will be discussed once the rest of the sub-surface data are discussed.

The data presented in this chapter indicate that throughout the development of the Gamtoos Basin the two principal structures (Gamtoos Fault and western basement high) have

controlled the basin's evolution and have been re-activated during various phases of deformation. Although the evolution of the extensional system will be discussed with respect to fault growth models in Chapter 10, the importance of structural inheritance is discussed below.

The primary feature of the basin is of course the Gamtoos Fault, and throughout the evolution of the basin extension has been focused on it. Regardless of whether the Gamtoos Fault is a structure inherited from the CFB (to be discussed in Chapter 9), there is evidence that it has had a fundamental control on the development of the basin. From a very early stage it has almost entirely controlled sedimentation to the exclusion of any other faults. Therefore, when the relative extensional direction changed in the upper Principal Syn-Rift and Late Syn-Rift packages, instead of new extensional structures being created the change was accommodated by the Gamtoos Fault. In much of the basin this was possible with reactivation of the pre-existing structure. However, proximal to the north-south fault section, the north-south extension could not be accommodated by the pre-existing structure and was transferred to the basin and resulted in significant deformation. Subsequently, when the basin underwent compression and uplift, the Gamtoos Fault was structurally inverted as a high angle reverse fault, and it is likely that the high angle reverse faulting in the west was also utilising an underlying structure. The early structures appear to be long lived and have had a significant influence on resultant basin-fill geometry.

In addition to addressing the issue of structural inheritance, the data presented constrain some of the models proposed by previous workers to explain some of the features in the basin. This is possible because this study has examined and mapped the evolution of the basin on a sequence scale in order to understand its development on a smaller timescale than previous studies. This study has also modeled the formation of some of the complex deformation and does not require complicated scenarios in which some parts of the basin are in compression and others are in extension.

The main issues raised by previous studies that will be addressed are: the role of the Agulhas Falklands Fracture Zone (AFFZ); the timing of the transition from the syn-rift to post-rift; and folding of the basin fill.

In many of the previous studies (Bate & Malan, 1992; McMillan *et al.*, 1997; Thomson, 1999) it has been suggested that the AFFZ has played an important part in the development of the basin, from exaggerating the curve of the Gamtoos Fault, to deforming the basin fill.

Some of these issues are discussed below, although the more regional effect of the AFFZ will be discussed in Chapter 9.

The rift to drift transition unconformity has traditionally been mapped as the *top-l-valanginian* horizon (Bate & Malan, 1992; McMillan *et al.*, 1997). The results from this study indicate that there is substantial syn-rift in the Latest Valanginian and Hauterivian. Therefore this study puts the rift-drift transition at the end of the Hauterivian.

The formation of the monoclinical folding (Gamtoos Anticline) has been much discussed in the literature and attributed to various mechanisms. Bate & Malan (1992) account for the folding through Late Valanginian extensional rejuvenation of the Gamtoos Fault in a dip-slip displacement with a minor strike-slip component. This resulted in extension and rotation adjacent to the east-west part of the fault and compression and uplift adjacent to the north-south fault.

McMillan *et al.* (1997) suggest that the timing of the Gamtoos Anticline is contemporaneous with the reverse faults in the western basement high and is related to localised compression as a result of right-lateral strike slip motion on the AFFZ. They support this by suggesting that the intra-basin faults are formed in response to strike-slip motion along the north-south Gamtoos Fault. This seems unlikely for a number of reasons. This study has demonstrated that the reverse faulting is not contemporaneous with the monoclinical folding. Furthermore, if the anticline formed from strike slip motion then folding and faulting would be expected to be oblique to the north-south fault, and this is not the case. The AFFZ, or a pre-cursor to it, would have been present through most of the evolution of the basin, therefore any deformation in the basin associated with the AFFZ strike slip motion would be expected to be manifested throughout the basin's evolution and not only in the Hauterivian.

Thomson (1999) has a similar explanation to McMillan *et al.* (1997) and associates the compression with strike-slip motion on the AFFZ. Thomson discusses the presence, though not the three dimensional geometry, of the eastern most anticline (Section 6.1.1) and attributes it to roll-over above a listric Gamtoos Fault as modeled by McClay *et al.* (1991). Although in some sections that are oblique to the Gamtoos Fault, the fault geometry can appear listric, this study has demonstrated the planar nature throughout its length. It is also uncertain why the roll-over geometry would be transitory, only occurring in the Hauterivian and not throughout the evolution of the syn-rift packages.

The only problem with the model of the basin's evolution outlined in this study is the non-depositional hiatus in the Aptian. It is unclear why the basin undergoes uplift, compression

and erosion in the late Hauterivian, then Barremian sediments are deposited in a slope environment with no obvious clastic input prior to the non-depositional hiatus. It is also uncertain what its genesis is.

6.9 Conclusions

By integrating offshore seismic data with borehole, sedimentological and age data the evolution of the Gamtoos Basin has been documented. The observed complex deformation, especially of the basin fill, can be explained predominantly by extension with a short phase of uplift and compression. Various models have been proposed to explain the genesis of the observed deformation. Throughout the development of the basin, structural inheritance has played an important role in controlling where sedimentation has occurred and in its subsequent deformation.

This chapter has only addressed the offshore Gamtoos Basin and it is therefore impossible to determine if the features observed in this basin are representative of the other South African basins. The following two chapters will form tectono-stratigraphic frameworks for the neighboring basins, the Pletmos and Algoa, in order to put the Gamtoos Basin into a regional context.

CHAPTER 7: Tectonic Evolution of the Offshore Pletmos Basin

7.1 Introduction

It is evident from the data presented in Chapter 6 that structural inheritance has played a role on the development of the Gamtoos Basin. However, deductions based on a single basin can not be reliably extrapolated to conclusions about inheritance on a regional scale, the interaction between the onshore basement and the offshore extension, or about the more general role of inheritance in the development of extensional systems. This chapter will therefore use the same techniques used in the previous Chapter to determine the tectonic framework for the Pletmos Basin, directly to the west of the Gamtoos Basin.

As in the Gamtoos Basin chapter, the overall structural framework will be established prior to evaluating the nature of faulting and basin-fill deformation. These observations will be integrated with published sedimentological observations to determine the evolution of the basin.

7.2 Pletmos data

Approximately 8,000 km of 2D multi channel 2D seismic data, and 21 boreholes have been utilised to establish the evolution of the Pletmos Data (Figure 7.1). The seismic data are of 1979, 1981, 1982, 1983, 1984, 1985, 1986, 1987, 1988, 1989, 1990 and 1991 vintage (cf. Table 5.1) with a maximum recording time of either 5000 or 6000 ms two-way-time (TWT). About 75% of the seismic data have been migrated, while the remainder has been stacked. There have been no problems in correlating between the two data sets. The locations of sections that are reproduced as figures are highlighted on Enclosure 9. The well data have only been used to age tie the seismic data (Appendix B) because no stratigraphic, lithofacies, or palaeo-environment data were available for the study.

7.3 Tectonic and stratigraphic framework

This section discusses the determination and characterisation of mega-sequences within the Pletmos Basin and integrates them with well age data to establish a tectonic framework. This framework comprises the four mega-sequences (Basement, Principal Syn-Rift, Late Syn-Rift and Post-Rift) that were established in Chapter 5, and used in the Gamtoos Basin, although the individual sequences within the mega-sequences differ (Figure 7.2). The

seismic character, areal extent and thickness of each mega-sequence, and corresponding sequences, will be discussed.

7.3.1 Basement

The nature and continuity of the *top_basement* reflector varies significantly across the basin. In the centre and west it is evident as a strong, traceable, double reflector onto which the Principal Syn-Rift onlaps; in the north and east, it is either deeper than the maximum recording time of 5.0s Two-Way-Time (TWT), or is poorly imaged, and therefore difficult to pick. The extent of the accurately picked Top Basement is plotted on the horizon's TWT map (Figure 7.3a).

The *top_basement* geometry is dominated by two faults, the south dipping Plettenberg Fault and the north dipping Pletmos Fault (Figure 7.3b), which define two sub-basins separated by the Springbok High. This high is formed from a complex array of smaller anastomosing faults. A third controlling fault, the Superior Fault, is present in the west of the basin, although its extent is difficult to assess because it is at the very edge of the data set. For much of the basin the overall geometry is dominated by east-west trending structures, except in the east where there is a significant change in trend of the both the Plettenberg Fault and the Springbok High from east-west to north-south.

The wells that have penetrated to basement (McMillan *et al.*, 1997) indicate that it is composed of Cape Super Group lithologies and is therefore consistent with the onshore basement geology (Chapter 3).

The basement generally has a transparent internal character, except in the west, where it is shallower and better imaged, and there is evidence of deformation of intra-basement reflectors (Figure 7.4). Although the data coverage does not permit detailed mapping of the structures it is evident that they have a broadly east-west trend, i.e. parallel to the regional fabric in that area. These features are well-tied within the basement and are probably not multiples. The geometry is therefore likely to be imaged folds within the Cape Fold Belt (CFB) and the scale of them is not dissimilar to that observed onshore (Chapter 3).

Unlike the Gamtoos Basin, it is not possible to pick a pseudo-basement horizon across the basin because much of the syn-rift is deeper than 5s TWT.

7.3.2 Principal Syn-Rift (Middle? Jurassic-Late Valanginian)

This mega-sequence is present across the entire basin, and is unconformably above *top_basement*, and conformably, or para-conformably below either the Late Syn-Rift or Post-Rift. The oldest horizon picked in the wells is Kimmeridgian and is present on the basin highs, although it has not been traced across the basin because of a lack of well control in the deepest portions.

The only well-tied horizons that can be reliably correlated are *top_portlandian*, *top_early-valanginian* and *top_late-valanginian*, and these have been used to define sequences within the Principal Syn-Rift mega-sequence. In addition to these age related sequences two other horizons, Earliest Syn-Rift and Early Syn-Rift, have been traced to study the pre-Portlandian syn-rift packages.

i) Earliest Syn-Rift(?)

Although the most prominent Principal Syn-Rift sequences occur against the basin controlling faults (Figure 7.2) there is evidence of a localised syn-rift package at the base of the Principal Syn-Rift to the south of the Plettenberg Fault. This package is traceable across much of the northern sub-basin although the eastern extent is unknown because of the reduction in seismic data quality (Figure 7.5a). No wells penetrate it therefore the age is uncertain.

Seismically the package is relatively transparent although weak internal reflectors are visible. It thickens towards a controlling fault in the south and varies between being fault bound or thinning and onlapping onto *top_basement* in the north (Figure 7.2).

ii) Early Syn-Rift

The lack of a correlative pick for the *top_kimmeridgian* results in the pre-Portlandian geometry being poorly understood. To overcome this, a seismically correlative, but not well-tied reflector (called *top_esr*), has been picked across the north and east of the basin; it defines the top of the Early Syn-Rift (ESR) sequence which either onlaps conformably onto *top_basement*, or conformably onto the Earliest Syn-Rift sequence. It has not been possible to trace the *top_esr* reflector across the Springbok High, although it is probably present.

The reflector chosen is the first strong reflector above the predominantly transparent ESR sequence and is traceable along much of the Plettenberg Fault's sub-basin. In the south-east it becomes increasingly difficult to pick the horizon for three reasons. Firstly, the lowermost

syn-rift package becomes less transparent, therefore the chosen reflector is less discrete. Secondly, there is only one line that ties the north of the data set to the south-east therefore making the tie impossible to cross-correlate. This problem is accentuated because the tie between the areas occurs on the basement high, therefore it is difficult to trace the reflector into the deeper depocentre. Thirdly, in the south-east sub-basin there are at least 2s TWT of Post-Rift sedimentation, and at this depth the geometry of the ESR is poorly constrained. As a result, subsequent isochron plots may be mis-leading in this area and have to be treated with caution.

The areal extent of the horizon (TWT map in Figure 7.5b) is confined in the north by the Plettenberg Fault and either onlaps onto, or is faulted against the basement in the south. As the horizon is not well correlated it is impossible to tie the reflector across the basin high.

The isochron plot of the ESR thickness is problematic because of the undefined nature of the *top_basement* in the south-east (Figure 7.6a). To overcome this, two additional horizons (*top_pseudo_basement*, and *basement>5s*) have been picked. The isochron is then the calculated thickness between ESR and the relevant horizon for the section where *top_basement* is uncertain. Therefore, in the isochron plot (Figure 7.6a) the south-east corner is thinner than the true thickness. Despite this, it is evident that the thickest sediment accumulation is in the north and east of the basin (up to 1100 ms thick) with only limited accumulation in the west (250 ms). In this plot it should be re-iterated that ESR is probably present to the south of the Springbok High, but as there is no substantiating data to the south it has not been correlated across the high.

iii) Portlandian

Conformably on top of the ESR sequence where it is present, and unconformably on top of the basement where ESR is not present, is a transparent package that does not have any significant internal reflectors, but is capped by a strong reflector that is well-tied to a *top_portlandian* time-top age. This reflector is well-tied across the basin, allowing it to be confidently traced across both the Springbok High (Figure 7.5c), and the Plettenberg Fault footwall, hence into the Gamtoos Basin. In addition to the three basin-controlling faults, there are various other intra-basin faults evident in the TWT map that will be discussed in Section 7.4.

During the Portlandian the basin was divided into two smaller graben basins with the dominant sediment accumulation occurring against the Plettenberg and Pletmos Faults, and with smaller faults on the Springbok High acting as the other graben controlling faults

(Figure 7.6b). The Portlandian thickness plot (Figure 7.6b) has to be considered with care because to the north of the Springbok High the isochron was calculated between *top_portlandian* and *top_esr* while to the south it was between *top_portlandian* and *top_basement*. The plot in the south therefore accounts for a larger sequence. Against the Plettenberg Fault accumulation occurs along its mapped length on both east-west and north-south trending portions, although the greatest mappable accumulation occurs to the west end of the east-west portion (maximum of 1050 ms). Sedimentation also occurs on the Springbok High and on the footwall to the eastern Plettenberg Fault.

iv) Early Valanginian

The Berriasian sequence was picked in the Gamtoos Basin between the Portlandian and Valanginian, however, in the Pletmos Basin there are insufficient well-ties to accurately correlate the horizon across the basin. The next pickable horizon above *top_portlandian* is the *top_e-valanginian* reflector that defines the top of the Early Valanginian sequence. The reflector is generally strong, which along with the well ties makes it relatively easy to trace and correlate.

In a similar geometry to the underlying sequences, it is bounded in the north and south by the Plettenberg and Pletmos Faults, and to a lesser extent the Superior Fault (Figure 7.5d). In the east the geometry is less clear as it forms a monoclinial structure above the north-south trending portion of the Plettenberg Fault (cf. Section 7.5). To the east of the monocline, it is correlatable with the *top_e-valanginian* of the Gamtoos Basin. Intra-basin faults are evident from the TWT map (Figure 7.5d), and have a general east-west trend.

The two sub-basin grabens are still evident from the isochron plot of the Early Valanginian (Figure 7.6c), although the relative importance of the Springbok High is reduced. The locus of maximum sediment accumulation is now positioned approximately at the apex of the Plettenberg Fault curve, and has therefore migrated towards the east compared to the Portlandian sequence (maximum of 1050 ms). Accumulation still occurs against the Pletmos Fault (500 ms), although in this sequence the Superior Fault becomes relatively more important (1000 ms). The intra-basin faults that are evident in the TWT map do not show any sediment growth across them.

v) Late Valanginian

The *top_l-valanginian* horizon defines the top of the Principal Syn-Rift mega-sequence and the top of the Late Valanginian sequence, which is conformably above the Early Valanginian

sequence across the basin. The package is composed of a series of very strong reflectors that are broadly sub-parallel, and the *top_l-valanginian* is evident as the uppermost strong reflector. The nature of this reflector is either conformable onlap of the subsequent sequences, or non-depositional hiatus with a minor degree of erosion.

The reflector is traceable across the whole basin (TWT map in Figure 7.5e) with its distribution being controlled by the basin-bounding faults. The north-south trending Plettenberg Fault has not been traced to the south because *top_l-valanginian* has a similar monoclinical geometry to that of the *top_e-valanginian*.

In comparison to the Early Valanginian, there are fewer faults, in particular intra-basin faults, (cf. TWT map Figure 7.5e), and this is discussed in Section 7.4.7. There are minor amounts of erosion at the top of the Late Valanginian commonly associated with small rotated fault blocks. (cf. Section 7.4.7).

Sedimentation occurs across the basin (isochron plot of *top_l-valanginian* to *top_e-valanginian*, Figure 7.5d) with accumulation continuing to be focused on the Plettenberg and Pletmos Fault (maxima of 850 ms and 700 ms respectively). The two grabens, and the Springbok High are no longer discernable. The locus of sediment accumulation remains adjacent to the Plettenberg Fault although it migrates from the apex of the fault curve (cf. Early Valanginian) to the centre of the east-west trending fault portion. Despite this migration of the locus, there is still active sedimentation in the hangingwall of the north-south trending fault portion.

7.3.3 Late Syn-Rift (Latest Valanginian – Late Hauterivian)

Despite the Late Syn-Rift (LSR) mega-sequence locally being conformable with the Principal Syn-Rift mega-sequence, the majority of it is either unconformable or para-conformable with the PSR (Figure 7.2). The presence of this unconformity and the dramatic change in areal extent of the LSR compared to the PSR results in this package being characterised as a separate mega-sequence.

i) Early Hauterivian and Pseudo Early Hauterivian

The *top_e-hauterivian* reflector has been picked in various wells in the north of basin and results in the defining of two sub basins, one associated with the Plettenberg Fault and the other with the Superior Fault (Figure 7.7a). In both of these locations the sequence is conformable with, and onlaps onto *top_l-valanginian*. In the south there is no *top_e-hauterivian* well pick, however, the same geometry above the Late Valanginian sequence is

present. As neither well nor seismic data show either an unconformity or non-depositional hiatus between *top_l-valanginian* and *top-l-hauterivian*, it is inferred that *top_e-hauterivian* is present. Therefore, a reflector with similar character to that in the north has been picked as *top_pseudo-e-hauterivian* in the southern sub-basin. Of particular importance is the dramatic reduction in areal extent of the sequence compared to the Principal Syn-Rift.

The Early Hauterivian package, regardless of position, forms a strongly divergent seismic package into the appropriate bounding faults (Figure 7.2) with its top defined by a correlatable, strong reflector. The sequence against the Plettenberg Fault is bounded by a smaller-north dipping antithetic fault for much of its southern extent, and in the south east it onlaps onto *top_l-valanginian*. At its eastern extent, it crosses the north-south fault without deformation and is correlatable with the equivalent sequence in the western Gamtoos Basin. The north-west sub-basin is fault-bound to the south by the northward dipping Superior Fault, and onlaps onto the *top_l-valanginian* in the north and east. The southern sub-basin, where the *top_pseudo-e-hauterivian* has been picked, is more difficult to map. Although it onlaps onto the *top_l-valanginian* in the north, the data coverage to the south is not extensive enough to determine its southern limit, although it is inferred that the east-west trending Pletmos Fault continues to the east and controls its deposition.

There is no evidence of faulting except for the principal basin-bounding faults.

The isochron plots highlight the dramatic thickening of the sequence into the Plettenberg Fault (1250 ms; Figure 7.8a) with only minor thickening into the other two faults (Pletmos Fault – 300 ms; Superior Fault – 275 ms). The locus of maximum sediment accumulation against the Plettenberg Fault is in the centre of the east-west trending portion, in a similar location to that of the Late Valanginian (cf. Figure 7.6d).

ii) Late Hauterivian

The *top_l-hauterivian* reflector is well-tied across the basin and is therefore correlatable to the south, unlike the *top_e-hauterivian* (Figure 7.7b). Its distribution continues to be controlled by the Plettenberg, Pletmos and Superior Faults, and the areal extent of the horizon is relatively limited, although greater than that of the Early Hauterivian sequence.

The sequence is a relatively transparent package conformably on top of either the *top_e-hauterivian* or the *top_l-valanginian* and the uppermost defining reflector is a moderately strong, correlatable feature. As in the underlying sequence it diverges into the bounding faults, although not as much as the Early Hauterivian. Where it is not fault bounded it onlaps

onto *top_l-valanginian*. The uppermost reflectors of the sequence do not show evidence of erosional truncation anywhere across the basin except in eastern extent of the data, on the Plettenberg Fault footwall. Figure 7.9 suggests that on the footwall the *top_l-hauterivian* reflector becomes the correlatable conformity of the Gamtoos Basin's *basin-wide unconformity* (cf. Chapter 6).

Despite the increase in areal extent of the Late Hauterivian, sediment accumulation is still dominated by the east-west trending portion of the Plettenberg Fault (Figure 7.8b), with no deposition along the north-south trending portion (maximum of 1250 ms). As in the Early Hauterivian, the Pletmos and Superior Faults define the areal extent of the Late Hauterivian in the south and west without significant thickening (Pletmos Fault – 550 ms; Superior Fault – 175 ms).

7.3.4 Post Rift

The transition from Syn-Rift to Post-Rift phases in the Pletmos Basin is highlighted in the restored section in Figure 7.10c with the Late Hauterivian sequence diverging into the Plettenberg Fault and being overlain by non-diverging Early Barremian and younger sequences. Therefore the Early Barremian and younger sequences are defined as the Post Rift.

i) Early Barremian

The Early Barremian sequence (defined by *top_e-barremian*) is dominated by a southward prograding system with well imaged 100 ms (~100m) high clinofolds (Figure 7.10c) that aggrade at a shallow angle towards the south. The sequence lies conformably above the Late Hauterivian and is constrained in the south by the *top_l-valanginian* horizon (Figure 7.11) with a geometry implying that it infills a pre-existing topography. This topography results in the sequence only being present immediately adjacent to the east-west trending portion of the Plettenberg Fault (Figure 7.12a).

The progradational nature of the sequence results in the thinning of the sequence towards the south (from 400 ms to 100 ms; Figure 7.13a). It is important to re-iterate that the observed thickening in the north is a consequence of southern progradation rather than divergence into the Plettenberg Fault.

ii) Late Barremian

The Late Barremian sequence (defined by *top_l-barremian*) forms the middle part of the progradation system containing the Early Barremian with the clinoform break point to the south of that of the Early Barremian (Figure 7.14). It has a significantly greater areal extent compared to the Early Barremian and is present in all of the wells. However, although it is present on the western Springbok High (well Hb-Spk1) it is ambiguous from the seismic data whether the horizon onlaps, and terminates against the Late Valanginian, or is draped across the western part of the high (Figure 7.15) and has therefore not been included in the TWT map (Figure 7.12b). The thickness of the Late Barremian (isochron plot in Figure 13b) is similar to the Early Barremian except that the break in slope of the progradational system is further to the south (625 ms in the north to 100 ms in the south).

iii) Early Cenomanian

The *top_e-cenomanian* horizon forms a planar surface that dips uniformly towards the south and despite being in the Post-Rift, some localised faulting is present (Figure 7.12c). The majority of these faults have no growth across them and are associated with the Springbok High, however, one of the faults in the west can be shown to have growth across it (cf. Section 7.4.7).

The package is characterised by relatively sub-parallel reflectors, although the lowest reflectors are included with the progradational system of the Barremian. The isochron plot (Figure 6.13c) shows a dramatic thickness change because of the nature of the underlying Late Barremian progradational system (175 ms in the north and 475 ms in the south). It is uncertain whether there is no progradation within the upper Early Cenomanian, or whether the clinoforms occur to the south of the data coverage.

iv) Early Turonian

The Early Turonian sequence (defined by *top_e-turonian*) is seismically conformable with the Early Cenomanian, although the absence of the Late Cenomanian in all of the well data indicates that there is a depositional hiatus. Although the horizon forms a planar southward dipping surface with no significant faults (Figure 7.12 d), it is evident from the isochron plot (Figure 7.13d) that there is a ribbon of thicker sediment at the south of the basin (385 ms compared to 75 ms), which is a result of the progradational nature of the sequence.

v) Late Turonian to Present

Although this sequence contains various progradational systems and small scale unconformities, it is dominated by two features. There is a significant thickening of the package towards the south and it appears that the fulcrum of this is the Springbok High (Figure 7.2). The other feature evident across the basin is the late stage uplift of the coastal region which is equivalent to that discussed in the Gamtoos Basin (Figures 7.2, 7.9 and 7.14).

7.4 Faulting

It is evident from the tectonic framework discussed in Section 7.3 that unlike the Gamtoos Fault (with its one fault), the Pletmos Basin is more complex with three principal faults, and various other growth faults. The three controlling faults will be discussed before the other faults. Where possible the geometry of the faults will be demonstrated and the timing and interaction between the faults will be established.

7.4.1 Plettenberg Fault

The Plettenberg Fault is the principal controlling fault in the north and east of the basin.

i) Geometry

The east-west trending section of the Plettenberg Fault is a plane that dips at approximately 45° towards the south, has an identical trend to the onshore basement structure, and is traceable along its length of 160 km as a discrete and continuous structure (Figure 7.16). The hangingwall is dominated by the Principal and Late Syn-Rift mega-sequence sediments and in the deepest portions of the basin the *top_basement* reflector is at least 5.0s TWT with occasional sections suggesting that it is deeper than 5.5s TWT. There are no wells that penetrate its footwall, although the transparent character of the package is similar to that observed in the Gamtoos Basin, and as it is close to the onshore basement it is inferred that the footwall is formed from CFB basement. There is no evidence of syn-rift deposits on the footwall with only minor Post-Rift sediments. When the fault surface is mapped out it is evident that towards the east it changes trend dramatically becoming a north-south trending fault. Despite this curve, the fault plane remains as a single traceable feature and there is no evidence of any cross-cutting faults.

The imaging of the north-south trending portion of the Plettenberg Fault is poor compared to the east-west section, although it is evident as a change in character between the transparent

basement and structured syn-rift reflectors. In this area there is a much greater thickness of Post-Rift sediments, therefore the syn-rift megasequences are considerably deeper and the fault is less well imaged at depth. The Principal Syn-Rift mega-sequence is cut by the fault, while the Late Syn-Rift megasequence is draped across. This observation will be discussed in Section 7.5.

ii) Evolution

The evolution of the Plettenberg Fault can be ascertained using sediment accumulation as a proxy for fault growth and activity (cf. Chapter 5).

The isochron plots presented for individual sequences (Figures 7.6 and 7.8) indicate that the position of maximum sediment accumulation, and hence the inferred position of maximum fault displacement, has changed through time. As discussed for the Gamtoos Basin, the switching in the position of the maximum accumulation for individual sequences makes it difficult to understand the overall evolution of the fault. To overcome this, cumulative isochron plots have been formed from the syn-rift horizons to *top_basement* (Figure 7.17). These plots are subjected to the same limitations as the Early Syn-Rift isochron plots of the *top_basement* being either difficult to pick, or below the maximum recording time of 5.0 or 5.5 s TWT. Furthermore, the lack of seismic coverage, especially in the north-east results in artificial depocentres where the contour grid spacing approaches that of the line spacing.

From the cumulative plots (Figure 7.17) the migration of the locus of maximum sedimentation can be assessed. In the Portlandian (Figure 7.17a) sedimentation occurs along the full extent of the fault (including the north-south trending portion) with little differential accumulation, while in the Early Valanginian the locus is more pronounced and located near to the apex of the Plettenberg Fault curve. In the Late Valanginian the locus becomes more diffuse again (Figure 7.17c), although is more focused along the east-west fault portion, despite continued deposition in the east.

The dramatic change in deposition during the Late Syn-Rift (Section 7.3.3) is evident in the cumulative isochron plots for the Early and Late Hauterivian (Figure 7.18). The Late Syn-Rift mega-sequence is only present along the east-west portion of the Plettenberg Fault and not the north-south, with maximum accumulation occurring at the centre of the fault portion. This is reflected in the cumulative isochron to *top_basement* plot (Figure 7.18b and c) that demonstrates the dominance of the east-west portion of the Plettenberg Fault at the end of the syn-rift deposition.

A further technique for assessing the evolution of a fault is by plotting Displacement / Length profiles (cf. Chapter 5). As determination of displacement requires depth conversion of all sections (which is beyond the scope of this project), fault throws (in TWT) have been plotted against length (Figure 7.19). This has the advantage that it can be compared with other fault studies that will be discussed in Chapter 10. This plot shows that although accumulation varies along strike, there is the continuous presence of each sequence without localised and confined depocentres, hence no significant local maxima and minima, an observation that will be discussed in Chapter 10.

7.4.2 Gemsbok Fault

The isochron plots in the previous section and Section 7.3 show the presence of a north-south fault that forms the western margin of a north-south trending graben in the east of the basin. Although this east-dipping fault, the Gemsbok Fault, is visible on the seismic data (Figure 7.20), its total displacement is unknown because of the limitations of imaging at depth. From the plots (Figure 7.17) the fault continues to the north before changing to an east-west trend.

The thickening of the Principal Syn-Rift mega-sequence into the Gemsbok Fault suggests that it was active throughout this time, although the amount of sediment accumulation diminishes during the Early Valanginian before a brief re-generation in the Late Valanginian. During the Hauterivian there is no evidence of accumulation and it is inferred that the fault has switched off, although the presence of its footwall appears to control the extent of the Hauterivian depocentre (Figure 7.18a).

7.4.3 Pletmos Fault

The lateral extent of the Pletmos Fault, in the south of the basin, is not mappable because only a portion of it is imaged on sections at the south-west area of the coverage, although from the isochron plots (Figure 7.17) it can be inferred that it continues to the east. These isochron plots also suggest that the sediment accumulation, and hence inferred fault displacement, reduces towards the west. The fault itself is a planar dipping structure with a dip of approximately 45° (Figure 7.21) and is imaged for at least 60 km. The centre of the depocentre is to the east of the mappable fault section implying that the fault may continue considerably further to the east, and be much longer than 60 km.

The data coverage does not enable the full extent of the Pletmos Fault to be established, however it is important to notice the substantial increase of throw on the fault towards the

east trend on the throw vs. length plot (Figure 7.22). This plot will be used later in this chapter to compare the Pletmos Fault with the Superior Fault.

As discussed (Section 7.3.2), the Early Syn-Rift, *top_esr* reflector, has not been traced across the basin high into this sub-basin, although the *top_kimmeridgian* reflectors on the flank of the rotated fault block suggest that the fault was active during the same time as the Plettenberg Fault (Figure 7.21b). Flattening of the *top_l-valanginian* reflector indicates that it was still an active fault throughout the Principal Syn-Rift mega-sequence (Figure 7.21c). Extension continued during the Hauterivian (Figure 7.21d), although this section, and the areal plots (Figure 7.18a) indicate that its lateral extent was significantly reduced. Furthermore, the fulcrum of extension and hangingwall rotation is very close to the fault compared to the much broader Principal Syn-Rift package.

7.4.4 Superior Fault

Despite the Superior Fault being at the western extent of the data, it is imaged relatively well and its position is obvious from the isochron plots (Figure 7.17). In many sections it has an approximately planar geometry with a dip to the north of 45°, however at the western extent of the data it has an unusual geometry with a dramatic reduction in dip towards the top of the fault (Figure 7.23). The geometry of the fault appears to be paralleled by the underlying intra-basement reflectors. As discussed in the Section 7.3.1, such reflectors are unlikely to be multiples, or side swipe from the fault plane, and are most likely to be primary. Therefore, as the fault parallels these reflectors, it is inferred that the geometry of the fault is being inherited from the basement structure.

Restoration of the section demonstrates that the fault has a very similar evolution to the other faults discussed, with deposition from pre-Kimmeridgian times through to the Early Valanginian (Figure 7.23). There is then renewed subsidence in the Late Valanginian prior to localised extension in the Hauterivian. However, unlike the other faults, the eastern end of the Superior Fault was re-activated during the Post-Rift. When the section in Figure 7.24 is restored to *top_e-turonian*, the Turonian sequence, and in particular the Early Cenomanian sequence thickens into the north dipping fault. This is supported by the isochron plot of the Early Cenomanian (Figure 7.13).

In all of the thickening packages the maximum sediment thickness in the isochron plots (Figure 7.17 and 18) is at the western extent of the data set, therefore it is inferred that only the eastern end of the Superior fault is present in the data coverage. This is supported by the

throw vs. length plot (Figure 7.22) that shows substantial thickening of the sequences towards the west.

7.4.5 En-echelon nature of the Pletmos and Superior Faults

The isochron plots (Figure 7.17), and throw vs. length plots (Figure 7.22) indicate that while sediment accumulation in the hangingwall of the Pletmos Fault reduces to the west, the accumulation associated with the Superior Fault increases to the west, suggestive of an en-echelon geometry. This is supported by Figure 7.23, onto which north-south sections are plotted to show the gradual reduction in displacement of the Superior Fault and associated increase on the Pletmos Fault from west to east.

7.4.6 Springbok High

Although the Springbok High, in the centre of the basin, is a complex array of anastomosing faults, the overall structure is a basement high defined by north- and south-dipping normal faults.

The north end of the high is dominated by a north-dipping fault that is continuous along the mappable length of the high. To the west, a lack of data makes it difficult to ascertain its true geometry although it is evident from the series of sections (Figure 7.26) that its displacement dramatically reduces before the fault becomes insignificant at the western extent. The south-dipping fault that defines the southern Springbok High is similar to that of the northern fault in that it dies out to the west, although it also dies out towards the east.

The timing constraint of the high's development comes from well Gb-Spk1 and indicates various stages of extension on the different fault arrays (Figure 7.27). The reconstructions of the high (Figure 7.27c, d and e) suggest that the faults on either side were active prior to the Portlandian and then switched off between the Portlandian and the Early Valanginian. Further extension occurred between the Early and Late Valanginian.

7.4.7 Intra-basin faults

In addition to the principal fault arrays there are a number of smaller faults that do not show significant growth but are still important to understanding the evolution of the basin. One problem with such faults is their scale, as it is often difficult to correlate single fault surfaces between horizons, especially where line spacing is large.

One fault that is traceable between sections is a north-dipping normal fault that occurs in the immediate hangingwall to the Plettenberg Fault (Figure 7.28) and is at least 40 km long with

an east-west trend. This fault is unusual as it offsets the Late Valanginian and Early Valanginian although does not offset the underlying Portlandian. It appears to décolle onto a mid-Principal Syn-Rift horizon, and was active during the Hauterivian, resulting in the formation of a rollover geometry of the Late Valanginian reflector.

Other intra-basin fault arrays are evident from the TWT maps, especially that of *top_e-valanginian* (Figure 7.5c), and tend to be focused around the Springbok High. One such array to the south of the high (Figure 7.29a) trends east-west with small displacements (largest is 200 ms but with average 60 ms). These faults are a combination of south and north dipping faults that delimit a small graben structure that is associated with the furthest extent of the Hauterivian. It is interesting to note that these faults die out rapidly towards the west, as shown by the parallel section in Figure 7.29b. A similar array occurs north of the high with a very similar geometry, including delimiting the extent of the Hauterivian deposition. The timing of both of these arrays is post *top_l-valanginian* and probably prior to, or during the Early Hauterivian (Figure 7.29a). One problem that arises from these sections is the specific position of the *top_l-valanginian* reflector. From the resolution of the data it is difficult to determine whether the horizon is faulted and rotated in domino fault block fashion, or whether the horizon is an erosional surface that truncates the top of the faults and sequence.

A similar array of Late Valanginian intra-basin faults is evident in the north of the basin. These are all north dipping faults with small throws (up to 50 ms) and occur at the limit of Hauterivian deposition. As discussed for Figure 7.29, the specific position of the *top_l-valanginian*.

7.4.8 Summary of faulting

It has been demonstrated that although the Plettenberg Fault dominates the control of sediment accumulation through much of the evolution of the basin, there are various other faults that control either localised, or sub-basin accumulation.

7.5 Basin-fill deformational styles

In comparison to the complex basin fill deformation of the Gamtoos Basin, there is very little present in the Pletmos Basin. There are three areas in which basin fill deformation occurs: the north; the east; and south, although the lack of suitable data coverage makes it difficult to describe and map the features in three dimensions.

In the north, folding of the PSR occurs in the hangingwall of the Plettenberg Fault with an anticline of an amplitude of 400 ms, and a wavelength of approximately 8 km (Figure 7.31a and b). This feature is dissected by one of the arrays of intra-basin faults discussed in Section 7.4.7, and they have a similar east-west trending nature (Figure 7.31 is along strike of Figure 7.30 and illustrates the same feature). In the Gamtoos Basin it was discussed whether the genesis of such structures was compressional or extensional, and a similar argument is valid here. If the folding was a result of compression it would have to have been synchronous with the extension during the Late Syn-Rift, which seems unlikely. Midland Valley's 2D Move programme was used to sequentially restore the basin to determine if the deformation could be extensionally related (Figure 7.31 d to i). After the deposition of the Late Valanginian sequence the Early Hauterivian syn-rift was deposited immediately adjacent to the Plettenberg Fault. The localised re-activation of the Plettenberg Fault results in arc flexure of the Principal Syn-Rift mega-sequence forming both the folding of the Late Valanginian, and the intra-basin faulting (cf. Figures 7.29 & 30). The early Post-Rift package progrades to the south prior to regional southern tilting in the post Early Turonian. Of particular importance in this model is that: i) folding and deformation can be explained by simply changing the extent of active extension; ii) there is no requirement for uplift or inversion during the Late Syn-Rift or early Post-Rift; and iii) there is regional tilting to the south in the post Early Turonian.

In the east of the basin, proximal to the north-south trending Plettenberg Fault, it has been discussed that the Late Valanginian forms a monoclinical structure (Section 7.3.2e), not dissimilar to the Gamtoos Anticline (Chapter 6) but on a smaller scale. 2D Move restoration of this area (Figure 7.32) suggests that such folding can be achieved by the progressive deposition of the Late Syn-Rift mega-sequence along the east-west trending Plettenberg Fault. The north-south portion remains passive and acts as a buttress preventing Late Syn-Rift subsidence.

The folding in the south is difficult to map out because of the limitations of the data, although it is evident that the Late Valanginian is deformed into a broad low amplitude fold train (Figure 7.33). These folds occur directly in the hangingwall of the Pletmos Fault, and are of greatest intensity in the south, close to the fault. These folds result in the unusual outcrop pattern of the Pseudo-Early, Early, and Late Hauterivian sequences (Figure 7.7a). It is therefore suggested that these folds formed as a direct consequence of varying degrees of extension on the Pletmos Fault, and are not of a compressional genesis.

the immediate footwalls of the three basin-bounding faults there are additional faults that were active during this time and these were associated with folding of the syn-rift sequences. During the deposition of this sequence, the areal extent of the package increases, although continues to be dominated by the east-west faults (Figure 7.34e).

The increased subsidence is accompanied by a marked deepening of the depositional environment (McMillan *et al.*, 1997), and the deposition of organic rich claystones.

When sedimentation rates are calculated for the sequences picked in the Pletmos Basin, (Table 7.1) there is no discernible change between the Late Valanginian and Early Hauterivian. In the Gamtoos Basin (Chapter 6) it was argued that in order to source the basin with the relatively large amounts of claystone observed, a provenance that will erode into clay is required, and therefore is unlikely to be the Cape Super Group quartz and sandstones. Such a provenance may be either the Permian sediments of the Karoo Basin, or the upper Cape Supergroup.

These observations indicate that during the Principal and Late Syn-Rift mega-sequences the evolution of the Pletmos Basin is very similar to that of the Gamtoos Basin. The significant difference, however, is that the top of the mega-sequence is conformable with the overlying package, and there is no evidence of the erosional truncation at the top of the sequence, nor of the Basin-wide Unconformity. As discussed, the Late Hauterivian horizon can be correlated across the eastern Plettenberg footwall is correlatable with the Basin-wide Unconformity.

7.6.3 Post-Rift

During the early Post Rift the system was dominated by southward progradation (Figure 7.34f & g), prior to more general shelf deposition and regional southward tilting (Figure 7.34h). Within this mega-sequence there are many small unconformities that have not been mapped in this study, and have been correlated and attributed to glacio-eustatic fluctuations (Brown *et al.*, 1995).

Sedimentation is dominated by shallow marine sandstones often with abundant terrigenous input (McMillan *et al.*, 1997).

7.7 Discussion

The observations presented on the Gamtoos Basin (Chapter 6) suggest that structural inheritance played an important role in both the development and subsequent evolution of

7.6 Summary of basin evolution

The tectonic framework, fault evolution and basin-fill deformation for the Pletmos Basin has been established in the previous three sections and the purpose of this section is to integrate these observations. Although no stratigraphic or depositional environment data were available for this study, appropriate data from published literature have been used. This is particularly important for a comparison with the Gamtoos Basin in the discussion chapter (Chapter 9).

7.6.1 Principal Syn-Rift

i) Kimmeridgian

Although this sequence has been observed in some wells, the deeper wells have not penetrated to a great enough depth to test if this sequence is present. Despite the reflector not being reliably correlatable, the presence of the Kimmeridgian on the basement high is important because it implies that rifting initiated prior to the Kimmeridgian. There is no evidence of active faults, other than those already discussed, therefore it is inferred that the Kimmeridgian has a distribution similar to the Portlandian.

ii) Portlandian – Late Valanginian

During this period most of the faults were active, including the three principal faults (Plettenberg, Pletmos and Superior) and those that form the Springbok High, resulting in deposition across the basin (Figure 7.34a). In the Early Valanginian the faulting was localised on the bounding faults with little activity on the other growth faults (Figure 7.34b). In the Late Valanginian the extension was focused on the east-west trending portion of the Plettenberg Fault, although did occur across the whole basin (Figure 7.34c).

Sedimentologically (McMillan *et al.*, 1997), the Portlandian and Berriasian sequences are outer shelf argillaceous sandstones that change in the Valanginian to become a widespread shelly sandstones indicating a transition to a shallow marine setting. The exception is in the hangingwall of the Plettenberg Fault where middle to outer shelf claystones and sandstones continue during the Early and Late Valanginian.

7.6.2 Latest Valanginian-Hauterivian

Between the *top l-valanginian* and the Hauterivian there was a dramatic reduction in the areal extent of the deposition with sediment accumulation only occurring on the east-west trending faults, and the east-west trending portion of the Plettenberg Fault (Figure 7.34d). In

the extensional system. However, it is impossible to form regional scale conclusions, or discuss generic concepts from a single basin. The objective of this and the following chapter is to address these questions on a regional scale. Therefore the primary discussion will be in Chapter 9 after the Algoa Basin is evaluated. However, it is useful to briefly discuss some of the features more pertinent to the Pletmos Basin here.

The Pletmos Basin is dominated by east-west trending structures that change dramatically to a north-south trend in the south-east of the basin. The genesis of this change in trend in the Pletmos Basin has been attributed to the same mechanism as the trend change in the Gamtoos Basin, namely either inheritance from the basement, or late stage deformation in response to motion of the Aghulas Falkland Fracture Zone (AFFZ) (Malan *et al.*, 1990; McMillan *et al.*, 1997). These mechanism will be discussed further in Chapter 9.

On a basin scale, it has been demonstrated that structural inheritance plays as an important role in the Pletmos Basin as it does in the Gamtoos Basin. Structures that were controlling the evolution of the basin at a very early stage have been continually utilised throughout the evolution of the basin. Temporal changes in sediment accumulation have been used as a proxy of fault activity and to infer changes in the orientation of the maximum extension direction. In the Pletmos Basin, a change in the maximum extension direction is inferred from the migration of most active fault section. It is important to note that the pre-existing structures are used and are not cross cut.

Furthermore, it has been shown that some of the basin's structures can be switched on and off. For example the faulting on the Springbok High was active during the Portlandian, was inactive in the Early Valanginian, and then re-activated in the Late Valanginian and Hauterivian.

The overall tectonic framework established in this Chapter broadly agrees with published literature (Malan *et al.*, 1990; McMillan *et al.*, 1997), although as in the Gamtoos Basin the analysis on a sequence scale is more detailed than previous work. In particular the use of these sequences to understand fault evolution has not been conducted before. This framework does question the role of the AFFZ on the evolution of the basin. Roux (1992) attributes the formation of the basin to wrench tectonics on the AFFZ, and discusses oblique slip motion on the bounding faults. The strike-slip component is inferred to result in localised compression and basin fill folding which rotate during the evolution of the basin. The folds that Roux refers to have been discussed, and modelled in this Chapter and attributed to alterations in the extensional regime, and do not require a complex strike-slip or

compressional regime. Furthermore, there is no deformation observed within the basin that requires strike-slip motion.

7.8 Conclusions

This chapter has established a tectono-stratigraphic framework of the Pletmos Basin by integrating seismic and well data with published sedimentological data. This framework is broadly similar to that of the Gamtoos Basin obtained in Chapter 6, and will be fully compared in Chapter 9. The primary difference is that there is no phase of uplift and compression in the Late Hauterivian as there is in the Gamtoos Basin. The principal fault arrays have been analysed using cumulative isochron plots and throw vs. displacement plots and these will be used in Chapter 10 to compare the Pletmos Fault with normal faults in other tectonic settings. Intra-basin deformation has been modelled and accounted for using extensional tectonics, disagreeing with previous workers.

The next chapter will apply the same tectonic-stratigraphic framework technique to the Algoa Basin, which is located to the east of the Gamtoos Basin. The purpose of this is to assess the role of structural inheritance on a regional scale, and to determine whether the normal fault systems of southern South Africa conform to pre-existing fault models.

CHAPTER 8: Tectonic Evolution of the Offshore Algoa Basin

8.1 Introduction

In Chapters 6 and 7 the tectonic framework for both the Gamtoos and Pletmos Basins were established. The objective of this chapter is to apply the same techniques to understand the evolution of the Algoa Basin, which lies to the east of the Gamtoos Basin. This will enable a regional synthesis to be presented in Chapter 9, and hence allow the role of structural inheritance in the development of southern South Africa to be assessed.

As with the other basins, the evolution of the Algoa Basin was determined by establishing a tectonic and stratigraphic framework, understanding fault evolution, and documenting basin-fill deformation

8.2 Algoa Basin data

Evaluation of the Algoa Basin utilised 5,000 km of 1975, 1976, 1983, 1984, 1985, 1986 and 1989 vintage 2D multi-channel seismic data (Figure 8.1) of which 60% were migrated and 40% stacked sections. Nine exploration boreholes (containing composite, lithofacies, paleo-environment logs; Appendix C) were integrated with the seismic data to determine the sedimentology and age of the basin fill (Figure 8.2). The locations of sections reproduced as figures are highlighted on Enclosure 10.

The available seismic data was of a high quality, although two problems have been encountered. First, in the Port Elizabeth Trough poor migration of the data has resulted in significant problems in correlating between east-west and north-south trending sections. In order to assess the geometry of the principal structure (the north-south trending Port Elizabeth Fault) east-west lines were interpreted and one north-south line was used to correlate between them. It transpired that although there were difficulties, accurate correlation could be achieved if the specific horizon character was not used. Second, in the south-east of the basin the data quality is poor, making interpretation very difficult. This area has been excluded from the study.

8.3 Tectonic and stratigraphic framework

This section outlines the tectonic and stratigraphic framework established in this study for the Algoa Basin. The framework comprises four mega-sequences (Basement, Principal Syn-Rift, Late Syn-Rift, and Post-Rift, Figure 8.3), and is therefore very similar to that of the Gamtoos and Pletmos Basins (Chapters 6 and 7). Lithological well data is available, hence in addition to the seismic character, areal extent and thickness of each mega-sequence being discussed, appropriate sedimentology will be summarised.

8.3.1 Basement (*top_basement*)

The *top_basement* horizon is a high amplitude, positive polarity reflector onto which the syn-rift packages onlap (Figure 8.3). It is mappable across the Recife Arch in the west where it correlates with the *top_basement* of the Gamtoos Basin. Unlike the Gamtoos and Pletmos Basins, in the Algoa Basin the reflector is imaged across the entire basin and is never deeper than the maximum recording time of 5.0 s two-way-time (TWT). This negates the need to have the *pseudo-basement* reflector required in the other two basins. There is little internal basement structure in the west, even across the Recife Arch where the basement is shallow. In the east, strong parallel reflectors are imaged within the basement and these may be related to underlying basement structures (Figure 8.4; Bate & Malan, 1992).

The architecture of the offshore Algoa Basin is dominated by two sub-basins and corresponding controlling faults (*top_basement* TWT map, Figure 8.5). Both sub-basins have their controlling faults in the east. The western sub-basin, the Port Elizabeth Trough, is bounded in the east by the Port Elizabeth Fault, while the eastern sub-basin, the Uitenhage Trough, is bounded in the east by the St Croix Fault and dissected in the south by the Uitenhage Fault (Figure 8.5b).

Top_basement is well imaged with two exceptions. In the immediate hangingwall of the Port Elizabeth Fault the position of the horizon is poorly defined, and has been taken as the lowest imaged divergent reflector. This problem also applies to the St Croix Fault and is compounded by its complex geometry (Section 8.4.2).

The basement is penetrated by four wells and in each it is composed of either quartzite or micaceous schist and is therefore consistent with the onshore Cape Fold Belt lithologies (Chapter 3).

8.3.2 Principal Syn-Rift (Middle Jurassic?-Late Valanginian)

The Principal Syn-Rift (PSR) mega-sequence is unconformably above *top_basement* and below either *base_canyon*, or *basin-wide_unconformity*. It is sub-divided into the five sequences, Kimmeridgian, Portlandian, Berriasian, Early Valanginian, and Late Valanginian, with the name of each sequence defined by the uppermost reflector. The mega-sequence has been well-tied across much of the basin except for the northernmost Port Elizabeth Trough. In this area, the PSR mega-sequence terminates against the Northern P.E. Fault (Section 8.4.1) and although the reflector character of the package above the footwall of the fault is very similar to that of the PSR, there is no well tie to confirm this. As it is impossible to correlate PSR sequences across the fault this area has been omitted from the study.

i) Kimmeridgian

The *top_kimmeridgian* reflector defines the lowest syn-rift sequence and is imaged as the first high amplitude, positive polarity reflector within the syn-rift package. In the Port Elizabeth Trough the package has relatively high amplitude reflectors with sub-parallel geometries that diverge into the bounding faults. In the Uitenhage Trough the sequence is more transparent, although *top_kimmeridgian* remains a high amplitude reflector. Both the seismic and well data indicate that the reflector is present only in the deepest portions of the troughs, and onlaps onto *top_basement* on the western flanks of both troughs (Figure 8.6a). The horizon is truncated against the Port Elizabeth and St Croix Faults, and is dissected by an array of small intra-basin faults in the south of the Port Elizabeth Trough. In the south of the Uitenhage Trough, *top_kimmeridgian* is not picked in well Hb-C1 as the younger Portlandian sequence is present directly on top of *top_basement*. In the seismic data *top_kimmeridgian* can be traced across this area and it is suggested that it has not been observed in the well because the lowest most sediments (dated as Portlandian) are continental sandstones and conglomerates.

This continentally dominated sedimentation is characteristic of the Kimmeridgian sequence in the Uitenhage Trough with interbedded red conglomerates, sandstones and minor red claystones. The conglomerates are dominated by fractured, rounded quartz clasts while the sandstones are quartz arenites with minor lithics. The sequence is only present in one of the Port Elizabeth Trough wells where it comprises alternating coarse and fining sandstones, silstones and claystone sequences with occasional coal beds.

During the deposition of the Kimmeridgian sequence sediment accumulation is at a maximum in the immediate footwalls of the Port Elizabeth and St Croix Faults (600 ms and 800 ms respectively; isochron plot of *top_basement* to *top_kimmeridgian*, Figure 8.7a). The localised increase in sediment thickness in the north of the Port Elizabeth Trough is attributed to a small east-west trending fault (Section 8.4.1.ii). There is no evidence of growth across either the Uitenhage Fault or the intra-basin faults.

ii) Portlandian

The *top_portlandian* reflector is well-tied and traceable in both troughs and is a high amplitude reflector capping the package above *top_kimmeridgian*. The areal extent of the reflector is very similar to that of *top_kimmeridgian* with onlap onto *top_basement* at the flanks of the basin and truncation against the Port Elizabeth and St Croix Faults (Figure 8.6b). It is dissected by the Uitenhage and intra-basin faults, and in the centre of the Uitenhage Trough there is minor truncation against a later stage canyon system.

Sedimentologically, the conglomerates and quartz sandstones of the Kimmeridgian are replaced by fine to medium grained lithic sandstones with occasional siltstones in the Uitenhage Trough, and argillaceous sandstones, siltstones and claystones in the Port Elizabeth Trough. Deposition remained focused on the Port Elizabeth and St Croix Faults, and the loci of maximum accumulation was more pronounced and occurred further to the south-west compared to the Kimmeridgian (maximum of 650 ms for both; Figure 8.7b).

iii) Berriasian

The Berriasian sequence has a transparent seismic character with the top defined by a moderately high amplitude reflector (*top_berriasian*) that is either conformable with the overlying Valanginian sequence, or erosionally truncated against the *basin-wide_unconformity* or *base_canyon*. The base of the sequence is either conformably ontop of the Portlandian sequence, or unconformably onto *top_basement*. The sequence is laterally continuous across the basin, however, as in the underlying sequences, it is dissected by the Port Elizabeth, St Croix, Uitenhage and intra-basin faults.

The two troughs continue to have different sedimentary fills. The Uitenhage Trough remains more sand dominated with upward coarsening quartitic sandstone units changing to lithic sandstones towards the sequence top, while in the Port Elizabeth Trough there are interbedded shelly sandstones and siltstones in the north-west and siltstones containing deep marine radiolaria and shallow marine ostracods in the south-east.

The loci of maximum sediment accumulation remained in the immediate hangingwall of the Port Elizabeth and St Croix Faults, although the former only had 750 ms compared to 1250 ms of the latter (Figure 8.7c). The sediment accumulation in the south-east of the basin increased (maximum of 500 ms), although the position of the controlling fault is uncertain because it does not appear to be consistent with growth on the Uitenhage Fault.

iv) Early Valanginian

The *top_e-valanginian* reflector is a high amplitude, negative phase reflector that is well-tied and correlateable across the basin, although it is less extensive than the *top_berriasian* because of erosion by the canyon system and the *basin-wide_unconformity* (Figure 8.3 & 8.6d). The seismic character of the sequence differs significantly depending on location with the Port Elizabeth Trough dominated by high amplitude sub-parallel reflectors with moderate divergence into the bounding fault. The sequence in the Uitenhage Trough is more transparent and the *top_e-valanginian* is a moderate amplitude, negative phase reflector below a sequence of stronger reflectors. Where the horizon is not erosionally truncated against either the canyon or the *basin-wide_unconformity*, it is truncated against one of the basin bounding faults. In comparison to the underlying sequences, few intra-basin faults are evident, although this may be a result of the lower areal extent of the preserved horizon.

The sequence in the Uitenhage Trough comprises a mixture of lithic and quartz sandstones interbedded with coal and claystones. In the Port Elizabeth Trough it is dominated by upward coarsening, fine-grained sandstones, siltstones and shales

The isochron plots demonstrate that both the Port Elizabeth and St Croix Faults continue to control sediment accumulation (maximum of 1000 ms in the latter) although the loci of maximum accumulation have migrated towards the north-west in both faults compared to that in the Berriasian (Figure 8.7d). There is an east-west trending depocentre evident in the Port Elizabeth Trough (maximum of 1000 ms compared to average of 750 ms); this is probably associated with post-deposition deformation.

v) Late Valanginian

The areal extent of this sequence is significantly smaller than the Early Valanginian package with the uppermost defining horizon (*top_l-valanginian*) not being preserved in the Port Elizabeth Trough and only present in the hangingwall of the St Croix Fault where it is well-tied (Figure 8.6e). This reduction is a result of significant erosion of this upper Principal Syn-Rift sequence by both the *basin-wide_unconformity* and the canyon system. The

sequence is characterised by relatively transparent reflectors with little or no divergence towards the St Croix Fault.

Where present, the sequence is sedimentologically similar to the Early Valanginian with interbedded silstones and argillaceous sandstones in the Uitenhage Trough, and shales and claystones in the Port Elizabeth Trough.

As a result of the limited extent of the *top_l-valanginian* reflector, the isochron plot (Figure 8.7e) is relatively inconclusive. However, the data presented are not incompatible with the continued northward migration of the locus of maximum sedimentation that was observed in the Early Valanginian.

8.3.3 Late Syn-Rift (Latest Valanginian – Hauterivian)

Conformably on top of the *top_l-valanginian* horizon is a sequence that is dated by wells Hb-P1 and Hb-D1 as Latest Valanginian and Hauterivian. Although these well picks are limited by the significant canyon erosion, the horizon can be tentatively correlated across the canyon into the hangingwall of the St Croix Fault (Figure 8.8a). The sequence contains a series of reflector packages with upward increasing reflector amplitude and the top of the first of these packages has been picked as *latest_valanginian*. Furthermore, the reflectors within these packages diverge into the St Croix Fault and have therefore been assigned to the Late Syn-Rift (LSR) mega-sequence (Figure 8.3). The areal extent of the sequence is restricted by the *basin-wide_unconformity* and canyon system erosion (Figure 8.8a).

Two wells penetrate the sequence and in contrast to the sandstones and siltstones of the Late Valanginian, the Late Syn-Rift mega-sequence is dominated by claystone with occasional silty claystone.

Despite the LSR's limited extent, the *latest_valanginian* to *top_basement* package thickens into the east-west trending portion of the St Croix Fault, and thins to the east (isochron plot in Figure 8.8b). The locus of maximum sediment accumulation has migrated to the west compared its position during the Late Valanginian.

8.3.4 Canyonisation and canyon fill

Many of the Principal Syn-Rift sequences are observed to have erosional truncation either against the *basin-wide_unconformity* or *base_canyon*. The canyon system, defined by the *base_canyon* reflector will be discussed in this section, and the *basin-wide_unconformity* will be discussed in Section 8.3.5.

To understand the geometry and development of the canyon system, three horizons have been picked: *base_canyon*; *base_transp* (defining an inter-canyon horizon); and *top_canyon*. The *base_canyon* reflector is of variable amplitude, although it is evident because it consistently truncates the Principal Syn-Rift reflectors. The seismic character of the canyon fill is moderately transparent, and because it is overlain by high amplitude post-rift reflectors many of the internal reflector geometries are poorly imaged (Figure 8.9). The extent of the canyon system can be determined from the TWT of *base_canyon* and is approximately 30 by 60 kilometres, accounting for at least 40% of the areal extent of the Algoa Basin (Figure 8.10a). The main system occurs in the Uitenhage Trough, although there is a smaller subsidiary canyon in the Port Elizabeth Trough.

The *base_transp* horizon is an intra-canyon reflector that is approximately tied to the Late Aptian and separates the more transparent upper package from the less transparent lower package. The reflectors within the lower package (below *base_transp*) are better imaged, sub-horizontal and onlap against the sides of the canyon, suggesting that the canyon was passively infilled (Figure 8.10b). This is apparent in Figure 8.9c in which the canyon system has been flattened to *base_transp*. Also apparent in these figures is the minor amount of erosion present at the *base_transp* level. The age of the canyoning is constrained to the Late Hauterivian /Early Aptian because the oldest sediments into which the canyon erode are Hauterivian and the earliest sediments that infill the canyon are Late Aptian. The canyon fill sediments consist of claystones interbedded with cycles of upward fining sandstone to siltstones beds.

Towards the top of the transparent package there is a south-eastward progradational package that fills the rest of the canyon (Figure 8.11). The base of this unit is dated as Mid-Albian (well Hb-C1). This progradational package corresponds to an influx of coarser grained quartz or carbonaceous sandstones.

The majority of the canyon system occurs in the Uitenhage Trough where it reaches a maximum incision of 750 ms (isochron of *top_canyon* to *base_canyon*, Figure 8.12a). There is a smaller system in the Port Elizabeth Trough that is approximately 300 ms deep. The locus of maximum accumulation migrated from the north to the south (compare *top_transp* to *base_canyon* isochron with *top_canyon* to *top_transp*, Figure 8.12b & c) although there is no evidence of growth into any of the faults. The Uitenhage Trough canyon opens towards the south, however, the geometry of the Port Elizabeth Trough canyon is less evident. This later canyon has closure in the north, east and south and is truncated against the Port

Elizabeth Fault in the east (Figure 8.8). There is no growth into Port Elizabeth Fault during or after the deposition of the canyon fill, indicating that the fault was inactive by the time the canyon was established. It is inferred that the exit point of the canyon is narrow and beyond the resolution of the data.

8.3.5 Top canyon / basin-wide unconformity

Across the basin there is a traceable, high amplitude, positive reflector that either defines the top of the canyon (*top_canyon*) or is the *basin-wide_unconformity* (Figure 8.3). When the horizon is mapped out (either as *top_canyon* or *basin-wide_unconformity*) it forms a uniform south dipping plane (Figure 8.13a).

Where the reflector is *top_canyon* there is no evidence of erosional truncation of seismic reflectors at the top of the canyon and this is supported by the non-existence of an unconformity in the available well data (Figure 8.9). This implies that the canyon fill is conformable with the overlying Post-Rift.

Where the reflector is the *basin-wide_unconformity* there is significant erosional truncation of the syn-rift packages (Figure 8.3 & 14). This erosion has resulted in the removal of the majority of the Late Syn-Rift mega-sequence and much of the Late and Early Valanginian sequences. In places it also erodes the entire Principal Syn-Rift mega-sequence with a sub-crop of basement (Figure 8.13b).

The relative timing of the *basin-wide_unconformity* and canyon formation will be discussed in Section 8.7.

8.3.6 Principal Post-Rift

To understand the development of the Post-Rift mega-sequence above the canyon fill, three horizons (*top_e-cenomanian*, *top_e-turonian* and *top_maastrichtian*) have been picked and correlated from well ties. The *top_e-cenomanian* reflector is a high amplitude, negative polarity trace that is at the top of the parallel Cenomanian reflectors. For much of the basin this package is para-conformable with the *basin-wide_unconformity* and conformable with the *top_canyon* (Figures 8.11 & 14) except in the north of the Port Elizabeth Trough where it onlaps onto *basin-wide_unconformity*. In the north of the Uitenhage Trough it is erosional truncated against the sea-bed (Figure 8.15a). In a proximal setting (i.e. in the north), there is an influx of fine to coarse grained quartz rich sandstones while, to the south sedimentation is dominantly claystone with frequent floating quartz grains.

The *top_e-turonian* is present in the south-east of the basin and onlaps onto the *top_e-cenomanian* (Figure 8.15b) with very similar sedimentation to that of the Cenomanian. The *top_maastrichtian* reflector is tracable across the basin, except where it is erosionally truncated against the sea-bed.

During the Cenomanian and the Turonian there is only moderate thickening towards the south (Figure 8.16). This is in contrast to higher sequences (in particular above *top_maastrichtian*, Figure 8.17) where there is evidence of significant subsidence in the south, and the development of large scale southward prograding sequences. This subsidence in the south is accompanied by uplift of the coastal regions and truncation of the nearshore Post-Rift sediments.

The scale of the subsidence in the south is evident in sections across the southern Algoa Basin into the Southern Outeniqua Basin (Figure 8.18) that indicate the dramatic deepening of the water depth and thickening of the Post-Rift packages towards the Agulhas Falklands Fracture Zone.

8.4 Faulting

It is evident from the TWT map of *top_basement* (Figure 8.5), and from the tectonic and stratigraphic framework (Section 8.3) that there are various fault arrays present in both the Port Elizabeth and Uitenhage Troughs (Figure 8.19). This section will discuss the geometry and timing of the arrays and where possible model their evolution.

8.4.1 Port Elizabeth Trough

i) Port Elizabeth Fault

This is a north-south trending fault that defines the eastern margin of the Port Elizabeth Trough and controls the majority of sedimentation within the trough. The cross-sectional geometry is consistent with a west dipping, planar structure (Figure 8.20) traceable for at least 30 km and continues to the south of the data limit. The exception to the uniform geometry is in the north where the presence of the Northern Port Elizabeth Trough Fault (NPETF) results in the depth to *top_basement* in the hangingwall of the Port Elizabeth Fault being dramatically reduced (Figure 8.20a). The isochron thickness plots for the individual Principal Syn-Rift sequences (Figure 8.7) and the cumulative isochron plots from *top_basement* to sequential Principal Syn-Rift sequences (Figure 8.21) both indicate that sedimentation was controlled by the Port Elizabeth Fault throughout the deposition of the

mega-sequence. The maximum sediment accumulation of 2800 ms occurs at the southern extent of the data. From the available data it is difficult to determine whether the locus of maximum sediment accumulation has migrated during the evolution of the fault, although the *top_e-valanginian* cumulative plot (Figure 8.21d) implies that it may have migrated to the north.

The sediment accumulation (in TWT) vs. length plot (Figure 8.22) for the Port Elizabeth Fault indicates that throughout the Principal Syn-Rift mega-sequence sediment accumulation is focussed to the south of the fault. From this plot there is no evidence of accumulation minima along the fault trend. The decrease in sediment thickness at 17 km in Figure 8.22 is a result of the interaction between the Port Elizabeth Fault and the Central Port Elizabeth Trough Fault (CPETF; Section 8.4.1.ii) rather than fault segmentation. It is important to note that this graph only accounts for sediment accumulation in the hangingwall of the fault. From Figure 8.20c it is evident that sediment was deposited onto the footwall, hence fault throw can be determined. However, the deposition on the footwall is not preserved in the north of the trough, therefore to maintain a consistent datum along the fault length, only hangingwall sediment accumulation has been calculated.

ii) Central Port Elizabeth Trough Fault (CPETF)

This fault is a small east-west trending structure that is 10 km long and is only active during the deposition of the Kimmeridgian (Figure 8.23). Its maximum throw of 400 ms occurs in the centre of the basin although it is not imaged towards the east where the Port Elizabeth Fault is present (Figure 8.19).

iii) Northern Port Elizabeth Trough Fault (NPETF)

The east-west trending NPETF is mappable for 13 kilometres and the throw on it varies significantly (Figure 8.24). In the west there is no single fault plane and extension is accommodated by various small throw faults (maximum of 600 ms). The throw increases towards the centre of the mapped fault with the maximum achieved of 1250 ms. To the east of the maximum, the throw reduces slightly before the fault intersects the Port Elizabeth Fault. There is no evidence that the fault continues to the west of the Port Elizabeth Fault although the cross-cutting of the Port Elizabeth Fault by the NPETF results in the decrease in depth to *top_basement* observed in Figure 8.20a.

Although the NPETF is a significant east-west trending structure that is well imaged, its geometry is difficult to evaluate. The Principal Syn-Rift is truncated against the fault (Figure

8.24), crucially however, there is neither evidence of growth into it, nor reflectors diverging towards it, implying that the fault was in-active during post Principal Syn-Rift deposition. This however cannot be fully verified because although there is a package above *top_basement* on the footwall of the fault that has the same seismic character as the Principal Syn-Rift, there is no well tie to confirm this.

It is proposed that the NPETF was active after the deposition of the Principal Syn-Rift and that a northward thickening Late-Syn-Rift sequence may have been associated with it. This sequence would subsequently have been eroded by the *basin-wide unconformity*. This model will be discussed further in Section 8.5.1.ii.

iv) One fault or two faults?

The two principal faults in the Port Elizabeth Trough have very different trends with the Port Elizabeth Fault in a north-south orientation and the NPETF trending east-west. In the Gamtoos Basin (Chapter 7) it was discussed whether a similar change in trend was a result of it being either one curved fault or two independent faults, and the same arguments apply here. The two models proposed are that the north-south fault was active first resulting in the formation of a depocentre in its hangingwall during the Principal Syn-Rift. Subsequently, a new fault developed in an east-west orientation, possibly in the Late Syn-Rift, that cross-cut the pre-existing fault. In the alternative model, the fault is a single structure with a dramatic change in trend from north-south to east-west. Sediment accumulation was originally accrued on the north-south portion with little sediment on the east-west portion. In the late Principal Syn-Rift, or Late Syn-Rift, sedimentation occurred only along the east-west portion.

The first model is preferred because there is evidence of cross-cutting of the Port Elizabeth Fault by the Northern P.E. Fault. Furthermore, Principal Syn-Rift sediments are preserved in the footwall of the Northern P.E. fault and there is no growth into it during the deposition of this mega-sequence indicating that it was not present until later.

8.4.2 Uitenhage Trough

i) St Croix Fault

The St Croix Fault is traceable for at least 60 km in a north-west to south-east orientation at the north of the Uitenhage Trough. Cross-sections perpendicular to the fault trace illustrate both the complex geometry and lateral variability of the structure (Figure 8.25).

The cross-sectional geometry of the St Croix Fault is a south-west dipping structure that is listric at depth. At its western extent it is a single fault plane with few faults in the adjacent hangingwall (Figure 8.25a). Late Syn-Rift extension is accommodated on the principal fault. In the next section to the east (Figure 8.25b), the St Croix Fault plane is dissected by a steeper fault plane into which there is growth of the Late Syn-Rift sequence. This latter structure is spatially limited and is not present further east where the fault returns to being a single plane, although there is the continued growth of the Late Syn-Rift package (Figure 8.25c). The basement fault remains a single fault plane to the east, although it has an increasingly listric geometry at depth. This increase in listric geometry, and corresponding decrease in fault dip, is accompanied by the increase in the importance of steeper, short-cut Late Syn-Rift faults. These high angle faults merge with the St Croix Fault at depth. The throw across the St Croix Fault dramatically reduces towards the south-east from 3500 ms in the north-west to 500 ms in the south-east (Figure 8.25g).

Sections parallel to the St Croix Fault highlight the complexity of the fault geometry, especially in the west of the fault system. In Figure 8.26a, the high amplitude reflector is the trace of the St Croix Fault plane. The two, shallow, high amplitude reflectors are cross-correlated to the steep structures observed in Figures 8.25b & d, implying that these structures are oblique to the St Croix Fault.

The eastern extent of the St Croix Fault is uncertain because the sediment accumulation in its adjacent hangingwall reduces abruptly towards the south-east (Figure 8.26b). This coincides with the presence of a north-south trending, west dipping normal fault that is evident as two discrete reflectors; a shallow dipping reflector that is correlated to the St Croix Fault, and a steeper structure. This fault could either be a continuation of the St Croix Fault with an arcuate plan geometry (cf. Gamtoos Fault, Chapter 6), or a late stage structure that cross-cuts the St Croix Fault. The footwall of the north-south fault is predominantly basement with a small (100 ms) thickness of syn-rift preserved on its footwall compared to its hangingwall (1500 ms). As this would require significant throw on the north-south fault, and there is growth into the fault during the Principal Syn-Rift, the preferred model is the former with the arcuate fault.

Despite the complexity of the fault geometry, the Principal Syn-Rift mega-sequence consistently thickens into the fault. There is minor along-trend variation in sediment accumulation with the locus of maximum accumulation remaining static towards the south-east of the fault (Figure 8.21). Sediment accumulation varies along the length of the St Croix

Fault (Figure 8.27a) with the maximum occurring towards the south-east. The general trend of the plot is an increase towards the maximum, although there are two local maxima. Although the locus of maximum accumulation remains static in the south-east, the thickness plots for the individual sequences (Figure 8.7) imply that the most active part of the fault migrates towards the north-west during the Principal Syn-Rift.

Understanding the deposition of the Late Syn-Rift package is problematic because of the substantial erosion. Cumulative sediment accumulation has not been plotted because of the very limited extent of the mega-sequence. However, TWT map of the *top_l-valanginian* reflector, and the associated sequence isochron plots, suggest that the St Croix Fault was active, and that the west end of it was more active than the east.

It is proposed that the St Croix Fault was active along its length during the deposition of the Principal Syn-Rift as a single fault plane. The fault was undulatory and listric at depth. During the Late Syn-Rift the complex array of faults was established (Figure 8.28). In the west, the St Croix Fault plane was used whilst at the centre of the St Croix Fault a number of smaller faults became active that had a trend slightly oblique to the St Croix Fault. In some sections these later faults cross-cut the St Croix Fault, whilst in others new short-cut faults were established.

ii) Uitenhage Fault

The Uitenhage Fault is an east-west trending structure that exhibits significant along strike variation in both geometry and throw (Figure 8.29), in particular between the eastern and western portions. In the west it is a planar fault with limited throw across it that reduces towards the west (Figure 8.29b). Although the data coverage is limited in the west, the fault throw reduces to beyond seismic resolution to the east of the Port Elizabeth Fault. There is limited syn-rift sedimentation preserved in its hangingwall as a result of the canyon erosion. In the east the throw on the fault increases dramatically, and the cross-sectional geometry becomes increasingly listric. The maximum throw on the fault is at the eastern extent of the data where it is 2800 ms (Figure 8.20b). The change in geometry is also evident from the TWT map of the fault plane (Figure 8.19). In the eastern portion the depth to *top_basement* increases, and the depth of canyon incision decreases, resulting in the preservation of much of the Principal Syn-Rift. The geometry of the Principal Syn-Rift package adjacent to the eastern portion of the fault is unexpected in two ways: first, there is no thickening into the fault (Figure 8.29c & d); secondly, the sediment thickness in the footwall is significantly greater than that of the hangingwall (in Figure 8.29c this is most evident with

top_portlandian to *top_berriasian*). When the Principal Syn-Rift sequences are restored across the fault (in Figure 8.29ciii it is restored to flattened *top_berriasian*) they thicken into the St Croix Fault with no apparent deformation by the Uitenhage Fault. It is proposed that the Uitenhage Fault was not active during the Principal Syn-Rift and became active in the Late Syn-Rift as an east-west trending extensional fault. This is substantiated as there are Hauterivian sediments preserved in the hangingwall of the Uitenhage Fault, although their extent is limited because of canyon erosion.

8.4.3 Intra-basin faults

In addition to the principal controlling faults, there are also intra-basin faults that dissect the basin fill in both the Uitenhage and Port Elizabeth Troughs.

In the Port Elizabeth Trough two intra-basin fault arrays are evident (Figure 8.19). The geometry of the northern array is evident in Figure 8.23 with multiple, parallel, south dipping faults that have average throws of 50-80 ms cross-cutting the entire Principal Syn-Rift mega-sequence and *top_basement* reflector. This array has an east-west trend that is parallel to both the Northern and Central P.E. Faults. The timing of the faults is poorly constrained, but they are post-deposition of the Principal Syn-Rift and pre *base_canyon/basin-wide_unconformity*. It is inferred that the timing of these faults is contemporaneous with the NPETF and is probably associated with the Late Syn-Rift age of Latest Valanginian / Hauterivian.

The other Port Elizabeth Trough fault array is in the south of the trough (Figure 8.19) and has a WNW-ESE trend. This array is therefore not parallel to the northern array, although the geometry and timing of the two arrays are identical (Figure 8.30a).

The Uitenhage Trough also has two arrays of intra-basin faults, one in the north and the other in the south (Figure 8.19). The northern array (Figure 8.30b) has a similar geometry to the Port Elizabeth Trough arrays with north dipping, parallel faults that have an average throw of 50 ms. These faults offset the Principal Syn-Rift and *top_basement* reflectors but do not cut the *latest_valanginian* reflector. In some sections the early Late Syn-Rift reflectors are back tilted by these faults and there is evidence of growth into them. This northern array has an east-west trend.

The southern array in the Uitenhage Trough has a very different geometry to the other intra-basin fault arrays (Figure 8.30c). The faults in this array also trend east-west but are a combination of south and north dipping faults. The upper Principal Syn-Rift reflectors are

offset by up to 80 ms while the lower Principal Syn-Rift show no visible offset. The faults also coincide with anticlinal folding of *top_e-valanginian* and *top_berriasian* reflectors (cf. Section 8.5.1ii). The age of the faults are post Principal Syn-Rift and pre canyon formation, and the genesis of them will be discussed in Section 8.5.1ii.

8.4.4 Summary of faulting

Faulting in the Algoa Basin is more complex than in either the Gamtoos or Pletmos Basins. Two principal faults control the deposition of the Principal Syn-Rift package and these have approximately north-south trends. As a result of the significant erosion by the *basin-wide_unconformity* and the canyon system there is only a small amount of the Late Syn-Rift preserved. However, it has been inferred that during the Late Syn-Rift extensional phase east-west trending faults were established resulting in the formation of the Uitenhage Fault, the NPETF and the four arrays of smaller intra-basin faults. These faults frequently cross-cut the pre-existing structures.

8.5 Basin-fill deformational styles

The basin-fill deformation within the Algoa Basin is more limited than that observed in the Gamtoos Basin, although the geometries that are present are important to furthering the understanding of the basin. The most significant features are folding of the Principal Syn-Rift in both the Port Elizabeth and Uitenhage Troughs, and the *basin-wide_unconformity* and the correlatable *top_canyon* reflectors.

8.5.1 Folding

i) Port Elizabeth Trough

In the hangingwall of the CPETF there is east-west trending anticlinal folding of the Principal Syn-Rift sequences. The fold hinge is directly above the fault's hangingwall and the displacement on the fault is approximately proportional to the amount of folding, although this is very difficult to quantify (Figure 8.31).

Modelling using Midland Valley's 2D Move software was undertaken to determine if the geometry has an extensional or compressional genesis. In the extensional model (Figure 8.32) deposition of the Principal Syn-Rift occurs across the trough and is controlled by the Port Elizabeth Fault. In the Late Syn-Rift, extension occurs on a narrow axis in response to the east-west trending NPETF becoming active; the intra-basin faults also develop. This

narrow axis of extension is a valid assumption in light of the evidence from the other two basins (Chapter 6 & 7). Subsequent to the Late Syn-Rift extension, uplift occurs with significant erosion of the Late Syn-Rift and much of the Principal Syn-Rift, resulting in the development of the *basin-wide_unconformity* and the canyon system. The *basin-wide_unconformity* horizon is assumed to be sub-horizontal because flattening of the horizon restores both the canyon fill and the overlying Cenomanian reflectors to the horizontal. Following the infilling of the canyon, deposition of the post-rift sequences is accompanied by subsidence in the south. Therefore in this model the folding is formed by extension on the NPETF inducing tilting of the northern region, and tilting in the south by regional subsidence.

In the inversion model, re-activation of the CPETF as a high angle reverse fault occurs after the deposition of the Principal Syn-Rift mega-sequence. This re-activation results in the inversion of the syn-rift package in a harpoon structure (cf. Chapter 2). Subsequent uplift erodes the anticlinal closure prior to the deposition of the Post-Rift.

Both of these models can explain the observed geometry. The critical test is the geometry of the truncation of the anticline. The extensional model implies that the *basin-wide_unconformity* and the Principal Syn-Rift reflectors were folded synchronously in response to subsidence in the south, hence the PSR reflectors should be broadly sub-parallel to the *basin-wide_unconformity*. In contrast, the inversion model requires that the anticline be eroded by the *basin-wide_unconformity*, prior to southern tilting. This would result in a significantly greater southern dip on the PSR reflectors compared to the *basin-wide_unconformity*. When the *basin-wide_unconformity* is restored to the horizontal, the reflectors directly below the unconformity at the fold hinge are sub-horizontal (Figure 8.33) implying that the extensional model is more feasible. Furthermore, this negates the requirement for a phase of inversion, and the geometry agrees well with the extensionally derived geometries in the Uitenhage Trough and the other two basins.

ii) Uitenhage Trough

Folding of the *top_berriasian* and *top_e-valanginian* reflectors has been observed in the sections that show the intra-basin faults in the southern Uitenhage Trough (Figure 8.29b & c). The extent of the folding is difficult to ascertain because of the limited data in a suitable orientation, however, from the available data, the fold axis is inferred to have an east-west trend and is in the immediate hangingwall to the Uitenhage Fault. The fold is dissected by the intra-basin faults (Section 8.4.3) and it is proposed that they formed in response to outer

arc extension associated with Late Syn-Rift extension on the Uitenhage Fault, in a similar mechanism to that discussed in the Gamtoos Basin (Chapter 6). As a result of the subsequent erosion there is no syn-rift sequence evident, although there are the remnants of Hauterivian sediments, which this model would predict.

8.5.2 Port Elizabeth Trough basin-wide unconformity

The section across the Port Elizabeth Trough presented in Section 8.3.5 (Figure 8.14) illustrated the significance of the *basin-wide unconformity*. It is evident that the truncated horizons continued to the west, and therefore by projecting them an estimate of the amount of erosion can be determined. In Figure 8.32b the Principal Syn-Rift horizons are projected using the assumptions: a) they converge towards the flank of the basin (i.e. west); b) the geometry of the projection is a continuation of the geometry of where the horizon is present; c) there is no significant feature, e.g. fault on the Recife Arch. This last assumption is validated by sections that cross the arch. The projection (Figure 8.34) is approximately depth converted by pinning the section at sea-level and using the compilation depth-time conversion plot for the Algoa Basin (Appendix C-iii) to estimate that 3.5s TWT of syn-rift sedimentation is equivalent to 6 km depth (see Chapter 9 for method). This depth converted section is then juxtaposed against a similarly depth converted sections from the Gamtoos Basin in order to estimate the amount of erosion (Figure 8.32c). Despite the projections being taken as the lowest elevations that the observed geometries allow, it is estimated that at least 3 km of sediments and basement were eroded.

8.6 Summary of basin evolution

This section will integrate the data from the previous three sections to understand the evolution of the Algoa Basin. The spatial and temporal development of faults and basin fill deformation will be integrated with the tectonic and stratigraphic framework (Figure 8.35). In addition, paleo-environmental data from well logs will also be included.

8.6.1 Principal Syn-Rift

i) Kimmeridgian

The oldest recorded sediments in the Algoa Basin are of Kimmeridgian age. However, no well penetrates to the deepest sediments in the hangingwall of the controlling faults, therefore the initiation of rifting may be older. During the Kimmeridgian the two principal controlling faults were the St Croix and Port Elizabeth Faults, with minor activity on the

NPETF (Figure 8.35a). The depocentres were immediately adjacent to the two faults with the sequences overlapping onto *top_basement*. None of the other faults were active.

The depositional environment varied across the basin with terrestrially dominated braided fluvial systems and alluvial fans in the Uitenhage Trough, and Shallow marine sandstones in the Port Elizabeth Trough.

ii) Portlandian – Late Valanginian

Sedimentation continued to be focussed on the St Croix and Port Elizabeth Faults throughout this period. The areal extent of the sequences increased with the spatially limited Kimmeridgian and Portlandian packages being overlain by Berriasian and Valanginian sequences (Figure 8.35b). These two later packages are inferred to have been deposited across the entire basin. The NPETF becomes inactive prior to the Portlandian and there is no suggestion of any of the mapped faults being active other than the St Croix and Port Elizabeth Faults. There is evidence of sediment accumulation in the south-east of the basin, however, the controlling fault is not present within the available seismic data. Between the Kimmeridgian and Portlandian, the locus of maximum accumulation migrates towards the south-east of the St Croix Fault. During the Portlandian to Early Valanginian it migrates back towards the north-west. The locus of maximum accumulation associated with the Port Elizabeth Fault remains relatively static throughout the period at the fault's southern extent. Although the Late Valanginian has limited preservation (Figure 8.35d), the laterally extensive nature of the horizon from the Pletmos Basin (Chapter 7) across the Gamtoos Basin (Chapter 6) and into the Algoa Basin implies that it was probably present across the entire Algoa Basin.

The northern part of the Uitenhage Trough remains terrestrially dominated with meandering river systems and clay overbank interludes while the southern part increasingly marine dominated in the Berriasian and Valanginian.

The shallow marine conditions of the Kimmeridgian in the Port Elizabeth Trough deepen to distal slope deposits during the Portlandian. This deepening is short lived and the depositional environment of the trough gradually shallows during the Berriasian until it becomes inter-tidal in the Valanginian (Soekor well reports).

8.6.2 Late Syn-Rift : Latest Valanginian-Hauterivian

This sequence is only preserved in the immediate hangingwall wall of the St Croix Fault (Figure 8.35d). However, Section 8.4 has demonstrated that during this Late Syn-Rift phase

there is a dramatic change in the distribution of active faults. It is inferred that the NPETF and Uitenhage Faults become active while activity on the Port Elizabeth Fault ceases. The St Croix Fault continues to be active, although much of the extension is inferred to have occurred along new structures that are slightly oblique to the St Croix Fault.

As a result of the subsequent erosion by the *basin-wide_unconformity* and the canyon system it is uncertain how extensive Late Syn-Rift sedimentation was. However, in both the Gamtoos and Pletmos Basins, the LSR package was not extensive and only occurred immediately adjacent to the active faults. Therefore it is proposed that sediment only occurred in the immediate hangingwalls of the NPETF, Uitenhage and western St Croix Faults. In addition to these faults, smaller intra-basin faults developed to enable the basin-fill to accommodate this late stage extension. In the southern Uitenhage Trough and to the south of the NPETF localised folding of the Principal Syn-Rift mega-sequence developed. The orientation of the active controlling faults, intra-basin faults and basin-fill folding is east-west, implying that during this period extension was north-south with respect to the present orientation.

Where the sequence is preserved the sediments are interpreted to be lower slope claystones (Appendix C). There is, therefore, a significant deepening of the depositional environment between the Principal and Late Syn-Rift mega-sequences.

8.6.3 Late Hauterivian-Aptian

This period is characterised by a period of uplift, erosion and canyon formation (Figure 8.35e). The age is constrained by pre-erosion deposition of Hauterivian slope deposits and post-erosion deposition of Aptian sediments. In addition to the peneplanation by the *basin-wide_unconformity*, there was at least 750m of incision by the canyon system. The setting for, and genesis of, this canyon system will be discussed in Section

8.6.4 Aptian

Despite the significant erosion, the canyon system is passively infilled during the Aptian with slope claystones that are not in a dissimilar depositional environment to the Late Syn-Rift (Figure 8.35f). Therefore there is very little change in depositional environment between the Late Syn-Rift and the Aptian despite the significant amount of erosion that occurred. This will be discussed further in Section 8.7.

The northern section of the Uitenhage Trough canyon has more accumulation below the *base_transp* horizon than the south (Figure 8.12b) that suggests the presence of two sub-

basins. Sediment supply was sourced from the north, and filled the northern sub-basin first with occasional spills to the south and the deposition of parallel reflectors. After the northern sub-basin was filled, sediment influxed to the south, resulting in the minor unconformity at the base of the transparent package. A possible analogue would be the fill-and spill processes documented by Sinclair & Tomasso (2002) from the Coyer Canyon in the French Alpine foreland basin. The depositional environment become gradually shallower, with the southern migration of the shelf inferred from the prograding sand units towards the top of the canyon fill.

8.6.5 Post Rift : Albian - Recent

Subsequent to the infilling of the canyon, post rift sedimentation occurred across the basin from the Albian to present. During the Albian and Cenomanian there is a gradual thickening towards the south and deposition of quartz rich sandstones (Figure 8.35g). These sandstones are most probably sourced from the Table Mountain Group.

From the Maastrichtian to the present day there is increased subsidence in the south with the development of a substantial southward progradational system with sedimentation continuing to be dominated by quartz sandstones (Figure 8.35f). This is accompanied by onlap onto *top_e.cenomanian* and the subsequent uplift of the coastal areas.

8.7 Discussion and role of structural inheritance

The evolution of the Algoa Basin will be integrated with the data from the Gamtoos and Pletmos Basins into a regional synthesis in Chapter 9, therefore this discussion will be limited to specific features of the Algoa Basin.

The key observation is that structural inheritance does not play a significant role during the development of the basin. Although the two principal structures, the Port Elizabeth and St Croix Faults, are present through out the deposition of the Principal Syn-Rift sequences, there is a dramatic change in active structures during the Late Syn-Rift phase. The Port Elizabeth Fault is not utilised, instead new structures become active and cross cut the existing fault. With the St Croix Fault it is more complicated, although there is substantial evidence suggesting that it is also cross cut by new structures and only partly utilised. There is no evidence of the Uitenhage Fault during the Principal Syn-Rift package, and it becomes active during the Late Syn-Rift.

The interpretation of the St Croix Fault geometry differs from previous workers. The complex nature had been observed and explained by an array of overlapping fault segments on the main St Croix Fault (Cartwright, 1989; Bate & Malan *et al*, 1992). Such segmentation would be expected to be preserved through variation in sediment accumulation in the fault's depocentre; no such variation is observed. Furthermore, the complex faulting appears to be intimately linked to the development of the Late Syn-Rift sequences, and not to the Principal Syn-Rift, as the previous model implies.

The *basin-wide_unconformity* is present in the Gamtoos Basin, and therefore is a regional scale feature, and will be discussed in Chapter 9. The canyon system is more localised and will be briefly discussed here, although because it is closely associated with the *basin-wide_unconformity*, a full discussion of it will also occur in Chapter 9. The nature of the system is perplexing because of its timing and the depositional environments immediately prior to, and post incision.

The principal timing constraints are: the canyon system incises both Principal and Late Syn-Rift packages, implying that erosion was post Late Syn-Rift; the *top_canyon* is not an unconformity, therefore erosion / incision ceased by the earliest canyon fill (Late Aptian). Hence, erosion is confined to being between the Late Hauterivian and the Late Aptian but does not constrain the number, nor relative timing of erosional events.

The relative timing of the canyon incision is one of three possibilities: canyon system incision followed by *basin-wide_unconformity* erosion; *basin-wide_unconformity* occurs across the whole basin and then canyon system cuts into the basin; or synchronous canyon and *basin-wide_unconformity* formation. In all possibilities, erosion occurred prior to canyon infilling.

Each of the models raises specific questions or there are problems with validating them. In the first model, the canyon would be present during the erosion associated with the *basin-wide_unconformity*, hence the base of the canyon would be expected to contain deposits associated with this erosion. The local provenance is the silt and claystones of the Principal Syn-Rift; any erosionally derived deposits therefore may not be distinguishable from the deposits expected in a slope setting.

Both the first and second models require two phase of uplift and incision / erosion in a relatively short period of time (see below), a suitable mechanism is therefore required.

The third model invokes synchronous *basin-wide_unconformity* erosion and canyon incision. This model only requires one phase of uplift, and no erosional canyon fill deposit would be predicted. However, when *basin-wide_unconformity* and *top_canyon* are plotted together, a uniform, south dipping plane is formed, suggesting that the area has been peneplained (Figure 8.13). Peneplanation, and canyon incision, are unlikely to be the result of a single erosional mechanism; incision is a localised event, while peneplanation is regional. Therefore, if canyon incision occurred synchronously with *basin-wide_unconformity* erosion, then they are the result of two different mechanisms. For example, peneplanation may be the result of regional uplift and erosion, while canyonisation is the incision related to a localised drainage network.

A further problem with the canyon system is that of the depositional and erosional environments. Immediately prior to, and post erosion, the depositional environment is a deep marine setting. The basin, between these slope depositional events, underwent significant *basin-wide_unconformity*, and approximately 750 m of incision by the canyon system. Such a change is too great to be related to only glacio-eustatic fluctuations, and requires an uplift event. This uplift and erosion occurred between the Late Hauterivian (~130 Ma) and the Mid Aptian (~115 Ma), corresponding to a relatively short period of time. Therefore, within 15 Ma the basin went from a deep marine setting, was uplifted to either shallow marine, or sub-aerial setting, underwent up to 3 km of erosion (including quartz basement), had incision of 750 m, and then subsided rapidly to deep marine setting.

The canyon system is a significant basin feature, and large by continental margin scales (e.g. Daly, 1936; Satterfield & Behrens, 1990; Cronin & Kidd, 1998; Wonham *et al.*, 2000), further work is required to fully understand its erosional genesis and fill history.

8.8 Conclusions

This chapter has established the tectonic and stratigraphic framework for the Algoa Basin, which is the eastern most of the three South African basins used in this study. It has been demonstrated that the Principal Syn-Rift deposition is controlled by two faults. To accommodate the extension in the Late Syn-Rift phase, new faults evolve rather than utilising the pre-existing structures. The basin has undergone significant erosion and canyonisation, and the timing and extent of these erosional events produces constraints to any uplift model invoked.

The following chapter will integrate the observations from all three offshore basins and the onshore basement transects to address the role of structural inheritance in the evolution of the region.

CHAPTER 9: Regional Synthesis

9.1 Introduction

The study of the onshore geology, and analyses of the offshore sedimentary basins in the preceding chapters have revealed that structural inheritance has had a significant influence on the evolution of southern South Africa. This chapter will integrate the onshore and offshore data through the modification of the Cape Fold Belt (CFB) schematic section presented in Chapter 4 (Onshore Mesozoic) with the sub-surface data derived from the seismic studies. Second, to evaluate the evolution of the offshore sedimentary systems by combining the observations from the three basins. Additionally, the influence of regional events on the development of the Mesozoic Basins will be addressed.

This chapter is intended to be a synthesis of the key observations from this study with conclusions specific to understanding South Africa. The next chapter will use this synthesis firstly to address generic questions of structural inheritance and the effect of pre-existing structures on normal fault growth.

9.2 Onshore structures

Five transects (each ~ 100 km long), orientated perpendicular to the regional structural trend, were compiled to evaluate the Permo-Triassic Cape Fold Belt (CFB) and the superimposition of Mesozoic extension (chapters 3 & 4). A comparison of the transects reveals that in an east-west orientation there is remarkable similarity in the foldbelt geometry over 500 km, whilst there is significant variations in structural styles between the north and south of the region.

In the north, the CFB is characterised by asymmetric, northward verging folds with wavelengths of approximately 5 km (Figure 9.1a). In the centre and south, steep limbed box folds, cored with Peninsula Formation or Pre-Cape Units, are evident with wavelengths of 10-15 km. The northern limbs of the box folds tend to be steeply dipping to overturned. In Chapter 3 it was discussed that as there are no large scale thrusts, significant metamorphism, evidence of exotic block transport or klippen, the architecture of the CFB is atypical of continental compressional orogenies associated with thrusting and décollements (e.g. McClay, 1992 and references therein; Mattaur, 1986; Ricou & Siddans, 1986; Coward, 1983; Butler, 1982a & b; Boyer & Elliot, 1982).

Normal faults, commonly containing Mesozoic age syn-rift sediments (Chapter 2 & 4), are superimposed upon the CFB with an east-west strike parallel to the foldbelt. These faults are restricted to the central and southern regions (Chapter 4). In cross-section, the normal faults consistently occur at the northern end of the central box-fold flats (Figure 9.1b). As the position of the normal faults occurs in a structurally similar setting, it is inferred that the location of extension is structurally inherited from the pre-existing foldbelt (Chapter 4). Despite some of these observations having been presented by previous workers (Dingle *et al.*, 1983; de Wit & Ransome, 1992), the question of structural control at depth has not been raised. In Chapter 4, two models were proposed, the first was reactivation of a thrustal décollement system, the second, normal reactivation of high angle reverse faults. From the onshore data it is impossible to constrain these models at depth, or differentiate between.

9.3 Offshore Mesozoic structures and evolution

The two objectives of studying the offshore data (Chapters 6, 7 and 8) were to determine the geometry of the Mesozoic extension at depth, thereby constraining the structural inheritance models proposed from the onshore data, and to understand the evolution of the extensional system. An understanding of the extensional system will be used in Chapter 10 to address whether structural inheritance influences normal fault growth.

9.3.1 Overall structure

The south-east offshore region of South Africa is comprised of three Mesozoic sedimentary basins (Pletmos, Gamtoos and Algoa; Figure 9.2), and these basins are principally controlled by the Plettenberg, Gamtoos, Port Elizabeth and St Croix Faults (Chapters 6, 7 & 8). The Pletmos Basin also contains the Pletmos and Superior Faults (Chapter 7), although they occur at the periphery of the available data are therefore not discussed in this chapter. There are no significant intra-basin faults in the Gamtoos Basin (Chapter 6), and the other faults present in the Algoa Basin are late rift stage structures (Chapter 8). The Plettenberg, Gamtoos, Port Elizabeth and St Croix Faults have east-west trends, which swing towards the south-east at the southern limit of the data coverage. The offshore Gamtoos Fault is a direct continuation of the onshore Gamtoos Fault (Chapter 6), while there are no direct equivalent onshore portions of the other faults. The width of the basin ranges from approximately 20 km for the western Pletmos Basin to 60 km for the Gamtoos Basin and Port Elizabeth Trough. In cross-section (Figure 9.3) the Plettenberg, Gamtoos and Port Elizabeth Faults are very planar, with throws of approximately 5.0s TWT for the former two, and 3.5s TWT for

the latter. The St Croix Fault has a more undulating, listric geometry with a throw of 3.5s TWT. From the throw (in TWT) it is impossible to determine the true displacement or dip, therefore it is necessary to depth convert these sections.

i) Representative sections

Four sections are presented to illustrate the overall geometry of the basin-bounding faults (Pletmos, Gamtoos, Port Elizabeth and St Croix Faults; Figure 9.3). These sections have been chosen because they illustrate the appropriate fault with maximum observed throw. Although the data available to this study is insufficient to permit accurate depth conversion of sections from depth in ms TWT to depth in metres, an approximate conversion of each of these sections have been undertaken to allow basin dimensions and fault throw, dip and displacement to be estimated. The method and errors corresponding to this conversion are discussed in the following section.

ii) Depth conversions and limitations

Accurate depth conversion of sections is beyond this project, and as it is the overall geometry on a basin scale that is important, in particular the dimensions and dip of the basin bounding faults, the conversion has been approximated. Using check shot data and time-depth data (Chapter 5) from 41 wells, depth in time was plotted against depth in metres. Data from all wells have been plotted together (Figure 9.4) and a best-fit time-depth function was calculated using Table Curve 3.0 graph package. As a consequence of insufficient data across the basins, this function was used for the four sections in Figure 9.3. The time-depth function suggests that the range of values are approximately ± 400 ms TWT from the predicted best-rift. This value is used as an approximate error for the calculated data. The *top_basement* hangingwall and footwall cut-off points were obtained from the sections in depth (TWT) and converted to depth in metres using this function. A linear velocity function between the two cut-off points is assumed. The true dip and vertical sediment thickness accumulation for each of the sections is then calculated (Table 10.1).

There are various limitations with this method. The first is that as there is no well penetration deeper than 4,374m (2920 ms TWT), the velocity structure for the deeper portions of the basin has to be estimated. As the seismic velocity in sediments increases with depth due to increasing compaction, the gradient of the depth-time curve correspondingly increases with depth. To conservatively estimate the depth-time correlation at depth, the

curve is projected using the gradient of the lowest well velocity data to estimate depths beyond well penetration. In reality, the gradient will continue to increase, therefore this method will underestimate the true depth. Lithological variations of the basin fill also introduce an error. The lithology from which the velocity data are derived is predominantly shale, the dominant basin fill, although evidence from the basin margins suggest that the early syn-rift fill may be more sandstone dominated (as predicted by Prosser, 1993). As sandstones have a higher internal velocity than shales, by assuming that the unpenetrated basin fill is shale, the calculated sediment thickness will again underestimate the true sediment thickness. It is impossible to estimate an error for the projection at depth, however, the range of known data from the best-fit line is approximately 20%; a similar error is assumed for the depth to footwall cut-offs.

A further error is introduced because the calculated sediment accumulation is underestimated because of erosion of hangingwall sediments against the Gamtoos, Port Elizabeth and St Croix Faults, although the observations from Chapters 6 & 8, suggest that there is less than 250 ms of erosion (equivalent to less than 5 %).

As the minimum resolution of faults is generally considered to be a quarter of a wavelet (e.g. Badley *et al.*, 1990; Pickering *et al.*, 1997), and the wavelength of a wavelet increases with depth, the resolution of the fault cut-off pick decreases with depth. It is estimated that the resolution varies between 10-40 ms (Chapter 5), which is a negligible error compared to the scale of the half-graben bounding faulting. The errors in determining heave are negligible for hangingwall cut-off and are estimated to be approximately 100-200 m for footwall cut-offs, which is equivalent to 1-2%.

In Chapter 5 it was discussed that sediment accumulation is used as a proxy for displacement. By assuming that calculated total sediment thickness is equivalent to total fault displacement, as is done here, further errors are introduced. The formation of accommodation space is a result of the interaction of tectonic subsidence and eustatic fluctuations (e.g. Gawthorpe & Leeder, 2000). As the thickness of sediments is significantly larger than eustatic fluctuations (~12 km compared to 100 m), eustatic effects have been ignored. The basins were probably underfilled for much of their evolution because syn-rift sedimentation was dominantly shelf to slope deposits (cf. Chapters 6, 7 & 8). This introduces an error because sediment supply was not filling all the available accommodation space, hence displacement is underestimated. In these calculations it is the total

displacement that is important; the underfilling of accommodation space would only increase inferred displacement by ~100m (cf. displacement of approximately 12 km).

A final consideration is that sediment accumulation does not account for elastic re-bound or isostatic restoration of the faults' footwalls (e.g. Stein & Barrientos, 1985; McKenzie & Jackson 1986; Anders *et al.*, 1993), resulting in further underestimation of displacement.

iii) Scale of faulting

The depth-conversion of the data in the previous section reveals that the maximum dimensions of the basins are: 60 km wide; fault lengths of up to 150 km; and up to 12 km throw on the bounding faults, which are moderately to steeply dipping (Table 9.1). It is important to note that these are minimum estimates (see previous section). The determination of the length of the faults is problematic. The lengths stated are the minima that are evident from the seismic data alone (except the Gamtoos Fault where both onshore and offshore portions are included). Previous workers (e.g. McLeod *et al.*, 2000) have used displacement/length profiles to estimate total fault length; this has not been undertaken here due to the uncertainty of errors in the displacement/length (D/L) profiles (see Chapter 10). The onshore portions of the faults will not be discussed because of a lack of accurate data.

iv) Implications for CFB model

The depth-conversion of the Mesozoic faulting can provide further constraints for the models of the CFB (Figure 9.1c & d). This assumes that there is continuity of structures between the onshore and offshore, which is reasonable given the similarity in structural styles across the foldbelt.

In both of the models, the north of the CFB is controlled by a shallow décollement thrust system, which is consistent with the listric geometry of the St Croix Fault flattening out at approximately 5 km. The two models differ with respect to the control of the southern CFB.

Inherent in the décollement model is that the normal faults become listric at depth, soling out onto a controlling décollement, and that the system undergoes complete, rather than partial, reactivation (see discussion in Chapter 3; Figure 9.1c). This last assumption is valid as the main compressional features are the box folds, which are inferred to be controlled by some structure at depth. This requires the controlling reverse fault to occur immediately to the south of the northern limb (i.e. northern end of the box-fold flat). As this is the position where the normal fault is observed, it is inferred to reactivate the pre-existing reverse fault.

The Gamtoos and Plettenberg Faults are planar structures with dips of 42.5° and 65° respectively. If reactivation is assumed, then the ramp structures of the pre-existing reverse faults have to have the equivalent dip. This invoked ramp dip is significantly steeper than most documented examples, where geometries tend to be shallower than 30° (Boyer & Elliot, 1982). The planar nature of the Gamtoos and Plettenberg Faults to at least 12 km confines the depth of the décollement to greater than 12 km, and it may be considerably deeper unless the steep ramps merge with the décollement without becoming listric. In Chapter 10 these observations will be integrated with the current understanding of structural inheritance (reviewed in Chapter 2) to assess which of the two proposed models is more applicable.

v) Evolution of South African offshore

The second aim in studying the offshore data was to establish a tectono-stratigraphic framework to understand the evolution of the Mesozoic extensional setting. This has been established, and results from all three basins will be integrated in this section (Figure 9.5). As discussed in Chapter 5, and in Section 9.2.2, it is assumed that accommodation space is controlled by tectonic subsidence and that sediment accumulation is a proxy for accommodation space. Therefore variations in sediment accumulation are assumed to reflect variations in fault displacement.

The earliest syn-rift sediments are not penetrated in the deepest portions of the basins, and the oldest sediments dated in any borehole is Kimmeridgian; rifting is assumed to have initiated prior to the Kimmeridgian.

Onshore data in Chapter 3 suggests that the earliest syn-rift may be Enon conglomerate, although from the available data it is difficult to know how extensive this unit is and how it relates to the offshore units. Across most of the offshore region, the *top_kimmeridgian* well-tie is picked, and even at this early stage deposition is controlled by the principal faults with no evidence of other controlling faults. Borehole evidence suggests that sedimentation is dominantly fluvial, and deposition is greatest adjacent to the north-south trending faults, although it also occurs on the east-west portions (~800 ms compared to 400 ms for the Gamtoos Fault). It is inferred that the north-south fault portions have greater displacements compared to the east-west portions, and that extension is east-west orientated with respect to the current position. In the Algoa Basin, deposition does not occur across the whole basin, but is focussed on the controlling faults, and onlaps onto the flanks of the sub-basins. In the Pletmos Basin, other faults are active and have deposition associated with them.

Across the region in the Portlandian, Berriasian and Valanginian (Principal Syn-Rift megasequence), sediment accumulation continues to be focussed on the controlling faults, with the other faults in the Pletmos Basin becoming less significant. During this period there is at least 1800 ms TWT of sediments accumulated adjacent to the Plettenberg Fault, 2500 ms TWT against the Gamtoos Fault, 1200 ms for the Port Elizabeth Fault, and 2100 ms associated with the St Croix Fault. There is a migration of the loci of maximum accumulation towards the north-west in all of the basins, although this is less evident in the Algoa, where these sequences are less well preserved. The orientation of the regional stress system is inferred to have changed and become more north-east to south-west orientated. The depositional environment deepens dramatically between the Kimmeridgian and Portlandian, with fluvially dominated sediments being replaced by marine sediments, except in the proximal Algoa Basin where estuarine deposits dominate. Immediately adjacent to the Plettenberg and Gamtoos Faults, sediments were deposited in outer shelf conditions.

In the Latest Valanginian and Hauterivian (Late Syn-Rift mega-sequence), the loci of deposition migrate to the west in the three basins, with extension only occurring on the east-west trending fault portions. The total accumulations during this stage are: Plettenberg Fault, 1700 ms; Gamtoos Fault, 1750 ms; St Croix Fault, >500 ms. Sediment accumulation only occurs immediately adjacent to the bounding faults, and onlaps onto the underlying Principal Syn-Rift sequences. In the Gamtoos and Pletmos Basins the pre-existing bounding faults are utilised, whilst in the Algoa Basin, new faults evolve that cross-cut the pre-existing faults. Across the region, arrays of smaller extensional faults, trending east-west, evolve in the sedimentary fill of the basins, and folding of basin-fill sediments occurs proximal to the north-south trending Gamtoos and Plettenberg Faults. Features such as the Gamtoos Anticline develop at this stage in response to this localised phase of extension. There is no erosional truncation evident between the Principal Syn-Rift and the Late Syn-Rift mega-sequences.

The depositional environment changes between the Late and Latest Valanginian from shallow marine/shelf to deeper marine slope, and this is accompanied by a change in petrography from lithic sandstones to claystones. Such a petrographic variation may be in response to either a switch to a more distal depositional environment (and probably corresponding decrease in coarse clastic sediment supply), or a change in provenance. Despite the errors inherent in the calculation of sediment accumulation rates (see Chapter 5), there is no evidence of a dramatic reduction in sedimentation, therefore a change provenance

is the more probable cause. The lithic and quartz provenance is most likely to be from the upper Cape Supergroup, which are lithic, not quartz, dominated sandstones (Chapter 2). The claystone input may be a result of erosion of the Karoo Basin.

Subsequent to the Hauterivian, the east of the study area experienced a major erosional truncation event which affects the whole of the Algoa Basin, and 60% of the Gamtoos Basin (eastern portion). The reconstruction of the Port Elizabeth Trough (Chapter 8) reveals that there may have been at least 3 km vertical erosion. At this time, there is evidence of compression and reverse faulting on the Gamtoos Basin western flank, and possible reactivation of the east-west trending Gamtoos Fault. This erosion is synchronous across the Gamtoos and Algoa Basins and has been dated as Barremian.

In contrast, in the Pletmos Basin (150 km to the west), there is subsidence with the development of a southward prograding system.

A regional hiatus is evident in the Aptian, prior to the Algoa Basin's canyon infilling in the mid-Aptian. Mild regional subsidence in the south is followed by uplift of coastal areas and dramatic subsidence during the Late Cretaceous and Tertiary.

The key conclusions from this synthesis are:

- 1) There is evidence of fault growth along the entire length of the principal faults from a very early stage.
- 2) Associated with the early Principal and Late Syn-Rift stages there is a significant increase in water depth of the depositional environment.
- 3) There is the sequential migration of the loci of maximum sediment accumulation towards the north-west during the evolution of the basins. It is inferred that this reflects a variation in the location of maximum fault displacement.
- 4) During the Latest Valanginian and Hauterivian, when extension becomes north-south orientated, the east-west portions of the Plettenberg and Gamtoos Faults are re-used, resulting in the deformation of their basin-fill sequences, while in the Algoa Basin new faults cross-cut the pre-existing structures.

9.4 Modification of Mesozoic basins by regional events

Prior to discussing whether structural inheritance has influenced the development of the basins, it is necessary to discuss whether the Mesozoic evolution has been modified by regional events.

i) Aghulas Falkland Fracture Zone

The Aghulas Falkland Fracture Zone (AFFZ) has been much cited as a significant influence on the evolution of southern South Africa, from the overall geometry of the basins to localised deformation events (e.g. Ben-Avraham *et al.*, 1993; McMillan *et al.*, 1997). This section will briefly assess whether such claims are valid in light of the presented observations.

Arcuate basin geometries: On a regional scale, three mechanisms have been proposed to explain the arcuate nature of the Mesozoic extensional structures, two of which involve the AFFZ. Ben-Avraham *et al.* (1993) attribute the change in trend to rotation of the faults by the dextral AFFZ during initial rifting. Many others (Martin *et al.*, 1981; Thomson, 1999) propose that it is inherited from the arcuate shape of the CFB.

In Chapters 3 & 4 it was documented that the Cape Fold Belt deformation was identical regardless of whether it had an east-west or NE-SW orientation (as it does in the Gamtoos Basin) and that there was no discontinuity between the two areas. This suggests that the along trend variation in the CFB was not a result of brittle deformation. The deformation associated with the AFFZ would be expected to be of a brittle nature in the upper crust, and therefore does not explain the observations. It is concluded that the arcuate nature was inherited from the underlying foldbelt.

Strike-slip and compression due to AFFZ: Many of the deformational features within the Gamtoos and Pletmos Basins have been attributed to a strike-slip component of the normal faults displacement, often inducing localised compression (cf. Chapter 2). The dominant cause of this strike-slip motion has been attributed to AFFZ motion. In particular, the Gamtoos Anticline, the change in extension of the Gamtoos Basin to the east-west fault portion only, and the folding within the Pletmos Basin have been cited as examples of compressional deformation. In each of the chapters, the formation of these inferred compressional structures have been attributed to extensional strain being superimposed upon the specific conditions within the basin. For example, the Gamtoos Anticline had been attributed to subsidence in the west of the basin resulting in compression and uplift of the basin fill in the east adjacent to the curve of the basin fill (Fouché *et al.* 1992).

Reconstruction of the geometries has revealed (Chapter 6) that this apparent folding can be achieved by switching the locus of active extension to the east-west trending fault, resulting in the deformation of the pre-existing basin fill. There are no features within any of the basins that require strike-slip motion on the AFFZ.

Proximity to AFFZ: Interpretations of published sections from the Southern Outeniqua Basin, which lies between the study area and the AFFZ, demonstrate that there was little or no deformation during the period when the AFFZ was active. It is presumed that associated deformation would be expected to be more evident closer to the AFFZ. In a study of the region to the south of the Outeniqua Basin, Ben-Avraham *et al.* (1993) conclude that there is no evidence of post-Hauterivian motion or deformation of the Diaz Ridge because AFFZ deformation is localised to the south. This localisation of deformation on a relatively narrow zone beside a transform margin has been documented in analogous settings (e.g. Mascle *et al.*, 1987; Ben-Avraham & Zoback, 1992; Basile & Brun., 1993), by sand-box models (Basile *et al.*, 1999) and thermomechanical modelling (Gad & Scrutton, 1997).

There is therefore no evidence that the AFFZ has played a significant role in modifying the basins in the study area.

9.5 Gamtoos and Algoa Basin uplift

It has been documented in this study that the eastern Gamtoos and Algoa Basins underwent uplift and erosion during the Late Hauterivian. The Gamtoos Fault footwall has undergone the most significant erosion (~4 km), with evidence of uplift and erosion of the eastern Gamtoos Basin, and across much of the Algoa Basin. There is no evidence of this uplift either in the western most Gamtoos Basin, or the Pletmos Basin, implying that the width of deformation is in the order of 200 km.

As the deformation is on the scale of 200 km (i.e. significantly greater than basin scale), it is concluded that a local causal mechanism is not valid, and a more regional mechanism is required. In other regions where basin inversion / exhumation has occurred, the dominant mechanisms invoked are: uplift due to either hot spots, or a transient spreading centre; post-glaciation lithospheric isostatic rebound; intra-plate compression associated with collision, or spreading centre ridge-push; or underplating beneath continental crust (Dewey, 1989; Coblenz *et al.*, 1995; Ferreira *et al.*, 1998; Withjack *et al.*, 1995).

Thermal anomalies associated with hot spots typically have topographic expressions on a wavelength of approximately 2000 km (White and McKenzie, 1989), which does not correspond to the observed deformation, and no hot spots were nearby at this time (Martin, 1987, Morgan, 1983). The progression of the sea floor spreading ridge to the south of the AFFZ has been suggested as a possible mechanism (Thomson, 1999). However, the associated uplift would be expected to be transient with maximum uplift passing to the west with time. The uplift is synchronous across the area and does not effect the western portion.

Isostatic rebound is not valid as there is no evidence of glaciation since the Carboniferous/Permian Dwyka Tillite (Dingle *et al.*, 1983).

The principal plate driving force on the African plate during the Cenozoic has been compression as a result of ridge-push and Meijer & Wortel (1999) conclude that there is no relationship between ridge push torque and changes in the Africa-Eurasian collision. Therefore, as there has been no change in plate margin boundary conditions, except for the northern margin, ridge-push was the dominant driving force in Southern Africa during the Late Hauterivian. The timing of the sea floor spreading initiation has been determined using sea-ward dipping reflectors on both the Namibian and Argentinian margins, which give an age of 130Ma, and by the first sea floor magnetic anomaly, chron CM10 (Austin & Uchupi, 1982). Chron CM10 and 130Ma are recognised as being of Late Hauterivian age (Channel *et al.*, 1995) which is co-incident with the pulse of uplift/compression. The compressional effects of ridge-push have been documented both by geophysical modelling (Lithgow-Bertelloni & Richards, 1998; Vågnes, *et al.*, 1998; Meijer *et al.*, 1997; Richardson, 1992; Bott & Kusznir, 1979), and from studies of inverted margins and basins (Doré *et al.*, 1997; Coblenz *et al.*, 1998; Withjack *et al.*, 1995; 1998). The majority of these studies document inversion of the adjacent margin, and not a basin that is over 600 km from the spreading centre. It is also uncertain why the compression would be focussed on this particular area.

An alternative would be uplift associated with underplating and the emplacement of intrusive bodies under the area, however, there are no available geophysical data to either support or disprove this.

From the available data it is difficult to differentiate between horizontal and vertical compression, therefore the genesis of the uplift remains an enigma.

9.6 Variation in extension orientation

The regional synthesis documents a consistent rotation in the relative orientation of extension from east-west in the early syn-rift, to the northwest-southeast in the Valanginian, to north-south in the Hauterivian. From the available data it is uncertain whether this variation is a consequence of a variation in the regional stress system, or a result of African plate rotation about a static stress system.

9.7 Conclusion

The objective of this chapter was to integrate the onshore and offshore data. Through the approximate depth conversion of seismic sections, the proposed models for the CFB have been constrained further in depth.

Data from the offshore chapters reveal that the evolution of the three basins are very similar. In the Gamtoos and Pletmos Basins the controlling faults remain dominant throughout the evolution regardless of extension orientation. In the Algoa Basin, where the controlling structures are shallower, when the extension orientation changes, new structures are established to accommodate the new stress regime.

Chapter 10: Implications and Conclusions

10.1 Introduction

Studies of structural inheritance and extensional system evolution have both received significant attention over the last decade (see review in Chapter 2). However, until recently, there have been very few studies that have attempted to fully integrate these two important aspects of continental tectonics. The central objectives of this study are to understand the role of structural inheritance in the evolution of southern South Africa, and to address the role of structural inheritance during the growth of normal faults.

This chapter is divided into two parts. The first part will address whether structural inheritance, and fault reactivation, can adequately explain the observations from the Cape Fold Belt and Mesozoic extension outlined in Chapter 9. The second part will examine the observations from the Mesozoic system and discuss whether current fault growth models are applicable to a region with a significant pre-existing structural fabric.

10.2 Structural inheritance

The repeated use of a tectonic fabric by multiple phases of deformation, structural inheritance, is intimately associated with reactivation, which is the accommodation of geologically separable displacement events along pre-existing structures (Holdsworth *et al.*, 1997). Depending upon the change in stress regime, reactivation can result in either inversion, the compression of an extensional system and the uplift of syn-rift sequences; or negative inversion, the extension of a previously contractional system (Williams *et al.*, 1989; for discussion on nomenclature see Cooper *et al.*, 1989). Reactivation of a structure with the same sense of slip is more difficult to observe.

This section will discuss whether the concepts of reactivation, and associated inversion geometries, are applicable to, and aid the understanding of, the CFB and Mesozoic extension.

Controls on CFB formation: It is assumed that the Cape Fold Belt deformation is controlled by underlying reverse faults (Chapter 3). There is no surface expression of these contractional structures, therefore the dips and strikes have to be inferred from the available data.

The key observation from onshore studies in South Africa, presented in Chapter 3, is the very different style of deformation between the northern foldbelt and the central and south areas. The former is dominated by 5 km wavelength, north-verging asymmetric folds, while the latter (central and south) are dominated by 20 km wavelength, 10 km amplitude anticlinal box-folds separated by ~ 5 km wavelength synclines; there are no significant thrust faults, mylonites, klippen that are indicative of a fold and thrust system, especially in the south (cf. Chapter 3). The key questions are whether the nature of the controlling faults can be ascertained from these geometries, and why there is a difference between north and south.

The north region does not present a problem as the geometry of the surface folds are similar to those expected from blind thrusts (Boyer & Elliot, 1982; Coward, 1984; Mitra, 1990).

The south is problematic because the box-folds are very different in style to the north and to those expected in fold and thrust belts. In Chapter 3, three models for the genesis of the box folds were suggested: regional décollement with either back-thrusting or stacked duplexes forming the box-folds; or reactivation of high-angle reverse faults. From the available data it is difficult to conclude which model is more valid. In Chapter 2 it was shown that given a simple ramp-flat geometry, box-folds (similar to those of the CFB) were produced in analogue models (Buchanan & McClay, 1991; McClay, 1995; Mandal & Chattopadhyay, 1995; Bonni *et al.*, 2000) only when the ramp angle has a dip of between 45-60° (Figure 10.1). These model also predict that at these steep ramp angles, significant back-thrusts evolve resulting in the rear limb of the fold being steep. The implication of the analogue models is that faults coring the CFB are steep. These results support the modelling of Hålbich (1983) presented in Chapter 3. Although reverse faults are more commonly shallow structures (cf. Chapter 2), reverse slip on high angle faults (>40°) is possible, as the teleseismic data published by Jackson (1980) and Amato *et al.* (1992) reveals. The alternative explanation proposed in Chapter 3 (model 2) is that complex stacked duplexes, which are currently subsurface, result in a box-fold geometry in the overlying sequences (e.g. McDougall & Hussain, 1991). From the basement geometry alone it is impossible to differentiate between the models.

Mesozoic extension: In the onshore data, the extensional structures have the same trend as the basement fabric (Chapter 4) with an east-west orientation in the Central Cape (Figure 10.1a), and a north-west to south-east orientation in the Gamtoos Basin (Figure 10.1b). The offshore Plettenberg Fault (Chapter 7) has the same trend as the immediately adjacent onshore basement (Figure 10.2a), while the Gamtoos Fault offshore has a consistent trend to

that of the onshore fault, and the onshore basement (Figure 10.2b). Additionally, the regional transects (Chapter 3 & 4), have demonstrated that the normal faults consistently occur in the same structural setting within the foldbelt, that is, at the north end of the box-fold flat. Similarity in trend of the CFB folds and Mesozoic faults, and the consistent structural relationship between the two suggest that Mesozoic extensional architecture is inherited from the CFB, and that the CFB underwent negative inversion. As discussed in Chapter 3, assuming the reactivation of high angle faults, the location of the normal faults at the northern end of box fold flats tends to preclude the existence of a complex stacked duplex system underlying the CFB.

The observations from the offshore seismic data are high angle planar (42° , 65°), large (>12 km displacement) normal faults in the centre and south, with more listric (32°), shallower detachment depth ~ 5 km (32°) in the north (cf. Chapter 6,7, 8 & 9). Therefore, there is a difference in the style of faulting between north and south (although the data set is very limited). If it is inferred that the position and character of the normal faults are inherited from the CFB, then the observations of the offshore faults imply that the northern faults may be shallow structures while the central and southern faults are deep rooted (to at least 12 km). The CFB models can therefore be tentatively constrained at depth (Figure 10.2).

The consensus from the studies of negative inversion and theoretical considerations discussed in Chapter 2 is reactivation of a reverse fault into extension is more likely to occur if the pre-existing fault is steep ($>35^\circ$), while a shallower reverse fault will be cross-cut by crustal scale faults (Table 10.1). Therefore, reactivation of a high angle reverse fault during Mesozoic extension is plausible.

The role of structural inheritance in South Africa: The integration of observations from the basement and the Mesozoic, both onshore and offshore, strongly suggest that structural inheritance has played a significant role in establishing the architecture of the Mesozoic system. What remains less certain is the controlling geometry at depth. The consensus from previous work (Chapter 2) is that there is a regional décollement (Figure 10.3a). The integration of observations presented in this study with the current understanding of structural inheritance presented in Chapter 2, suggests that an alternative model may be one of a décollement in the north and high angle faults in the south that, during Permian-Triassic compression, form box folds. In the subsequent Mesozoic extension, the northern faults relax, forming shallow listric faults, while the southern faults are crustal scale and accommodate the majority of the extensional strain.

These shallow (i.e. not crustal scale) faults in the north are more likely to be cross-cut (Chapter 2), as is evident in the Late Syn-Rift phase (Chapters 8 & 9). Furthermore, such a model may explain why the CFB has an atypical architecture when compared with other fold and thrust systems (cf. Chapter 3 & 9). Theoretical considerations discussed in Chapter 2 suggest that high angle ($> 45^\circ$) reverse faults are more likely to have initiated through reactivation of extensional faults; a premise that is also proposed by Bonini *et al.* (2000), and Jackson (1980) (cf. Chapter 2). It is speculated that these high angle faults may have been normal faults on the Cape Supergroup (Ordovician to Devonian) passive margin (Figure 10.3). Only by conducting further studies e.g. analysis of sediment variation within the Cape Supergroup, crustal scale seismic sections, will it be possible to ascertain which model is more appropriate.

10.3 Implications for normal fault evolution

10.3.1 Comparison of South African faults with fault growth models

Normal faults have been demonstrated to grow by both radial tip propagation, and segment linkage (Morley *et al.*, 1990; Roberts & Jackson, 1991; Peacock & Sanderson, 1991, 1994; Trudgill & Cartwright, 1994; Dawers & Anders, 1995; Cartwright *et al.*, 1996; Morley, 1999; Contreras *et al.*, 2000; Young *et al.*, 2001; McLeod *et al.*, 2002). The evolution of fully grown normal fault systems can be reconstructed through the identification of segment boundaries determined by: 1. changes in strike; 2. along strike-displacement variations; 3. footwall lows and intra-basin highs; 4. the growth of depocentres; and 5. abandoned fault tips. By determining whether these characteristic features are evident in observations presented in Chapters 6, 7 & 8, it is possible to determine the evolution of the South Africa faults. It then possible to assess whether the presence of the pre-existing structural fabric (as described in the previous section influences) fault growth.

1. Changes in strike: the principal fault planes in this study are mappable as discrete, continuous surfaces for 158 km (Plettenberg), 96 km (Gamtoos, offshore only), 52 km (St Croix), and 38 km (Port Elizabeth). There is no evidence from the TWT of the fault planes (Figure 10.4) of along strike changes in trend.

2. Along strike displacement variations: Sediment accumulation is used a proxy for fault displacement (Chapter 9), and sediment accumulation / length plots for the Plettenberg, Gamtoos, Port Elizabeth and St Croix Faults are shown in Figure 10.5. Even with the

earliest sequences there are no points at which the accumulation approaches zero. Therefore, the fault is accumulating displacement along its length even during the early syn-rift stages.

3. Footwall lows, intra-basin highs: There is no evidence of intra-basement highs (e.g. onlap and thinning of sequences parallel to the fault) in the observations presented in any of the basins (Chapters 6, 7 & 8).

4. Isolated depocentres: There is no evidence of isolated depocentres, even in the earliest mappable syn-rift packages, in the sediment accumulation – Length plots of the four principal faults (Plettenberg, Gamtoos, Port Elizabeth and St Croix Faults; Figure 5, 6, 7 & 8). In all of the sequences, sedimentation occurs across all of the basin area. Even accounting for the lack of available data on sediment supply, the basins have been underfilled and redistribution of marine sediments would be expected to result in the preferential preservation of depocentres (McLeod *et al.*, 2002).

5. Abandoned fault tips: There is no evidence in the observations of abandoned fault tips (Chapters 6, 7 & 8).

The faults of South Africa therefore do not show evidence of segmentation; the following section will compare the observations from the studied faults with predictions from the fault growth model reviewed in Chapter 2.

10.3.2 Normal fault growth in heterogeneous crust

It is proposed that the growth of the South African faults, without evidence for segmentation, is a consequence of the significant pre-existing fabric (cf. Section 10.2). A model is presented for extensional system evolution in a region with a significant pre-existing structural fabric, and compared with that of the near-homogenous lattice of Gupta *et al.* (1998) in Figure 10.16.

The model of Gupta *et al.* (1998) is initiated with a lattice containing randomly distributed, minor, strength heterogeneities. As stress is applied, the lattice points with least strength are the loci of fault nucleation, resulting in isolated fault segments across the lattice. With continued extension, interaction of local stresses (Willemese *et al.*, 1996; Willemese, 1997) and stress feedback mechanisms (Cowie, 1998) results in the progressive coalescing of the isolated segments. In the model presented in Figure 10.9, the pre-existing plane of weakness is used as a “seed-point” for new faults which grow radially. These faults grow and interact, however because they are on the same plane, there is no evidence of either abandoned tips, or en-echelon segments in plan view. Furthermore, because of the pre-existing weakness

there are no effective rupture barriers to prevent radial fault tip propagation (Cowie & Scholz, 1992), and the faults can become very long, despite being significantly underdisplaced. A consequence of stress being localised onto a few structures is that strain is accumulated rapidly, therefore in the heterogenous model, the system evolves from isolated segments to a single fault significantly quicker than in the Gupta *et al.* model. This is supported by the absence of both isolated depocentres adjacent to the principal faults, and intra-basin faults even during the early syn-rift phase. During the middle and late rift stage, faults in the Gupta *et al.* model are increasingly dominated by a few major faults that are still increasing in length and displacement. At this stage in the heterogenous model, the fault length has already been achieved, and displacement is accrued to redress the deficit.

A further feature of the fault growth models is the progressive localisation of strain on a few principal structures during the evolution of fault system (e.g. Gupta *et al.*, 1998; Cowie *et al.*, 2000), which has been demonstrated in sub-surface studies (Chapter 2; McLeod *et al.*, 2000). In all three basins, from at least the earliest syn-rift sequences, there is no evidence of any intra-basin faults. Instead, strain appears to be localised from a very early stage on the principal faults.

An alternative way to view the growth history is through the maximum displacement/length ratio (D_{\max}/L). Cartwright *et al.* (1996) demonstrate a step-like cycle of growth through a combination of segment linkage and propagation. When a fault grows by segment linkage, length increases with little accumulation of displacement, however, when it grows by propagation, displacement can be accumulated with little increase in length, resulting in a step-like plot (Figure 10.10). In South Africa, there is probably an initial period of growth as isolated segments (during the poorly resolved earliest syn-rift phase) followed by a rapid period of linkage to produce a long, under-displaced fault. Subsequently, there is a prolonged period of growth through the accumulation of displacement. The absence of isolated depocentres in the early syn-rift implies that the transition from segment linkage to displacement accrual must have occurred early in the basin's evolution.

10.3.3 Scale of South African faulting

A final consideration for the South African faults is their size. The Plettenberg and Gamtoos Faults have minimum lengths of 150 km and 96 km (150 km including onshore) respectively, and maximum displacements of 13 km and 16.5 km (Chapter 9). The Port Elizabeth and St Croix Faults are smaller with minimum lengths of 38 km and 52 km, and maximum displacements of 8.6 km and 12.7 km, respectively. It has been suggested that

fault displacements scale with length according to the relationship of $D=cL^n$, where c is a constant associated with rock properties (Watterson, 1986; Walsh & Watterson, 1988; Gillespie *et al.*, 1992; Marrett & Allmendinger, 1991; Cowie & Scholz, 1992; Dawers *et al.*, 1993; Schlische *et al.* 1996). The ratio of D_{\max}/L for the South African faults (0.08 for the Plettenberg Fault; 0.17 for the Gamtoos (0.11 if onshore is accounted for); 0.22 for the Port Elizabeth Fault; and 0.24 for the St Croix Fault) are considerably higher than the value of 0.03, which is predicted from Schlische *et al.*'s best fit line, and has been supported by various recent studies (Contreras *et al.*, 2000; McLeod *et al.*, 2000). From the available data it is uncertain whether this correlation between D_{\max} and L is not valid for this region, or whether the faults are significantly longer than the seismic coverage (for a D/L value of 0.03, the length of the Plettenberg and Gamtoos Faults would have to be at 433 km and 550 km).

The observed lengths of the Plettenberg and Gamtoos Faults are at the upper limit of normal faults documented on continental crust (Figure 10.11 & 12), therefore, the estimated lengths of 433 km and 550 km from the global D/L are considered to be unrealistic, suggesting that the D/L ration of 0.03 may not be globally applicable.

When the South African fault values are plotted onto the global data set compiled by Schlische *et al.* (1996), they have significantly larger D and L values compared to other normal fault arrays (Figure 10.11).

The faults in this study also have displacements considerably larger than previously documented for an extensional continental setting (cf. Chapter 2; Figure 10.12). Other regions with large displacement and long faults (e.g. East African Rift with faults of 150 km length and 7 km displacement; Baikal Rift with 140 km long faults) have been explained by large elastic and seismogenic thicknesses, abnormally mafic and dry lower crust, and low geothermal gradients (Déverchère *et al.*, 1991; Jackson & Blenkinsop, 1993, 1997; Hayward & Ebinger, 1996; Foster & Nimmo, 1996; Jackson & Blenkinsop, 1997; van der Beek, 1997; Ebinger *et al.*, 1999; Contreras *et al.*, 2000). Although such explanations may be applicable to southern Africa, without a better understanding of regional crustal dynamics, and geophysical characteristics, it is impossible to ascertain the genesis of such large faults in southern South Africa.

In conclusion, the faults in South Africa have grown through strain localisation from an unprecedentedly early stage, most likely in response to structural inheritance, and have dimensions that are larger than previously documented for an extensional, continental setting.

References

- Adie, R.J. 1952. The position of the Falkland Islands in a reconstruction of Gondwana. *Geological Magazine*, **89**, 401-410.
- Amato, A., Chiarabba, C., Malagnini, L. & Selvaggi, G. 1992. Three-dimensional P-velocity structures in the region of the Ms = 6.9 Irpinia, Italy, normal faulting earthquake, *Physics of the Earth and Planetary Interiors*, **75**, 111-119.
- Anders, M.H. & Schlische, R.W. 1994. Overlapping Faults, Intrabasin highs, and the growth of normal faults. *Journal of Geology*, **102**, 165-180.
- Anders, M.H., Speigelman, M., Rodgers, D.W. & Hagstrum, J.T. 1993. The growth of fault-bounded tilt blocks. *Tectonics*, **12**(6), 1451-1459.
- Anderson, E.M. 1905. The dynamics of faulting. *Transacts of the Geological Society, Edinburgh*, **8**, 393-402.
- Austin, J.A. & Uchupp, E. 1982. Continental-oceanic crustal transition off southwest Africa. *AAPG Bulletin*, **66**(9), 1328-1347.
- Austin, J.A.Jr., and Uchupi, E. 1982. Continental-oceanic crustal transition off Southwest Africa. *AAPG Bulletin*, **66**(9), 1328-1347.
- Badley, M.E., Freeman, B., Roberts, A.M., Thatcher, J.S., Walsh, J., Watterson, J. & Yielding, G. 1990. Fault interpretation during seismic interpretation and reservoir evaluation. In The integration of geology, geophysics and petroleum engineering in reservoir delineation, description and management, *Proceedings of the 1st Archie Conference*, Houston, Texas, p. 224-241.
- Badley, M.E., Price, J.D. & Backshall, L.C. 1989. Inversion, reactivated faults and related structures: seismic examples from the southern North Sea. In: Buchanan, J.G. & Buchanan, P.G. (eds), *Basin Inversion*, Special publication of the Geological Society, London, **88**, 201-219.
- Bally, A.W., Gordy, P.L., & Stewart, G.A., 1966. Structure seismic data and orogenic evolution of Southern Canadian Rocky Mountains, *Bull. Canadian Petroleum Geologists*, **14**, 337-381.
- Barker, P.F. 1999. Falkland Plateau evolution and a mobile southernmost South America. In Cameron, N.R., Bate, R.H. & Clure, V.S. (eds) *The oil and gas habitats of the South Atlantic*. Special publication of the Geological Society, London, **153**, 403-408.
- Basile, C. & Brun, J.P., 1999, Transtensional faulting patterns ranging from pull-apart basins to transform continental margins: an experimental investigation, *Journal of Structural Geology*, **21**, 23-37.
- Basile, C., Mascle, J., Popoff, M., Bouillin, J.P. & Mascle, G., 1993, The Ivory Coast-Ghana transform margin: a marginal ridge structure deduced from seismic data, *Tectonophysics*, **222**, 1-19.
- Bate, K.J. & Malan, J.A. 1992. Tectonostratigraphic evolution of the Algoa, Gamtoos and Pletmos Basins, offshore South Africa. In de Wit, M.J & Ransome, I.G.D. (eds) *Inversion tectonics of the Cape Fold Belt, Karoo and Cretaceous Basins of Southern Africa*. Rotterdam, Balkema, 61-73.
- Bate, K.J. 1993. Reassessment of the petroleum geology of the Gamtoos Basin. Soekor internal report (unpublished), 43 pp.
- Bell, C.M. 1980. Deformation of the Table Mountain Group in the Cape Fold Belt South of Port Elizabeth. *Transacts of the Geological Society of South Africa*, **83**, 115-124.

- Ben-Avraham, Z., Hartnady, C.J.H. & Kitchin, K.A. 1997. Structure and tectonics of the Agulhas-Falkland fracture zone. *Tectonophysics*, **282**, 83-98.
- Ben-Avraham, Z., Hartnady, C.J.H. & Malan, J.A. 1993. Early tectonic extension between the Agulhas Bank and the Falkland Plateau due to the rotation of the Lafonia microplate. *Earth and Planetary Science Letters*, **117**, 43-58.
- Ben-Avraham, Z. & Zoback, M.D. 1992. Transform-normal extension and asymmetric basins: an alternative to pull-apart models. *Geology*, **20**, 423-426.
- Bonini, M., Sokoutis, D., Mulugeta, G. & Katrivanos, E. 2000. Modelling hangingwall accommodation above rigid thrust ramps. *Journal of Structural Geology*, **22**, 1165-1179.
- Booth, P.W.K. 1996. The relationship between folding and thrusting in the Floriskaal Formation (upper Witteberg Group), Steytlerville, Eastern Cape. *South African Journal of Geology*, **99(3)**, 235-243.
- Booth, P.W.K. and Shone, R.W. 1992a. The Laurie's Bay fault: A pre-Cape-Table Mountain Group contact west of Port Elizabeth. In de Wit, M.J & Ransome, I.G.D. (eds) *Inversion tectonics of the Cape Fold Belt, Karoo and Cretaceous Basins of Southern Africa*. Rotterdam, Balkema, 211-216.
- Booth, P.W.K. & Shone, R.W. 1992b. Folding and thrusting of the Table Mountain Group at Port Elizabeth, eastern Cape, Republic of South Africa. In de Wit, M.J & Ransome, I.G.D. (eds) *Inversion tectonics of the Cape Fold Belt, Karoo and Cretaceous Basins of Southern Africa*. Rotterdam, Balkema, 207-210.
- Booth, P.W.K. & Shone, R.W. 1992c. Structure of the Table Mountain Group in the Port Elizabeth area. *South African Journal of Geology*, **95**, 29-33.
- Bosworth, W. 1985. Geometry of propagating continental rifts. *Nature*, **316**, 625-627.
- Bott, M.H.P. & Kasznir, N.J. 1979. Stress distributions associated with compensated plateau uplift structures with application to the continental splitting mechanism. *Geophys.J.R.astr.Soc*, **56**, 451-459.
- Bott, M.H.P. & Kasznir, N.J. 1984. The origin of tectonic stress in the lithosphere. *Tectonophysics*, **105**, 1-13.
- Boyer, S.E. & Elliot, D. 1982. Thrust Systems. *AAPG Bulletin*, **66(9)**, 1196-1230.
- Brink, G.J., Keenan, J.H.G. & Brown Jr, L.F. 1994. Depositional of Fourth-Order, Post-Rift Sequences and Sequence Sets, Lower Cretaceous (Lower Valanginian to Lower Aptian), Pletmos Basin, Southern Offshore, South Africa. In Weimer, P. & Posamentier, H. (eds) *Siliciclastic Sequence Stratigraphy. Recent Advances and Applications*. AAPG Memoir, **58**, 43-69.
- Broad, D.S. 1989. Petroleum geology and hydrocarbon potential of the Gamtoos Basin. Soekor internal report (unpublished), 56 pp.
- Broquet, C.A.M. 1992. The sedimentary record of the Cape Supergroup: A review. In de Wit, M.J & Ransome, I.G.D. (eds) *Inversion tectonics of the Cape Fold Belt, Karoo and Cretaceous Basins of Southern Africa*. Rotterdam, Balkema, 159-183.
- Brown, L.F., Benson, J.M., Brink, G.J., Doherty, S., Jollands, A., Jungslager, E.H.A., Keenan, J.H.G., Muntingh, A. & van Wyk, N.J.S. 1995. Sequence stratigraphy in offshore South African divergent basins: an atlas on exploration for Cretaceous lowstand traps by Soekor (Pty) Ltd. *AAPG Studies in Geology*, **41**.

- Buchanan, J.G. & Buchanan, P.G. 1995. *Basin Inversion*, Special publication of the Geological Society, London, **88**, 596pp.
- Buchanan, P.G. & McClay, K.R. 1991. Sandbox experiments of inverted listric and planar fault systems, *Tectonophysics*, **188**, 97-115.
- Buck, W.R. 1988. Flexural rotation of normal faults. *Tectonics*, **7**, 959-973.
- Buck, W.R. 1993. Effect of lithospheric thickness on the formation of high- and low-angle normal faults. *Geology*, **21**, 933-936.
- Bullard, E.C., Everett, J.E. & Smith, A.G. 1965. Fit of the continents around the Atlantic. In Blackett, P.M.S., Bullard, E.C. & Runcorn, K.S. (eds) *A symposium on Continental Drift*. Philosophical transactions of the Royal Society of London, **A258**, 419-426.
- Butler, R.W.H, Matthews, S.J. & Parish, M., 1986. The NW external Alpine Thrust Belt and its implications for the geometry of the Western Alpine Orogen, in Coward, M.P. & Reis, A.C. (eds), *Collision Tectonics*, Geological Society Special Publication, **19**, 245-260.
- Butler, R.W.H. 1982a. The terminology of structures in thrust belts. *Journal of Structural Geology*, **4(3)**, 239-245.
- Butler, R.W.H. 1982b. Hangingwall strain: A function of duplex shape and footwall topography. *Tectonophysics*, **22**, 235-246.
- Cartwright, J.A., & Mansfield, C.S. 1998. Lateral displacement variation and lateral tip geometry of normal faults in the Canyonlands National Park, Utah. *Journal of Structural Geology*, **20(1)**, 3-19.
- Cartwright, J.A., Mansfield, C. & Trudgill, B. 1996. The growth of normal faults by segment linkage. In Buchanan, P.G. & Nieuwland, D.A. (eds), *Modern developments in structural interpretation, validation and modelling*. Special publication of the Geological Society, London, **99**, 163-177.
- Cartwright, J.A., Trudgill, B.D. & Mansfield, C.S. 1995. Fault growth by segment linkage: an explanation for scatter in maximum displacement and trace length data from the Canyonlands Grabens of SE Utah. *Journal of Structural Geology*, **17(9)**, 1319-1326.
- Cartwright, J.A. 1989. The structural and stratigraphic development of the Gamtoos and Algoa Basin. Soekor internal report (unpublished), 25 pp.
- Cartwright, J.A. 1989b. The kinematics of inversion in the Danish Central Graben. In: Cooper, M.A. & Williams, G.D., *Inversion Tectonics*, Special publication of the Geological Society, London, **44**, 153-175.
- Channel, J.E.T, Erbas, E., Nakanishi, M. & Tamaki, K. 1995. Late Jurassic-Early Cretaceous Time Scales and Oceanic Magnetic Anomaly Block Models. In Geochronology Time Scales and Global Stratigraphic Correlation, SEPM Special Publication No **54**.
- Chen, W.P. & Molnar, P. 1983. The depth distribution of intracontinental and intraplate earthquakes and its implications for the thermal and mechanical properties of the lithosphere. *Journal of Geophysical Research*, **88**, 4183-4214.
- Cloetingh, S., Lankreijer, A., de Wit, M.J., & Martinez, I. 1992. Subsidence history analysis modelling of the Cape and Karoo Supergroups. In de Wit, M.J & Ransome, I.G.D.

- (eds) *Inversion tectonics of the Cape Fold Belt, Karoo and Cretaceous Basins of Southern Africa*. Rotterdam, Balkema, 239-248.
- Coblentz, D.D, Sandiford, M, Richardson, R.M, Zhou, S. & Hillis, R. 1995. The origins of the intraplate stress field in continental Australia. *Earth and Planetary Science Letters*, **133**, 299-309.
- Coetzee, D.S. 1983. The deformation style between Meiringspoort and Beaufort West. In Söhne, A.P.G. & Hälbig, I.W. (eds.) *Geodynamics of the Cape Fold Belt*. Special publication of the Geological Society of South Africa, **12**, 101-113.
- Cole, D.I. 1998. Paleogeography and palaeocurrent distribution of the Beaufort Group in the Karoo, South Africa during the Late Permian. In Almond, J., Anderson, J., Booth, P., Chinsamy-turan, A., Cole, D., De Wit, M., Rubridge, B., Smith., Van Bever Donker, J., Storey, B.C. (eds). Special abstract issue- Gondwana 10: event stratigraphy of Gondwana. *Journal of African Earth Sciences*, **27**, 46.
- Cole, D.J. 1992. Evolution and development of the Karoo Basin. In de Wit, M.J & Ransome, I.G.D. (eds) *Inversion tectonics of the Cape Fold Belt, Karoo and Cretaceous Basins of Southern Africa*. Rotterdam, Balkema, 87-99.
- Constenius, K.N., 1982. Relationship between the Kishenehn Basin, and the Flathead listric normal fault system and Lewis Thrust salient. In, Powers, R.B. (ed), *Geological Studies of the Cordilleran Thrust Belt*, Rocky Mountain Association of Geologists, 817-830.
- Contreras, J., Anders, M.H. & Scholz, C.H. 2000. Growth of a normal fault system: observations from the Lake Malawi basin of the East African Rift. *Journal of Structural Geology*, **22**, 159-168.
- Cooper, M.A. & Williams, G.D., 1989. *Inversion tectonics*. Special publication of the Geological Society, London. **44**, 375pp.
- Cooper, M.A., Williams, G.D., De Graciansky, P.C., Murphy, R.W., Needham, T., De Paor, D., Stoneley, R., Todd, S.P., Turner, J.P. & Ziegler, P.A. 1989. Inversion tectonics – a discussion. In: Cooper, M.A. & Williams, G.D., *Inversion Tectonics*, Special publication of the Geological Society, London, **44**, 335-350.
- Cotter, E. 1998. Late Devonian Milankovitch-scale sea-level cycles of Gondwana confirm global eustasy. In Almond, J., Anderson, J., Booth, P., Chinsamy-turan, A., Cole, D., De Wit, M., Rubridge, B., Smith., Van Bever Donker, J., Storey, B.C. (eds). Special abstract issue- Gondwana 10: event stratigraphy of Gondwana. *Journal of African Earth Sciences*, **27**, 48.
- Coward, M.P. 1983. Thrust tectonics, thin skinned or thick skinned, and the continuation of thrusts to deep in the crust. *Journal of Structural Geology*, **5**, 113-123.
- Coward, M.P. 1984. The strain and textural history of thin-skinned tectonic zones; examples from the Assynt region of the Moine thrust zone, NW Scotland. *Journal of Structural Geology*, **6**(1/2), 89-99.
- Coward, M.P. 1996. Balancing sections through inverted basins. In Buchanan, P.G. & Nieuwland, D.A. (eds) *Modern developments in structural interpretation, validation and modelling*. Special publication of the Geological Society, London, **99**, 51-77.
- Cowie, P.A., Gupta, S. & Dawers, N.H. 2000. Implications of fault array evolution for syn-rift depocentre development: insights from a numerical fault growth model. *Basin Research*, **12**, 241-261.

- Cowie, P.A., 1998. A healing-reloading feedback control on the growth rate of seismogenic faults. *Journal of Structural Geology*, **20**(8), 1075-1087.
- Cowie, P.A. & Scholz, C.H. 1992a. Physical explanation for displacement-length relationship of faults using post-yield fracture mechanics model. *Journal of Structural Geology*, **14**, 1133-1148.
- Cowie, P.A. & Scholz, C.H. 1992b. Displacement-length scaling relationship for faults using a post-yield fracture mechanics model. *Journal of Structural Geology*, **14**, 1149-1156.
- Cox, K.G. 1992. Karoo igneous activity, and the early stages of break-up of Gondwanaland. In Storey, B.C., Alabaster, T. & Pankhurst, R.J. (eds.) *Magmatism and the causes of continental breakup*. Special publication of the Geological Society, London, **68**, 137-148.
- Cronin, B.T. & Kidd, R.B. 1998. Heterogeneity and lithotype distribution in ancient deep-sea canyons: Point Lobos deep-sea canyon as a reservoir analogue. *Sedimentary Geology*, **115**, 315-349.
- Curtis, M.L. & Hyam, D.M. 1998. Late Paleozoic to Mesozoic structural evolution of the Falkland Islands: a displaced segment of the Cape Fold Belt. *Journal of the Geological Society*, **155**, 115-129.
- Dahlstrom, C. D. 1969. Balanced cross sections, Canadian Journal of Earth Science, **6**, 743-757.
- Daly, M.C., 1989. The intracratonic Irumide Belt of Zambia and its bearing on collision orogeny during the Proterozoic of Africa, in Coward, M.P. & Reis, A.C. (eds), *Collision Tectonics*, Geological Society London, Special Publication, **19**, 321-328.
- Daly, R.A. 1936. Origin of submarine "canyons". *American Journal of Science*, **51-186**, 401-420.
- Dalziel, I.W.D., Lawver, L.A. & Murphy, J.B. 2000. Plumes, orogenesis, and supercontinental fragmentation. *Earth and Planetary Science Letters*, **178**, 1-11.
- Dawers, N. & Underhill, J.R. 2000. The role of fault interaction and linkage in controlling synrift stratigraphic sequences: Late Jurassic, Statfjord East Area, northern North Sea. *AAPG Bulletin*, **84**(1), 45-64.
- Dawers, N.H. and Anders, M.H. 1995. Displacement-length scaling and fault linkage. *Journal of Structural Geology*, **17**(5), 607-614.
- Dawers, N.H., Anders, M.H., Scholz, C.H. 1993. Growth of normal faults: Displacement-length scaling. *Geology*, **21**, 1107-1110.
- de Beer, C.H. 1995. Fold interference from simultaneous shortening in different directions: the Cape Fold Belt syntaxis. *Journal of African Earth Sciences*, **21**, 157-169.
- de Beer, C.H. 1992. Structural evolution of the Cape Fold Belt syntaxis and its influence on syntectonic sedimentation in the SW Karoo Basin. In de Wit, M.J & Ransome, I.G.D. (eds) *Inversion tectonics of the Cape Fold Belt, Karoo and Cretaceous Basins of Southern Africa*. Rotterdam, Balkema, 197-206.
- de Beer, C.H. 1990. Simultaneous folding in the western and southern branches of the Cape Fold Belt. *South African Journal of Geology*, **93**(4), 583-591.
- de Beer, J.H. 1983. Geophysical studies in the southern Cape Province and models of the lithosphere in the Cape Fold Belt. In Söhnge, A.P.G. & Hälbig, I.W. (eds.)

- Geodynamics of the Cape Fold Belt*. Special publication of the Geological Society of South Africa, **12**, 57-64.
- de Polo, C.M., Clark, D.G., Slemmons, D.B. & Ramelli, A.R. 1991. Historic surface faulting in the Basin and Range Province, western North America- implications for fault segmentation. *Journal of Structural Geology*, **13**, 123-136.
- de Wit, M.J. 1992. The Cape Fold Belt; A challenge for an integrated approach to inversion tectonics. In de Wit, M.J & Ransome, I.G.D. (eds) *Inversion tectonics of the Cape Fold Belt, Karoo and Cretaceous Basins of Southern Africa*. Rotterdam, Balkema, 3-14.
- de Wit, M.J. & Ransome, I.G.D. 1992. Regional Inversion tectonics along the Southern Margin of Gondwana. In de Wit, M.J & Ransome, I.G.D. (eds) *Inversion tectonics of the Cape Fold Belt, Karoo and Cretaceous Basins of Southern Africa*. Rotterdam, Balkema, 15-22.
- Déverchère, J., Houdry, F., Diament, M., Solonenko, N.V. & Solonenko, A.V. 1991. Evidence for a seismogenic upper mantle and lower crust in the Baikal rift. *Geophysical Research Letters*, **18**, 1099-1102.
- Dewey, J.F., Hempton, M.R., Kidd, W.S.F., Saroglu, F. & Şengör, A.M.C. 1986. Shortening of continental lithosphere: the neotectonics of Eastern Anatolia – a young collision zone. In Coward, M.P. & Reis, A.C. (eds), *Collision tectonics*. Special publication of the Geological Society, London, **19**, 3-36.
- Dewey, J.F. 1982. Kinematics and dynamics of basin inversion. In Cooper, M.A. & Williams, G.D. (eds), *Inversion tectonics*. Special publication of the Geological Society, London, **44**, 352.
- Dingle, R. V., Siesser, W.G. & Newton A.R. 1983. Mesozoic and Tertiary Geology of Southern Africa. Rotterdam, A.A.Balkema. 375 pp.
- Doré, A.G, Lundin, E.R, Fichler, C. & Olesen, O. 1997. Patterns of basement structure and reactivation along the NE Atlantic margin. *J.Geophysical Soc.*, **154**, 85-92.
- Du Toit, A.L. 1937. Our wandering continents: an hypothesis of continental drifting. Oliver and Boyd, London. 366 pp.
- Duane, M.J., & Brown, R. 1992. Geochemical open-system behaviour related to fluid-flow and metamorphism in the Karoo Basin. In de Wit, M.J & Ransome, I.G.D. (eds) *Inversion tectonics of the Cape Fold Belt, Karoo and Cretaceous Basins of Southern Africa*. Rotterdam, Balkema, 127-137.
- Dunbar, J.A. & Sawyer, D.S. 1989a. How preexisting weaknesses control the style of continental breakup. *Journal of Geophysical Research*, **94 B6**, 7278-7292.
- Dunbar, J.A. & Sawyer, D.S. 1989b. Patterns of continental extension along conjugate margins of the Central and North Atlantic Oceans and Labrador Sea. *Tectonics*, **8**, 1059-1077.
- Ebinger, C.J., Jackson, J.A., Foster, A.N., & Hayward, N.J. 1999. Extensional basin geometry and elastic lithosphere. *Philosophical Transacts of the Royal Society, London*, **A 357**, 741-765.
- Elliot, D. 1983. The construction of balanced cross-sections. *Journal of Structural Geology*, **5**, 101.

- Elliot, D. & Johnson, M.R.W. 1980. Structural evolution in the northern part of the Moine Thrust Belt, NW Scotland. *Transact of the Royal Society Edinburgh, Earth Sciences*, **71**, 69-96.
- England, P.C. & Jackson, J. 1989. Active deformation of the continents. *Annual review of Earth and Planetary Sciences*, **17**, 197-226.
- Faccenna, C., Nalpas, T., B., J.-P. & Davy, P. 1995. The influence of pre-existing thrust faults on normal fault geometry in nature and experiments *Journal of Structural Geology*, **17**(8), 1139-1149.
- Ferreira, J.M, Oliveira, R.T, Takeya, M.K & Assumpção. 1998. Superposition of local and regional stresses in northeast Brazil: evidence from focal mechanisms around the Potiguar marginal basin. *Geophys.J.Int.*, **134**, 341-355.
- Forsyth, D.W. 1992. Finite extension and low-angle normal faulting. *Geology*, **20**, 27-30.
- Foster, A. & Nimmo, F. 1996. Comparison between the rift systems of East Africa, Earth and Beta Regio, Venus. *Earth and Planetary Science Letters*, **143**, 183-195.
- Fouché, J., Bate, K.J. & Van der Merwe, R. 1992. Plate tectonic setting of Mesozoic Basins, southern offshore, South Africa: A review. In de Wit, M.J & Ransome, I.G.D. (eds) *Inversion tectonics of the Cape Fold Belt, Karoo and Cretaceous Basins of Southern Africa*. Rotterdam, Balkema, 33-48.
- Gadd, S.A. & Scrutton, R.A., 1997. An integrated thermomechanical model for transform continental margin evolution, *Geo-Marine Letters*, **17**, 21-30.
- Gawthorpe, R.L. & Leeder, R.L. 2000. Tectono-sedimentary evolution of active extensional basins. *Basin Research*, **12**, 195-218.
- Gawthorpe, R.L., Sharp, I., Underhill, J.R. & Gupta, S. 1997. Linked sequence stratigraphic and structural evolution of propagating normal faults. *Geology*, **25**(9), 795-798.
- Gawthorpe, R.L., Fraser, A.J. & Collier, R.E.L. 1994. Sequence stratigraphy in active extensional basins: implications for the interpretation of ancient basin-fills. *Marine and Petroleum Geology*, **11**, 6.
- Gawthorpe, R.L. & Hurst, J.M. 1993. Transfer zones in extensional basins: their structural style and influence on drainage development and stratigraphy. *Journal of the Geological Society, London*, **150**, 1137-1152.
- Gillespie, P.A., Walsh, J.J., & Watterson, J. 1992. Limitations of dimension and displacement data from single faults and the consequences for data analysis and interpretation. *Journal of Structural Geology*, **14**, 1157-1172.
- Gradstein, F.M., Agterberg, F.P., Ogg, J.G., Hardenbol, J., Van Veen, P., Thierry, J. & Huang, Z., 1995, A Triassic, Jurassic and Cretaceous time scale, *Geochronology Time Scales and Global Stratigraphic Correlation*, SPEM Special Publication, **54**.
- Gresse, P. 1983. Lithostratigraphy and structure of the Kaaimans Group. In Söhnge, A.P.G. & Hälbich, I.W. (eds.) *Geodynamics of the Cape Fold Belt*. Special publication of the Geological Society of South Africa, **12**, 7-19.
- Gresse, P.G., Theron, J.N., Fitch, F.J., & Miller, J.A. 1992. Tectonic inversion and radiometric resetting of the basement in the Cape Fold Belt. In de Wit, M.J & Ransome, I.G.D. (eds) *Inversion tectonics of the Cape Fold Belt, Karoo and Cretaceous Basins of Southern Africa*. Rotterdam, Balkema, 217-228.

- Gupta, S., Underhill, J.R., Sharp, I.R. & Gawthorpe, R.L. 1999. Role of fault interactions in controlling syn-rift sediment dispersal patterns: Miocene, Abu Alaqa Group, Suez Rift, Sinai, Egypt. *Basin Research*, **11**, 167-189.
- Gupta, S., Cowie, P.A., Dawers, N.H. & Underhill, J.R. 1998. A mechanism to explain rift-basin subsidence and stratigraphic patterns through fault array-evolution. *Geology*, **26**(7), 595-598.
- Hälbich, I.W. 1993. The Cape Fold Belt-Agulhas Bank transect across Gondwana Suture, Southern Africa. *Global Geoscience Transect 9*, American Geophysical Union; Publication No 202 of International Lithosphere Program. Washington. 18 pp.
- Hälbich, I.W. 1992. The Cape Fold Belt Orogeny; state of the art 1970's-1980's. In de Wit, M.J & Ransome, I.G.D. (eds) *Inversion tectonics of the Cape Fold Belt, Karoo and Cretaceous Basins of Southern Africa*. Rotterdam, Balkema, 141-158.
- Hälbich, I.W. 1983a. Disharmonic folding, detachment and thrusting in the Cape Fold Belt. In Söhnge, A.P.G. & Hälbich, I.W. (eds.) *Geodynamics of the Cape Fold Belt*. Special publication of the Geological Society of South Africa, **12**, 115-123.
- Hälbich, I.W. 1983b. A tectonogenesis of the Cape Fold Belt (CFB). In Söhnge, A.P.G. & Hälbich, I.W. (eds.) *Geodynamics of the Cape Fold Belt*. Special publication of the Geological Society of South Africa, **12**, 165-175.
- Hälbich, I.W. and Cornell, D.H. 1983. Metamorphic History of the Cape Fold Belt. In Söhnge, A.P.G. & Hälbich, I.W. (eds.) *Geodynamics of the Cape Fold Belt*. Special publication of the Geological Society of South Africa, **12**, 131-148.
- Hälbich, I.W., Fitch, F.J. and Miller, J.A. 1983. Dating the Cape orogeny. In Söhnge, A.P.G. & Hälbich, I.W. (eds.) *Geodynamics of the Cape Fold Belt*. Special publication of the Geological Society of South Africa, **12**, 149-164.
- Hälbich, I.W. & Swart, J. 1983. Structural zoning and dynamic history of the cover rocks of the Cape Fold Belt. In Söhnge, A.P.G. & Hälbich, I.W. (eds.) *Geodynamics of the Cape Fold Belt*. Special publication of the Geological Society of South Africa, **12**, 75-100.
- Hand, M. & Sandiford, M. 1999. Intraplate deformation in central Australia, the link between subsidence and fault reactivation, *Tectonophysics*, **305**, 121-140.
- Haq, B., Hardenbol, J. & Vail, P.R. 1988. Mesozoic and Cenozoic chronostratigraphy and eustatic cycles of sea-level change. In: Wilgus, C.K. (ed), *Sea-level change: an integrated approach*, SEPM Special Publication, **42**, 71-108.
- Harland, W.B., Armstrong, R.L., Cox, A.V., Craig, L.E., Smith, A.G. & Smith, D.G. 1990. *A Geological Time Scale 1989*, Cambridge, Cambridge University Press, 263 pp.
- Haughton, S.H. 1963. The Stratigraphic history of Africa south of the Sahara. Oliver and Boyd, Edinburgh. 365 pp.
- Hayward, N.J. & Ebinger, C.J. 1996. Variations in the along-axis segmentation of the Afar Rift System. *Tectonics*, **15**, 244-257.
- Hessami, K., Koyi, H.A., Talbot, C.J., Tabasi, H. & Shabaniyan, E. 2001. Progressive unconformities within an evolving foreland fold-thrust belt, Zagros Mountains. *Journal of the Geological Society, London*. **154**, 73-78.

- Holdsworth, R.E., Butler, C.A. & Roberts, A.M. 1997. The recognition of reactivation during continental deformation. *Journal of the Geological Society, London*, **154**, 73-78.
- Holdsworth, R.E., Hand, M., Miller, J.A. & Buick, I.S. 2001. Continental reactivation and reworking: an introduction. In Miller, J.A., Holdsworth, R.E., Buick, I.S. & Hand, M. (eds) *Continental reactivation and reworking*. Special publication of the Geological Society, London, **184**, 1-12.
- Hossack, J.R. 1983. A cross-section through the Scandinavian Caledonides constructed with the aid of branch-line maps. *Journal of Structural Geology*, **5**, 103-111.
- Hubbard, R.J., Pape, J. & Roberts, D.G. 1985a. Depositional sequence mapping as a technique to establish tectonic and stratigraphic framework and evaluate hydrocarbon potential on a passive continental margin. In (Beerg, O.R. & Wooverton, D.G.) *Seismic stratigraphy II*. AAPG Memoir, **29**, 79-92.
- Hubbard, R.J., Pape, J. & Roberts, D.G. 1985b. Depositional sequence mapping to illustrate the evolution of a passive continental margin. Depositional sequence mapping as a technique to establish tectonic and stratigraphic framework and evaluate hydrocarbon potential on a passive continental margin. In (Beerg, O.R. & Wooverton, D.G.) *Seismic stratigraphy II*. AAPG Memoir, **29**, 93-116.
- Hunter, M. 1989. Devonian sedimentary rocks on the Falkland Islands: part of the Cape Supergroup, South Africa?. In Almond, J., Anderson, J., Booth, P., Chinsamy-turan, A., Cole, D., De Wit, M., Rubridge, B., Smith, Van Bever Donker, J., Storey, B.C. (eds). Special abstract issue- Gondwana 10: event stratigraphy of Gondwana. *Journal of African Earth Sciences*, **27**, 117.
- Huyghe, P. & Mugnier, J.-L. 1992. The influence of depth on reactivation in normal faulting. *Journal of Structural Geology*, **14**, 991-998.
- Ivins, E.R., Dixon, T.H. & Golombek, M.P. 1990. Extensional reactivation of an abandoned thrust: a bound on shallowing in the brittle regime. *Journal of Structural Geology*, **12**(3), 303-314.
- Jackson, J.A. 1987. Active normal faulting and crustal extension. In Coward, M.P., Dewey, J.F. & Hancock, P.L. (eds), *Continental extensional tectonics*. Special publication of the Geological Society, London, **28**, 3-17.
- Jackson, J.A. 1980. Reactivation of basement faults and crustal shortening in orogenic belts, *Nature*, **283**, 343-346.
- Jackson, J. & Blenkinsop, T. 1997. The Bilila-Mtakataka fault in Malawi: an active, 100 km long, normal fault segment in thick seismogenic crust. *Tectonics*, **16**(1), 137-150.
- Jackson, J.A. & Leeder, M. 1994. Drainage systems and the development of normal faults: an example from the Pleasant Valley, Nevada. *Journal of Structural Geology*, **16**, 1041-1059.
- Jackson, J. & Blenkinsop, T. 1993. The Malawi earthquake of March 10, 1989: deep faulting within the East African Rift System. *Tectonics*, **12**(5), 1131-1139.
- Jackson, J. & McKenzie, D. 1983. The geometrical evolution of normal fault systems. *Journal of Structural Geology*, **5**(5), 471-482.
- Jackson, J.A. & White, N.J. 1989. Normal faulting in the upper continental crust: observations from regions of active extension. *Journal of Structural Geology*, **11**(1/2), 15-36.

- Jacobs, J., Thomas, R.J., Armstrong R.A. & Henjes-Kunst, F. 1998. Structure, geochronology and Rodinia-Gondwana correlations of the Mesoproterozoic Cape Meredith Complex, West Falklands. *The Geology of the Falkland Islands, abstract volume*. Geological Society, London, 7.
- Johnson, M.R. 1991. Sandstone petrography, provenance and plate tectonic setting in Gondwana context of the southeastern Cape-Karoo Basin. *South African Journal of Geology*, **94**, 137-154.
- Johnstone, S.T. 2000. The Cape Fold Belt and Syntaxis and the rotated Falkland Islands: dextral transpression tectonics along the southwest margin of Gondwana. *Journal of African Earth Sciences*, **31**, 51-63.
- Johnson, S.T. 1998. The Karoo Basin, the Cape Fold Belt and syntaxis, and the rotated Falkland Islands: a comprehensive tectonic model. In Almond, J., Anderson, J., Booth, P., Chinsamy-turan, A., Cole, D., De Wit, M., Rubridge, B., Smith, Van Bever Donker, J., Storey, B.C. (eds). Special abstract issue- Gondwana 10: event stratigraphy of Gondwana. *Journal of African Earth Sciences*, **27**, 120.
- Keenan, J.H.G. 1990. Application of seismic sequence concepts to basin evolution and petroleum exploration, Pletmos Basin, offshore South Africa. Geocongress 90, *Geological Society of South Africa*, abstract volume, 285-288.
- Keller, J.V.A. & McClay, K.R. 1995. 3D sandbox models of positive inversion. In: Buchanan, J.G. & Buchanan, P.G. (eds), *Basin Inversion*, Geological Society London, Special Publication, **88**, 137-146.
- Kelly, P.G., Peacock, D.C.P., Sanderson, D.J. & McGurk, A.C. 1999. Selective reverse-reactivation of normal faults, and deformation around reverse-reactivated faults in the Mesozoic of the Somerset coast. *Journal of Structural Geology*, **21**, 493-509.
- Kleywegt, R.J. 1971. Interpretation of a Gravity Profile across the Oudtshoorn Cretaceous Basin. *Annual Review of the Geological Society, South Africa*, **9**, 125-128.
- Koyi, H.A. & Skelton, A. 2001. Centrifuge modelling of the evolution of low-angle detachment faults from high-angle normal faults. *Journal of Structural Geology*, **23**, 1179-1185.
- Krynauw, J.R. 1983. Granite intrusion and metamorphism in the Kaaimans Group. In Söhne, A.P.G. & Hällich, I.W. (eds.) *Geodynamics of the Cape Fold Belt*. Special publication of the Geological Society of South Africa, **12**, 21-32.
- Kuzsnir, N.J. & Park, R.G. 1987. The extensional strength of the continental lithosphere: its dependence on geothermal gradient, and crustal composition and thickness. In Coward, M.P., Dewey, J.F. & Hancock, P.L. (eds), *Continental extensional tectonics*, Special publication of the Geological Society, London, **28**, 35-52.
- Lawrence, S.R.; Johnson, M., Tubb, S.R. & Marshallsea, S.J. 1999. Tectono-stratigraphic evolution of the North Falkland region. In Cameron, N.R., Bate, R.H. & Clure, V.S (eds) *The oil habitats of the South Atlantic*. Special publication of the Geological Society, London, **153**, 409-424.
- Lawver, L.A., Gahagan, L.M., Dalziel, I.W.D. & Macdonald, D.I.M. 1998. Breakup of a tight fit, early Mesozoic Gondwana: a plate reconstruction perspective. *CASP South Atlantic Project Report*, **7**, 56pp. (unpublished).

- Le Fort, P. 1986. Metamorphism and magmatism during the Himalayan collision. In Coward, M.P. & Reis, A.C. (eds), *Collision tectonics*. Special publication of the Geological Society, London, **19**, 159-172.
- Le Roux, D.M. 1983a. Geological Structure in the Little Karoo about 21°E Longitude. In Söhnge, A.P.G. & Hälbich, I.W. (eds.) *Geodynamics of the Cape Fold Belt*. Special publication of the Geological Society of South Africa, **12**, 65-74.
- Le Roux, J.P. & Gresse, P.G. 1983. The sedimentary-tectonic realm of the Kango Group. In Söhnge, A.P.G. & Hälbich, I.W. (eds.) *Geodynamics of the Cape Fold Belt*. Special publication of the Geological Society of South Africa, **12**, 33-45.
- Le Roux, J.P. 1983a. Structural evolution of the Kango Group. In Söhnge, A.P.G. & Hälbich, I.W. (eds.) *Geodynamics of the Cape Fold Belt*. Special publication of the Geological Society of South Africa, **12**, 47-56.
- Le Roux, J.P., Grobler, L.E. & Smit, P.H. 1994. Monoclines and paleochannels; evidence for syntectonic sedimentation in the Beaufort Group of the Karoo Basin, South Africa. *Journal of African Earth Sciences*, **18**(3), 219-226.
- Le Turdu, C., Tiercelin, J.J., Richert, J.P., Rolet, J., Xavier, J.P., Renaut, R.W., Lezzar, K.E. & Coussement, C. 1999. Influence of preexisting oblique discontinuities on the geometry and evolution of extensional fault patterns: evidence from the Kenya Rift using SPOT imagery, in Morley, C.K. (ed) *Geosceince of rift systems – evolution of East Africa*, AAPG Studies in Geology, **44**, 173-191.
- Leeder, M.R. & Gawthorpe, R.L. 1987. Sedimentary models for extensional tilt-block / half-graben basins. In Coward, M.P., Dewey, J.F. & Hancock, P.L. (eds), *Continental extensional tectonics*, Special publication of the Geological Society, London, **28**, 139-152.
- Lithgow-Bertelloni, C. & Richards, M.A. 1998. The dynamics of Cenozoic and Mesozoic plate motions. *Reviews of Geophysics*, **36**, 27-78.
- Lock, B.E. 1978. The Cape Fold Belt of South Africa; tectonic control of sedimentation. *Proceedings of the Geologists Association*, **89**, 263-281.
- Macdonald, D., Gómez-Pérez, Franzese, J., Spalletti, L., Paton, D., Gilpin, R., Lawver, L., Dalziel, I., Gahagan, L. & Anderson, L. 1998. Mesozoic evolution of the South Atlantic and its influence on the Tertiary development of the region, *CASP South Atlantic Report*, **10**, 18 pp (unpublished).
- Malan, J.A., Martin, A.K. & Cartwright, J.A. 1990. The structural and stratigraphic development of the Gamtoos and Algoa Basins, offshore South Africa. Geocongress 90, *Geological Society of South Africa*, abstract volume, 328-331.
- Malan, J.A. & Theron, J.N. 1987. Notes on an Enon Basin Northeast of Bredasdorp, Southern Cape Province. *Annals of the Geological Survey of South Africa*, 83-87.
- Mandal, N. & Chattopadhyay, A. 1995. Modes of reactivation of domino-type normal faults: experimental and theoretical approach. *Journal of Structural Geology*, **17**(8), 1151-1163.
- Marrett, R. & Allmendinger, R.W. 1991. Estimates of strain due to brittle faulting: sampling of fault populations. *Journal of Structural Geology*, **13**, 735-738.

- Marshall, J.E.A. 1994a. The Falkland Islands and the early fragmentation of Gondwana: implications for the hydrocarbon exploration in the Falkland Plateau. *Marine and Petroleum Geology*, **11**(5), 631-636.
- Marshall, J.E.A. 1994b. The Falkland Islands: A key element in Gondwana paleogeography. *Tectonics*, **13** (2), 499-514.
- Martin, A.K. 1987. Plate reorganisation around Southern Africa, hot-spots and extinctions. *Tectonophysics*, **142**, 309-316.
- Martin, A.K., Hartnady, C.J.H. & Goodlad, S.W. 1981. The revised fit of South America and South Central Africa. *Earth and Planetary Science Letters*, **54**(2), 293-305.
- Masclé, J., Mougénot, D., Blarez, E., Marinho, M., & Virlogeux, P. 1987. African transform continental margins: examples from Guinea, the Ivory Coast and Mozambique, *Geological Journal*, **22**, 537-561.
- Mattauer, M. 1986. Intracontinental subduction, crust-mantle décollement and crustal stacking wedge in the Himalayas and other collision belts. In Coward, M.P. & Reis, A.C. (eds), *Collision Tectonics*, Special publication of the Geological Society, London, **19**, 337-50.
- McClay, K.R. 1995. The geometries and kinematics of inverted fault systems: a review of analogue model studies. In Buchanan, J.G. & Buchanan, P.G. (eds), *Basin Inversion*, Special Publication of the Geological Society, London, **88**, 97-118.
- McClay, K.R. (ed.) 1992 Thrust tectonics. Chapman & Hall, London. 446pp
- McClay, K.R. 1989. Analogue models of inversion tectonics. In Cooper, M.A. & Williams, G.D. (eds) *Inversion Tectonics*. Special publication of the Geological Society, London, **44**, 41-59
- McClay, K.R. & White, M.J. 1995. Analogue modelling of orthogonal and oblique rifting. *Marine and Petroleum Geology*, **12**, 137-151.
- McClay, K.R., Waltham, D.A., Scott, A.D. & Abousetta, A. 1991. Physical and seismic modelling of listric normal fault geometries. In Knipe, R.J. & Rutter, E.H. (eds) *Geometry of normal faults*. Special publication of the Geological Society, London, **56**, 231-239.
- McDougall, J.W. & Hussain, A. 1991. Fold and thrust propagation in the Western Himalaya based on a balanced cross section of the Surghar Ranger and Kohat Plateau, Pakistan. *AAPG Bulletin*, **75**, 463-478.
- McKenzie, D. & Jackson, J. 1986. A block model of distributed deformation by faulting. *Journal of the Geological Society, London*, **143**, 349-353.
- McKenzie, D.P. 1978. Some remarks on the development of sedimentary basins, *Earth and Planetary Science Letters*, **40**, 25-32.
- McLachlan, I.R. & McMillan, I.K. 1976. Review and Stratigraphic Significance of Southern Cape Mesozoic Paleontology. *Transactions of the Geological Society of South Africa*, **79**, 197-212.
- McLeod, A.E., Dawers, N.H., & Underhill, J.R. 2000. The propagation and linkage of normal faults: insights from the Strathspey-Brent-Statfjord fault array, northern North Sea. *Basin Research*, **12**, 263-284.

- McLeod, A.E., Underhill, J.R., Davies, S.J. & Dawers, N.H. 2002 (*in press*). The influence of fault array evolution on syn-rift sedimentation patterns: controls on deposition in the Strathspey-Brent-Statfjord half-graben, Northern North Sea. *APPG Bulletin*.
- McMillan, I.K. 1999. Time tops database. Soekor internal report (unpublished).
- McMillan, I.K. 1998. The foraminifera of the Late Valanginian to Hauterivian (Early Cretaceous) Sundays River Formation of the Algoa Basin, Eastern Cape Province, South Africa. *Annals of South African Museum*, **106(1)**, 1-38.
- McMillan, I.K., Brink, G.J., Broad, D.S., and Maier, J.J. 1997. Late Mesozoic Sedimentary Basins off the South Coast of South Africa. In Selly, R.C. (ed.) *African Basin. Sedimentary Basins of the World*, 3. Elsevier, Amsterdam. 319-376.
- Meijer, P.Th. & Wortel, M.J.R. 1999. Cenozoic dynamics of the African plate with emphasis on the African-Eurasia collision. *J. Geophysical Res.* **104(B4)**, 7405-7418.
- Mercier, E., Outtani, F., Frizon de Lamotte, D. 1997. Late-stage evolution of fault propagation folds: principles and example. *Journal of Structural Geology*, **19**, 185-193.
- Miller, J.A., Holdsworth, R.E., Buick, I.S. & Hand, M. (eds) 2001. *Continental reactivation and reworking*. Special publication of the Geological Society, London, **184**, 408.
- Mitchell, C., Taylor, G.K., Cox, K.G. & Shaw, J. 1986. Are the Falklands a rotated microplate? *Nature*, **319**, 131-134.
- Mitchum, R.M. Jr, Vail, P.R. & Sangree, J.B. 1977. Seismic stratigraphy and global changes of sea-level part 6: seismic stratigraphic interpretation procedure. In Payton, C.E. (ed.) *Seismic stratigraphy- applications to hydrocarbon exploration*. AAPG Memoir, **26**, 117-134.
- Mitra, S. 1990. Fault propagation folds: geometry, kinematic evolution and hydrocarbon traps. *AAPG Bulletin*, **74**, 921-945.
- Morgan, W.J. 1983. Hotspot tracks and the early rifting of the Atlantic. *Tectonophysics*, **94**, 123-139.
- Morley, C.K. 1999. Patterns of displacement along large normal faults: implications for basin evolution and fault propagation, based on examples from East Africa. *AAPG Bulletin*, **83(4)**, 613-634.
- Morley, C.K. 1994. Fold-generated imbricates: examples from the Caledonides of Southern Norway. *Journal of Structural Geology*, **16**, 619-631.
- Morley, C.K. & Wonganan, N. 2000. Normal fault displacement characteristics, with particular reference to synthetic transfer zones, Mae Moh mine, northern Thailand. *Basin Research*, **12**, 307-327.
- Morley, C.K., Nelson, R.A., Patton, T.L. & Munn, S.G. 1990. Transfer zones in the East African Rift system and their relevance to hydrocarbon exploration in rifts, *AAPG Bulletin*, **74**, 1234-1253.
- Mussett, A.E. & Talyor, G.K. 1994. Ar-39Ar ages for dykes from the Falkland Islands with implications for the break-up of southern Gondwana. *Journal of the Geological Society*, **151**, 79-81.
- Newton, A.R. 1993. The Cape folding- a syntaxis or not? *South African Journal of Geology*, **96(4)**, 213-216.

- Newton, A.R. 1992. Thrusting on the northern margin of the Cape Fold Belt, near Laingsburg. In de Wit, M.J & Ransome, I.G.D. (eds) *Inversion tectonics of the Cape Fold Belt, Karoo and Cretaceous Basins of Southern Africa*. Rotterdam, Balkema, 193-197.
- Nürnberg, D. & Müller, D.R. 1991. The tectonic evolution of the South Atlantic from Late Jurassic to present. *Tectonophysics*, **191**, 27-53.
- Peacock, D.C.P. & Sanderson, D.J. 1994. Geometry and development of relay ramps in normal fault systems. *AAPG Bulletin*, **78**(2), 147-165.
- Peacock, D.C.P. & Sanderson, D.J. 1991. Displacements, segment linkage and relay ramps in normal fault zones. *Journal of Structural Geology*, **13**(6), 721-733.
- Philippe, Y., Deville, E. & Mascle, A. 1998. Thin-skinned inversion at oblique basin margins: example of the western Vercors and Chartreuse Subalpine massifs (SE France). In Mascle, A., Puigdefàbregas, C., Luterbacher, H.P. & Fernández, M. (eds) *Cenozoic foreland basins of Western Europe*. Special publication of the Geological Society, London, **134**, 239-262.
- Pickering, G., Peacock, D.C.P., Sanderson, D.J. & Bull, J.M. 1997. Modeling tip zones to predict the throw and length characteristics of faults. *AAPG Bulletin*, **81**, 82-99.
- Pitts, B.E., Maher, M.J., de Beer, J.H. & Gough, D.I. 1992. Interpretation of magnetic, gravity and magnetotelluric data across the Cape Fold Belt and Karoo Basin. In de Wit, M.J & Ransome, I.G.D. (eds) *Inversion tectonics of the Cape Fold Belt, Karoo and Cretaceous Basins of Southern Africa*. Rotterdam, Balkema, 27-32.
- Powell, C.M. & Williams, G.D., 1989, The Lewis Thrust/Rocky Mountain trench fault system in Northwest Montana, USA: an example of negative inversion tectonics? In Cooper, M.A. & Williams, G.D. (eds), *Inversion Tectonics*, Special publication of the Geological Society, London, **44**, 223-234.
- Proffett, J.M. 1977. Cenozoic geology of the Yerington district, Nevada, and implications for the nature of Basin and Range faulting. *Bulletin of the Geological Society of America*, **88**, 247-266.
- Prosser, S. 1993. Rift-related linked depositional systems and their seismic expression. In Williams, G.D. & Dobb, A. (eds.), *Tectonics and seismic sequence stratigraphy*. Special publication of the Geological Society, London, **71**, 35-66.
- Ranalli, G. 2000. Rheology of the crust and its role in tectonic reactivation. *Journal of Geodynamics*, **30**, 3-15.
- Ransome, I.G.D. & de Wit, M.J. 1992. Preliminary investigations into a microplate model for the South Western Cape. In de Wit, M.J & Ransome, I.G.D. (eds) *Inversion tectonics of the Cape Fold Belt, Karoo and Cretaceous Basins of Southern Africa*. Rotterdam, Balkema, 257-265.
- Rapela, C.W. & Pankhurst, R.J. 1992. The granites of northern Patagonia and the Gastre Fault system in relation to the break-up of Gondwana. In Storey, B.C., Alabaster, T. & Pankhurst, R.J. (eds) *Magmatism and the Causes of Continental Break-up*. Special publication of the Geological Society, London, **68**, 209-220.
- Ratcliffe, N.M., Burton, W.C., D'Angelo, R.M. & Costain, J.K. 1986, Low-angle extensional faulting, reactivated mylonites, and seismic reflection geometries of the Newark basin margin in eastern Pennsylvania, *Geology*, **14**, 766-770.

- Richards, P.C., Gatliff, R.W., Quinn, M.F., Williamson, J.P., & Fannin, N.G.T. 1996. The geological evolution of the Falkland Islands continental shelf. In Storey, B.C., King, E.C. & Livermore, R.A. (eds) *Weddel sea tectonics and Gondwana break-up*. Special publication of the Geological Society. London, **108**, 105-128.
- Richardson, R.M. 1992. Ridge forces, absolute plate motions, and intraplate stress field. *Journal of Geophysical Research*, **97**, 11739-11748. Journal
- Ricou, L.E. & Siddans, A.W.B. 1986. Collision tectonics in the Western Alps, in Coward, M.P. & Reis, A.C. (eds), *Collision Tectonics*, Special publication of the Geological Society, London, **19**, 229-244.
- Ring, U. 1994. The influence of preexisting structure on the evolution of the Cenozoic Malawi rift (East Africa rift system). *Tectonics*, **13**(2), 313-326.
- Roberts, S. & Jackson, J.A. 1991. Active normal faulting in Greece: an overview. In Roberts, A.M., Yielding, G. & Freeman, B. (eds), *The geometry of normal faults*. Special publication of the Geological Society, London, **56**, 125-142.
- Roux, J. 1992. A study of the structural evolution of the Pletmos Basin, South Africa. Soekor internal report (unpublished), 12 pp.
- Salvini, F., Stori, F. & McClay, K., 2001, Self-determining numerical modelling of compressional fault-bend folding, *Geology*, **29**(9), 839-842.
- Sandiford, M. 1999. Mechanics of basin inversion. *Tectonophysics*, **305**, 109-120.
- Sandiford, M. & Hand, M. 1998. Controls on the locus of Phanerozoic intraplate deformation in central Australia. *Earth and Planetary Science Letters*, **162**, 97-110.
- Sattarzadeh, Y., Cosgrove, J.W. & Vita-Finzi, C., 2000, The interplay of faulting and folding during the evolution of the Zagros deformation belt. In : Cosgrove, J.W. & Ameen, M.S. (eds) *Forced folds and fractures*, Geological Society London, Special Publication, **169**, 187-189.
- Satterfield, W.M. & Behrens, E.W. 1990. A late Quaternary canyon / channel system, Northwest Gulf of Mexico continental slope. *Marine Geology*, **92**, 51-67.
- Schlische, R.W. 1995. Geometry and origin of fault related folds in extensional settings. *AAPG Bulletin*, **79**, 1661-1678.
- Schlische, R.W., Young, S.S., Ackermann, R.V. & Gupta, A. 1996. Geometry and scaling relations of a population of very small rift-related normal faults. *Geology*, **24**(8), 683-686.
- Scholz, C.H. & Contreras, J.C. 1998. Mechanics of continental rift architecture. *Geology*, **26**(11), 967-970.
- Scholz, C.H. & Cowie, P.A. 1990. Determination of total strain from faulting using slip measurements. *Nature*, **364**, 837-839.
- Sharp, I.R., Gawthorpe, R.L., Armstrong, B. & Underhill, J.R. 2000. Propagation history and passive rotation of mesoscale normal faults: implications for syn-rift stratigraphic development. *Basin Research*, **12**, 285-305.
- Shone, R.W. 1978. A case for lateral gradation between the Kirkwood and Sundays river formations, Algoa Basin. *Transactions of the Geological Society of South Africa*, **81**, 319-326.

- Shone, R.W. & Booth, P.W.K. 1993. Thrusting in the Bokkeveld Group of the southern Cape. *South African Journal of Geology*, **96**(4), 220-225.
- Shone, R.W., Nolte, C.C., & Booth, P.W.K. 1990. Pre-Cape rocks of the Gamtoos area—a complex tectonostratigraphic package preserved as a horst block. *South African Journal of Geology*, **93**(4), 616-621.
- Sibson, R.H. 1995. Selective fault reactivation during basin inversion: potential for fluid redistribution through fault-valve action, in Buchanan, J.G. & Buchanan, P.G. (eds), *Basin Inversion*, Special publication of the Geological Society, London, **88**, 3-19.
- Sibson, R.H. 1985. A note on fault reactivation *Journal of Structural Geology*, **7**(6), 751-754.
- Sinclair, H.D. & Tomasso, M. 2002 (*in press*) Depositional evolution of confined turbidite basins. *Journal of Sedimentary Research*.
- Smythe, D.K., Dobinson, A., McQuillin, R., Brewer, J.A., Matthews, D.H., Blundell, D.J. & Kelk, B. 1982. Deep structures of the Scottish Caledonides revealed by MOIST reflection profile, *Nature*, **299**, 338-340.
- Snyder, D.B., England, R.W. & Bride J.H. 1997. Linkage between mantle and crustal structures and its bearing on inherited structures in northwest Scotland. *Journal of the Geological Society, London*, **154**, 79-83.
- Söhnge, A.P.G. 1983. The Cape Fold Belt—Perspective. In Söhnge, A.P.G. & Hälbig, I.W. (eds.) *Geodynamics of the Cape Fold Belt*. Special publication of the Geological Society of South Africa, **12**, 1-6.
- Spring, L. & Crespo-Blanc, A. 1992. Nappe tectonics, extension and metamorphic evolution in the Indian Tethys Himalaya (Higher Himalaya, SE Zaskar and NW Lahul). *Tectonics*, **11**, 978-98.
- Stein, R.S. & Barrientos, S.E. 1985. Planar high-angle faulting in the Basin and Range: geodetic analysis of the 1983 Borah Peak, Idaho, earthquake. *Journal of Geophysical Research*, **90** B13, 11355-11366.
- Storey, B.C., Curtis, M. L., Ferris, J. K., Hunter, M. A. & Livermore, R. A. 1999. Reconstruction and break-out model for the Falkland Islands within Gondwana. *Journal of African Earth Sciences*, **29**(1), 153-163.
- Storey, B.C. & Kyle, P.R. 1997. An active mantle mechanism for Gondwana breakup. *South African Journal of Geology*, **100**(4), 283-290.
- Storey, B.C., Alabaster, T., Hole, M.J., Pankhurst, R.J. & Wever, H.E. 1992. Role of subduction-plate boundary forces during the initial stages of Gondwanan break-up: evidence from the proto-Pacific margin of Antarctica. In Storey, B.C., Alabaster, T. & Pankhurst, R.J. (eds.) *Magmatism and the causes of continental breakup*. Special publication of the Geological Society, London, **68**, 149-163.
- Tankard, A.J., Jackson, M.P.A., Eriksson, K.A., Hobday, D.K., Hunter, D.R., & Minter, W.E.L. 1982. *Crustal Evolution of Southern Africa*. Springer-Verlag, New York. 520pp.
- Thomas, R.J., von Veh, M.W., and McCourt, S. 1993. The tectonic evolution of southern Africa: an overview. *Journal of African Earth Sciences*, **16**, 5-24.

- Thomson, K. 1999. Role of continental break-up, mantle plume development and fault reactivation in the evolution of the Gamtoos Basin, South Africa. *Marine and Petroleum Geology*, **16**, 409-429.
- Thomson, K. 1998. When did the Falklands rotate? *Marine and Petroleum Geology*, **15**, 723-736.
- Thomson, K. & Underhill, J.R. 1999. Frontier exploration in the South Atlantic : structural prosperity in the North Falkland Basin. *AAPG Bulletin*, **83(5)**, 778-797.
- Toerien, D.K. 1979. Explanation : Sheet 3322, 1:250,000; Oudtshoorn, Republic of South Africa, Department of Mineral and Energy Affairs, Geological Survey, Pretoria 13pp.
- Toerien, D.K. and Hill, R.S. 1989. Explanation: Sheet 3324, 1:250,000; Port Elizabeth, Republic of South Africa, Department of Mineral and Energy Affairs, Geological Survey, Pretoria 35pp.
- Trewin, N.H., Macdonald, D.I.M. & Thomas, C.G.C. 2002. Stratigraphy and sedimentology of the Permian of the Falkland Islands: lithostratigraphic and palaeoenvironmental links with South Africa. *Journal of Geological Society, London*, **159**, 5-20.
- Trouw, R.A.J. & de Wit, M.J. 1999. Relation between the Gondwanide Orogen and contemporaneous intracratonic deformation. *Journal of African Earth Sciences*, **28**, 203-213.
- Trudgill, B. & Cartwright, J. 1994. Relay-ramp forms and normal-fault linkages, Canyonlands National Parl, Utah. *Geological Society of America Bulletin*, **106**, 1143-1157.
- Turner, B.R. 1999. Tectonostratigraphical development of the Upper Karoo foreland basin: orogenic unloading versus thermally induced Gondwana rifting. *Journal of African Earth Sciences*, **28**, 215-238.
- Turner, B.R. 1986. Tectonic and climatic controls on continental depositional facies in the Karoo Basin of Northern Natal, South Africa. *Sedimentary Geology*, **46**, 231-257.
- Underhill, J.R. & Paterson, S. 1998. Genesis of tectonic structures: seismic evidence for the development of key structures along the Purbeck-Isle of Wight Disturbance, *J. Geol. Soc. Lon.*, **155**, 975-992.
- Våagnes, E., Gabrielsen, R.H. & Haremo, P. 1998. Late Cretaceous – Cenozoic intraplate contractional deformation at the Norwegian continental shelf: timing, agnitude and regional implications. *Tectonophysics*, **300**, 29-46.
- Van der Beek, P. 1997. Flank uplift and topography at the central Baikal Rift (SE Siberia): a test of kinematic models for continental extension. *Tectonics*, **16**, 122-136.
- Vann, I.R., Graham, R.H. & Hayward, A.B. 1986. The structure of mountain fronts. *Journal of Structural Geology*, **8(3/4)**, 215-227.
- Van Wees, J.D. & Beekman, F. 2000. Lithosphere rheology during intraplate basin extension and inversion Inferences from automated modeling of four basins in western Europe. *Tectonophysics*, **320**, 219-242.
- Veevers, J.J., Cole, D.I., & Cowan, E.J. 1994. Southern Africa: Karoo Basin and Cape Fold Belt. In Veevers, J.J. & Powell, C. McA. (eds) *Permian-Triassic Pangean Basins and Foldbelts Along the Panthalassan Margin of Gondwanaland*, GSA Memoir **184**, Boulder, Colorado, 223-279.

- Viljoen, J.H.A. 1990. K-bentonites in the Ecca Group of the south and central Karoo Basin. Geocongress 90, *Geological Society of South Africa*, abstract volume, 576-579.
- Visser, 1992. Basin Tectonics in South West Gondwana in the Carboniferous and Permian. In de Wit, M.J & Ransome, I.G.D. (eds) *Inversion tectonics of the Cape Fold Belt, Karoo and Cretaceous Basins of Southern Africa*. Rotterdam, Balkerna, 109-116.
- Visser, J.N.J., Van Niekerk, B.N. & Van der Merwe, S.W. 1997. Sediment transport of the Late Paleozoic glacial Dwyka Group in the southwestern Karoo Basin. *South African Journal of Geology*, **100**(3), 223-236.
- Walsh, J.J. & Watterson, J. 1988. Analysis of the relationship between displacements and dimensions of faults. *Journal of Structural Geology*, **10**, 239-247.
- Watterson, J. 1986. Fault dimensions, displacements and growth. *Pure & Applied Geophysics*, **124**, 365-373.
- Wernicke, B. 1995. Low-angle normal faults and seismicity: A review. *Journal of Geophysical Research*, **100**, B10, 20159-20174.
- Wernicke, B. & Burchfiel, B.C. 1982. Modes of extensional tectonics. *Journal of Structural Tectonics*, **4**, 105-115.
- Wernicke, B. 1981. Low-angle normal faults in the Basin and Range Province: nappe tectonics in an extending orogen. *Nature*, **291**, 645-648.
- White, R.S. & McKenzie, D.P. 1989. Magmatism at rift zones: the generation of volcanic continental margins and flood basalts. *Journal of Geophysical Research*, **94**, 7685-7729.
- Willemse, J.M. 1997. Segmented normal faults: correspondence between three-dimensional mechanical models and field data. *J. Geophysical Res.*, **102**(B1), 675-692.
- Willemse, J.M., Pollard, D.D. & Aydin, A. 1996. Three-dimensional analyses of slip distributions on normal fault arrays with consequences for fault scaling. *Journal of Structural Geology*, **18**, 295-309.
- Williams, G.D., Powell, C.M. & Cooper, M.A. 1989. Geometry and kinematics of inversion tectonics, in, Cooper, M.A. & Williams, G.D., *Inversion Tectonics*, Special publication of the Geological Society, London, **44**, 3-16.
- Williams, G.D. & Chapam, T.J. 1986. The Bristol-Mendip foreland thrust belt. *Journal of the Geological Society London*, **143**, 63-73.
- Withjack, M.O., Olsen, P.E. & Schlische, R.W. 1995. Tectonic evolution of the Fundy rift basin, Canada: evidence of extension and shortening during passive margin development. *Tectonics*, **14**, 390-405.
- Withjack, M.O., Schlische, R.W. & Olsen, P.E., 1998. Diachronous rifting, drifting, and inversion on the passive margin of central eastern North America: an analog for other passive margins. *AAPG Bulletin*, **82** (5A), 817-835
- Wonham, J.P., Jayr, S., Mougamba, R. & Chuilon, P. 2000. 3D sedimentary evolution of a canyon fill (Lower Miocene-age) from the Mandorove Formation, offshore Gabon. *Marine & Petroleum Geology*, **17**, 175-197.
- Young, M.J., Gawthorpe, R.L. & Hardy, S. 2001. Growth and linkage of a segmented normal fault zone; the Late Jurassic Murchison-Statfjord North Fault, northern North Sea. *Journal of Structural Geology*, **23**, 1933-1952

- Ziegler, P.A. 1989. Geodynamic model for Alpine intra-plate compressional deformation in Western and Central Europe. *In* Cooper, M.A. & Williams, G.D. (eds) *Inversion Tectonics*. Special publication of the Geological Society, London, **44**, 63-85.

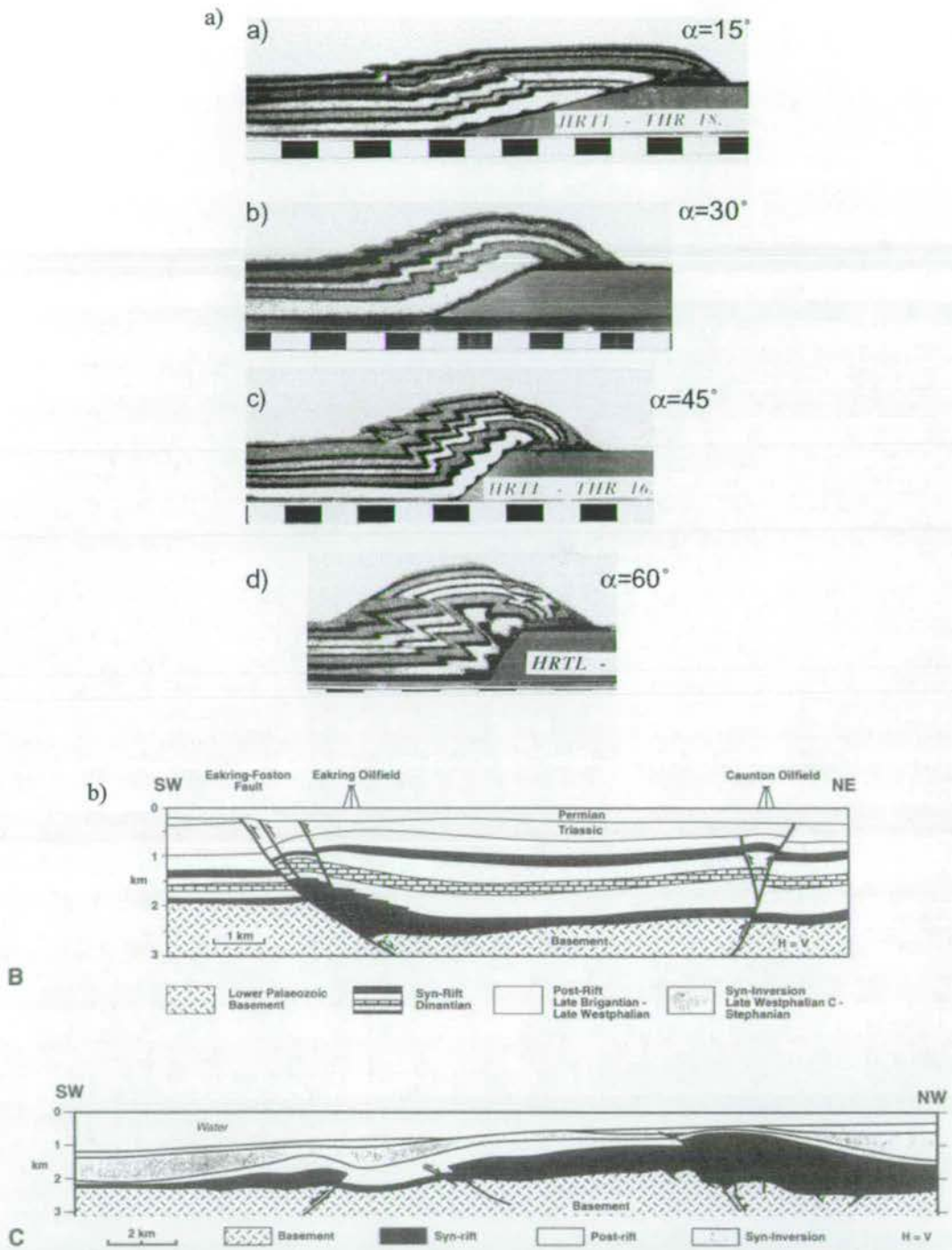


Figure 2.1: Examples of positive structural inversion. a) Sand-box modeling with a variable ramp angle (α) illustrating that the higher the ramp angle, the shorter the wavelength of the resultant hangingwall deformation (Bonini *et al.*, 2000). b) Two examples of inversions from seismic studies that illustrate the overall pop-up geometry that can be observed (after McClay, 1995).

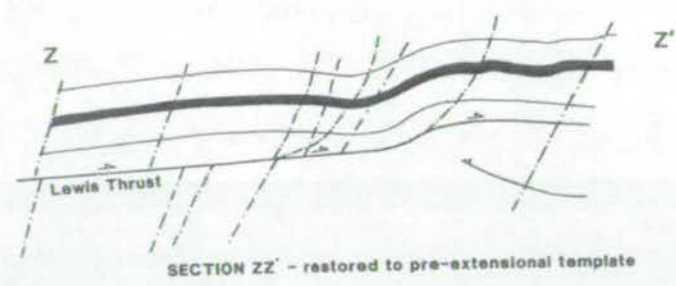
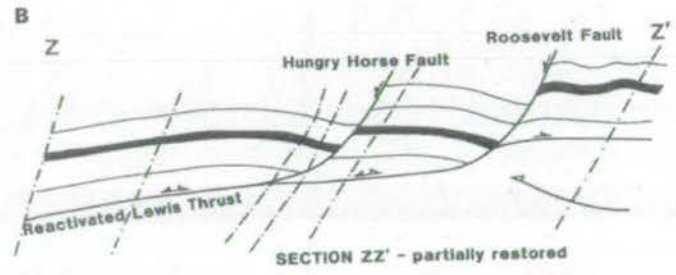
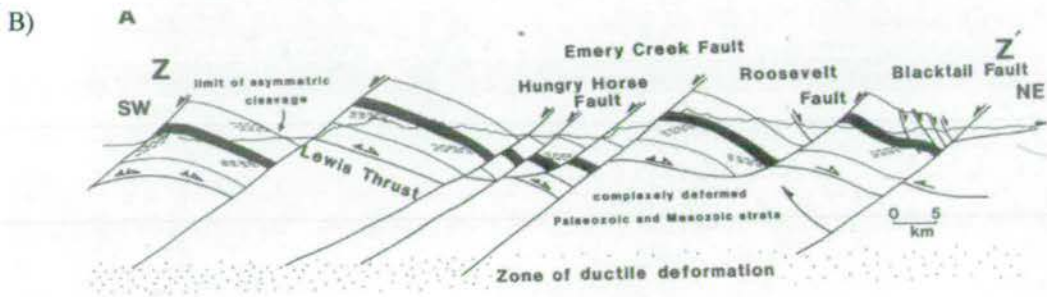
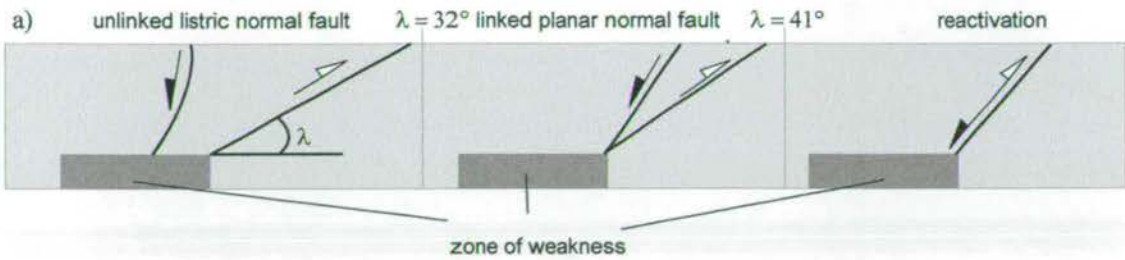


Figure 2.2: Two examples of negative structural inversion. a) Faccena *et al.* (1995)'s results from sandbox models show that the complete reactivation of an existing reverse fault into extension occurs if the dip of the structure is $> 41^\circ$. b) Structural cross-section across the Lewis thrust sheet, northwest Montana. Note that the majority of normal faults ignore the pre-existing low angle thrust fault. The lower two diagrams show partly and fully restored sections (after Powell & Williams, 1989).

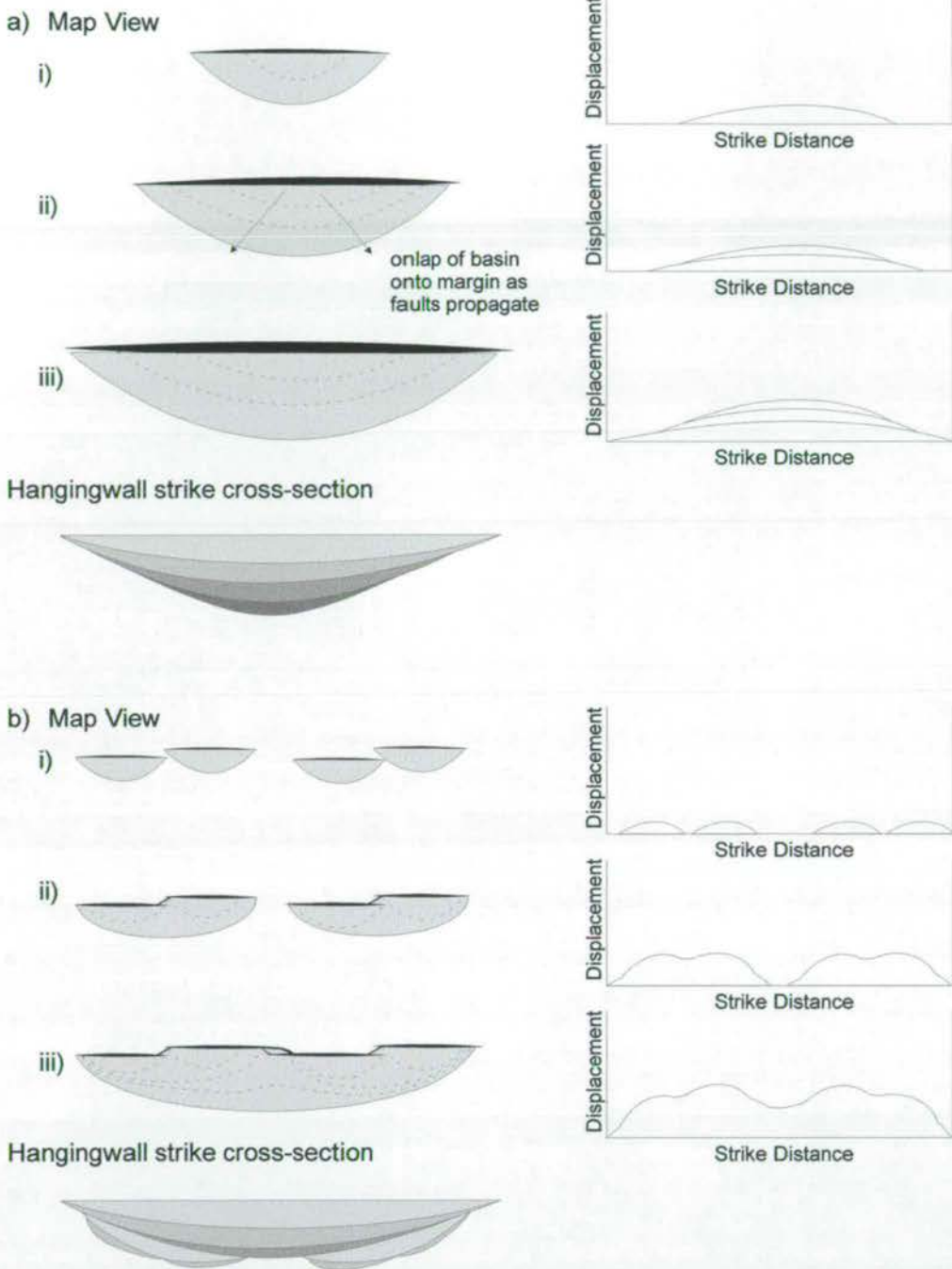
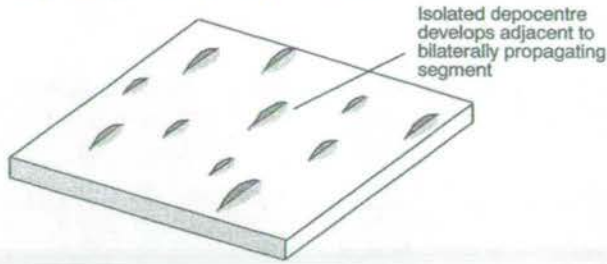


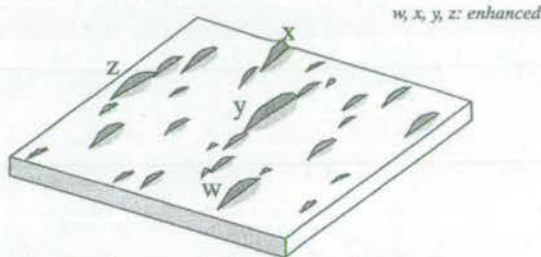
Figure 2.3: Two models of fault system evolution and associated sedimentary basin formation are illustrated, with growth controlled by a) isolated radial propagation, and b) segment linkage. For both models, map view and displacement/length profiles through time (i-iii) and final hangingwall strike sections are presented (after Cartwright *et al.* (1995); Morley & Wonganan, 2000). The evaluation of hangingwall strike cross-sections and displacement/length profiles can be used to establish the evolution of the fault system (cf. Chapter 5).

(1) Early Rift Initiation: Onset of fault nucleation and segment growth in relative isolation



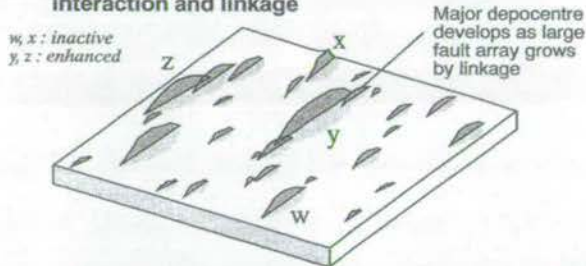
- Initiation and growth of numerous small isolated depocentres adjacent to early formed faults

(2) Mid-rift Initiation: Continued nucleation, and onset of segment interaction and linkage



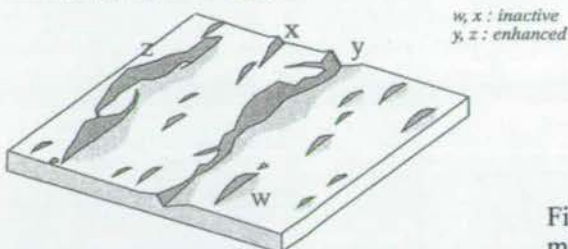
- Abrupt enlargement of early formed depocentres by linkage of adjacent fault segments.
- Major depocentres established in hangingwall of longer segments.

(3) Late Rift Initiation: Dominant fault segment interaction and linkage



- Growth of major depocentres by coalescence of smaller depocentres as deformation localises on major fault segments. Maximum subsidence rates at segment centres
- Depocentres adjacent to inactive fault segments cease to subside

(4) Rift Initiation – Rift Climax Transition: Full linkage of fault segments to produce a through-going fault system



- Single large depocentre develops adjacent to the major linked fault
- More uniform subsidence rate along strike

Figure 2.4: Tectono-stratigraphic model for the evolution of a normal fault array and the associated evolution of syn-rift depocentres (after Cowie *et al.*, 2000)

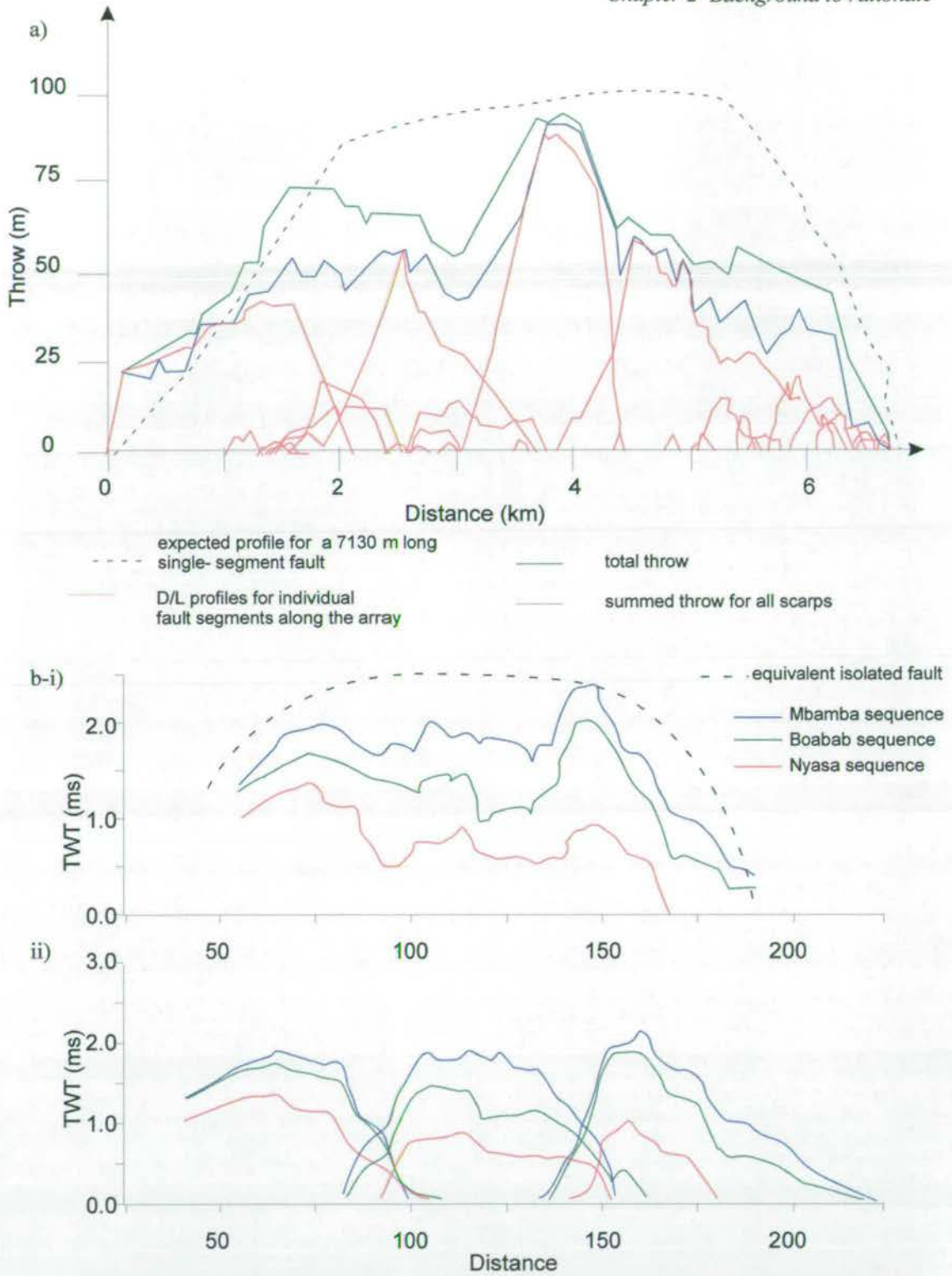


Figure 2.5: Two examples illustrating how the displacement-length profile of an evolved fault can be composed of individual segments. In a) the total throw is 93 m, and the cumulative throw on individual segments approaches that of an isolated fault (after Dawers & Anders, 1995). In b) the fault system is much larger (2.0 s TWT ~ 3 km), with cumulative displacement plot for the entire system (i) being formed from sequences associated with three segments (ii) (after Contreras *et al.*, 2000).

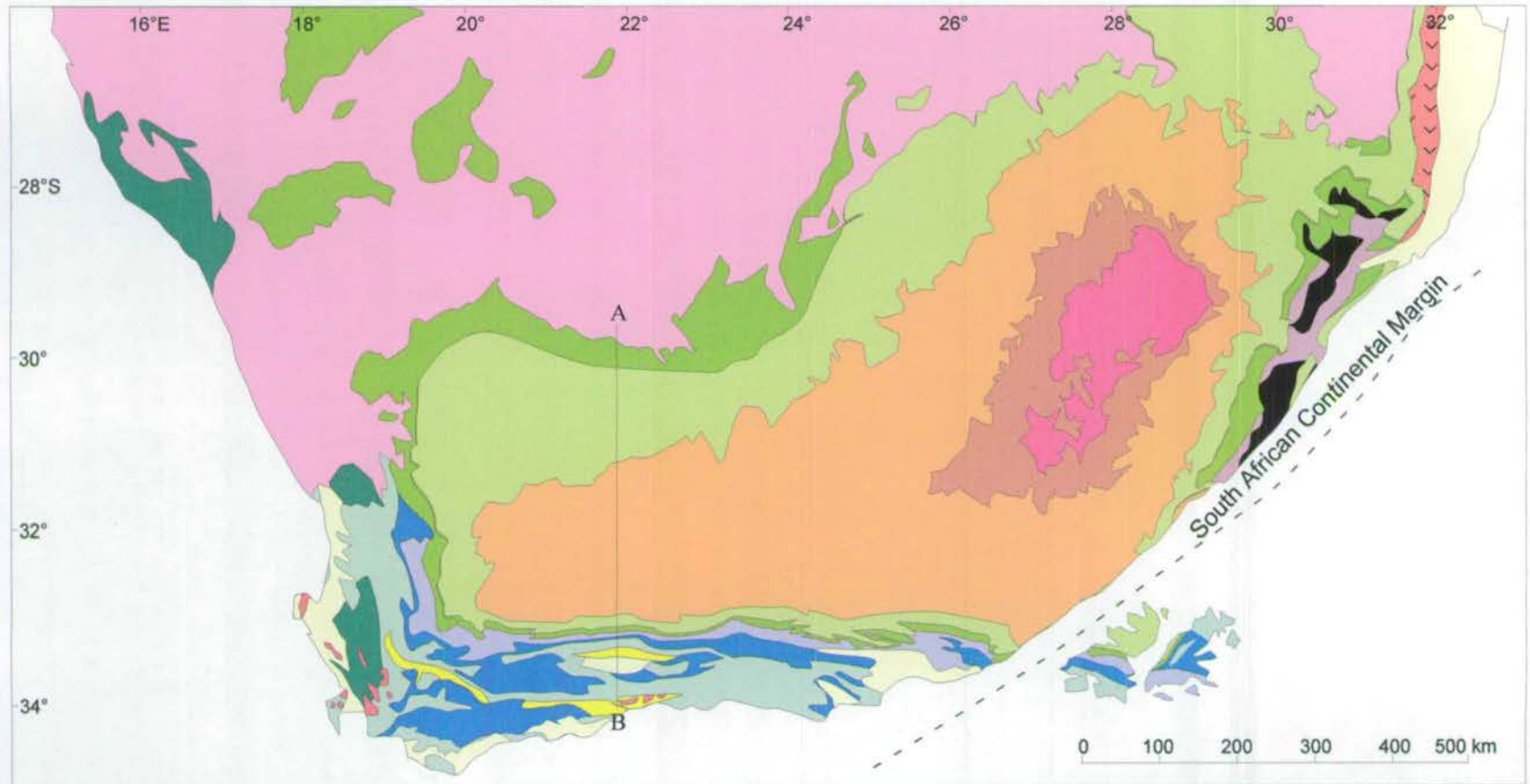


Figure 2.6: Geological map of South Africa and the Falkland Islands in a pre-Gondwana break-up position (see Section 2.5 for discussion), after Veevers *et al.*, 1994; Trewin *et al.*, 2002. Position of section in Figure 2.7 is shown. Equivalent Falkland Islands units: ¹-Port Stephens, ²-Fox Bay, ³-Port Stanley, ⁴-Lafonian Diamicite, ⁵-Upper Lafonian.

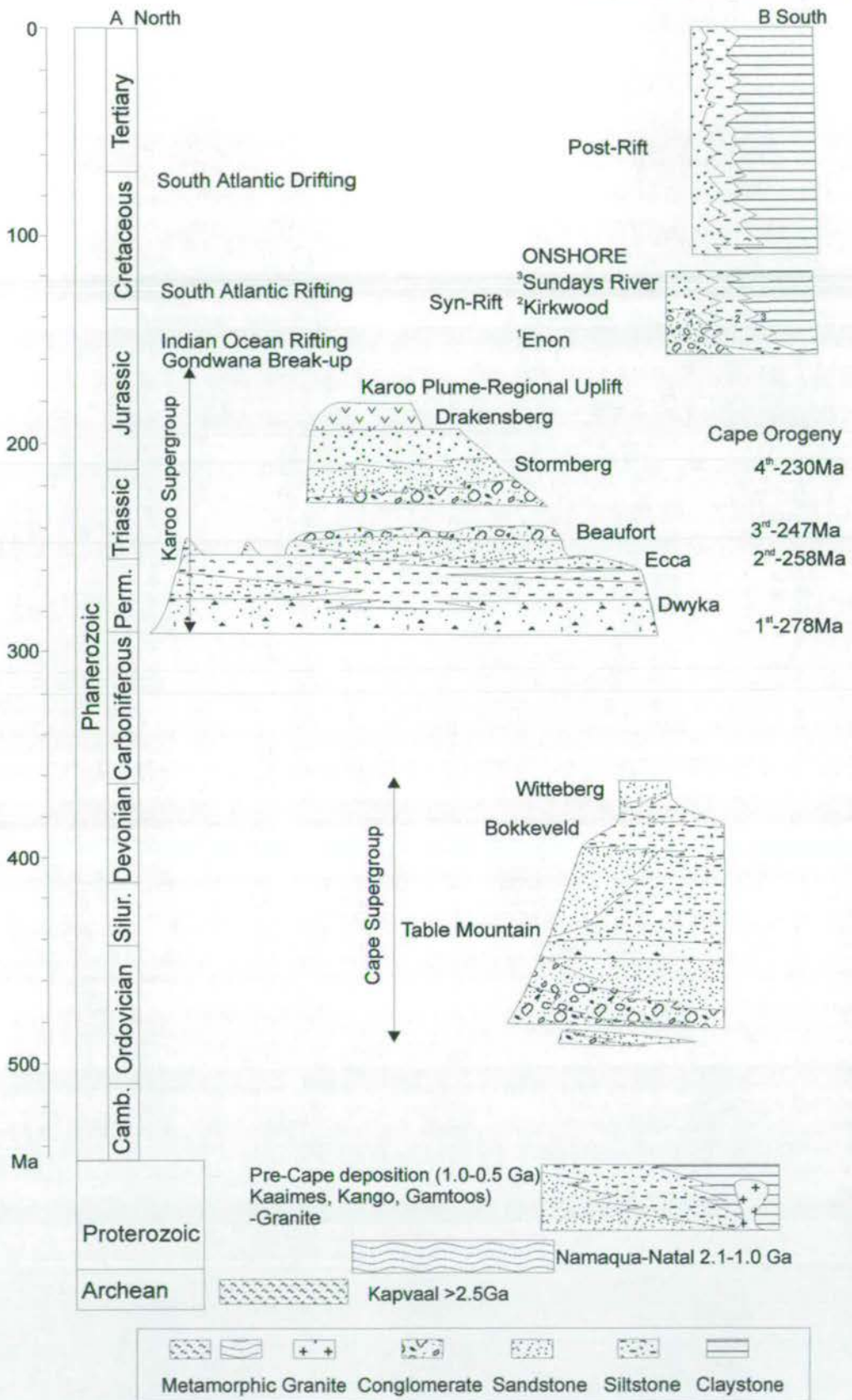


Figure 2.7: Chrono-stratigraphic diagram for South Africa showing sediment distribution and appropriate unit names. After Dingle *et al.*, 1983; Hällich & Swart, 1983; McMillan *et al.*, 1997; Veevers *et al.*, 1994..

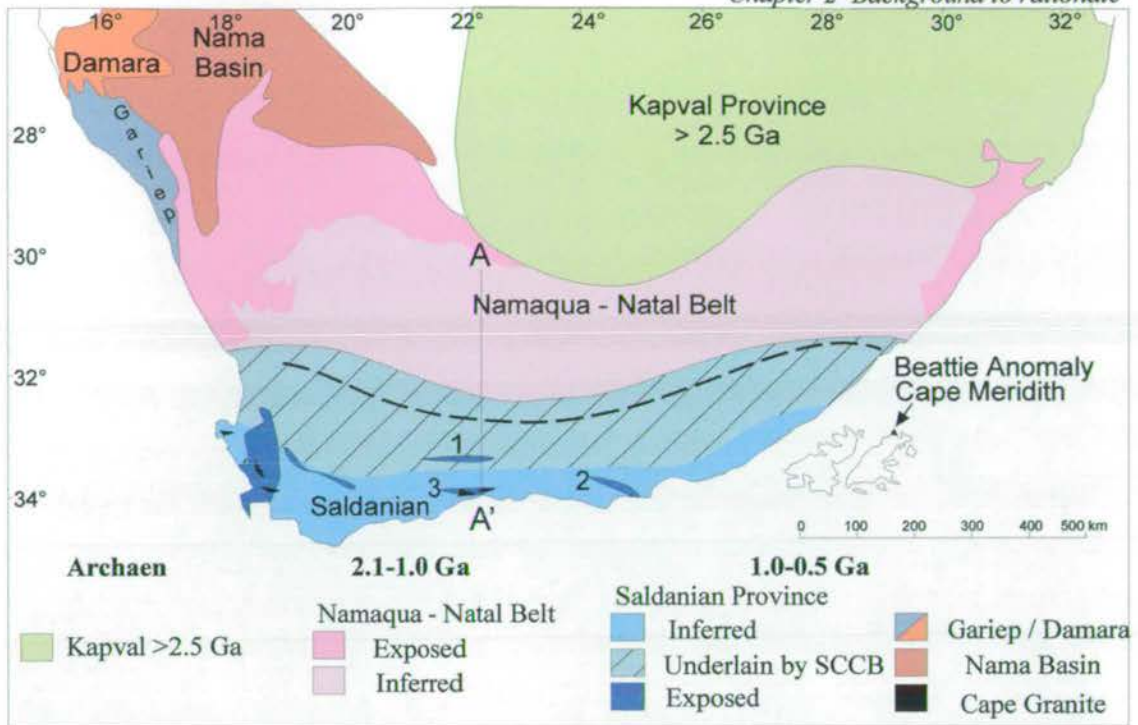


Figure 2.8: Pre-Cape geology of southern Africa highlighting the extent of the principal Proterozoic provinces (after Cole, 1992; Veevers *et al.*, 1994). The Falkland Islands have been placed in their pre-breakup position. SCCB - Southern Cape Conductive Belt. 1: Kango, 2: Gamtoos, 3: Kaaimes.

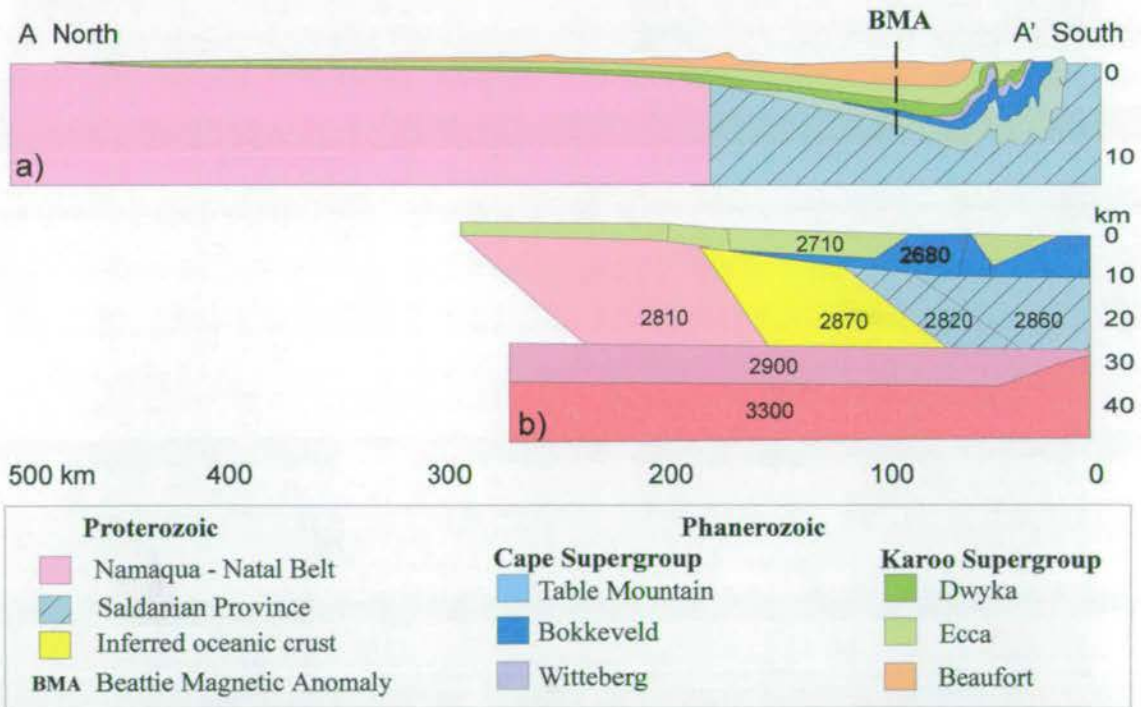


Figure 2.9: a) North-south section across South Africa showing the position of the Cape Supergroup and Karoo Basins with respect to the weaker crust of the Southern Cape Conductive Belt (including the Beattie Anomaly) and stronger Namaqua-Natal crust (after Cole, 1992). Position in Figure 2.8. b) Model of gravity profile of section in (a) showing the presence of the high density, highly conductive body (yellow) that is interpreted to be obducted oceanic crust (Pitts *et al.*, 1992).

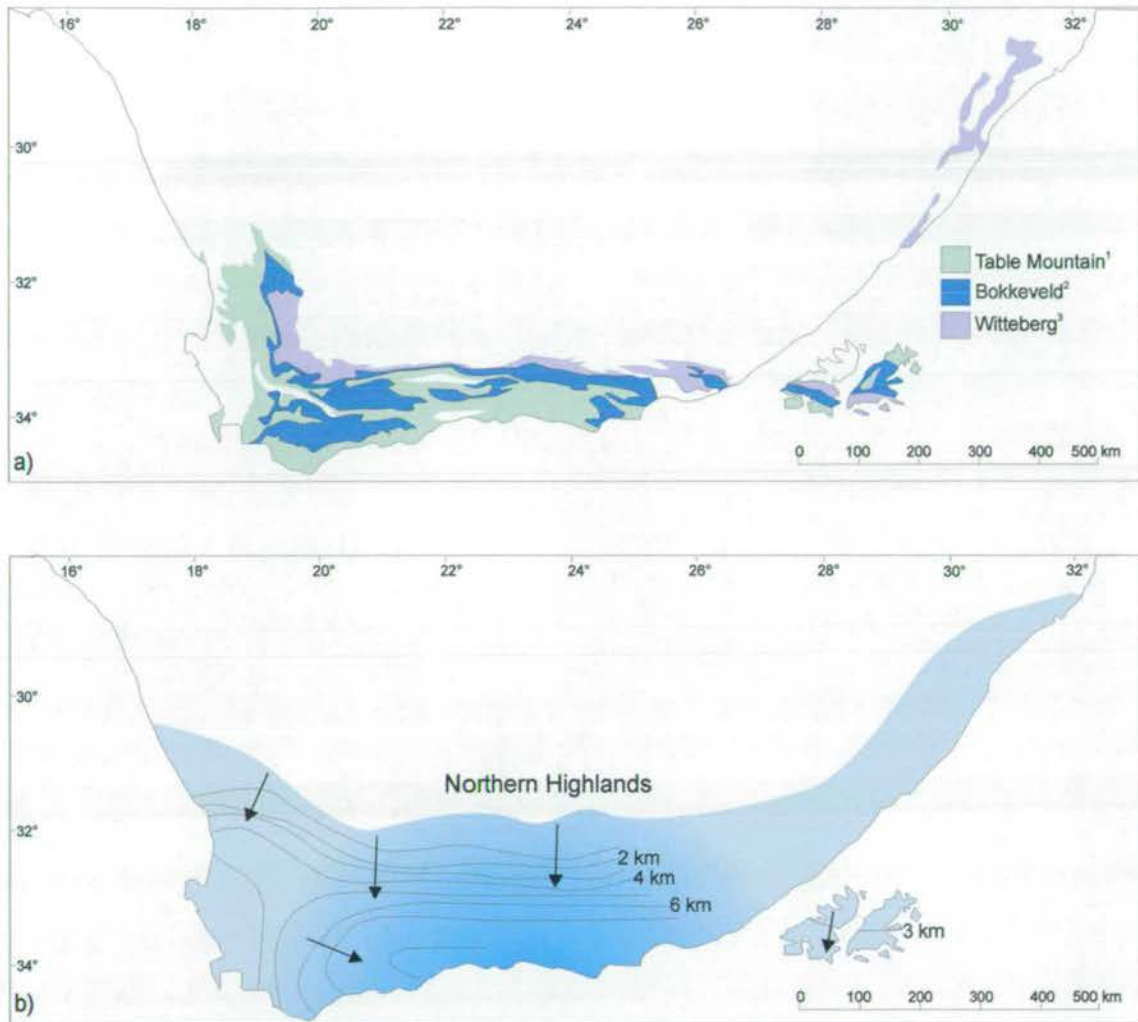


Figure 2.10: a) Outcrop map of South Africa showing the present day distribution of the Cape Supergroup units (Table Mountain, Bokkeveld, and Witteberg Groups; after Tankard *et al.*, 1983; Veevers *et al.*, 1994). Falkland Islands have been restored to pre-break-up position with the equivalent units mapped: ¹-Port Stephens, ²-Fox Bay, ³- Port Stanley (after Marshall, 1994a).
 b) Isochach map of the Cape Supergroup. The sediments were deposited from the north into an east-west trending basin with the basin axis directly to the south of the SCCB (cf. Figure 2.8 & 9), after Veevers *et al.*, 1994.

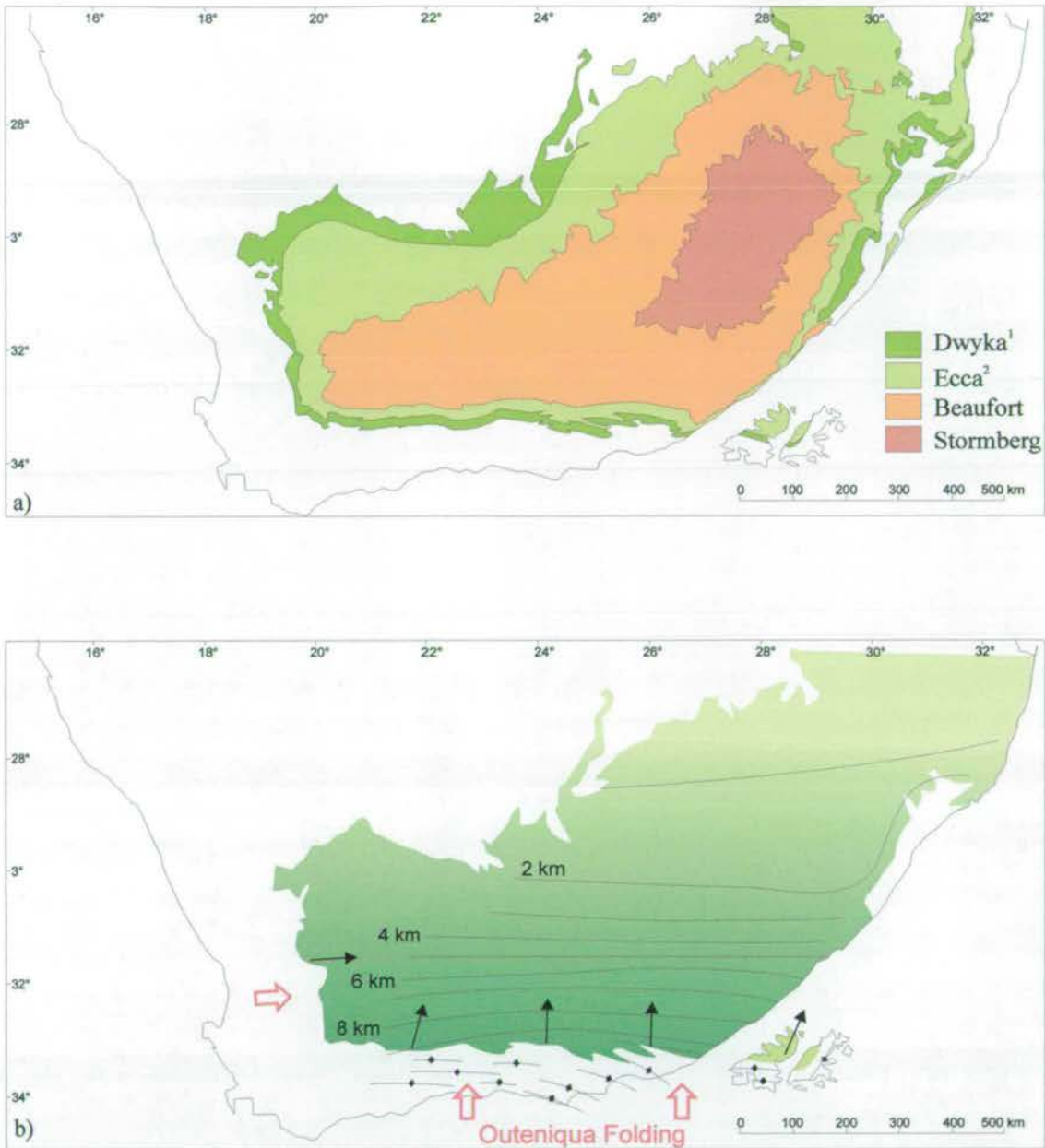


Figure 2.11: a) Outcrop map of South Africa showing the present distribution of the Karoo Supergroup units (Dwyka, Ecca, Beaufort, and Stormberg). (after Veevers *et al.*, 1994). Falkand Islands have been restored to pre-break-up position with the equivalent units mapped, ¹-Lafonian Diamictite, ²- Upper Lafonian Group (after Trewin *et al.*, 2002).

b) Isopach map of the Karoo Supergroup. The sediments were deposited from the south into an east-west trending basin with the basin axis immediately to the north of the SCCB (cf. Figure 2.8 & 9), after Veevers *et al.*, 1994. The change from north to south provenance (cf. Figure 2.10) is in response to the initiation and northward migration of the Cape Orogeny. Overall structural trend of anticlines associated with the orogeny are marked on.

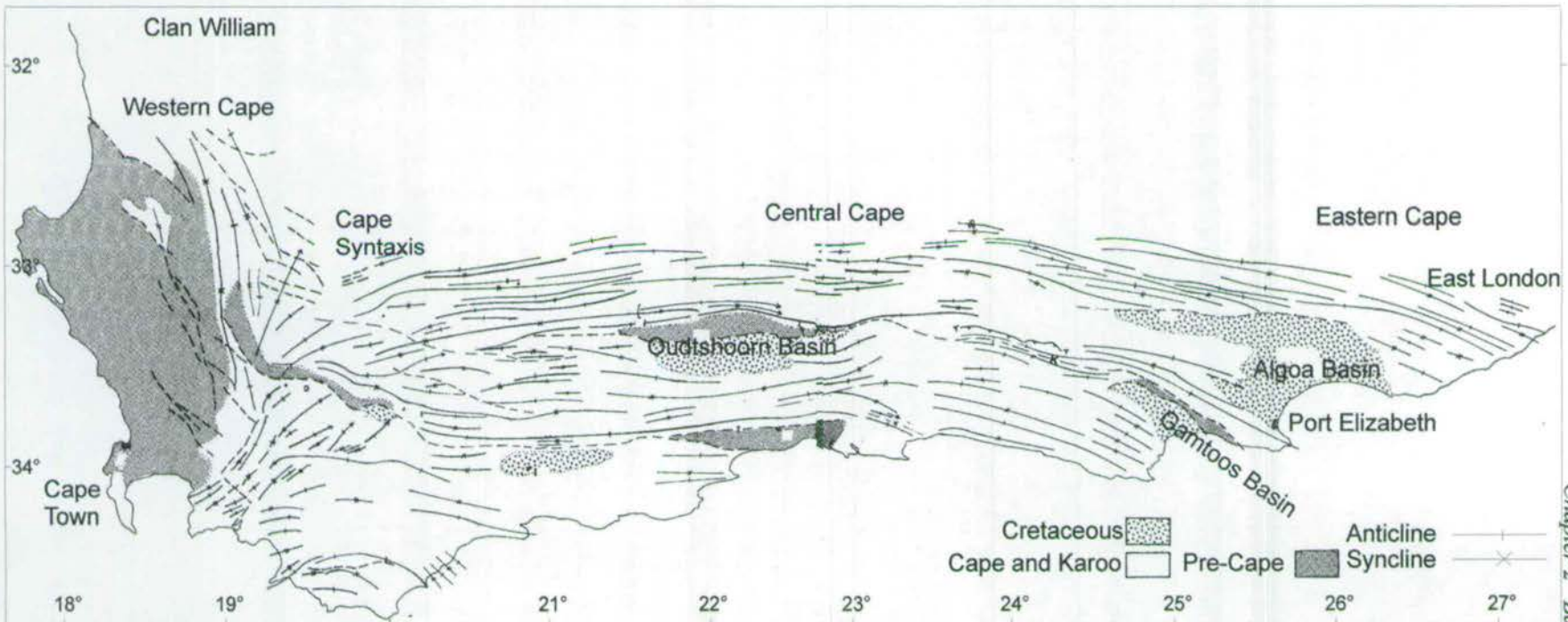


Figure 2.12: Structural geology of the Cape Fold Belt showing the position of the major folds and faults (after Dingle *et al.*, 1983).

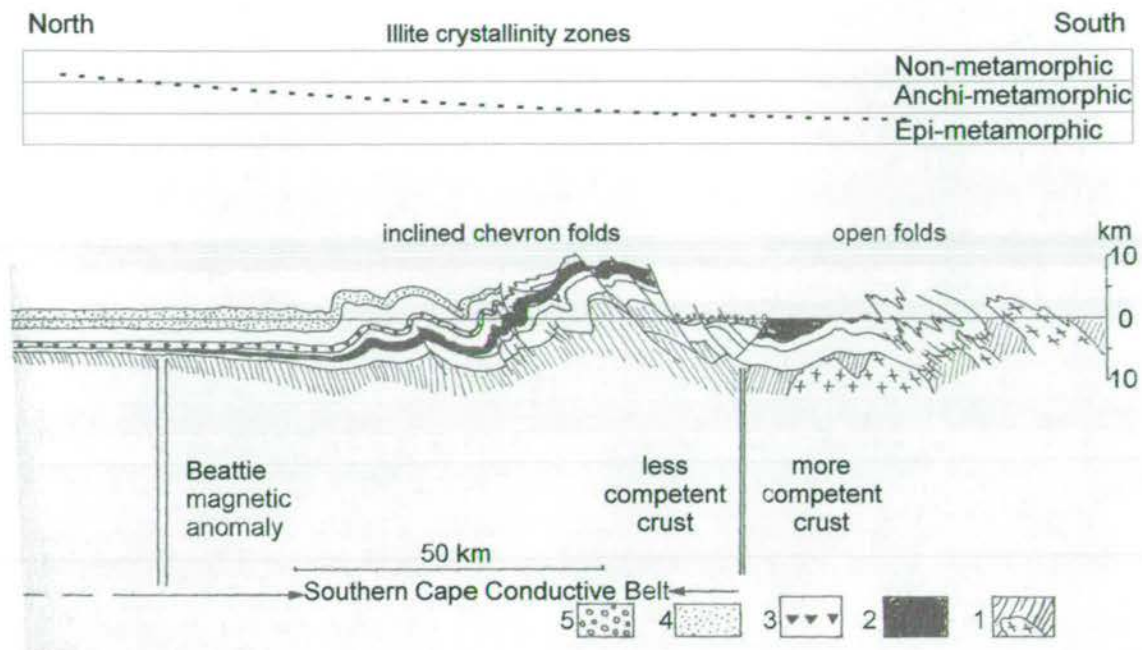


Figure 2.13: Stratigraphic and structural section across the Cape Fold Belt located at 22.5°E. 1-Pre-Cape sequences with granites, 2-Bokkeveld Group, 3-Dwyka Group, 4-Beaufort Group, 5- Jurassic-Cretaceous. (after Dingle *et al.*, 1983; Hälbig & Cornell, 1983). Illite crystallinity shows the gradual increase in metamorphic facies towards the south.

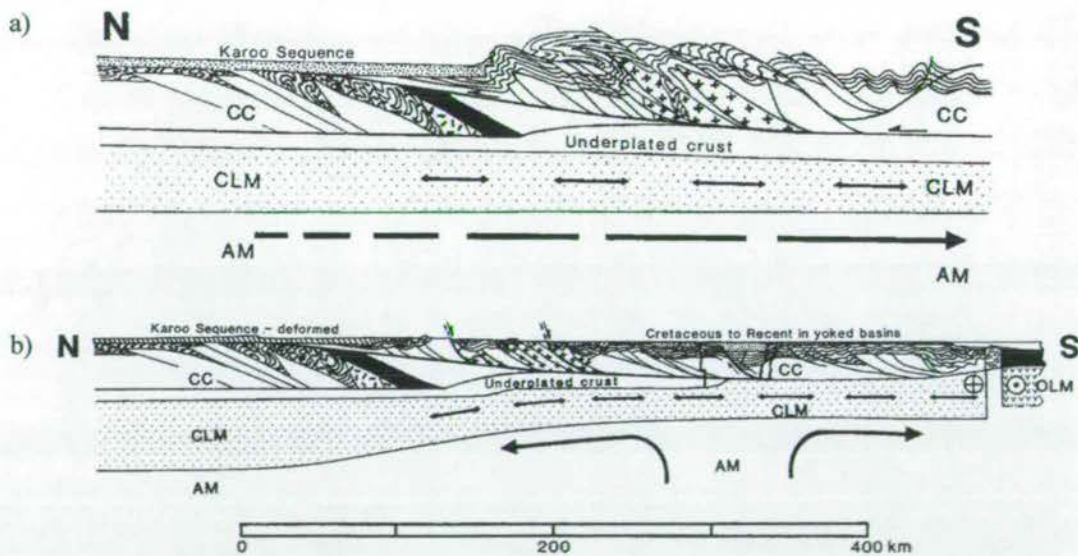


Figure 2.14: Model for the evolution of the Cape Fold Belt utilising the inferred low angle, pre-existing Pan-African décollement. b): Subsequent Mesozoic extension utilises the Cape Fold Belt structures. CC-Continental Crust, CLM-Continental Lithospheric Mantle, AM-Asthenospheric Mantle, OLM-Oceanic Lithospheric Mantle (after Hälbig, 1993).

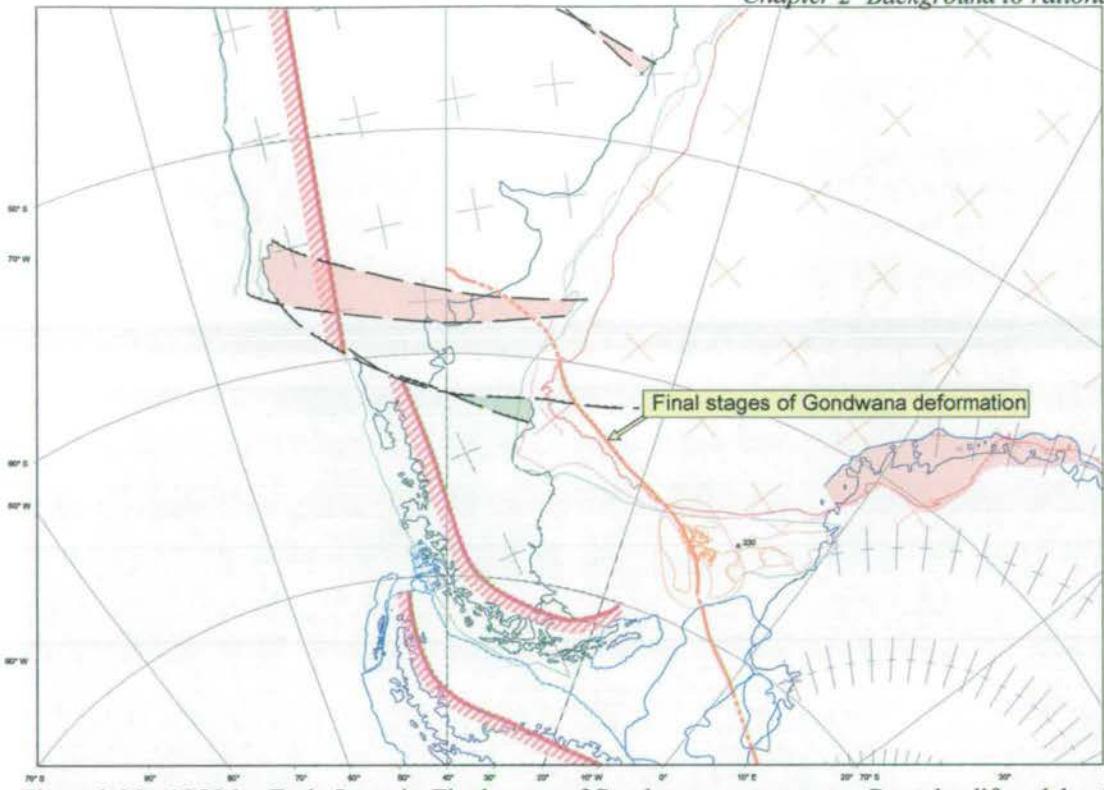


Figure 2.15a: 195 Ma - Early Jurassic. Final stages of Gondwana convergence. Crustal uplift and doming, as a result of Karoo volcanism, may have begun. After Macdonald *et al.*, (1998)

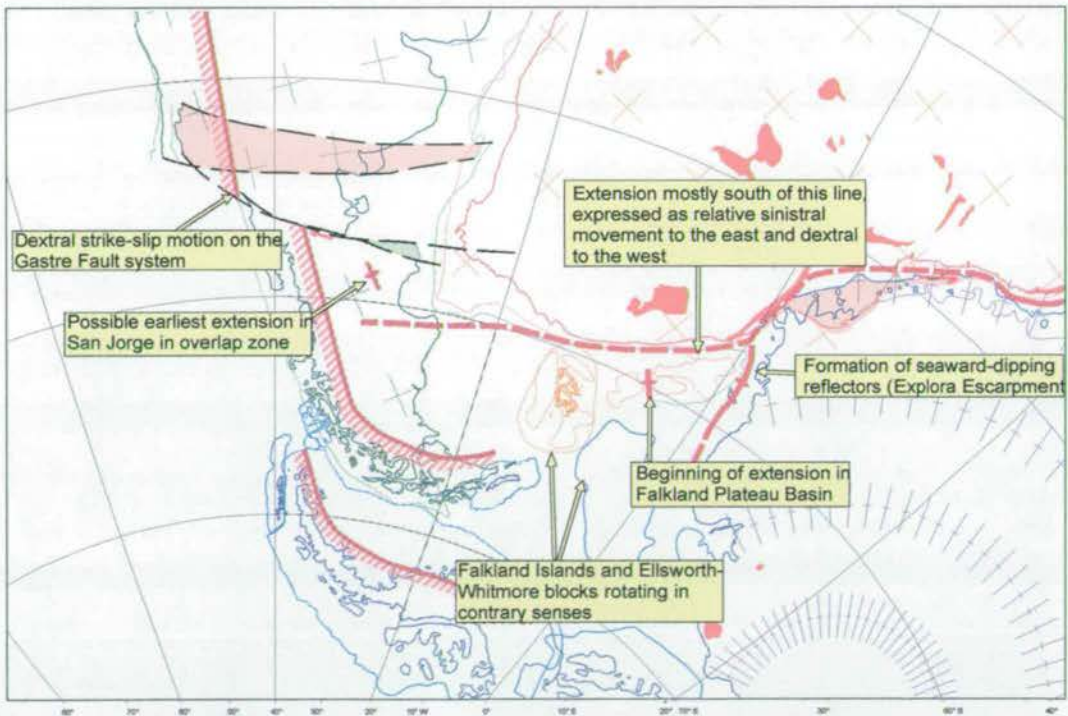


Figure 2.15b: 180 Ma - Early-Middle Jurassic. East and West Gondwana begin to rift. Major dextral strike-slip motion occurs, separating South Africa, the Falklands Plateau, Falkland Islands (clockwise rotation), and Ellsworth Mountains (counter-clockwise rotation). After Macdonald *et al.*, (1998).

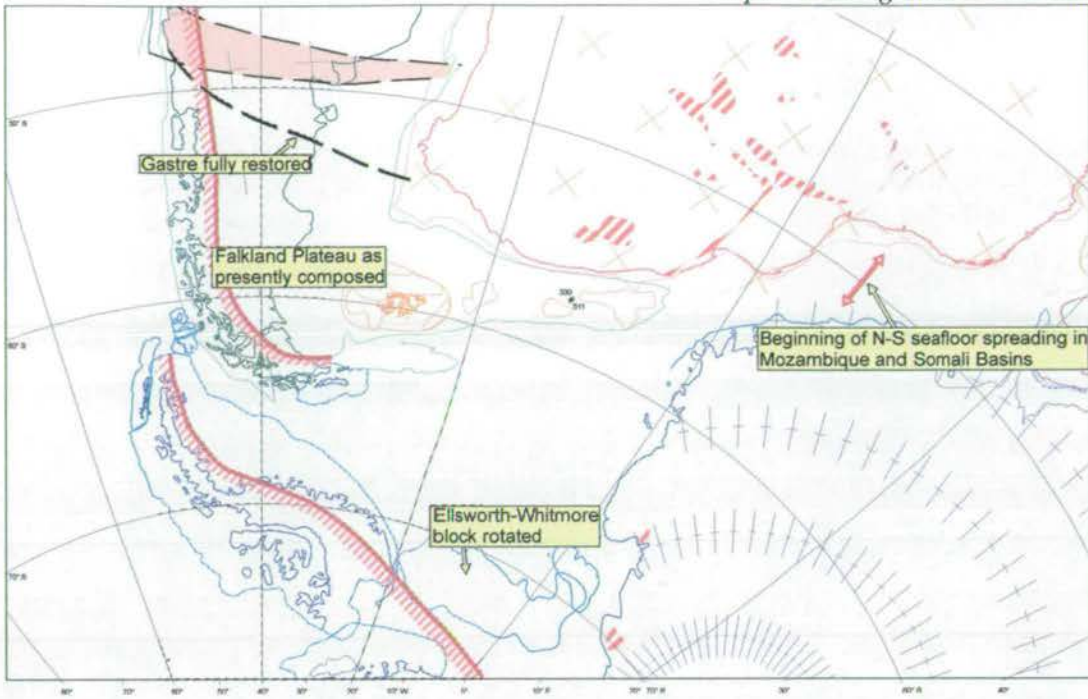


Figure 2.15c : 165 Ma - Middle Jurassic: . Southern South America restored by dextral strike-slip movement along the Gastre Fault System. The Falklands and Ellsworth Mountains are fully rotated. First rift-related volcanics in South Africa at 162 Ma (Dingle *et al.*, 1983). After Macdonald *et al.*, (1998)

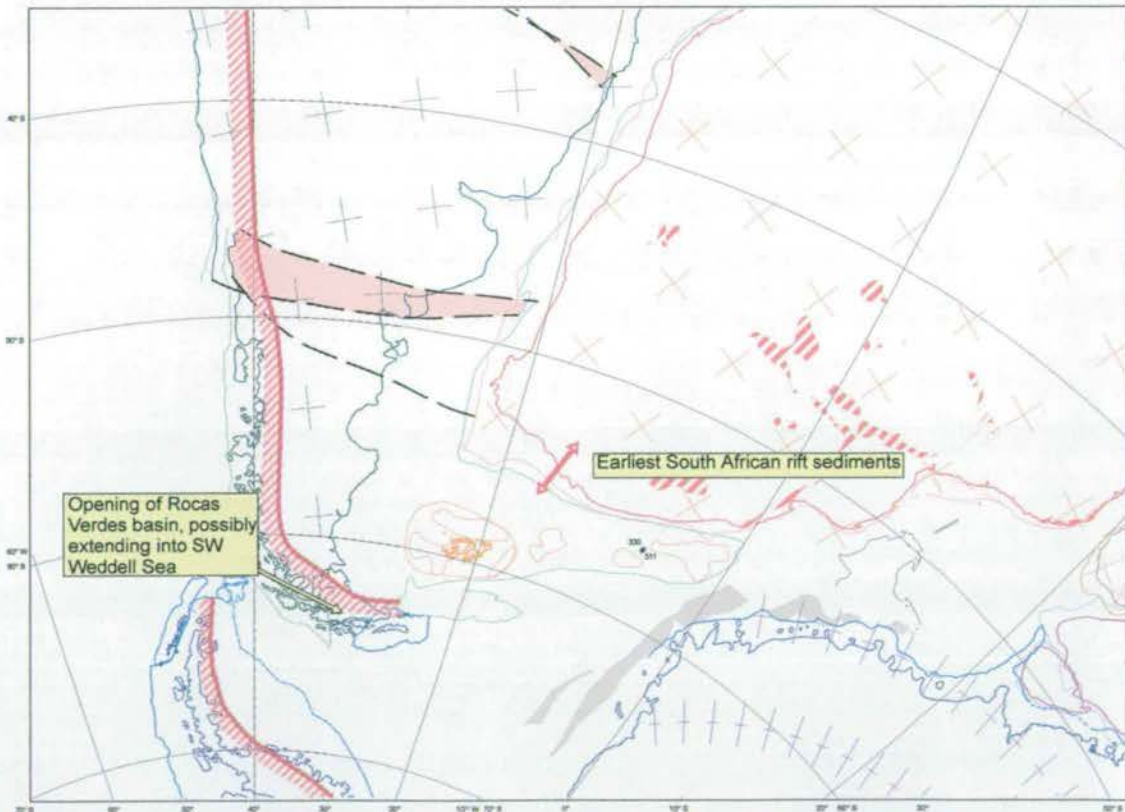


Figure 2.15d 150 Ma, Tithonian, Late Jurassic. Sea-floor spreading in the Weddell Sea. Initiation of the negative inversion of the Cape Fold Belt (South Africa). The oldest observed rift related sediments are Kimmeridgian. After Macdonald *et al.*, (1998)

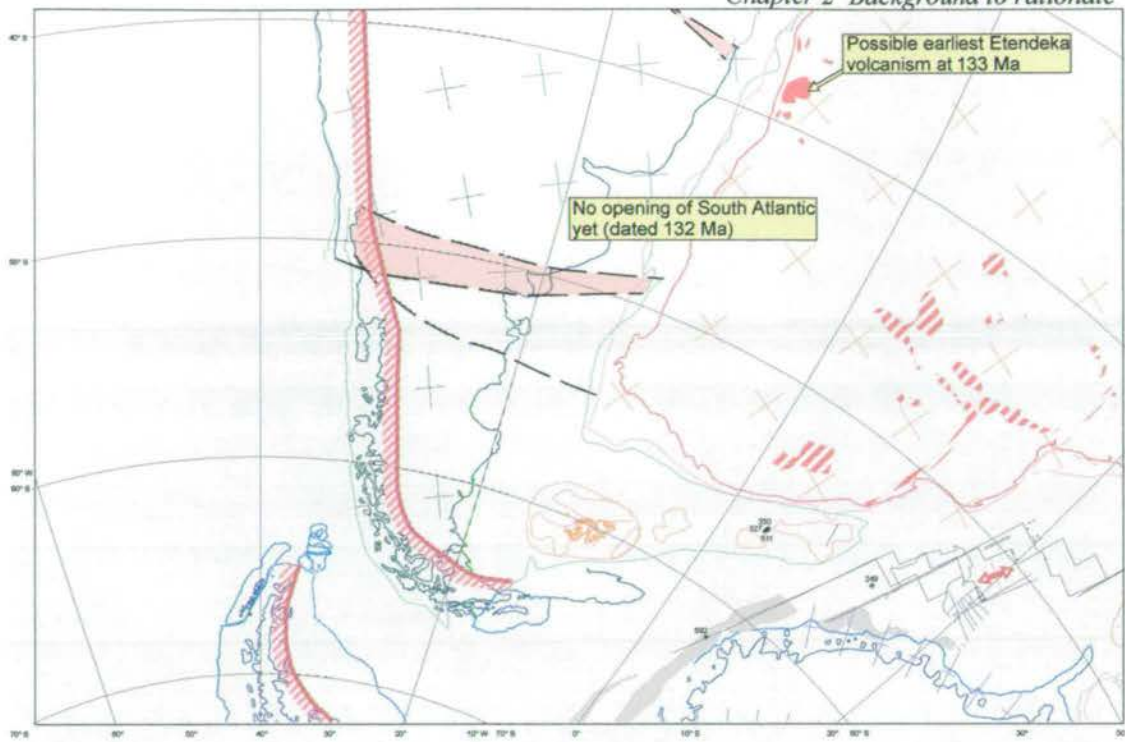


Figure 2.15e: 135 Ma- Valanginian-Hauterivian, Early Cretaceous. West Gondwana continues to break-up. The South Atlantic start to open at 132 Ma. After Macdonald *et al.*, (1998).

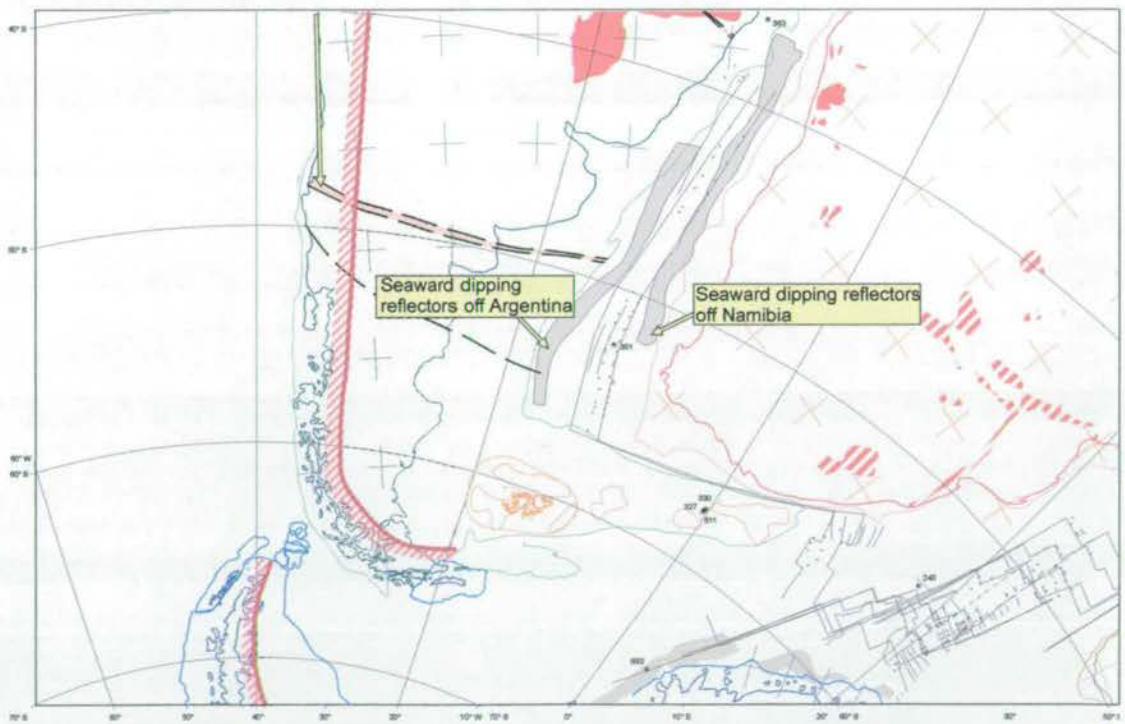


Figure 2.15f: 120 Ma - Aptian, Early Cretaceous. South Atlantic sea floor spreading, indicated by seaward dipping reflectors on both the Namibian and Argentinian passive margins. After Macdonald *et al.* (1998).

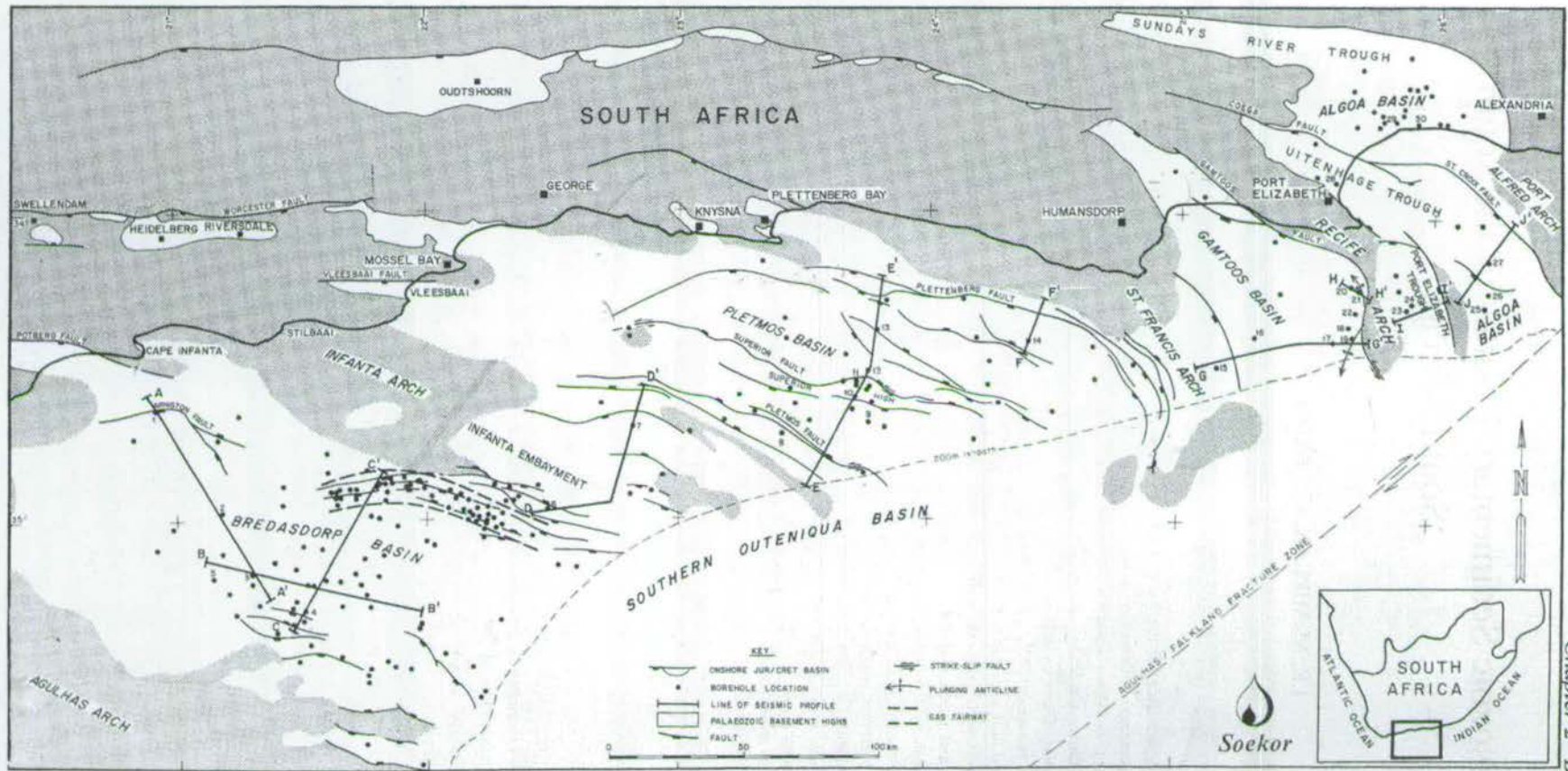


Figure 2.16: Structural map of the onshore and offshore Mesozoic basins of South Africa. Fault lines correspond to normal faults (after McMillan *et al.*, 1997).

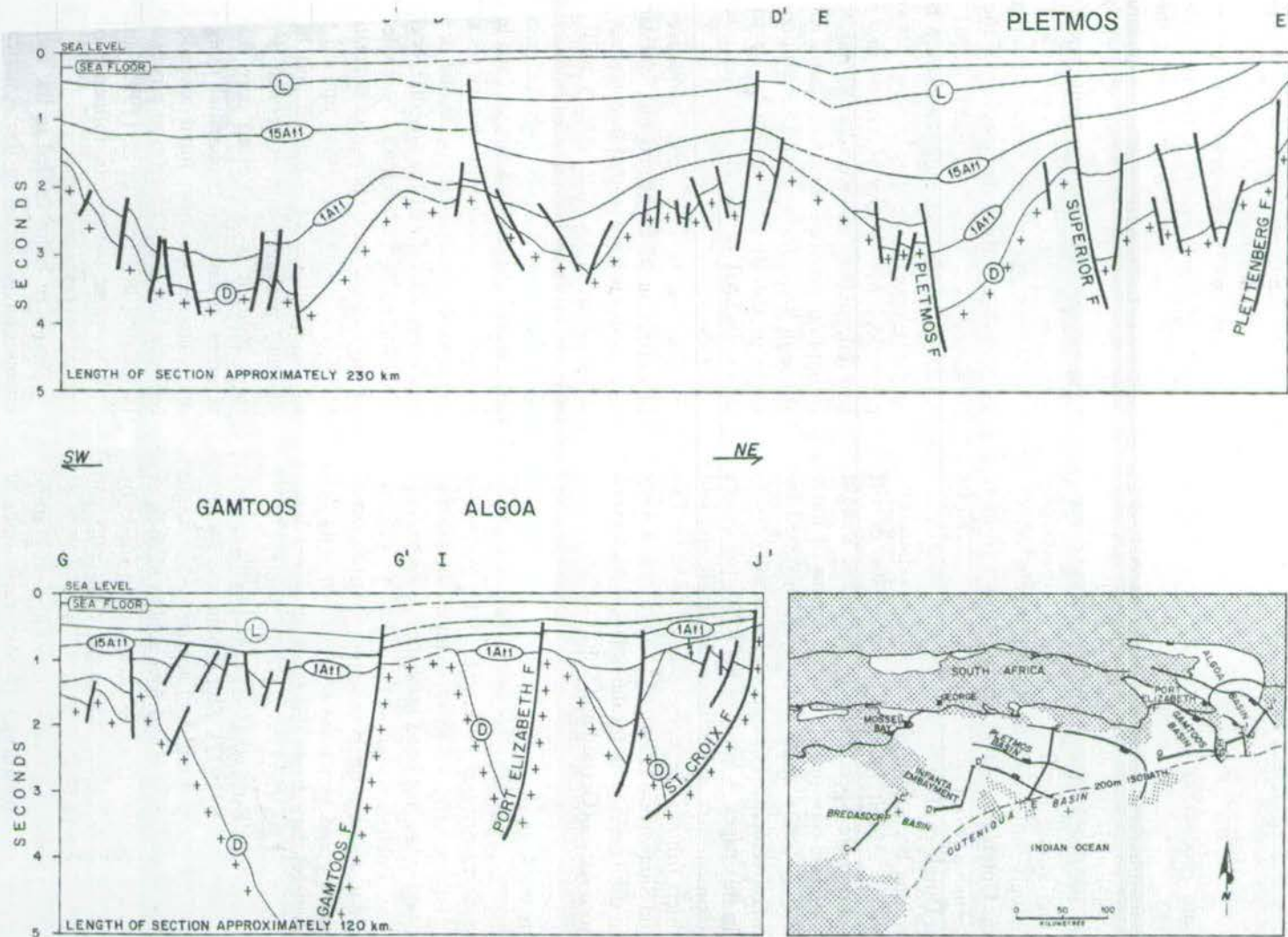


Figure 2.17: Compilation of seismic sections highlighting the principal structural features of the offshore Mesozoic basins. Terminology in figure corresponds to Soekoro horizon names: D-Top Basement, 1A11-End Syn-Rift, 15A11 & L-Post Rift (after McMillan *et al.*, 1997). Map shows position of section.

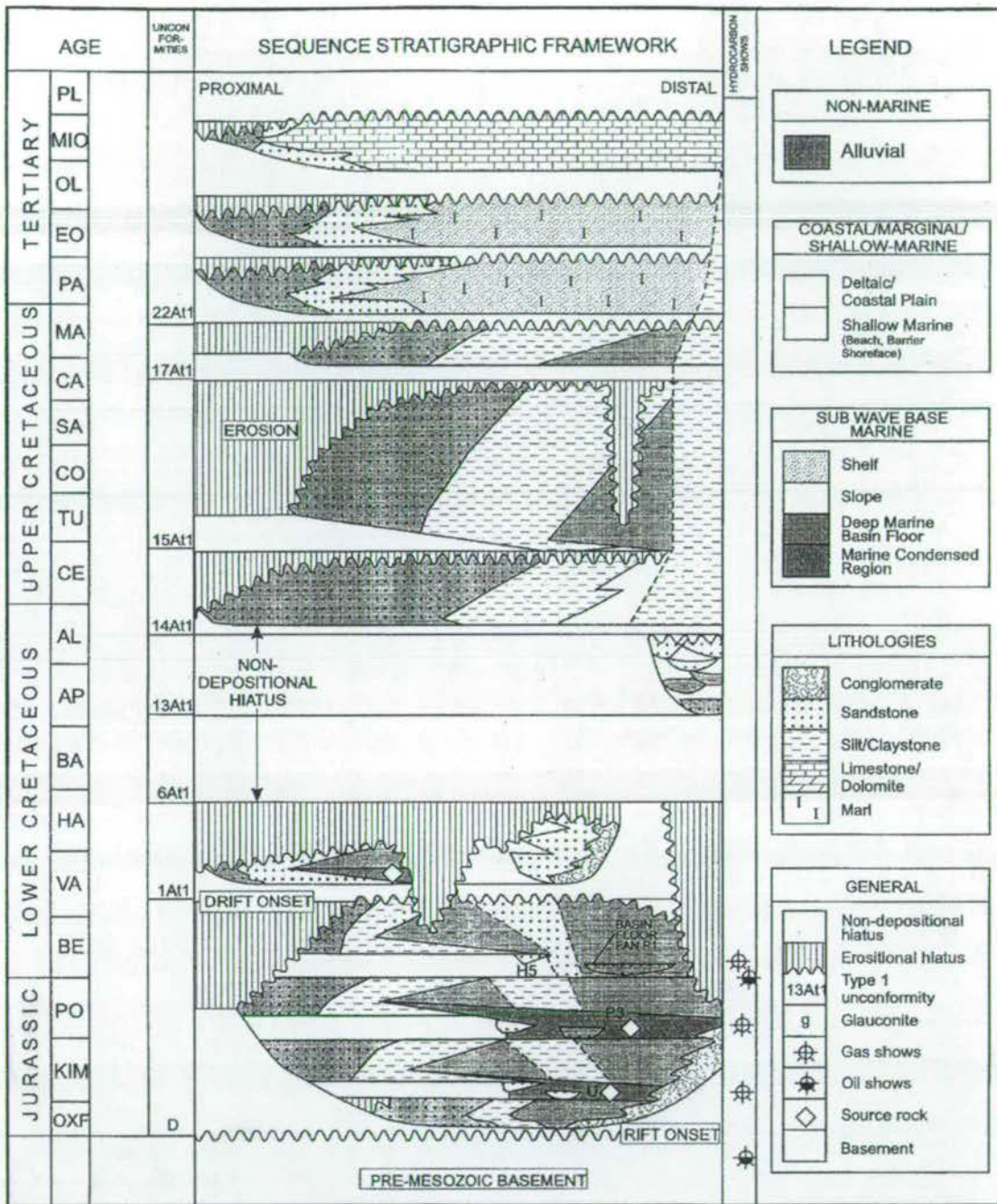


Figure 2.18: Sequence stratigraphic framework for the offshore South African Mesozoic Basins. Abbreviations: OXF- Oxfordian, KIM- Kimmeridgian, PO-Portlandian, BE- Berriasian, VA- Valanginian, HA-Hauterivian, BA- Barremian, AP-Aptian, Al- Albian, CE- Cenomanian, TU- Turonian, CO-Coniacian, SA- Santonian, CA- Campanian, MA-Maastrichtian, PA- Paleocene, EO- Eocene, OL- Oligocene, MIO- Miocene, PL- Pliocene. After McMillan *et al.*, 1997.


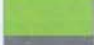
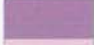
Formation	Subgroup	Group	Age
 Enon, Kirkwood, Sunday's River			Mesozoic
 Abrahamskraal	Beaufort	Karoo	Permian
 Waterford			
 Fort Brown			
 Ripon	Ecca		
 Prince Albert, Whitehill Collingham			
 Dwyka			Permian/ Carboniferous
 Floriskaal, Waaiport	Witteberg	Cape Supergroup	Devonian
 Witpoort			
 Weltevrede			
 Traka			
 Boplass	Ceres		
 Tra-Tra			
 Hex River			
 Swartkrans			
 Gamka			
 Gydo			
 Baviaanskloof	Table Mountain	Silurian	
 Kouga			
 Tchando			
 Cedarberg	Table Mountain	Odrovician	
 Peninsula			
 Sardinia Bay			
	Pre-Cape		Pre Cambrian

Table 3.1: Key to stratigraphic units used in the five regional transects in this chapter. For complete list of mapped units, and correlation between maps, see Enclosure 1.

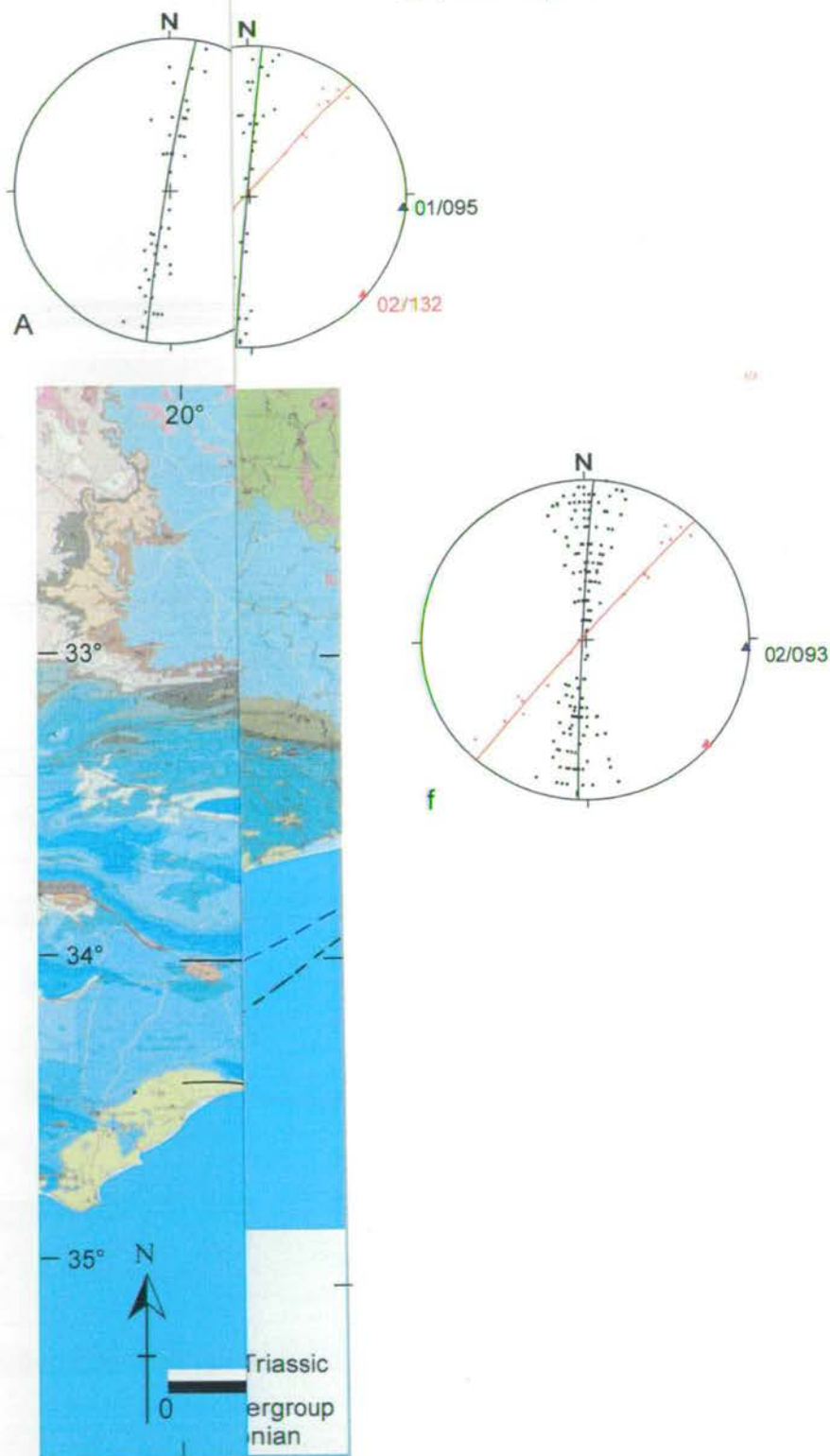


Figure 3.1: Geological structures are shown. The Mesozoic structures are shown by bedding from data used to construct a change in trend and data from the two

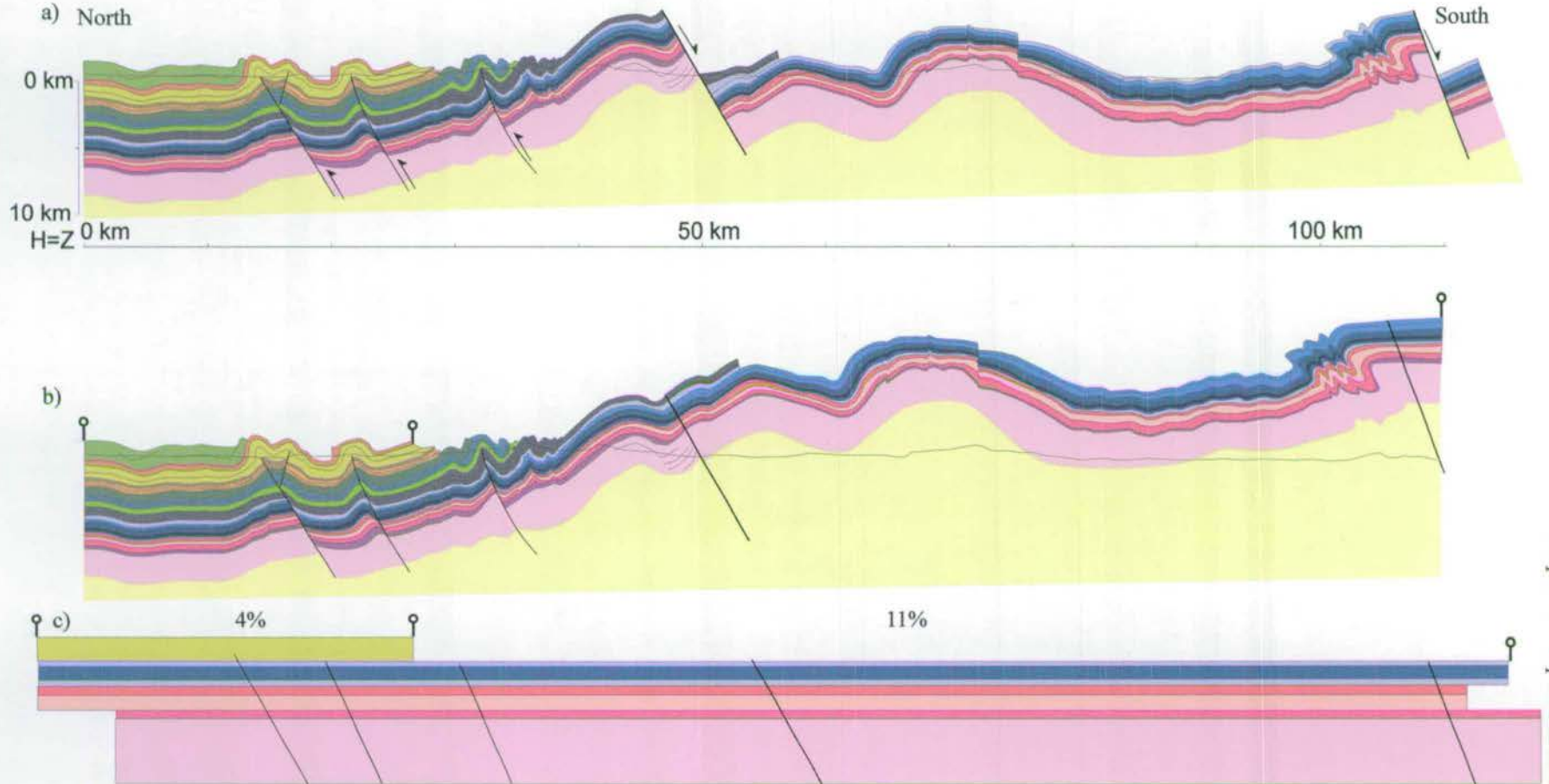


Figure 3.2 : a) Summary of Transect A (see Enclosure 2 for full transect and data). b) Transect A restored to pre-extension Cape Fold Belt geometry. c) Balanced restoration removing compressional deformation with tie-points and corresponding percentages of compression shown. The incomplete restoration of the section is discussed in the text. Faults have been approximately projected to depth as planar structures, although they may décolle (see text for discussion). See Table 3.1 for complete key.

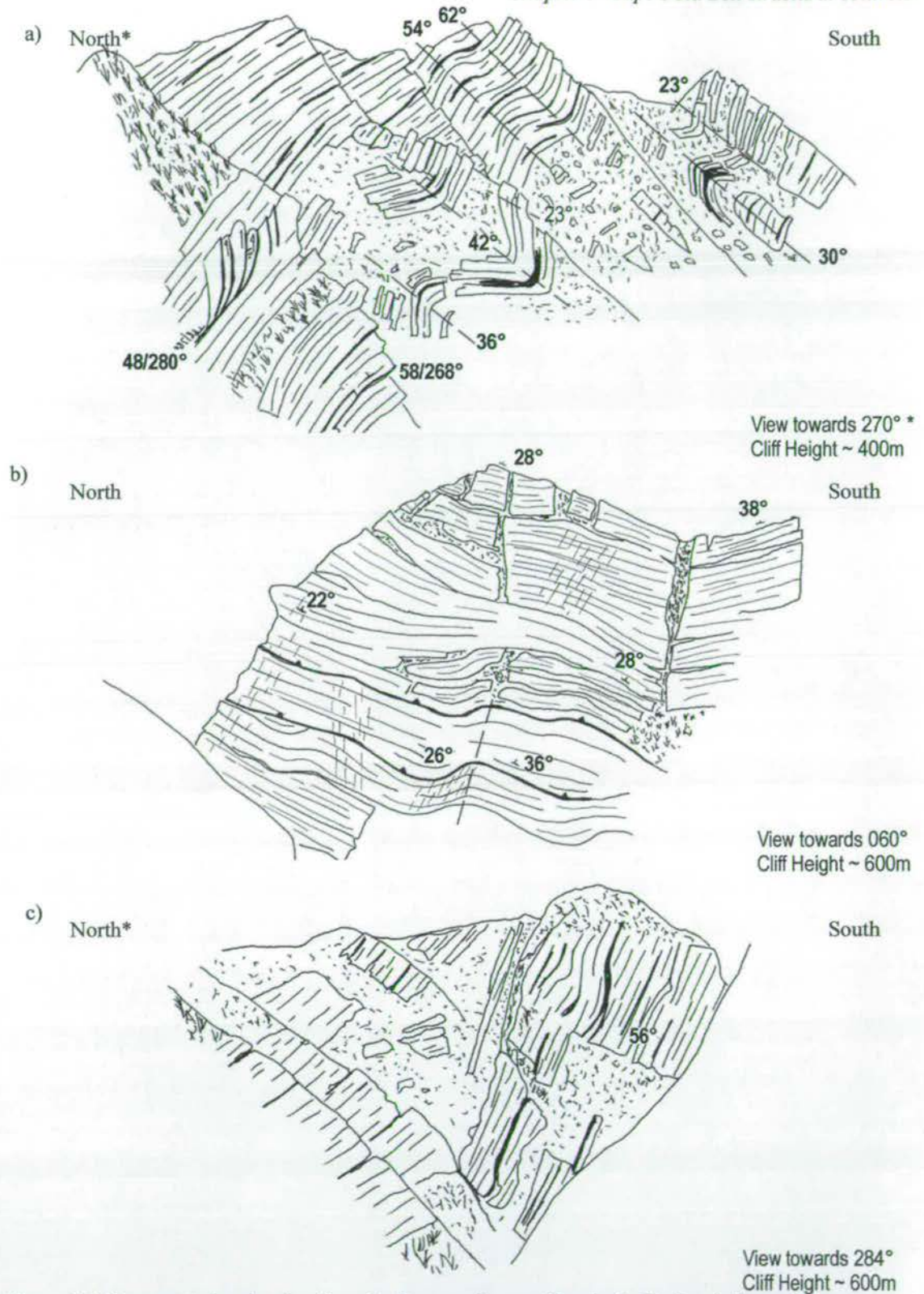


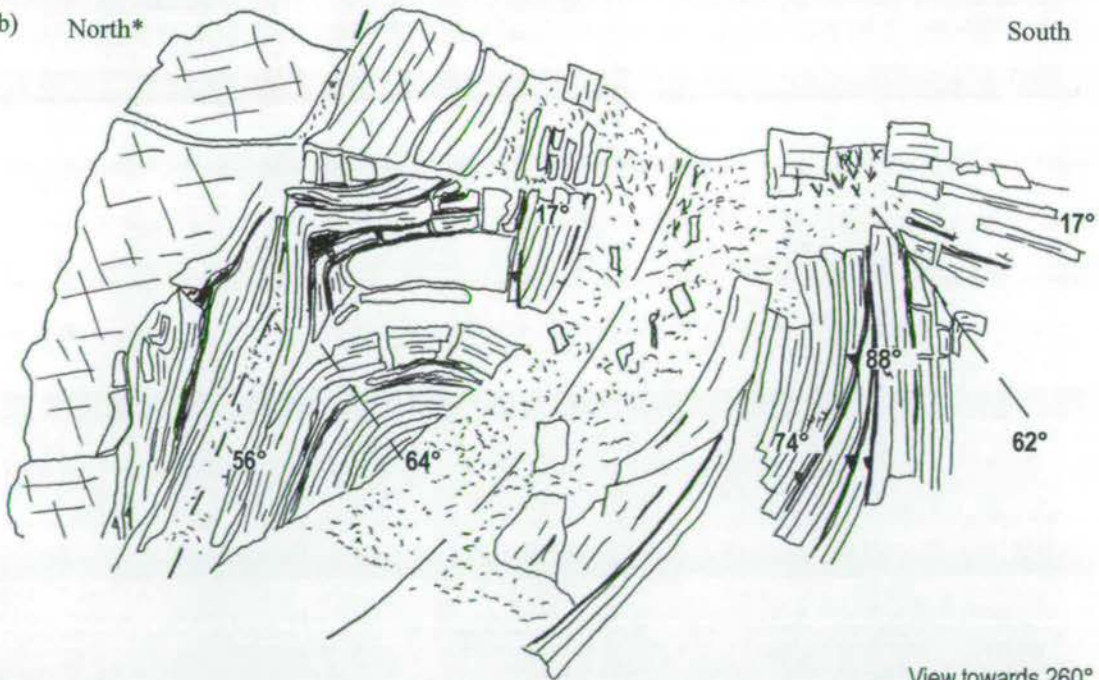
Figure 3.3: Representative sketches from the Seweweekspoort Pass in the Peninsula Formation outcrop at the north of Transect A. a) Northern end of transect - gentle folding with northern limb dipping towards the north; b) Middle - relatively little deformation and obvious bedding-parallel thrusts; c) Southern end - little deformation with open fold and southern limb dipping towards the north.* **The orientation of these sketches has been reversed so that north is consistently towards the left throughout this chapter.**

a) North



South

b) North*



View towards 260°
Cliff Height ~ 350m

Figure 3.4: An example from the Seweweekspoort Pass (Transect A) of later brittle deformation cross-cutting pre-existing folding. Age of the later faulting is unknown, although is possibly Mesozoic. See Enclosure 2 for position. * The orientation of these sketches has been reversed so that North is consistently towards the left throughout this chapter.

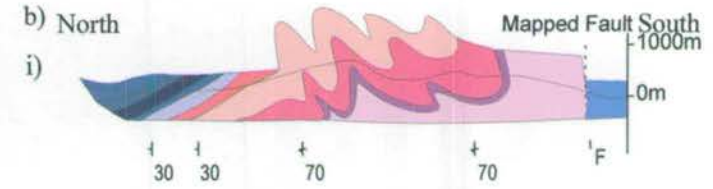
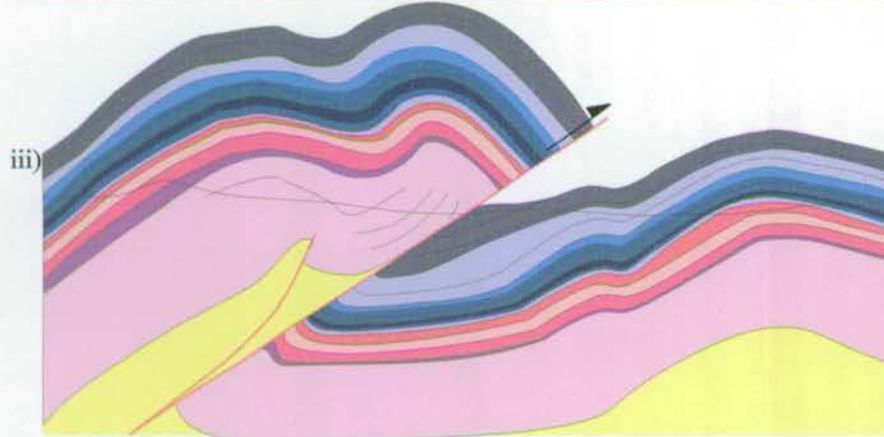
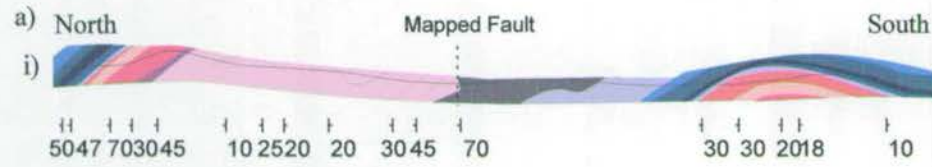


Figure 3.5: Two localities in Transect A have ambiguous fault geometries, a) is in the centre of the transect and b) at the south coast (see Transect A for locations). i) Map data, ii) south dipping normal fault, iii) north dipping reverse fault. In both instances the south dipping normal fault model is preferred, see text for discussion.

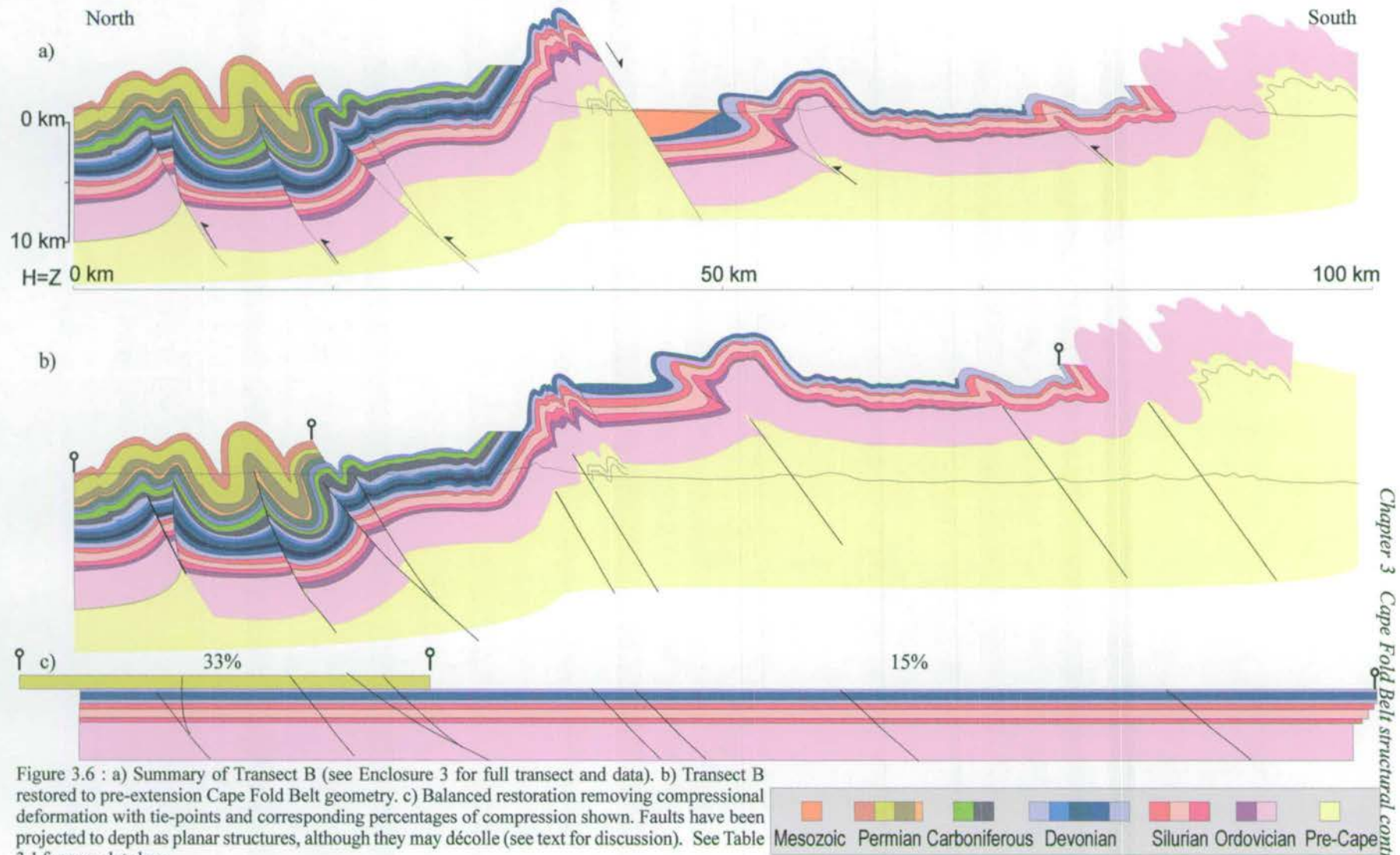
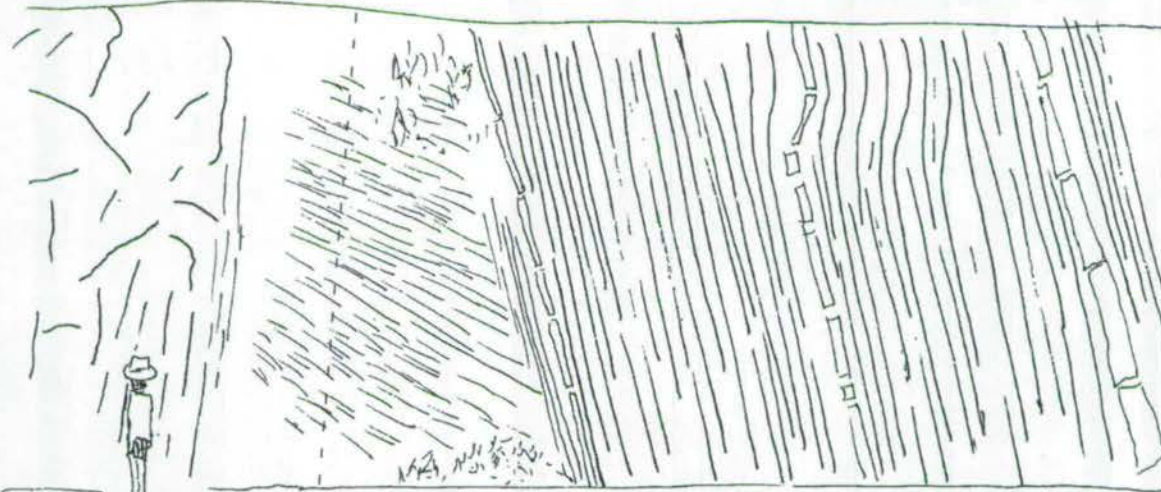


Figure 3.6 : a) Summary of Transect B (see Enclosure 3 for full transect and data). b) Transect B restored to pre-extension Cape Fold Belt geometry. c) Balanced restoration removing compressional deformation with tie-points and corresponding percentages of compression shown. Faults have been projected to depth as planar structures, although they may décolle (see text for discussion). See Table 3.1 for complete key.

North

South



Indurated siltstone

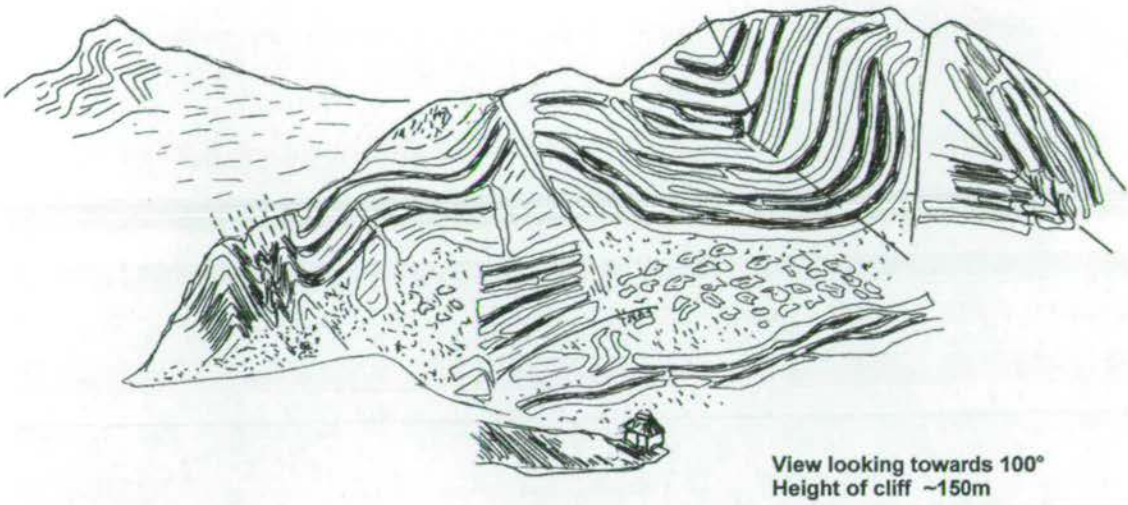
Black shale with strong cleavage evident cross-cutting high angle structure

5cm rhythmically bedded siltstone and interbeds of flakey fine sandstone (~1cm) Occasional sandstone beds of 50cm.

Figure 3.7 : Road cutting through the Whitehill Formation at the north of Transect B. Despite steep dip of bedding very little deformation except for strong south dipping cleavage. View looking East.

a) North

South



b) North*

South

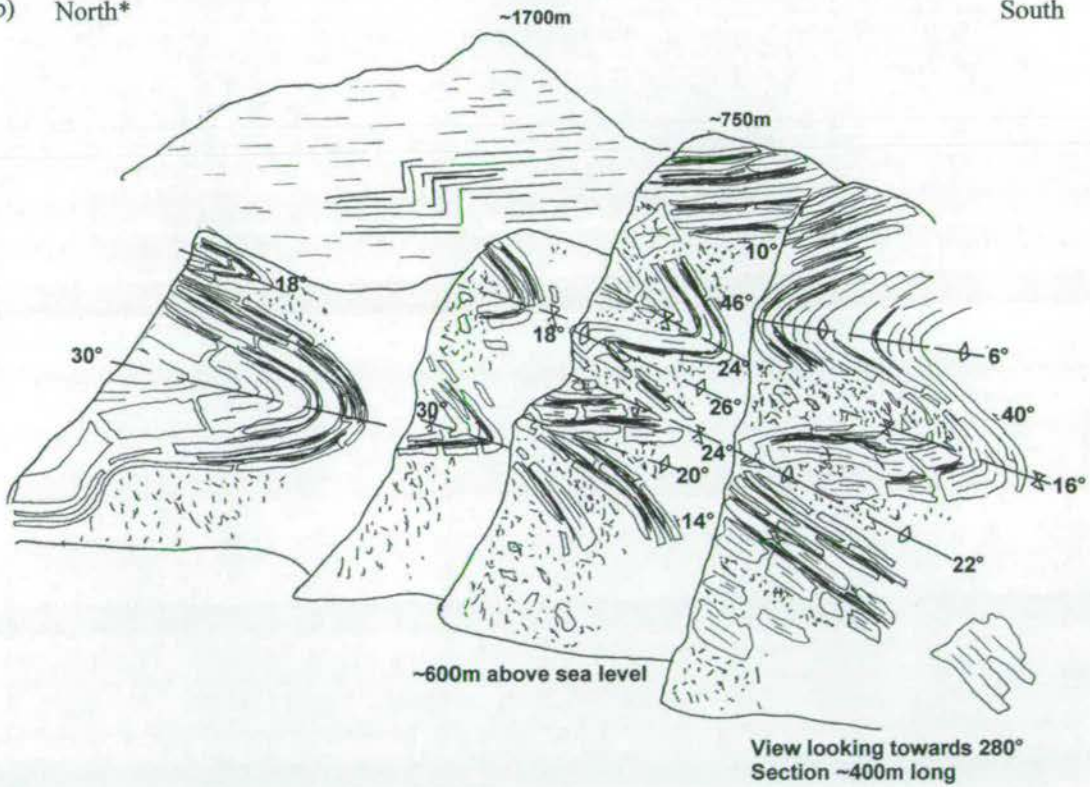


Figure 3.8 : Sketches from the Meeringspoort Pass (Positions shown on Transect B). a) a variety of deformation styles are present with high amplitude, short wavelength folding in the north and longer wavelength folds in the south. This section is also cross-cut by later brittle faults. b) Chevron folds showing consistent northward verging fold axial planes (data shown on sketches). * The orientation of this sketch has been reversed so that North is consistently towards the left throughout this Chapter.

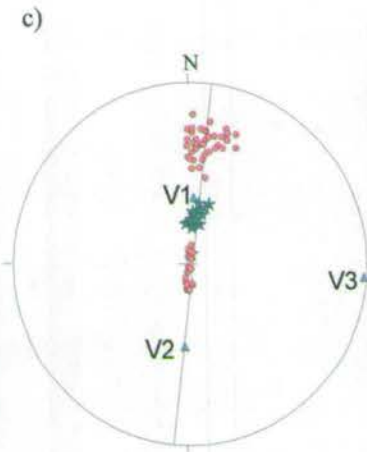
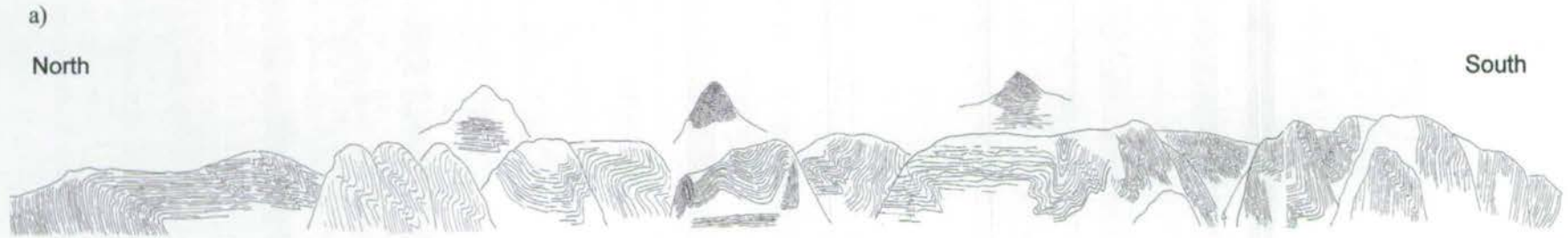


Figure 3.9: a) Summary section through the Meeringspoort Pass Transect B. See Enclosure 4 for position and Enclosure 4 for complete section. Section is approximately 8 km long and is perpendicular to the fold belt structural trend. b) Reverse faults utilising ~ 0.5m spaced bedding planes in Peninsula Formation quartzites. Reverse shear indicators are commonly present within interbedded siltstone. Such deformation is common throughout the fold belt. c) Stereonet of compiled field data from the Meeringspoort Pass showing poles to bedding (red dots; $n=80$), and measured fold axes (green stars, $n=30$). Blue triangles indicate eigenvectors calculated from bedding data ($V1=54$ to 006 ; $V2=35$ to 186 ; $V3=00.2$ to 096). This plot shows that despite variations in deformation styles, the data are consistent with an east-west trend and shallow plunging fold axes with a northward verging nature.

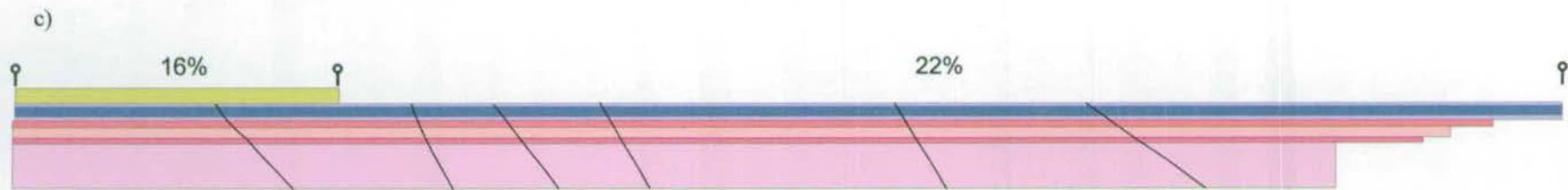
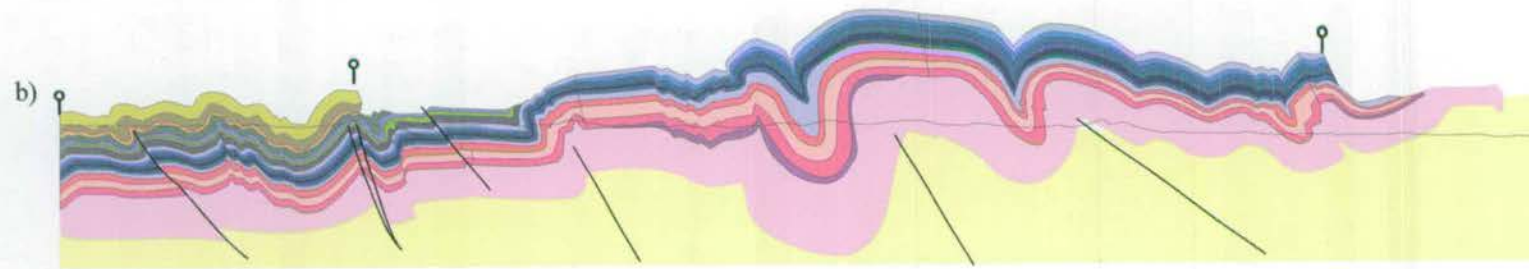
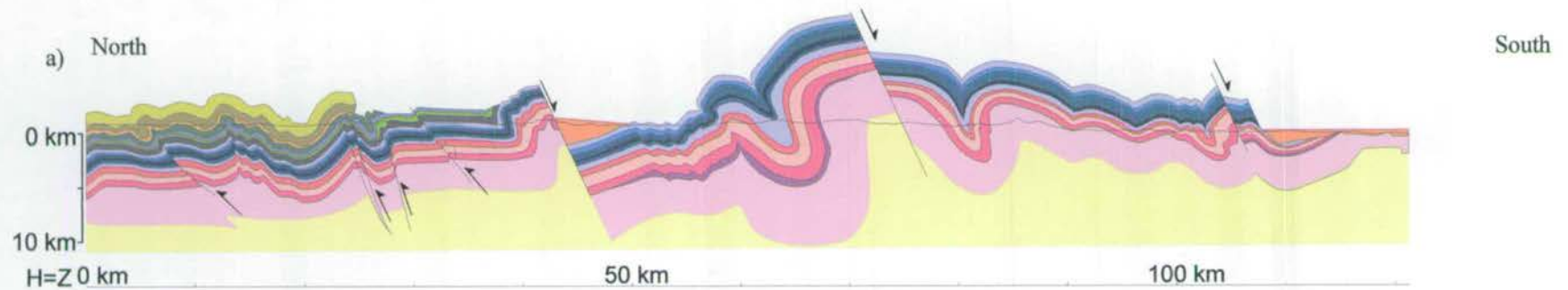


Figure 3.10 : a) Summary of Transect C (see Enclosure 54 for full transect and data). b) Transect C restored to pre-extension Cape Fold Belt geometry. b) Balanced restoration removing compressional deformation with tie-points and corresponding percentages of compression shown. Faults have been projected to depth as planar structures, although they may décolle (text for discussion). See Table 3.1 for complete key.



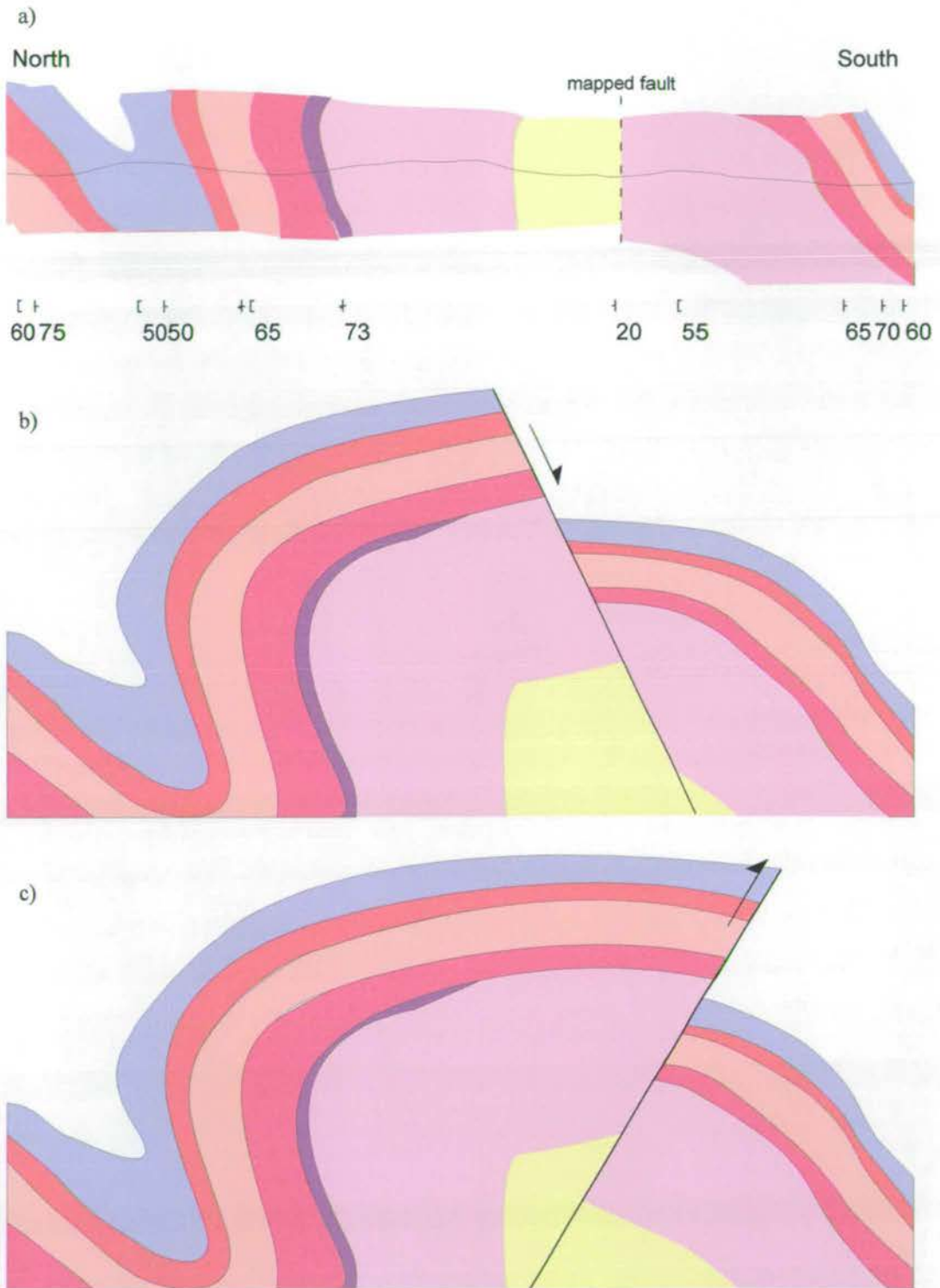


Figure 3.11 : Ambiguous geometry in centre of Transect C (see Enclosure 5 for position). Unknown type of fault that down-throws towards the south. a) Map data, b) south-dipping normal fault, c) north-dipping reverse fault. When compared with the complete transect, the normal fault geometry is preferred.

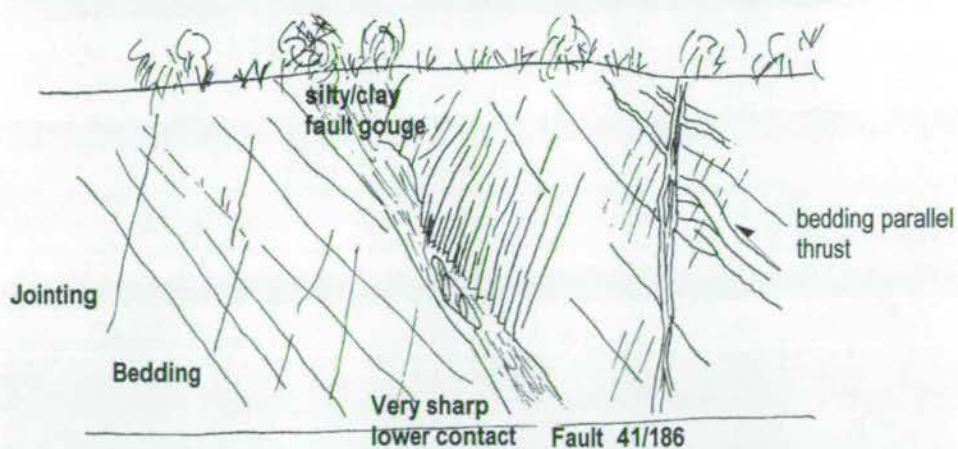
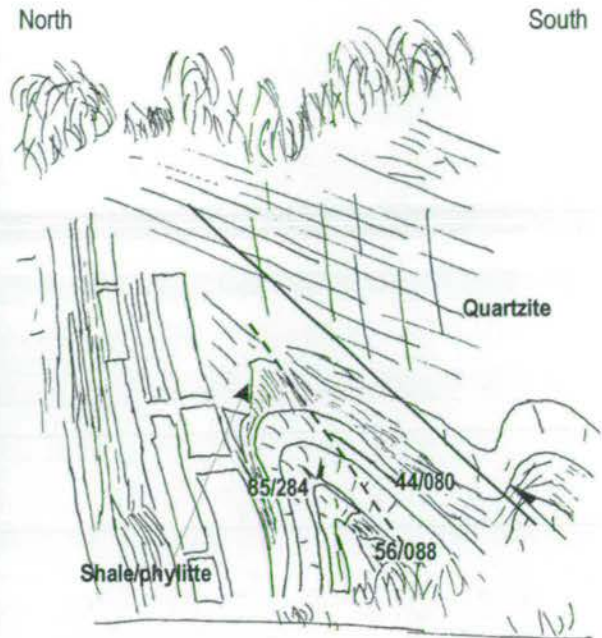


Figure 3.12 : Structures within the Peninsula Formation in Transect C, positions shown in Enclosure 5. a) Small scale kink folds (north verging). Notice similarity of structures compared to the much larger scale kink bands of Figure F, Enclosure 4. b) Outcrop is cross-cut by brittle fault.

a)



b)



Section 3.13 : a) Northward verging, tight fold which is dissected by a north verging thrust.
b) Southern coast of section showing sub-horizontal Mesozoic sediments unconformably on top of moderately south dipping Peninsula Formation quartzites. Height of cliff ~30m.

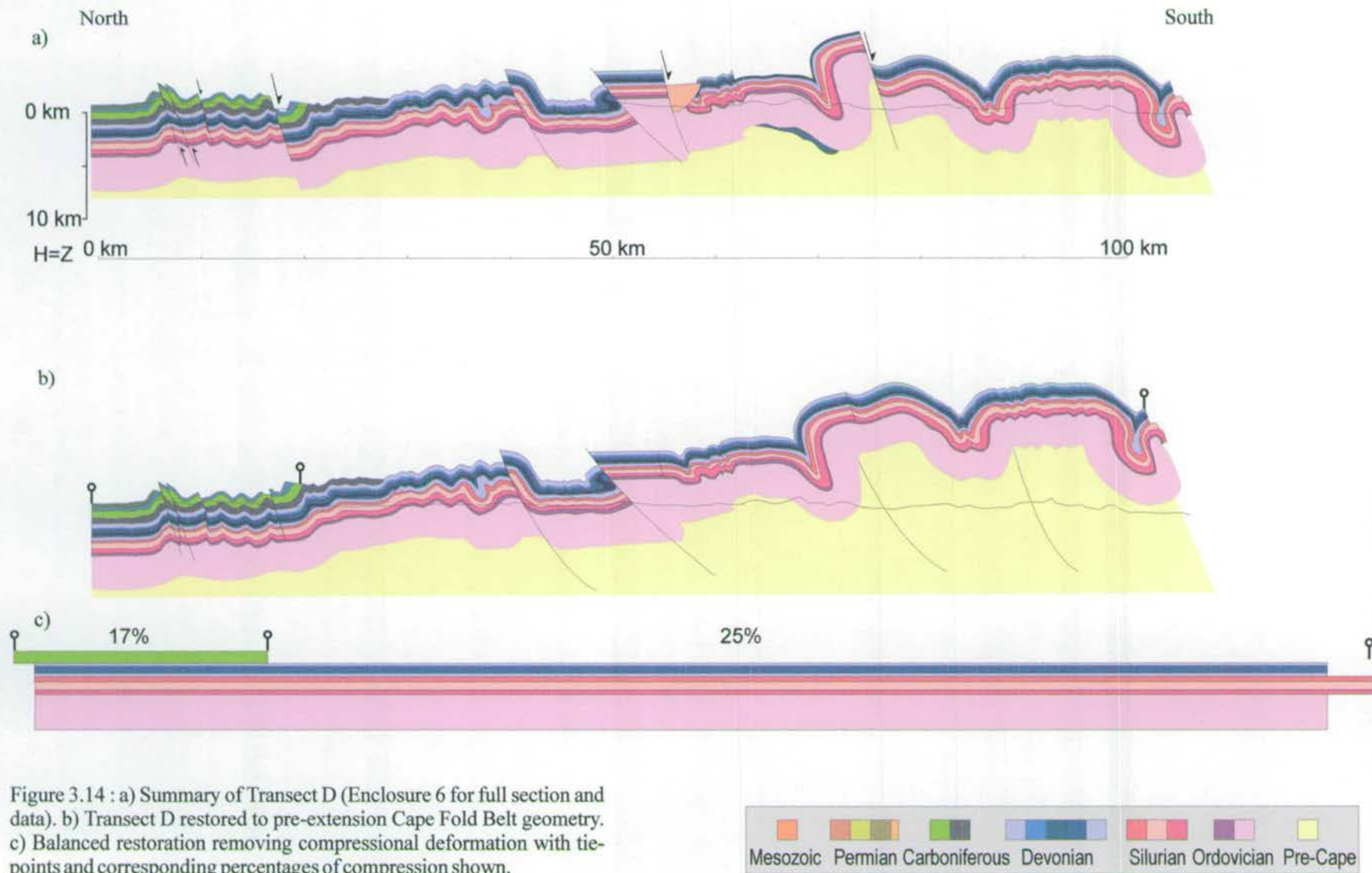
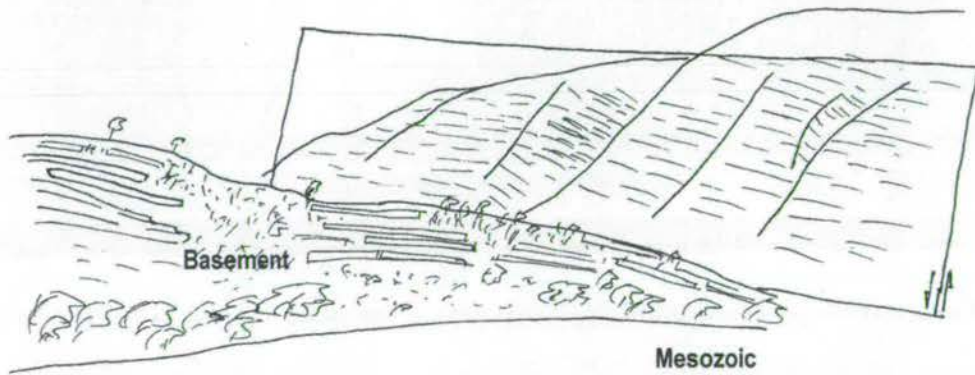


Figure 3.14 : a) Summary of Transect D (Enclosure 6 for full section and data). b) Transect D restored to pre-extension Cape Fold Belt geometry. c) Balanced restoration removing compressional deformation with tie-points and corresponding percentages of compression shown.

a)



b)

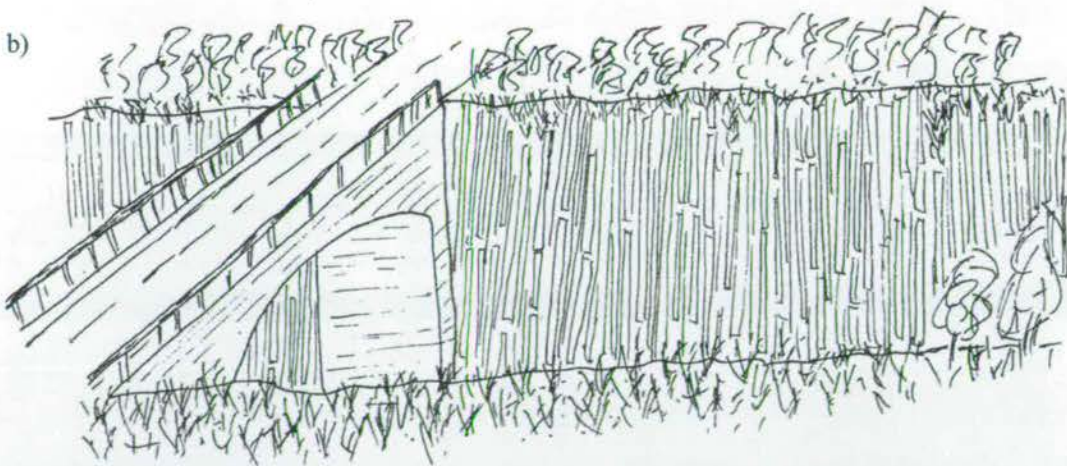


Figure 3.15: a) Normal fault at southern end of Transect D. View looking north-west showing Peninsula Formation faulted against itself in the background, and Mesozoic in the foreground. Height of cliff is ~ 40m.

b) River gorge at Storms River, 10 km East of section showing sub-vertical, undeformed Peninsula Formation; looking East.

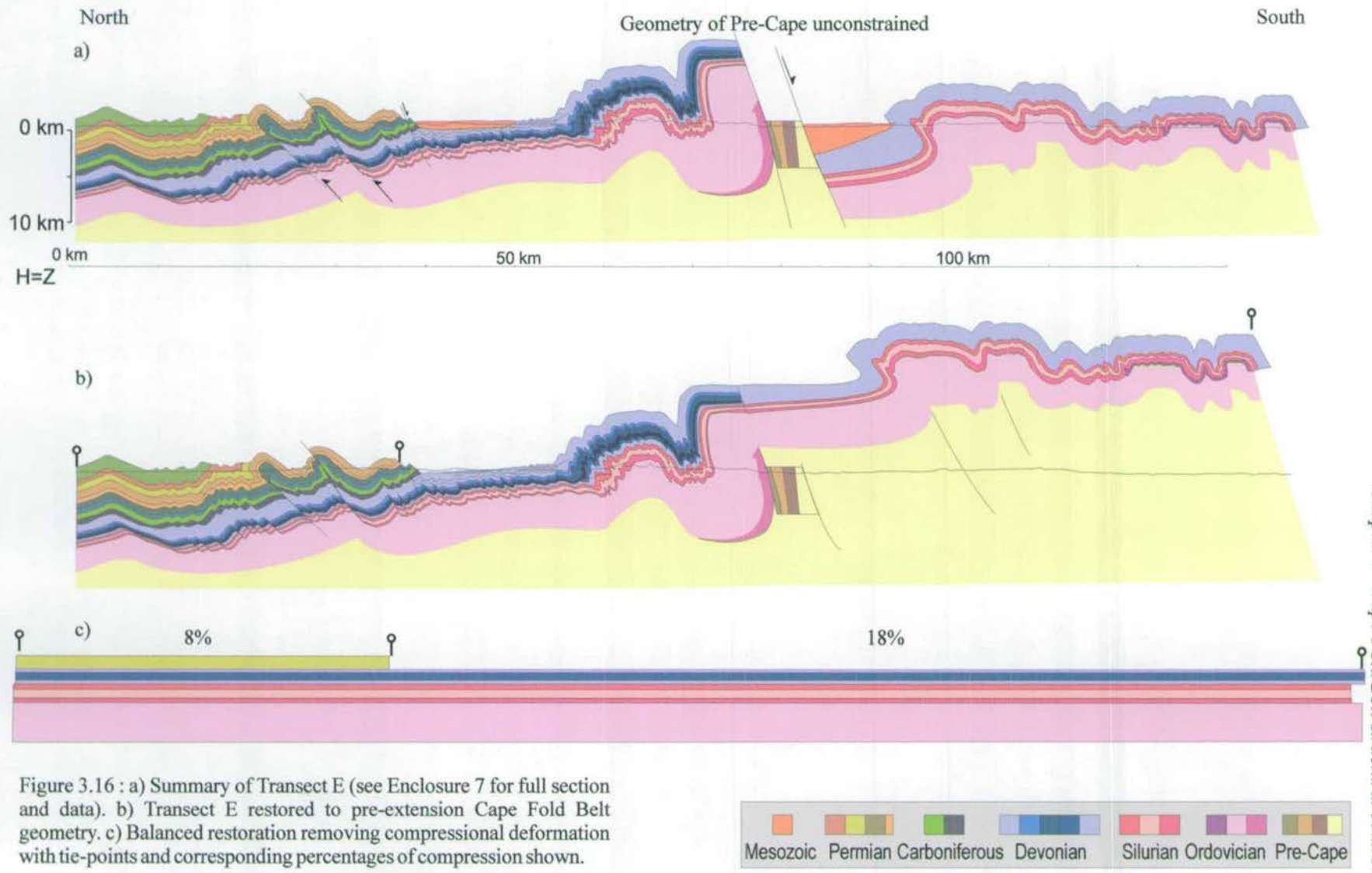


Figure 3.16 : a) Summary of Transect E (see Enclosure 7 for full section and data). b) Transect E restored to pre-extension Cape Fold Belt geometry. c) Balanced restoration removing compressional deformation with tie-points and corresponding percentages of compression shown.

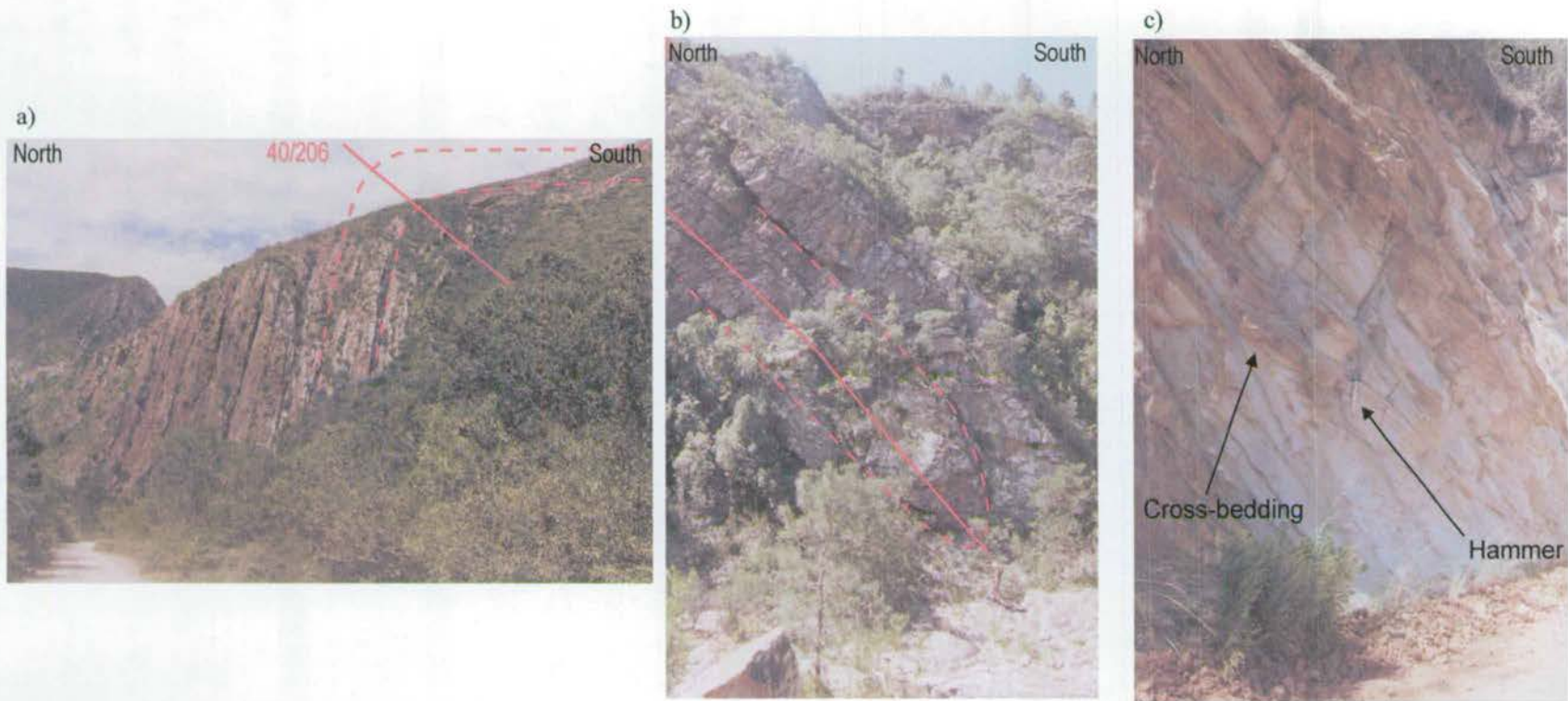


Figure 3.17: Photographs from the Gamtoos transect (Transect E). These structures are very similar to those observed in the Meeringspoort Pass (Transect b). a) Open, northward verging folds, height of cliff ~ 80m, b) isoclinal folding, height of cliff ~ 30m, c) overturned cross-bedding in the Pre-Cape unit, 30 cm hammer for scale.

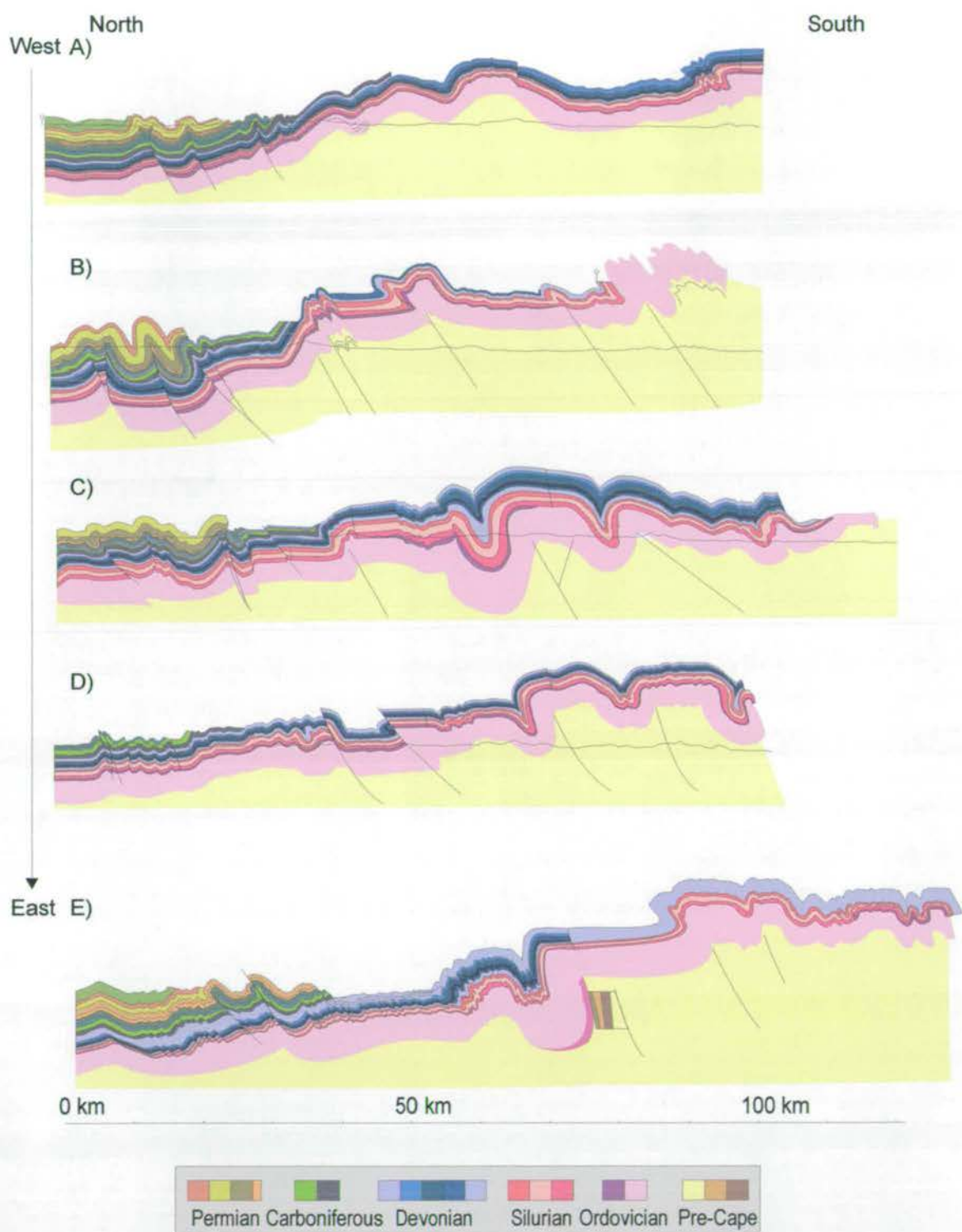


Figure 3.18 : Compilation of transects restored to pre-extensional foldbelt geometry. The important observation is deformation in the north is characterised by asymmetric, north verging folds, while the centre and south typically have anticlinal box folds.

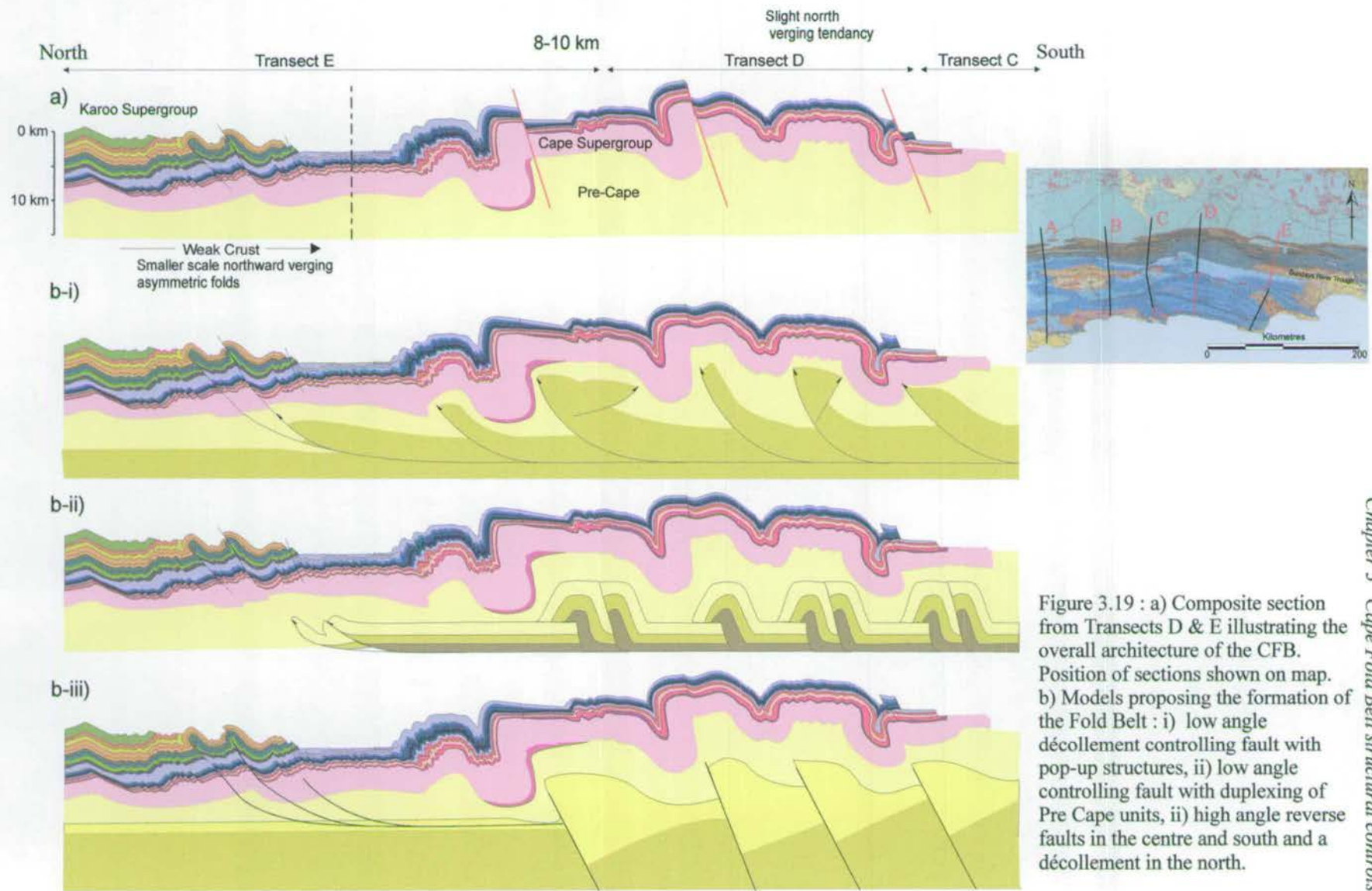


Figure 3.19 : a) Composite section from Transects D & E illustrating the overall architecture of the CFB. Position of sections shown on map. b) Models proposing the formation of the Fold Belt : i) low angle décollement controlling fault with pop-up structures, ii) low angle controlling fault with duplexing of Pre Cape units, ii) high angle reverse faults in the centre and south and a décollement in the north.

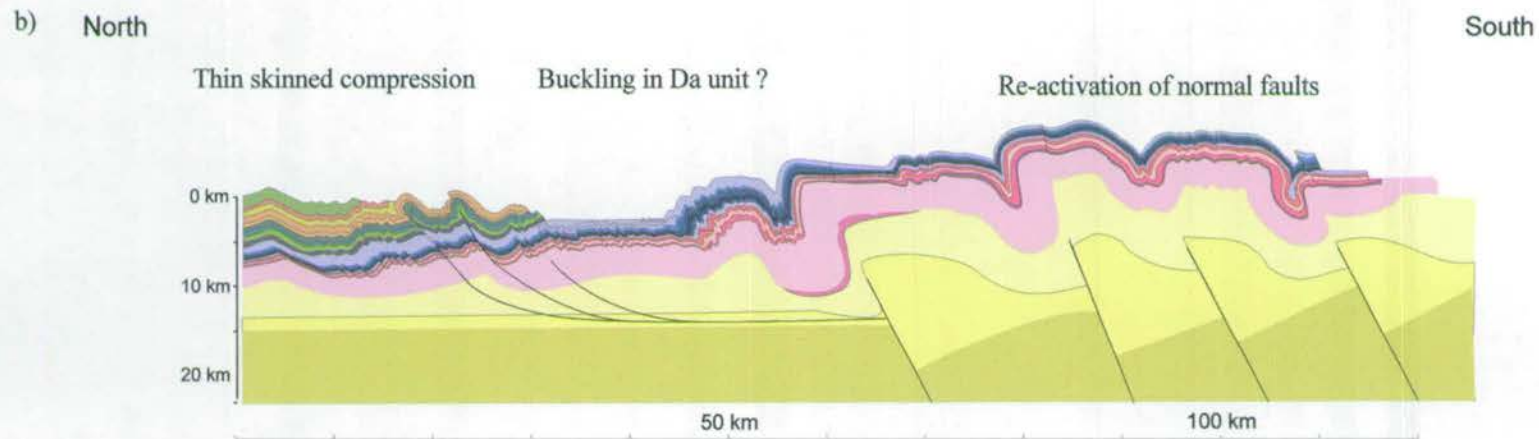
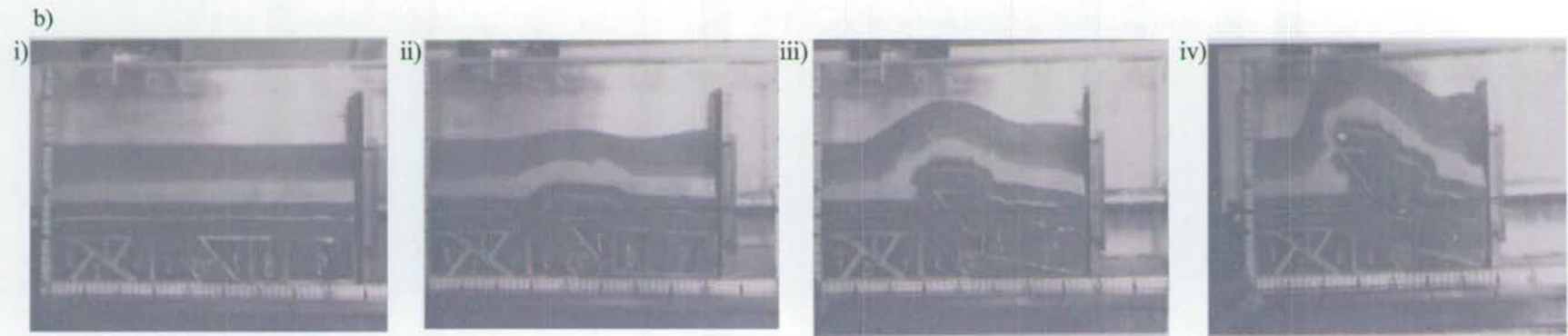


Figure 3.20 : a) i-iv : Sequential compression of sand box model with deformation being controlled by high angle basement faults (Hälbich & Swart, 1983). b) High angle faults in Figure 3.19 model (iii) are proposed to be pre-existing extensional structures (associated with a previous passive margin?) that are reactivated in compression during the Cape Orogeny. The passive margin may not have extended to the north of the sections, therefore compressional deformation is accommodated by thin skinned thrust tectonics. NB. scale is approximate.

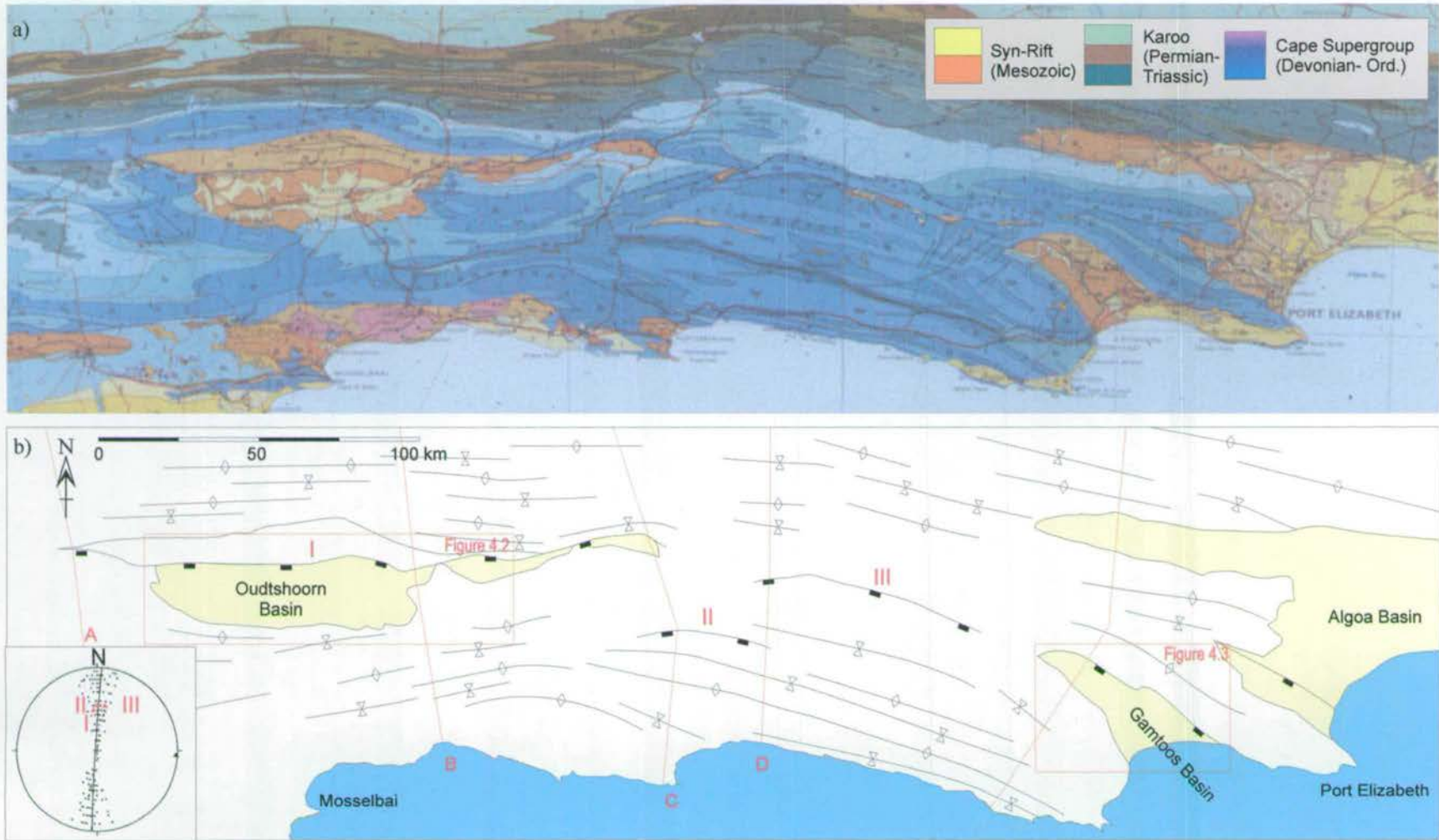
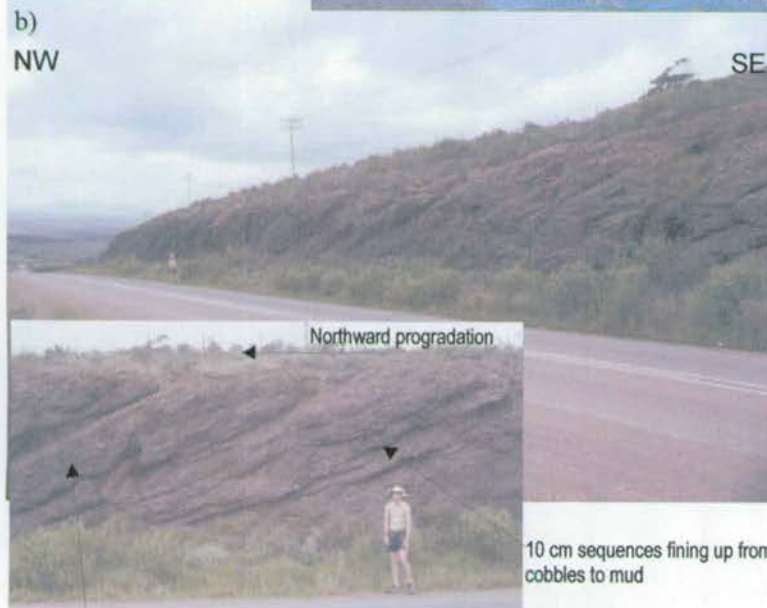
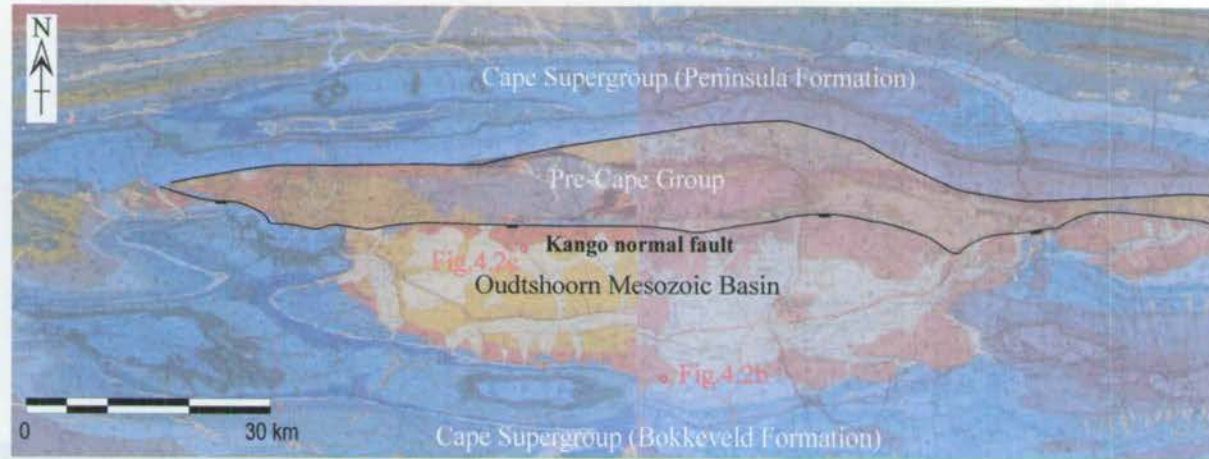


Figure 4.1 : a) Geological map of southern South Africa with the principal structural elements shown in the sketch map (b). Extensional faults are marked with rectangles on the down-thrown side, and extensional basins are yellow. All other lines correspond to compressional features. Stereonet of basement structures (Chapter 3) has the three extensional fault plotted. Position of transects (A-E) from Chapter 3 shown in red.



Red/purple clast-supported, poorly sorted conglomerate (1-30cm elongated clasts-indurated, finely laminated grey siltstone derived from Bokkeveld Formation?)

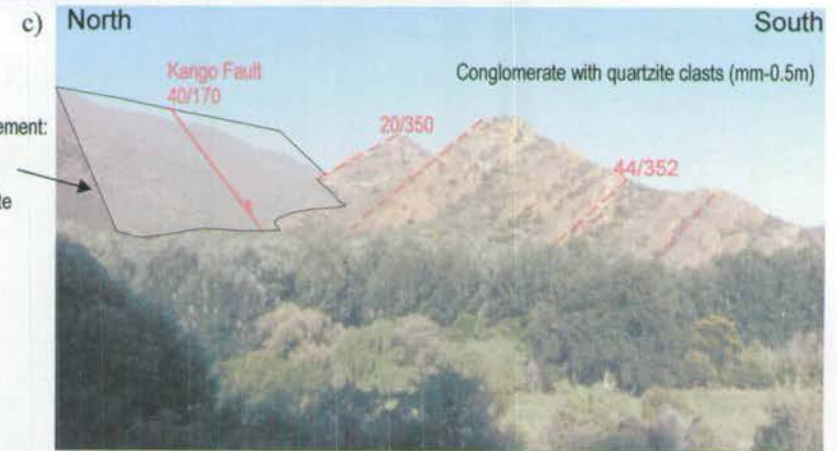


Figure 4.2 : Overview of the geology of the Oudtshoorn Basin (see Figure 4.1b for location). a) Geological map showing the position of the Mesozoic basin with respect to the outcrop of Pre-Cape and Cape Supergroup units. b) Southern flank of the basin, where Mesozoic sediments onlap onto the Cape Supergroup, shows foresets of northward prograding alluvial system. c) Near to the Kango Fault in the north. Syn-rift sediments dip and thicken northwards into the controlling fault (Redstone Hill Location). View to the east.

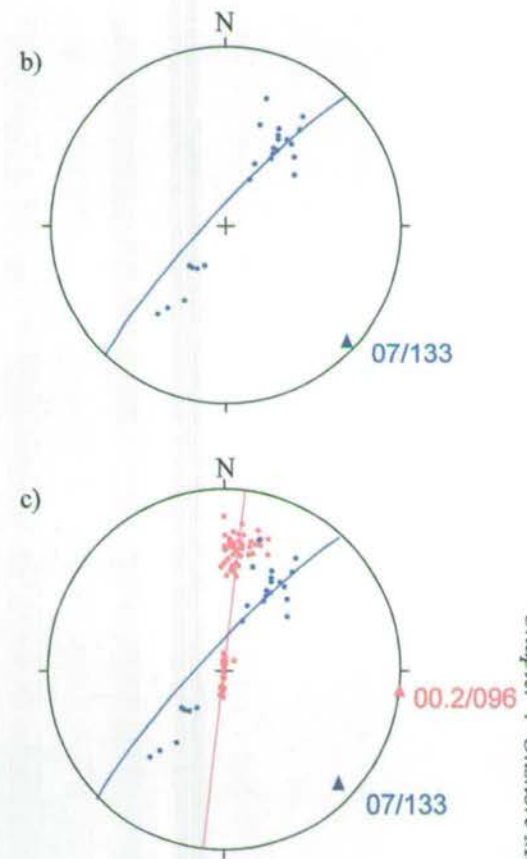
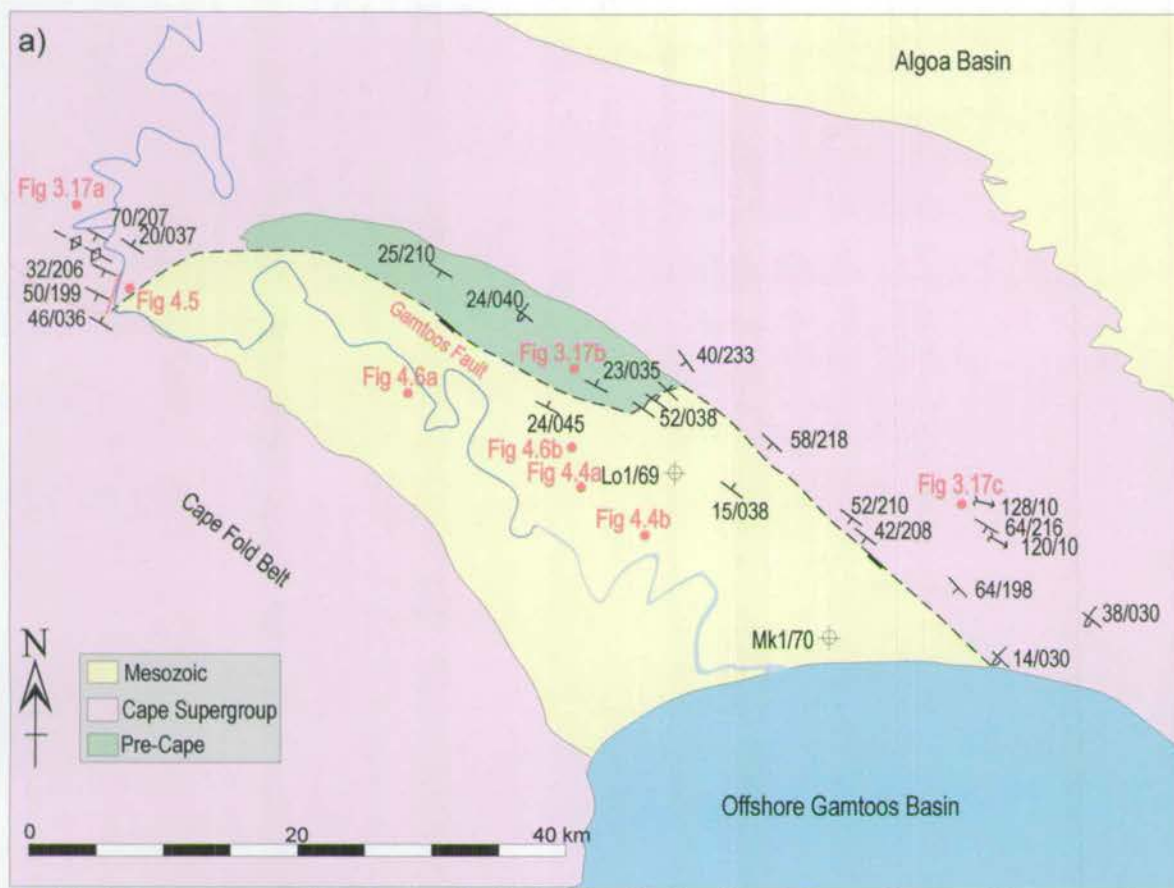
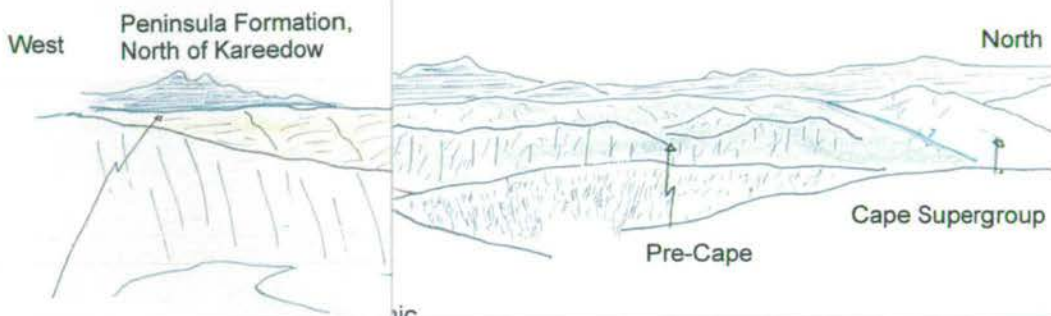
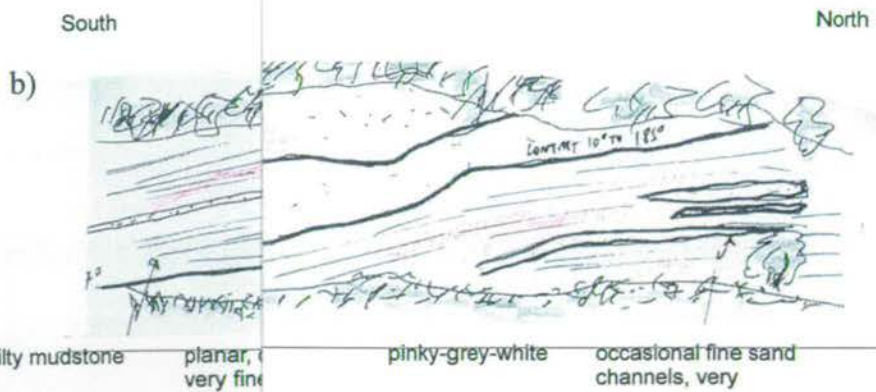


Figure 4.3: a) Structural map of the Gamtoos Basin also showing location of chapter figures and the two exploration wells Lo1/69 and Mk1/70. See Figure 4.1 for location. Note the Gamtoos Fault is parallel to the basement trend. b) Stereonet of pole to bedding from Gamtoos Basin. c) Comparison of structural data (including π -girdles) from Gamtoos Basin (blue) and Central Cape (red, data taken from Figure 3.9) show that there is a significant change in structural trend. Triangles show poles to π -girdles.



basement high

nic
os
c is
re-



pink/grey silty mudstone

planar, very fine

pinkish-grey-white

occasional fine sand channels, very

section ~50m long 4m high

Figure 4.4 : a) Overview of the contact between the Mesozoic and Pre-Cape units which is where the Gamtoos Fault occurs. Panoramic view of the contact.

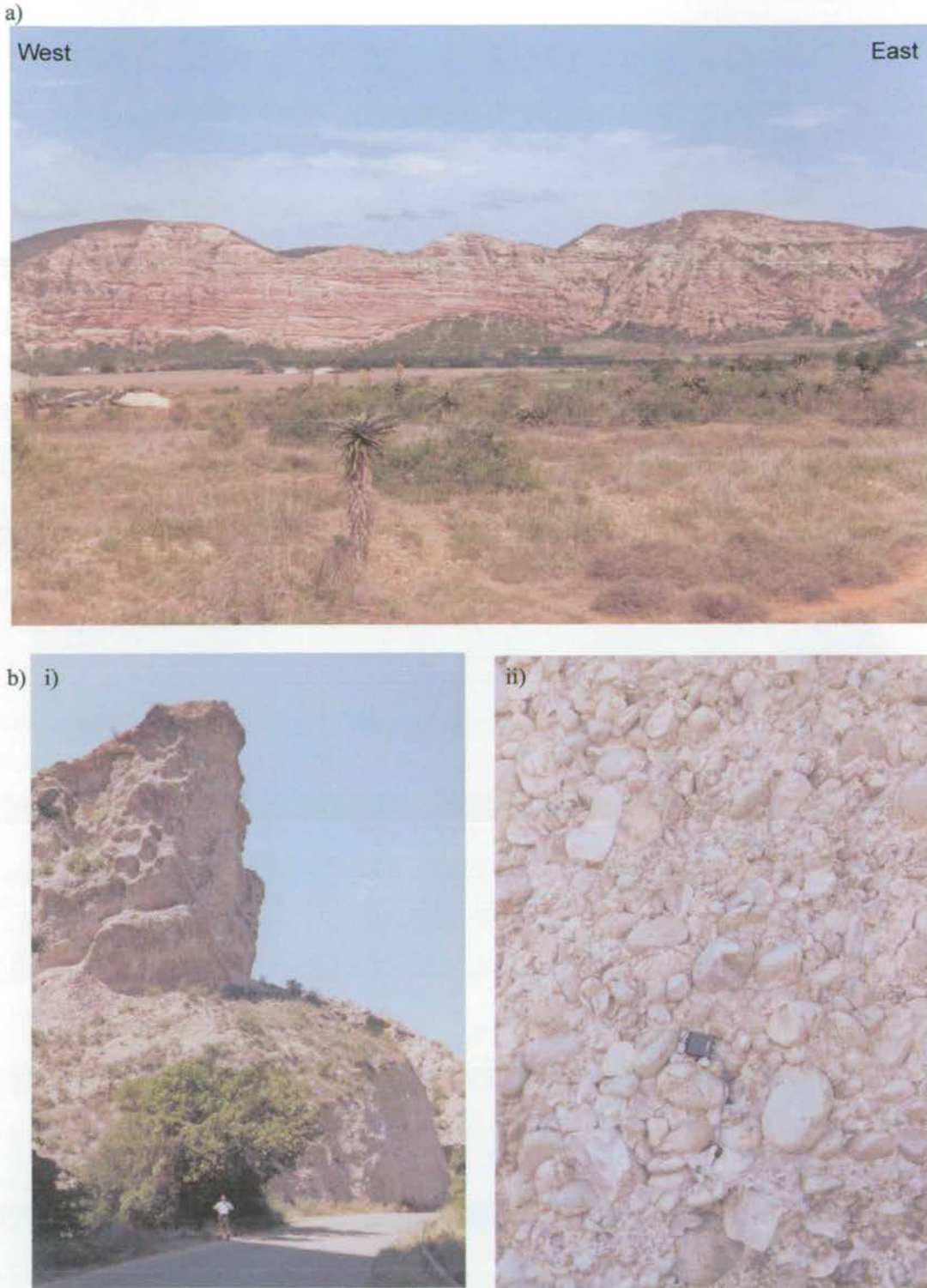
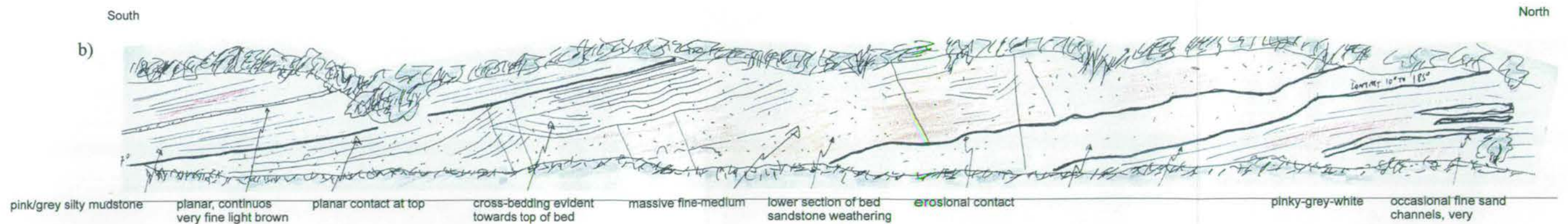
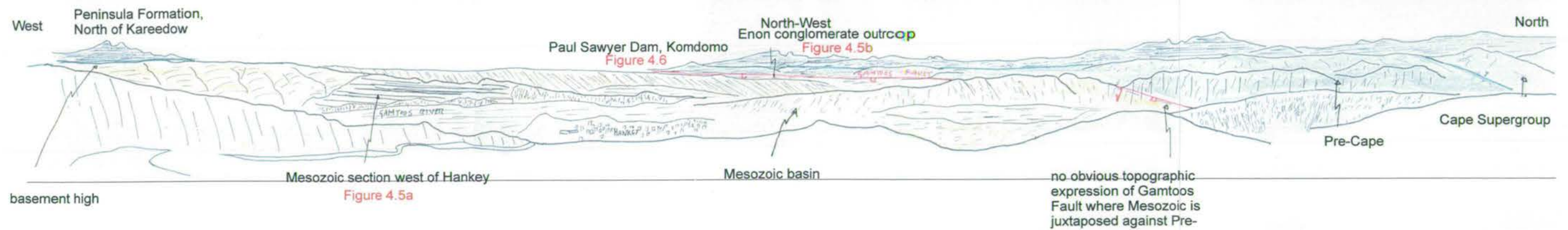


Figure 4.5 : Examples of syn-rift sedimentation in the Gamtoos Basin. See Figure 4.3 & 4.4 for locations. a) Cliff section west of Hankey showing undeformed Kirkwood Formation - fluvial sandstone interbedded with bentonites and overbank silts (Dingle *et al.*, 1983). Cliff ~30m high, 250m long. b i) Large Enon conglomerate outcrop in the north-west of the basin. Cliff ~30m high. ii) The Enon is a very mature, polymodal quartz conglomerate containing boulders up to 1-2m diameter, all well rounded and frequently fractured. Matrix is quartz sandstone with occasional blocks of silt and sandstone.



section ~50m long 4m high

Figure 4.4 : a) Overview of the north-west section of the Gamtoos Basin from a viewpoint 5 km south-east of Hankey. Of particular importance is the very poorly exposed nature of the contact between the Mesozoic and Pre-Cape units which is where the Gamtoos Fault occurs. Panorama is approximately 25 km across. b) Sketch of road-cutting section through part of the Mesozoic syn-rift basin fill, 10 km north-west of Hankey.

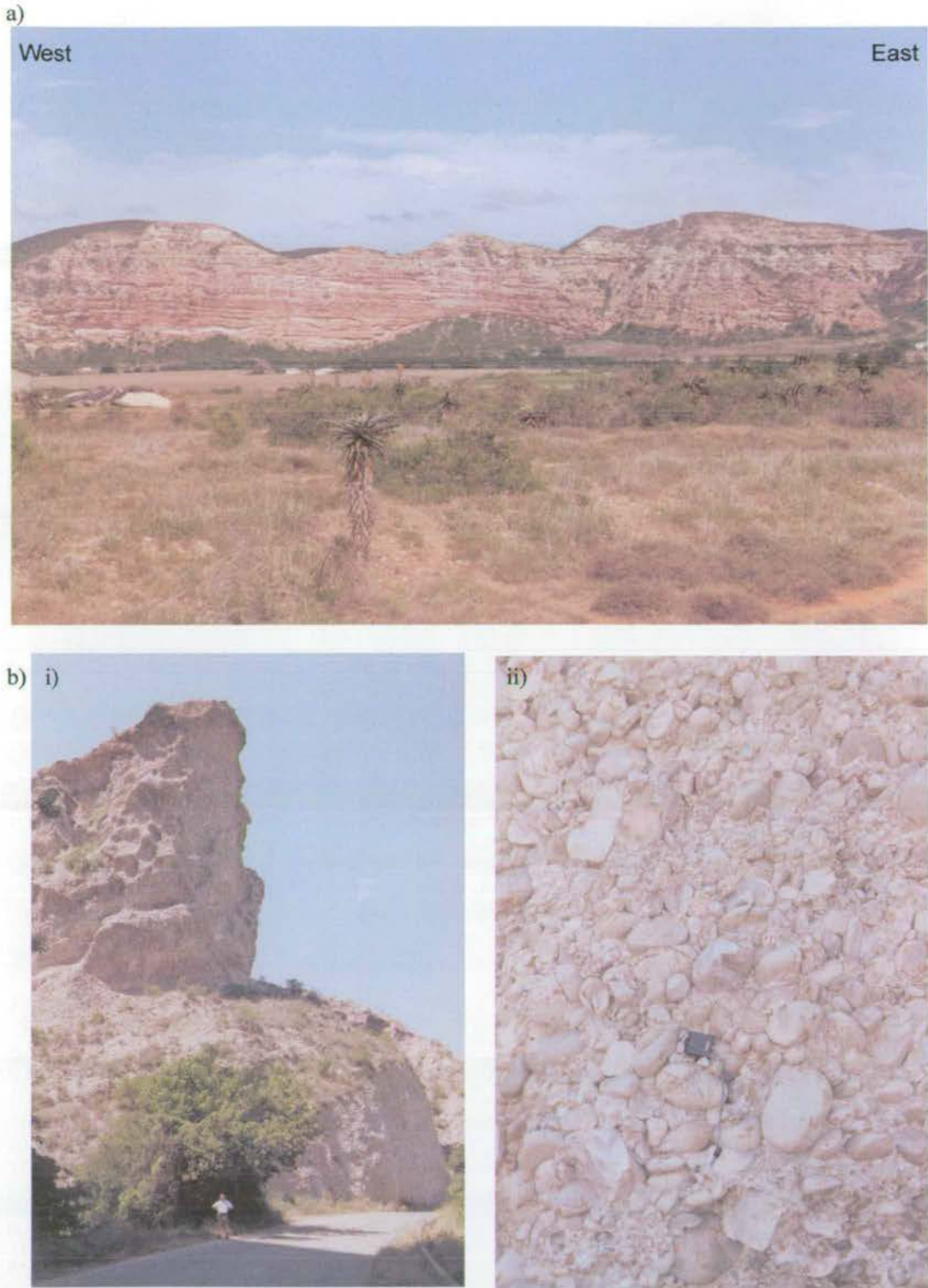
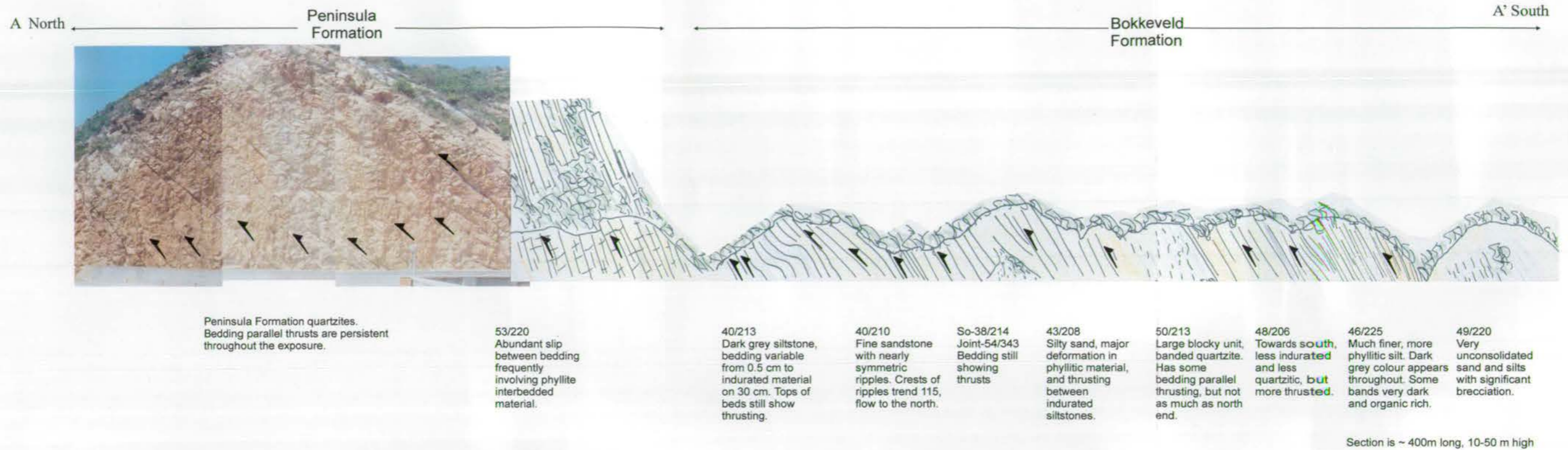
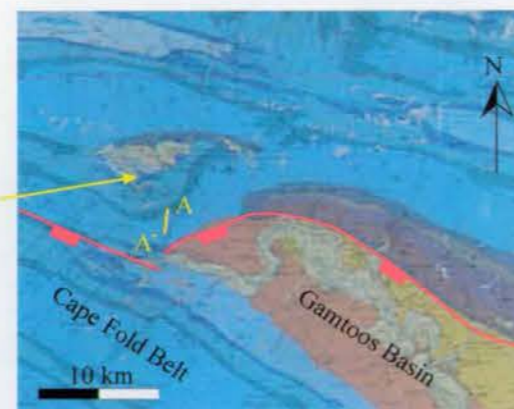


Figure 4.5 : Examples of syn-rift sedimentation in the Gamtoos Basin. See Figure 4.3 & 4.4 for locations. a) Cliff section west of Hankey showing undeformed Kirkwood Formation - fluvial sandstone interbedded with bentonites and overbank silts (Dingle *et al.*, 1983). Cliff ~30m high, 250m long. b i) Large Enon conglomerate outcrop in the north-west of the basin. Cliff ~30m high. ii) The Enon is a very mature, polymodal quartz conglomerate containing boulders up to 1-2m diameter, all well rounded and frequently fractured. Matrix is quartz sandstone with occasional blocks of silt and sandstone.



No evidence of extensional deformation in section. If strain was dissipated would evidence of extension, hence inferred that strain is localised on NE-SW trending Gamtoos Fault.



Gamtoos Fault

Figure 4.6a : Outcrop of Peninsula Formation at the Paul Sawyer Dam, Komdomo that is due west of NE--SW trending section of the Gamtoos Fault (b).. Despite the proximity to the Gamtoos Fault there is no evidence of extensional structures, see text for discussion. In the north the principal features are 0.5 -1m scale quartzite beds with parallel and shallowly cross-cutting thrust faults. To the south there are pervasive thrust and no kinematic indicators of extension. See Figure 4.3 for position of map.

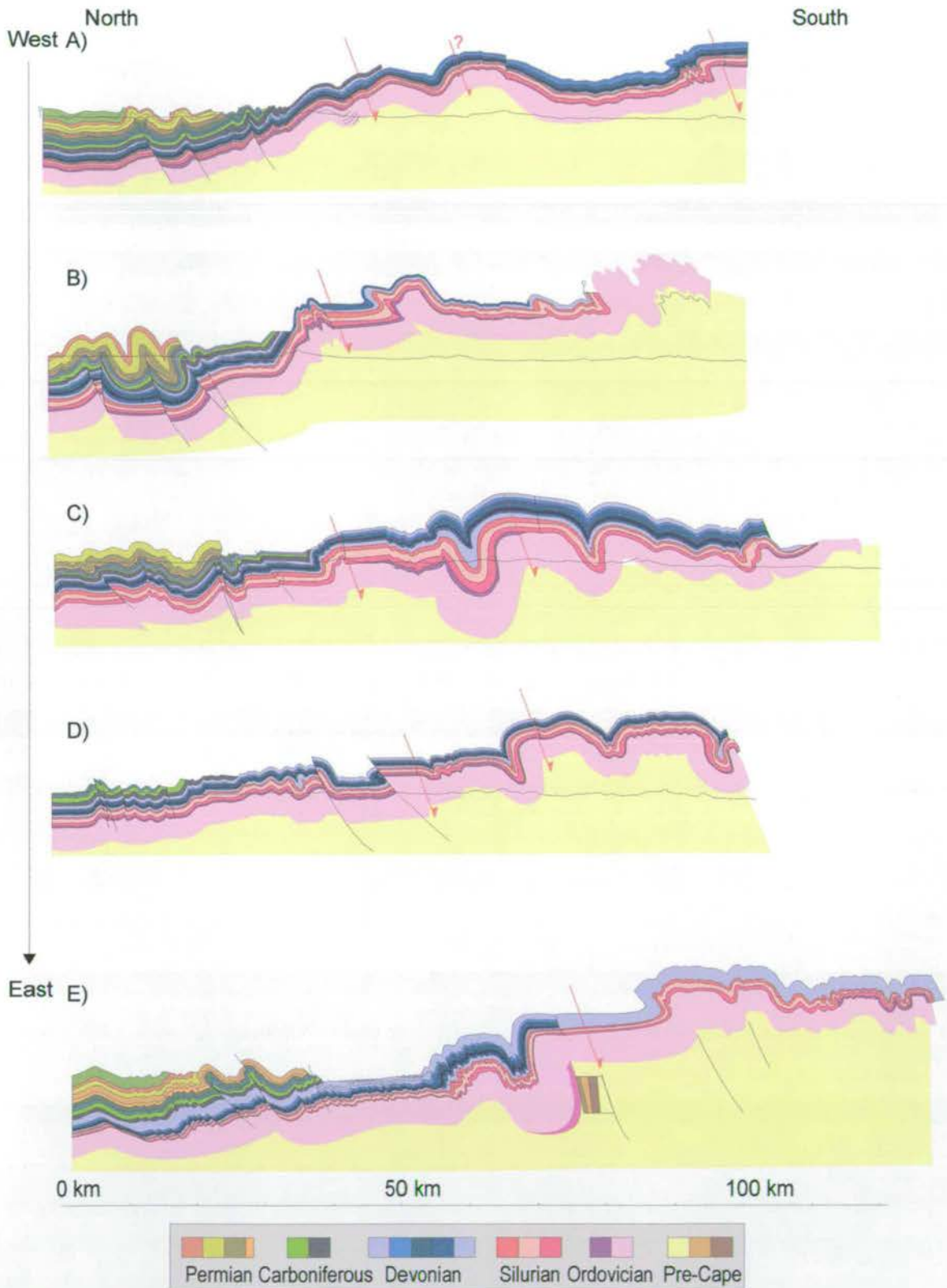


Figure 4.7 : Compilation of transects restored to pre-extensional foldbelt geometry from Figure 3.18 with the position of Mesozoic extensional faults (red) superimposed. Extension consistently occurs at the northern end of the anticlinal box fold flats..

North

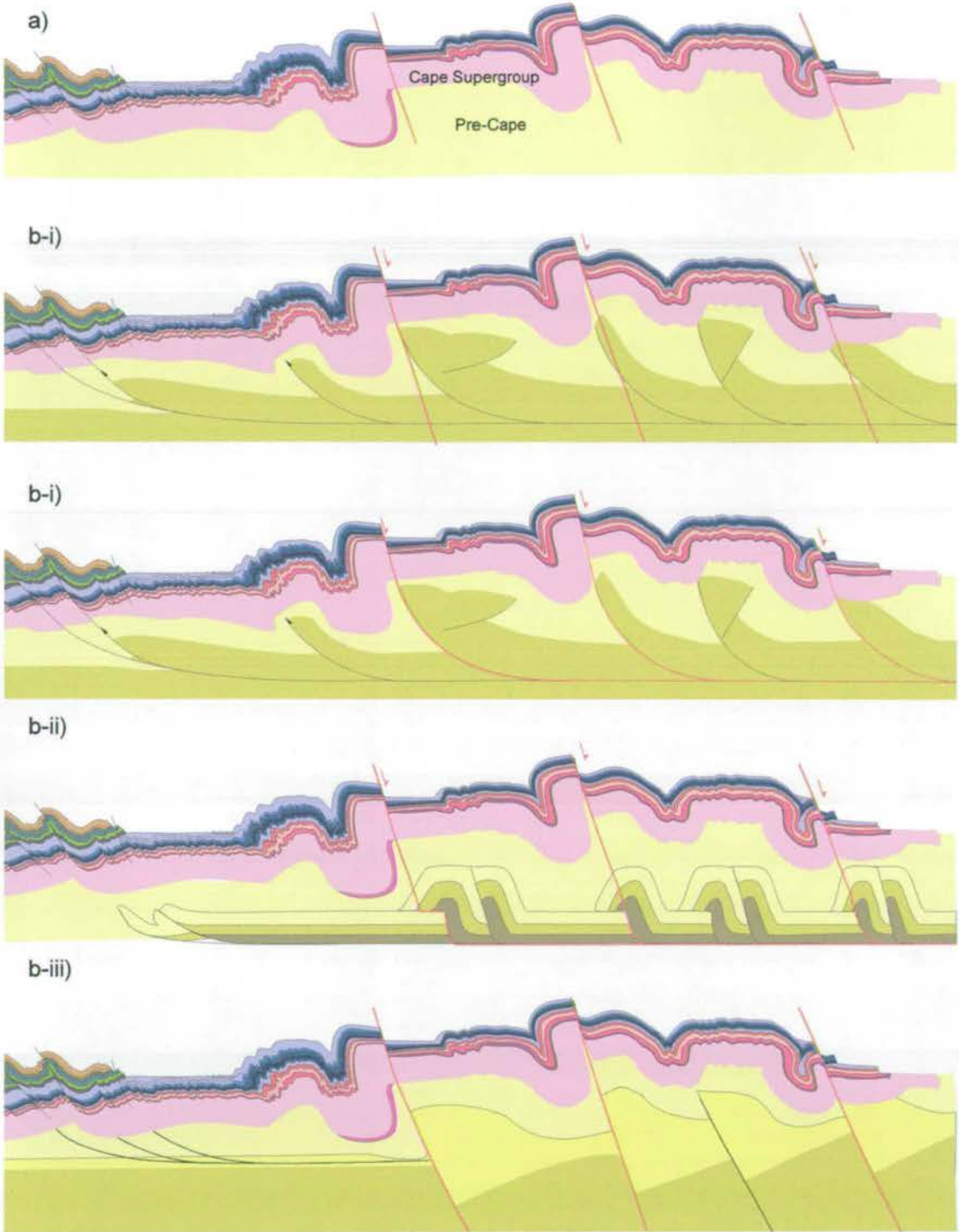


Figure 4.8 : a) Summary of the observations from the transects across the Cape Fold Belt (Figure 3.19) with the location of the Mesozoic extension superimposed. b) Model in which there is no structural control at depth. c) i) Low angle controlling fault with pop-up in which the southern faults are reactivated, ii) reactivation of ramp and flat thrust geometries in extension, iii) reactivation of high angle reverse faults.

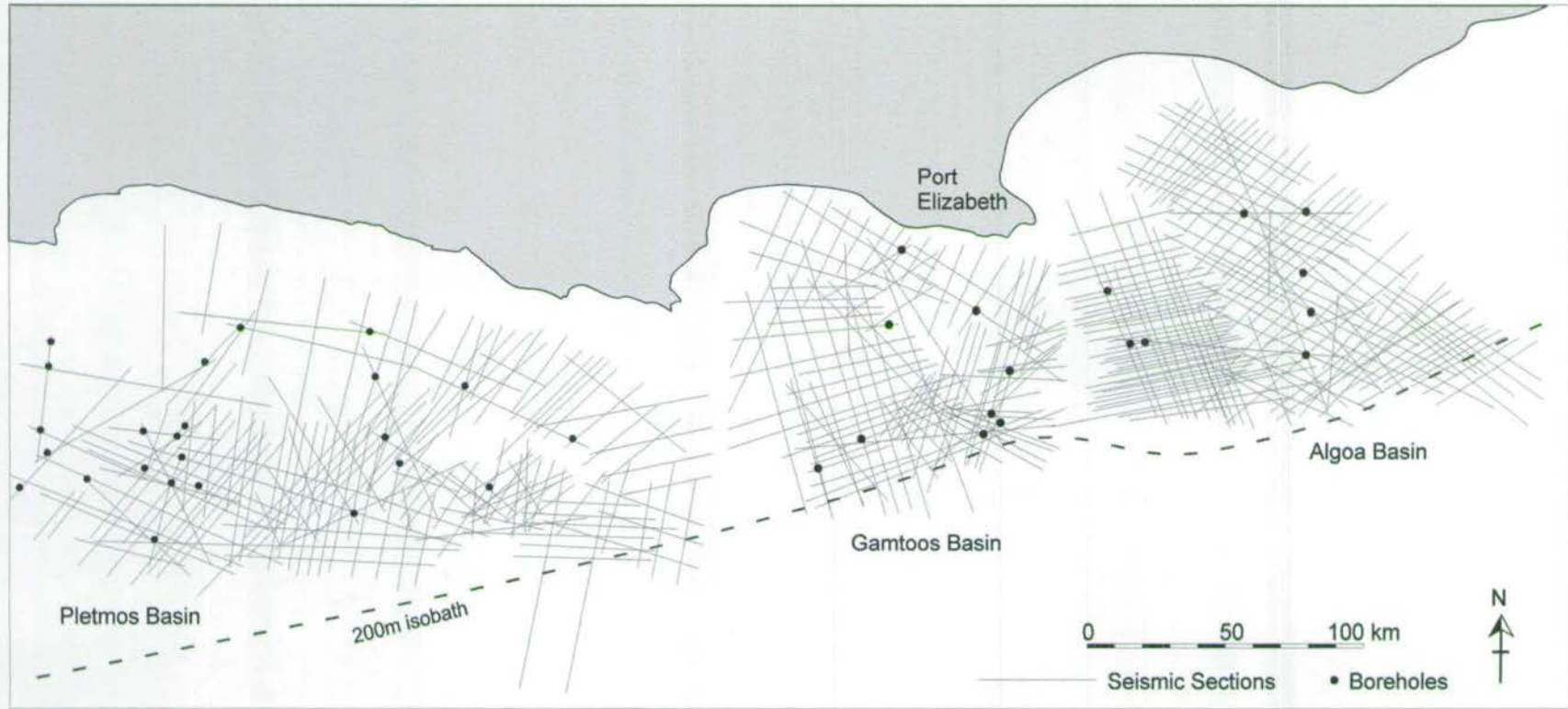


Figure 5.1: Seismic array and borehole utilised in this study to evaluate the Pletmos, Gamtoos and Algoa Basins. The data set consists of 18,000 km of 2-D seismic data and 41 wells.

	Seismic Array	High Filter (Hz)	Low Filter (Hz)
Pletmos Basin	Ga 79	62	8
	Ga 81	64	5
	Ga 82	64	5.3
	Ga 84	64	5.3
	Ga 85	180	5
	Ga 86	154	4
	Ga 87	250	3
	Ga 88	188	8
	Ga 89	218	8
	Ga 90	218	8
	Ga 91	218	8
Pletmos Basin	Gb 81	64	5
	Gb 82	64	5.3
	Gb 83	64	5.0
	Gb 84	64	5.3
	Gb 85	180	5.5
	Gb 87	250	3
	Gb 89	218	8
	Gb 91	102	8
Gamtoos Basin	Ha 76	62	8
	Ha 82	90	3
	Ha 83	64	5
	Ha 85	250	3
	Ha 87	64	5
Algoa Basin	Hb 75	62	12
	Hb76	62	8
	Hb 83	64	5
	Hb 84	64	5
	Hb 85	180	5
	Hb 86	154	4
	Hb 89	218	8

Table 5.1: The various vintages of 2D seismic arrays are shown for the three basins that are studied. Acquisition frequency data are also shown, and discussed in text with respect to seismic resolution.

		Age ¹	Mega-sequence	Pletmos	Gamtoos	Algoa
TERTIARY	Pliocene					
	Miocene					
	Oligocene					
	Eocene					
	Paleocene					
UPPER CRETACEOUS	Maastrichtian	65	POST-RIFT			— <i>top_late-mass.</i>
	Campanian	71				
	Santonian	83				
	Coniacian	85				
	Turonian	89		— <i>top_early-tur.</i>	— <i>top_early-tur.</i>	
	Cenomanian	93		— <i>top_early-cen.</i>	— <i>top_early-cen.</i>	— <i>top_early-cen.</i>
		99				
	LOWER CRETACEOUS	Albian		112		
Aptian		121		— <i>top_late-barr.</i>		
Barremian		127		— <i>top_early-barr.</i>		
				— <i>top_late-haut.</i>	— <i>b.wide u/c</i>	— <i>b.wide u/c/</i>
Hauterivian		132	Late Syn-Rift	— <i>top_early-haut.</i>	— <i>top_LSR III</i>	— <i>base_canyon</i>
				— <i>top_late-val.</i>	— <i>top_LSR II</i>	— <i>top_early-haut.</i>
Valanginian		137		— <i>top_early-val.</i>	— <i>top_late-val.</i>	— <i>top_late-val.</i>
				— <i>top_berr.</i>	— <i>top_early-val.</i>	— <i>top_early-val.</i>
Berriasian		144		— <i>top_berr.</i>	— <i>top_berr.</i>	— <i>top_berr.</i>
				— <i>top_port.</i>	— <i>top_port.</i>	— <i>top_port.</i>
UPPER JURASSIC	Portlandian ²	150	Principal Syn-Rift	— <i>top_kimm./</i>	— <i>top_kimm.</i>	— <i>top_kimm.</i>
	Kimmeridgian	154		— <i>top_esr.</i>		
		Oxfordian				
			Basement	— <i>top_basement.</i>	— <i>top_basement.</i>	— <i>top_basement.</i>

Figure 5.2: The seismic stratigraphy, and mega-sequences established for each of the basins is shown, and are based on McMillan (1999) time-top well data.

¹-Age data are from Gradstein *et al.* 1995. ²- there is a discrepancy between McMillan using 'Portlandian', and Gradstein *et al.* (1995) using 'Tithonian' (see text for discussion).

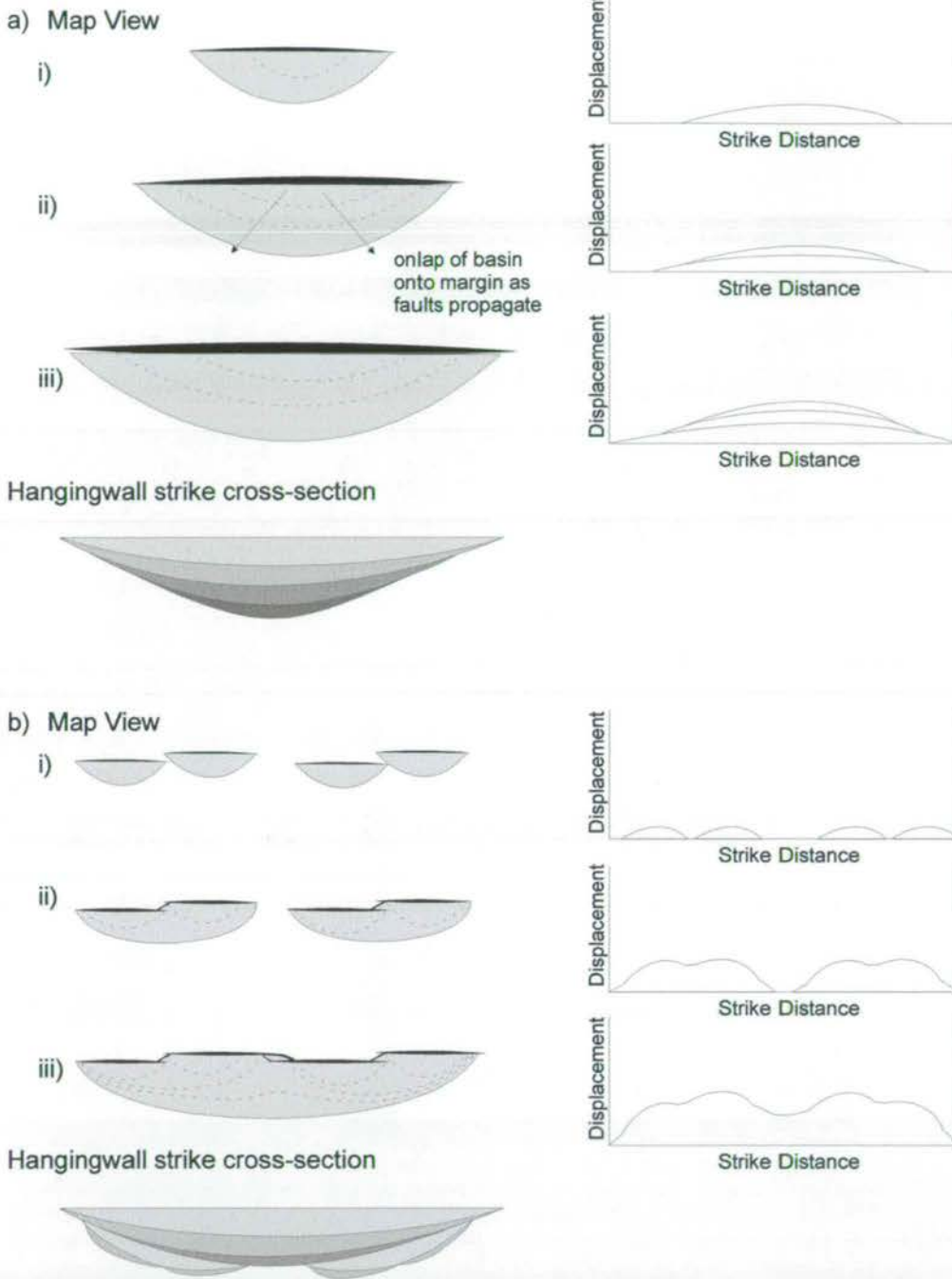


Figure 5.3: Two models of fault system evolution and associated sedimentary basin formation are illustrated, with growth controlled by a) isolated radial propagation, and b) segment linkage. For both models, map view and displacement/length profiles through time (i-iii) and final hangingwall strike sections are presented (after Cartwright *et al.*, 1996; Morley & Wonganan, 2000). The evaluation of hangingwall strike cross-sections and displacement/length profiles can be used to establish the evolution of the fault system (see text).

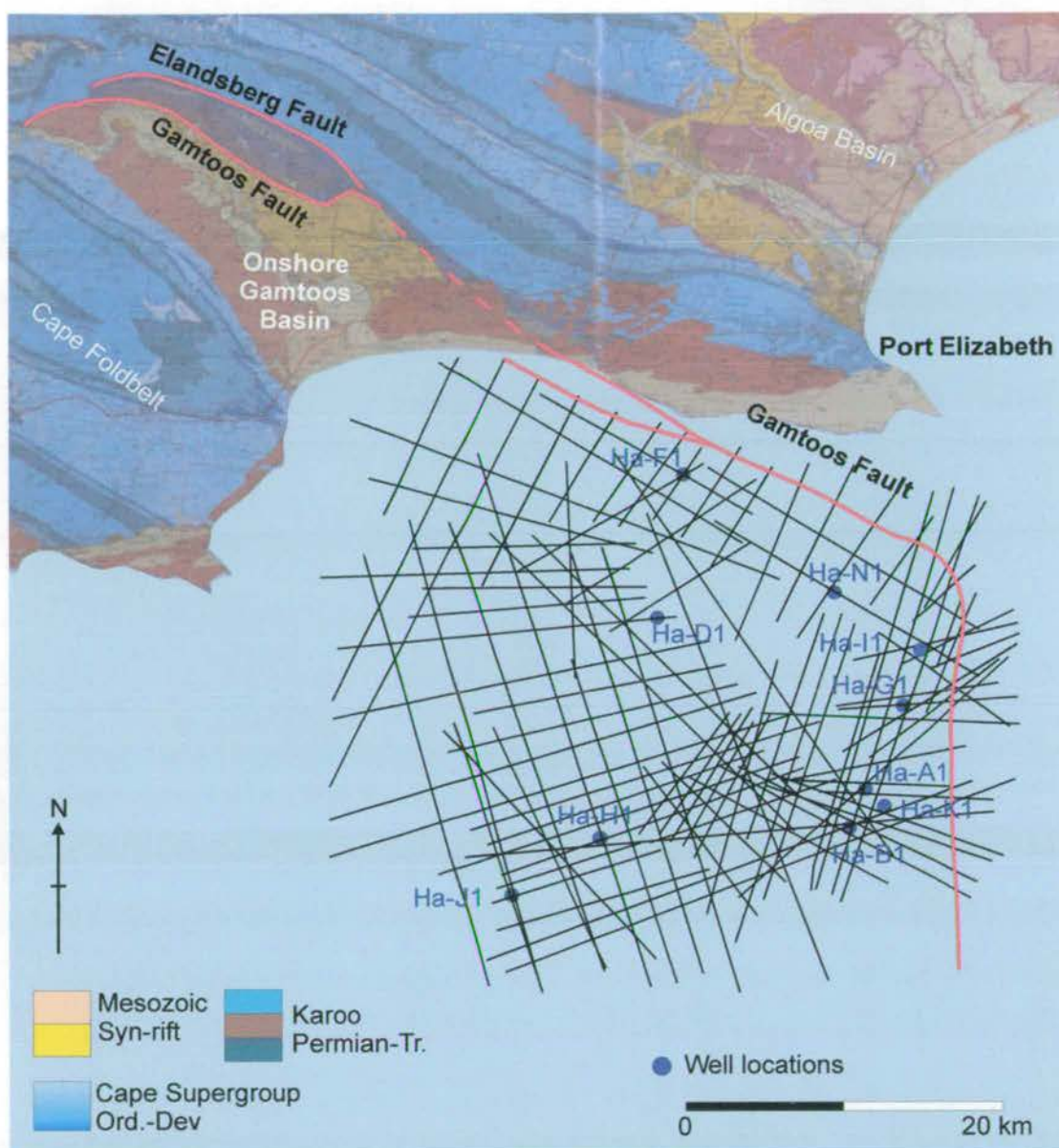


Figure 6.1: The location of the offshore seismic and well data set used to establish the tectono-stratigraphic framework of the Gamtoos Basin. In the north-west offshore the Gamtoos Fault forms two splays (Figure 6.19) that are possible along strike continuations of the onshore Gamtoos and Elandsberg Faults (Shone *et al.* 1990). The principal onshore geological units are shown (after Toerien, 1989). The position of sections used in this chapter are shown in Enclosure 8.

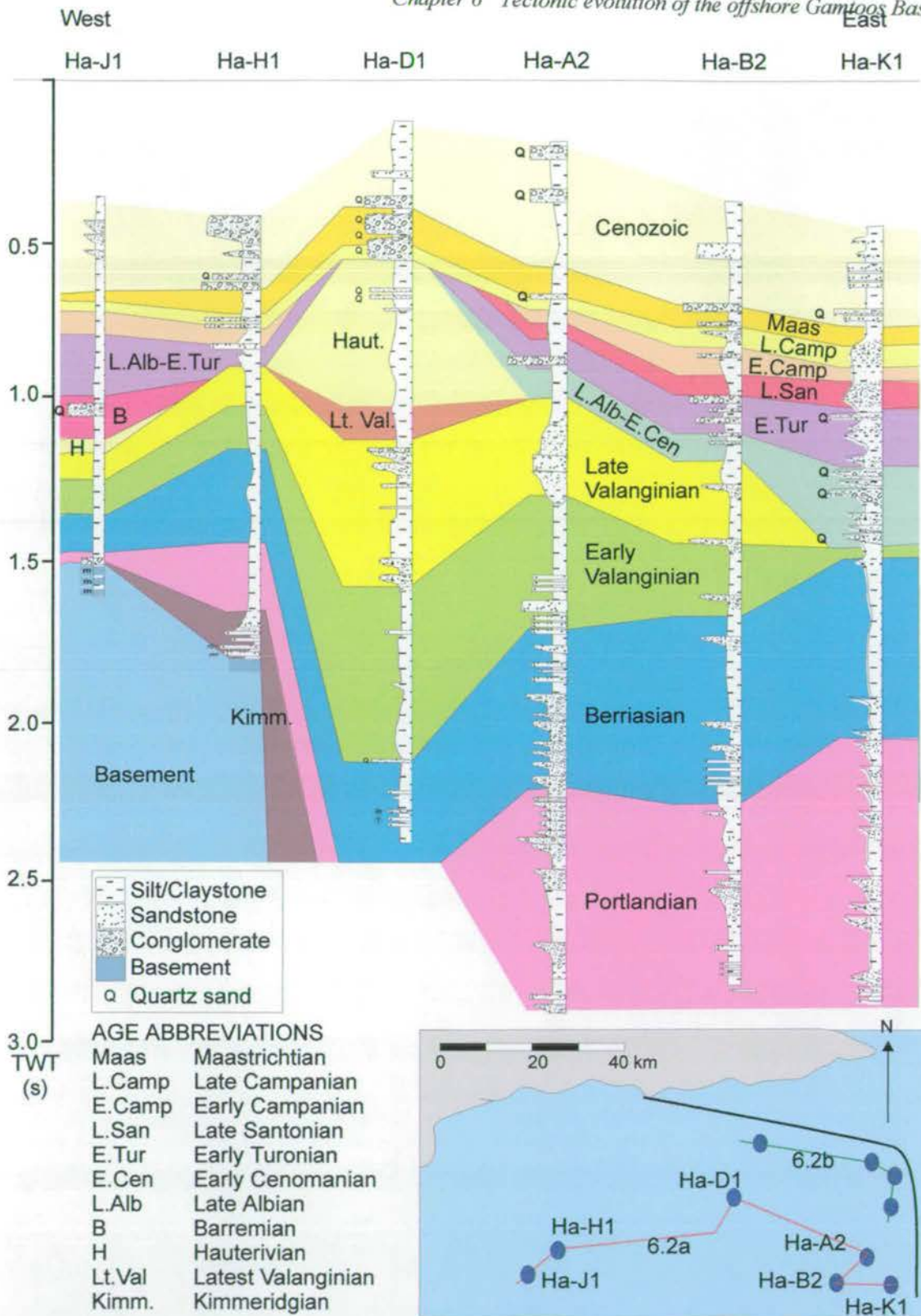
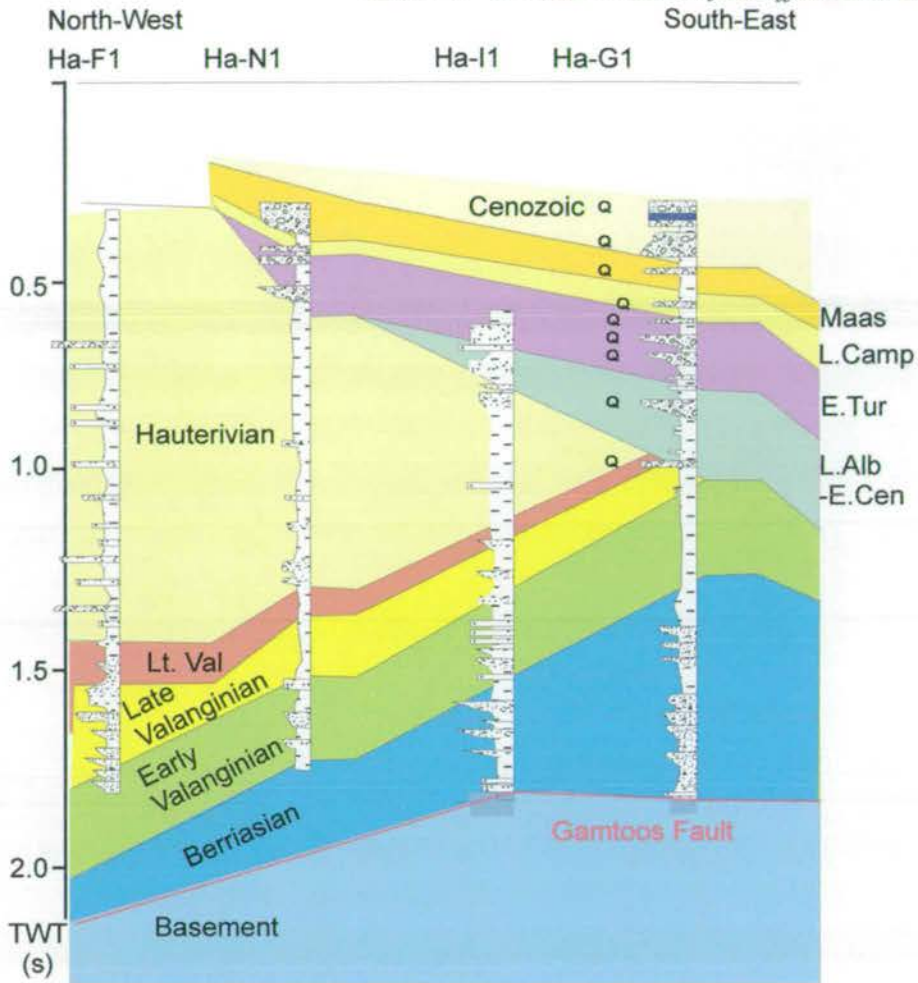


Figure 6.2a: Summary of wells in the southern area of the Gamtoos Basin displayed from west to east and positions marked on map inset. Age data between wells have been correlated. Full well logs are included in Appendix A. Although wells have been plotted against time, depth/conversion data (Appendix A) suggests that time/depth relationships are comparable amongst wells.



AGE ABBREVIATIONS

Maas	Maastrichtian
L.Camp	Late Campanian
E.Camp	Early Campanian
L.San	Late Santonian
E.Tur	Early Turonian
E.Cen	Early Cenomanian
L.Alb	Late Albian
B	Barremian
H	Hauterivian
Lt.Val	Latest Valanginian
Kimm.	Kimmeridgian

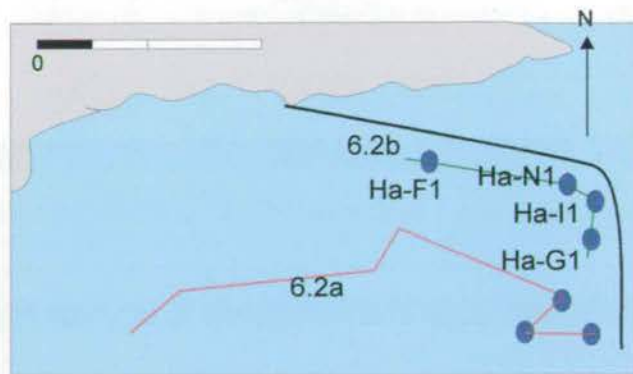


Figure 6.2b: Summary of wells along the trace of the Gamtoos Fault plane from the north-west to the south-east with positions marked on the map inset. Age data between wells have been correlated. Full well logs are included in Appendix A. Although wells have been plotted against time, depth/conversion data (Appendix A) suggests that time/depth relationships are comparable amongst wells.

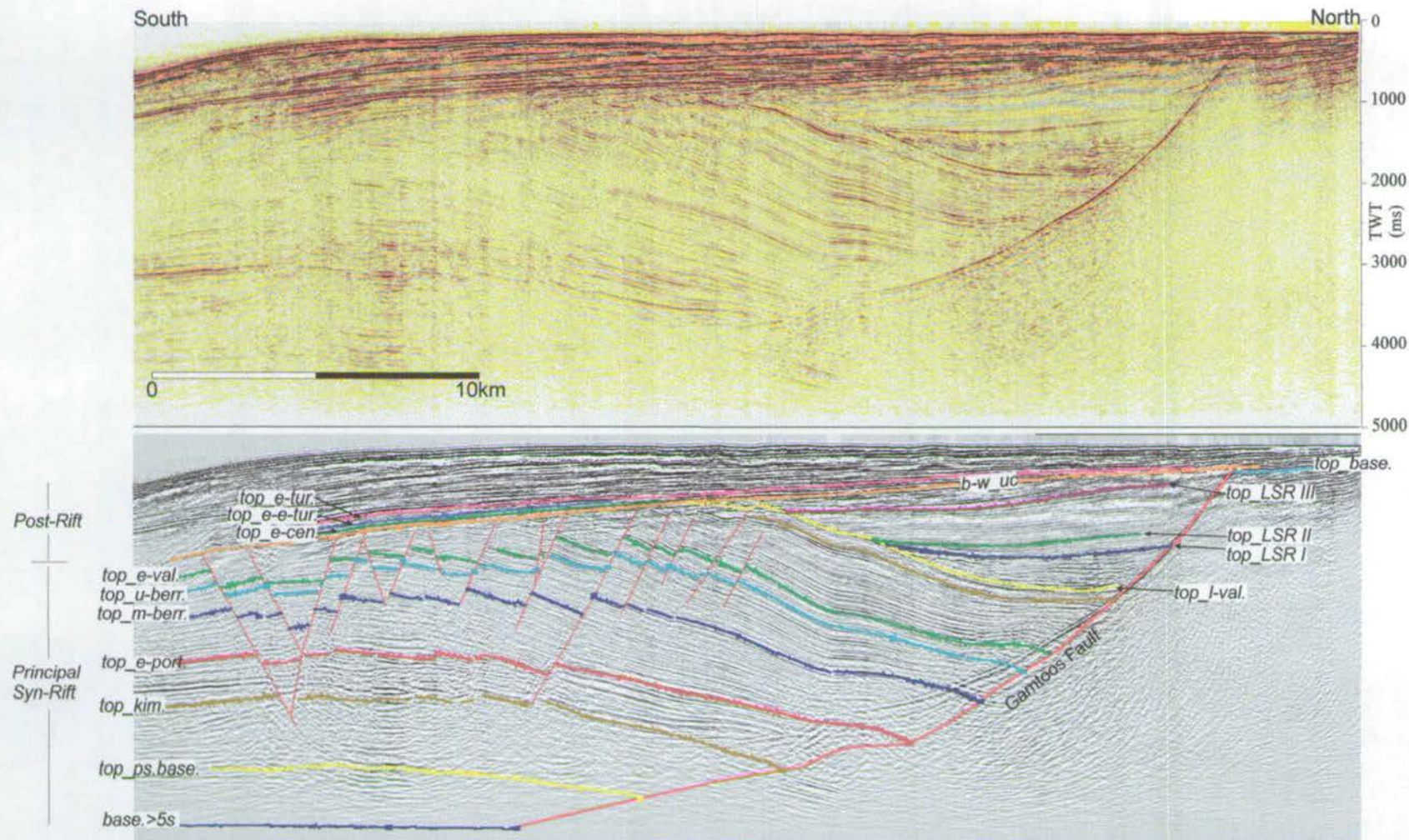
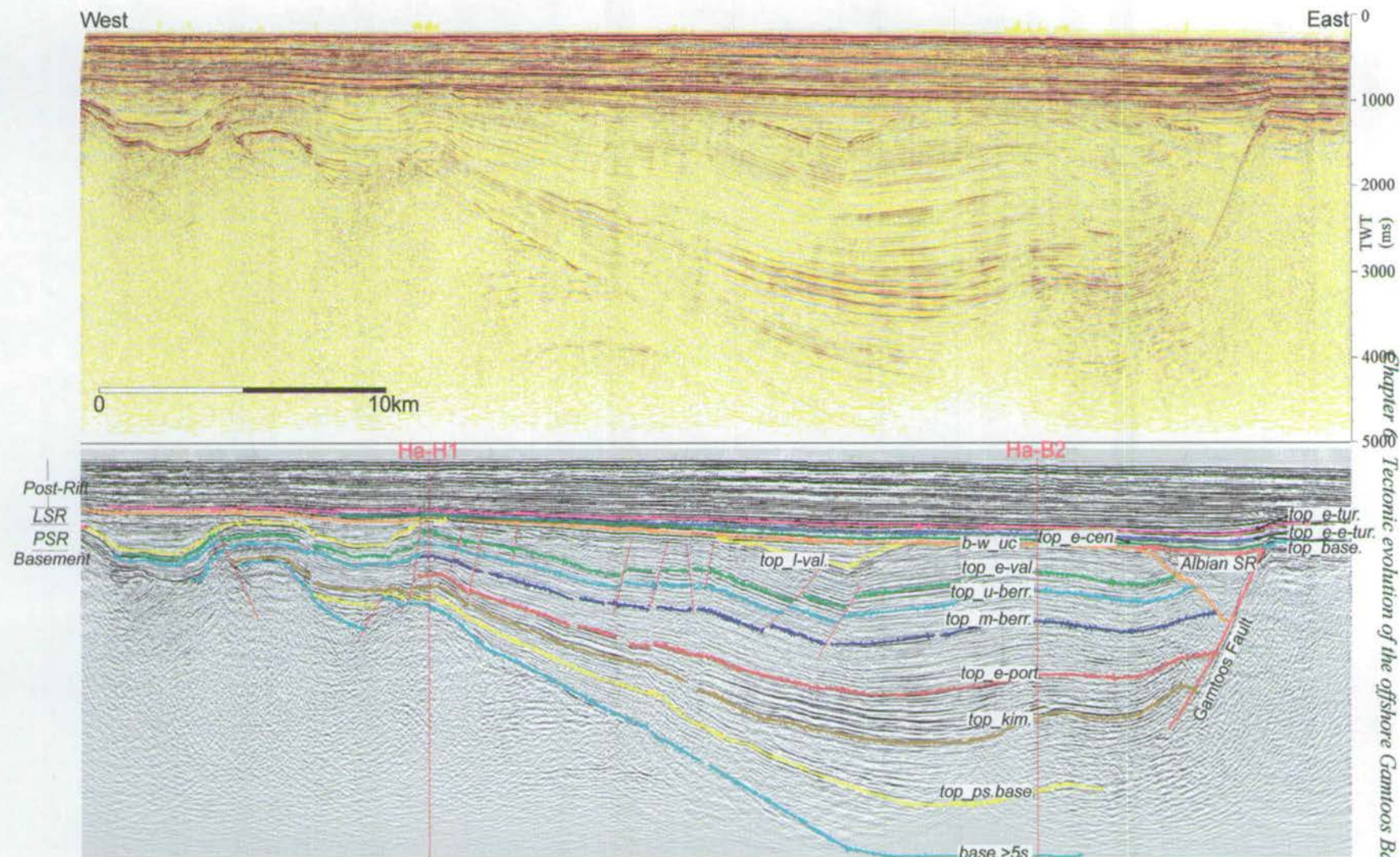


Figure 6.3a: North-south section across the Gamtoos Basin showing the overall basin geometry, mega-sequences and sequences. The Gamtoos Fault appears to be listric because the section is oblique to the fault trend. Line Ha87-026. Abbreviations: *base.* - basement; *base > 5s* - basement deeper than 5s; *ps_base.* - pseudo basement; *kimm.* - Kimmeridgian; *e-port.* - Early Portlandian; *m_berr.* - Middle Berriasian; *u_berr.* - Upper Berriasian; *e-val.* - Early Valanginian; *l-val.* - Late Valanginian; *LSR* - Late Syn-Rift; *b-w_uc* - basin-wide unconformity; *e-cen.* - Early Cenomanian; *e-e-tur.* - Early Early Turonian; *e-tur.* - Early Turonian.



Chapter 6
Tectonic evolution of the offshore Gamtoos Basin

Figure 6.3b: East-west section across the Gamtoos Basin. The Principal Syn-Rift (PSR), Late Syn-Rift (LSR) and Post Rift mega-sequences are evident as is the localised Albian Syn-Rift package. The positions of wells Ha-B2 and Ha-H1 are shown. Line Ha87-45. Abbreviations - as in Figure 6.3a

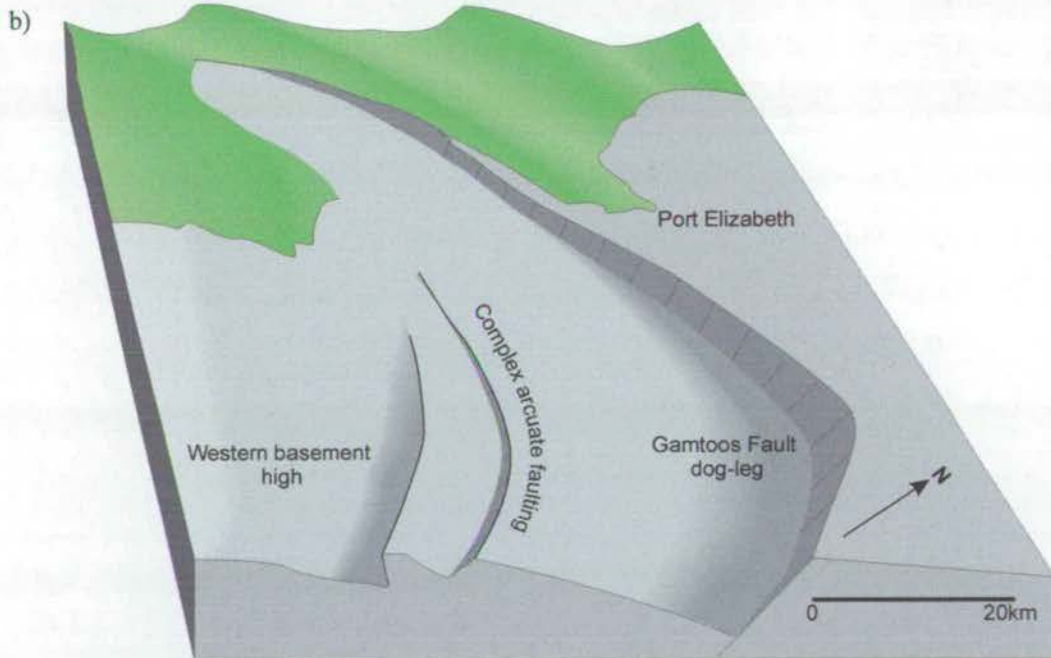
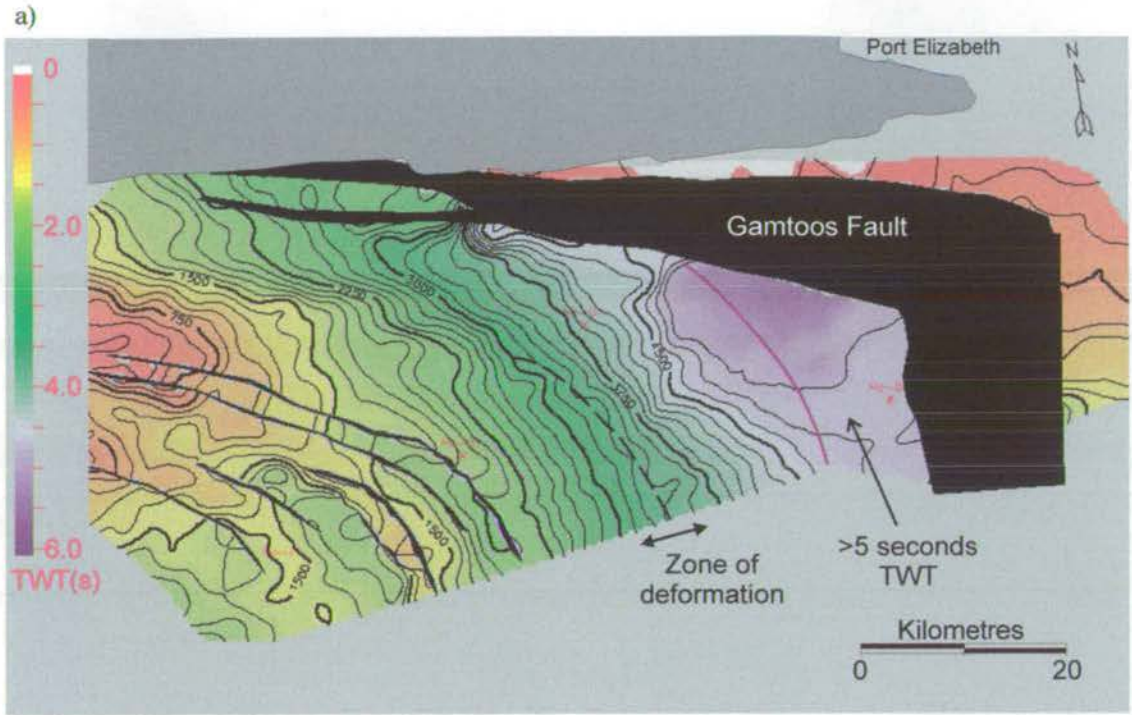


Figure 6.4: a) TWT map of *top* basement with fault polygons plotted, and coastline marked on (used as reference for all other maps). b) 3D sketch of the Gamtoos Basin to highlight the salient features. Of particular importance are : the dog-leg in the Gamtoos Fault; *top* basement adjacent to the fault is deeper than 5 s TWT; and the complex faulting on the western basement high.

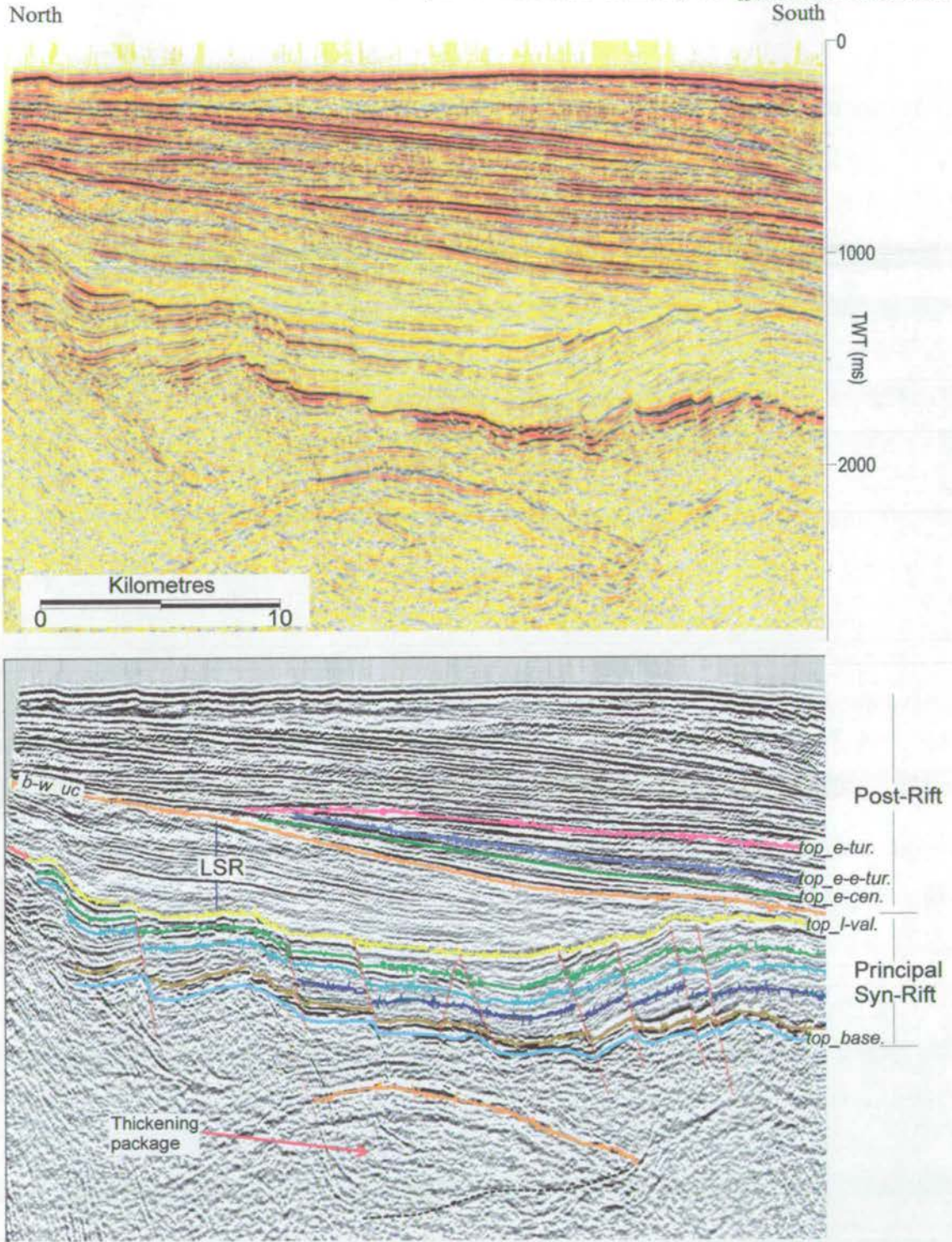
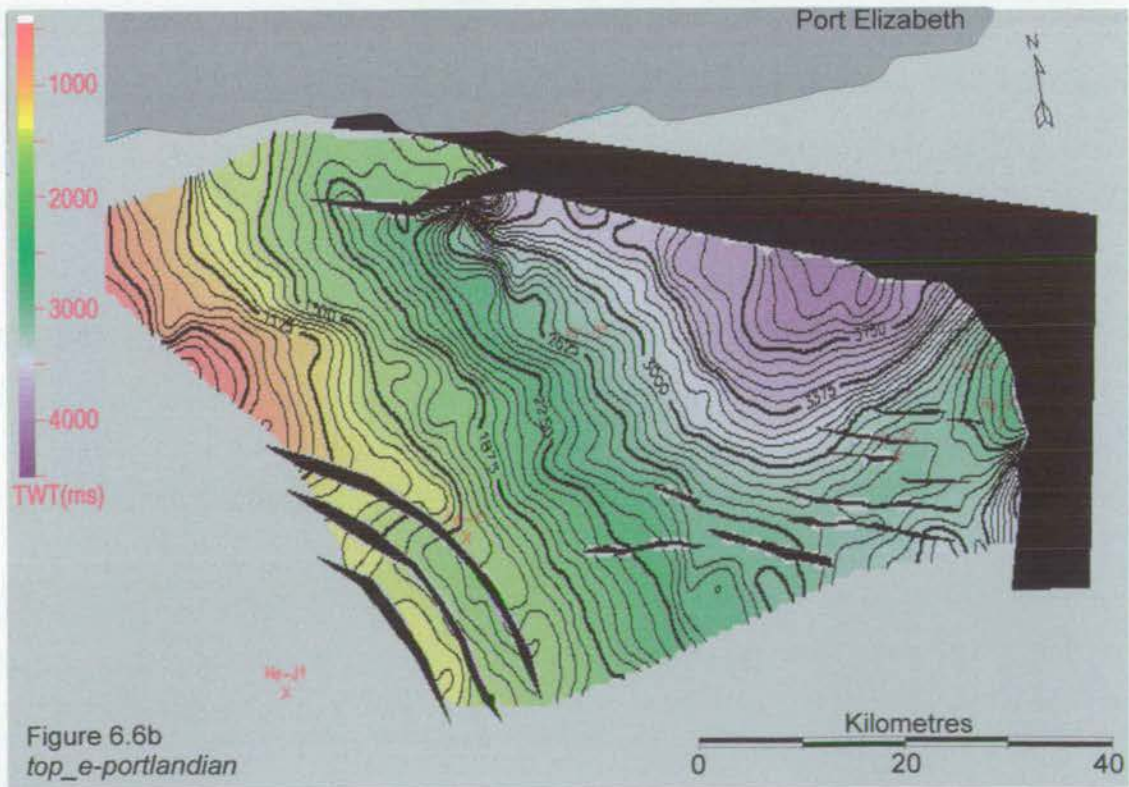
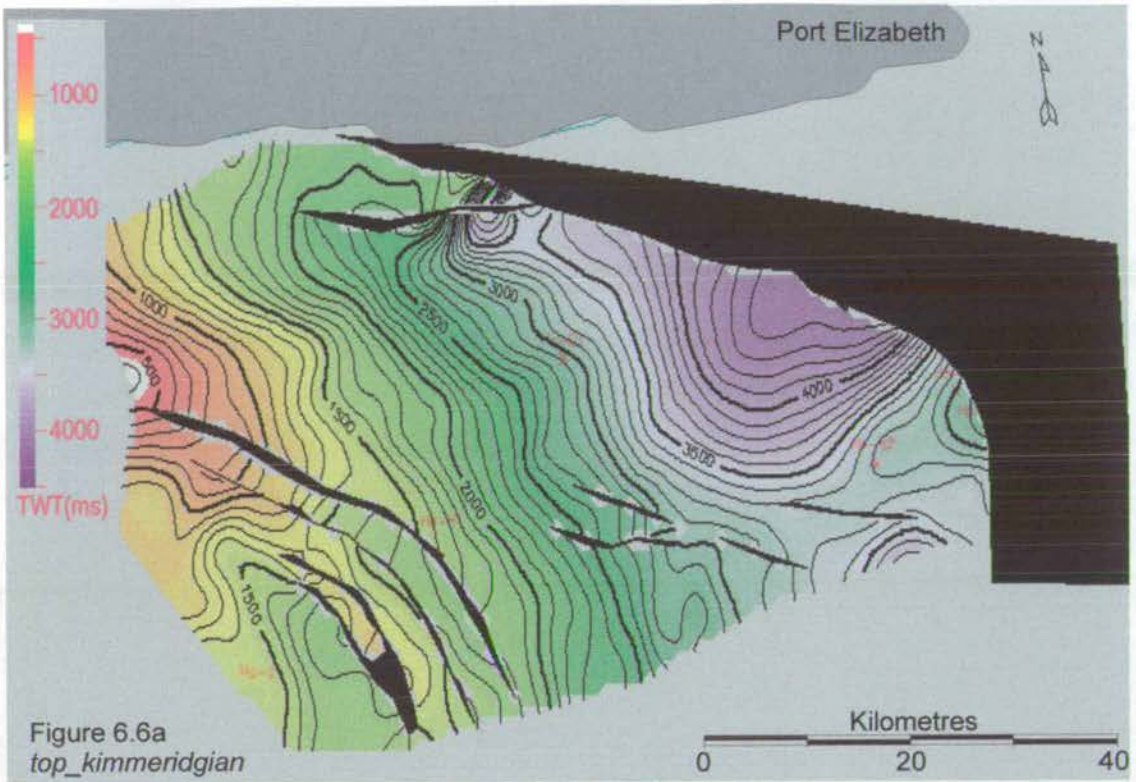
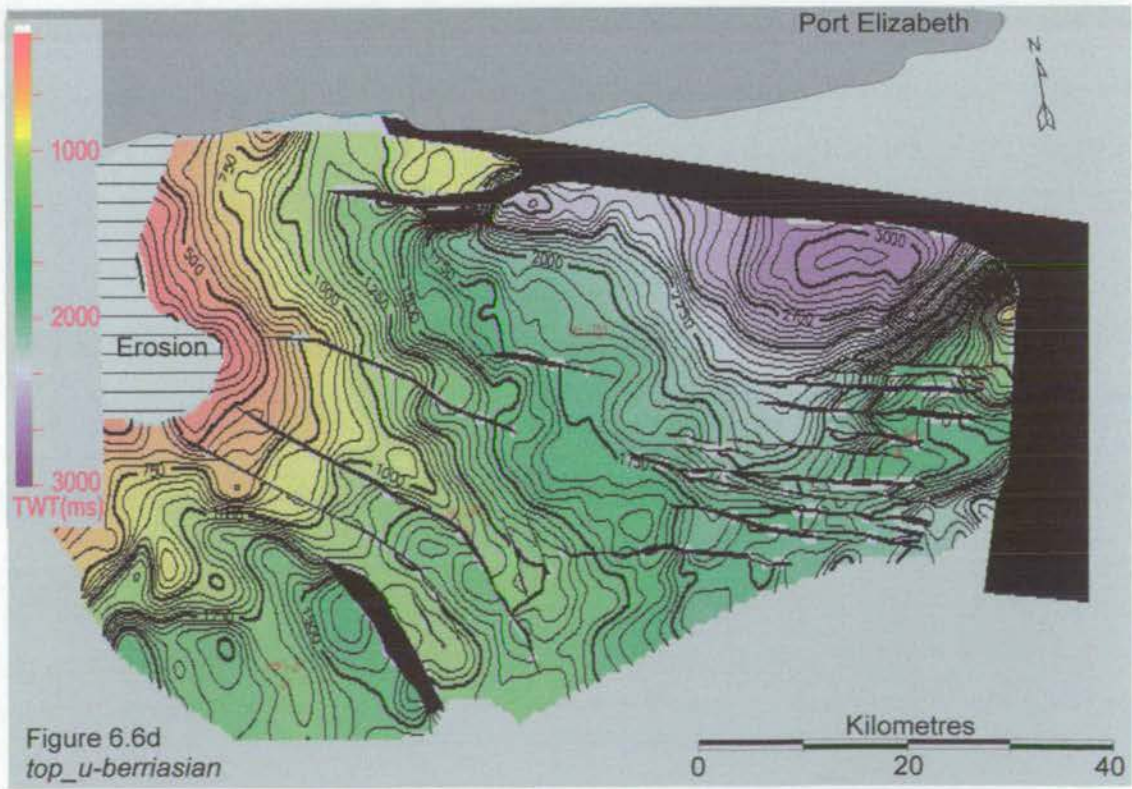
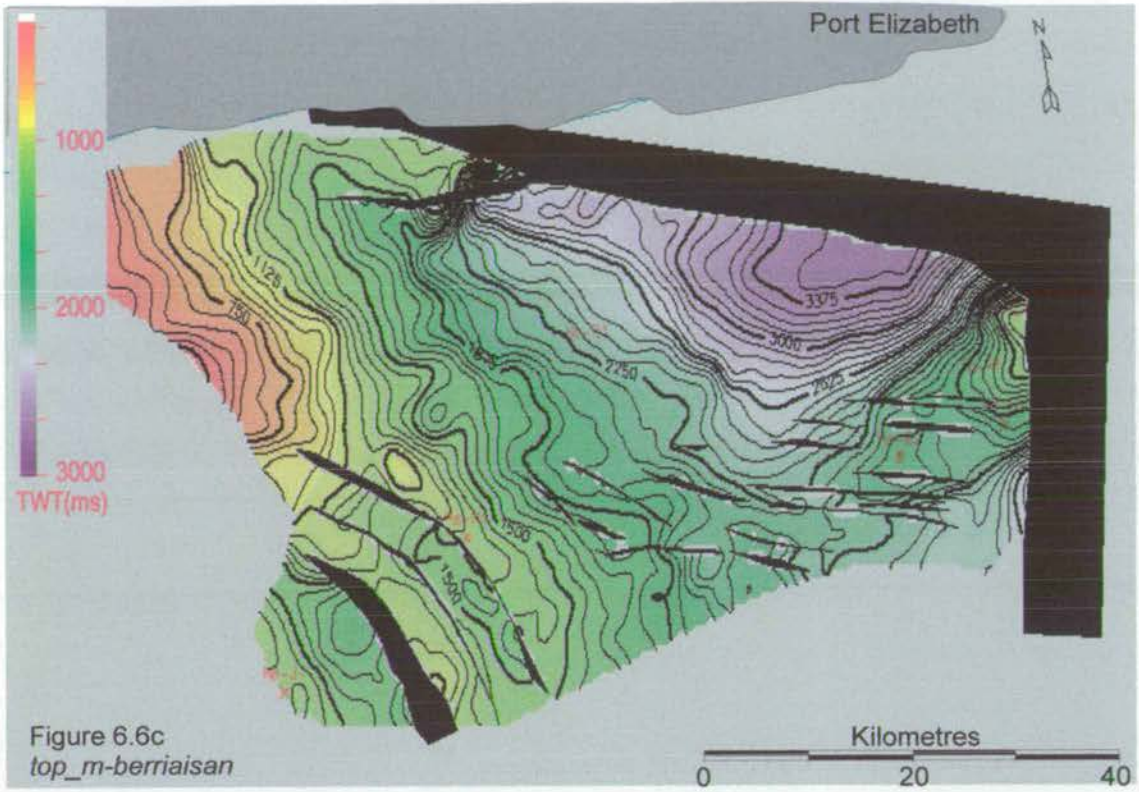


Figure 6.5: North-south section in the western Gamtoos Basin. The Principal Syn-Rift package shows abundant faults that terminate at *top_l-valanginian* horizon and at the base of the Late Syn-Rift Package (LSR). The lower Post-Rift sequences onlap on to the *basin-wide unconformity*. Below *top_base* there is an apparent package thickening in towards a normal fault that may be an earliest syn-rift package.





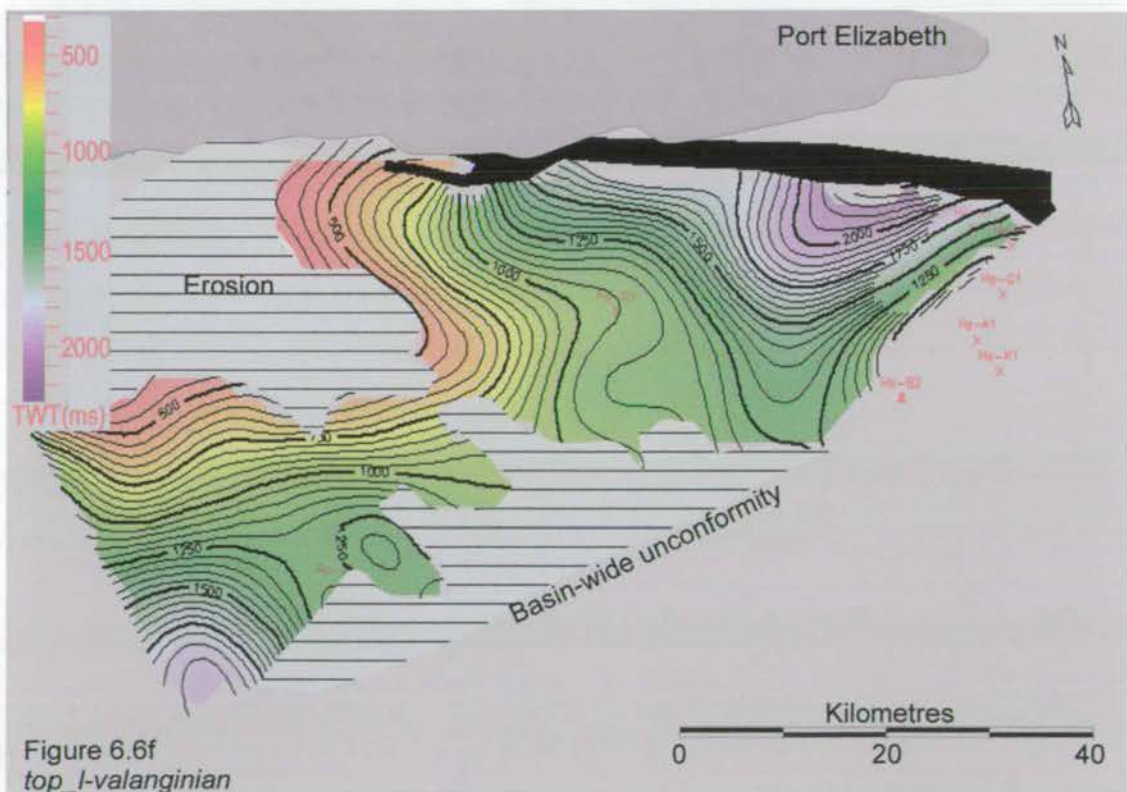
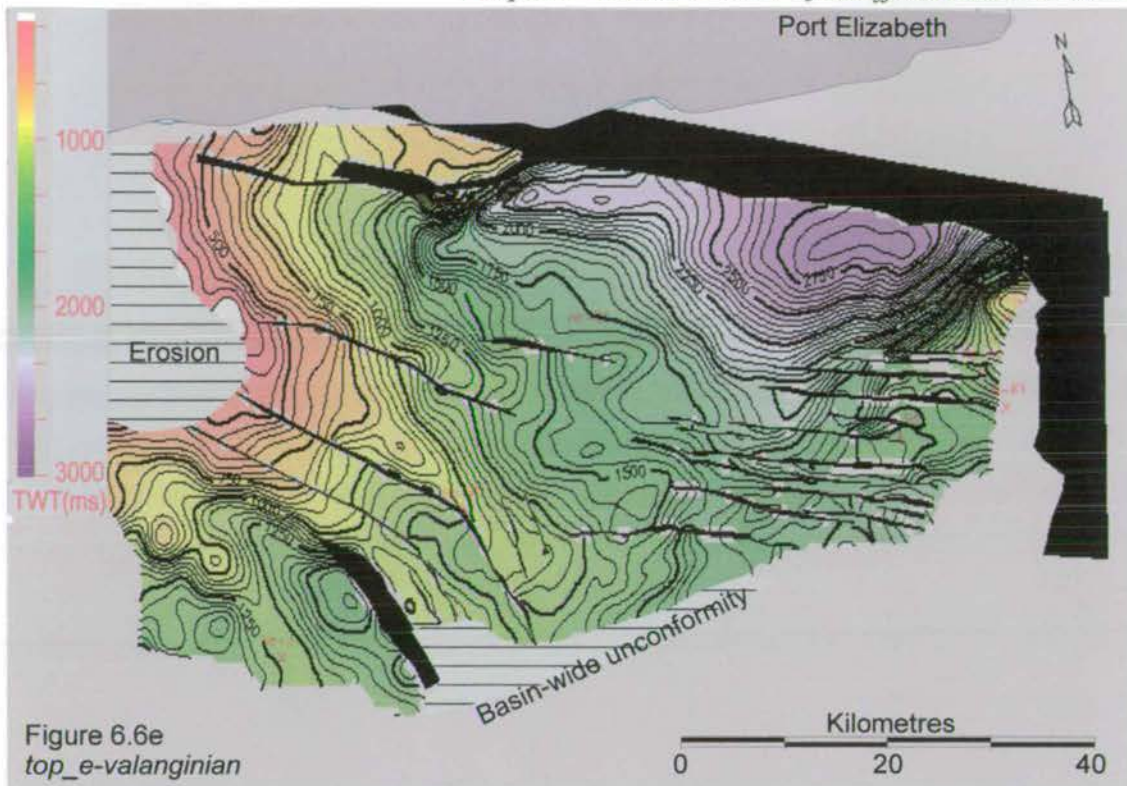
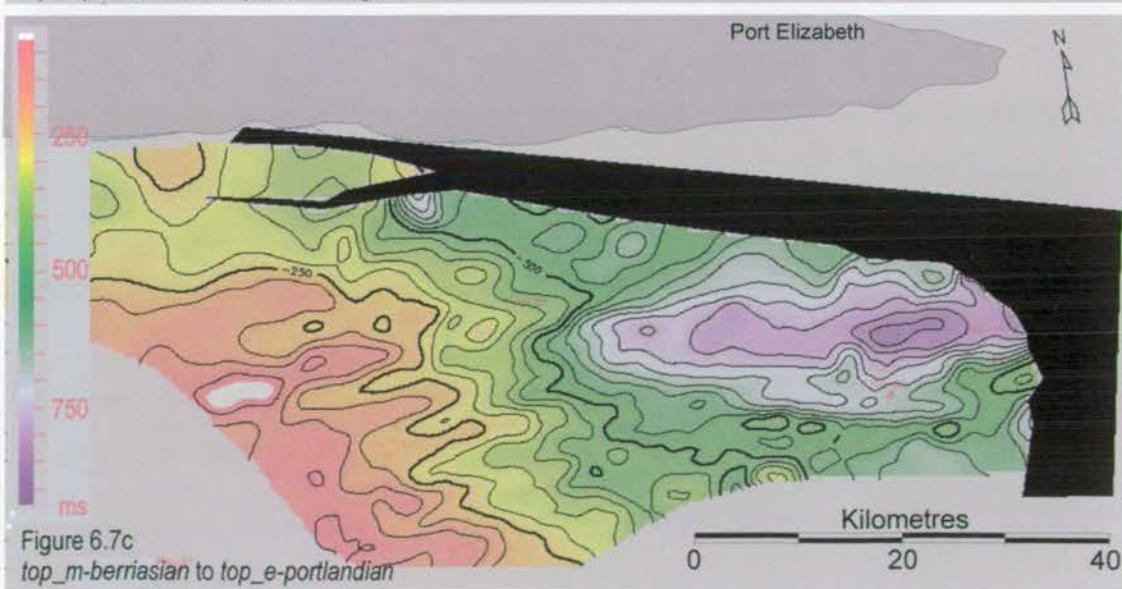
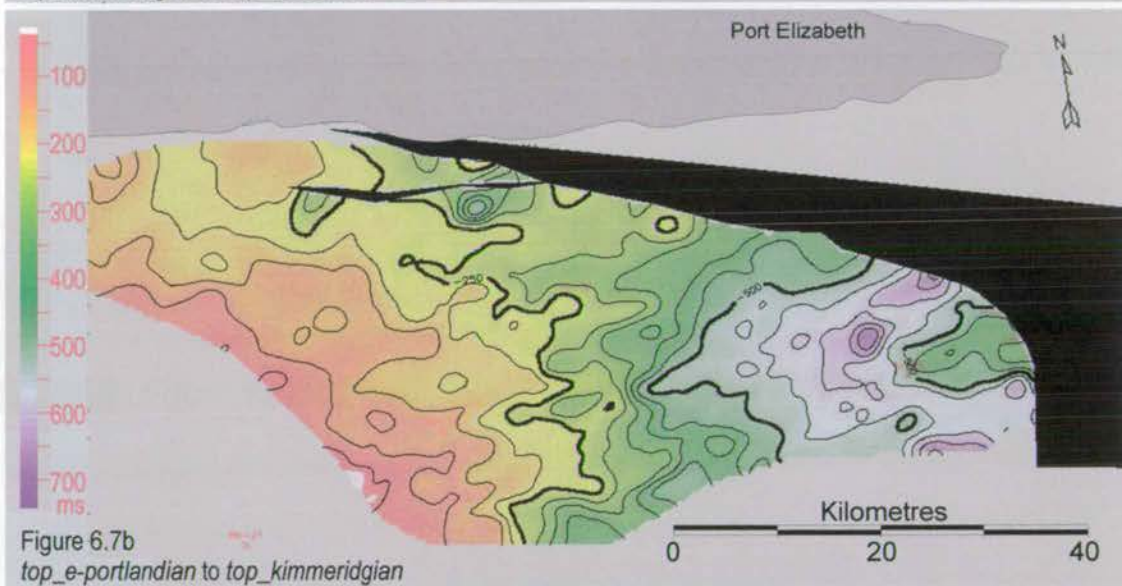
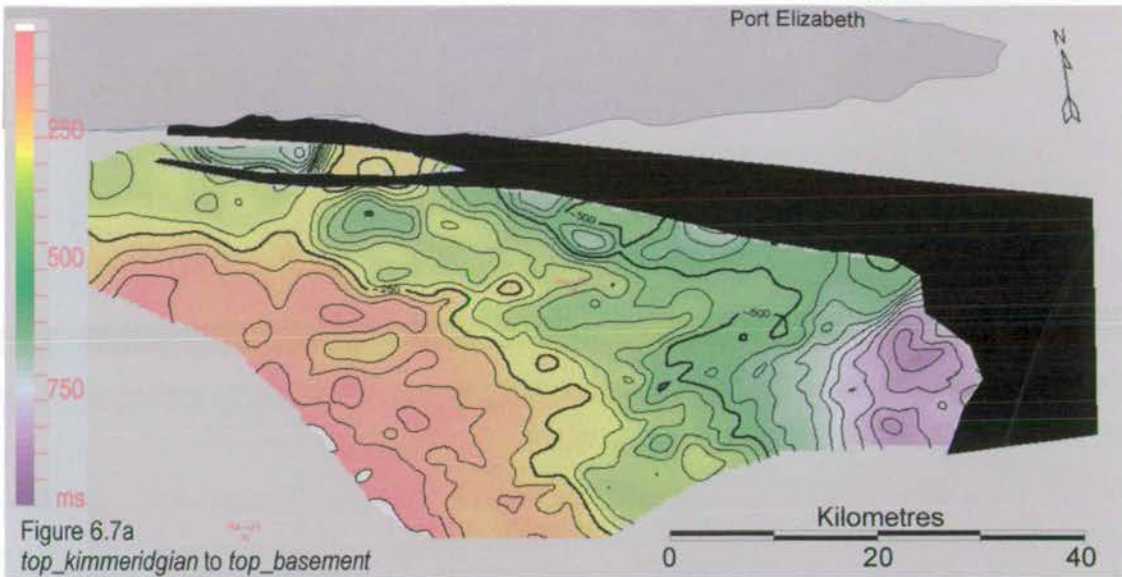


Figure 6.6 : TWT maps for the picked Principal Syn-Rift seismic horizons. a) *top_kimmeridgian*, b) *top_e-portlandian*, c) *top_m-berriasian*, d) *top_l-berriasian*, e) *top_e-valanginian*, f) *top_l-valanginian*. Note the increase in the number of intra-basin faults throughout the mega-sequence, the substantial amount of erosion in the later sequences, and the increased deformation against the apex of the fault curve (c-e).



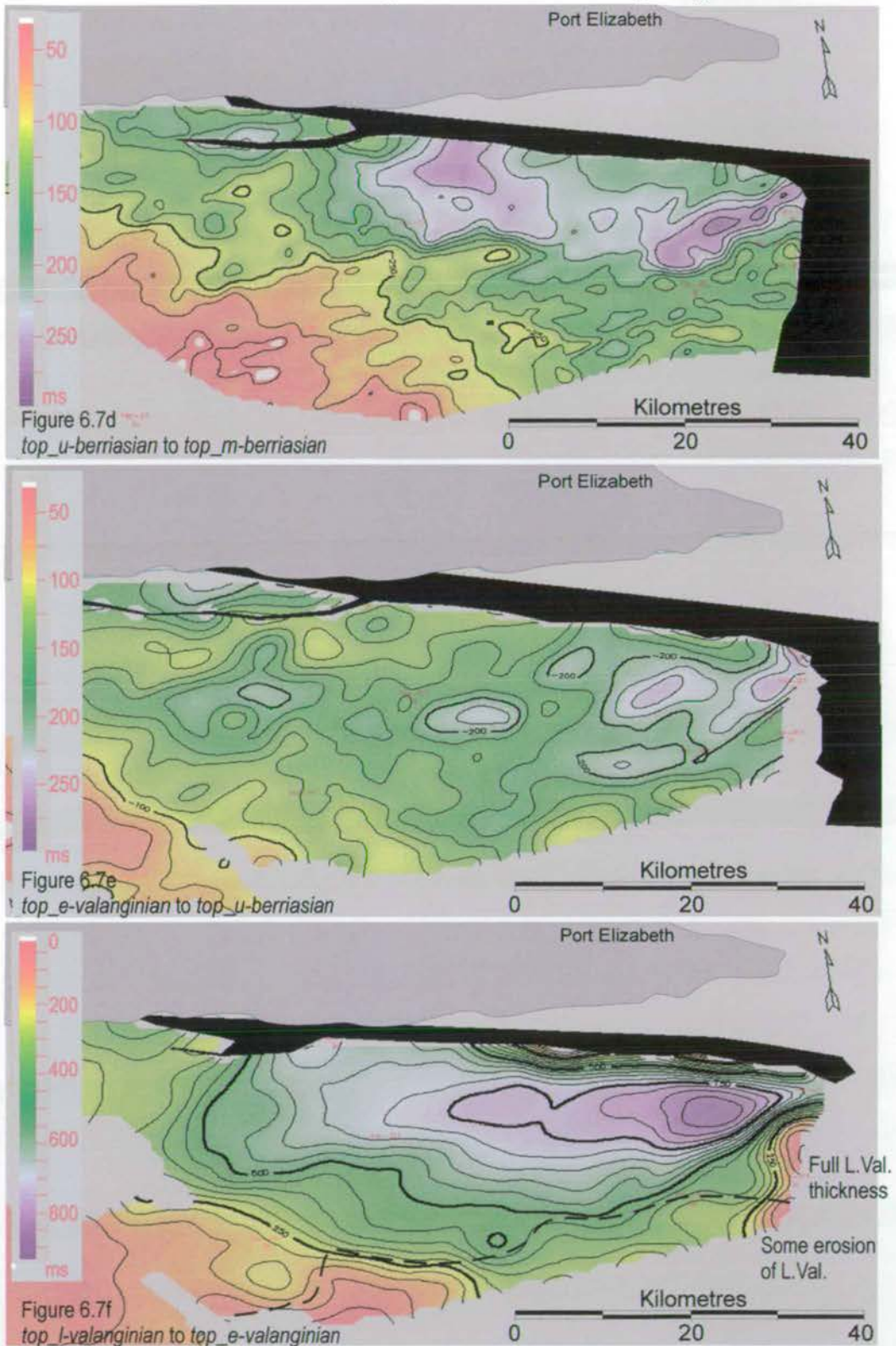


Figure 6.7 : Isochron plots of Principal Syn-Rift sequences. a) Kimmeridgian, b) Early Portlandian, c) Mid Berriasian, d) Upper Berriasian, e) Early Valanginian, f) Late Valanginian. The Late Valanginian to Early Valanginian plot does not have the full sediment thickness because of erosion by the basin-wide unconformity (extent of erosion shown).

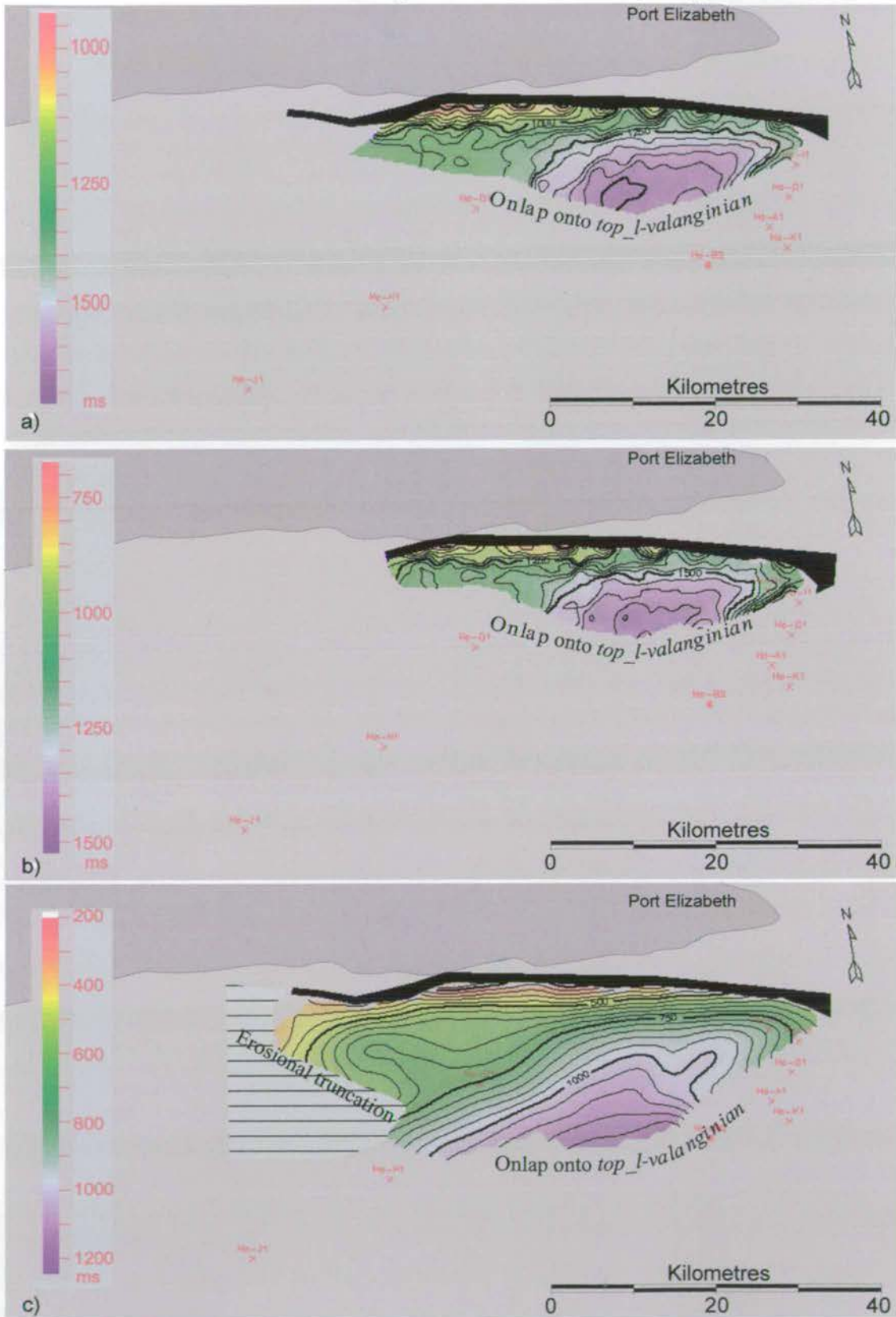


Figure 6.8: TWT maps of the Late Syn-Rift sequences. a) *top_LSR I*, b) *top_LSR II*, c) *top_LSR III*. Notice the dramatic reduction in areal extent of sedimentation compared to the Principal Syn-Rift mega-sequence (cf. Figure 6.7).

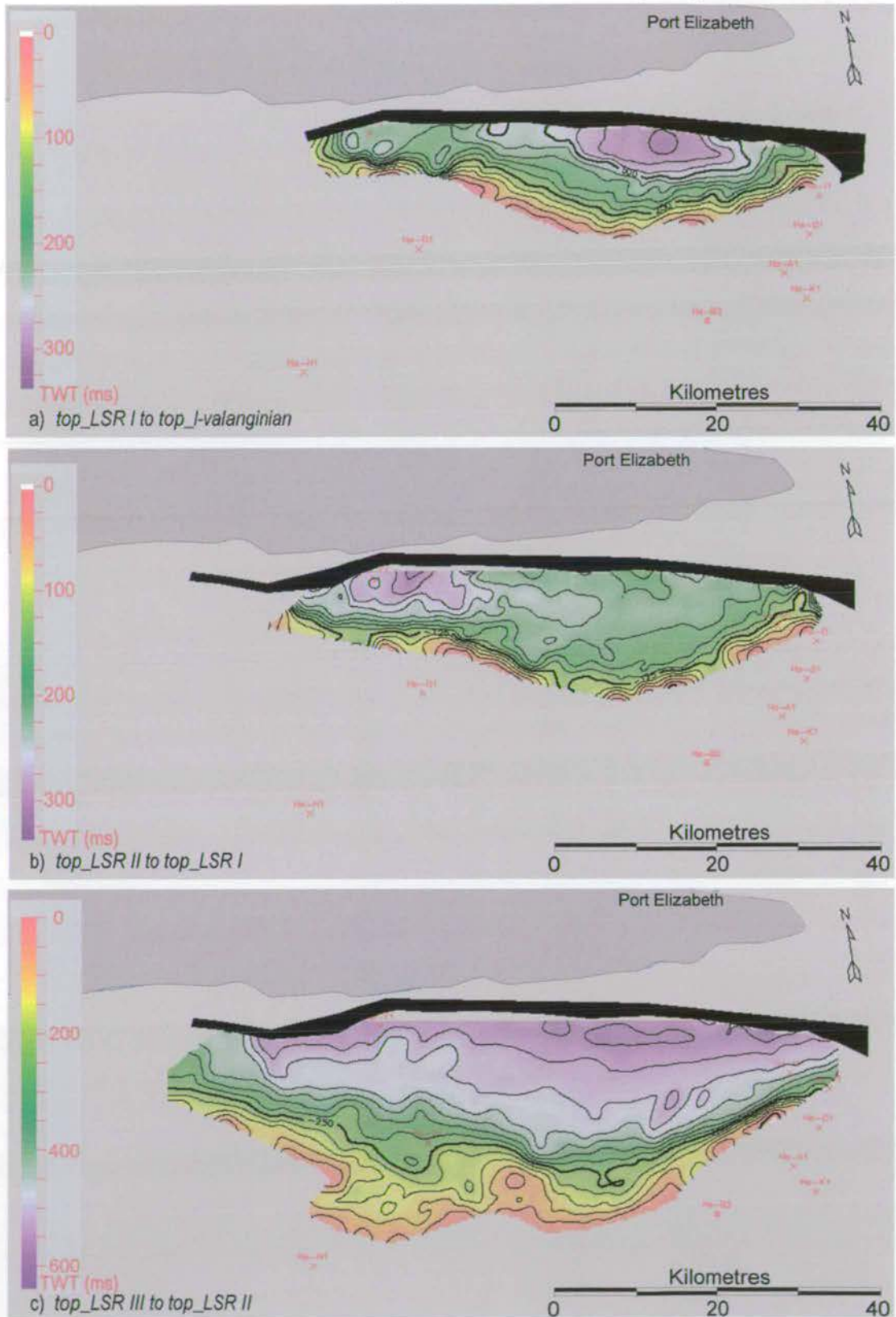


Figure 6.9 : Isochron plots of Late Syn-Rift sequence thickness. a) LSR I, b) LSR II, c) LSR III. Although the sequences generally thicken into the East-West Gamtoos Fault portion (b) shows very little thickening. The areal extent of the packages increases through time.

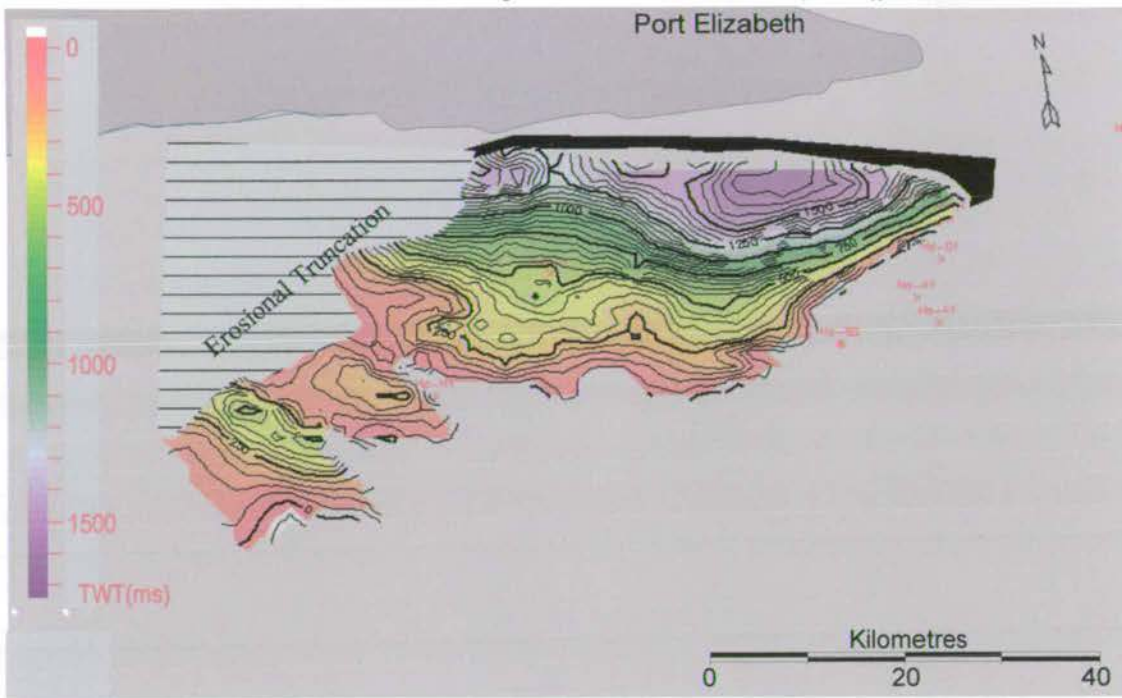


Figure 6.10: Isochron plot of the *basin-wide unconformity to top l-valanginian*, i.e. preserved thickness of the Late Syn-Rift package. Although it is uncertain how much erosion has occurred, it is evident from this plot that between LSR III and the basin-wide unconformity the areal extent of the deposition increased from the lower LSR packages (c.f. Figure 6.9).

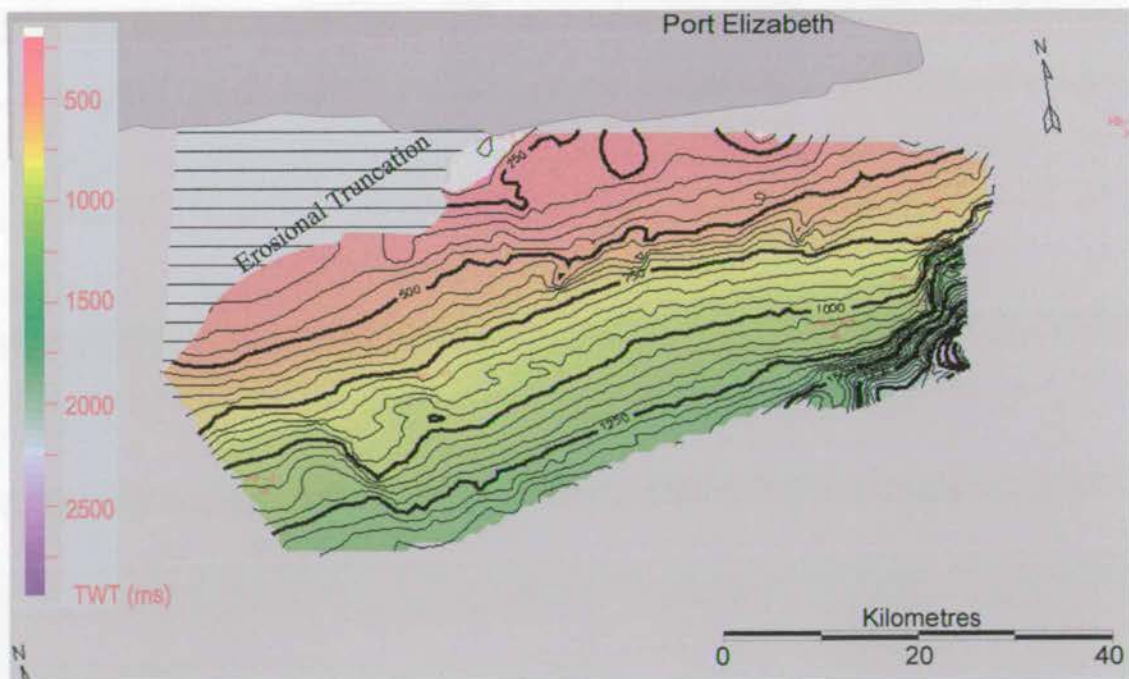


Figure 6.11 : TWT map of the *basin-wide unconformity*. Despite this being a significant unconformity the horizon forms a planar surface that dips towards the south.

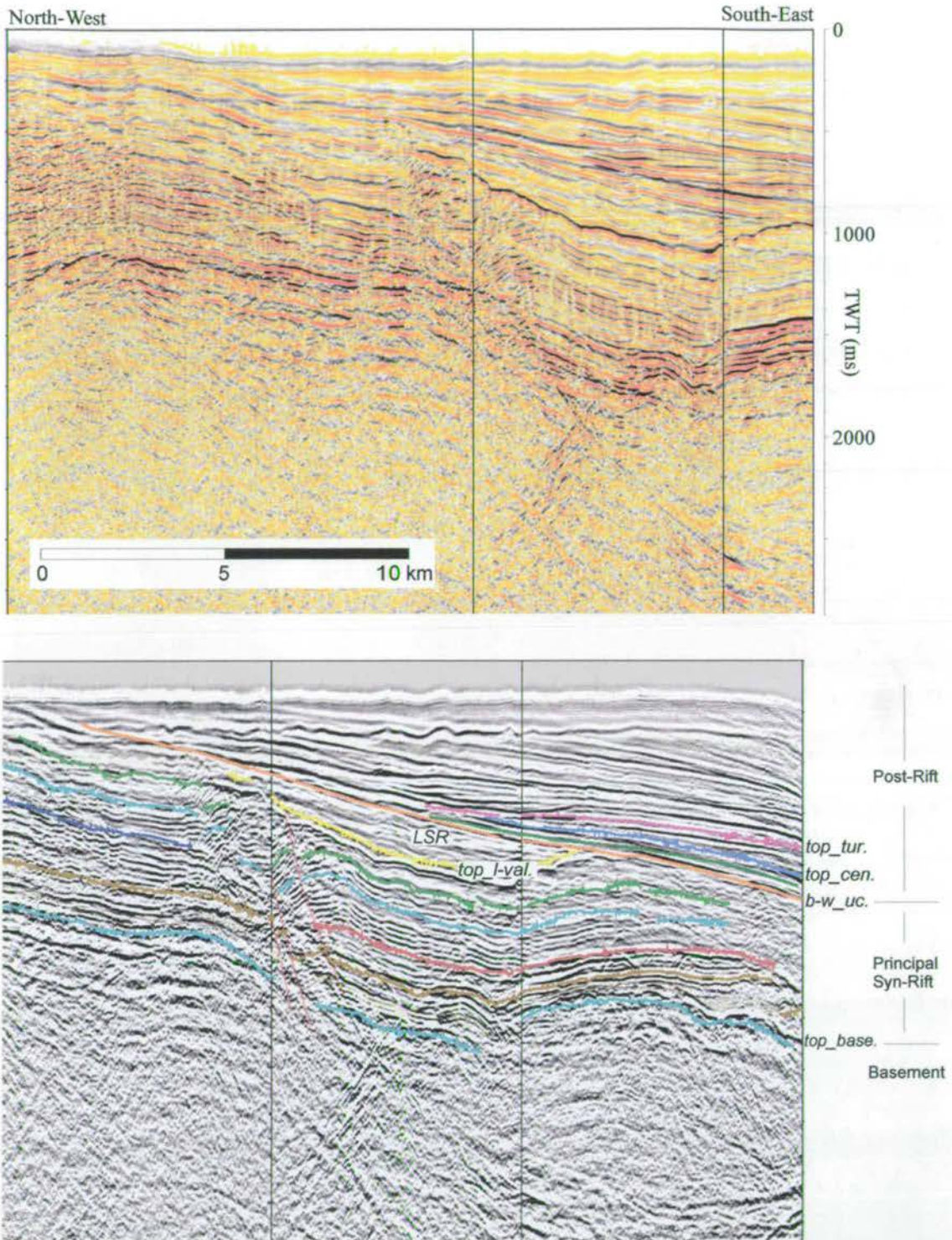


Figure 6.12: North-west margin of the Gamtoos Basin. The *top_e-cenomanian* and *top_e-turonian* horizons onlapping onto the *basin-wide_unconformity* that is subsequently uplifted and eroded by a later unconformity. Line Ha 82-036.

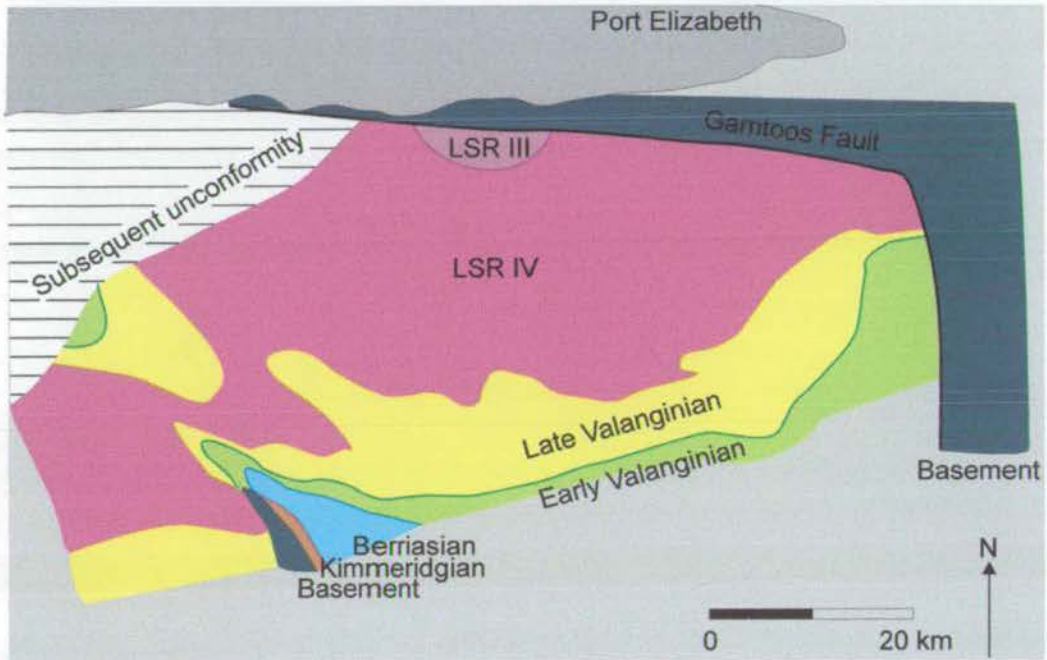


Figure 6.13: Sub-crop map to the *basin-wide_unconformity*. The intersect between a horizon and the unconformity is shown by a line with the colour corresponding to the appropriate horizon. LSR - Late Syn-Rift.

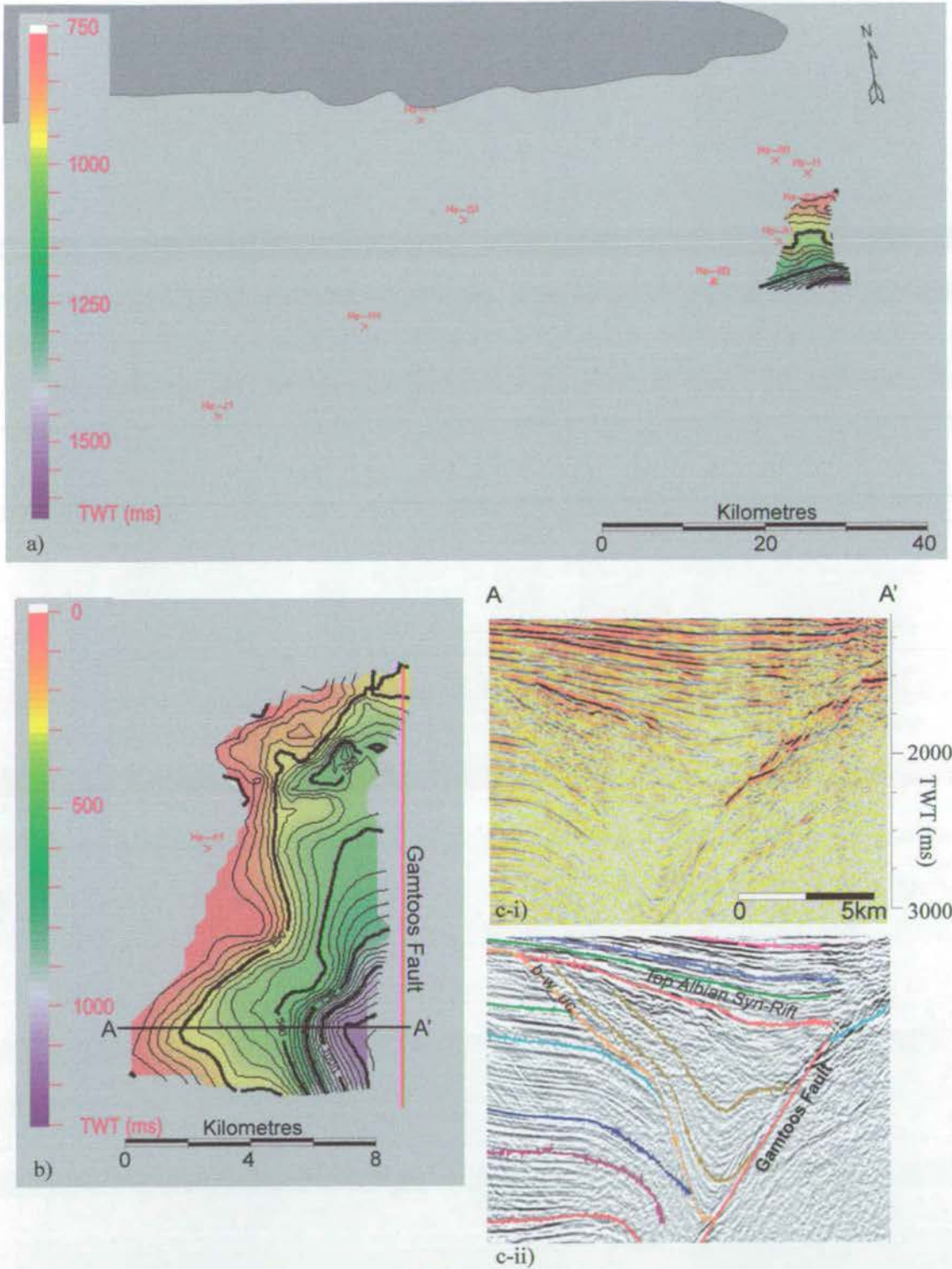


Figure 6.14 : a) TWT map of *top_albian* Syn-Rift package.
 b) Isochron plot of *top_albian* reflector to *basin-wide unconformity* showing thickening of the package into the Gamtoos Fault. The brown reflectors within the seismic section (c-i, ii) are progressively folded towards the base of the package indicating that it is a syn-rift sequence rather than simple canyon in-filling.

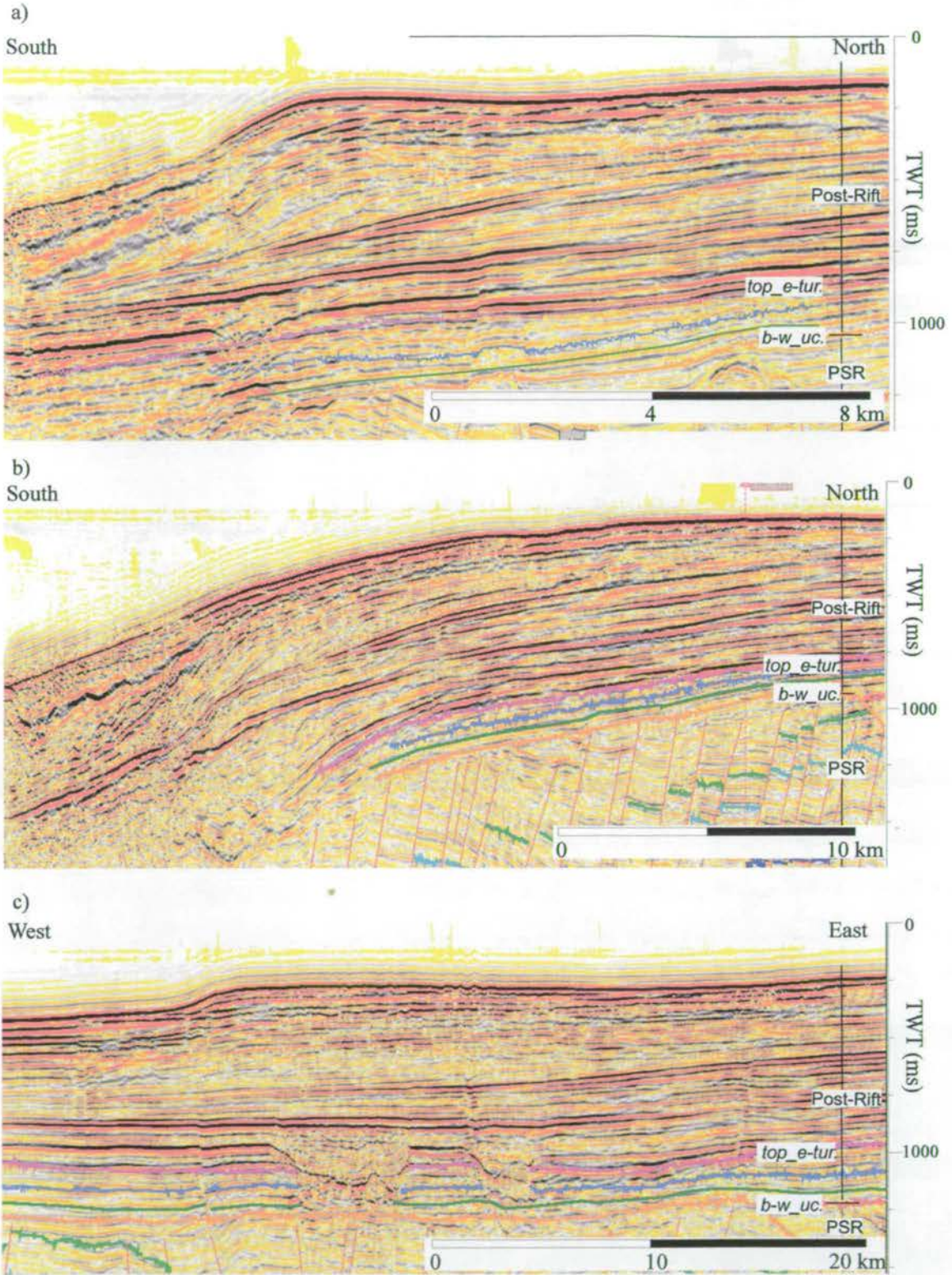


Figure 6.15: Sections showing Post-Rift deformation. Figures a) Line Ha 87-032 and b) Line Ha 87-31, both highlight the varying amounts of sediment accumulation during the Post Rift interval. In both sections there is very little accumulation below *top_e-turonian* and significant progradational packages above *top_e-turonian*. Localised canyoning above the *top_e-turonian* is also present (c), Line 87-008.

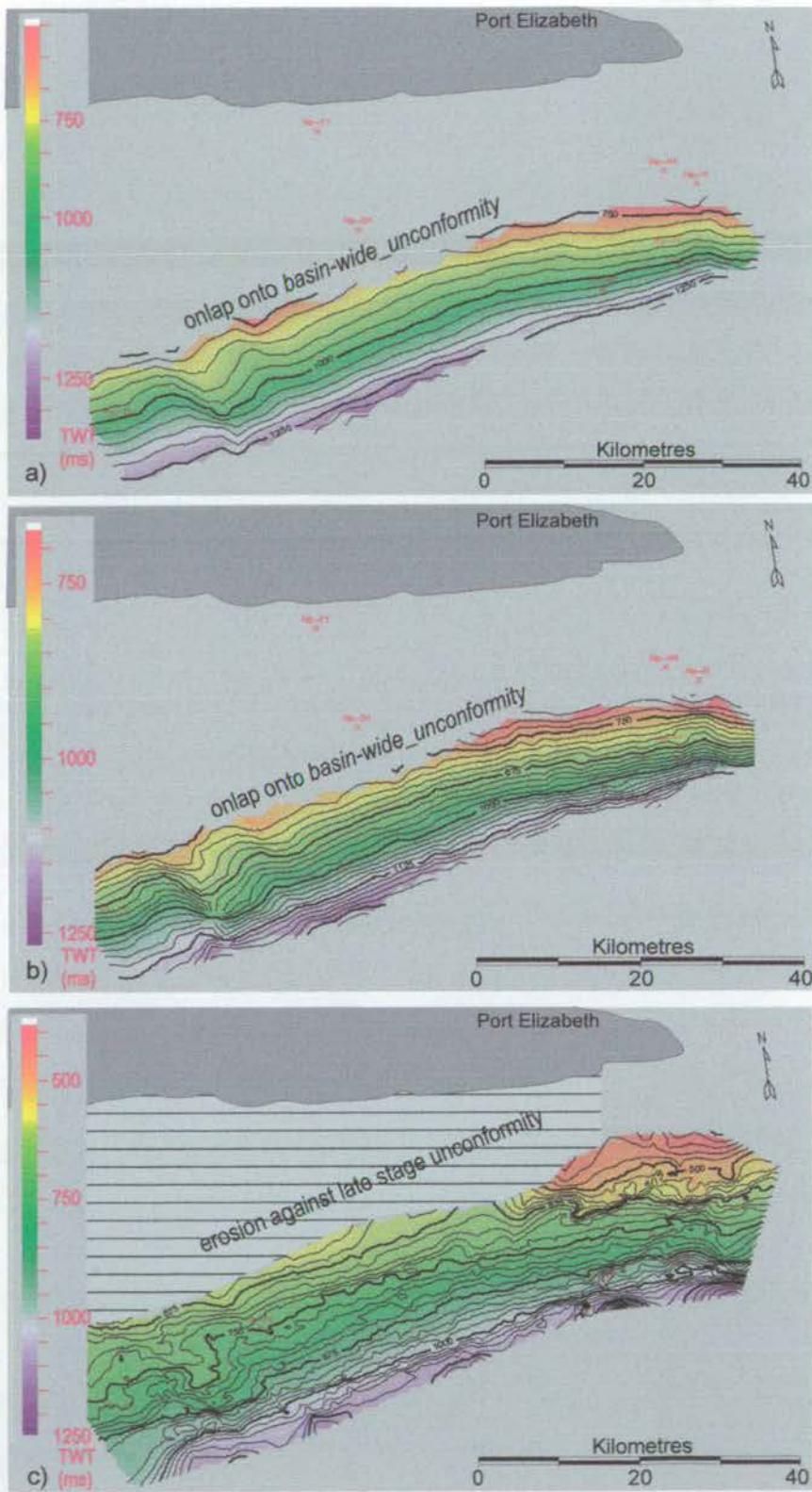


Figure 6.16: TWT maps of the Post-Rift mega-sequence horizons, a) *top_e-cenomanian*, b) *top_e-e-turonian* and c) *top_e-turonian*.

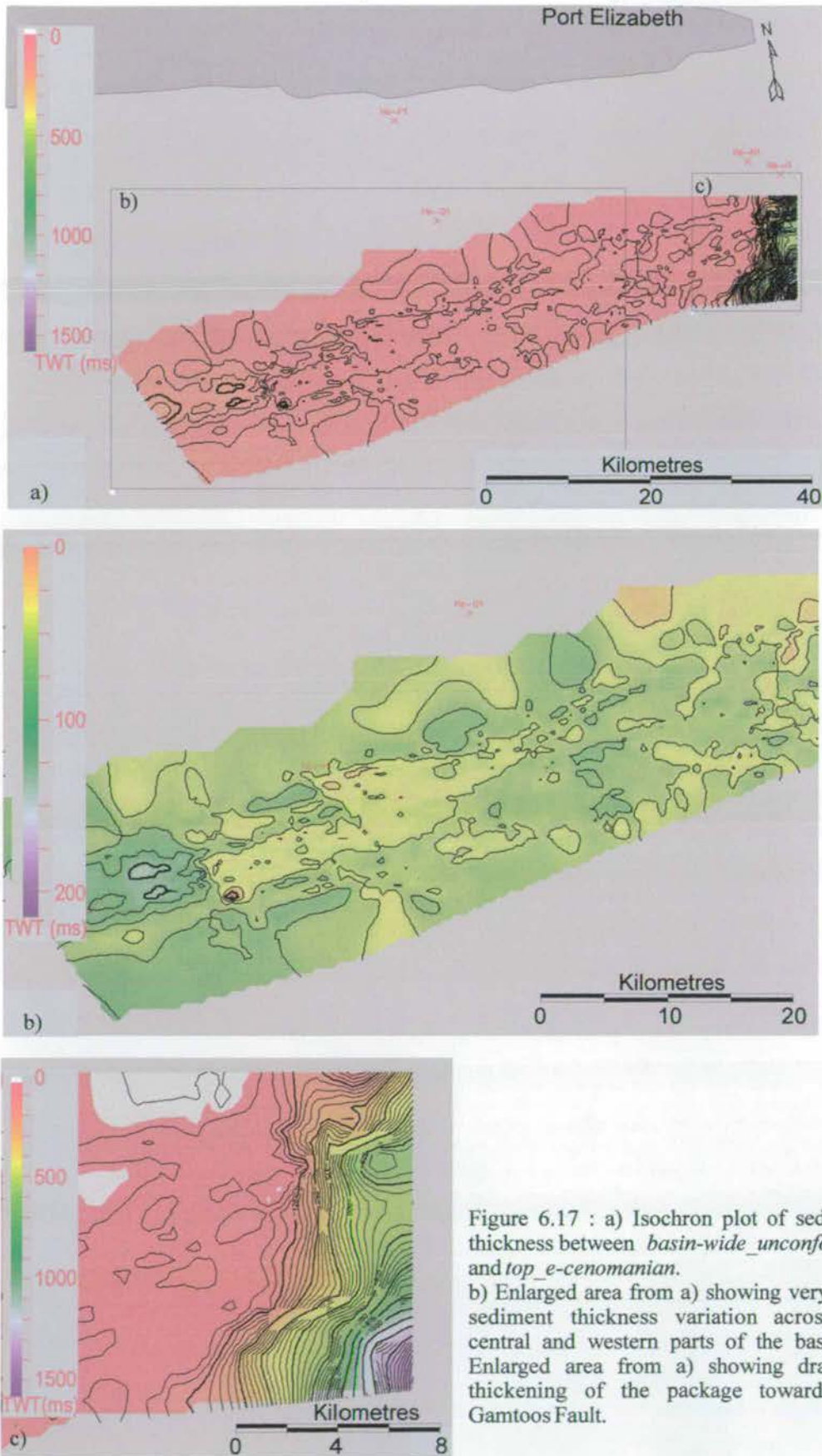


Figure 6.17 : a) Isochron plot of sediment thickness between *basin-wide_unconformity* and *top_e-cenomanian*. b) Enlarged area from a) showing very little sediment thickness variation across the central and western parts of the basin. c) Enlarged area from a) showing dramatic thickening of the package towards the Gamtoos Fault.

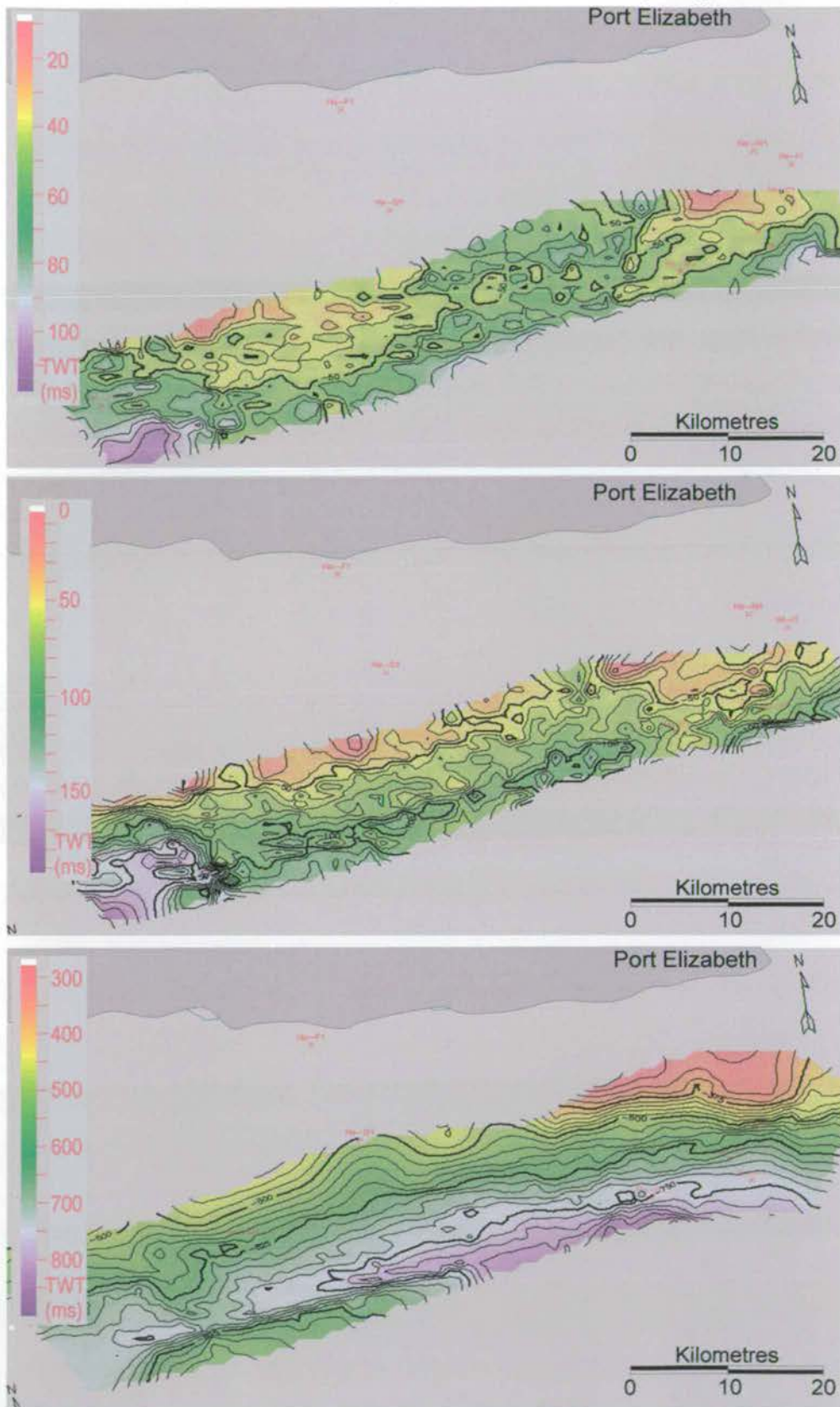


Figure 6.18 : Isochron thickness plots of a) Early Cenomanian, b) Turonian and c) sea bed to Early Turonian. There is very little sediment accumulation until after the Turonian (cf. progradational packages in Figure 6.15).

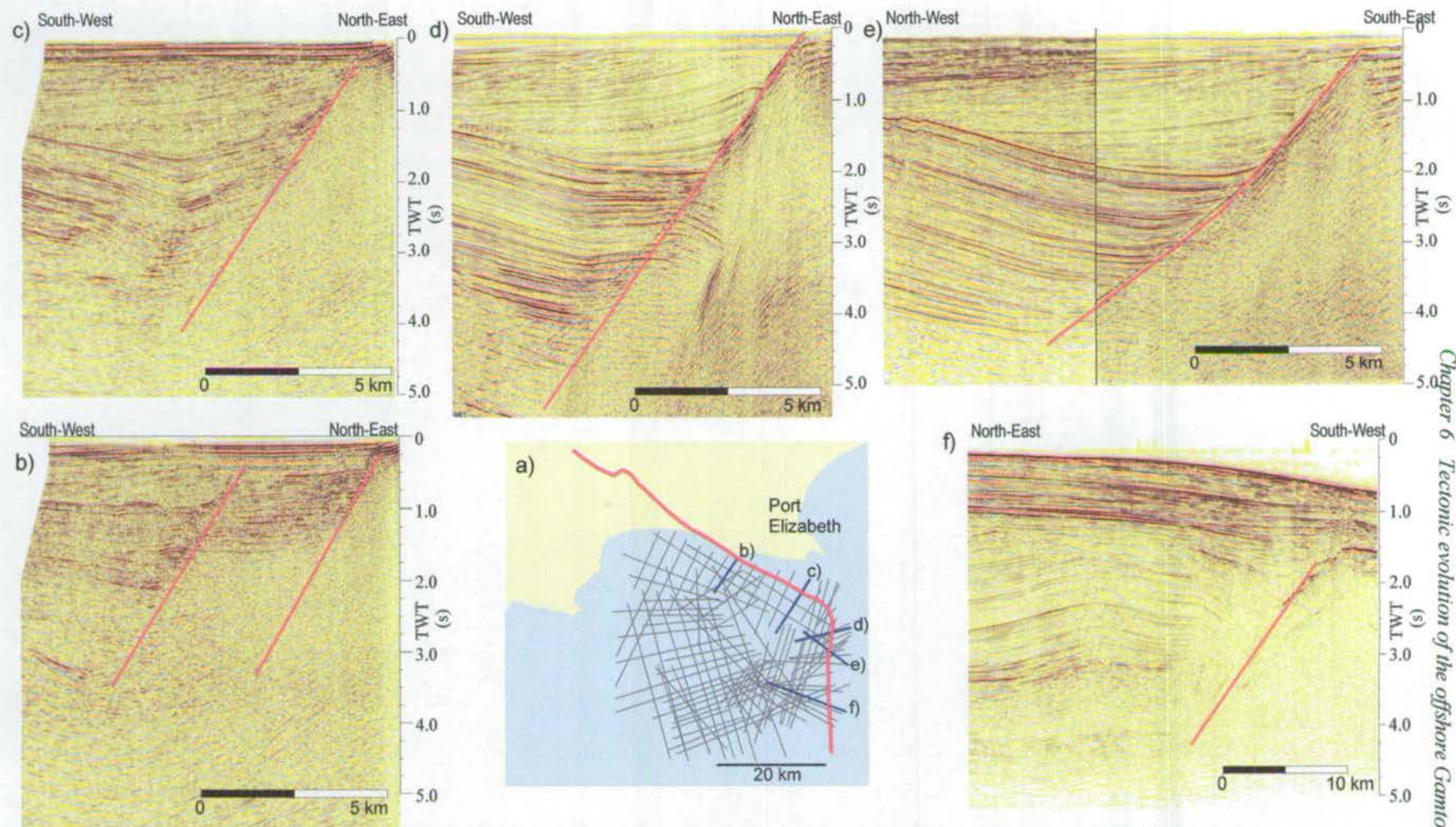
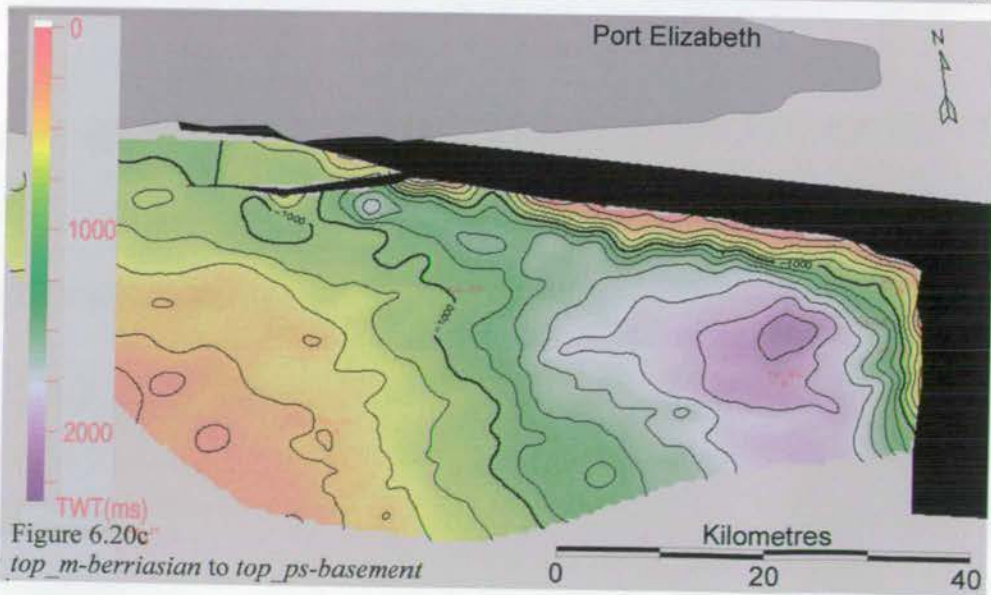
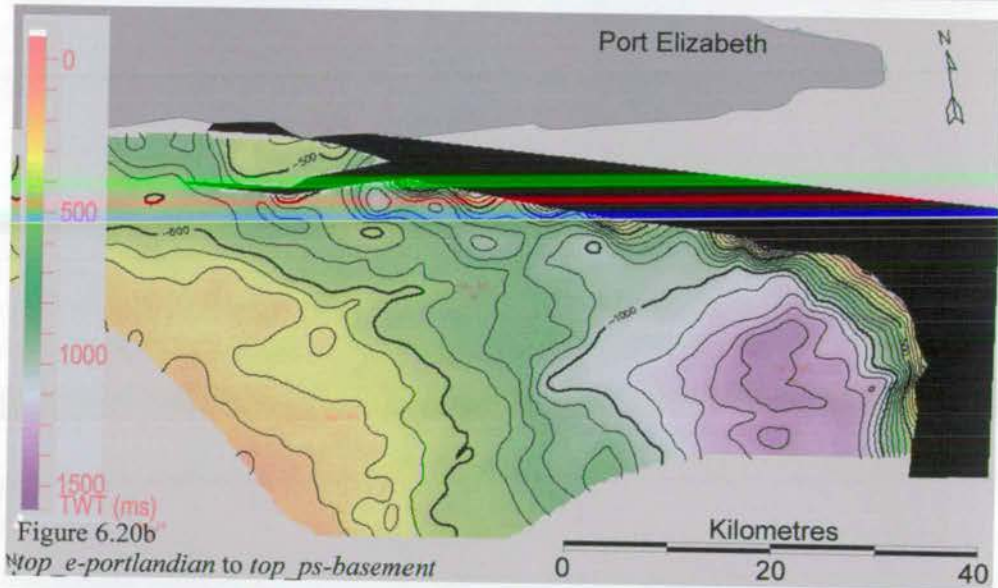
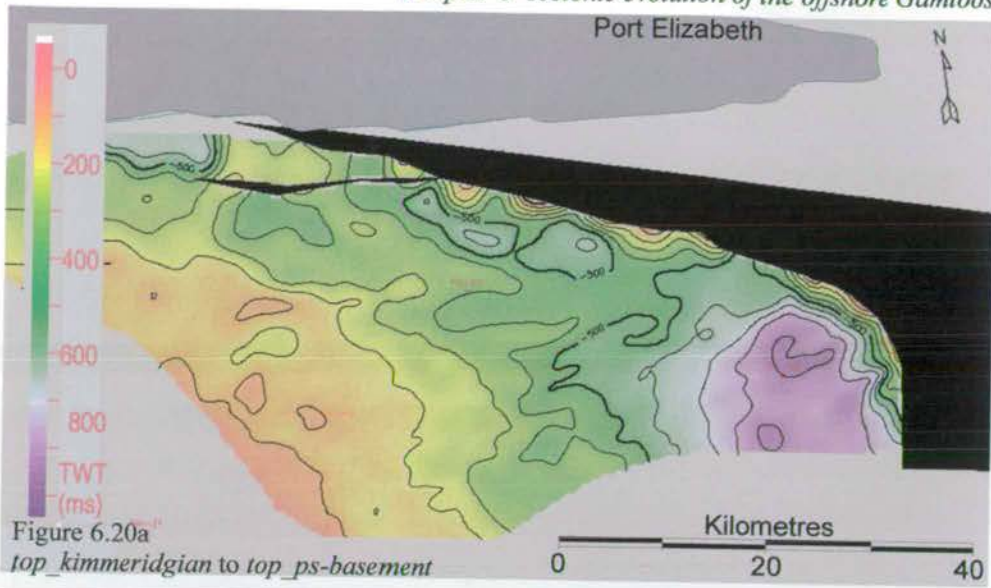


Figure 6.19: Seismic sections perpendicular to the Gamtoos Fault with locations in Figure (a) (Gamtoos Fault shown in red). Apart from (b) the Gamtoos Fault appears as a discrete planar fault that continues to at least 5 seconds twtt (~12 km) and has a very similar geometry regardless of orientation. There is also no indication of any cross cutting faults. In (b) there are two fault splays (cf. Figure 6.1). Line Names: b) Ha76-006, c) Ha76-019, d) Ha76-019, e) Ha75-017 (west), Ha82-011 (east), f) Ha82-042.



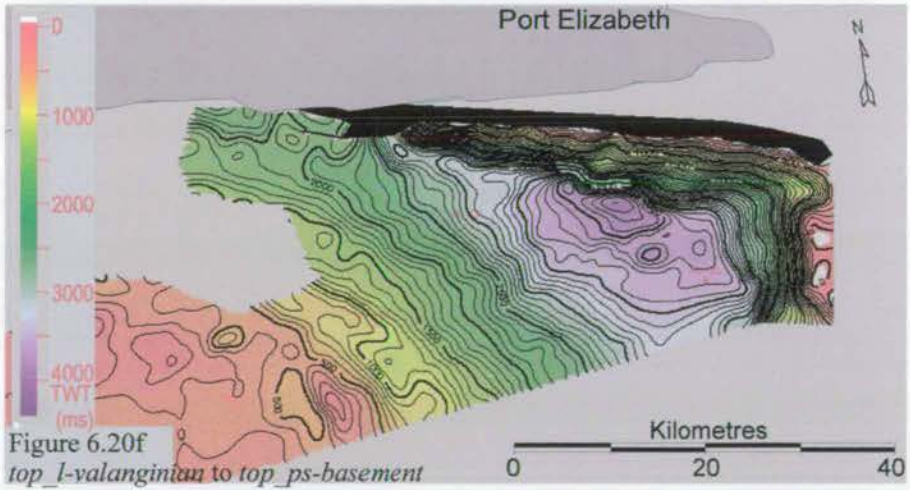
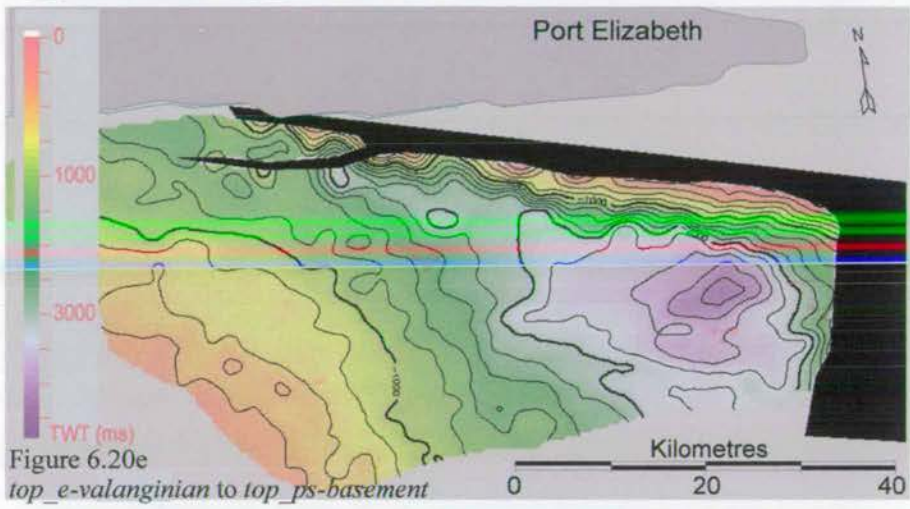
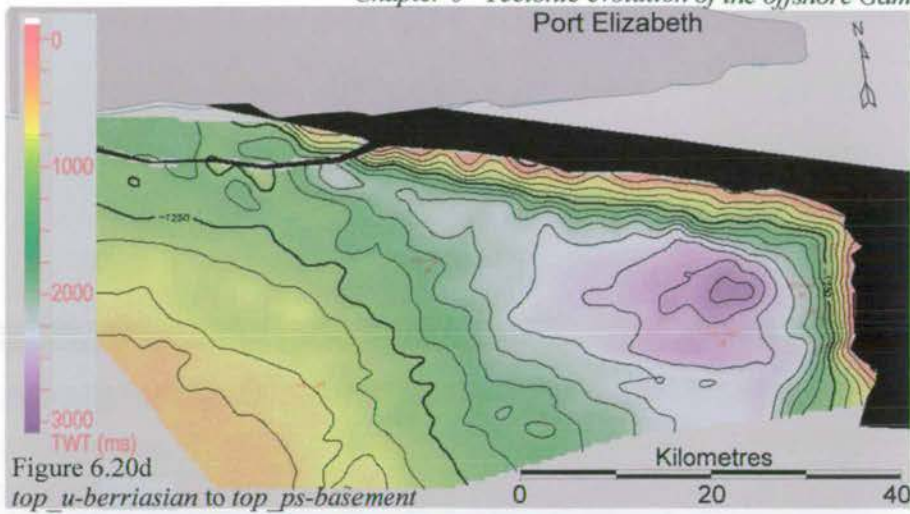


Figure 6.20 : Isochron thickness plots between the Principal Syn-Rift reflectors and *top_ps-basement* reflector. Sediments between the Gamtoos Fault plane and the appropriate reflector have been include. Plots show thickness of *top_ps-basement* to a) Kimmeridgian, b) Early Portlandian, c) Middle Berriasian, d) Late Berriasian, e) Early Valanginian, f) Late Valanginian (incomplete because of erosion in the south). These plots show that through time the locus of maximum sediment accumulation migrates from the south-east towards the east-west section of the Gamtoos Fault in the Late Valanginian.

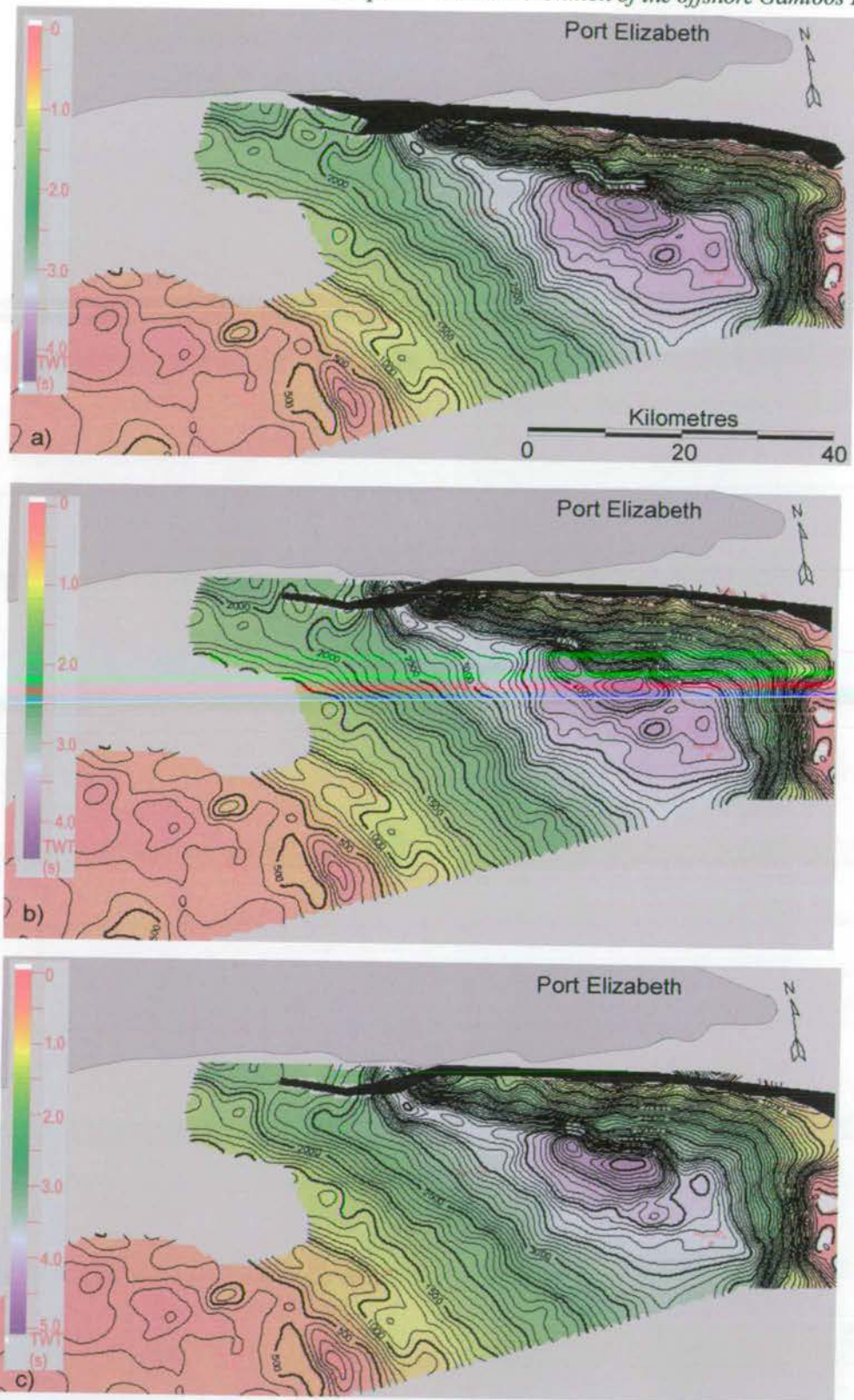


Figure 6.21: Cumulative isochron plots from *top_ps-basement* to a) *top_LSR I*, b) *top_LSR II*, c) *top_LSR III* (including sediments above the Gamtoos Fault). The locus of maximum sediment accumulation remains static adjacent to the east-west section of the Gamtoos Fault.

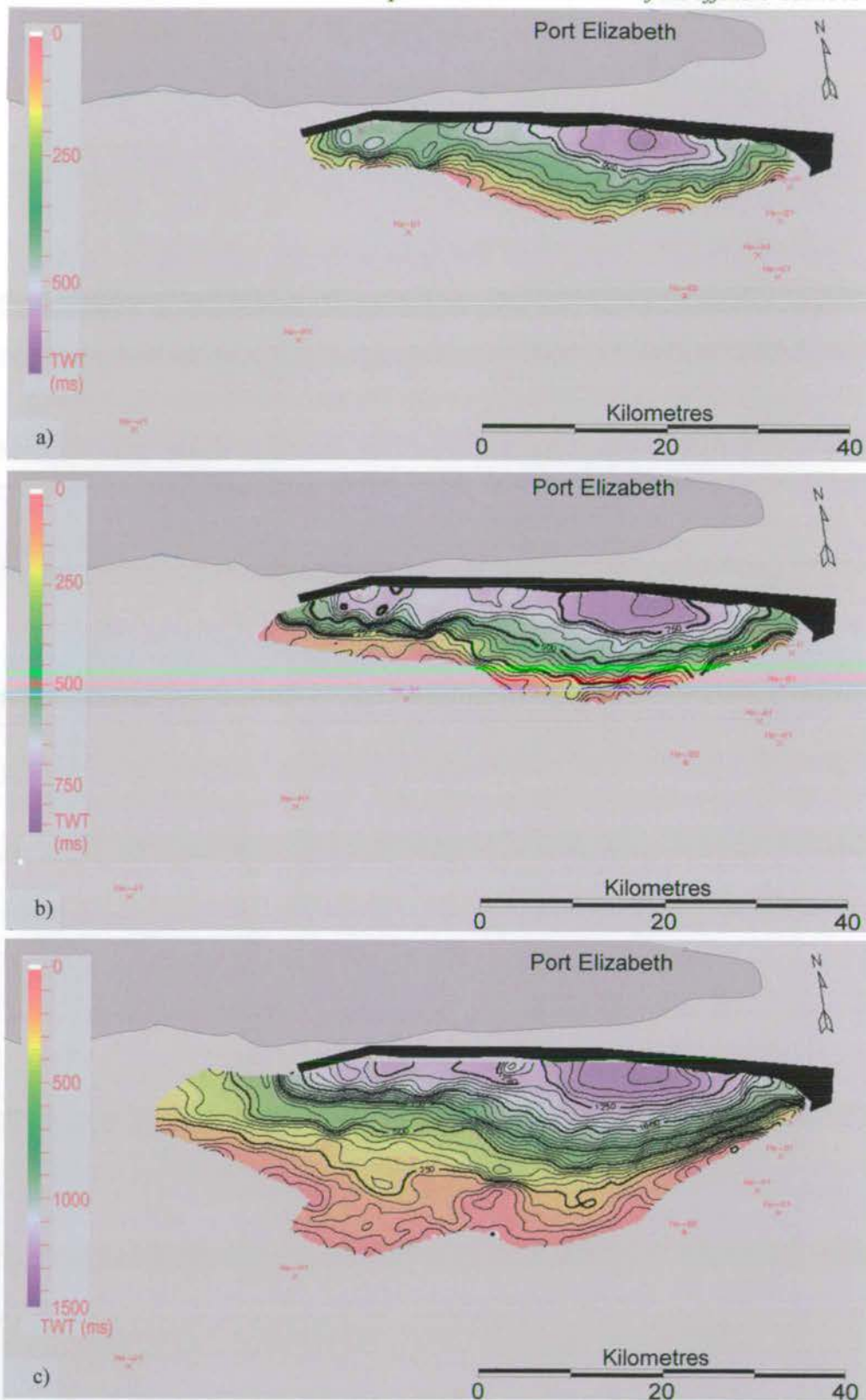


Figure 6.22: Isochron thickness plots between *top_l-valanginian* and Late Syn-Rift horizons, a) *top_LSR I*, b) *top_LSR II*, c) *top_LSR III*. Note, unlike Figure 6.20 (Principal Syn-Rift isochrons) these plots do not include sediments above the Gamtoos Fault. Loci of maximum sediment accumulation remains in approximately the same position through the development of the mega-sequence.

Figure 6.23a

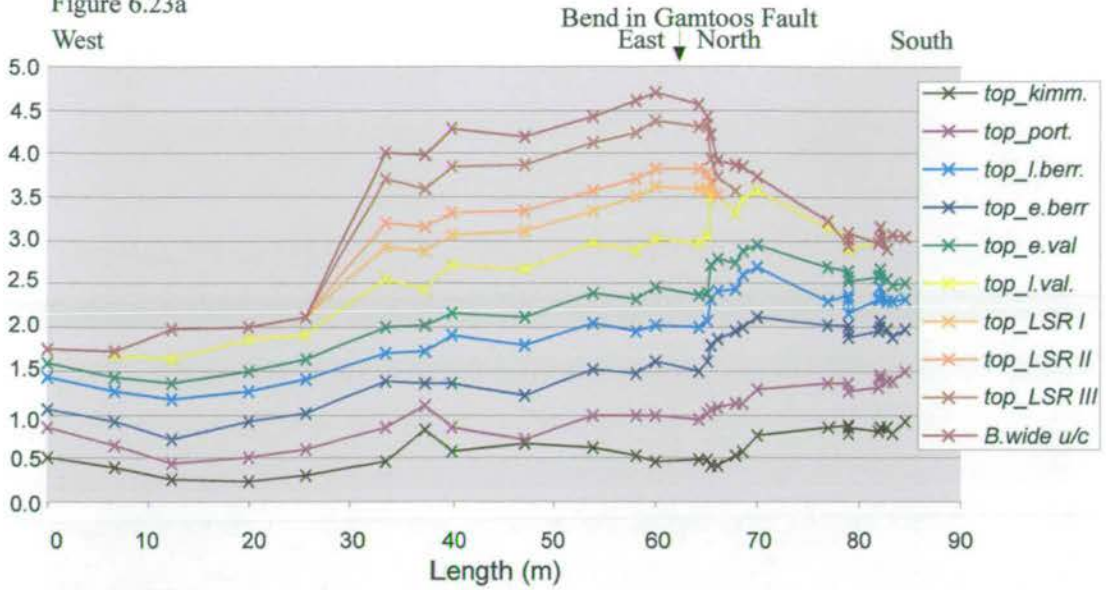
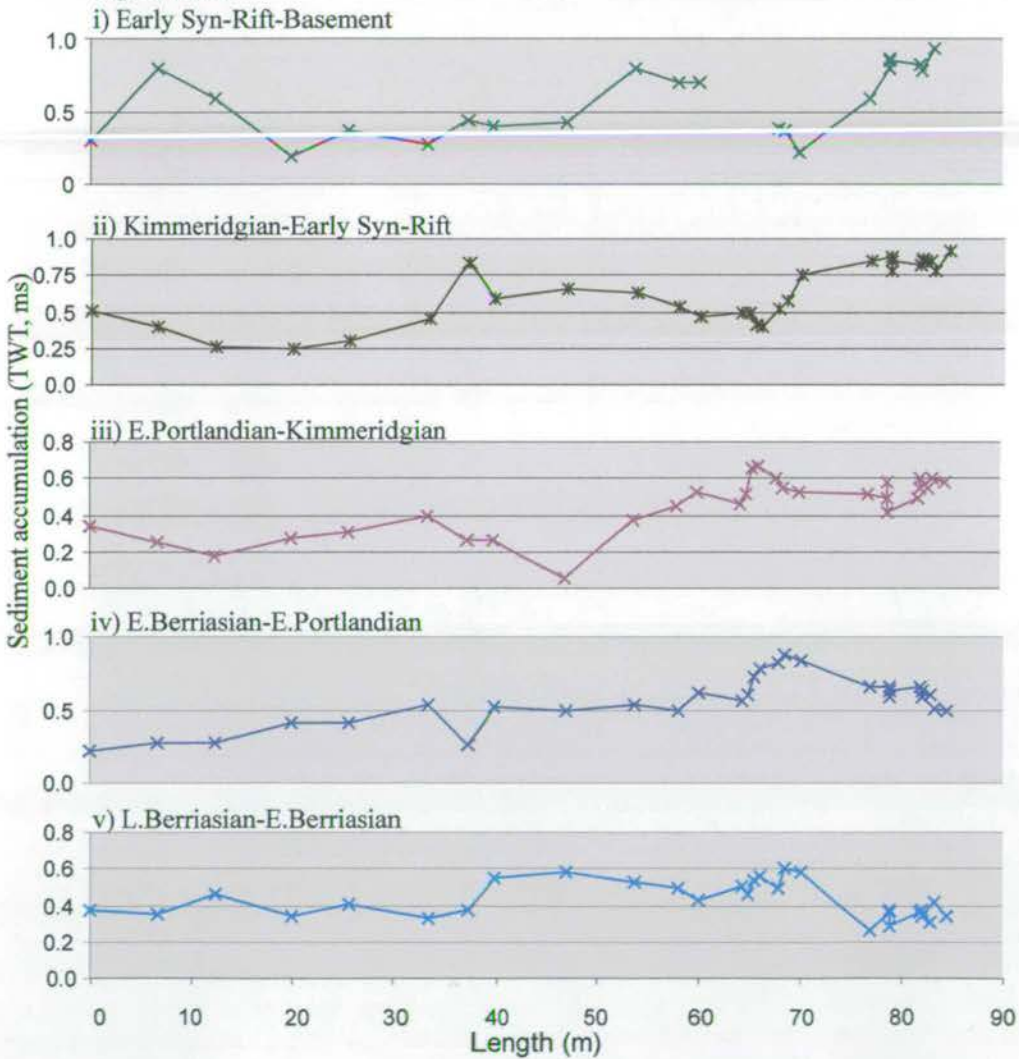


Figure 6.23b



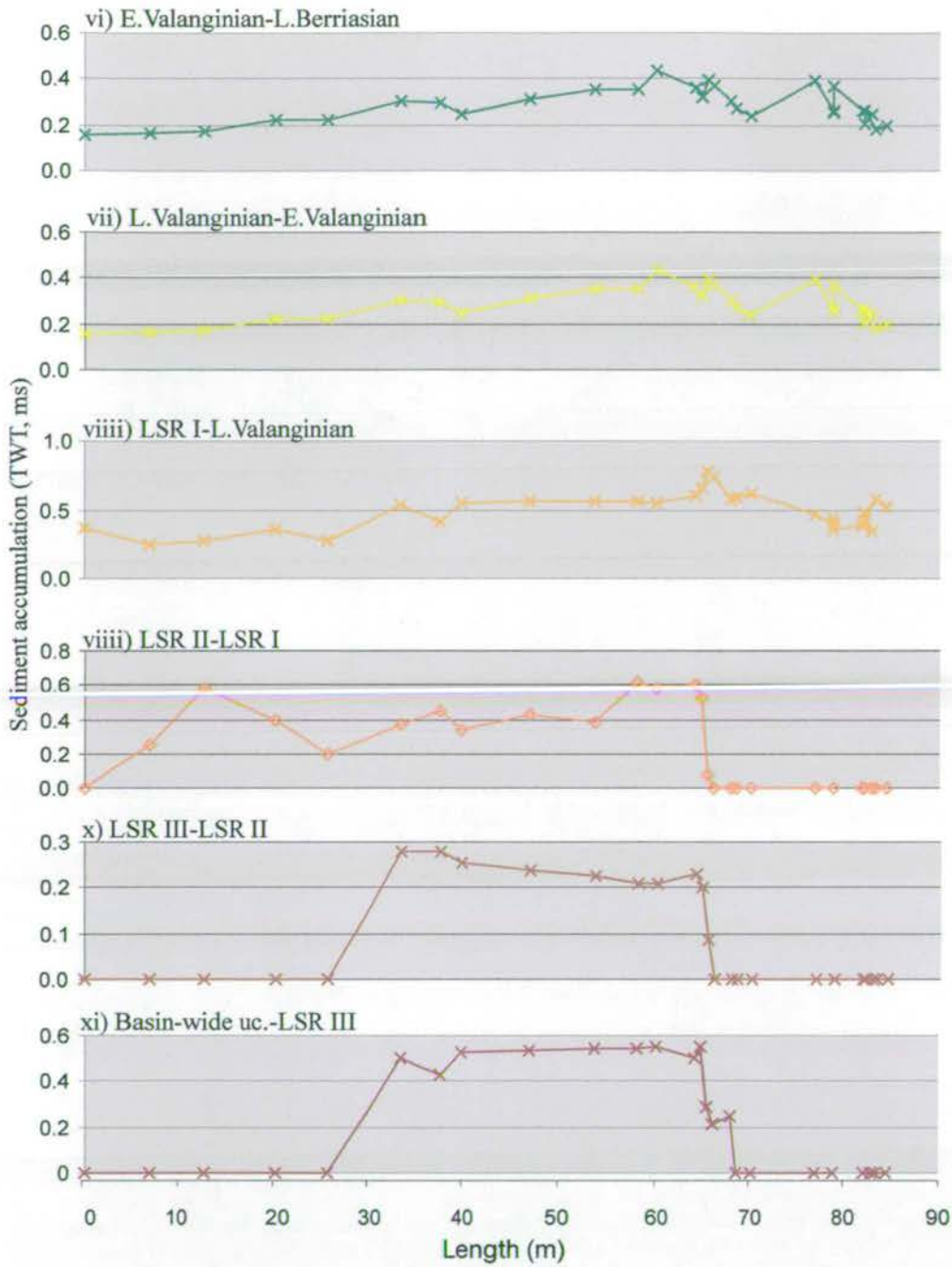
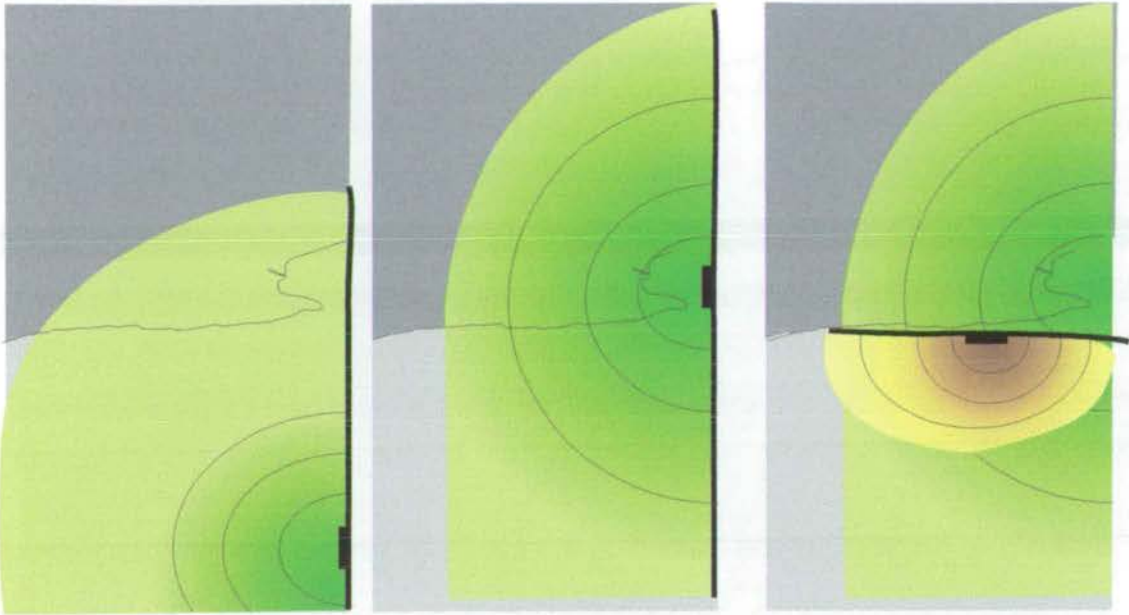


Figure 6.23: Sediment accumulation-length profiles along the Gamtoos Fault. a) Cumulative isochron from top pseudo-basement. b) Isochron plots of individual syn-rift sequences. Note the significant decrease in active fault length between the Late Valangian and Latest Valangian.

a)



b)

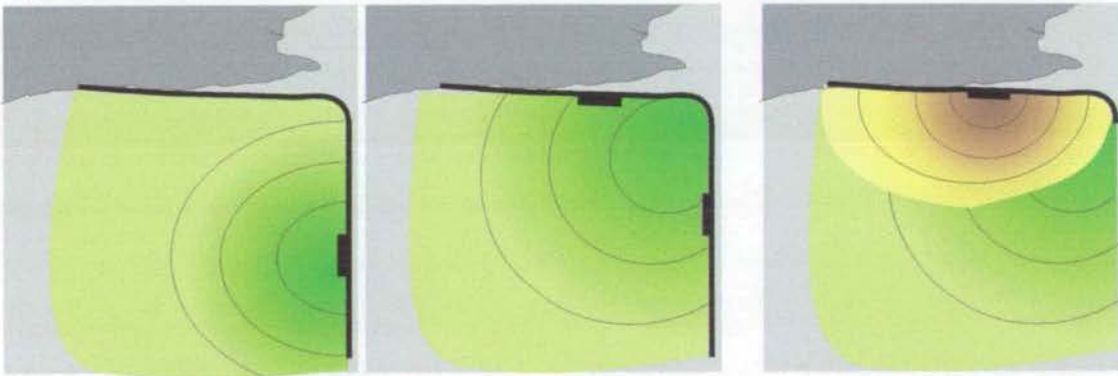


Figure 6.24: Two models proposing the evolution of the Gamtoos Fault. In both models light colour indicates thin sediment thickness and dark indicates thick sediment successions, green is deposition of the Principal Syn-Rift and yellow/brown is Late Syn-Rift. The present coastline and onshore area is shaded in grey, black line corresponds to active fault portion. The Principal Syn-Rift package is deposited on a north-south fault with the position of the locus of maximum sediment accumulation migrating north. In model a) sediment accumulation in the Principal Syn-Rift is controlled entirely by a north-south fault and Late Syn-Rift accumulation occurs against a separate east-west fault. In model b) there is one discrete fault controlling the sedimentation of both packages. The primary difference is that the footwall of the east-west fault is either Principal Syn-Rift sediments (model a) or basement (model b), see text for discussion..

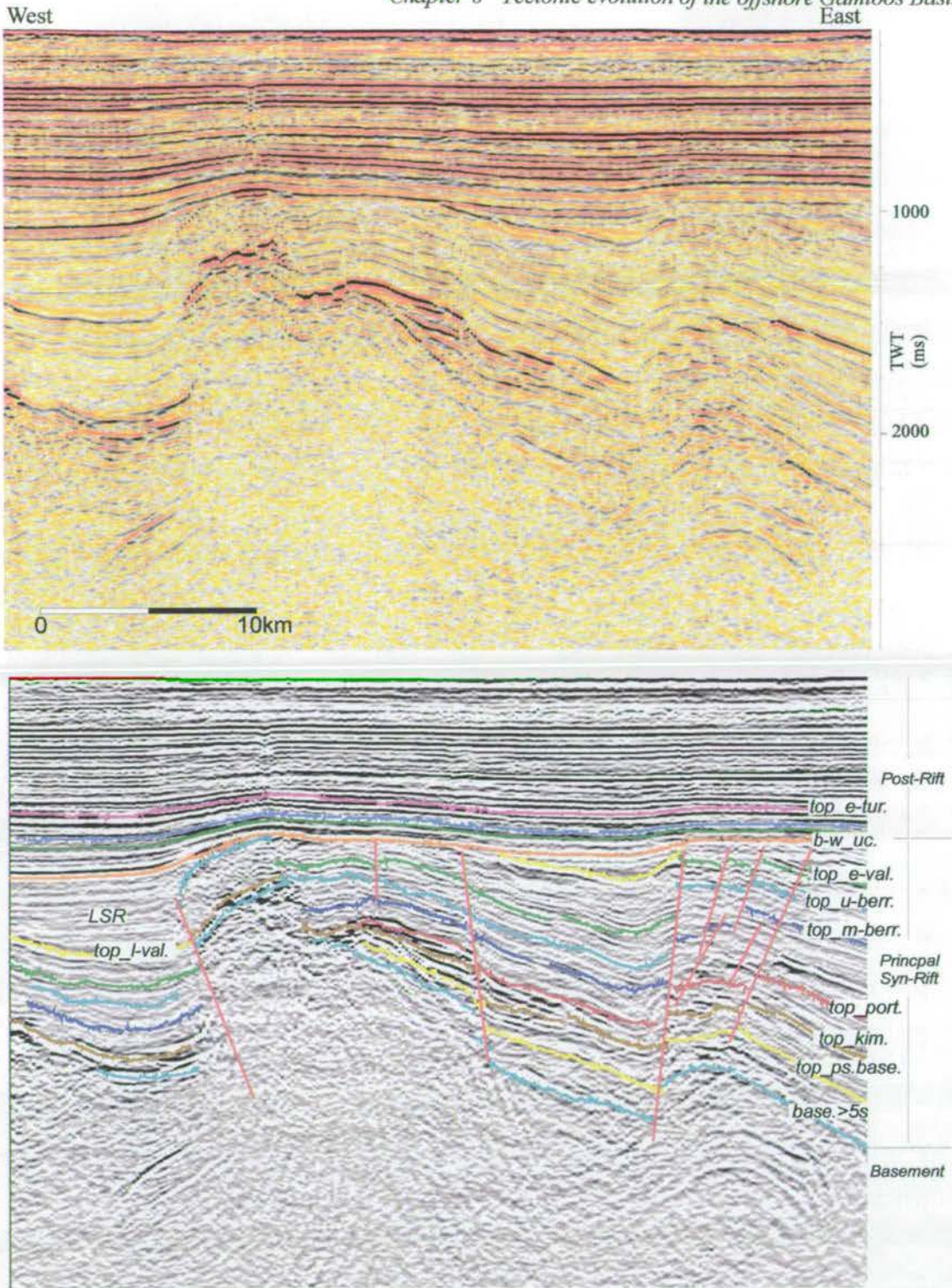


Figure 6.25: Section across the western basement high in which complex faulting is evident. Two arrays of normal faults define a small graben in the east, while a high angle reverse fault juxtaposes basement onto the Principal and Late Syn-Rift packages in the west. Line 87-002.

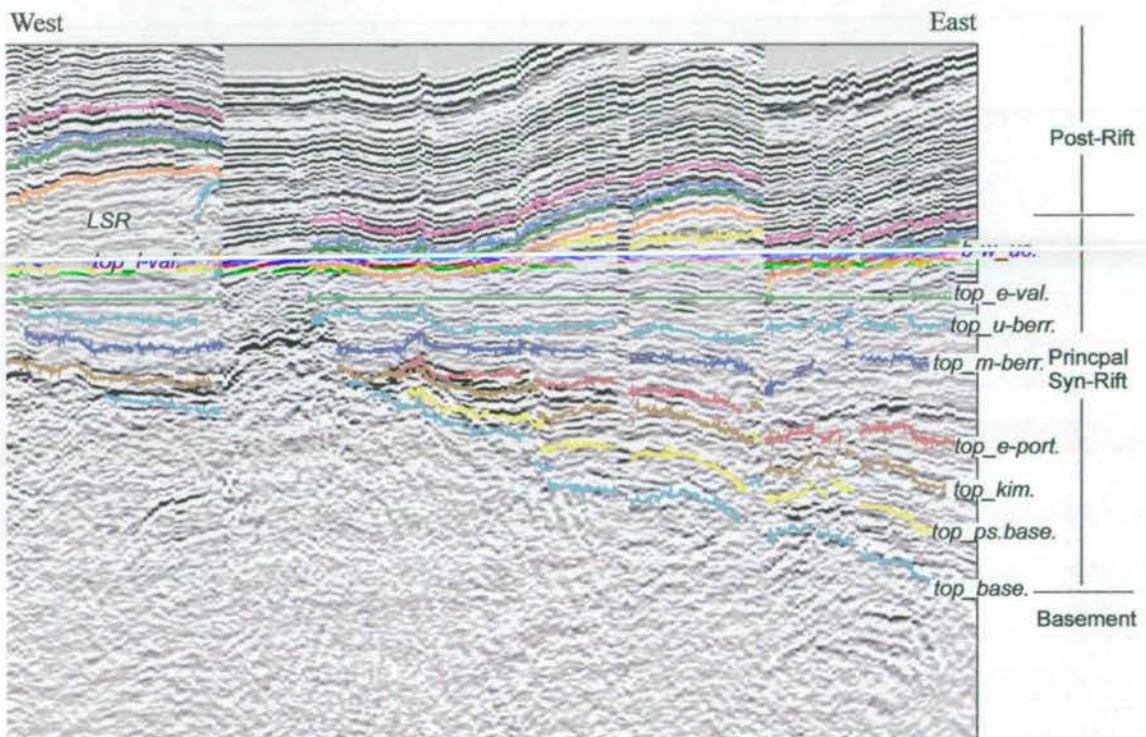


Figure 6.26: Section across the western basement high in Figure 6.25 with the *top_e-valanginian* reflector flattened to the horizontal. The restoration results in the removal of the high angle reverse faulting and much of the normal faulting to produce classic onlap geometry onto the basin margin.

South-West

North-East

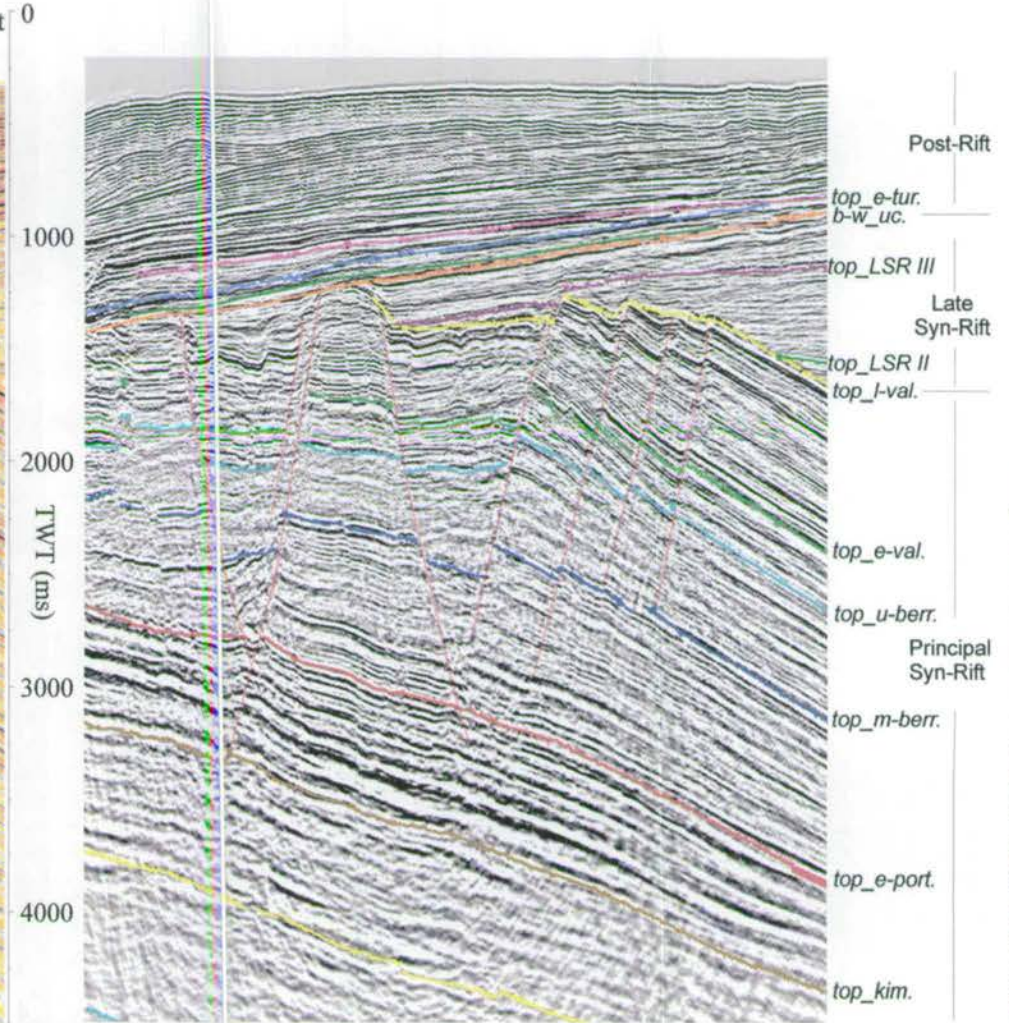
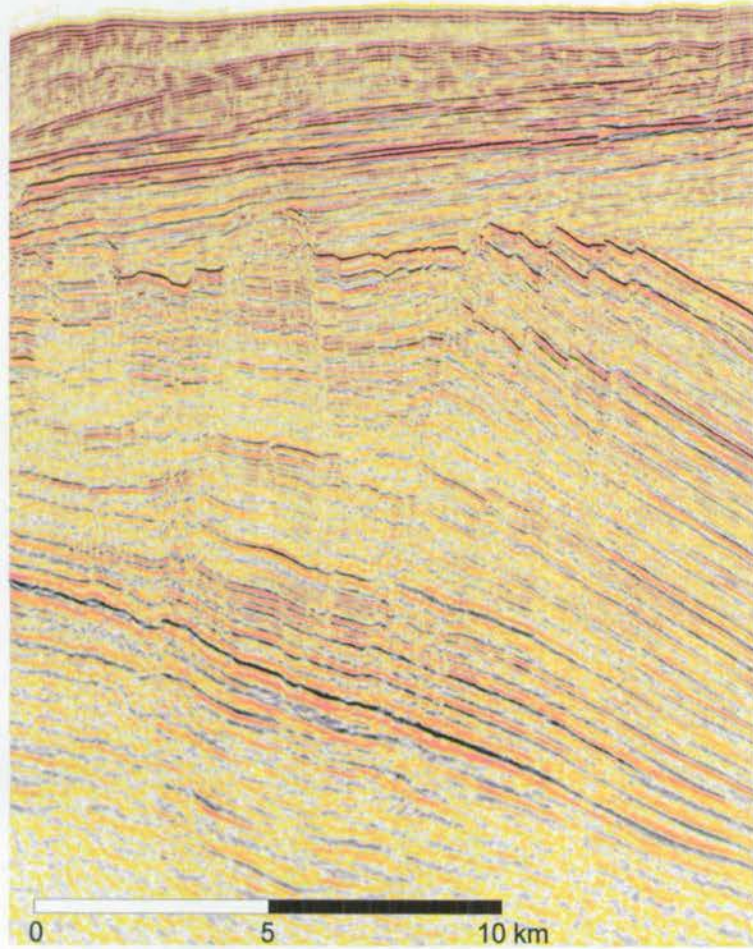


Figure 6.27: Intra-basin faulting commonly forms graben structures. Faulting is more pronounced in the upper Principal Syn-Rift package and population size and individual fault throws decrease with depth. The faulting does not significantly cross-cut *top_kimmeridgian* or *top_l-valanginian*. The majority of faults terminate at *top_l-valanginian*. Line Ha 75-017.

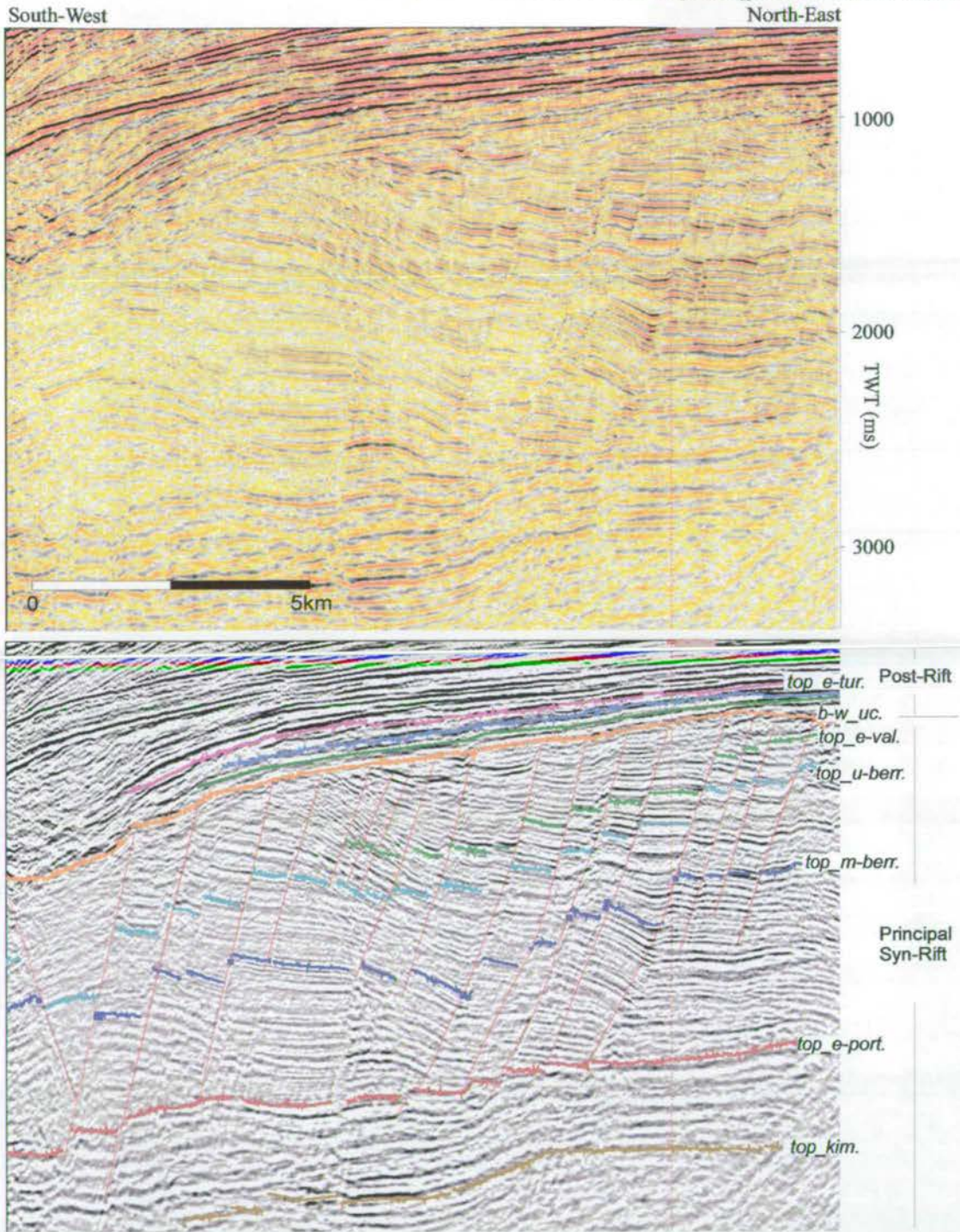


Figure 6.28: Intra-basin faulting in the Principal Syn-Rift mega-sequence. Some of the faulting appears to décolle below *top_portlandian* with associated folding directly above the *top_portlandian* reflector. Line Ha 87-032.

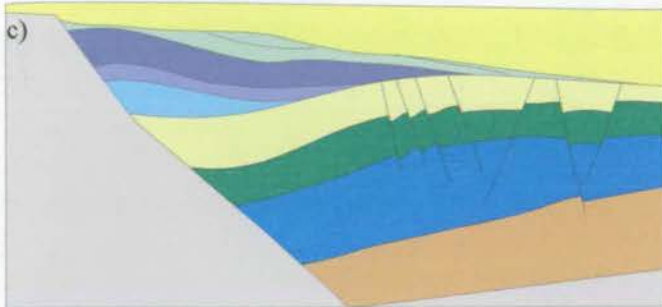
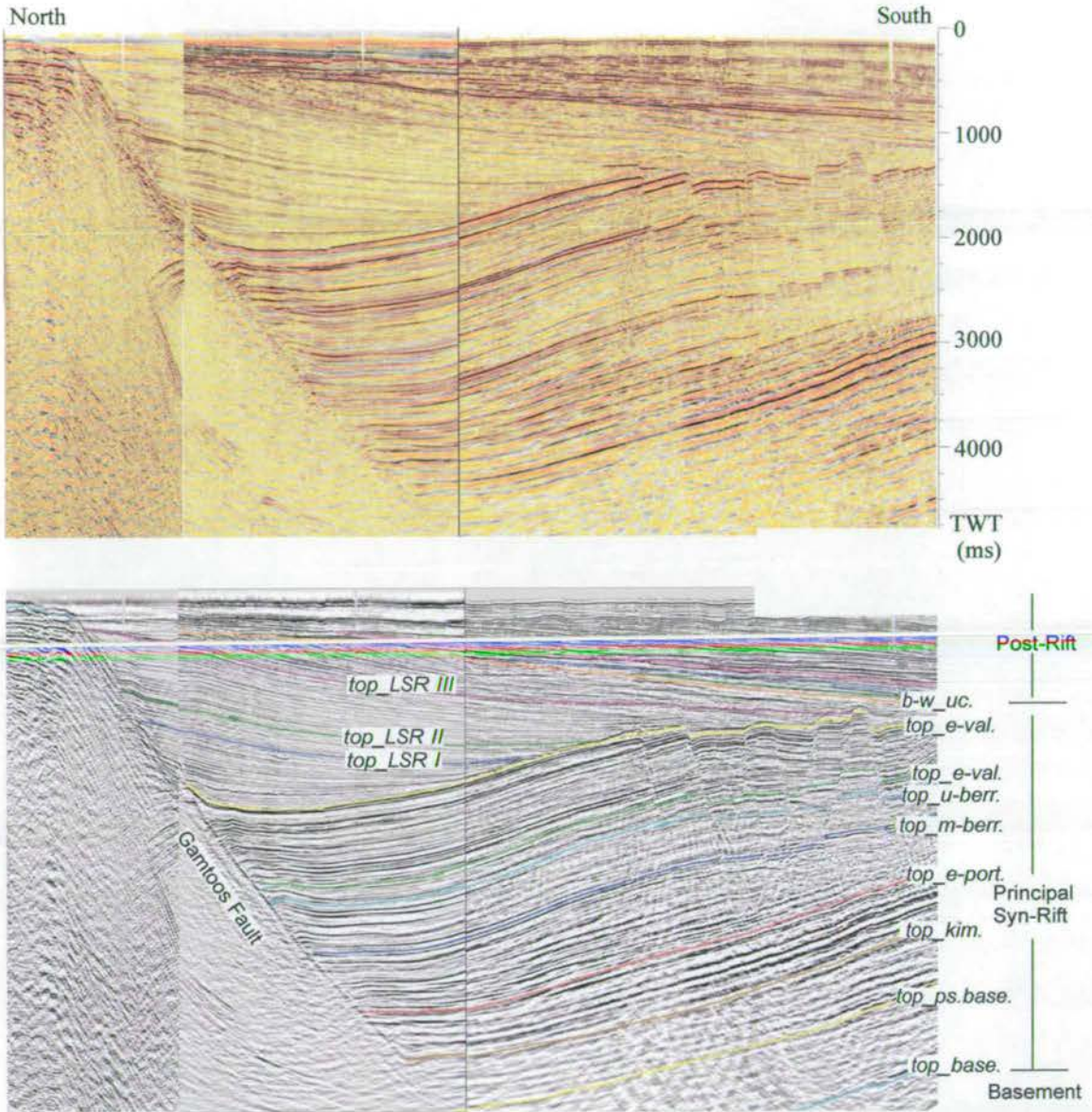


Figure 6.29: North-south section across the Gamtoos Fault that shows significant erosional truncation of the Late Syn-Rift (LSR) packages directly below the basin-wide unconformity. The simplified section (c) is used in the 2D-Move restoration in Figure 6.30.

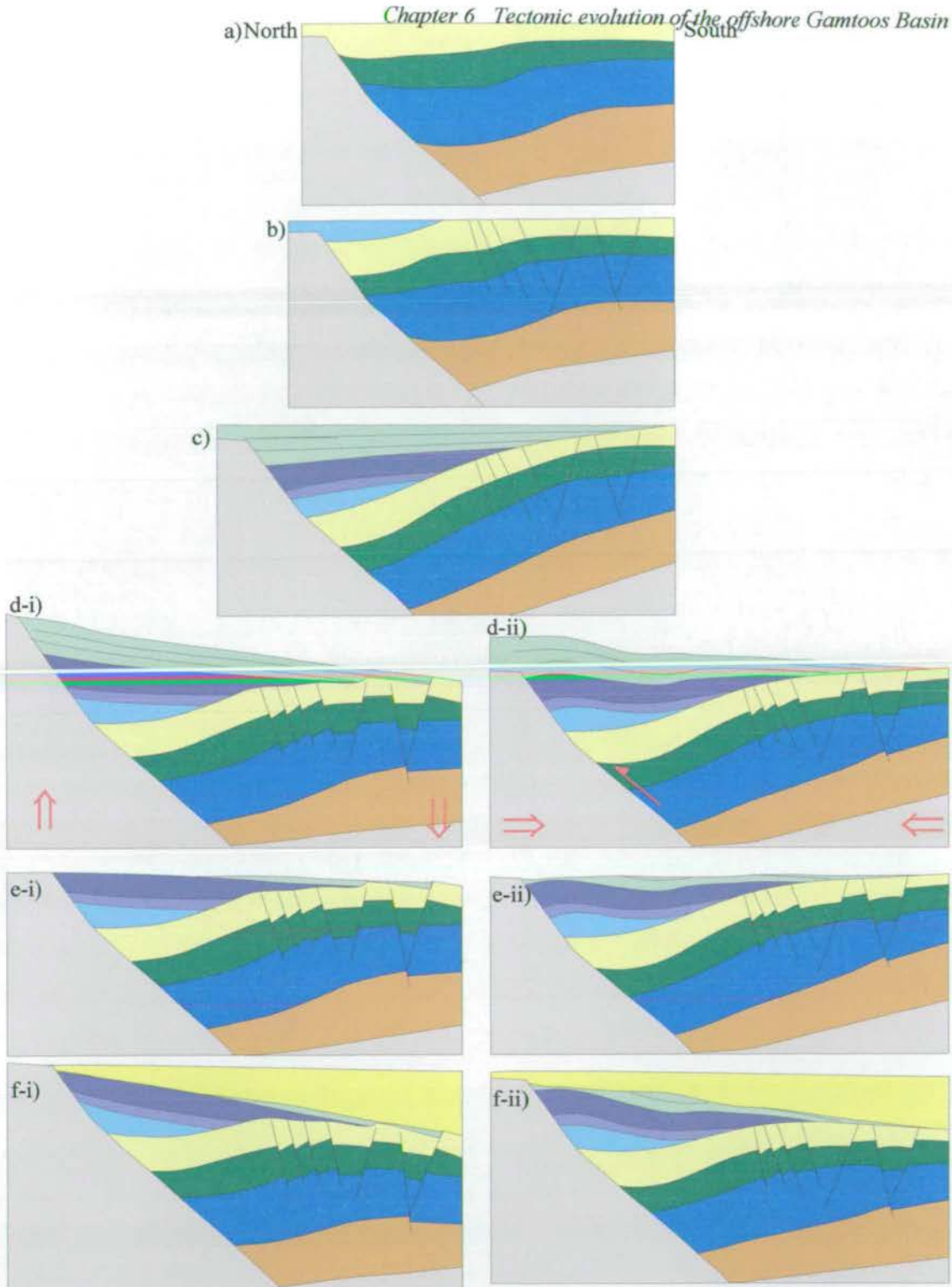


Figure 6.30: 2D Move restoration of the basin-fill deformation adjacent to the East-West Gamtoos Fault discussed in Figure 6.29. a) *Top 1 valanginian* deposited across the whole section. b) and c) deposition of the Late Syn-Rift sequences adjacent to the fault. Two models are proposed to obtain observed geometry. Model i (d-i) invokes differential uplift in the north and subsidence in the south (red arrows) while Model ii requires structural inversion against the fault with horizontal shortening (d-ii). e-i&ii) basin-wide unconformity prior to regional subsidence towards the south (f-i&ii). Model i does not result in the observed reflector geometries, especially in the upper LSR package, nor is there evidence of the regional tilting prior to the basin-wide unconformity, therefore Model ii is preferred.

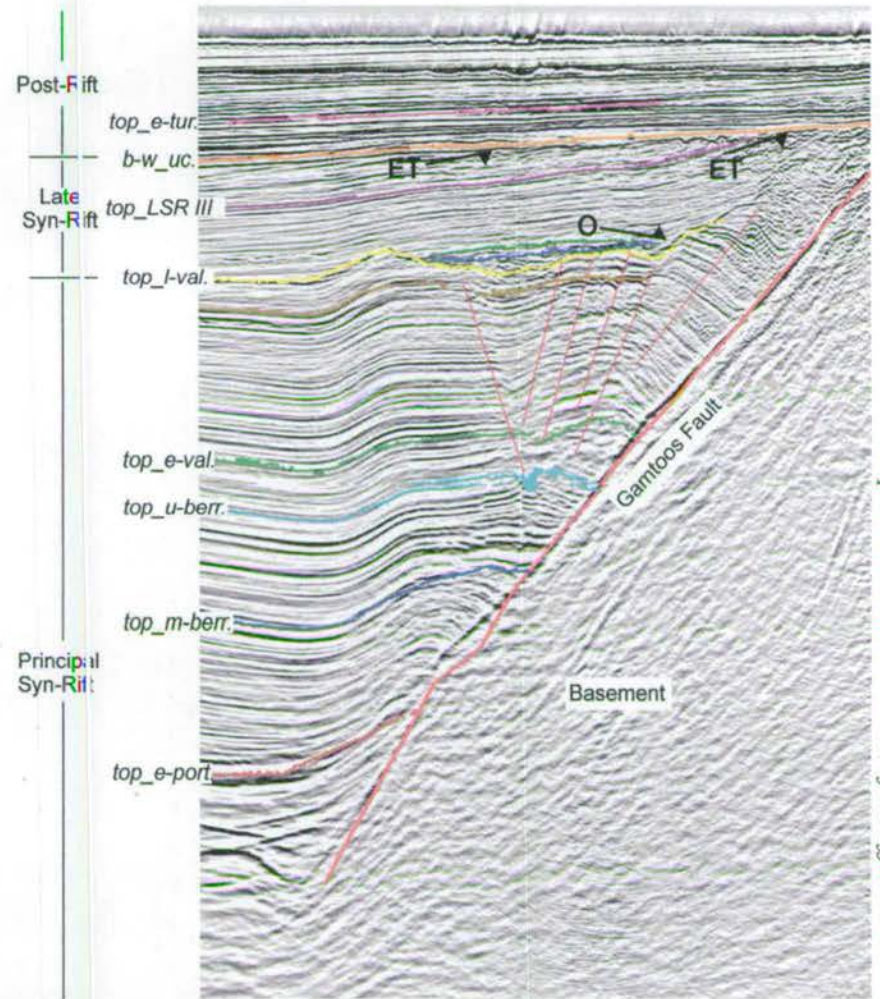
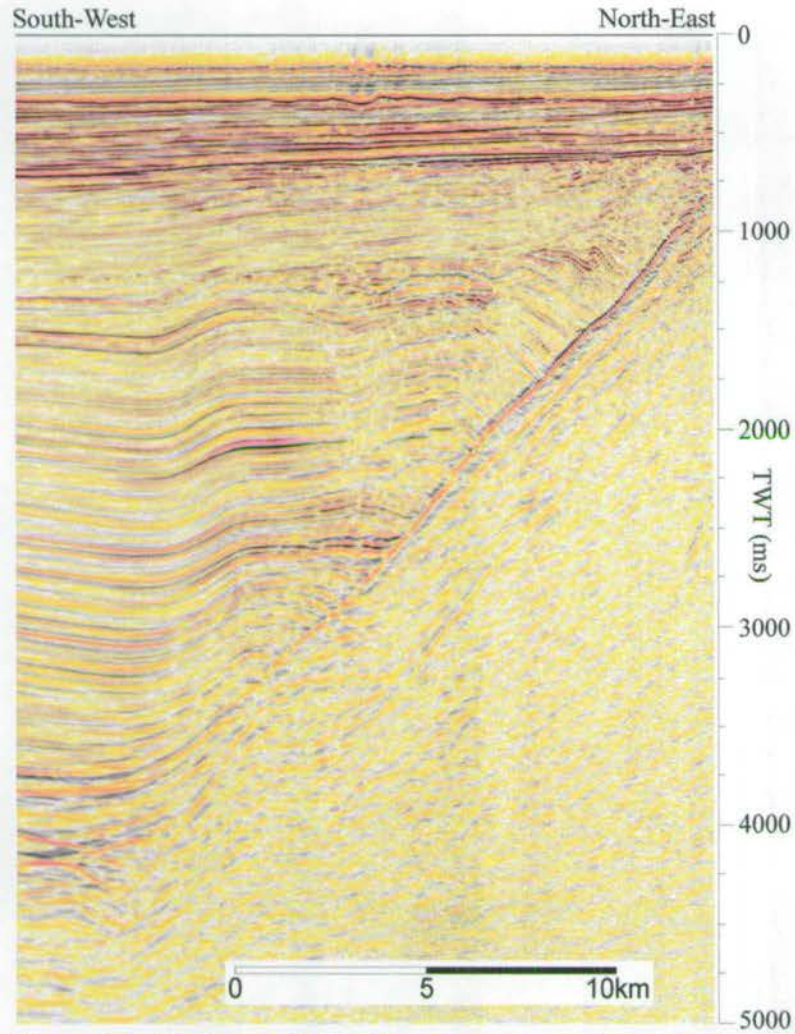


Figure 6.31a: Northern end of north-south trending section of the Gamtoos Fault. The Principal Syn-Rift Package is deformed directly above the Gamtoos Fault into a box fold composed of a series of smaller scale anticlines and synclines. Deformation dies away towards the south-east. The Late Syn-Rift (LSR) package onlaps (shown by O arrows) onto the lower structures and is truncated (ET) below the basin-wide unconformity. Line Ha 85-004.

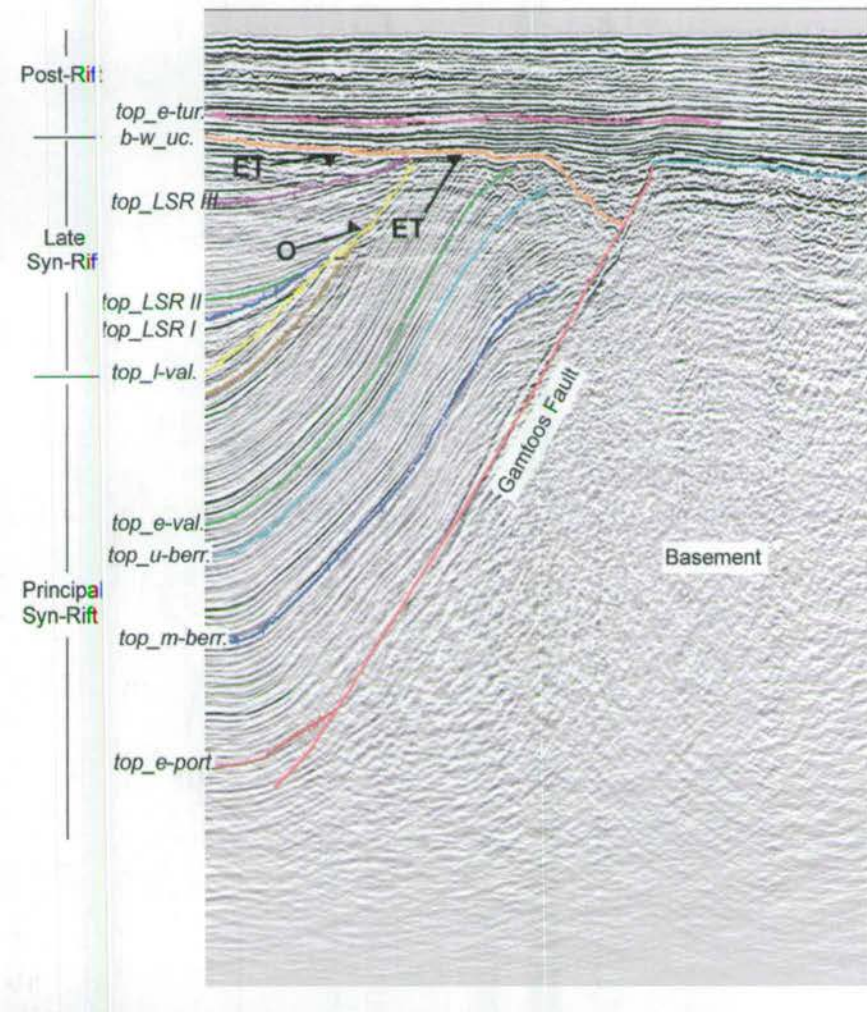
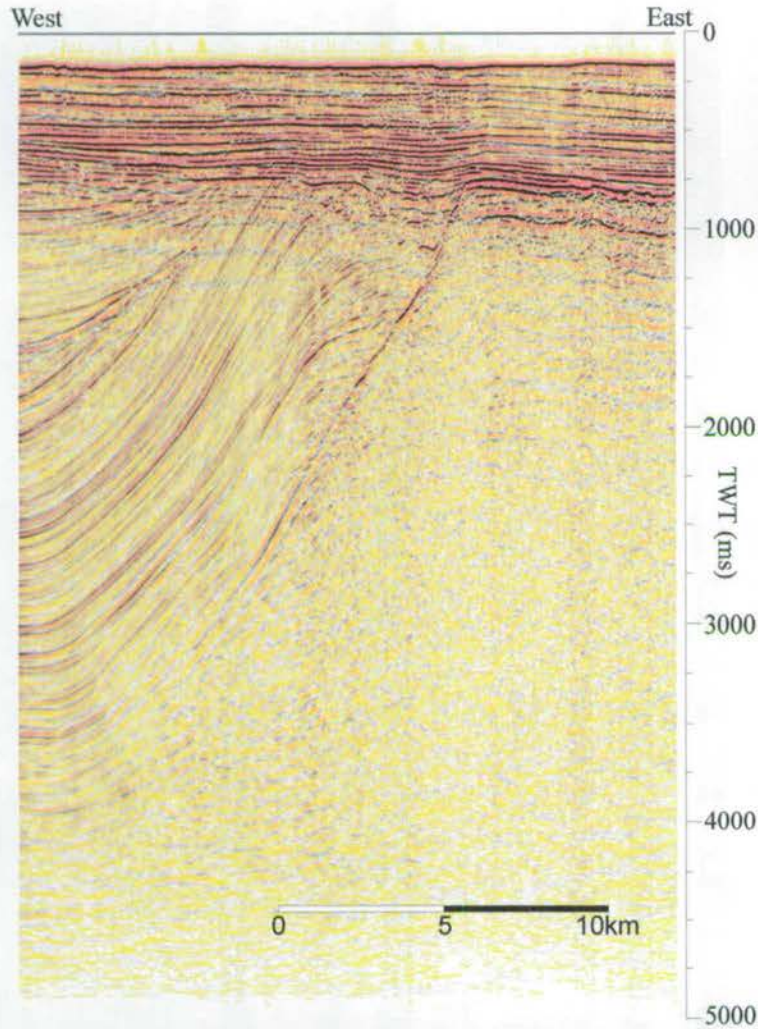


Figure 6.31b: Middle of north-south section of the Gamtoos Fault. Principal Syn-Rift package forms a monoclinial structure against the Gamtoos Fault. Late Syn-Rift package overlies onto *top_l-valanginian* (O) and shows sequential reflector rotation. Both the Principal and Late Syn-Rift packages are erosionally truncated against the *basin-wide_unconformity* (ET). Line Ha 87-052.

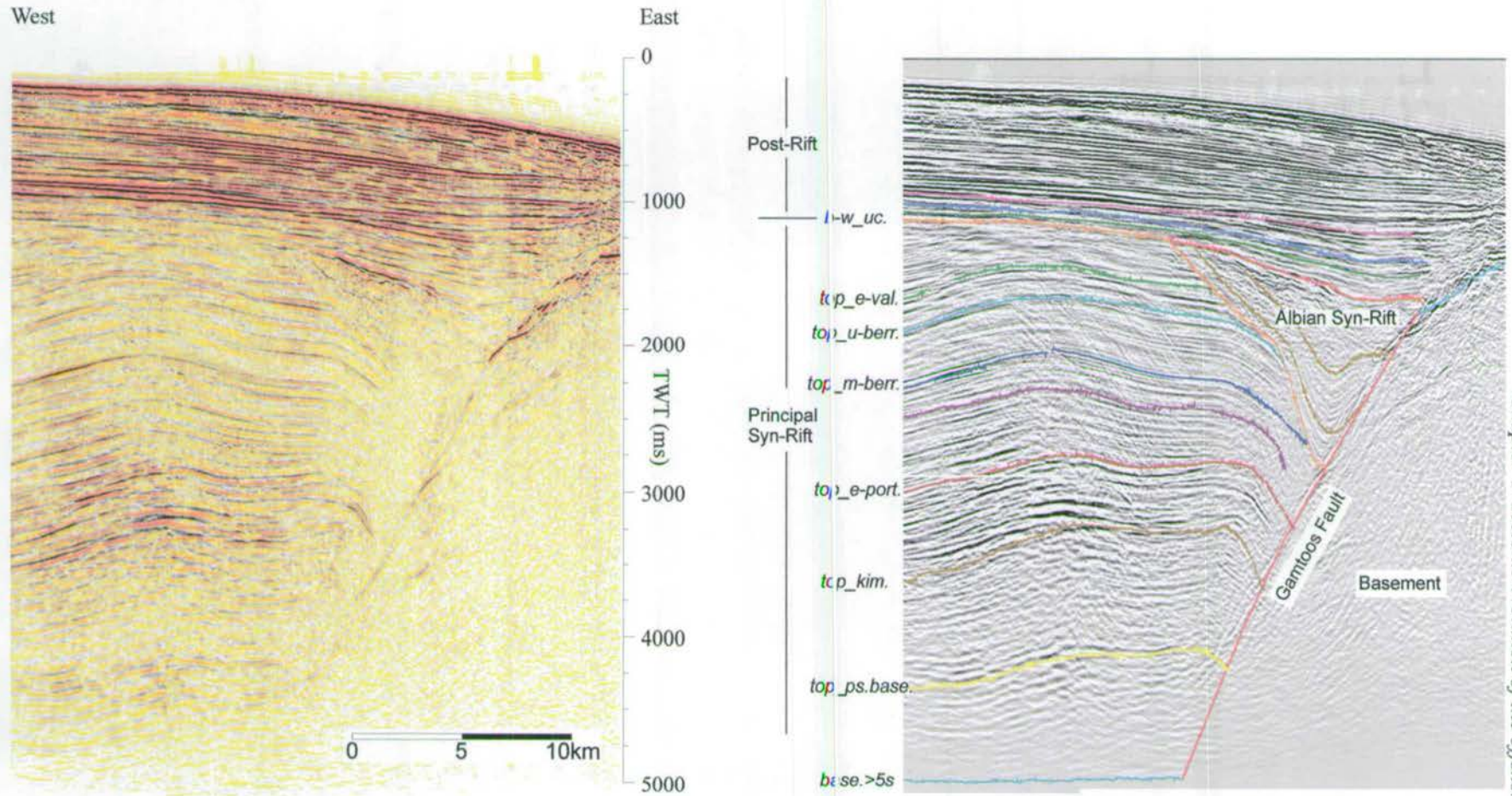


Figure 6.31c: Southern end of the north-south section of the Gamtoos Fault with the Principal Syn-Rift package forming a broad anticline against the Gamtoos Fault. The Late Syn-Rift package is not present in this section. Adjacent to the Gamtoos Fault is a localised Albian Syn-Rift package. Line Ha 87-042.

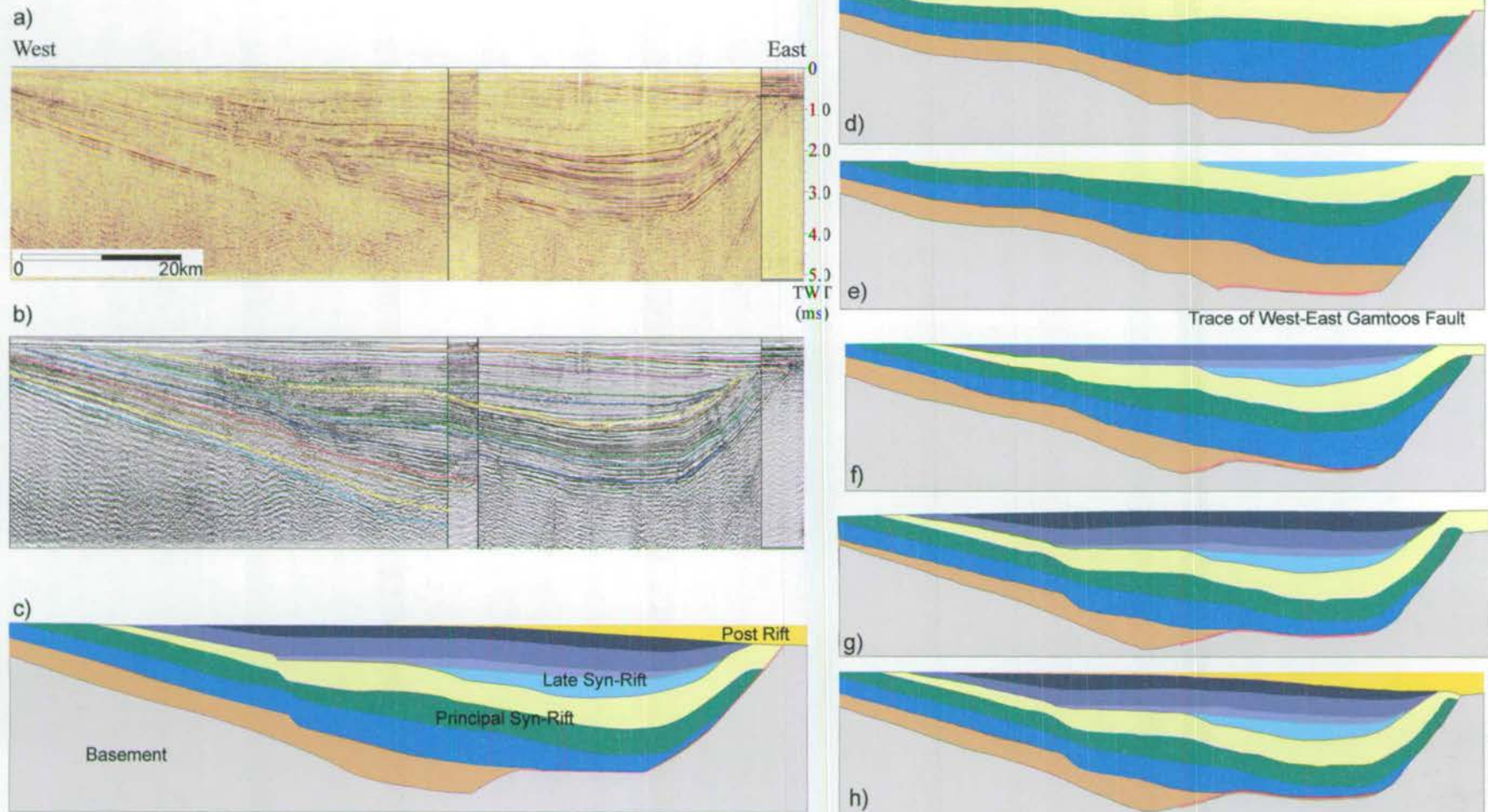
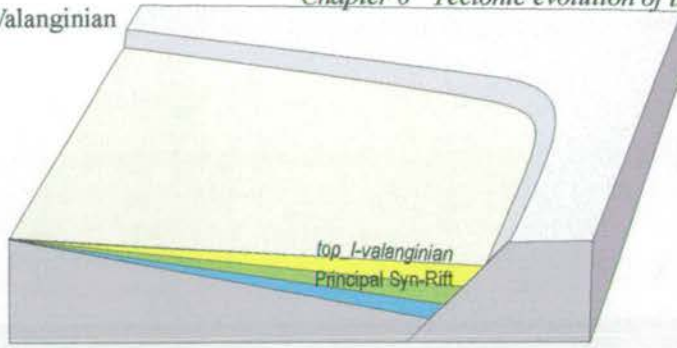
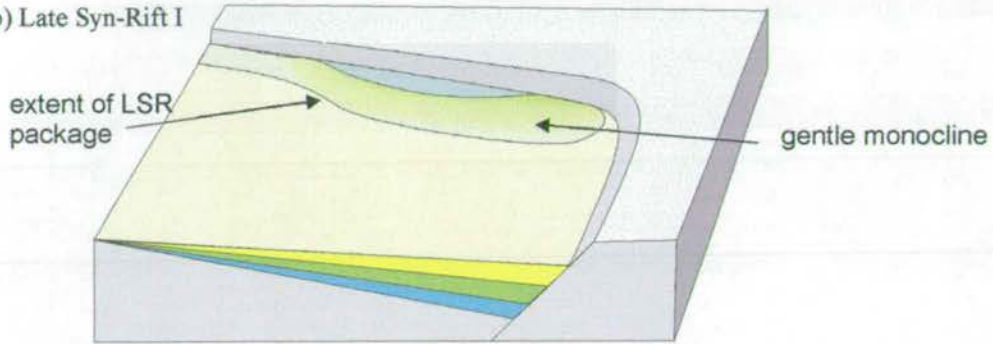


Figure 6.32: Section in the north of the basin parallel to, and in the immediate hangingwall of the east-west trending Gamtoos Fault section. The seismic section (a) with interpretation (b) was simplified to the model in (c). The model was restored to top *l-valangian* (d) and then Late Syn-Rift deposition on the East-West Gamtoos Fault was sequentially added, (e) top *LSR I*, (f) top *LSR II*, (g) top *LSR III*. As deposition occurs, the Principal Syn-Rift is folded to accommodate it, although in the east because the basement forms a buttress, the sediments deform more than expected and form a monoclinical structure. (h) the basin-wide unconformity erodes part of the monocline prior to regional subsidence and later uplift of the western flank.

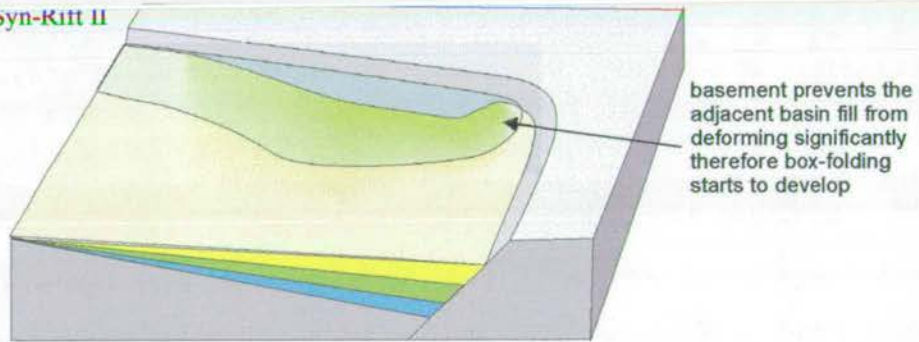
a) Late Valanginian



b) Late Syn-Rift I



c) Late Syn-Rift II



d) Late Syn-Rift III

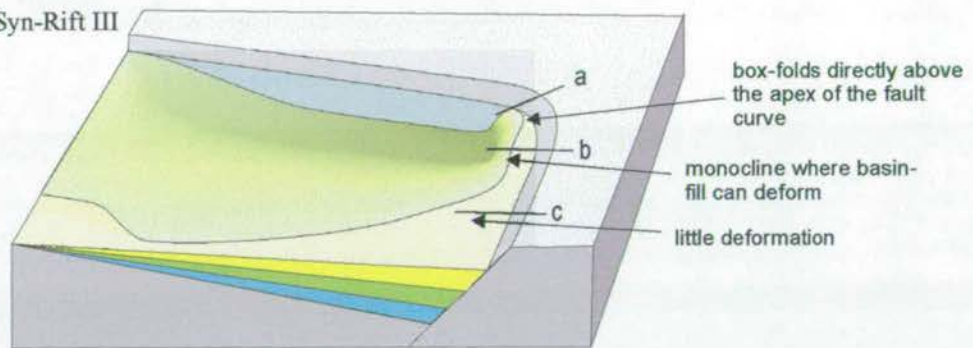


Figure 6.33: 3-D sketch to show the formation of the basin fill deformation proximal to the north-south Gamtoos Fault. Sketches correspond to deposition of : a) Late Valanginian, b) Late Syn-Rift (LSR) I, c) LSR II, and d) LSR III (includes position of sections in Figures 30a-c). The geometry of the *top I-valanginian* horizon is shown throughout and the lateral position of the appropriate LSR horizon is shown. The increase in the extent of the LSR is accompanied by increasing deformation of the basin fill and the progressive formation of the observed monoclinical structures.

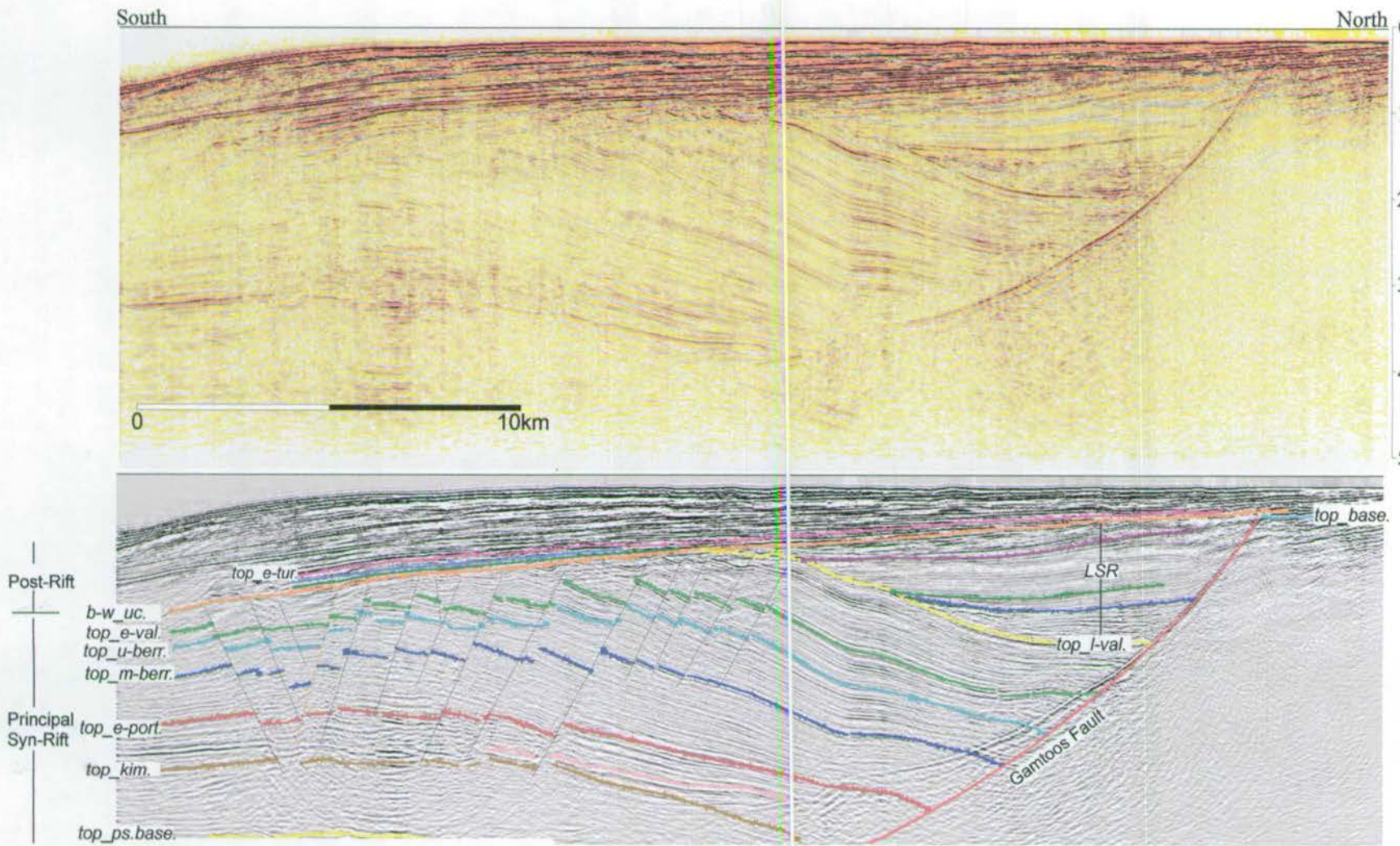


Figure 6.34: Section across the eastern part of the basin that shows folding of the Principal Syn-Rift package below the basin-wide unconformity. This package shows evidence of intra-basin folding and the onlap of the Late Syn-Rift Package (LSR). Note that the Gamtoos Fault appears to be listric because the section is oblique to the fault trend. Line Ha 89-026.

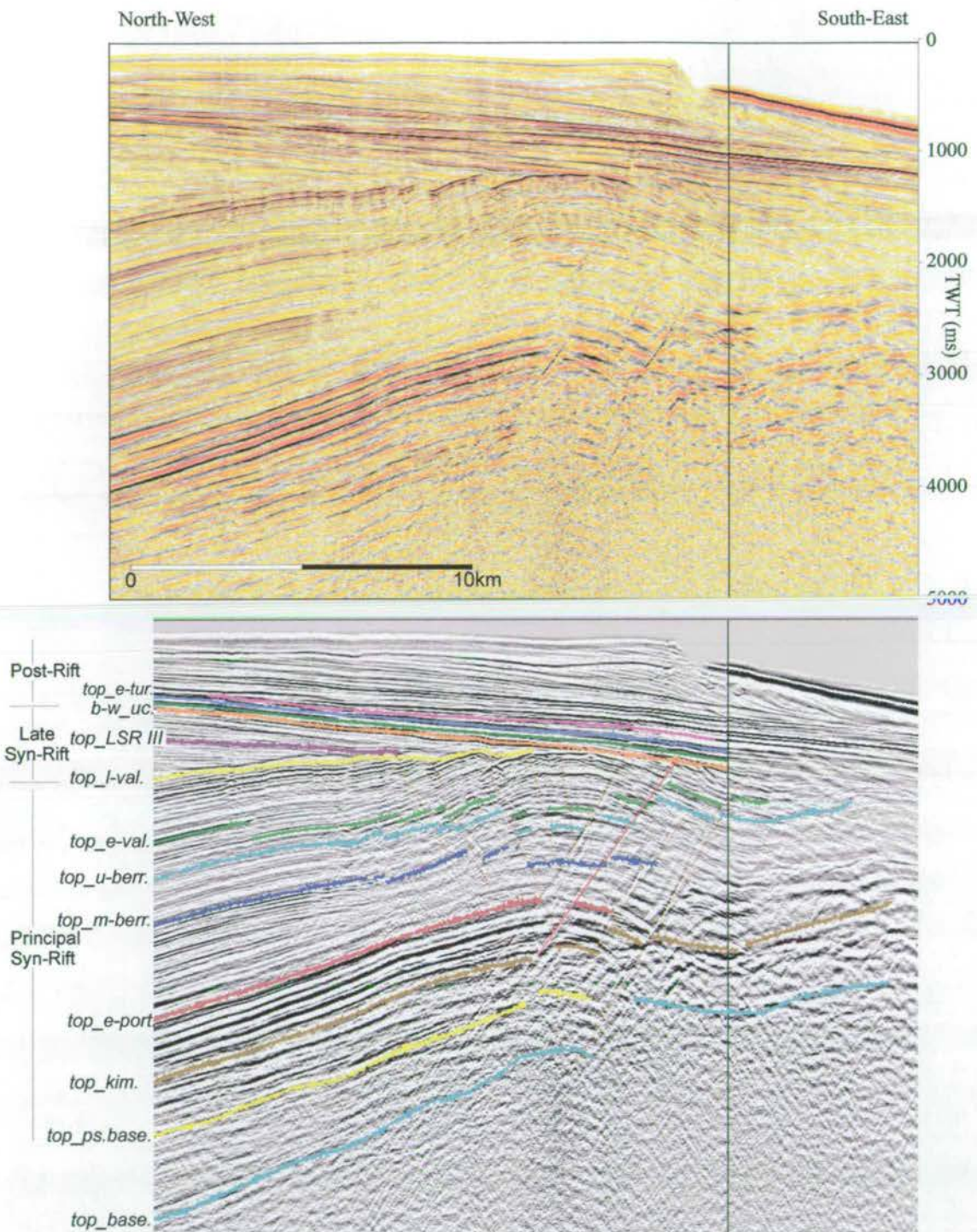


Figure 6.35: Folding of the Principal Syn-Rift package and the subsequent onlap of the Late Syn-Rift package. The basin-wide unconformity truncates the top of the anticline. Line HA 82-039.

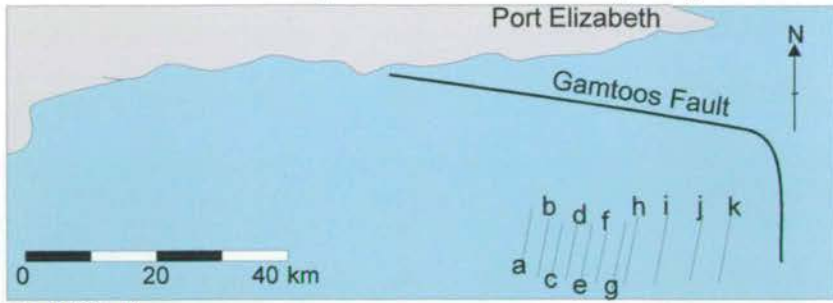
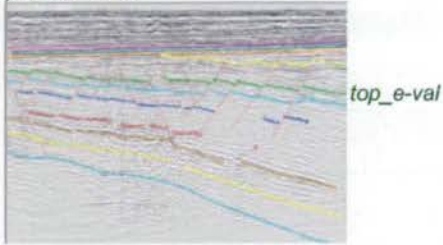


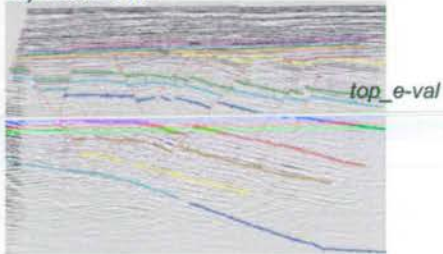
Figure 6.38 - i)

South

a) Ha87-016



b) Ha87-018



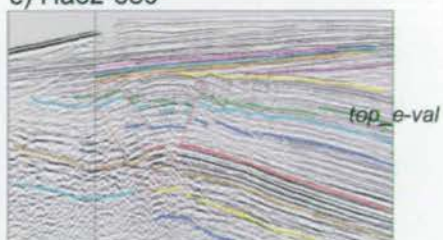
c) Ha87-020



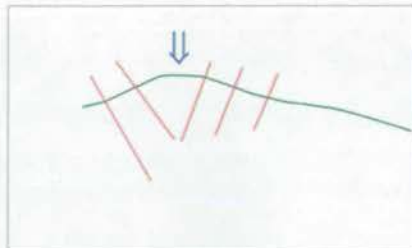
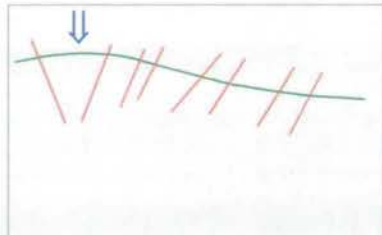
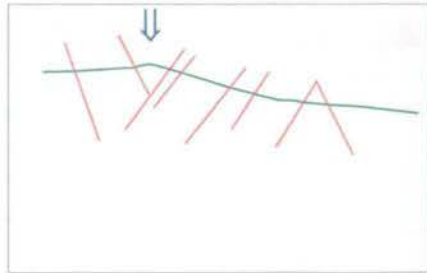
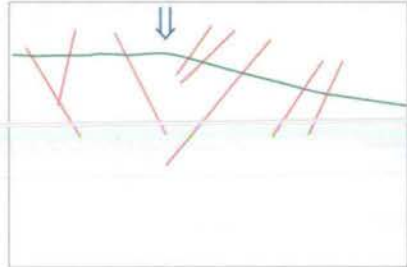
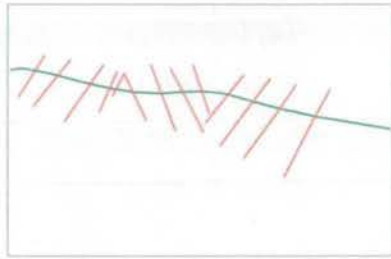
d) Ha87-021



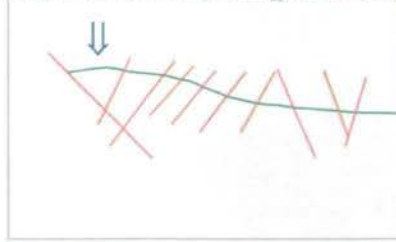
e) Ha82-039



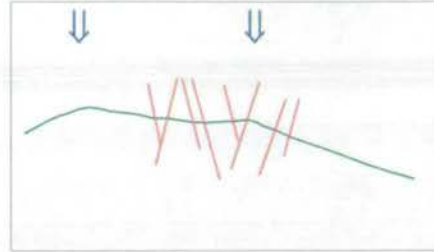
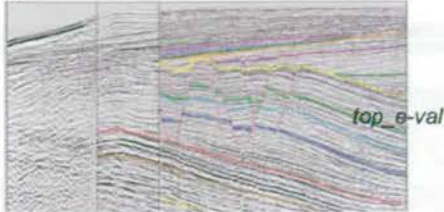
ii)



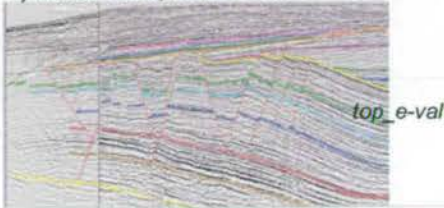
f) Ha87-022



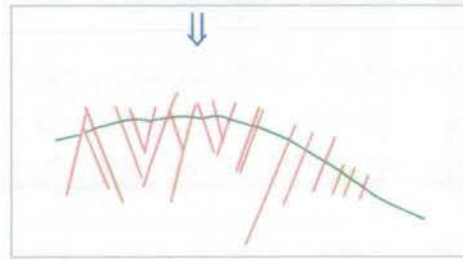
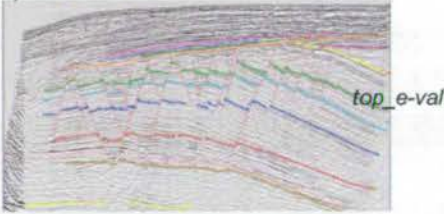
g) Ha87-023



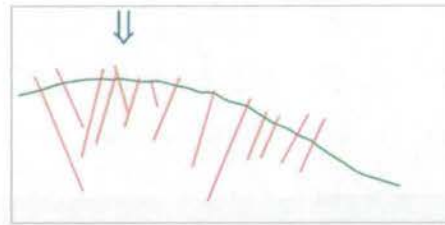
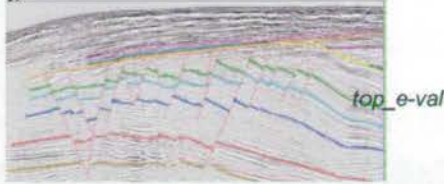
h) Ha87-024, Ha75-017



i) Ha87-025



j) Ha87-026



k) Ha87-028

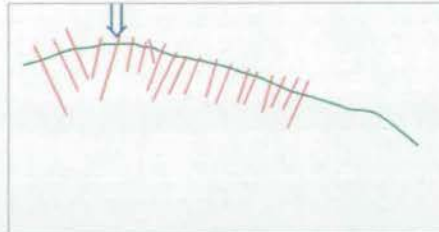
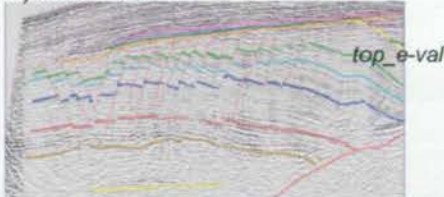


Figure 6.36: North-south sections in the centre and south of the basin that show evidence of folding; locations shown on map. a (i)-k(i) are the interpreted seismic sections from west to east. a(ii)-k(ii) is the restoration of the *top_e-valanginian* reflectors (green) to pre-intra-basin fault geometries that are used in Figure 6.36 to understand the 3-dimension geometries of the folds. Note that in the restored sections the point of inflexion/ hinge point are marked and that in many sections the southern limb of the anticlines are to the south of the data coverage.

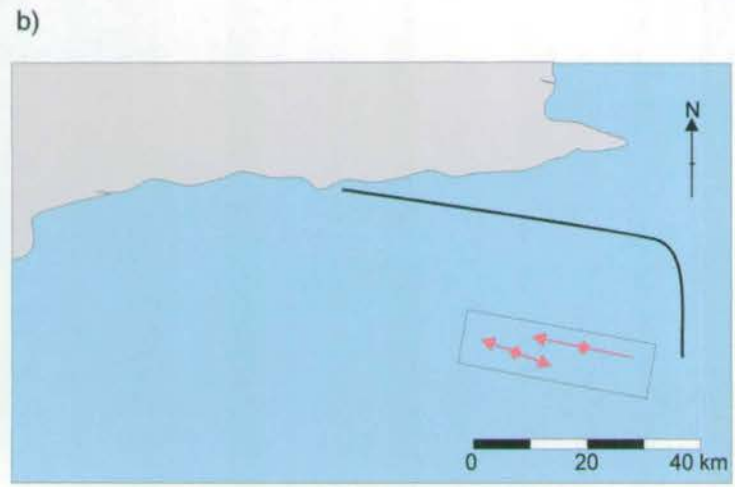
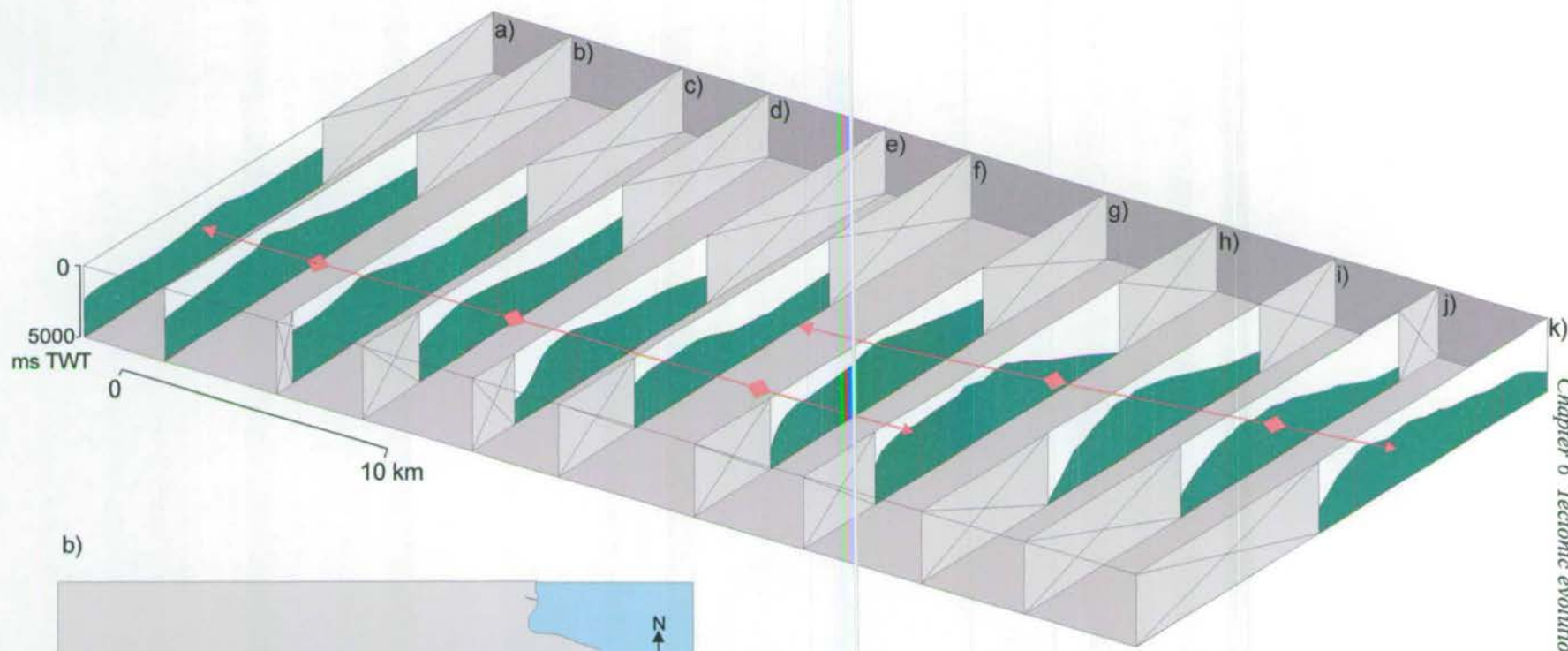


Figure 6.37: a) Reconstructed sections from Figure 6.36 have been plotted approximately in space to determine the 3-dimensional geometry of the Principal Syn-Rift folding in the southern part of the basin. When hinge points of each section are traced, an en-echelon relationship between a pericline and an anticline can be seen. b) Map of the Gamtoos Basin highlighting the position of (a) and the parallel trend of the fold hinges with respect to the east-west Gamtoos Fault.

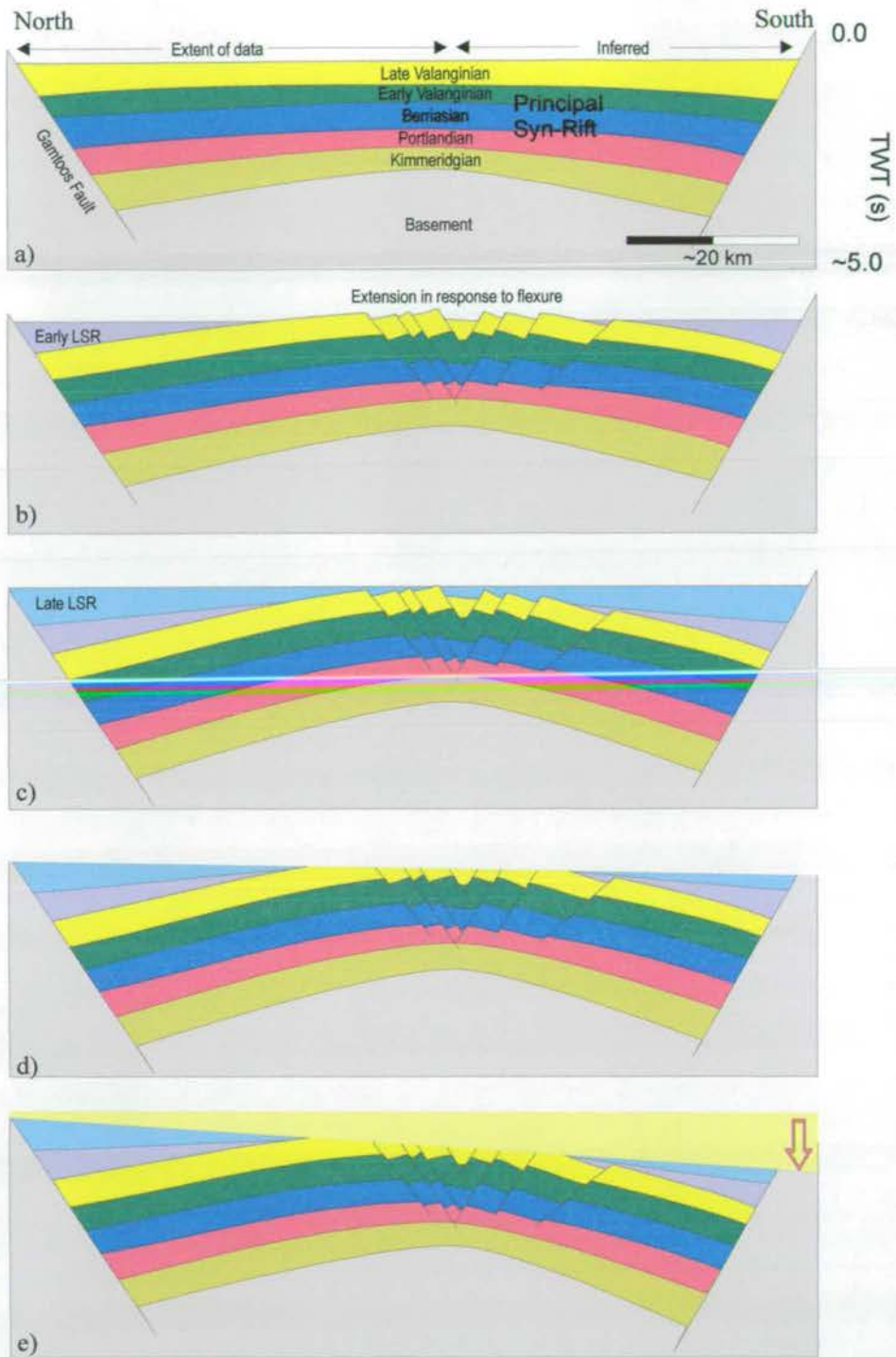


Figure 6.38: Modelling of the intra-basin folding in the south of the basin using a north-south section. The southern end of the section is inferred (see text). a) Deposition of the Late Valanginian sequence across the whole basin with minor growth into the two controlling fault. b) Early Late Syn-Rift (LSR) deposition (Hauterivian) is confined to adjacent to the controlling faults. The Principal Syn-Rift undergoes flexure in the centre of the basin resulting in localised normal faults that are more pronounced on the outer arc. c) Late LSR sedimentation across the basin followed by uplift, basin-wide unconformity and erosion (d). (e) Regional subsidence to the south.

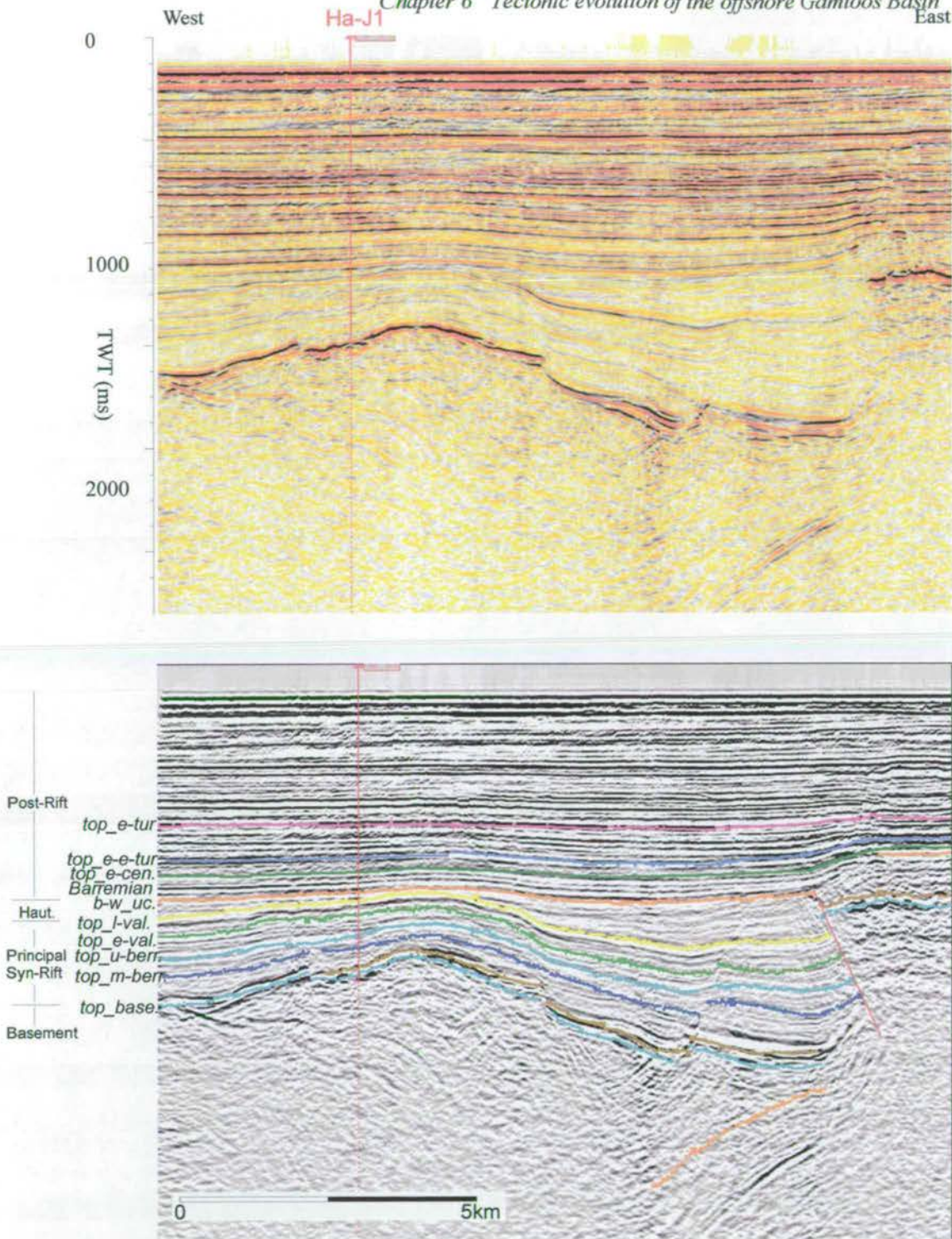


Figure 6.39: Section on the western margin with well Ha-J1 that confines the age of the basin-wide unconformity between Early Hauterivian and Barremian. A high angle reverse fault in the east of the section (cf. Figure 6.24) deforms the Hauterivian package while the Barremian is draped across it. Line Ha 87-003.

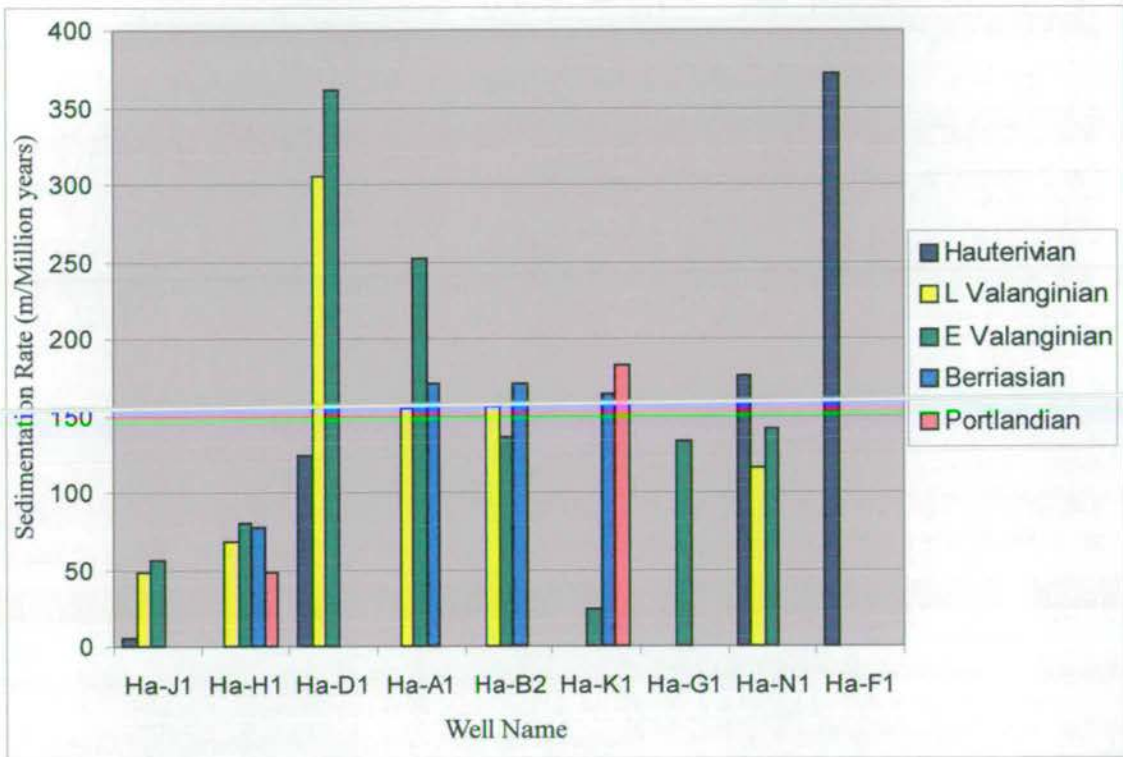
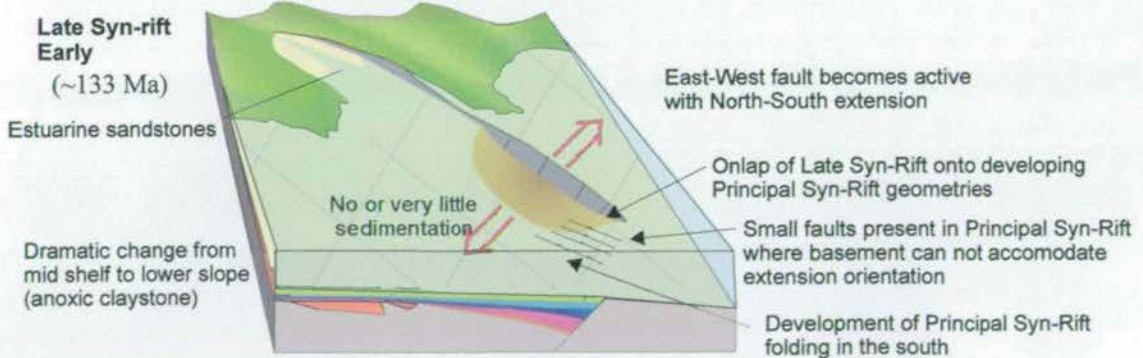
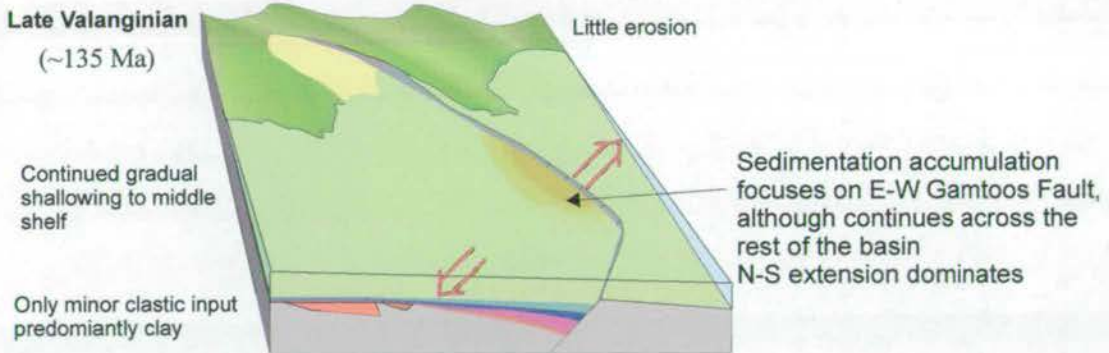
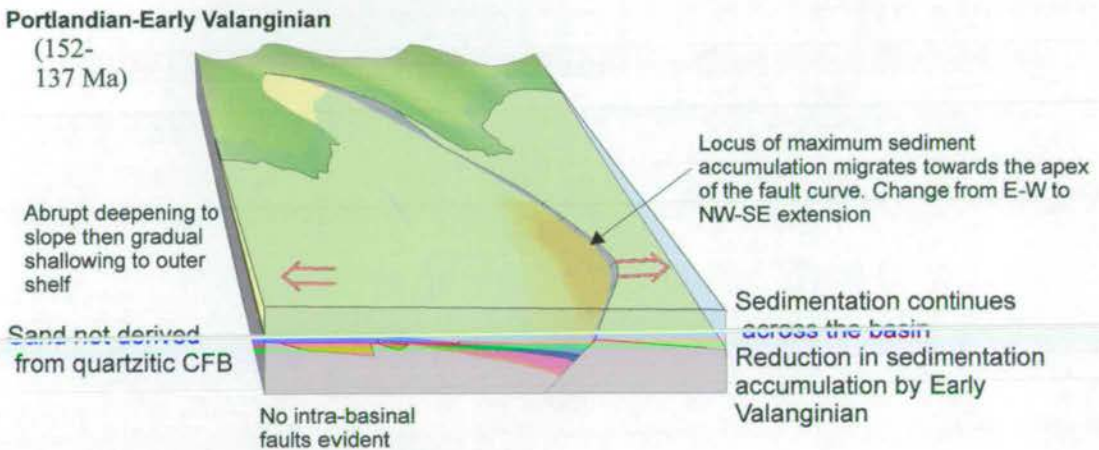
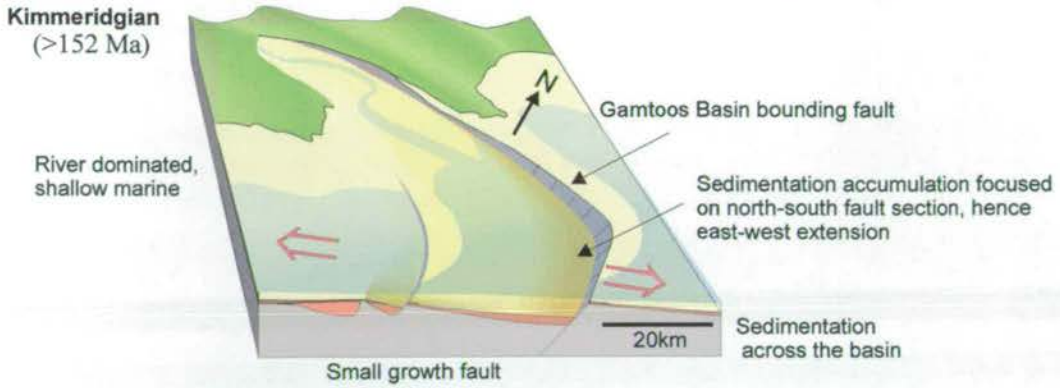
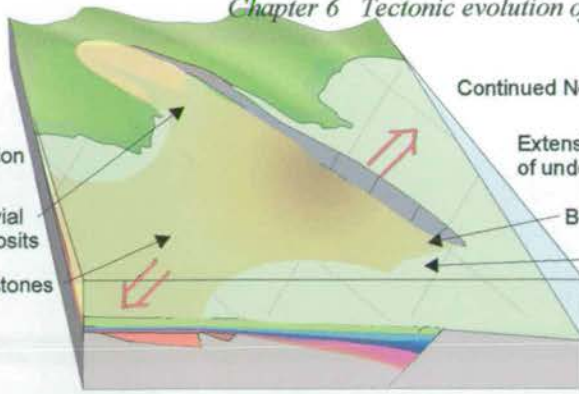


Table 6.1: Calculated sedimentation rates (in metres per million years) for the Principal Syn-Rift sequences and the Hauterivian from each of the Gamtoos Basin wells. Although the specific rates must be treated with caution (cf. Chapter 5) comparisons between different sequences are valid.



**Late Syn-rift
Late**
(130 Ma)

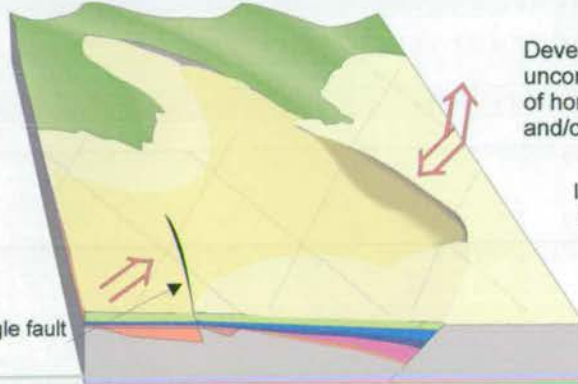
Onshore sedimentation
observed
Fluvial/alluvial
sandy deposits
Deep marine claystones



Continued North-South extension
Extension results in folding
of underlying Principal Syn-Rift package
Box-folds above fault curve
Monocline

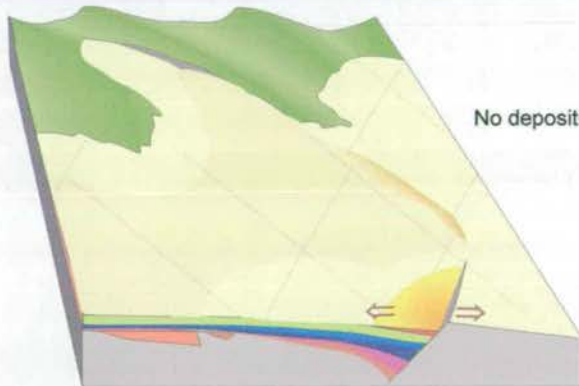
Post Hauterivian

High reverse angle fault



Development of Basin-wide
unconformity either as a result
of horizontal compression
and/or basin uplift
Inversion along East-West
Gamtoos Fault

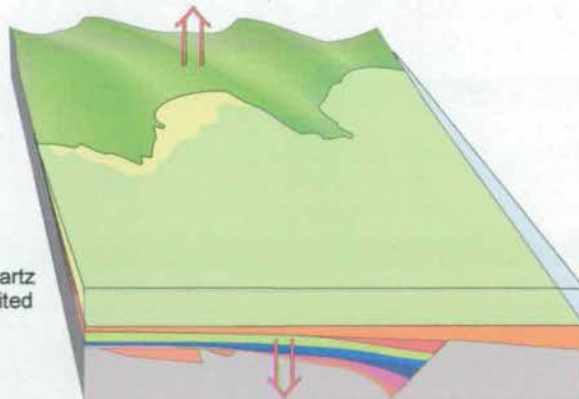
Albian
(~97 Ma)



No deposition except in localised syn-rift
Small localised syn-rift
results in folding of principal
syn-rift package

Post Albian

Progressive uplift
of coastal area
Shallow marine quartz
sandstone deposited
across the basin



Regional tilt to the south
Development of southward
progradational units

Figure 6.40: Summary sketches of the evolution of the Gamtoos Basin highlighting the principal tectonic events, relative sea-level, and type of sedimentation. Note that the coast is shown as it is today. Arrows indicate extension/compression orientation.

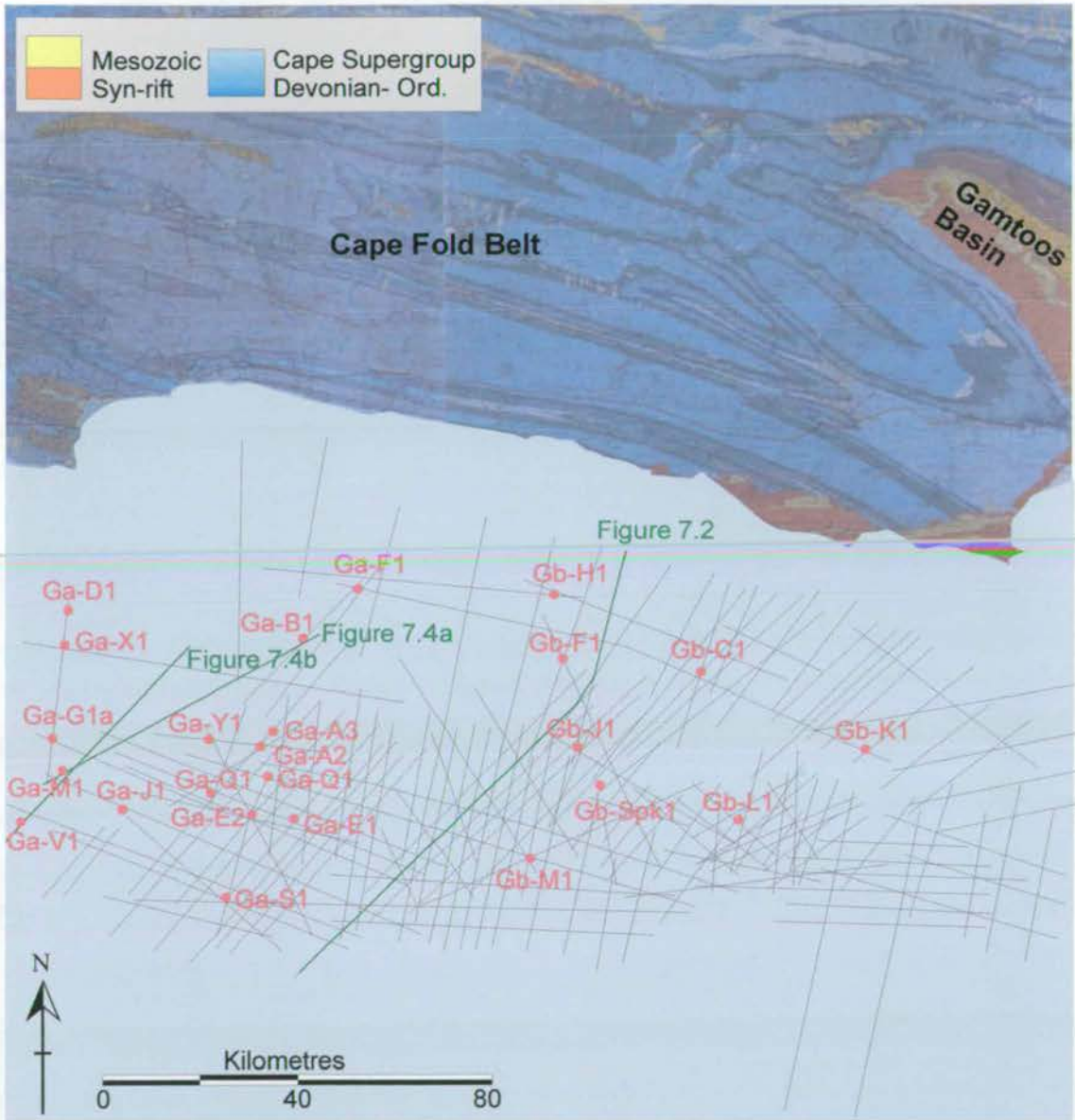


Figure 7.1: Map of the Pletmos Basin showing the location of seismic and well data used to establish the tectono-stratigraphic evolution of the basin. Although much of the basin has good data coverage there are limitations, especially in the north-east and north-west. The onshore geology has been shown. Position of Figures 7.2 & 7.4 are shown, and the location of other sections can be found in Enclosure 2.

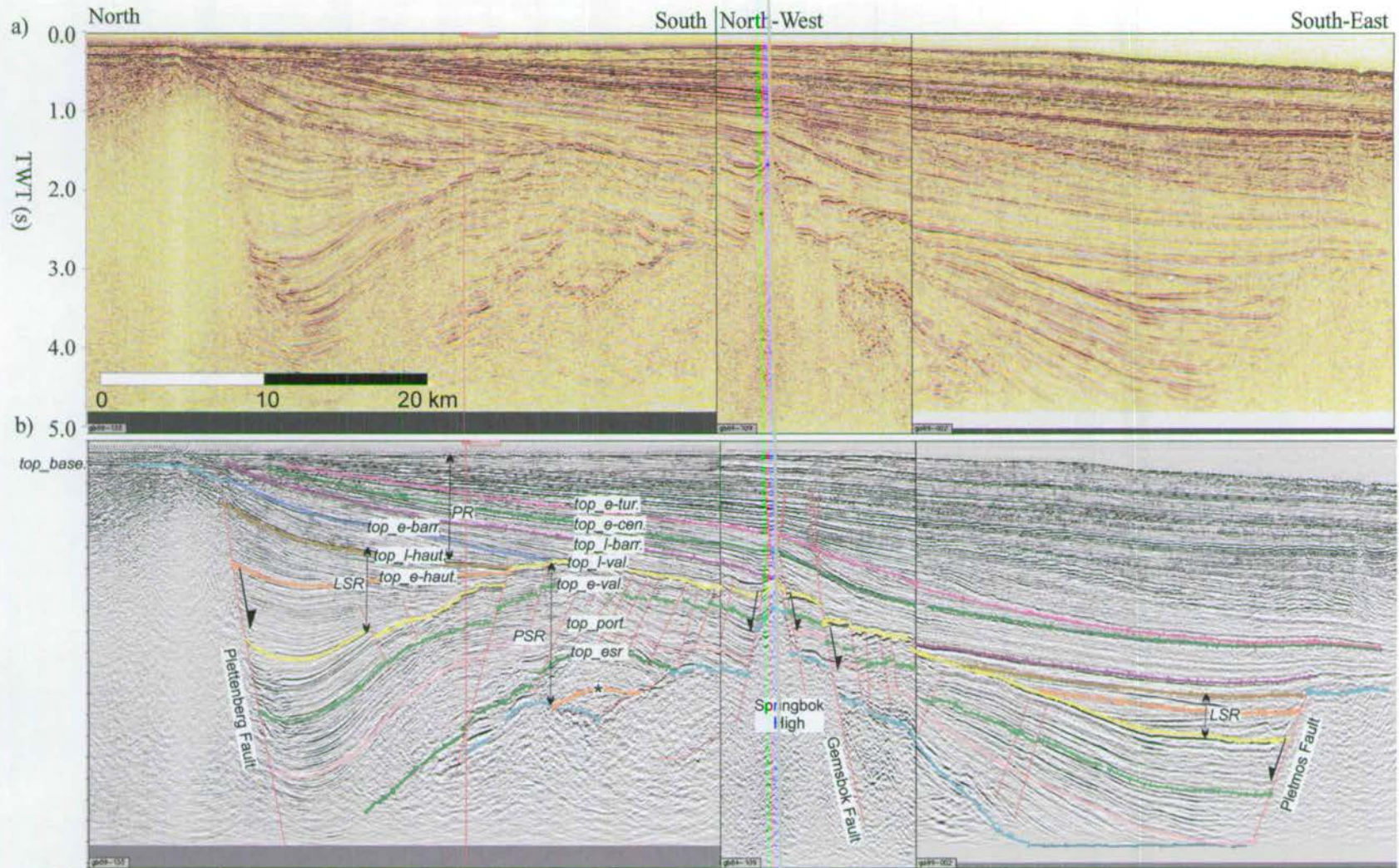


Figure 7.2: North-south section across the Pletmos Basin with the Plettenberg Fault in the north and Pletmos Fault in the south. The overall structure is two sub-basin separated by the Springbok High. The principal mega-sequences are indicated: Early Syn-Rift (ESR), Principal Syn-Rift (PSR), Late Syn-Rift (LSR), and Post-Rift (PR). * indicates the Earliest Syn-Rift package. Lines Gb89-135 (north), Gb89-109 (middle), Ga89-002 (south).

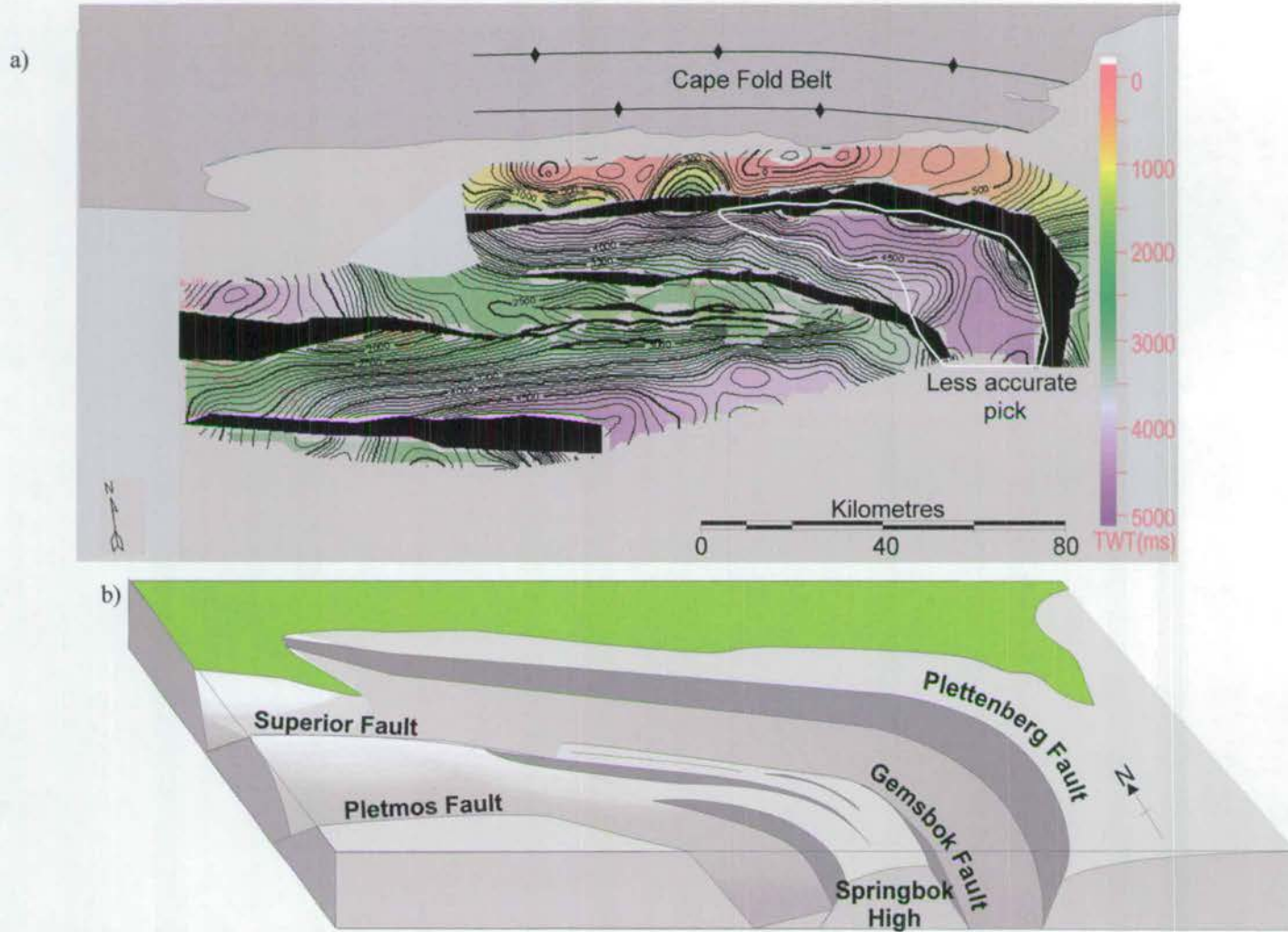


Figure 7.3: a) TWT map to *top_basement* with fault polygons. The trend of the onshore Cape Fold Belt is shown. b) 3-D cartoon of the basin highlighting its salient features.

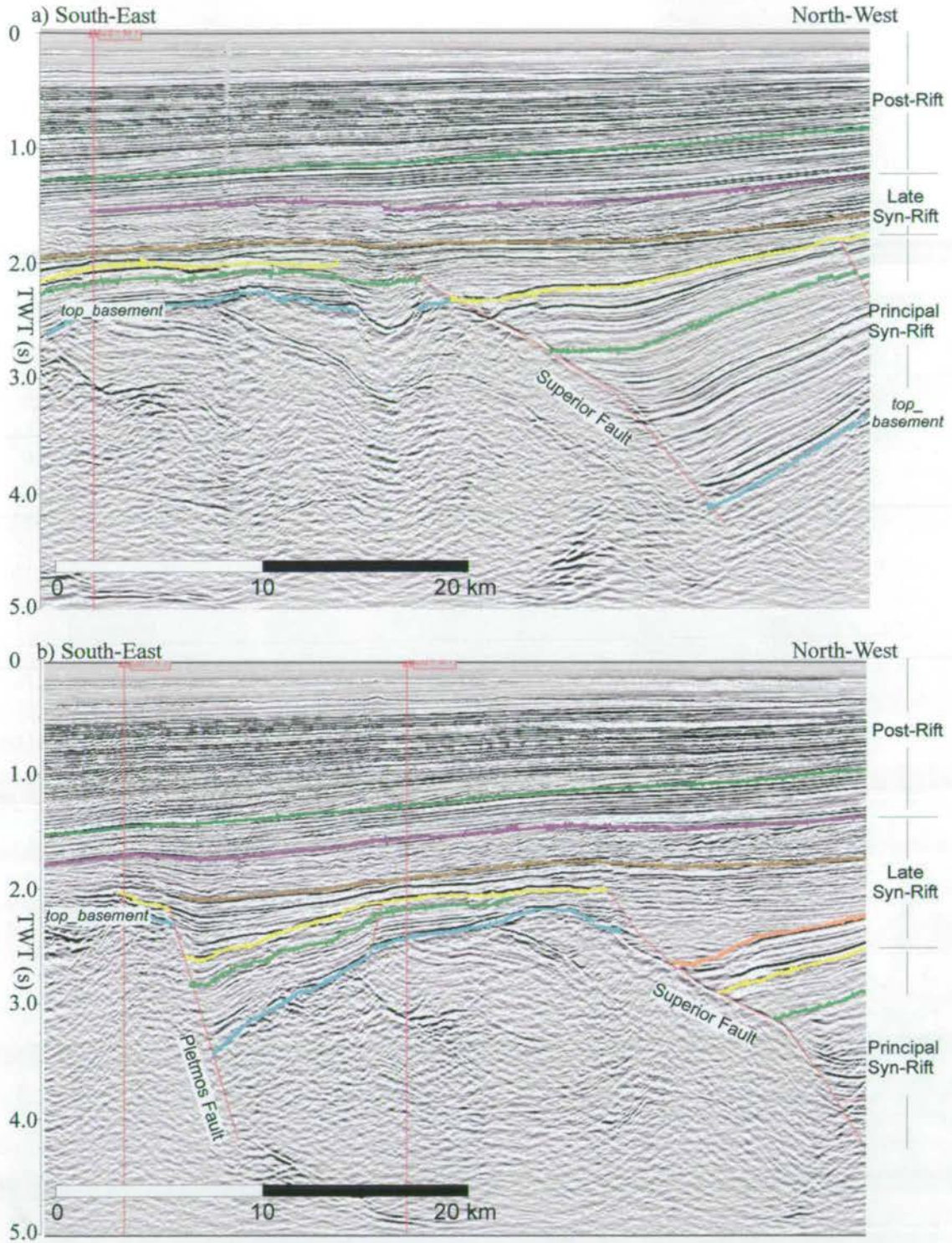
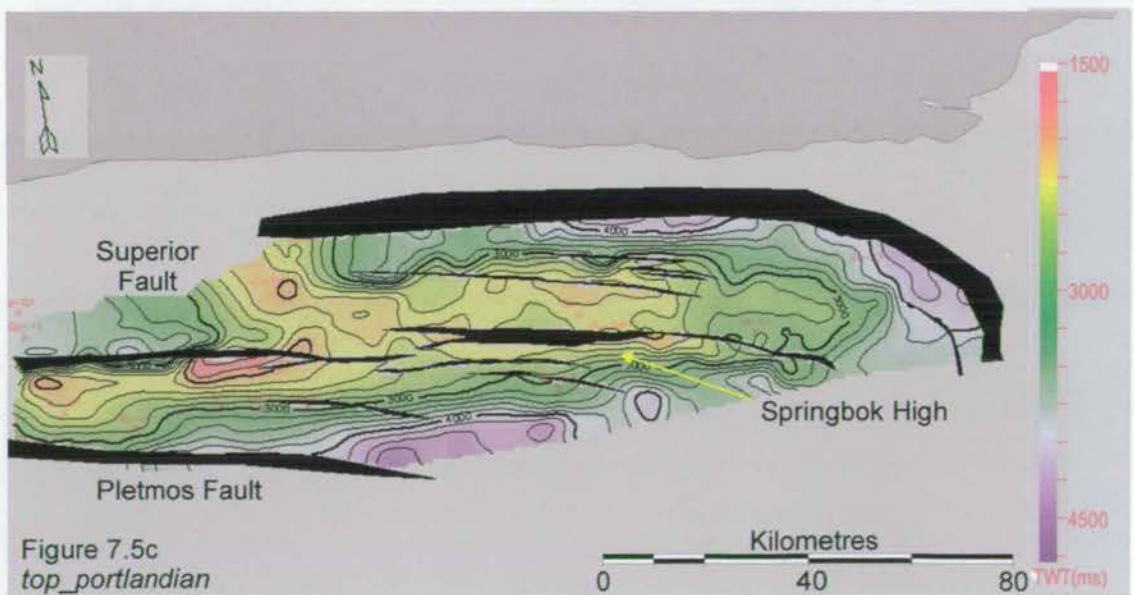
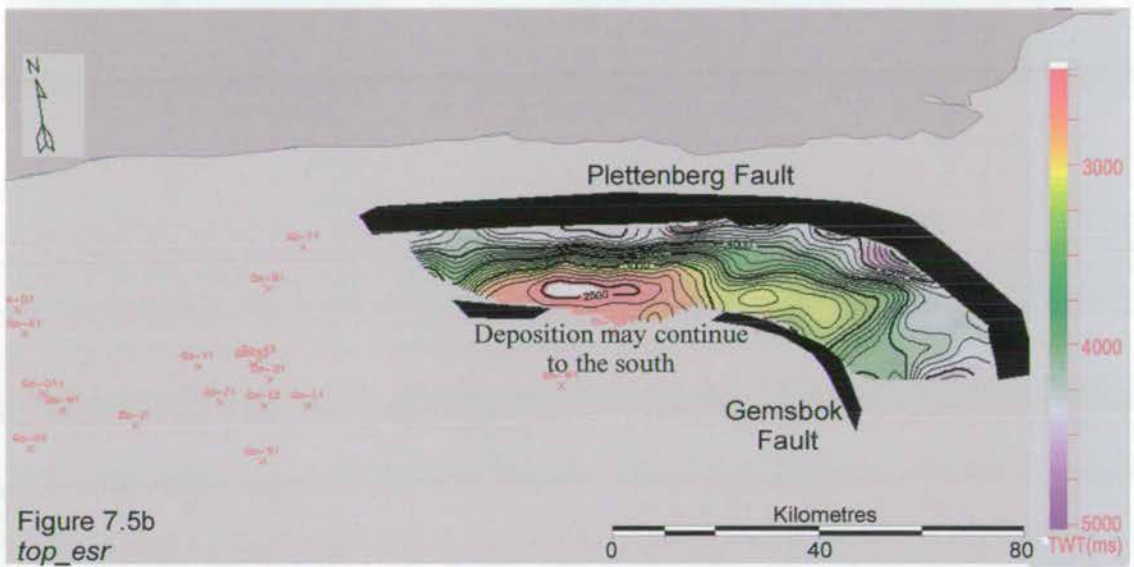
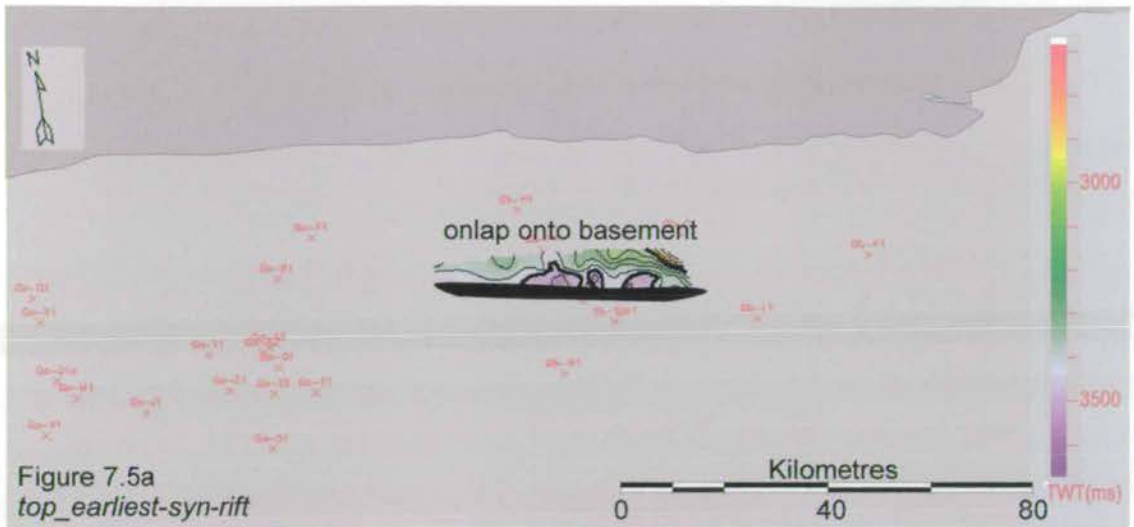


Figure 7.4: Although the basement is characteristically transparent, intra-basement reflectors are evident in these two sections. The folded geometry, including the inferred approximate east-west trend of the fold axes, are consistent with basement structures discussed in Chapter 4. Location on Figure 7.1. Line names: a) Ga 88-006, b) Ga 88-004



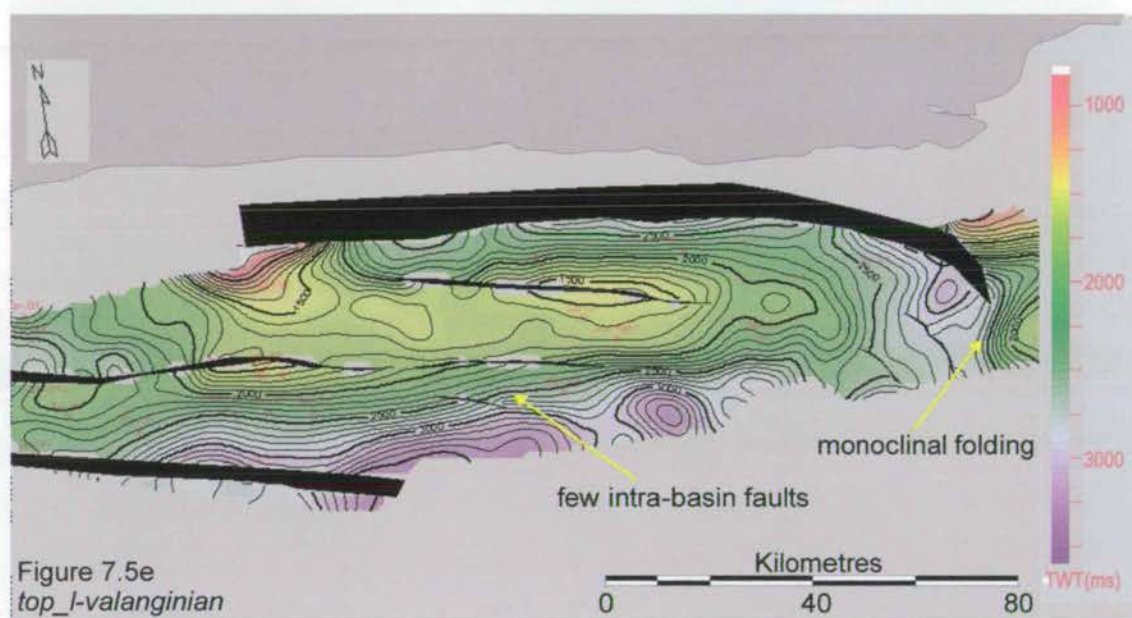
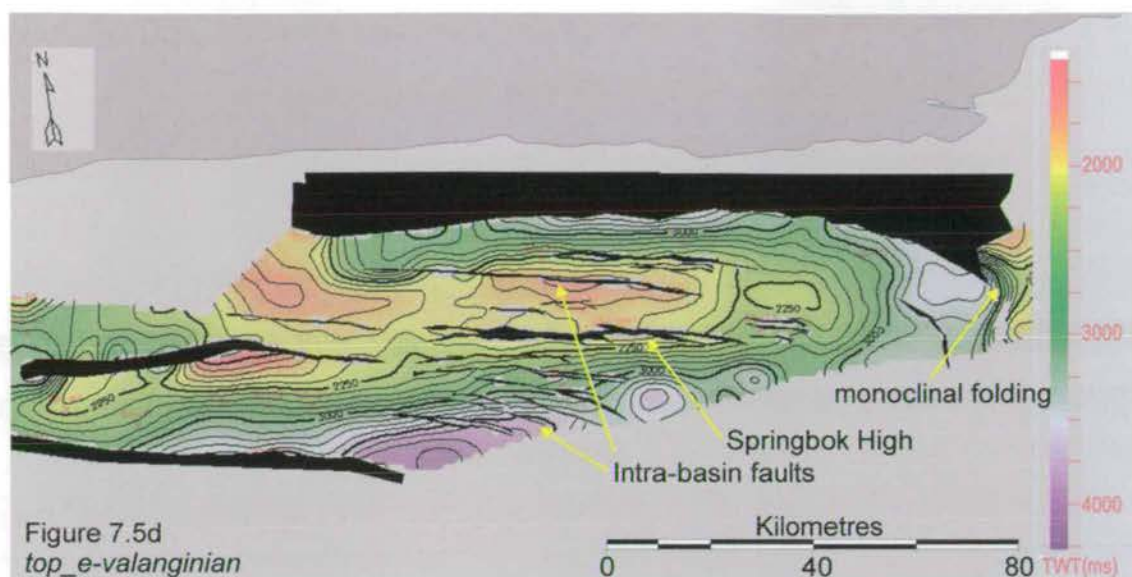


Figure 7.5: TWT maps for the Top Principal Syn-Rift sequences, a) Earliest Syn-Rift, b) Early Syn-Rift (not traced to the southern sub-basin), c) Portlandian, d) Early Valanginian, e) Late Valanginian.

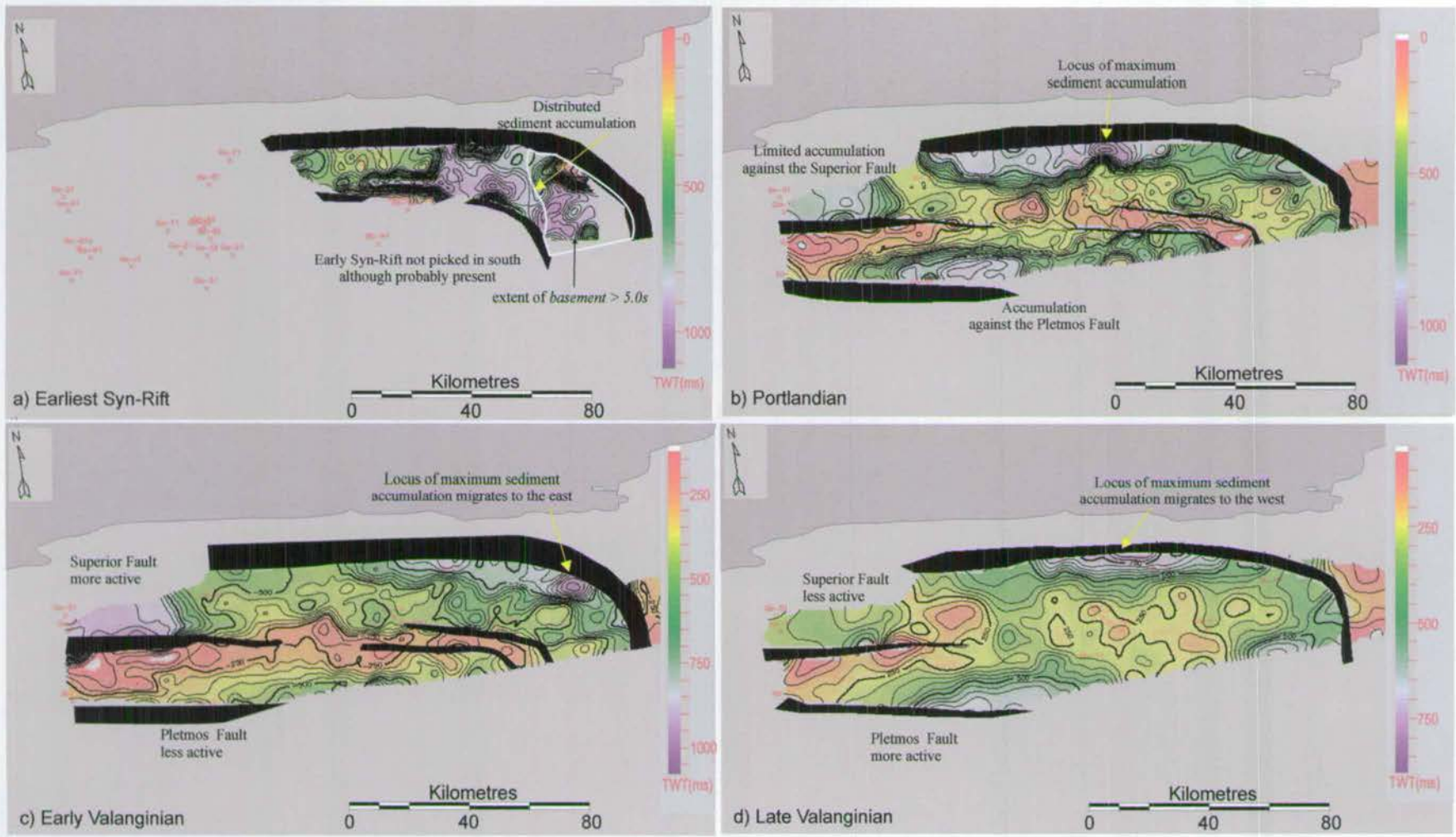


Figure 7.6. Isochron plots for sequence thicknesses within the Principal Syn-Rift package. a) *top_esr* to *top_basement* / *basement* > 5.0 s, b) *top_portlandian* to *top_esr* / *top_basement*, c) *top_e-valanginian* to *top_portlandian*, d) *top_l-valanginian* to *top_e-valanginian*.

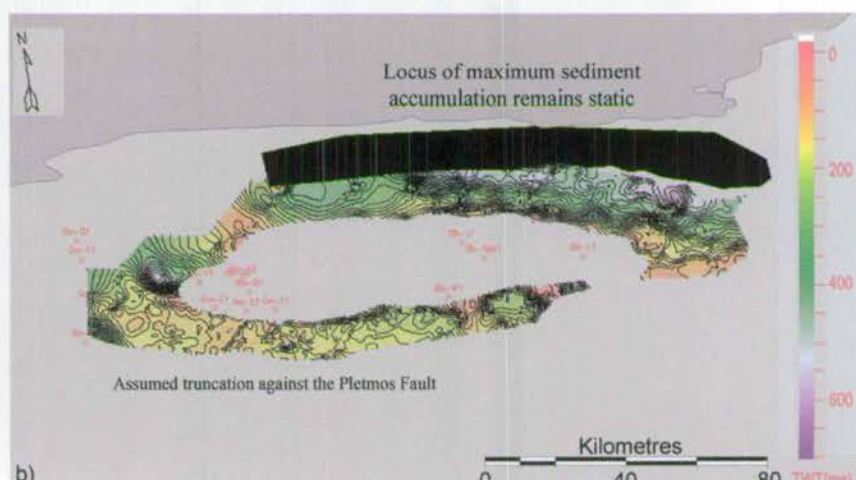
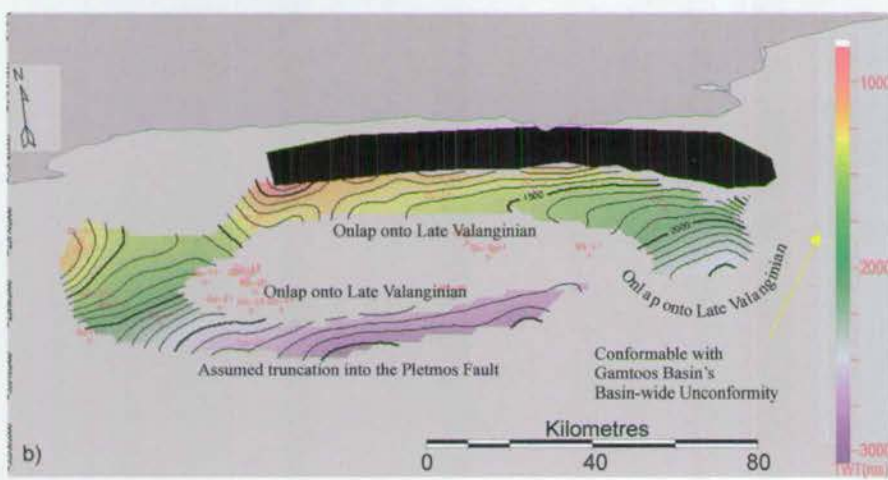
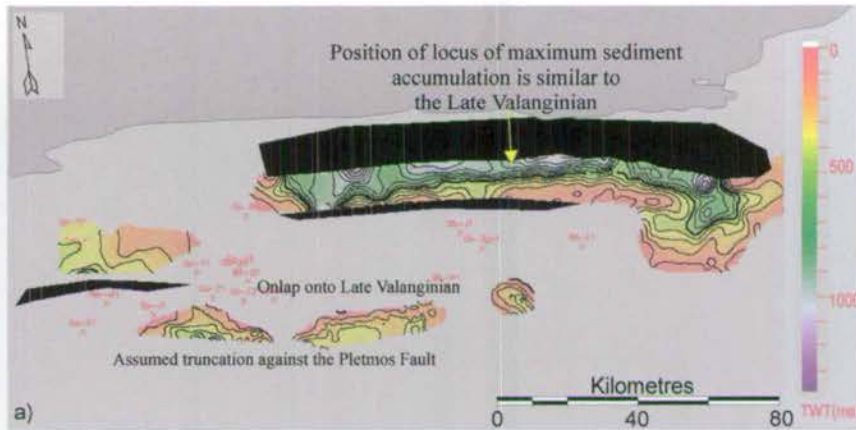
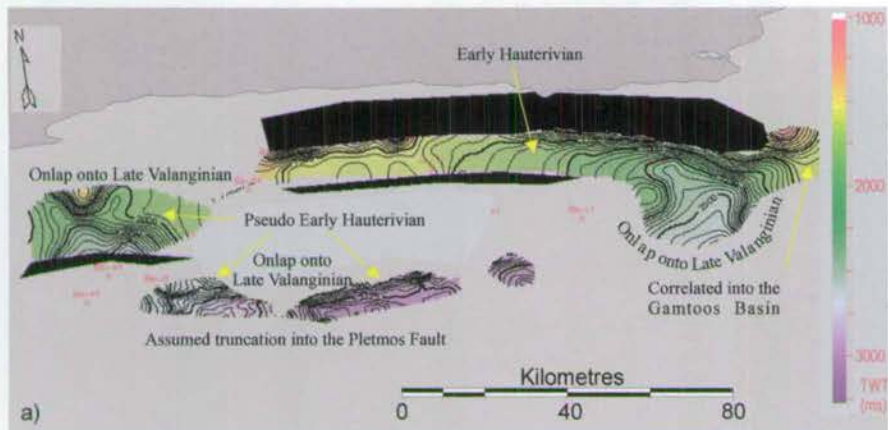


Figure 7.7: TWT maps of a) *top_e-hauterivian* (including *top-pseudo-e-hauterivian* in the south) and b) *top_l-hauterivian*.

Figure 7.8: Isochron plots of Late Syn-Rift sequences in TWT. a) *top_e-hauterivian* (and *top_pseudo-hauterivian* in the south) to *top_l-valanginian* b) *top_l-hauterivian* to *top_e-hauterivian* (and *top_pseudo_hauterivian* in the south).

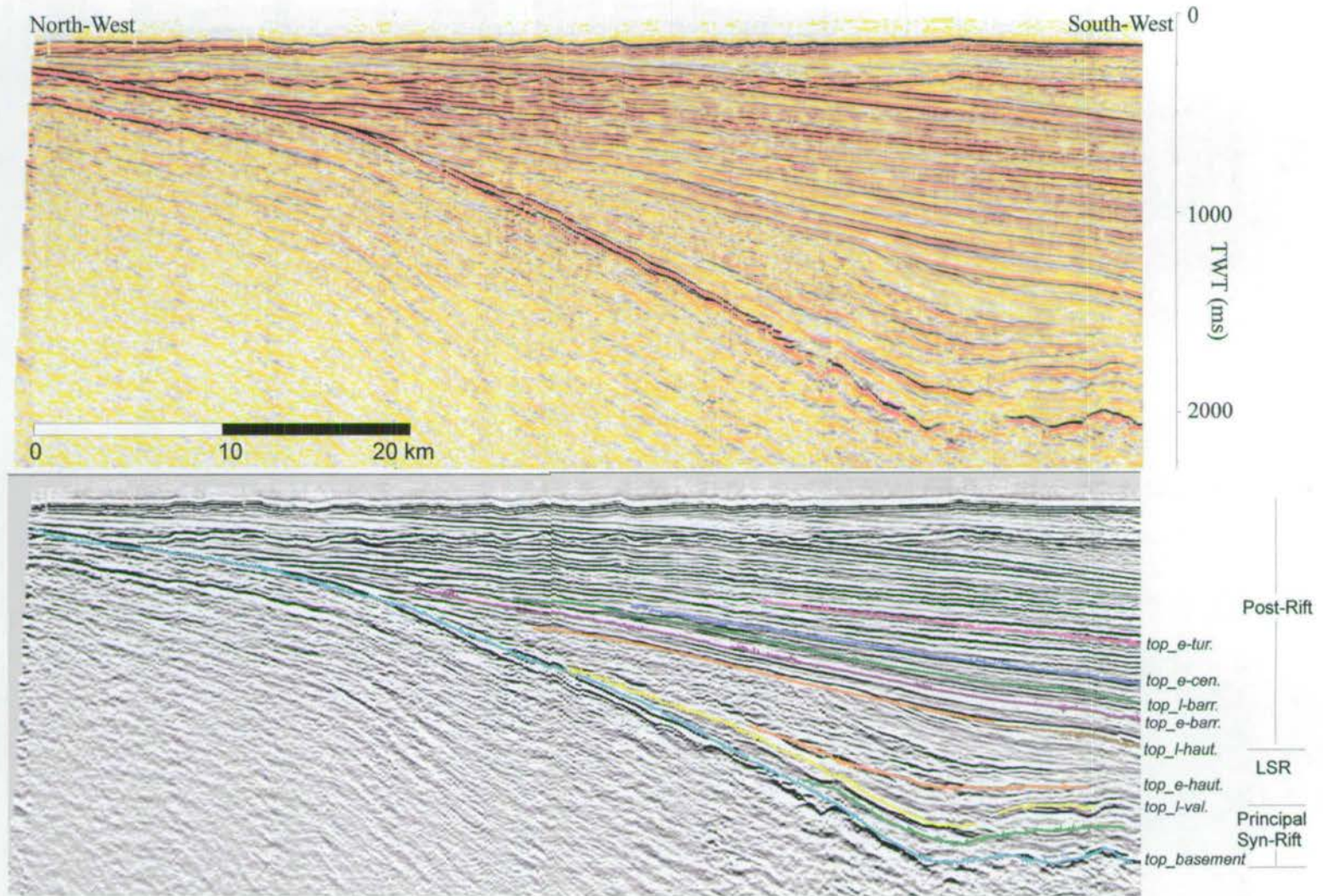


Figure 7.9: In this section, at the east of the Pletmos Basin, the *top_l-hauterivian* horizon becomes conformable with the basin-wide unconformity of the Gamtoos Basin, and is overlain by undeformed Late Barremian. The recent uplift and erosion through to the basement is evident towards the coast (north). Line Gb84-103.

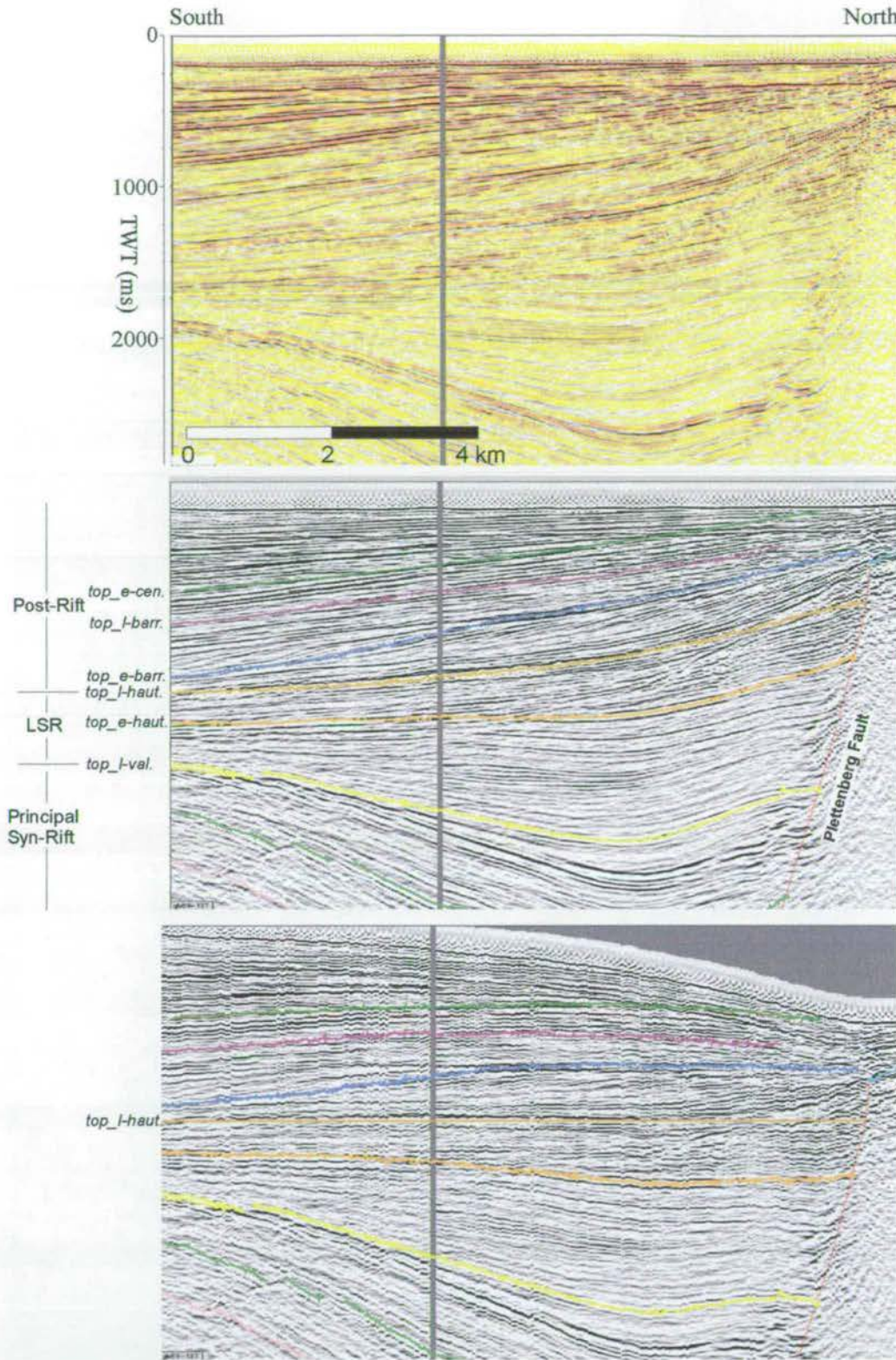


Figure 7.10: North-south section showing the geometries of the Principal Syn-Rift, Late Syn-Rift (LSR) and Post-Rift megasequences against the east-west trending Plettenberg Fault. a) un-interpreted section, b) interpreted section, c) interpreted section flattened to *top l-hauterivian*. While the Late Hauterivian package thickens into the fault as a syn-rift package, the Early Barremian package thins towards the south because it is a progradational package. Grey line is a data gap. Line Gb 89-037.

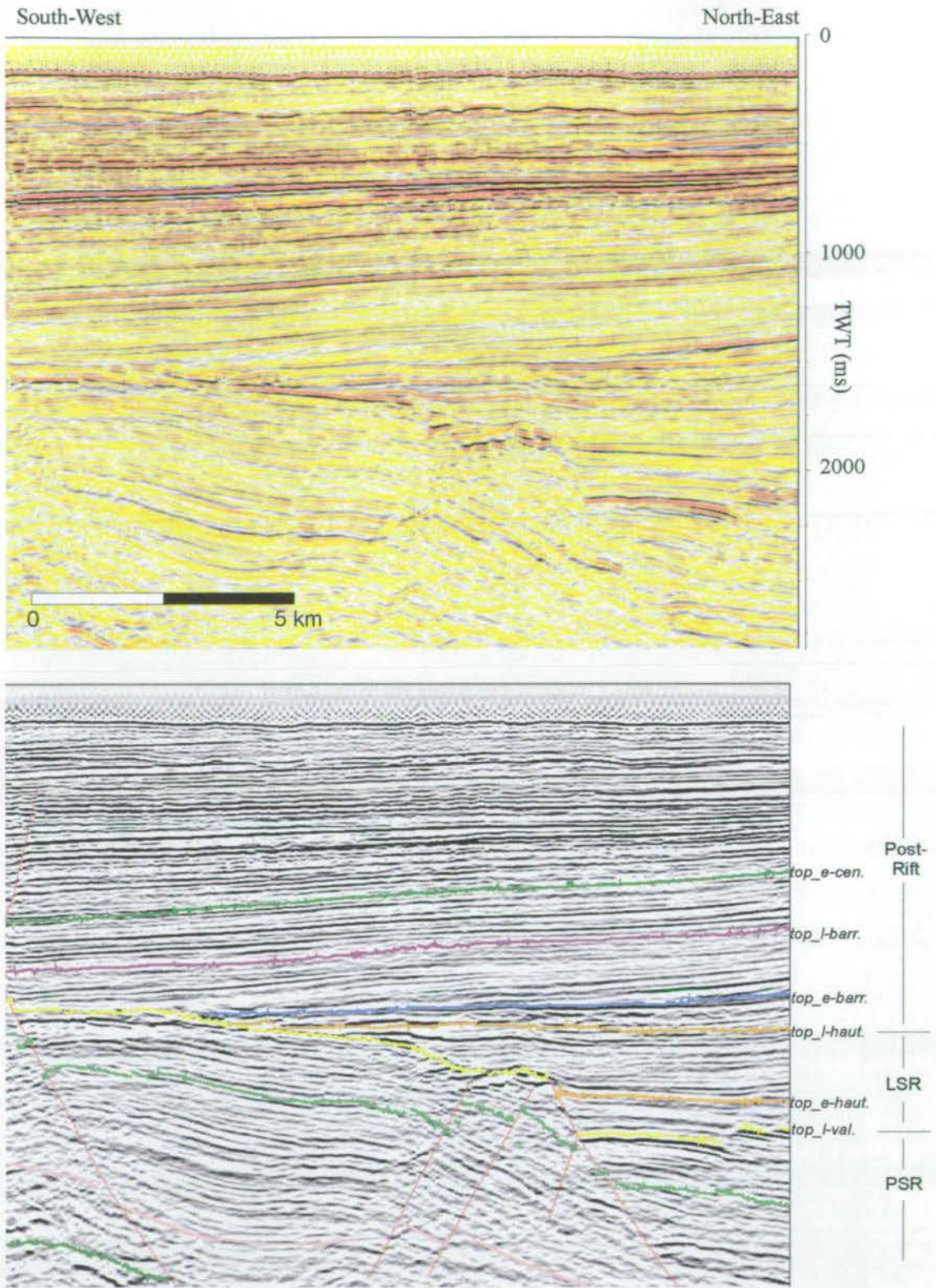


Figure 7.11: The Early Barremian horizon onlaps onto a folded Late Valanginian reflector. The Early Barremian package therefore does not condense onto the basement high and is filling in pre-existing topography.

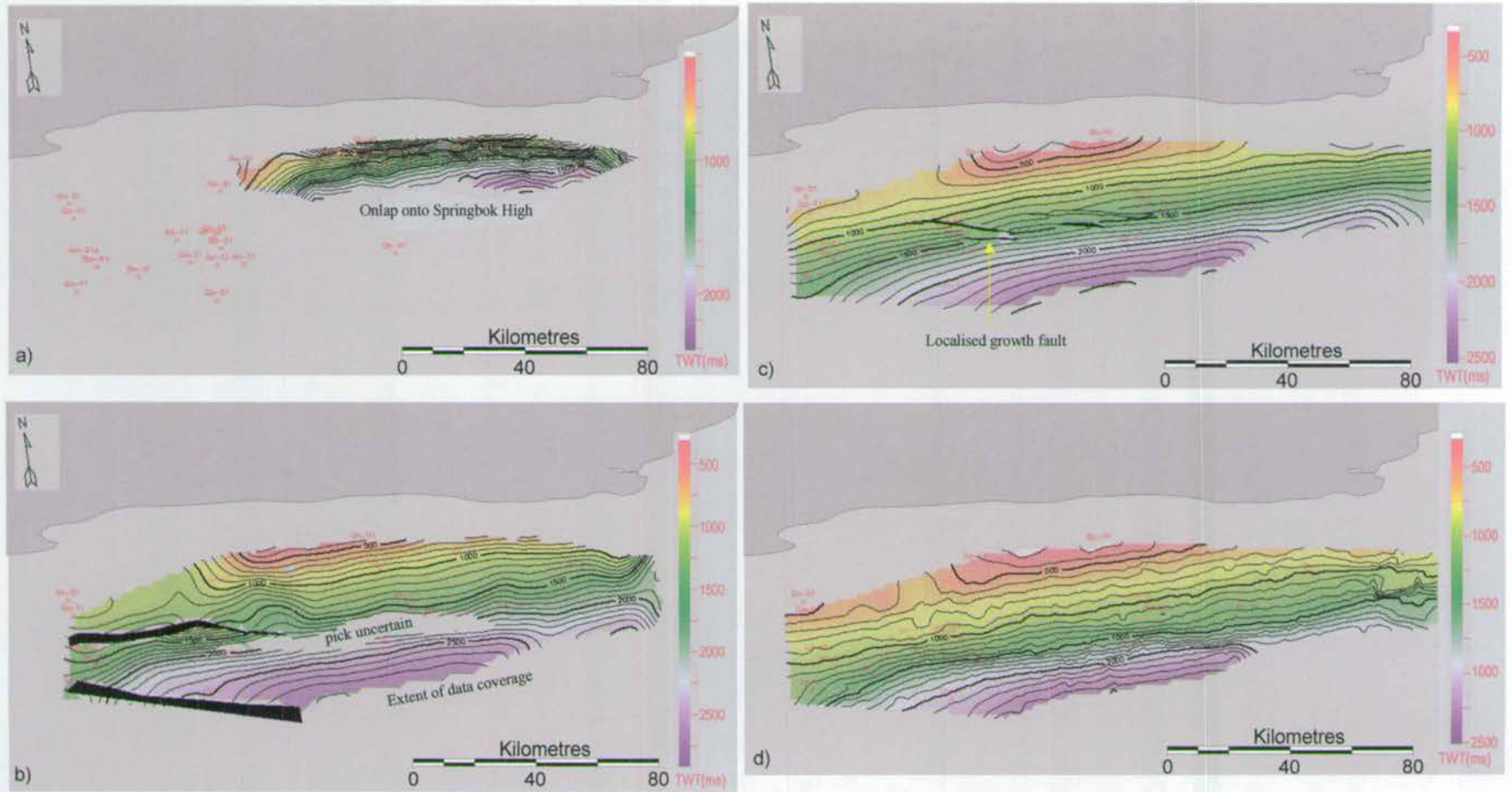


Figure 7.12: TWT maps to of Post-Rift sequences, a) *top_e-barremian*, b) *top_l-barremian*, c) *top_e-cenomanian*, d) *top_e-turonian*. Notice in (c) the presence of growth faults in the west of the basin.

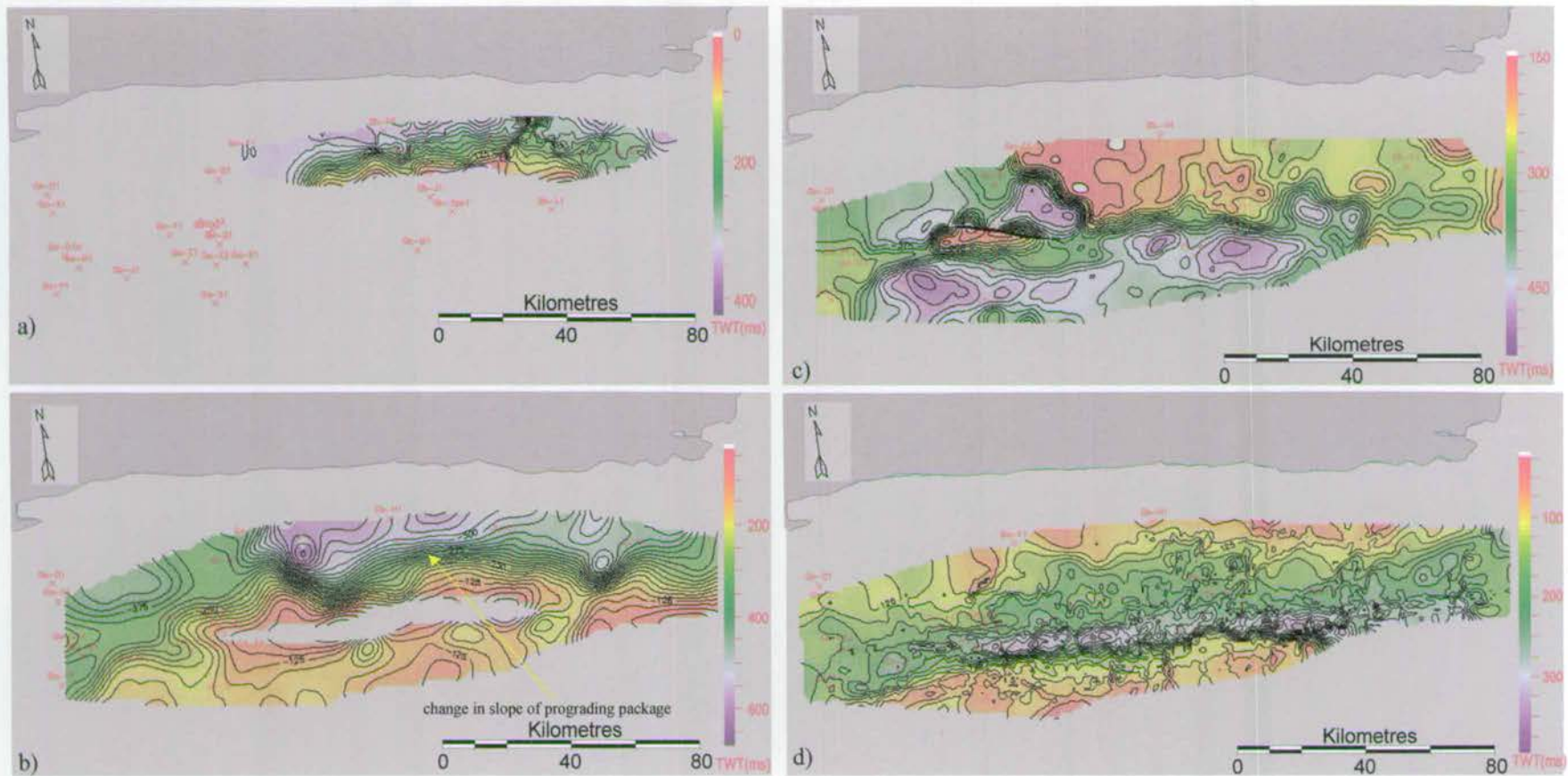


Figure 7.13: Isochron thicknesses of Post-Rift sequences, a) *top_e-barremian* to *top_l-hauterivian*, b) *top_l-barremian* to *top_e-barremian*, c) *top_e-cenomanian* to *top_l-barremian*, d) *top_e-turonian* to *top_e-cenomanian*. In (b) it is uncertain whether *top_e-barremian* horizon is draped across the intra-basin high, see Figure 7.12.

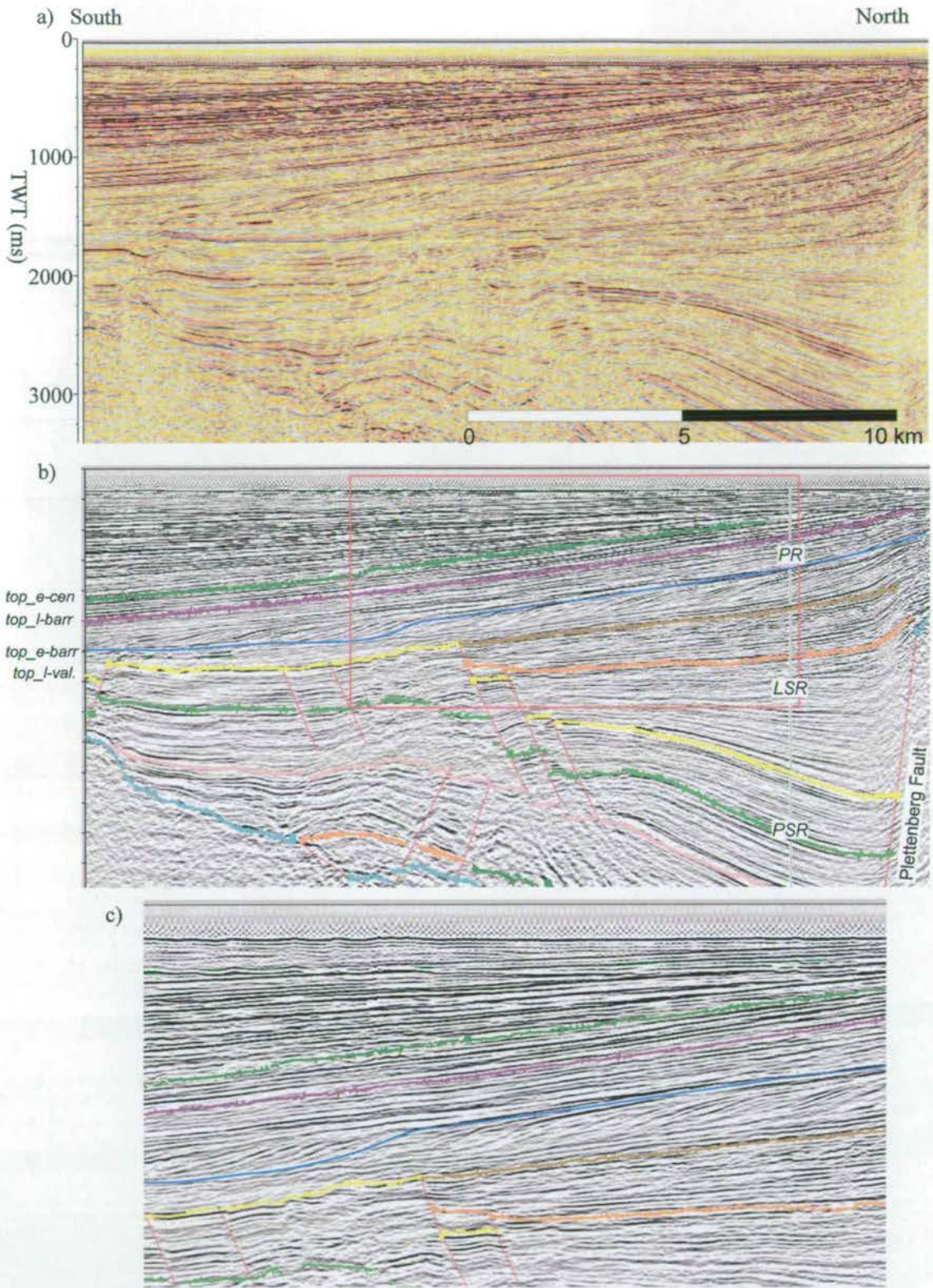


Figure 7.14: A large southward directed progradational system occurs in the Late Barremian sequence. Position of detailed section (c) is shown in (b). Line Gb89-139

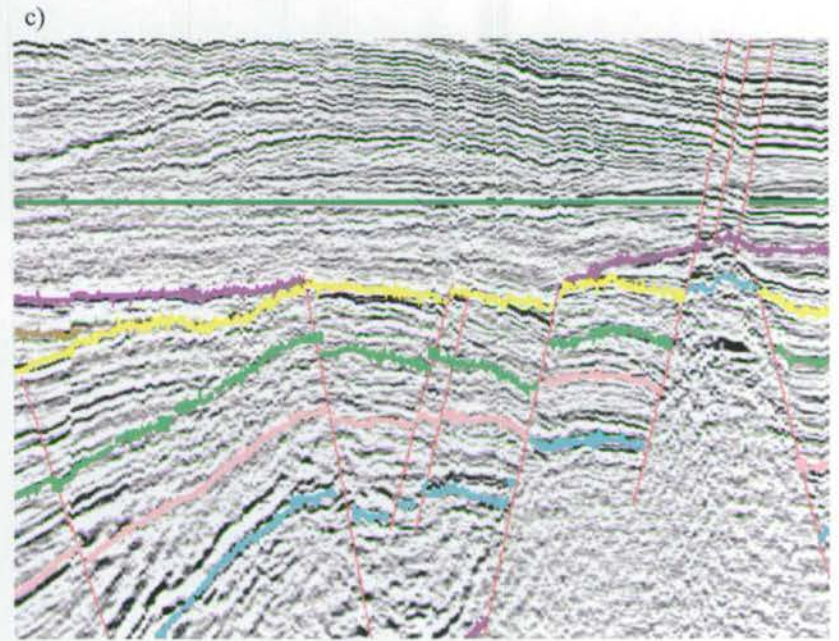
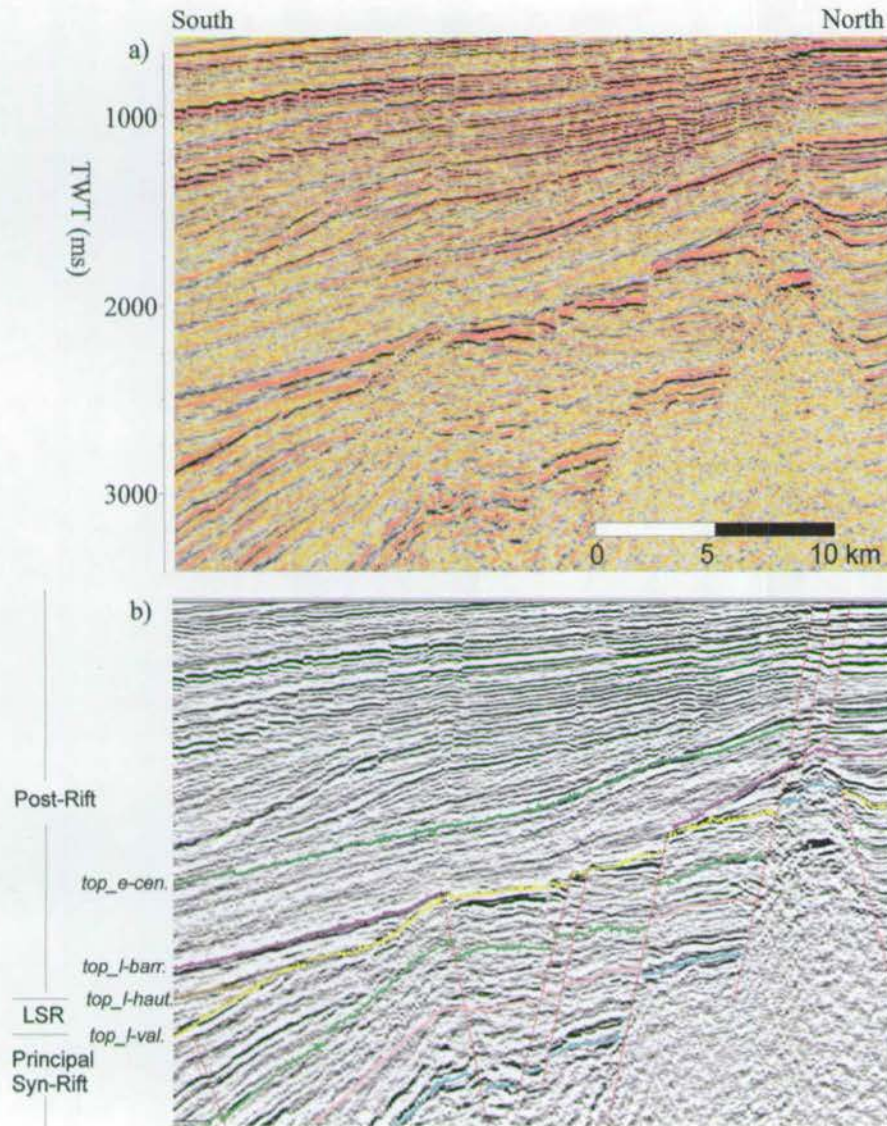


Figure 7.15: Section across the Springbok High showing the uncertainty of whether the *top l-barremian* reflector onlaps onto, or forms a condensed and draped sequence across, the *top l-valanginian* horizon. a) Un-interpreted section, b) interpreted section, c) interpreted section flattened to *top e-cenomanian* to obtain approximate depositional geometry of the Late Barremian. Line Gb 82-006.

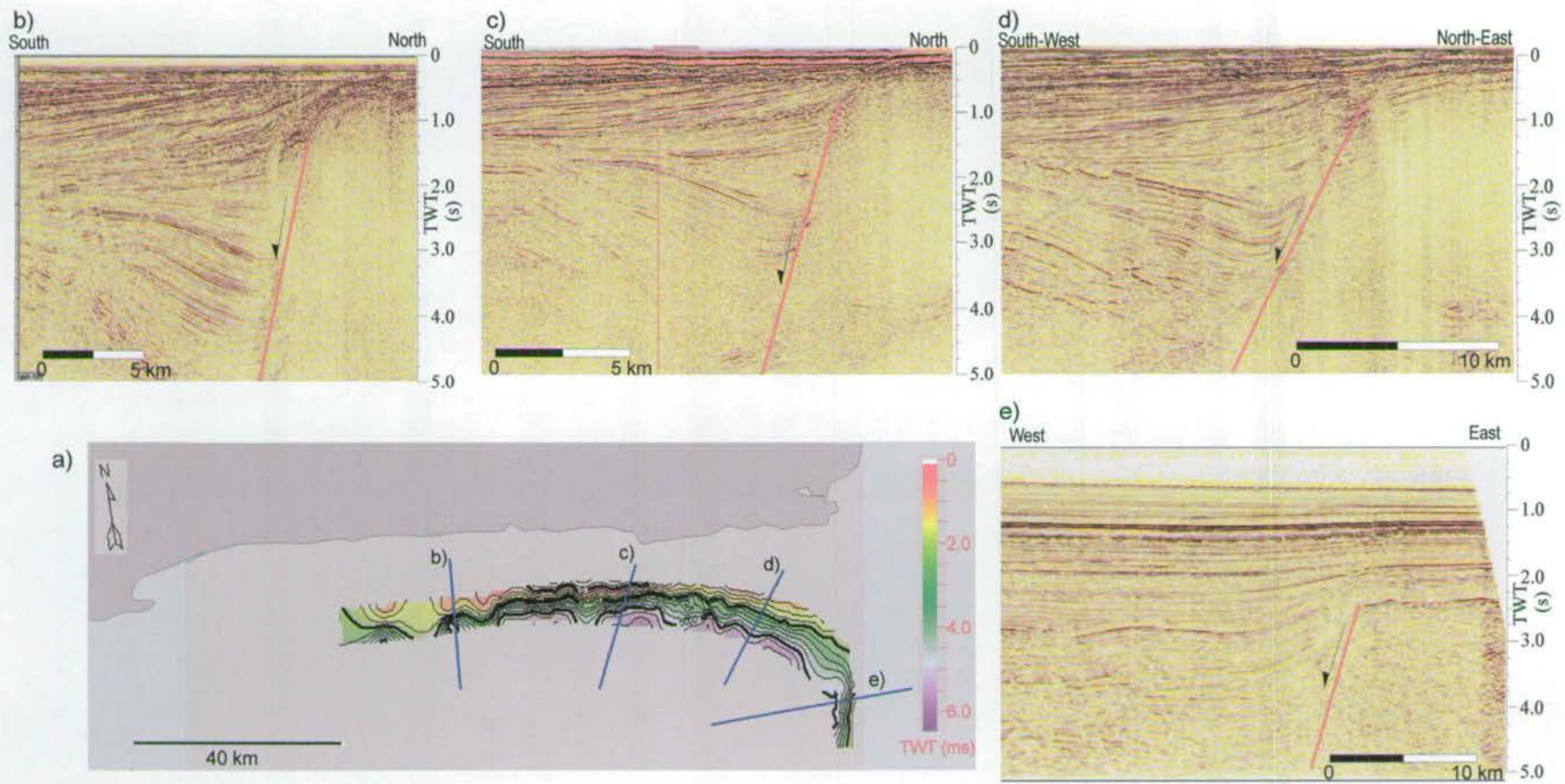


Figure 7.16: a) Map of the Pletmos Basin showing the TWT to the Plettenberg Fault and the location of seismic sections (b-e) perpendicular to the fault. The fault appears as a discrete planar surface that continues to at least 5 seconds TWT (~12 km) and has a very similar geometry regardless of orientation. There is also no indication of any cross cutting faults. Line: b) Gb 89-139, c) Gb 83-025, d) Gb 84-104, e) Gb 91-104

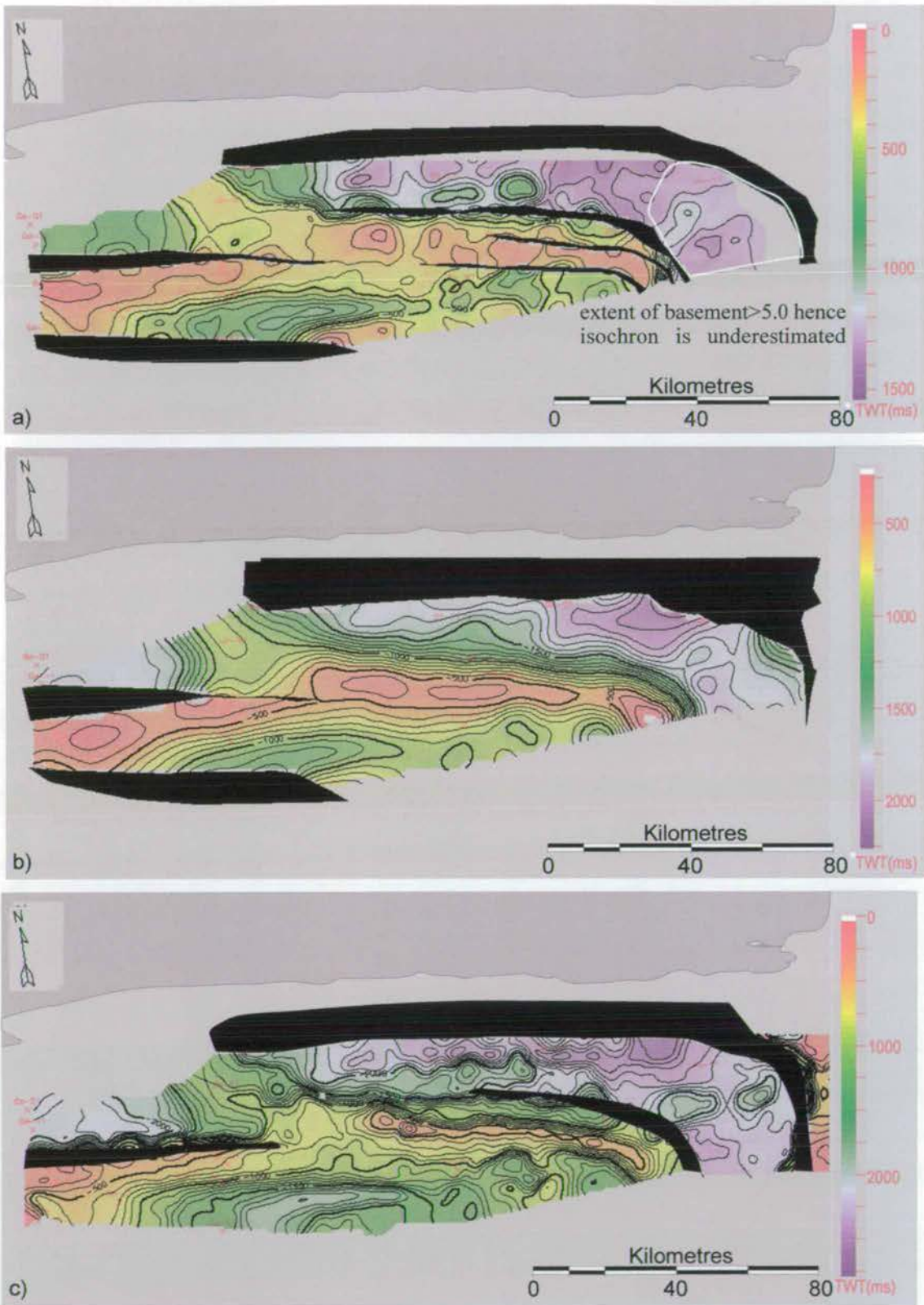


Figure 7.17: Cumulative isochron plots within the Principal Syn-Rift mega-sequence from *top_basement* (including *top_ps_basement* and *basement > 5.0s*) to, a) *top_portlandian*, b) *top_e-valanginian*, and c) *top_l-valanginian*.

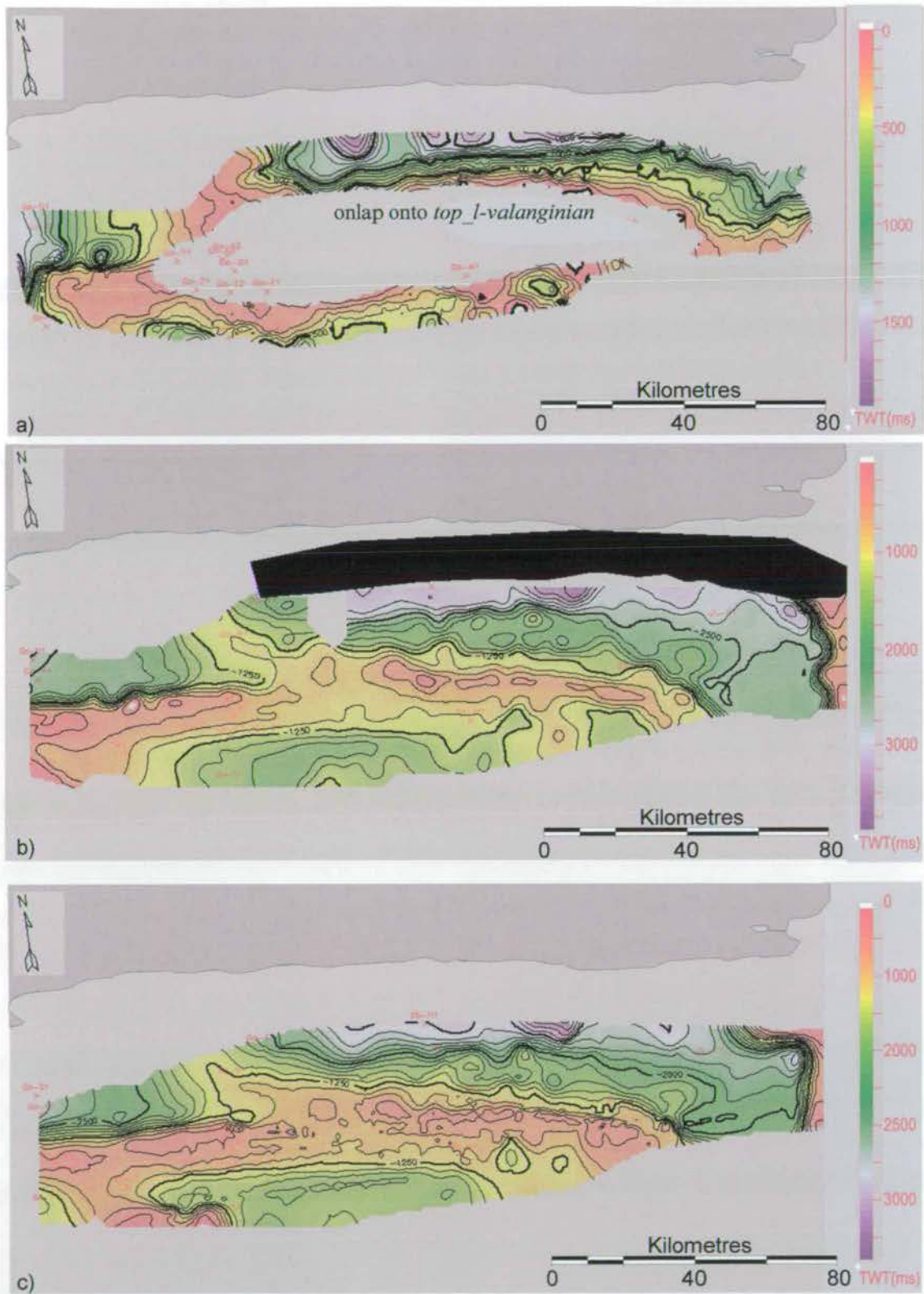


Figure 7.18: Cumulative isochron plots of a) Hauterivian (*top_l-hauterivian* to *top_l-valanginian*), b) *top_basement* to *top_e-hauterivian*, and c) *top_basement* to *top_l-hauterivian*. In b) and c) where Hauterivian is not present, *top_l-valanginian* to *top_basement* has been used.

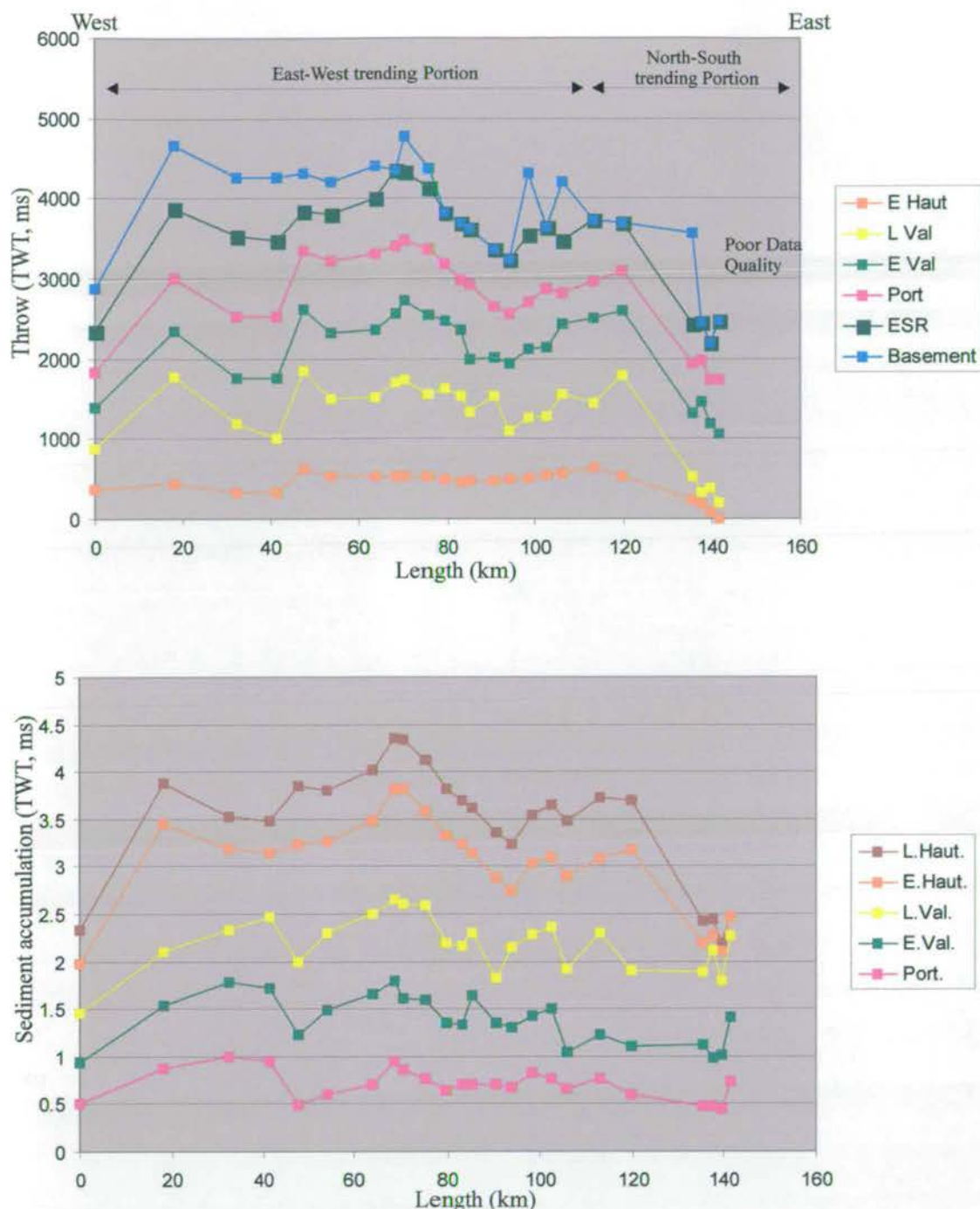


Figure 7.19: Throw and Sediment accumulation-Length graphs across the Plettenberg Fault. In both plots Length is the distance from the western extent of the data to the appropriate section, and the location of the change of trend of the fault is marked. a) Each line corresponds to the observed sediment thickness calculated from the Late Hauterivian (i.e. uppermost syn-rift) to the top of the appropriate horizon. This is approximately equivalent to throw on the Plettenberg Fault. The thickness to the Top Basement is generally under represented because it is frequently deeper than the maximum recording time of 5 s TWT and therefore will be plotted as being thinner than its true thickness. b) Cumulative sediment thickness from Top Early Syn-Rift to the appropriate horizon plotted. Top Basement can not be used because of the inaccuracy discussed in (a). From these plots it is evident that although there are variations in thickness along the fault, these are generally insignificant.

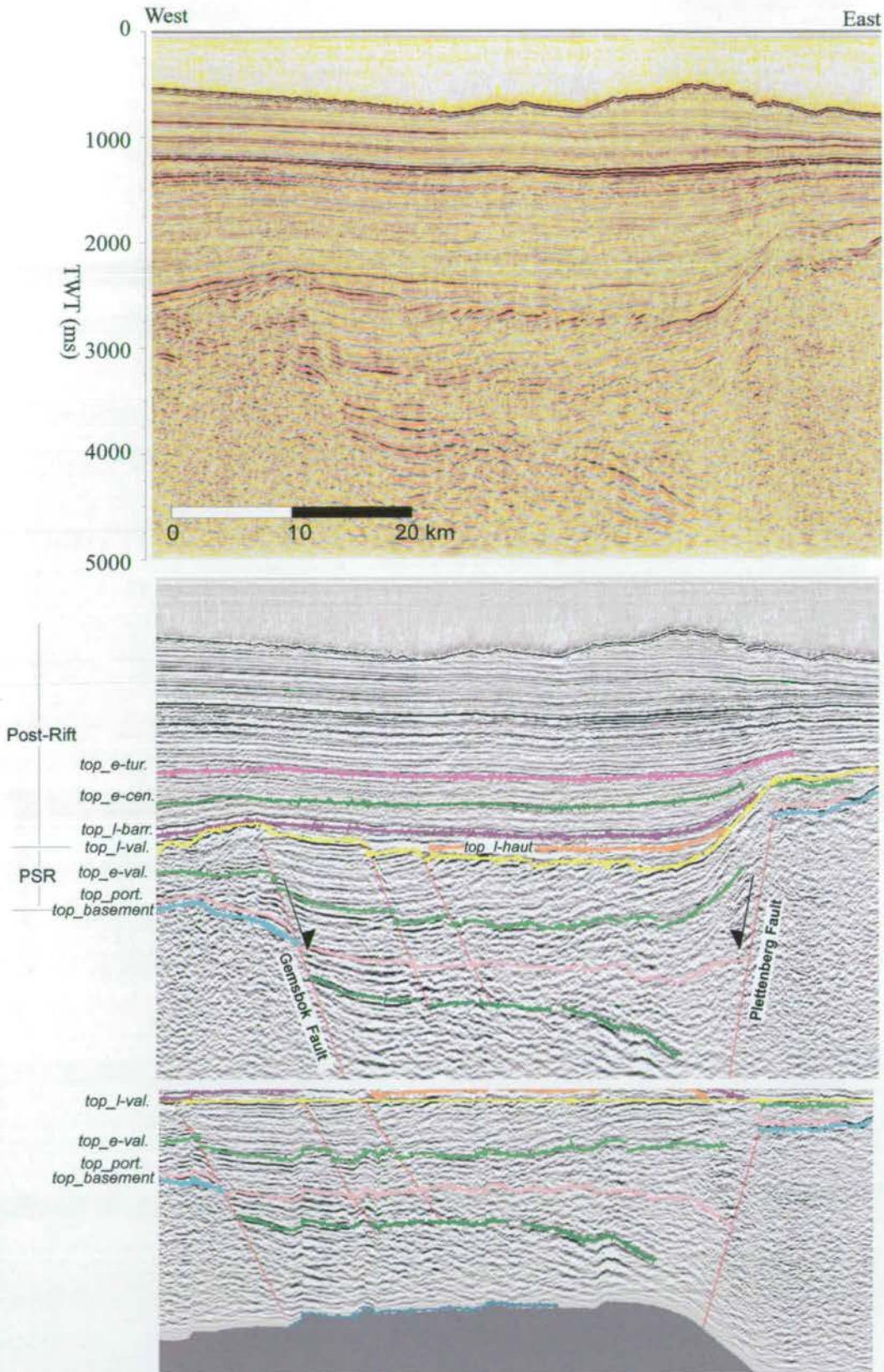


Figure 7.20: East-west section in the south-east of the basin showing the north-south trending Plettenberg Fault and Gembok Fault. The reconstruction (c) is flattened to *top_l-valanginian* and shows thickening in the Portlandian and Late Valanginian. Line Gb 91-106.

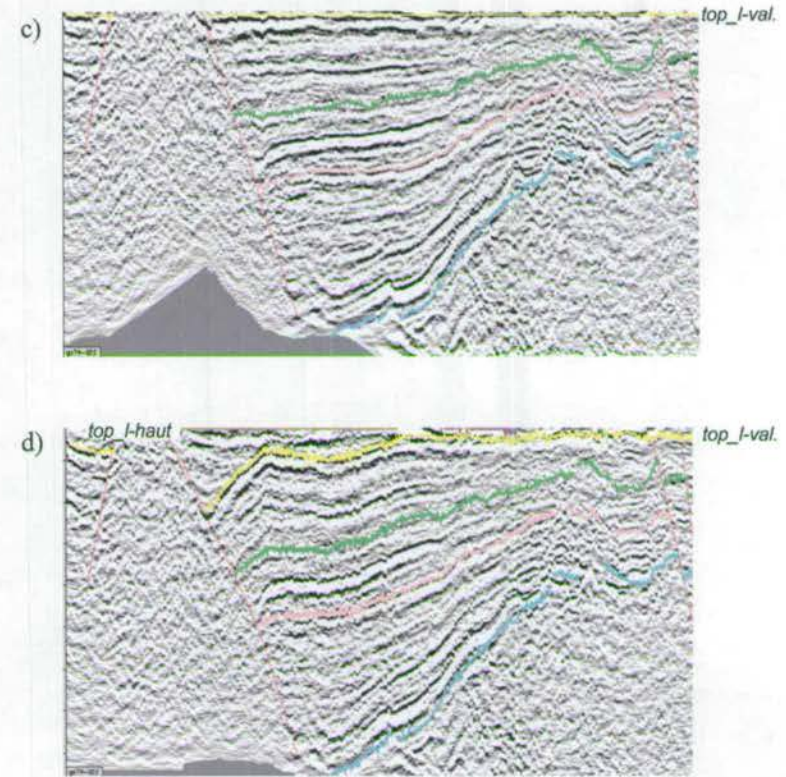
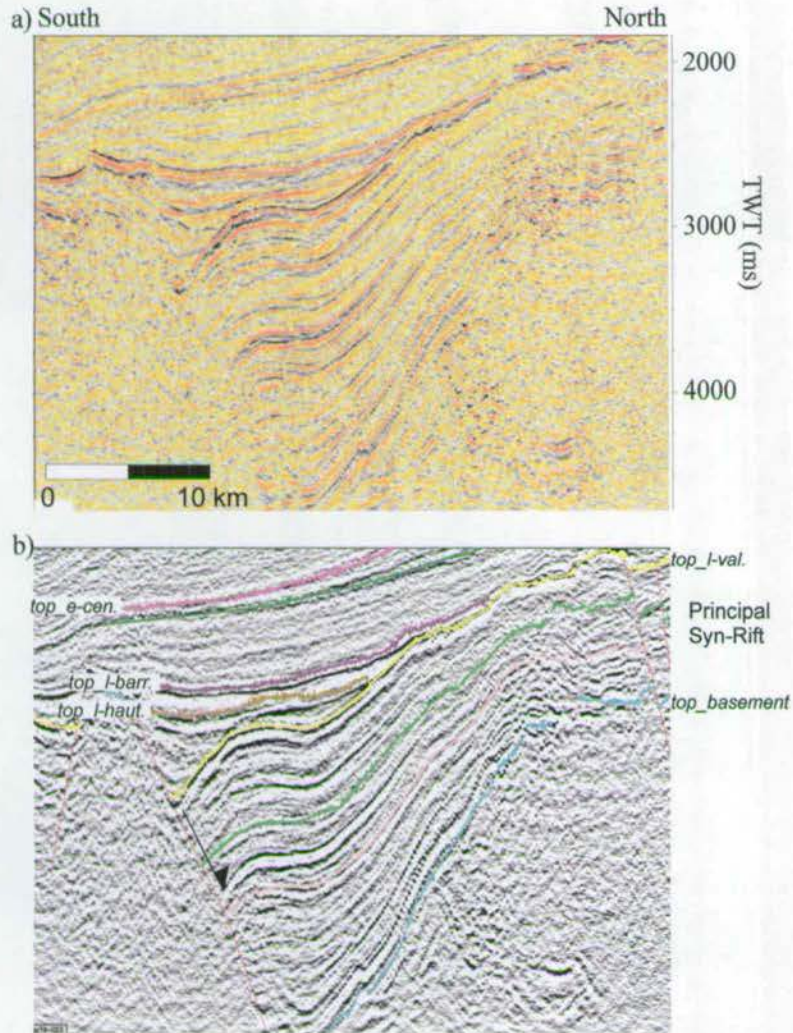


Figure 7.21: North-south section across the Pletmos Fault, a) un-interpreted section and b) interpreted section. c) Section flattened to top_l-valanginian to obtain end of Principal Syn-Rift (PSR) mega-sequence geometry, and (d) flattened on top_l-hauterivian to obtain end of Late Syn-Rift (LSR) geometry. Notice that PSR deposition occurs across the basin while LSR deposition occurs only proximally to the fault. Line Ga 87-022.

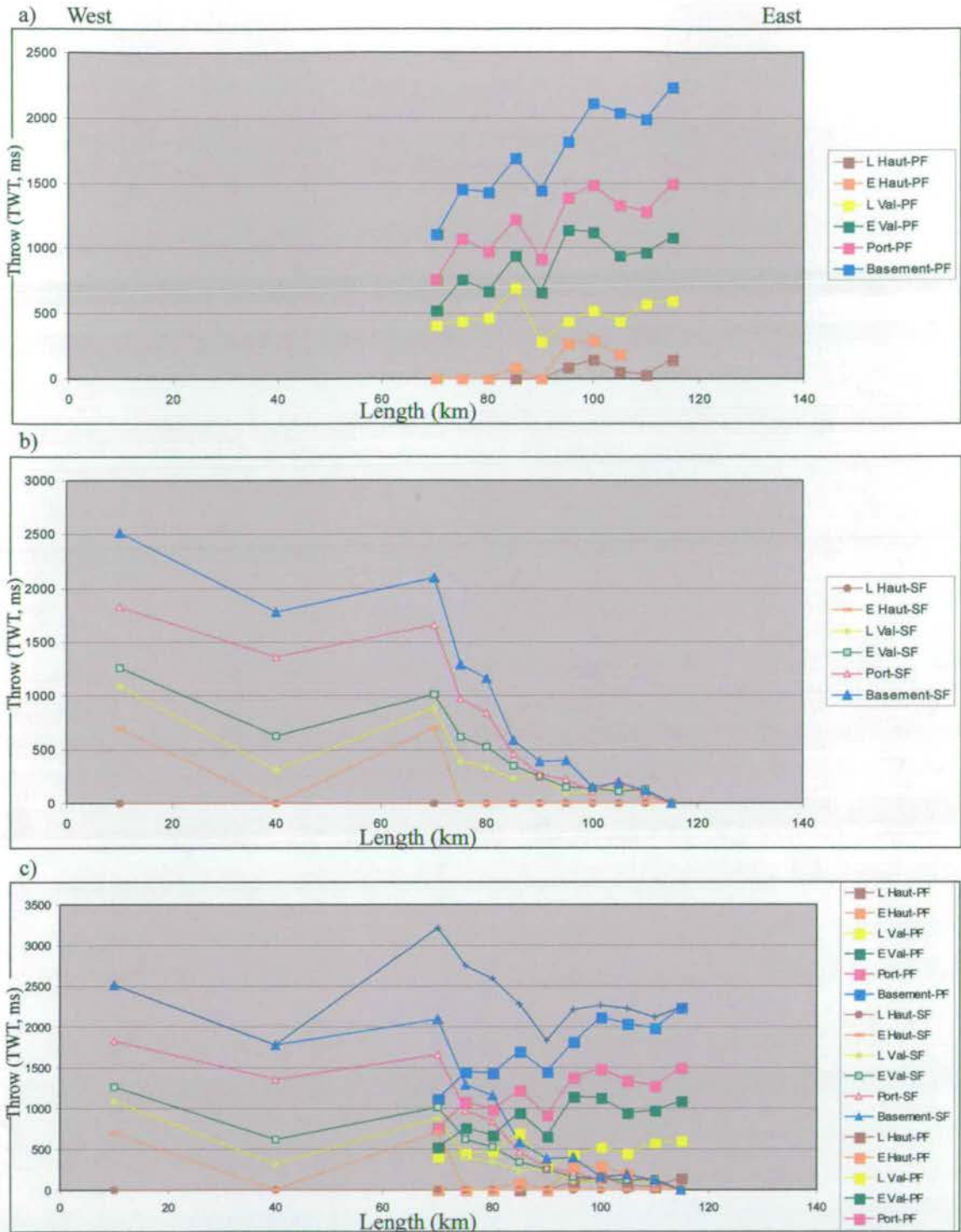


Figure 7.22: Throw-Length graphs across the (a) Pletmos, and (b) Superior Faults. The presence of Principal and Late Syn-Reflectors on the footwalls of both faults allows throw to be determined. Each line corresponds to the calculated throw for the top of each sequence, including basement. Length is the distance from the western extent of the data to the appropriate section. c) Both (a) and (b) plotted on one graph to show the transfer of throw from the Superior Fault in the west to the Pletmos Fault in the east. This graph also has the total throw of the *top_basement* (sum of throws from Pletmos and Superior Faults) plotted.

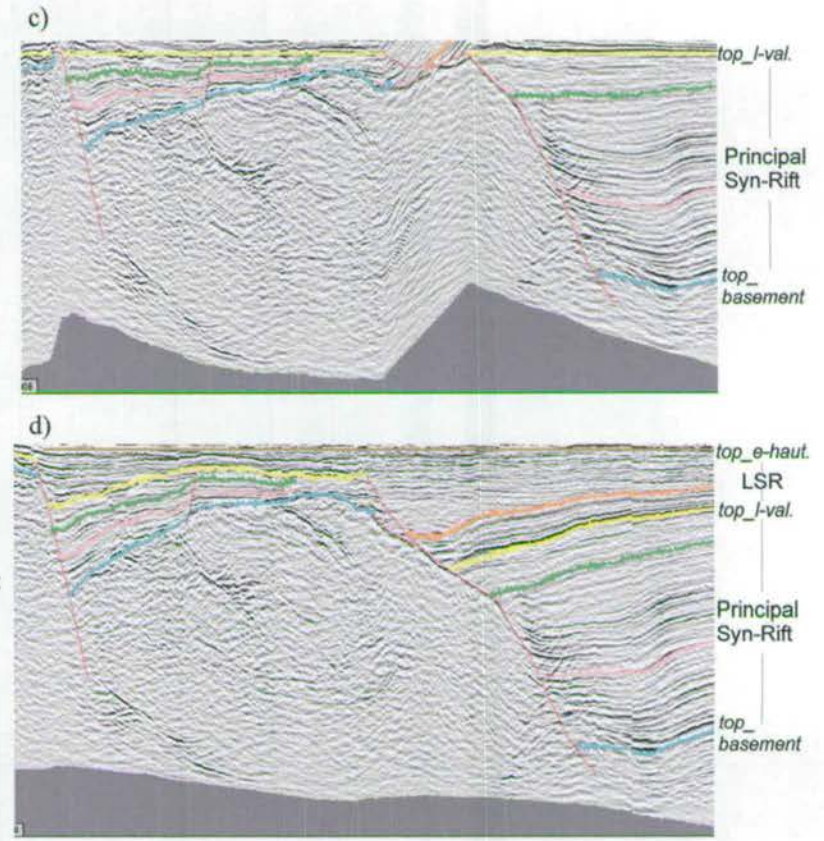
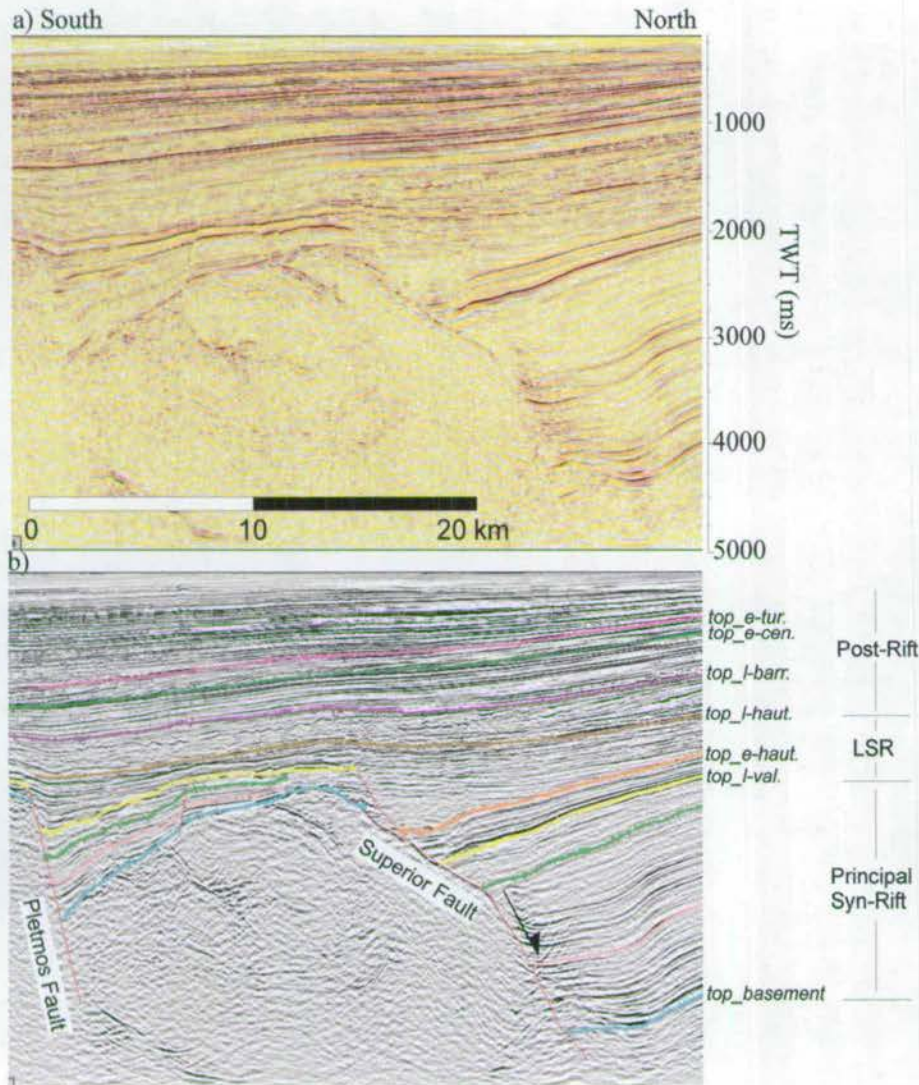


Figure 7.23: North-south section across the Pletmos and Superior Faults, a) un-interpreted, and b) interpreted. c) Section flattened to top_l-val. to obtain Principal Syn-Rift geometry, and d) flattened to top_l-hauterivian to obtain Syn-Rift (LSR) geometry.

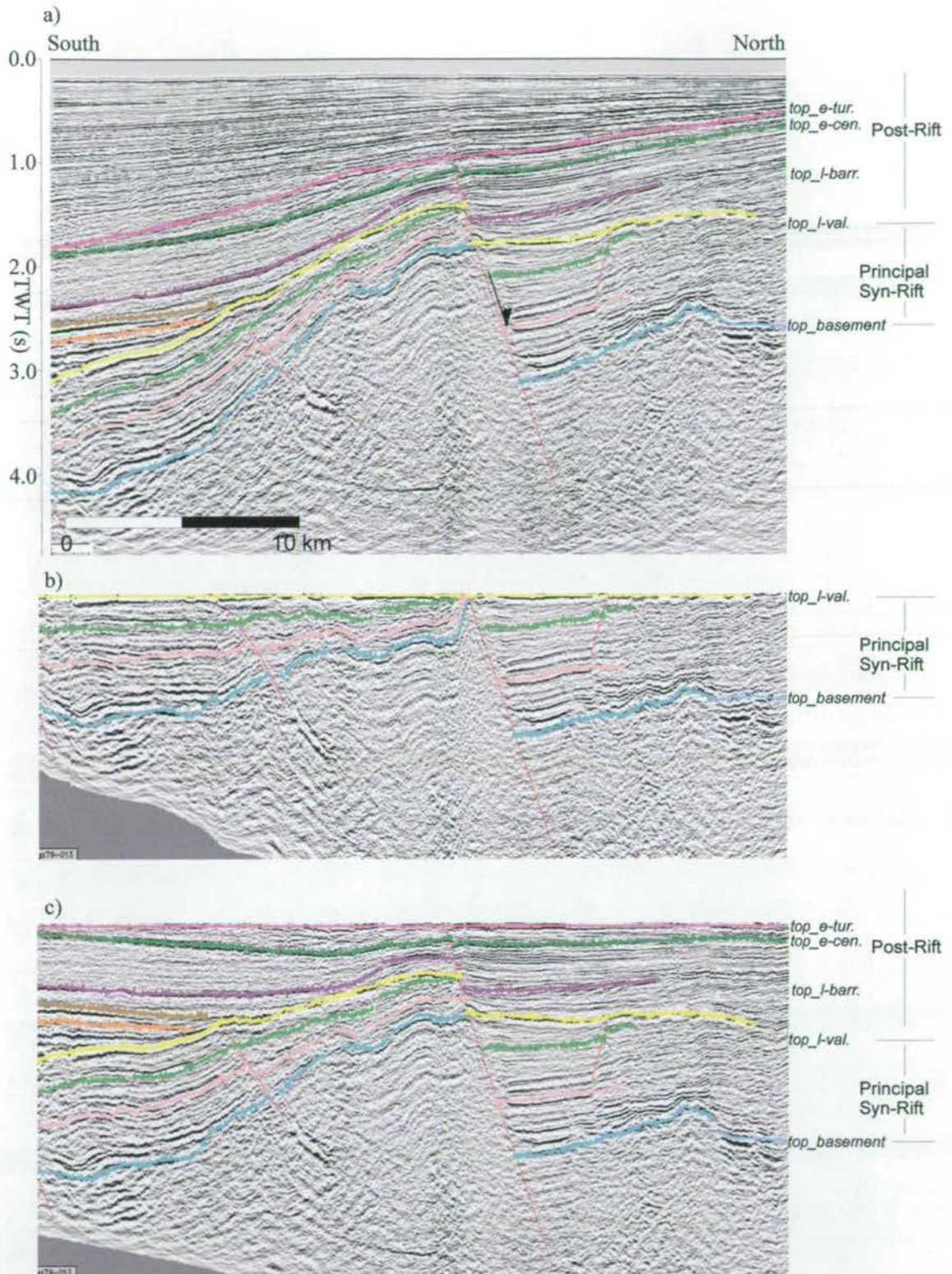


Figure 7.24: North-south section across the Superior Fault approximately 20 km east of Figure 7.23. a) Interpreted section that shows the Superior Fault with no Late Syn-Rift deposition against it. b) Section in (a) flattened to *top_l-valanginian*. c) Section in (a) flattened to *top_l-turonian* showing a growth in the thickness of the Early Cenomanian sequence (between Late Barremian, *top_l-barr.*, and Early Cenomanian, *top_e-cen.*). There is also minor growth into the fault in the Early Turonian. Line Ga 79-013.

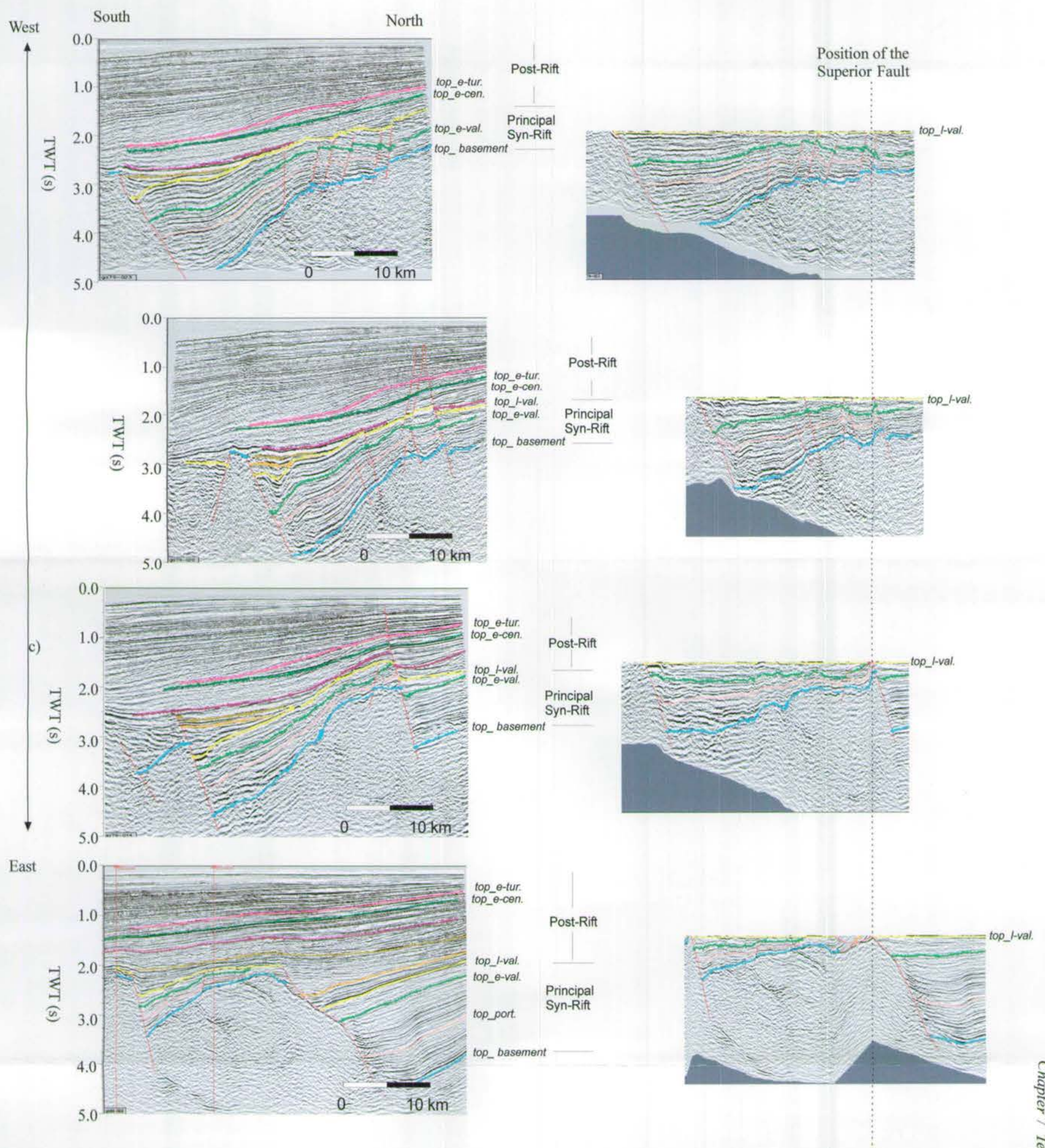


Figure 7.25: North-south sections across the Pletmos Fault (south) and Superior Fault (north) to highlight the en-echelon nature of the faulting. Throw in the west (a) is concentrated on the Superior Fault and towards the east throw is accrued on the Pletmos Fault (d). Sections i-a) to i-d) are interpreted sections, while ii-a) to ii-d) have been flattened to *top_lvalanginian* to show the gradual transition of deposition from the Superior to Pletmos Faults. Line names, a) Ga 79-023, b) Ga 79-020, c) Ga 79-014, and d) Ga 88-006.

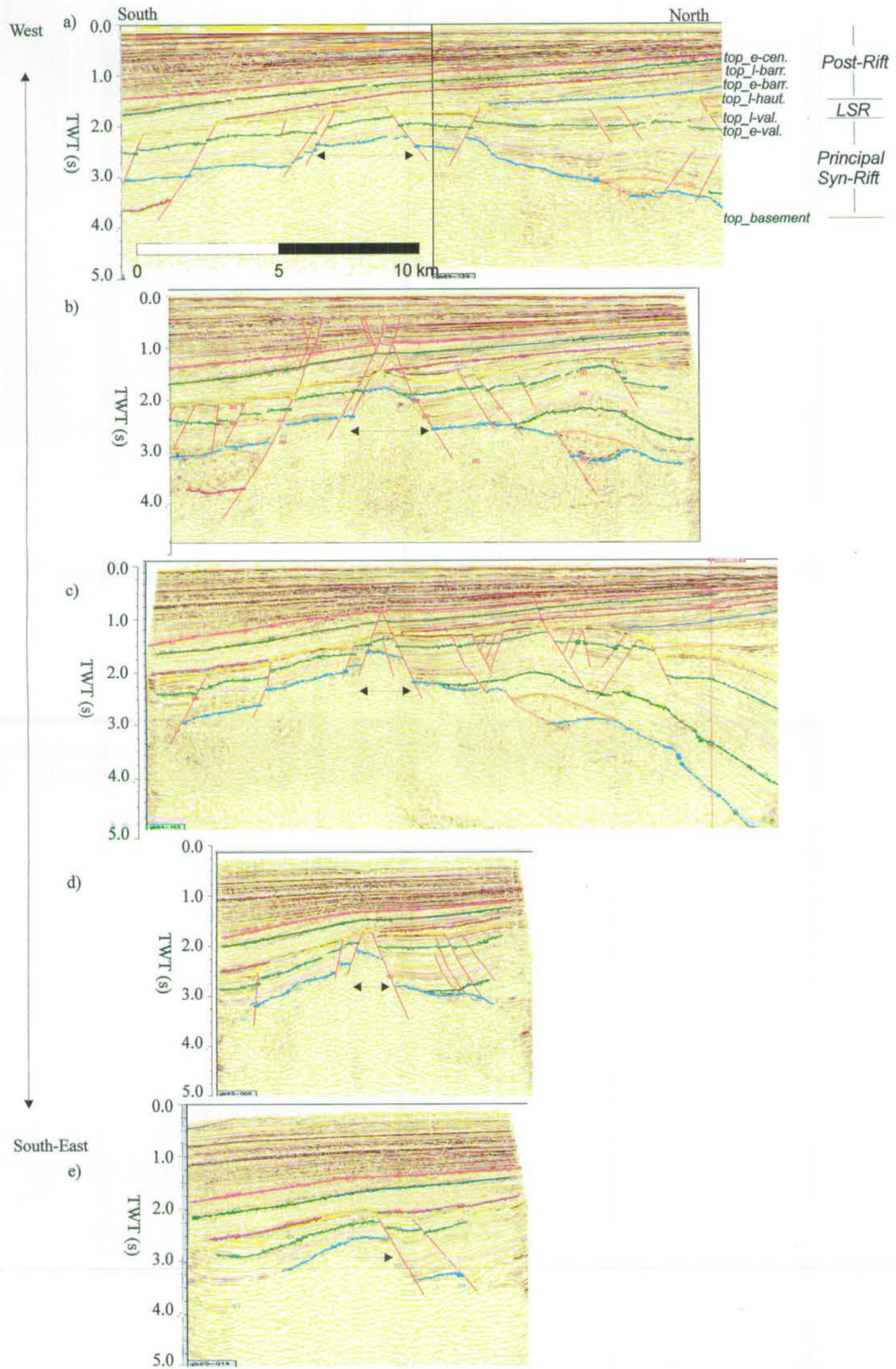


Figure 7.26: North-south sections displayed from west (a) to south-east (b) to show the structure of the Springbok High (arrows). The high is formed from complex north and south dipping faults. dies out towards the south-east while the northern fault increases throw. Lines Name: a) Gb87-140, b) Gb84-109, c) Gb84-105, d) Gb85-008, e) Gb85-014.

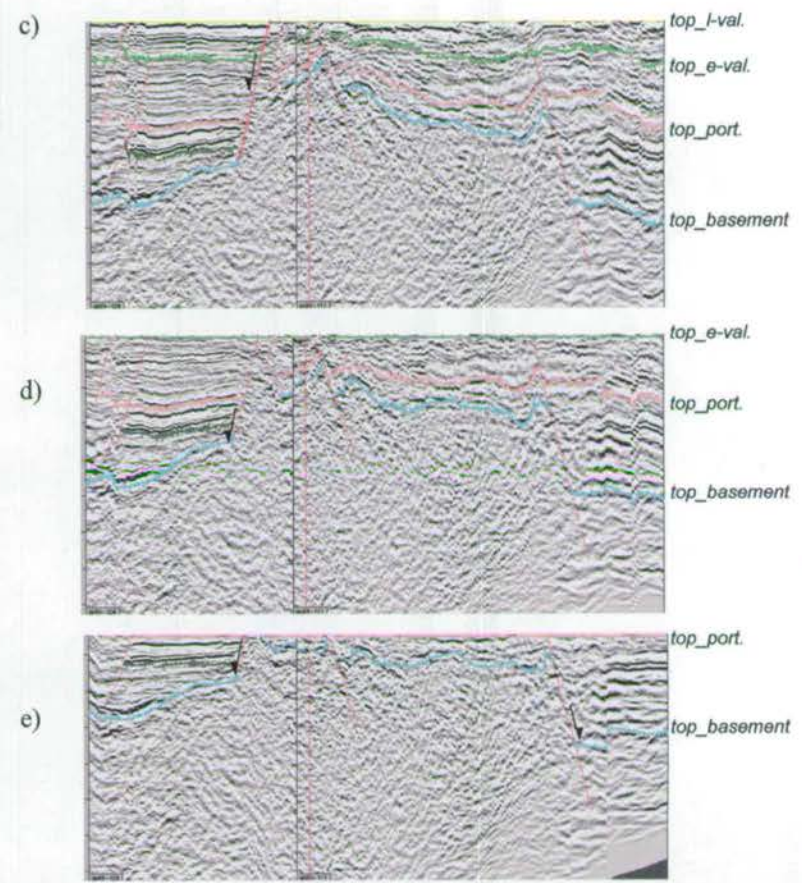
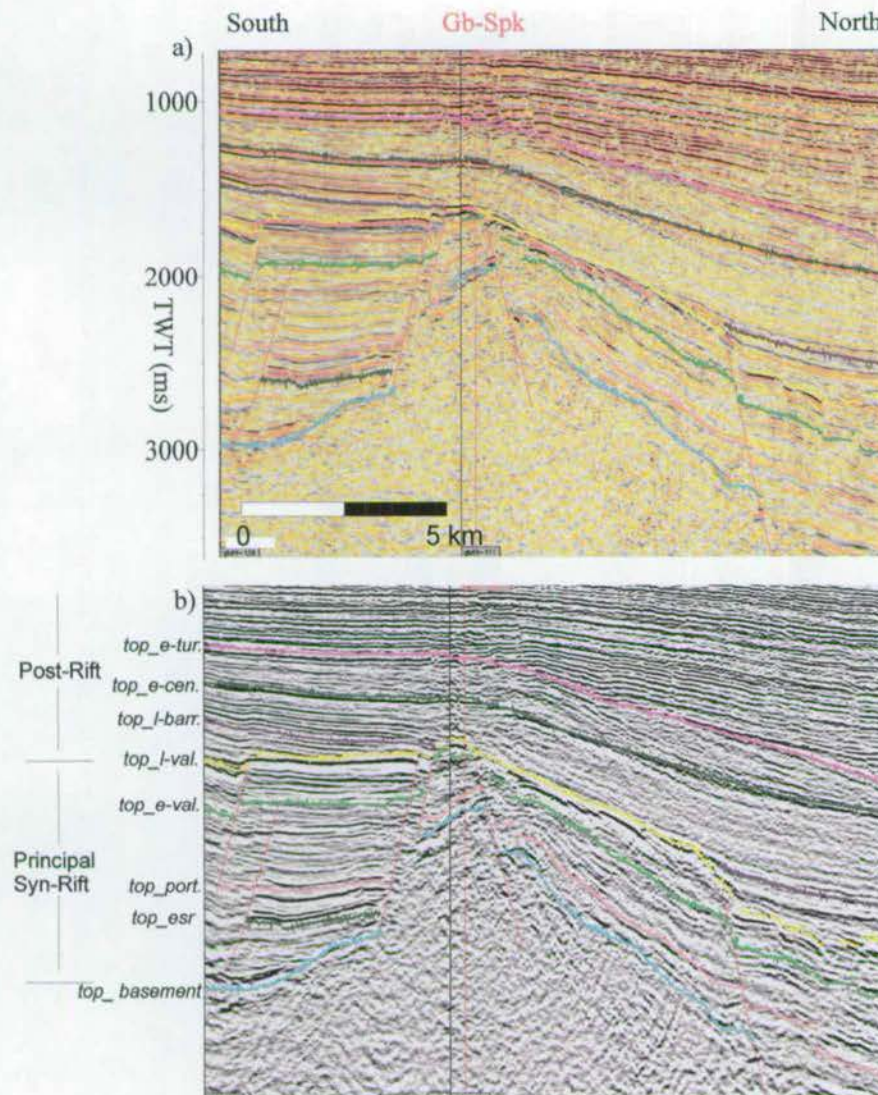


Figure 7.27: Section across the Springbok High, well tied to Gb-Spk1. a) un-interpreted section and (b) interpreted and age tied to the well. The sequential flattened sections of (c) *top_l-valanginian*, (d) *top_e-valanginian*, and (e) *top_portlandian* indicate that the basement high was present throughout the evolution of the basin, and that the faults were active at different times. Lines Gb89-128, Gb89-111.

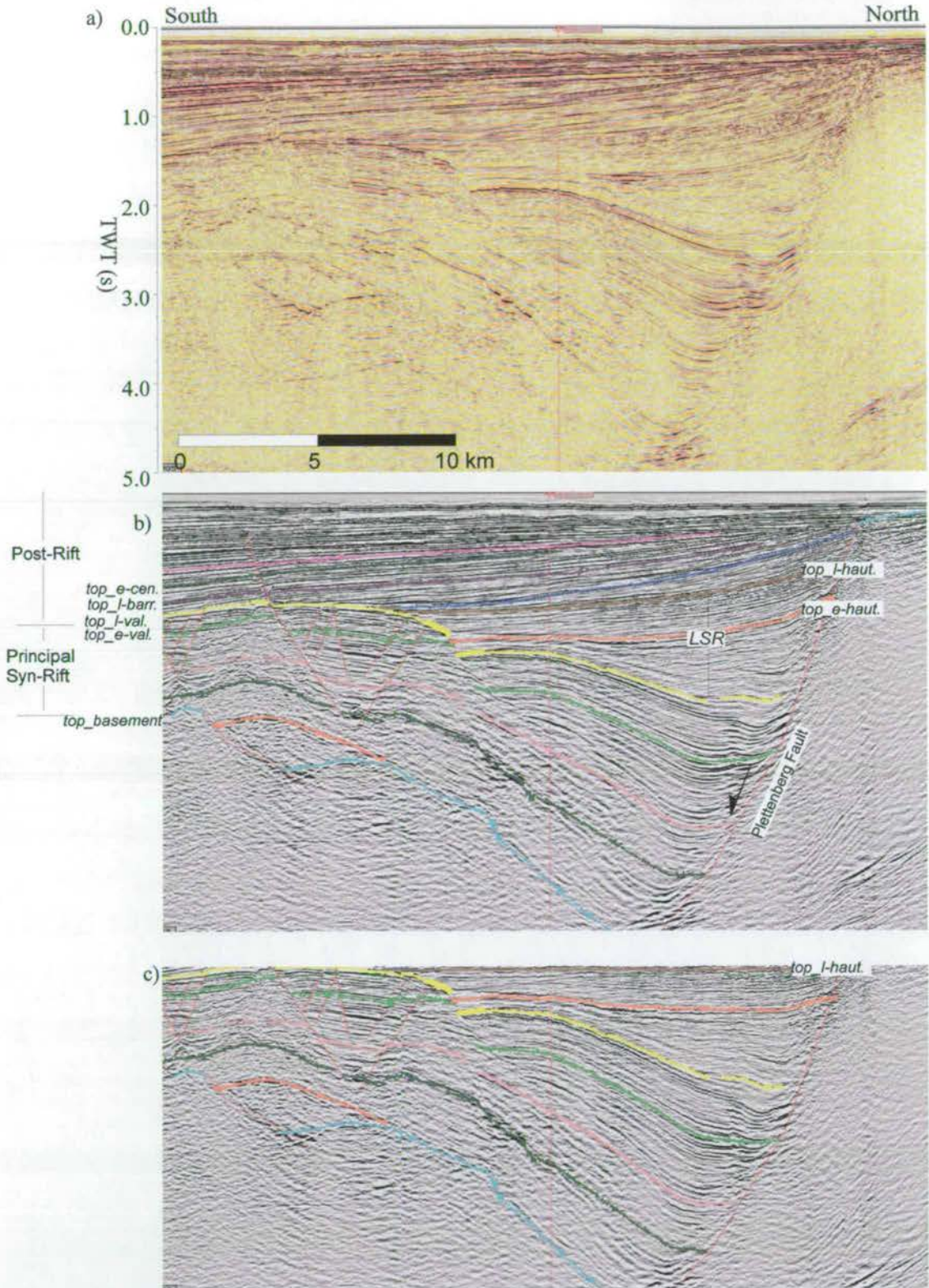


Figure 7.28: The antithetic fault to the Plettenberg Fault is a north dipping structure that appears to décolle in the Early Valanginian. When the section is flattened to *top_l-hauterivian* (c) it is evident that the fault was active in the Late Hauterivian. Gb84-105

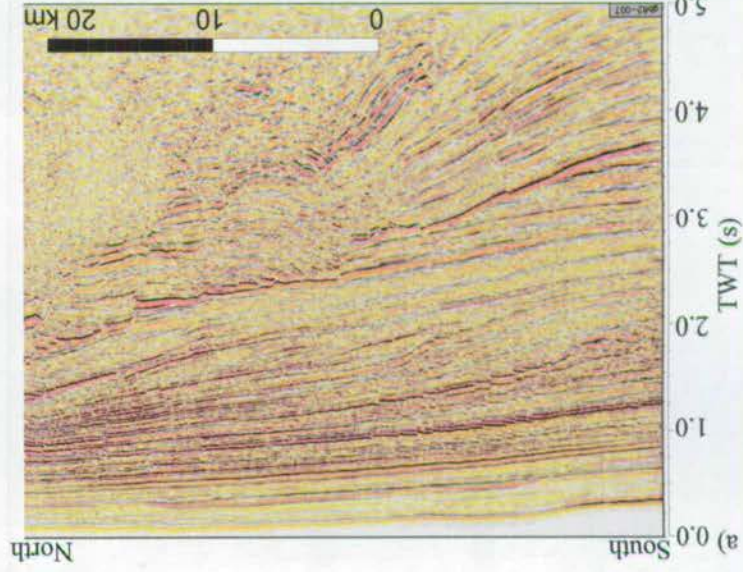
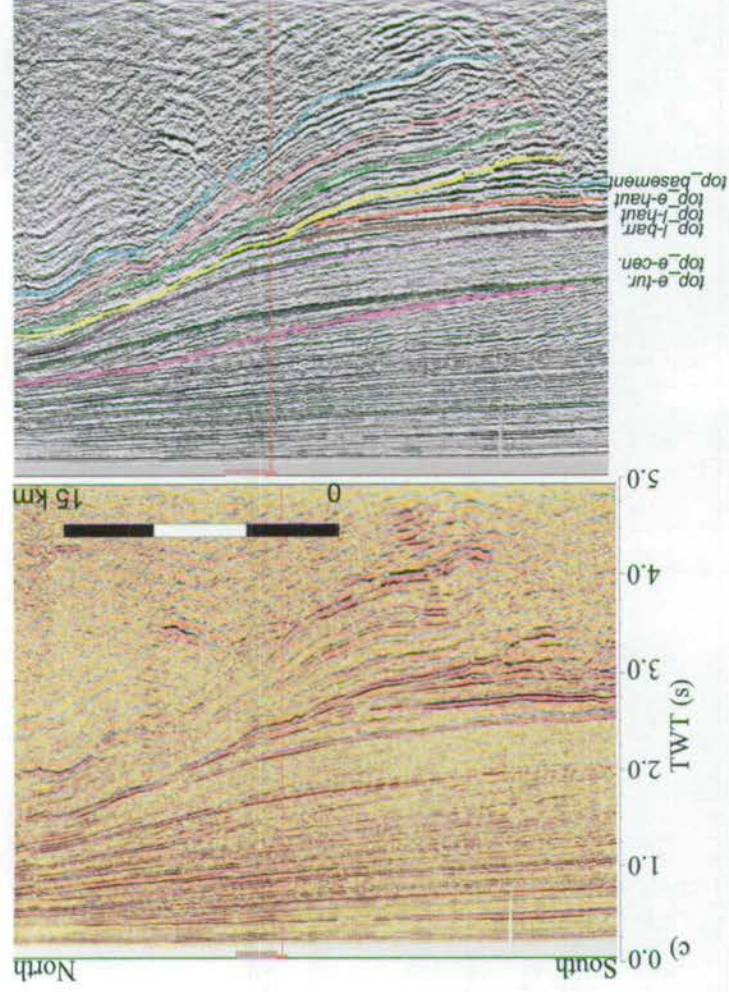


Figure 7.29: The section to the south of the Springbok High (a) uninterpreted and (b) interpreted shows many intra-basin faults that deform the *top_l-valanginian* horizon but do not deform Late Barremian. The section in (c) and (d) is only 10 km west of (a) but does not contain any of these faults.

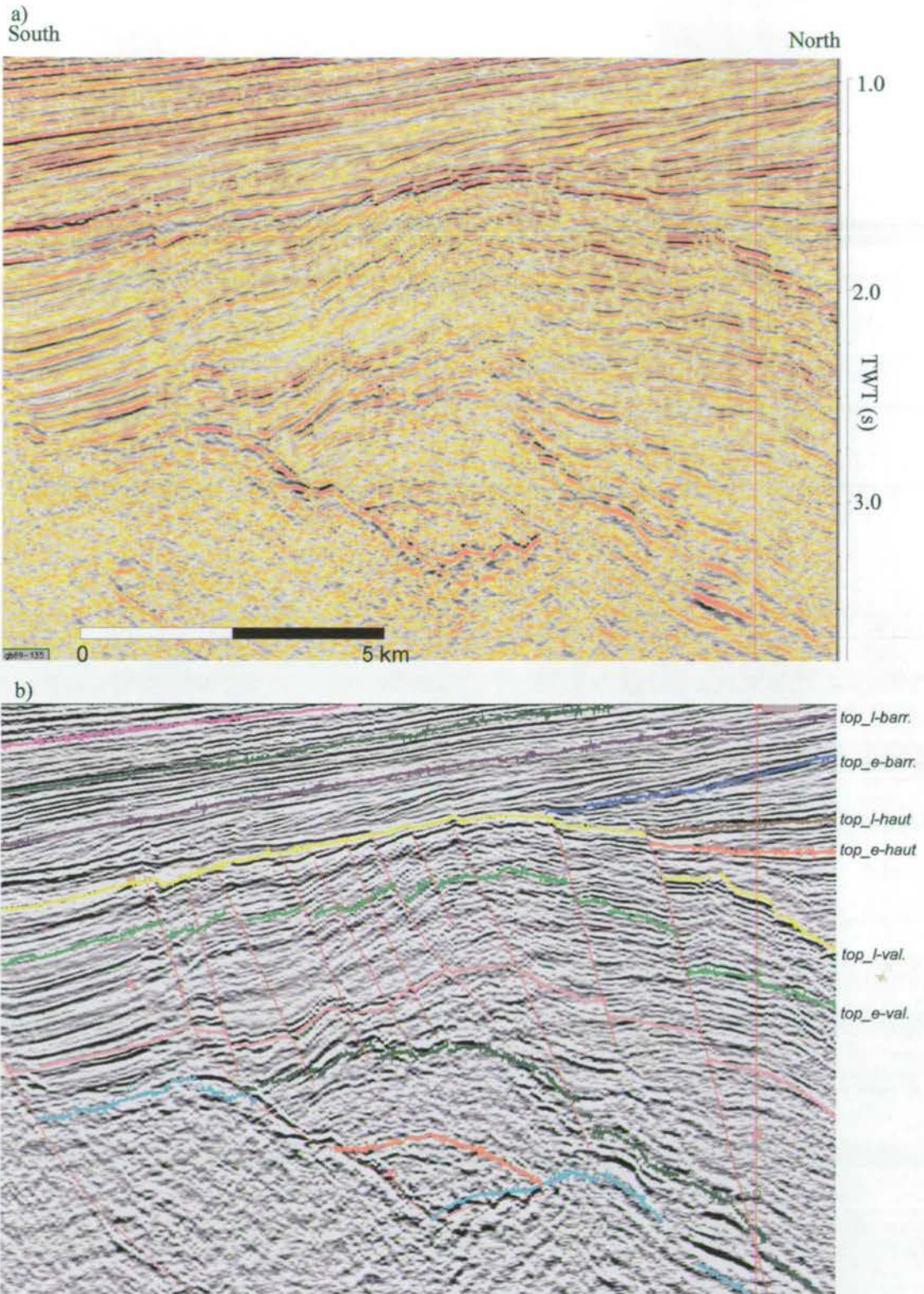


Figure 7.30: North-south section in the north of the basin showing folding of the *top_l-valanginian* which is dissected by numerous post-Late Valanginian extensional faults. Ga89-135

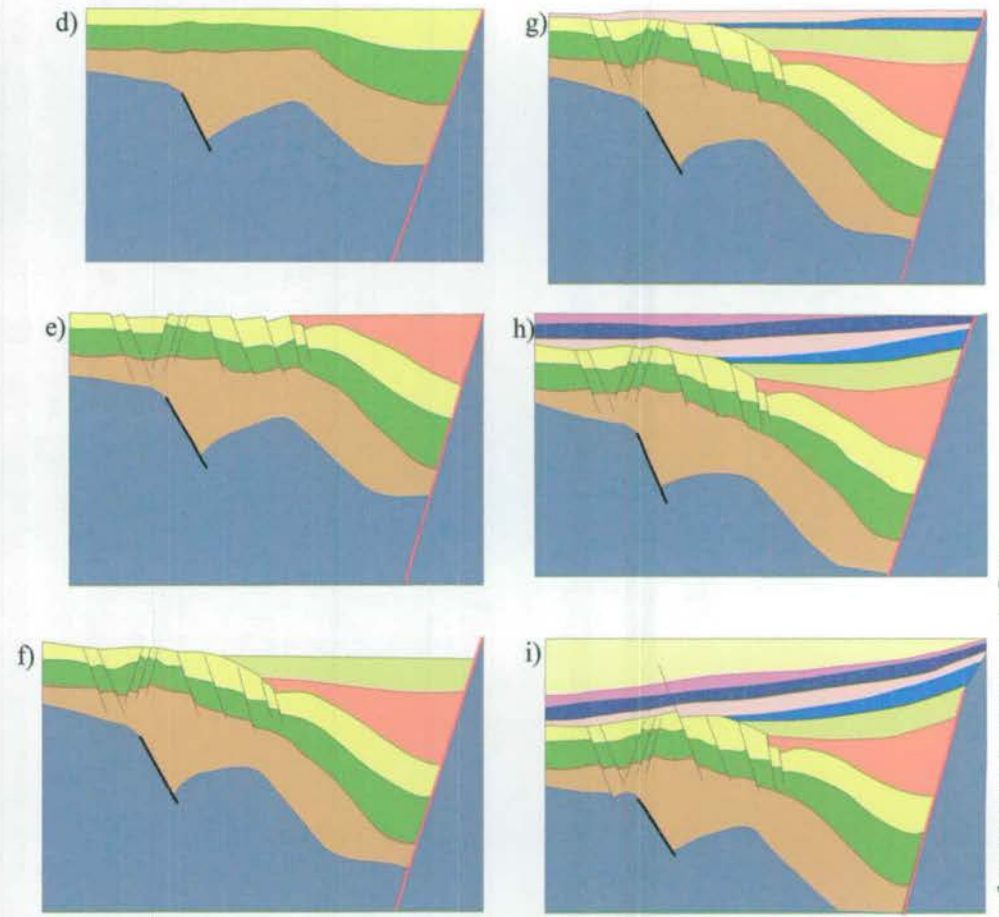
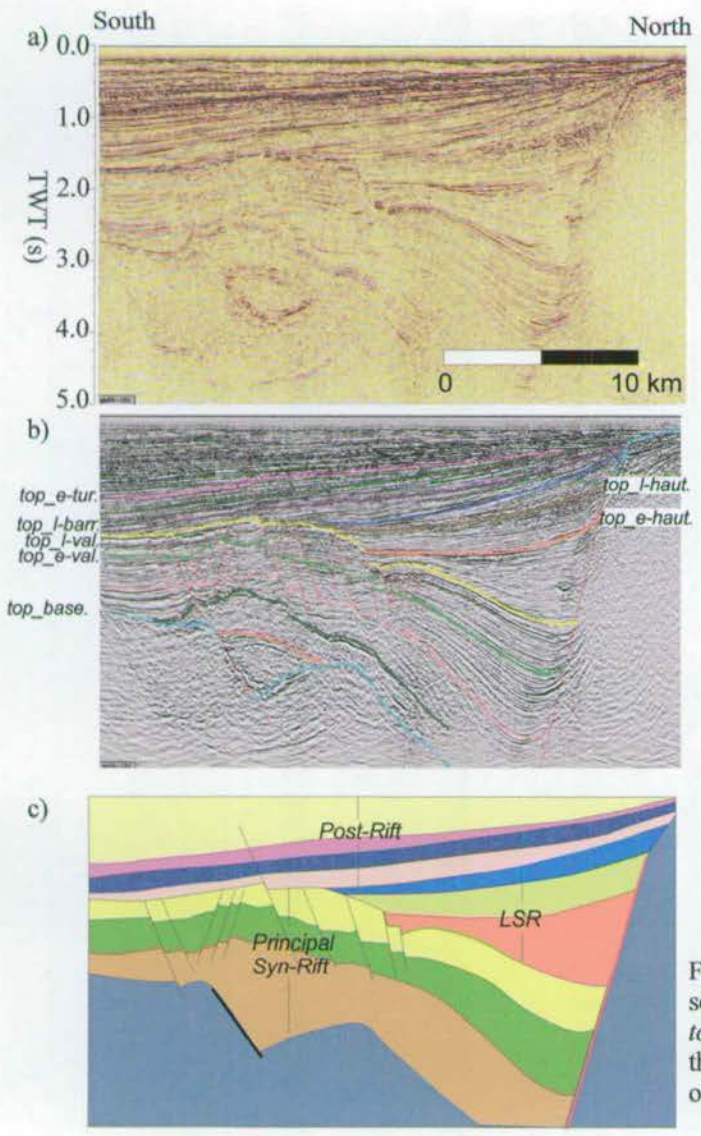


Figure 7.31: North-South section across the Plettenberg Fault. a) un-interpreted and b) interpreted section used to produce the model (c) that is restored to: d) *top_l-valanginian*; e) *top_e-hauterivian*; f) *top_l-hauterivian*; g) *top_l-barremian*; h) *top_e-turonian*; i) present. Of importance is the extent of the Principal Syn-Rift package compared to the Late Syn-Rift, the topographic infill and progradation of the Barremian sequences, and the regional southern tilt post Early Turonian. Line 89-130.

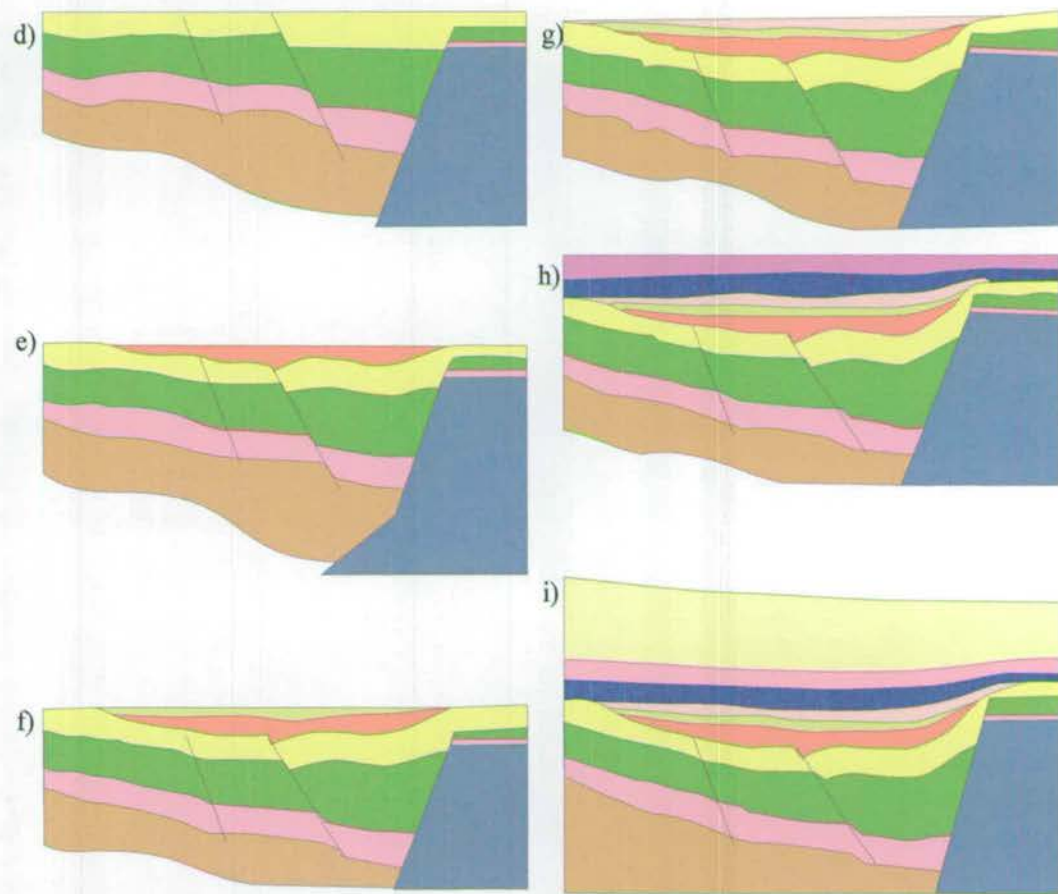
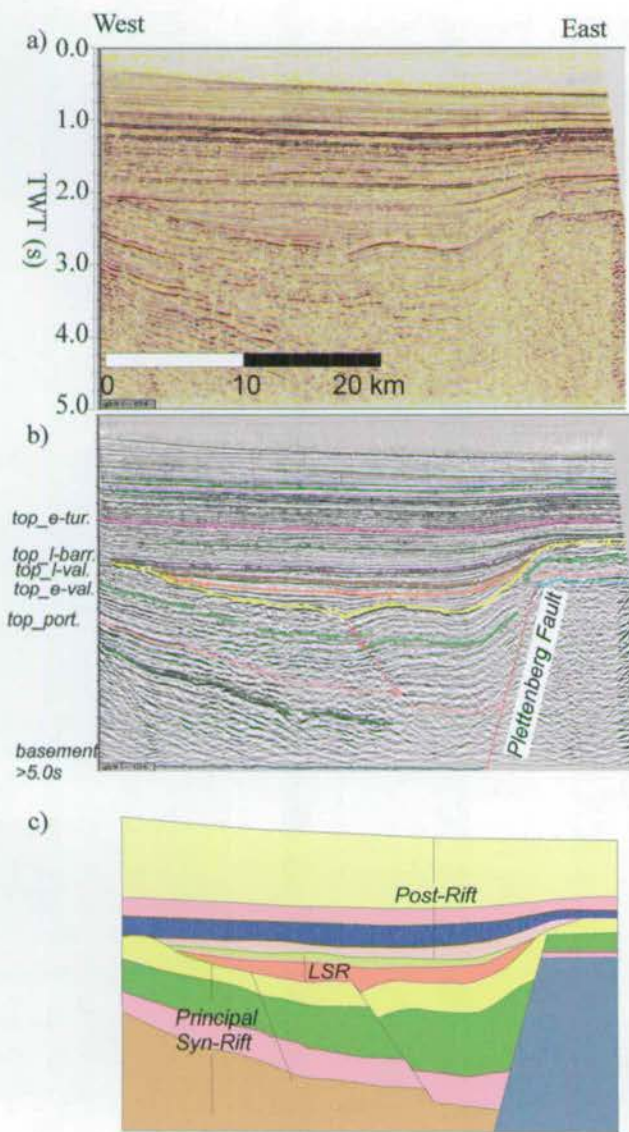


Figure 7.32: East-west section across the north-south trending Plettenberg Fault in the south-east of the basin. a) un-interpreted and b) interpreted section used to produce the model (c) that is restored to: top_l-valanginian; e) top_e-hauterivian; f) top_l-hauterivian; g) top_l-barremian; h) top_e-turonian; i) present. Of importance is the deformation of the Late Valanginian into a monoclinical structure with increasing deposition of the Late Syn-Rift (LSR) which is controlled by the east-west trending Plettenberg Fault.

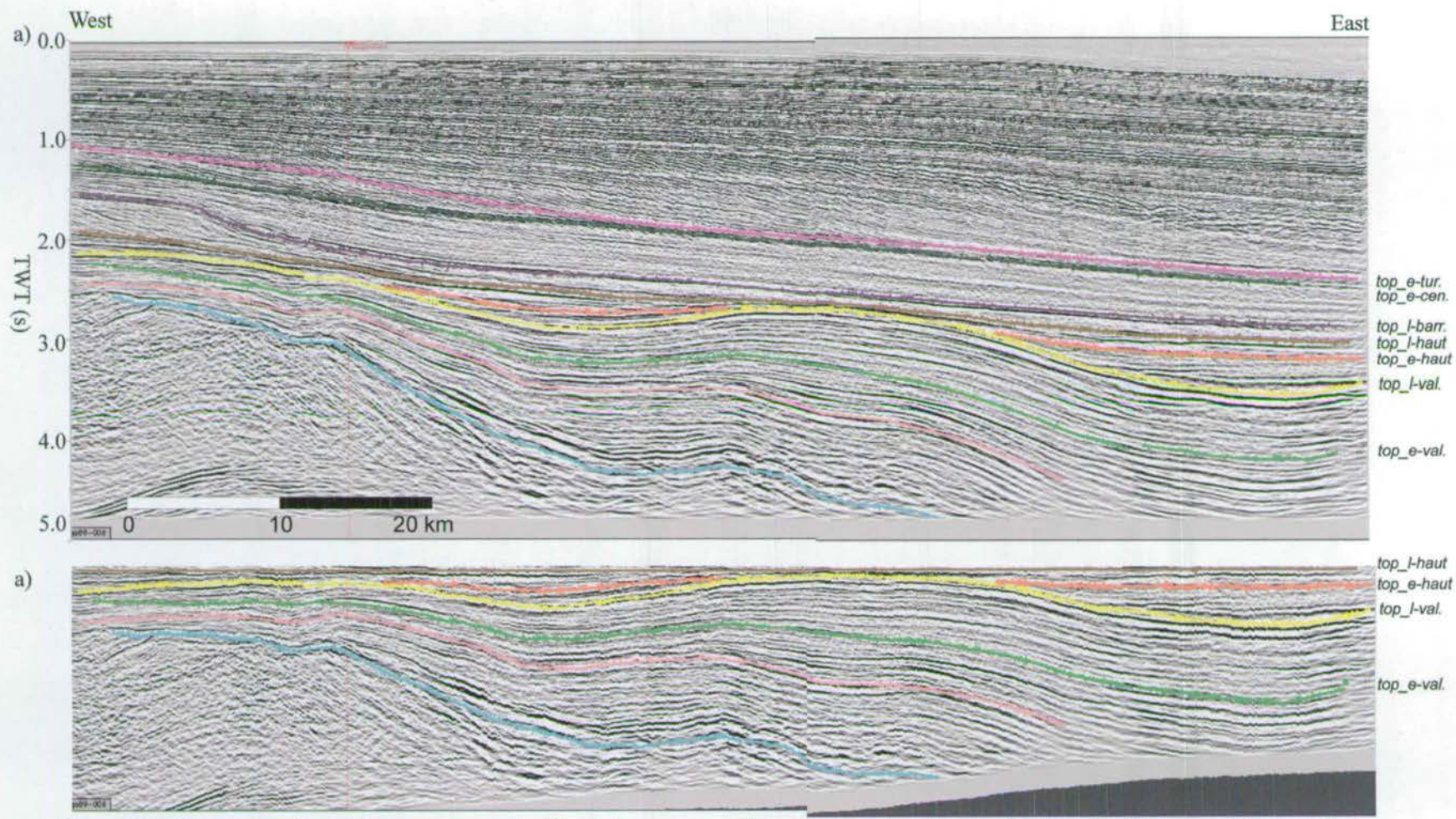
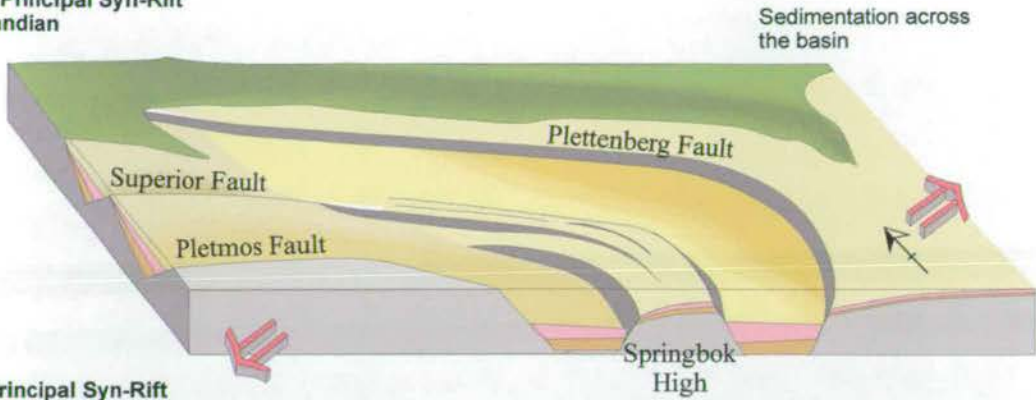
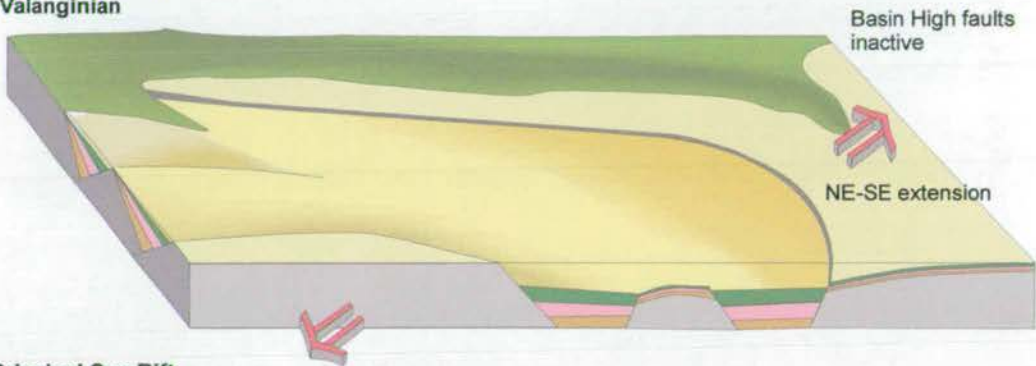


Figure 7.33: West-east section at the southern extent of the data coverage. a) Interpreted section showing the dramatic thickening of the post-Early Turonian sequence. b) Section (a) flattened to *top l-hauterivian* to show the undulatory nature of the *top l-valanginian* horizon with the onlap of the Hauterivian Syn-Rift sequence onto the anticlines. This folding suggests that the controlling Pletmos Fault may be separated into two fault segments during the Hauterivian. Line Ga 89-006.

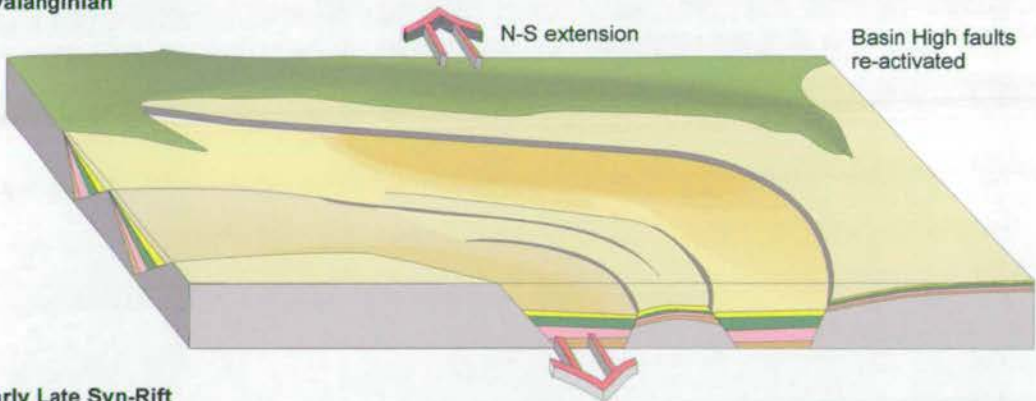
Early Principal Syn-Rift
Portlandian



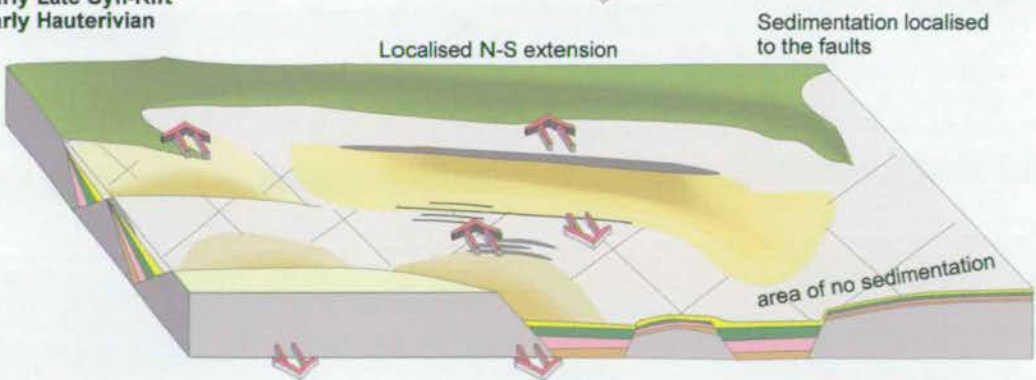
Mid Principal Syn-Rift
Early Valanginian



Late Principal Syn-Rift
Late Valanginian



Early Late Syn-Rift
Early Hauterivian



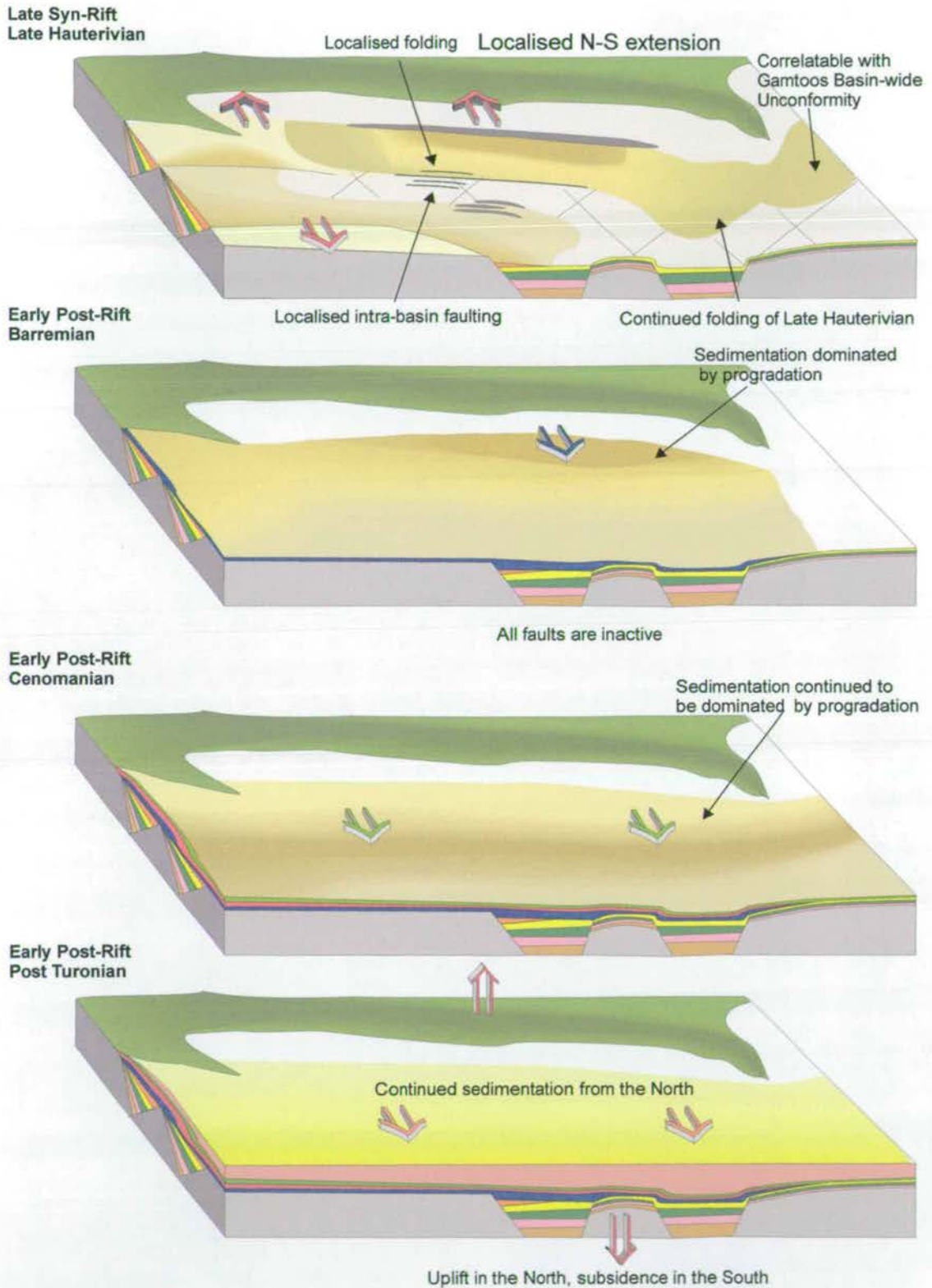


Figure 7.34: Summary sketches of the evolution of the Pletmos Basin highlighting the principal tectonic events, relative sea-level, and type of sedimentation. Note that the coast is shown as it is today. Red arrows indicating extension with respect to present orientation, other arrows indicate sediment progradational direction.

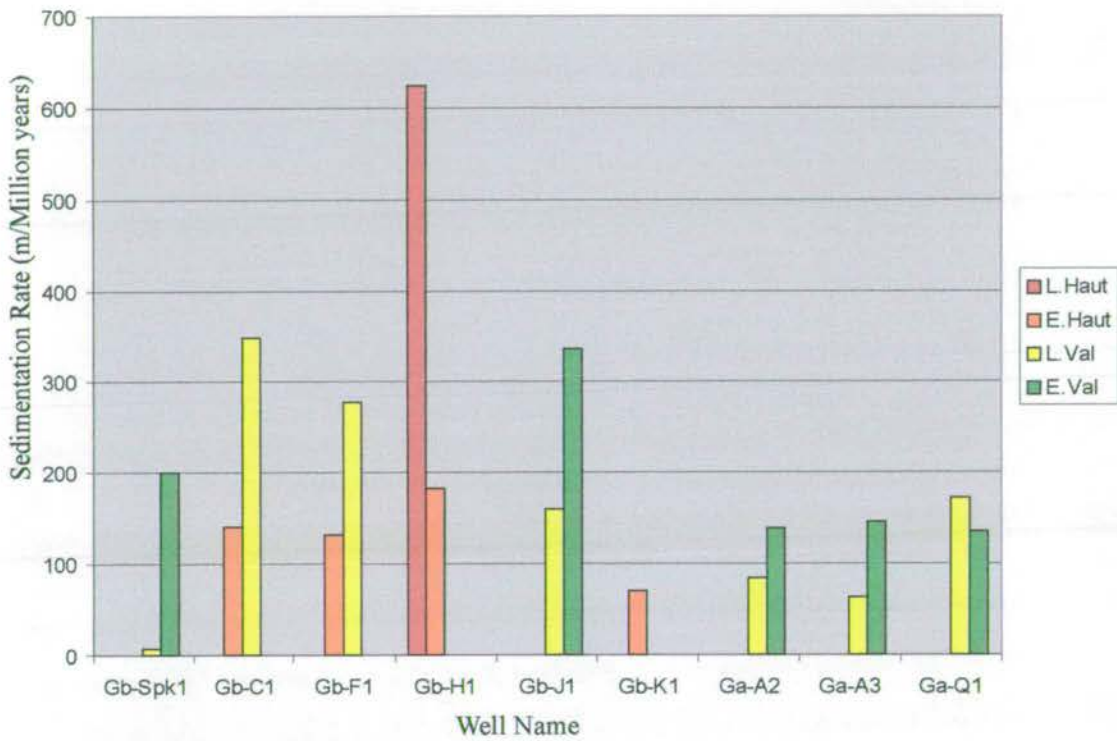


Table 7.1: Calculated sedimentation rates (in metres per million years) for the Principal Syn-Rift sequences and the Late Syn-Rift sequences. Although the specific rates must be treated with caution (cf. Chapter 7- methods) comparisons between different sequences are valid.

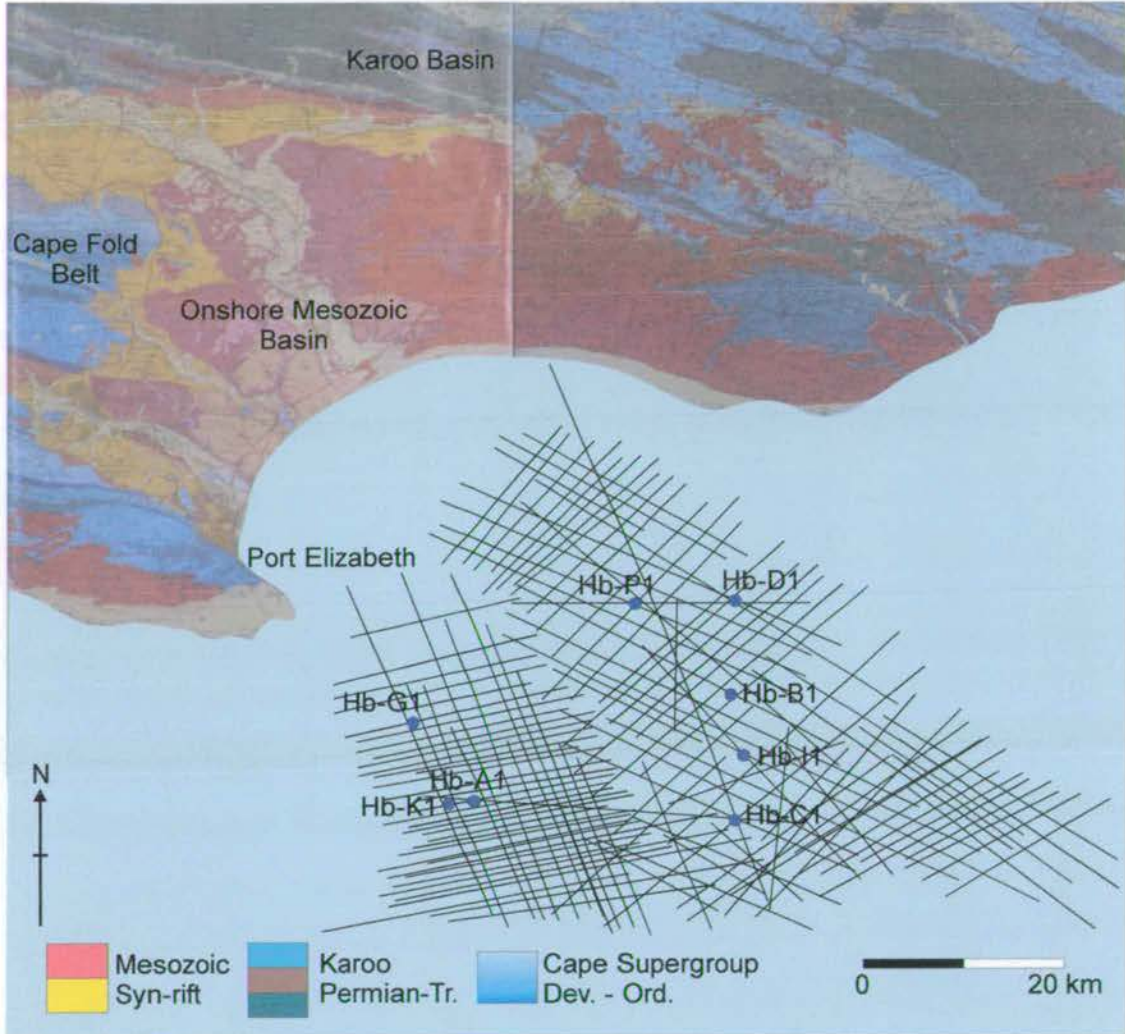


Figure 8.1: The location of the offshore seismic and well data set used to establish the tectono-stratigraphic framework of the Algoa Basin. The principal onshore geological units are shown (after Toerien, 1989). The position of sections used in this chapter are shown in Enclosure 10.

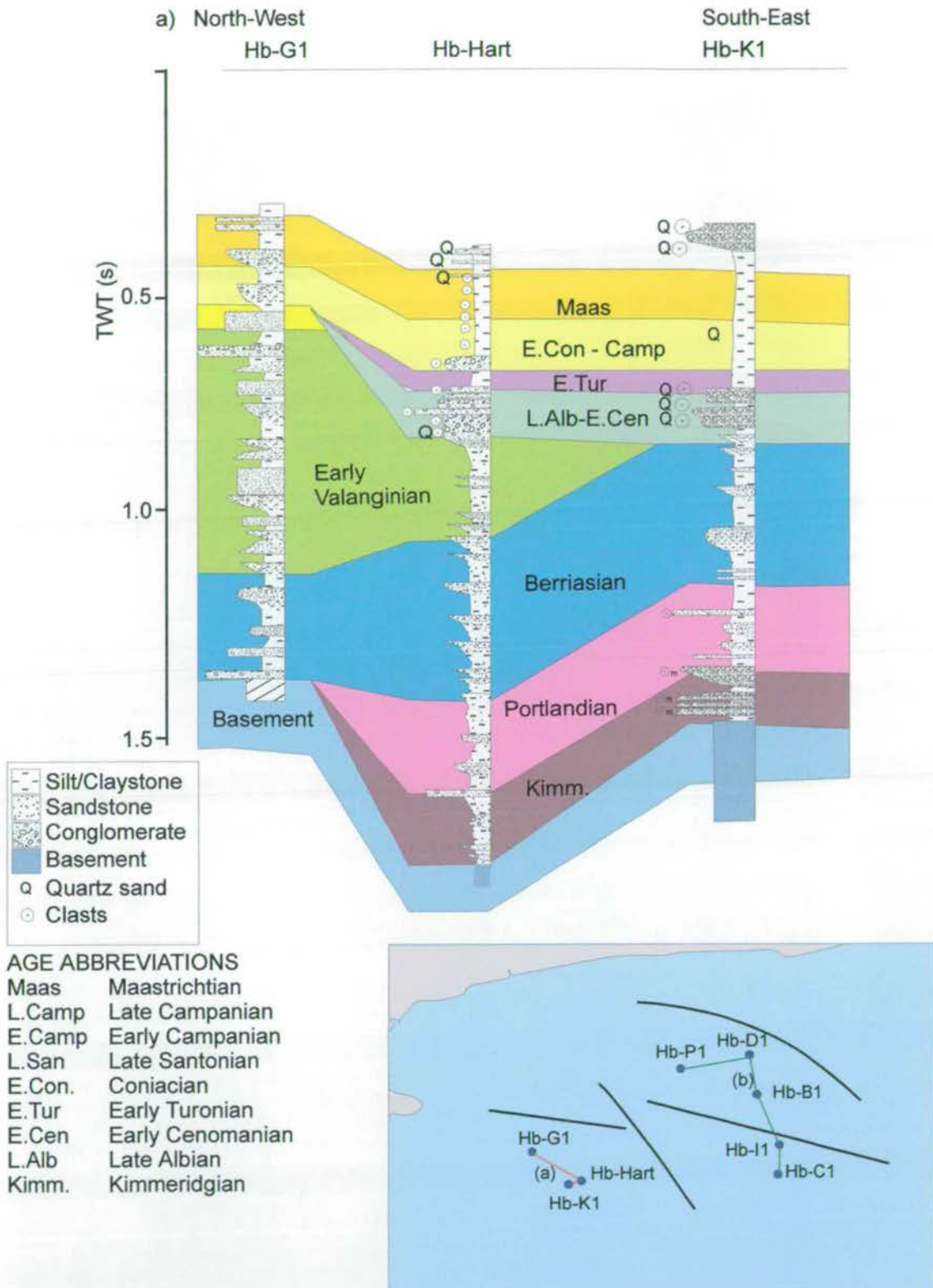
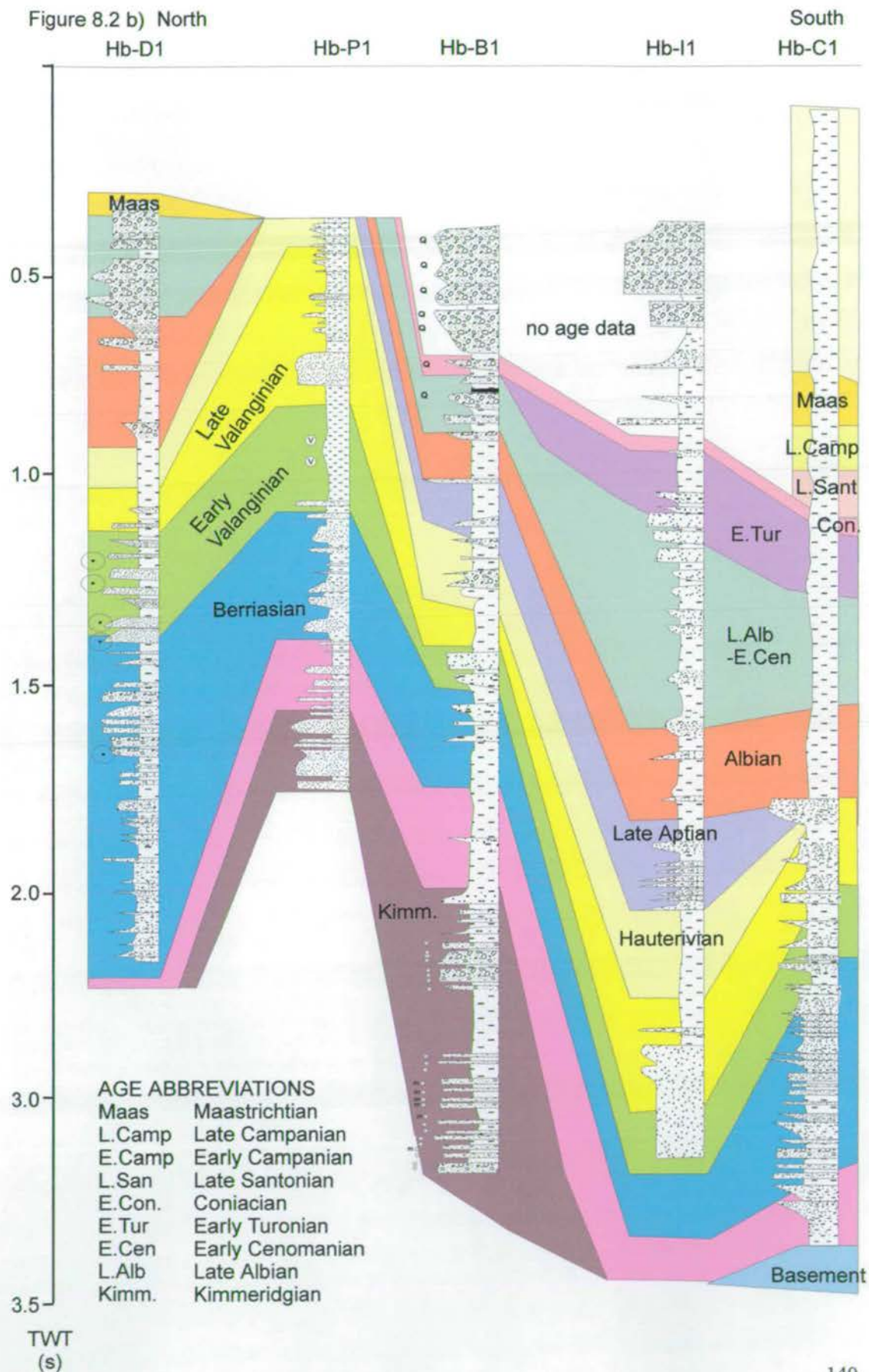


Figure 8.2: Summary of wells present in the Algoa Basin with (a) North-west south-east sections in the Port Elizabeth Trough, and (b) north-south section in the Uitenhage Trough. Well positions are marked on the map inset. Age data between wells have been correlated. Full well logs are included in Appendix C. Although wells have been plotted against time, depth/conversion data (Appendix C) suggests that time/depth relationships are comparable amongst wells.

Figure 8.2 b) North



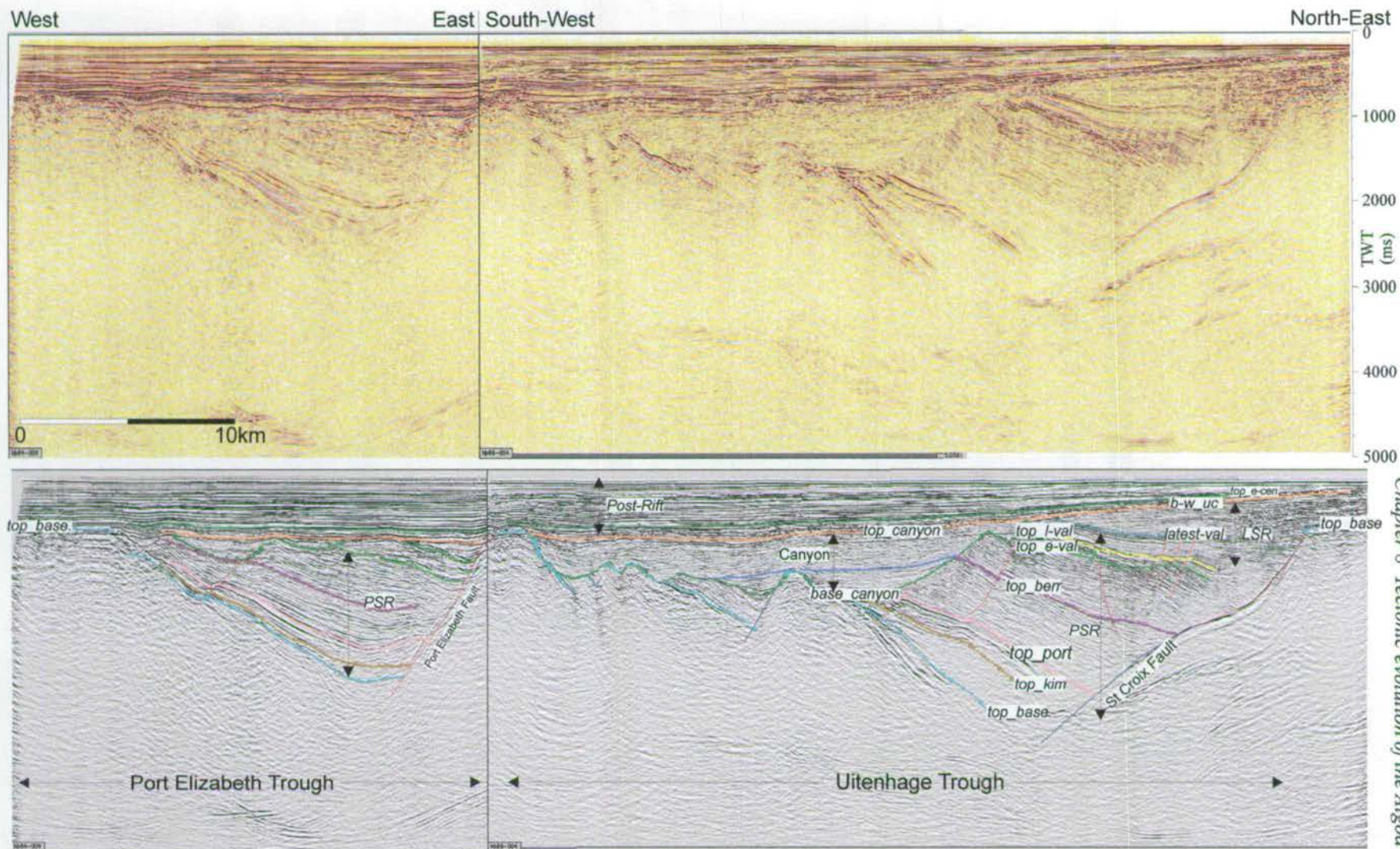


Figure 8.3: East-west section across the Algoa Basin. The Principal Syn-Rift (PSR), Late Syn-Rift (LSR) and Post Rift mega-sequences are evident in the two sub-basins, the Port Elizabeth and Uitenhage Troughs. Lines: Hb86-004 (west), Hb84-009 (east). Abbreviations - as in Figure 8.2

a)



b)

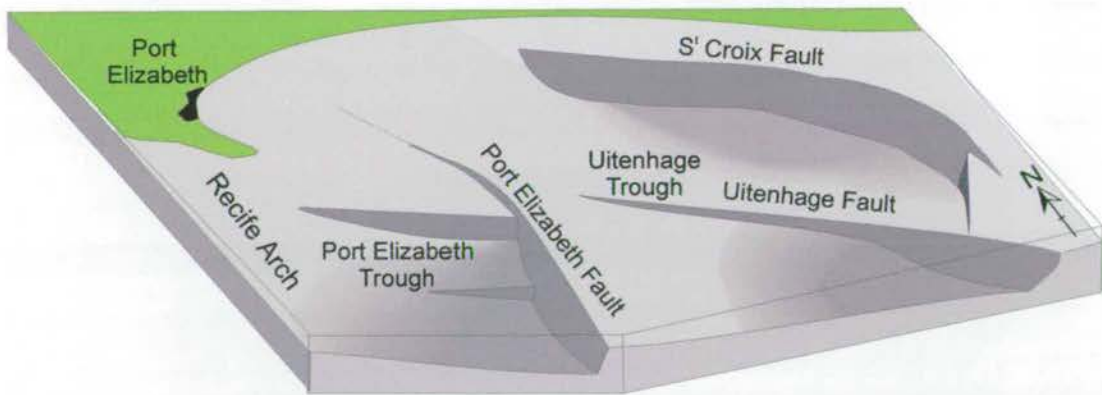


Figure 8.4: a) TWT map of *top basement* with fault polygons of the principal faults plotted. b) 3D cartoon of the basin highlighting its salient features.

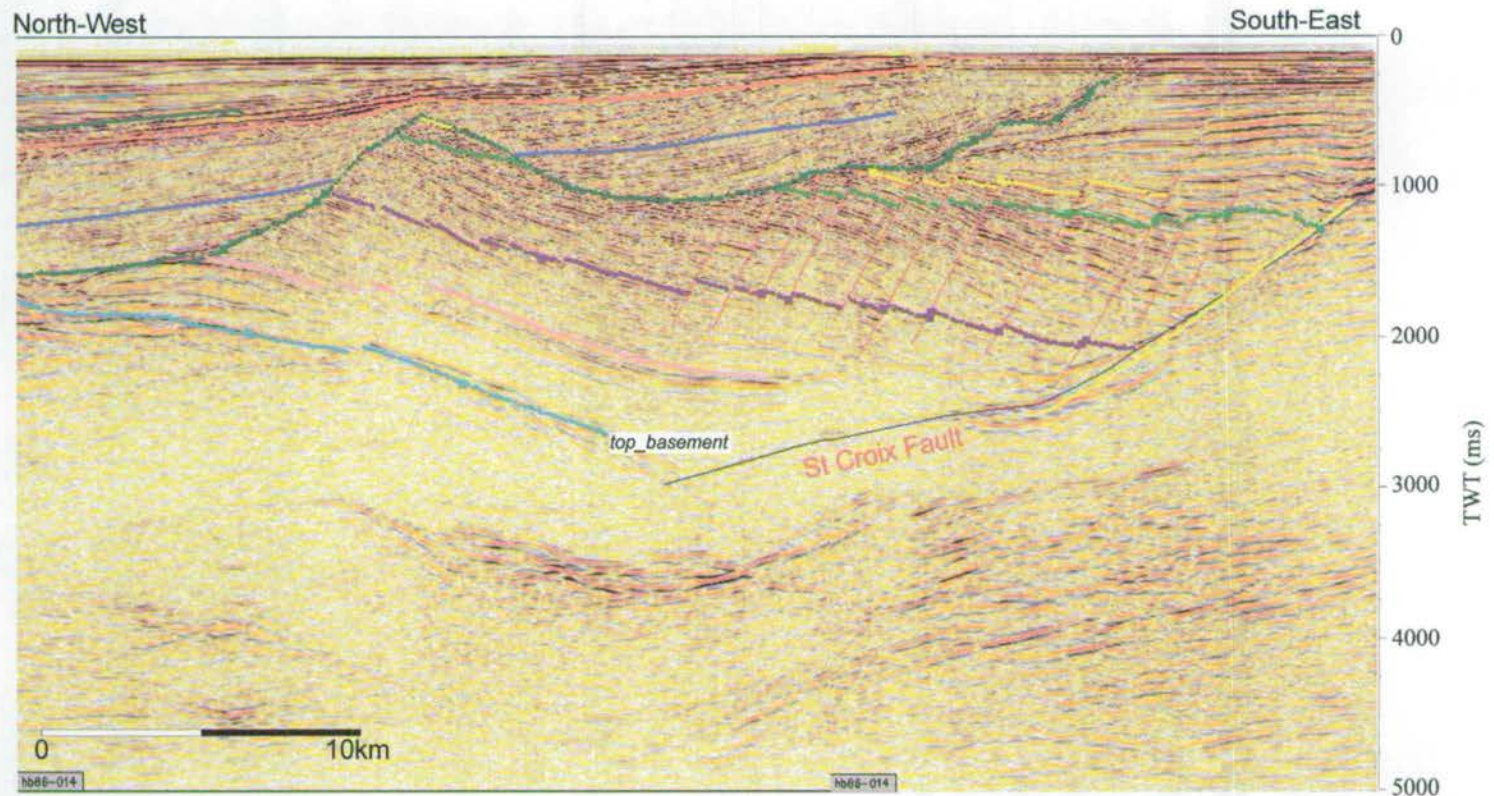
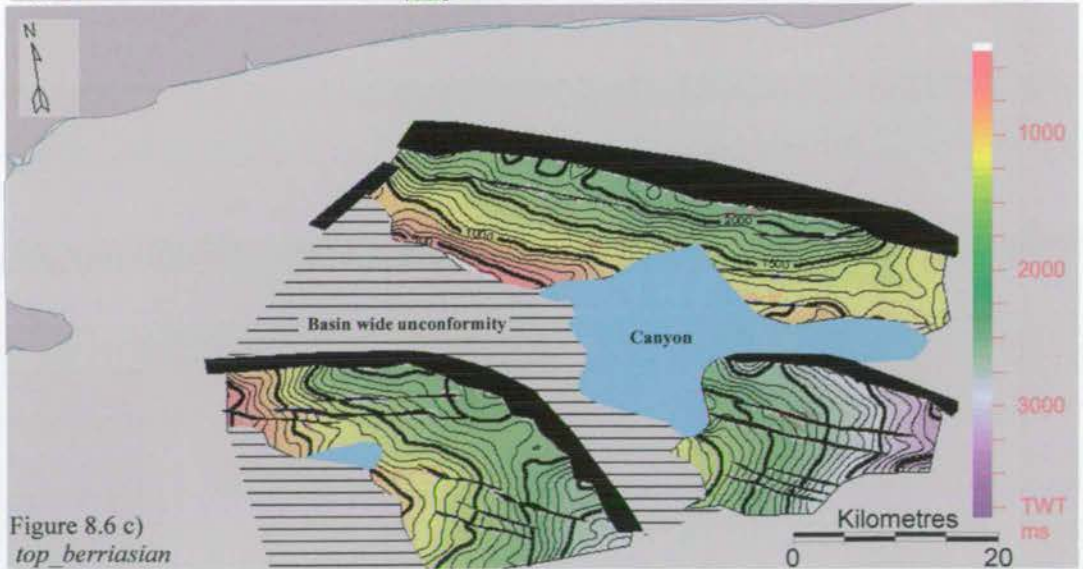
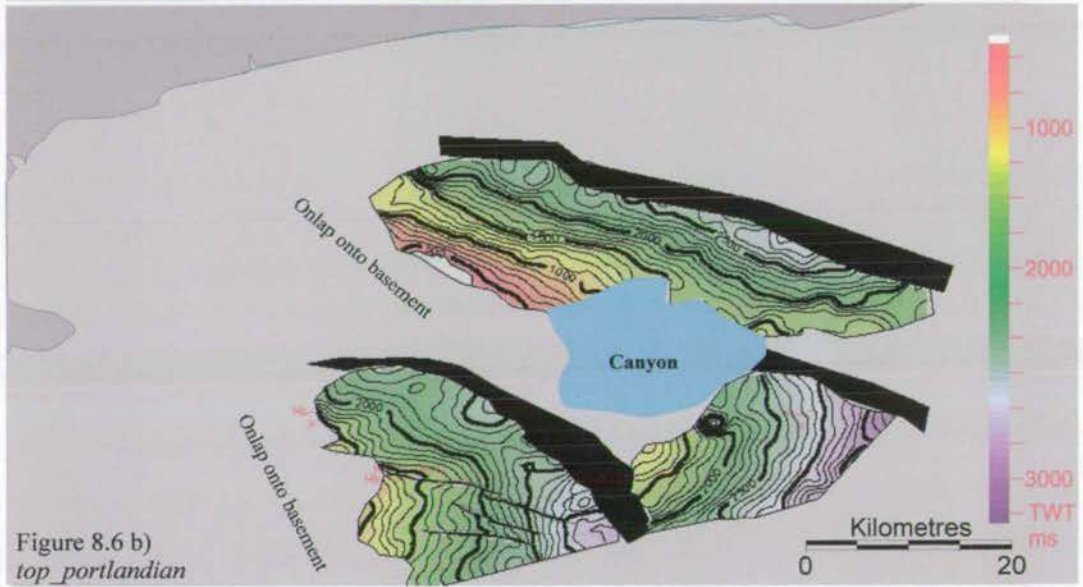
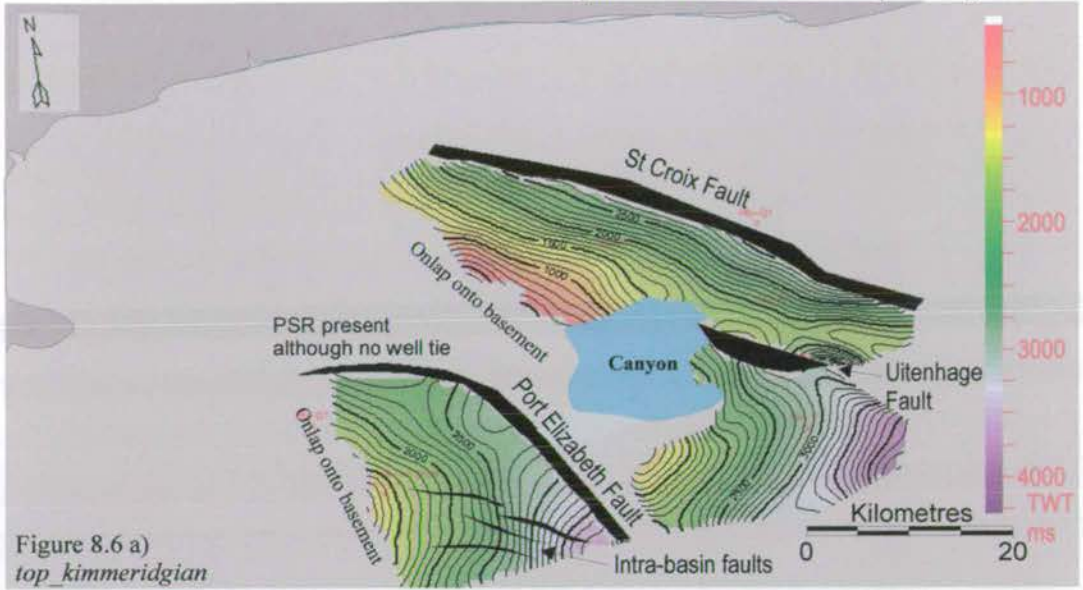


Figure 8.5: Section across the Uitenhage Trough that shows sub-parallel intra-basement reflectors. These have been attributed to either stratigraphic contacts or Cape Fold Belt shear zones (Bate & Malan, 1992). Line Hb86-014.



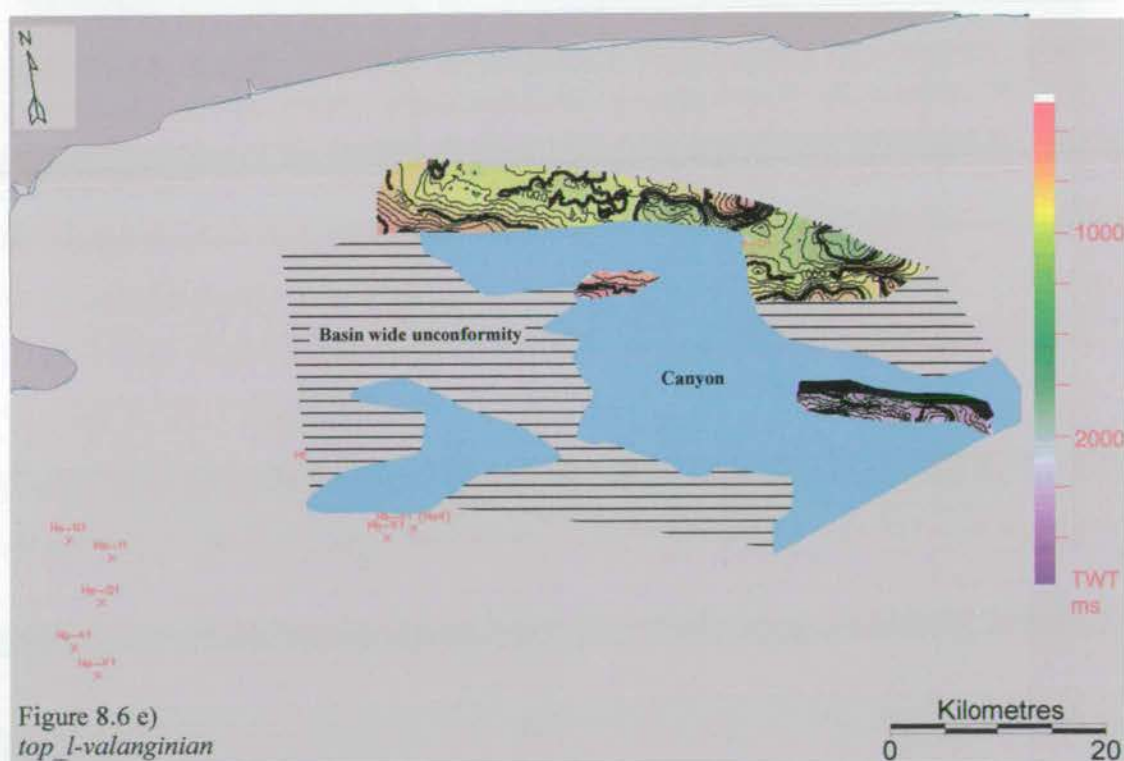
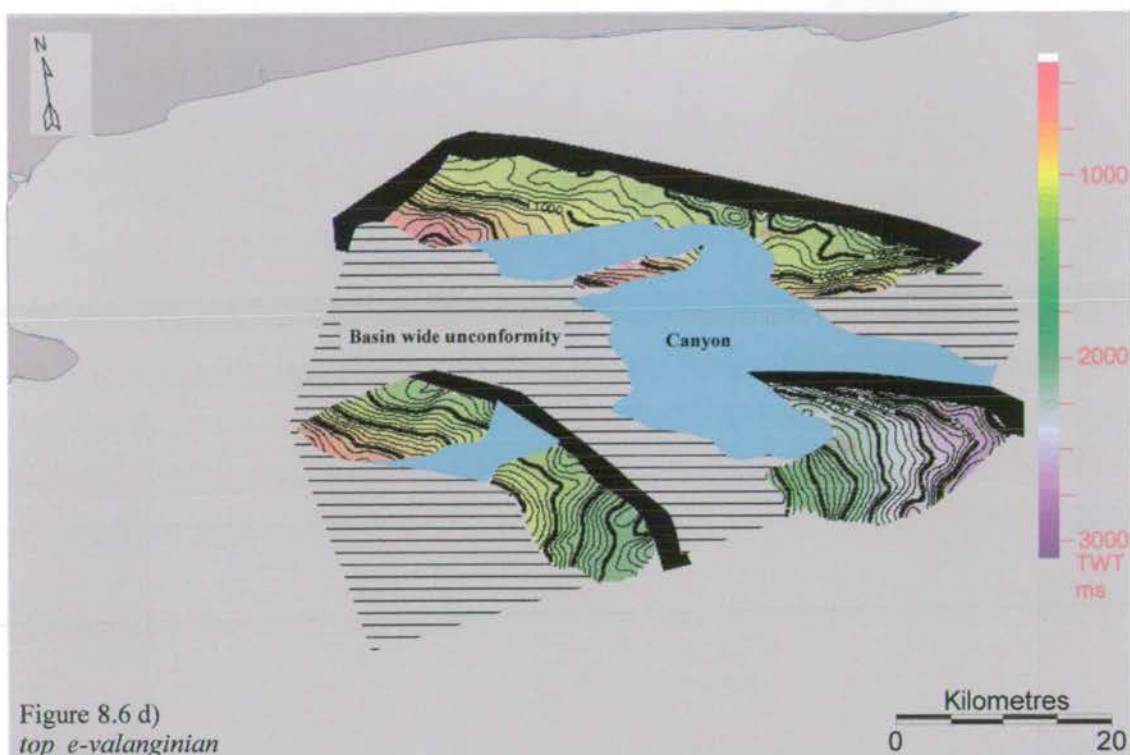
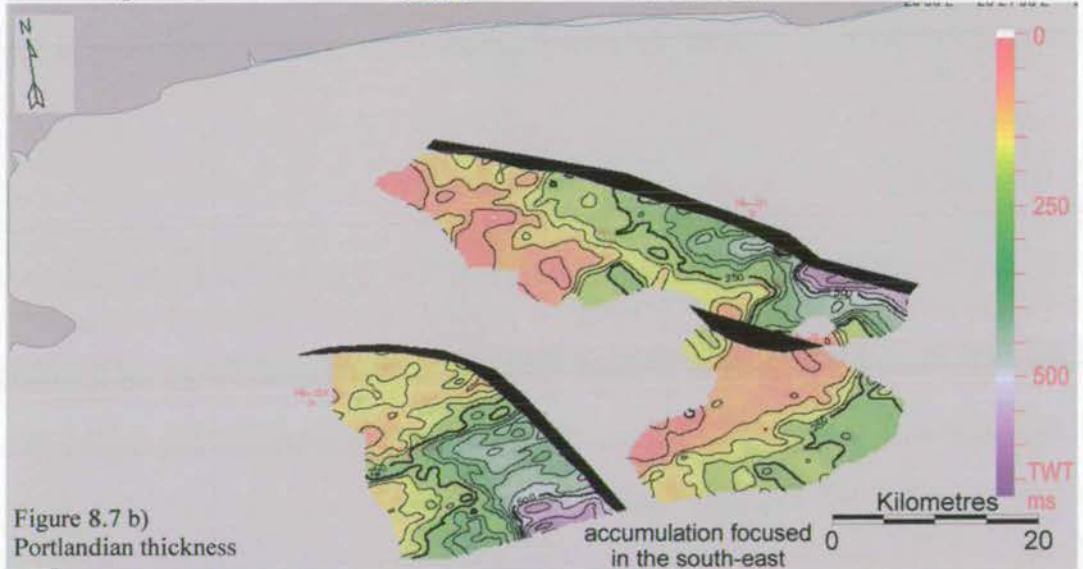
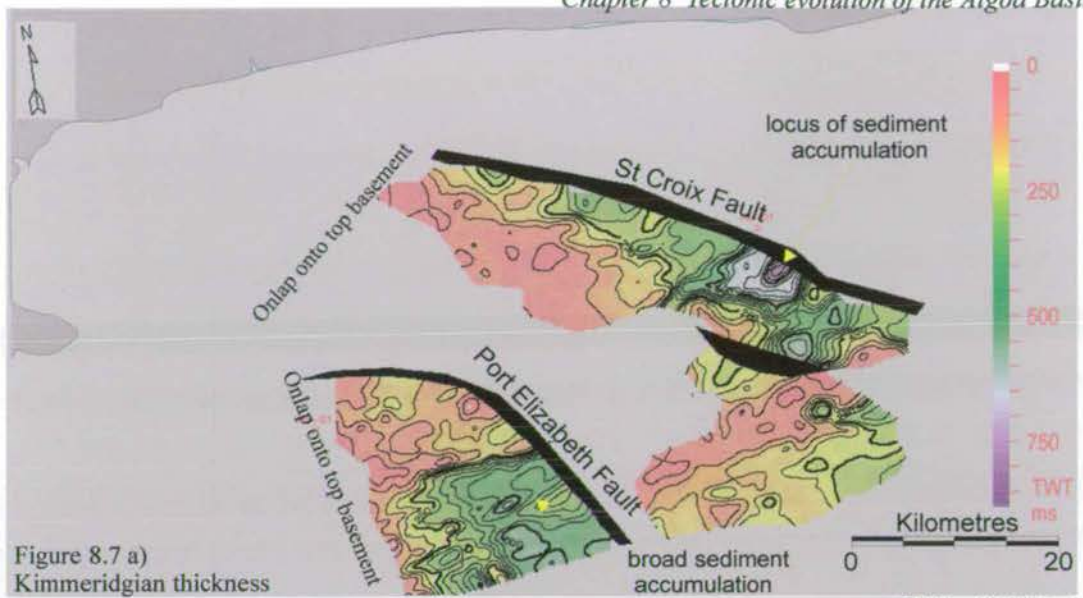


Figure 8.6: TWT maps to top of the Principal Syn-Rift (PSR) sequences: a) top_kimmeridgian, b) top_portlandian, c) top_berriasian, d) top_e-valanginian, e) top_l-valanginian. Fault polygons have been added to show the distribution of controlling faults and intra-basin faults. The extent of the canyon systems and the basin-wide unconformity have been plotted.



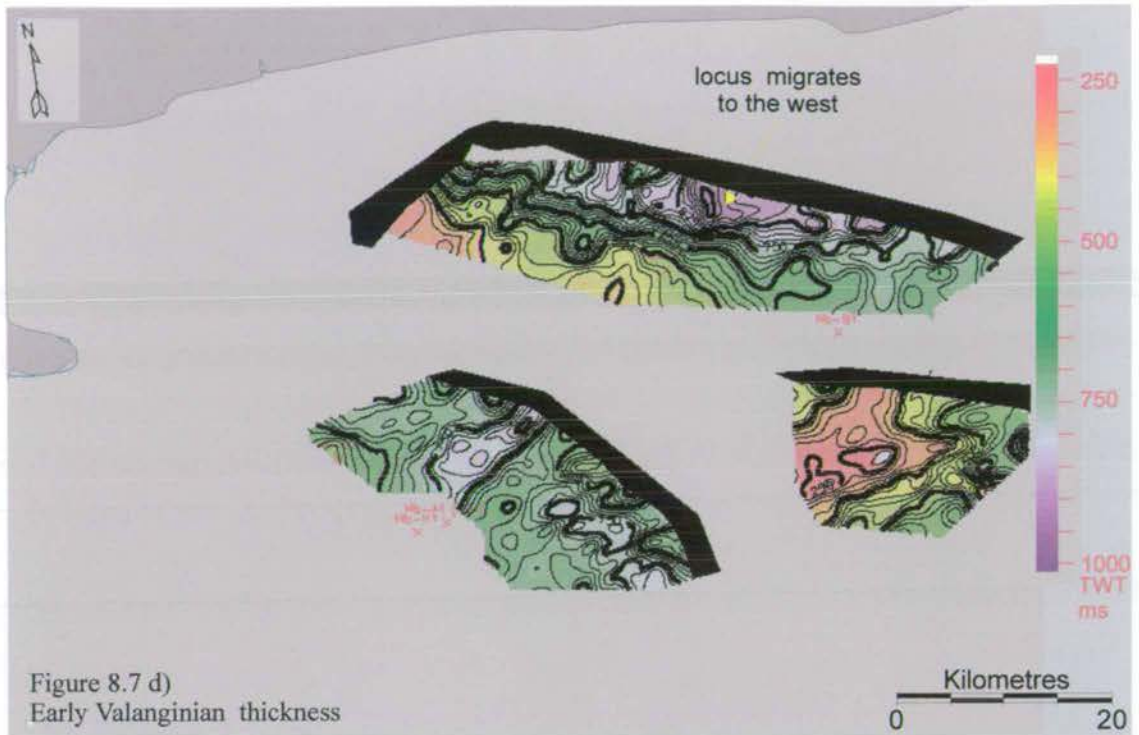


Figure 8.7: Thickness plots (in TWT) of the Principal Syn-rift sequences. a) Kimmeridgian thickness (*top_kimmeridgian* to *top_basement*) b) Portlandian thickness (*top_portlandian* to *top_kimmeridgian*), c) Berriasian thickness (*top_berriasian* to *top_portlandian*), d) Early Valanginian thickness (*top_e-valanginian* to *top_berriasian*), e) Late Valanginian thickness (*top_l-valanginian* to *top_e-valanginian*).

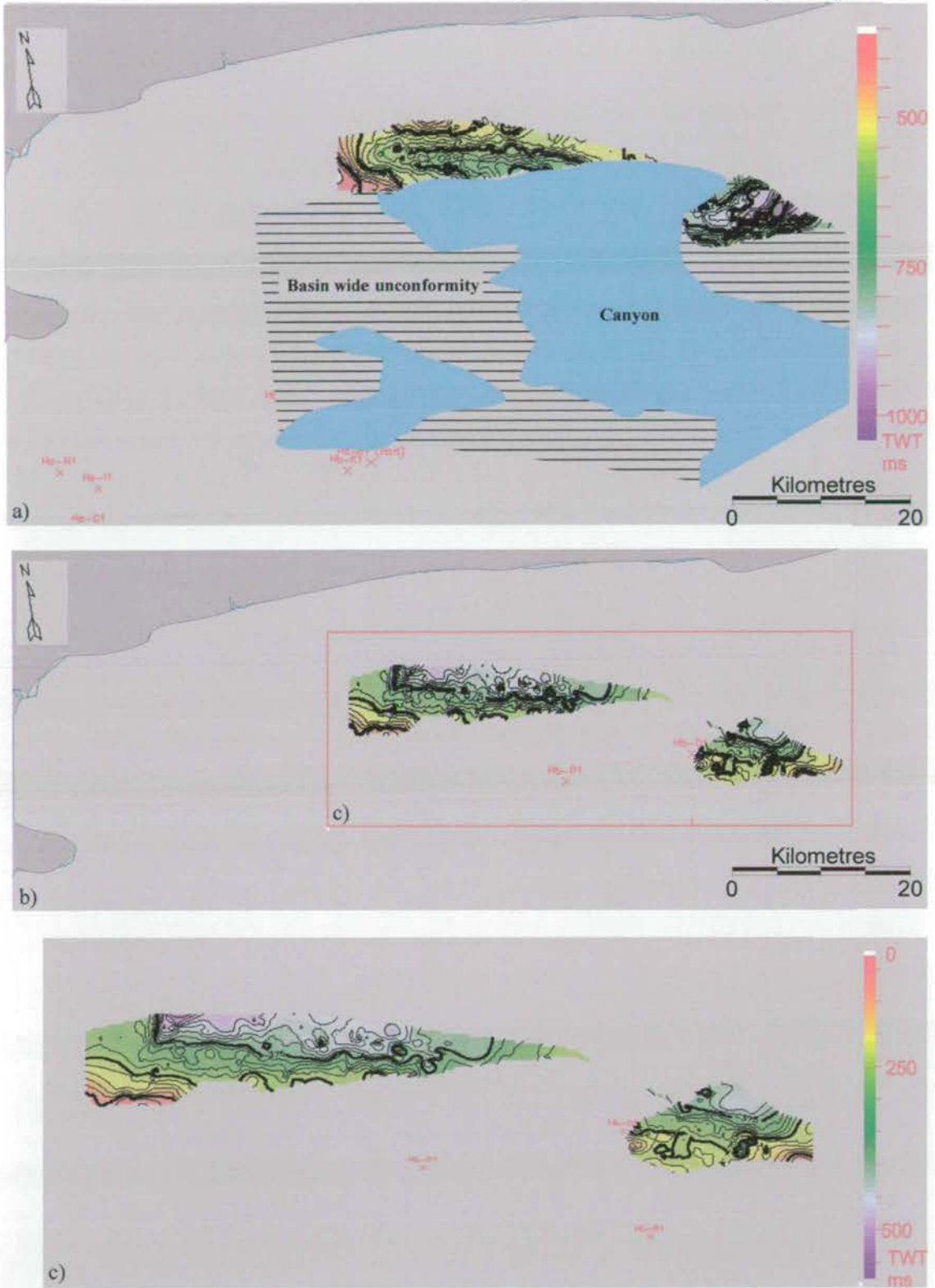


Figure 8.8: a) TWT map of *latest-valanginian*. b) Isopach of *latest-valanginian* to *top_l-valanginian*, c) enlargement of area shown in (b).

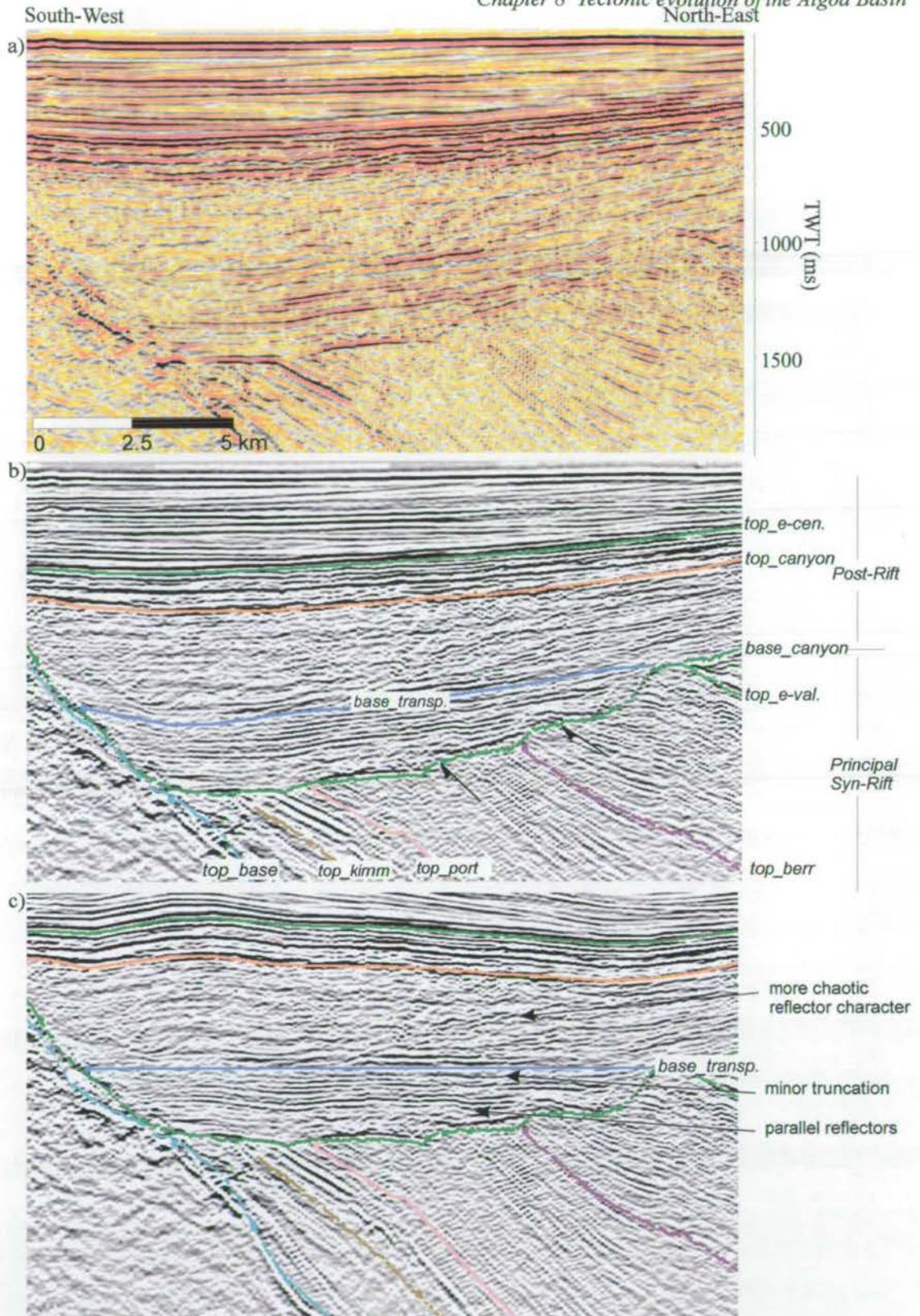


Figure 8.9: Uninterpreted (a) and interpreted (b) section across the canyon in the Uitenhage Trough. There is significant erosional truncation of the Principal Syn-Rift sequences against the *base_canyon* horizon. It is evident from the section, when it is flattened to *base_transp* (c) that the early canyon fill is a parallel laminated sequence that in-fills the topography.

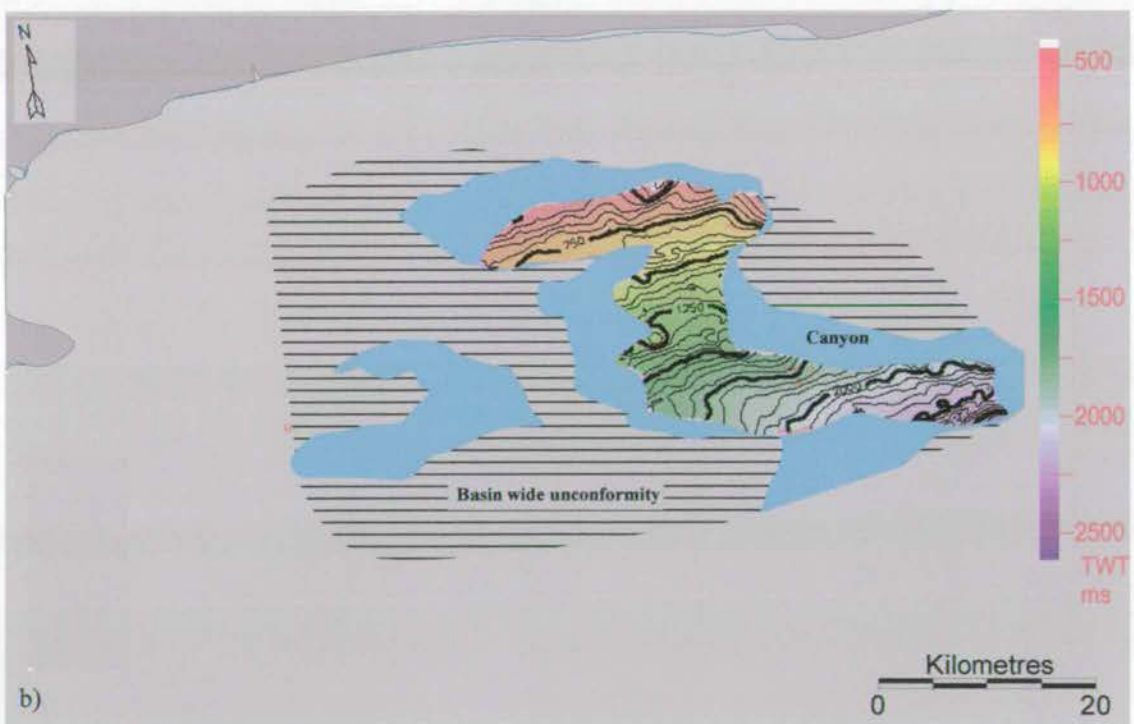
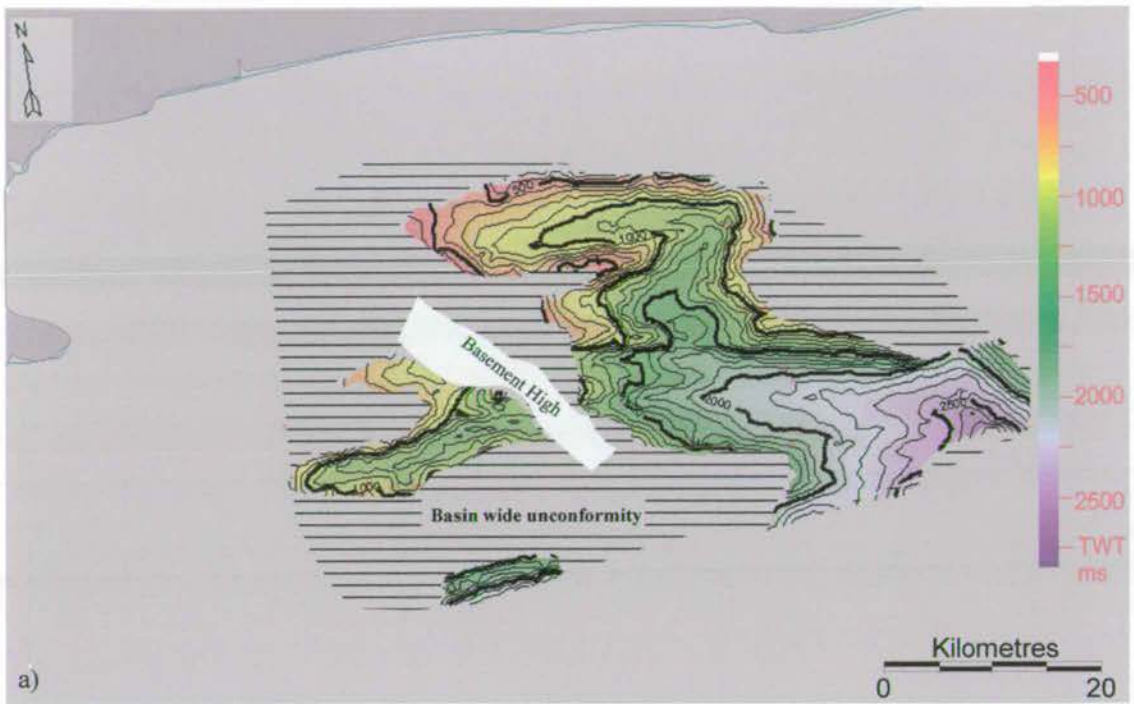


Figure 8.10: TWT maps of the canyon system: a) *base_canyon* reflector; b) *base_transparent* package.

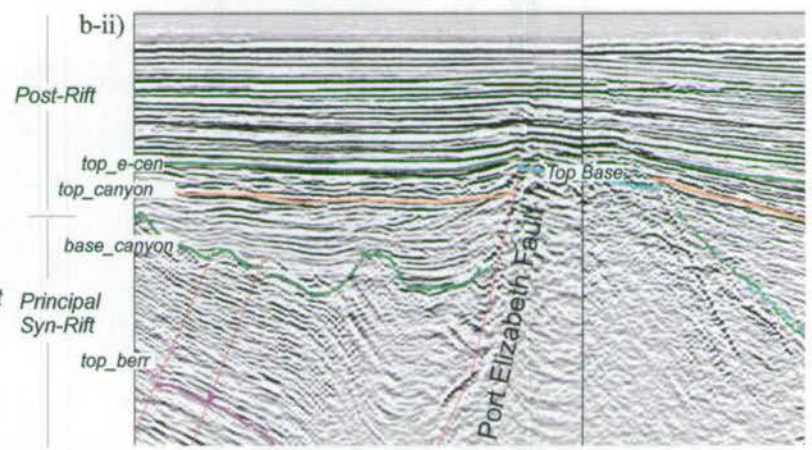
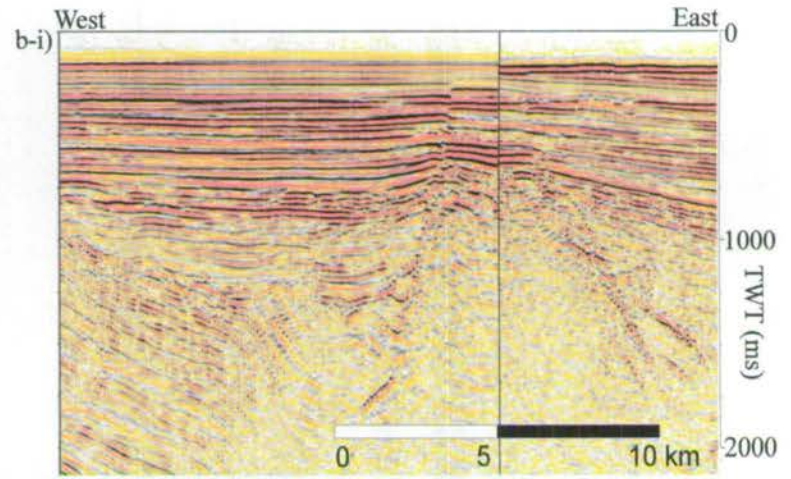
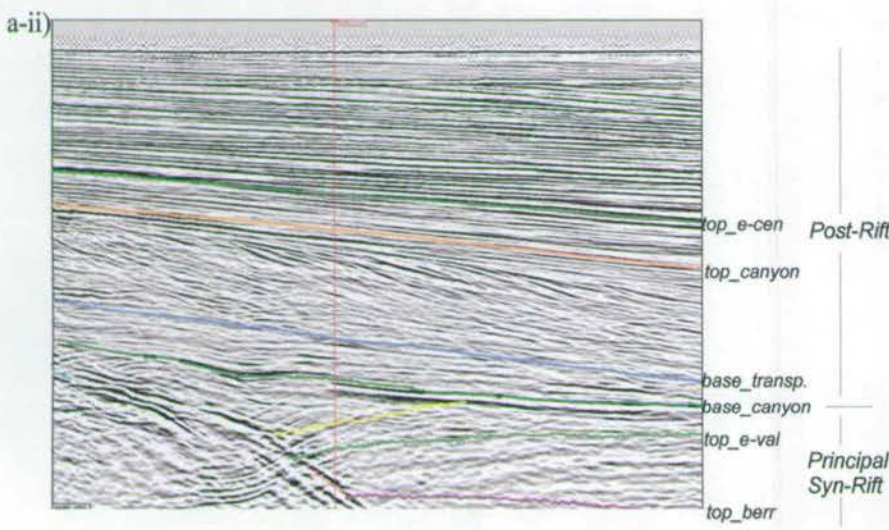
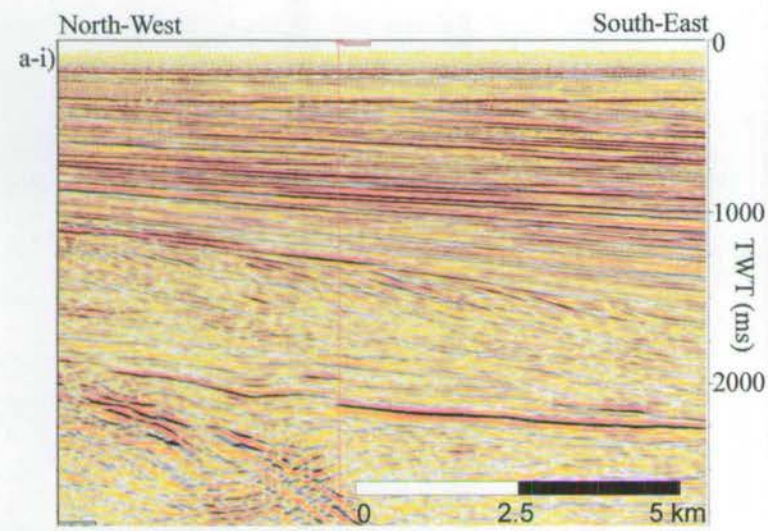


Figure 8.11: a) The lower canyon fill is characterised by sub-parallel reflectors that in-fill canyon topography. Towards the top of the canyon fill the system develops into a southward prograding system. b) The Port Elizabeth canyon is constrained in the east by the Port Elizabeth fault, although its geometry (Figure 8.10) suggests that it joins the Uitenhage Canyon across the fault. It is inferred that the canyon exit is not resolvable with the available line spacing.

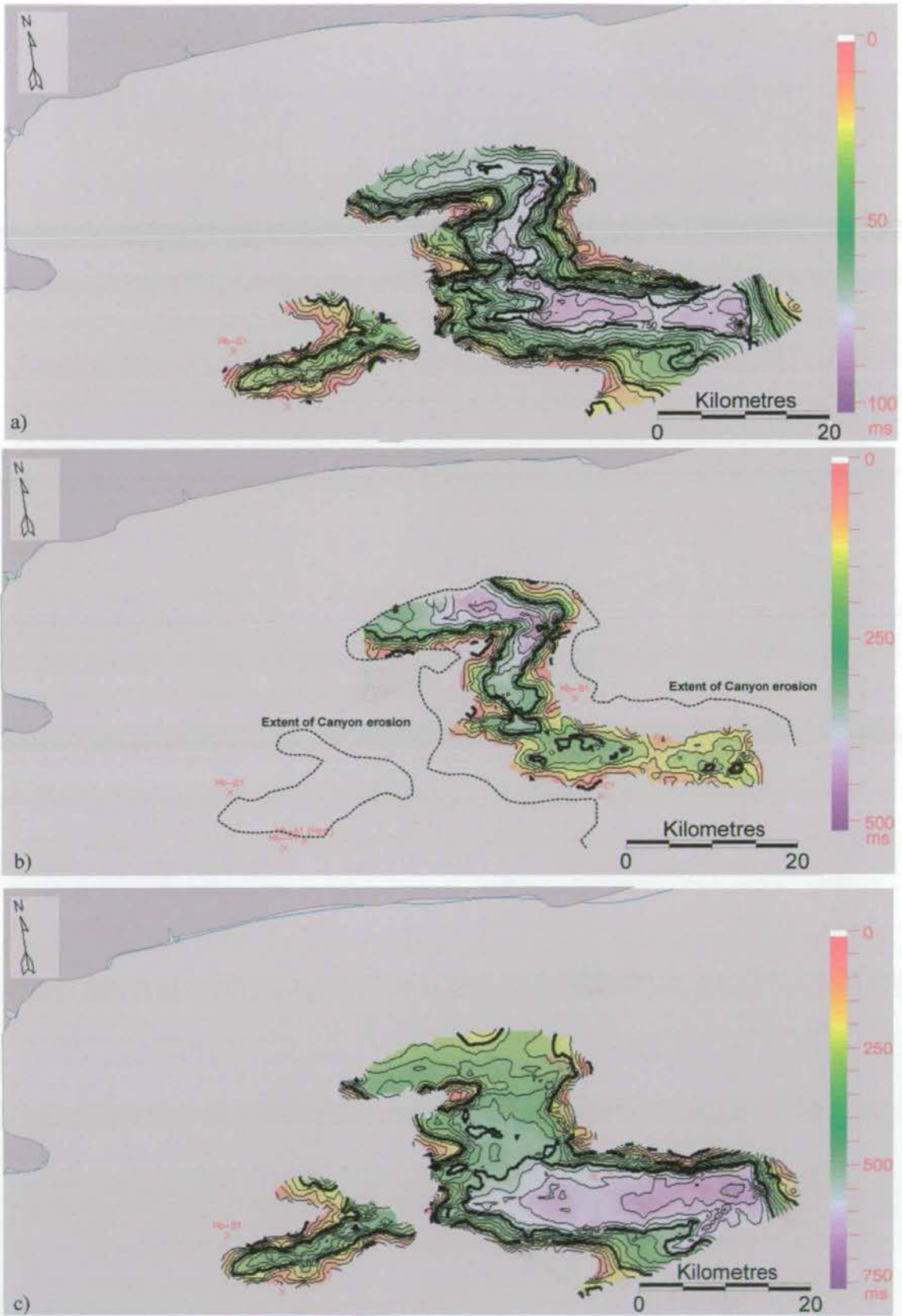


Figure 8.12: Isochron plots of sediment thickness (in TWT) within the canyon system: a) *top_canyon* to *base_canyon*; b) *base_transparent* to *base_canyon* c) *top_canyon* to *base_transparent*.

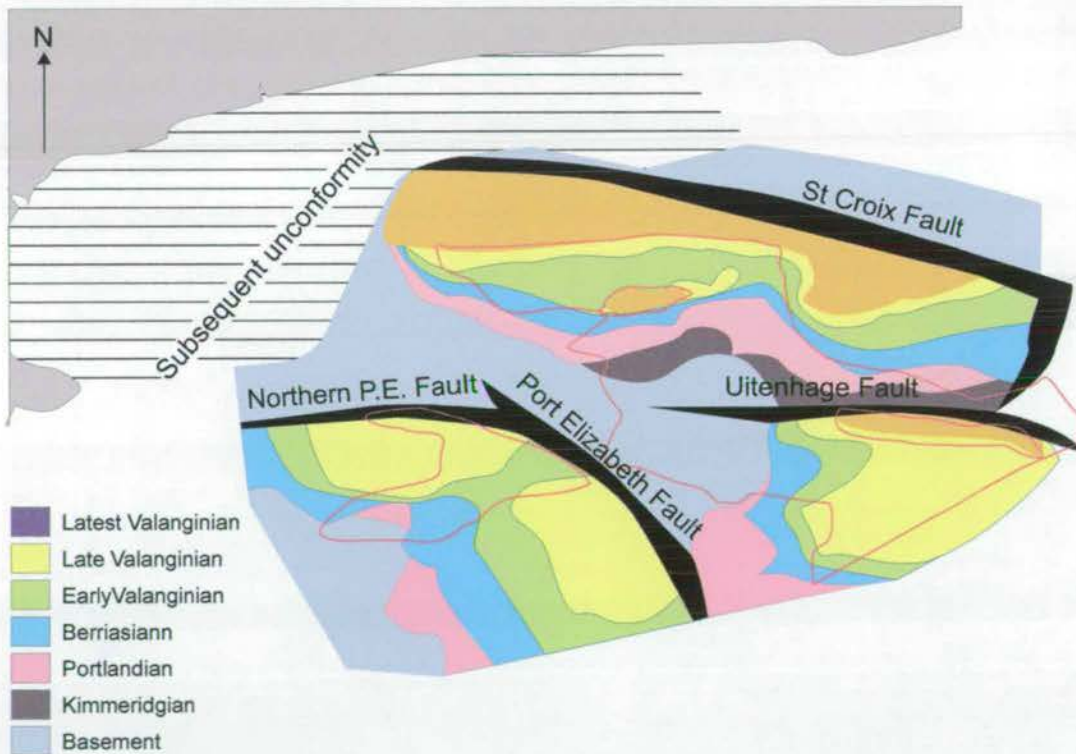
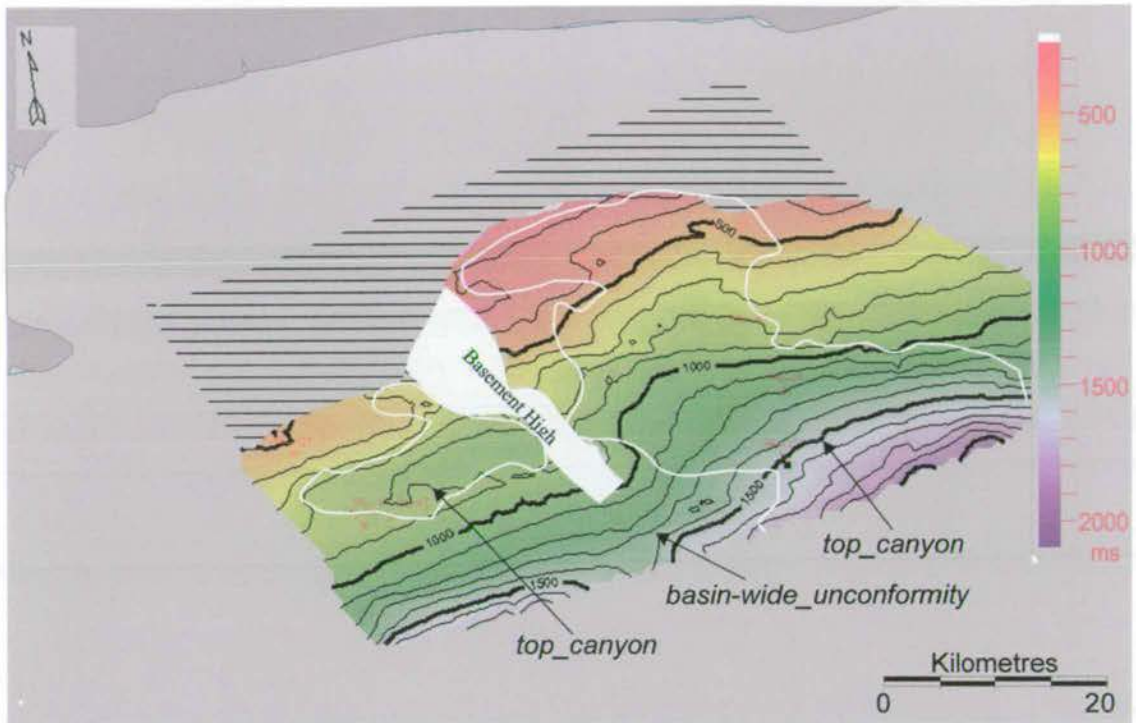


Figure 8.13: Basin-wide erosion events, a) TWT map of *basin-wide_unconformity* and *top_canyon* reflectors, b) sub-crop map to the *basin-wide_unconformity* and *base_canyon*. In (b) the extent of the canyon system is shown by the red line, and the controlling faults have been plotted.

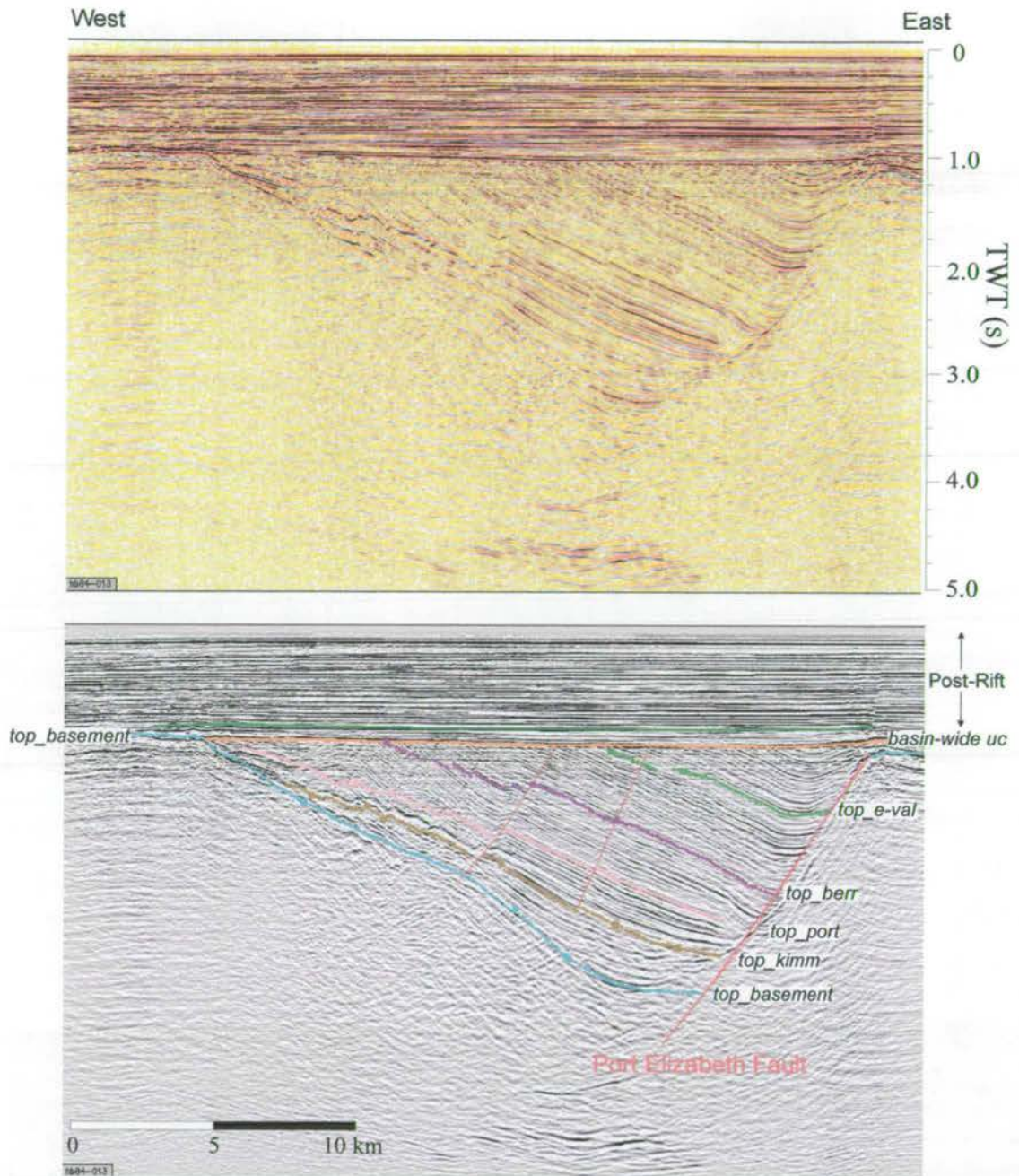


Figure 8.14: West-east section across the Port Elizabeth Trough that shows the significance of the *basin-wide_unconformity*. Line Hb84-013.

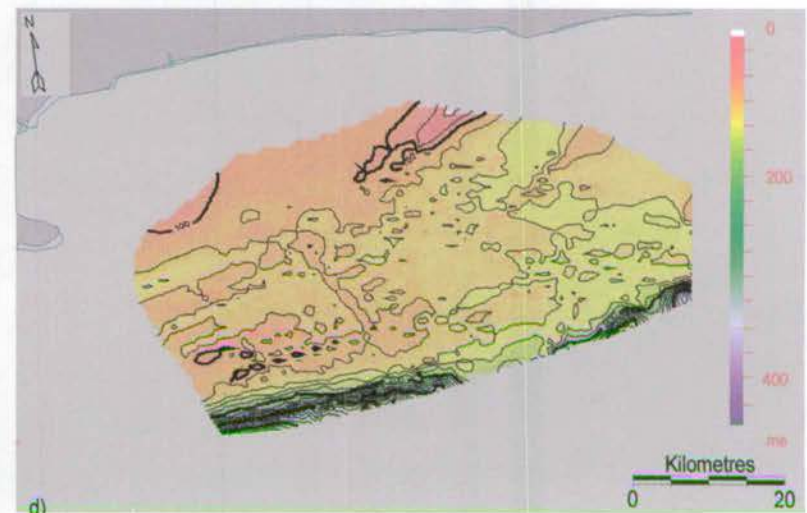
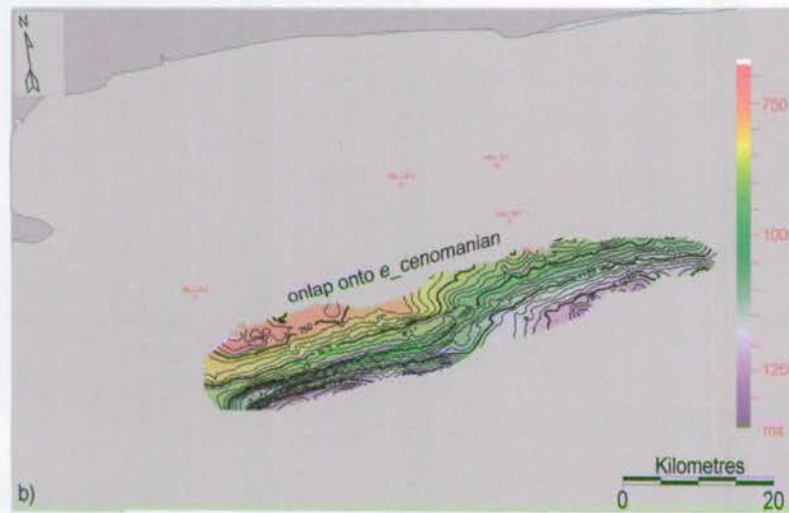
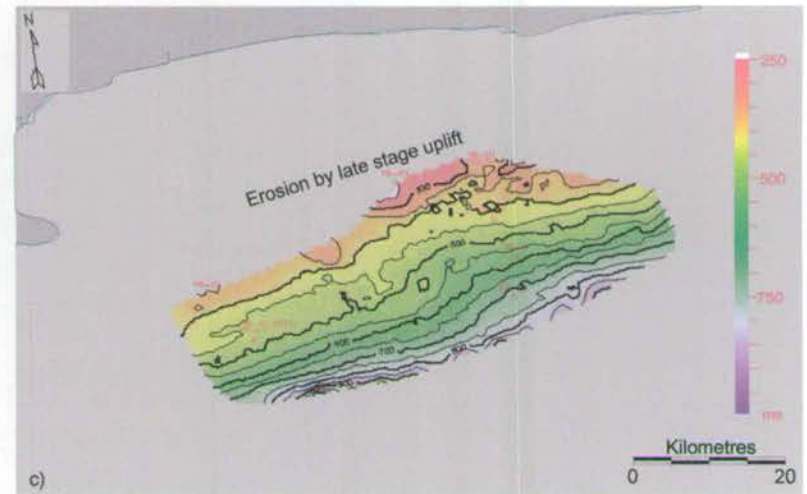
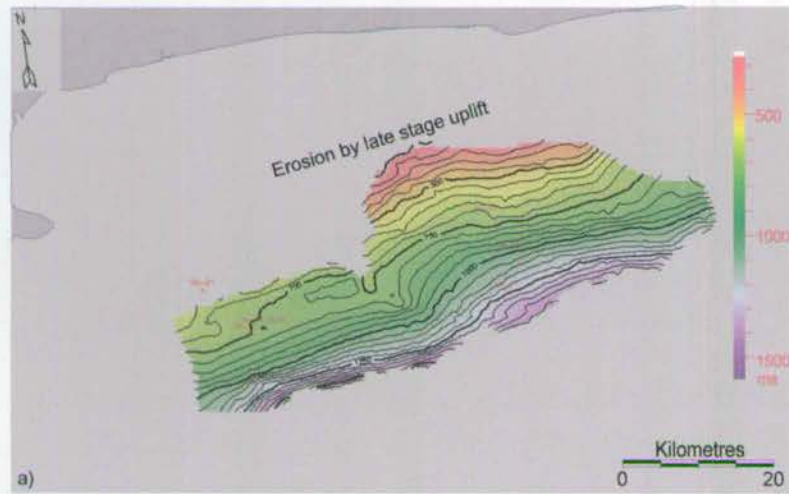


Figure 8.15: TWT maps of the Post-Rift rift sequences above *top_canyon/basin-wide_unconformity* a) *top_e-cenomanian*, b) *top_e-turonian*, c) *top_maastrichtian*, d) *sea_floor*.

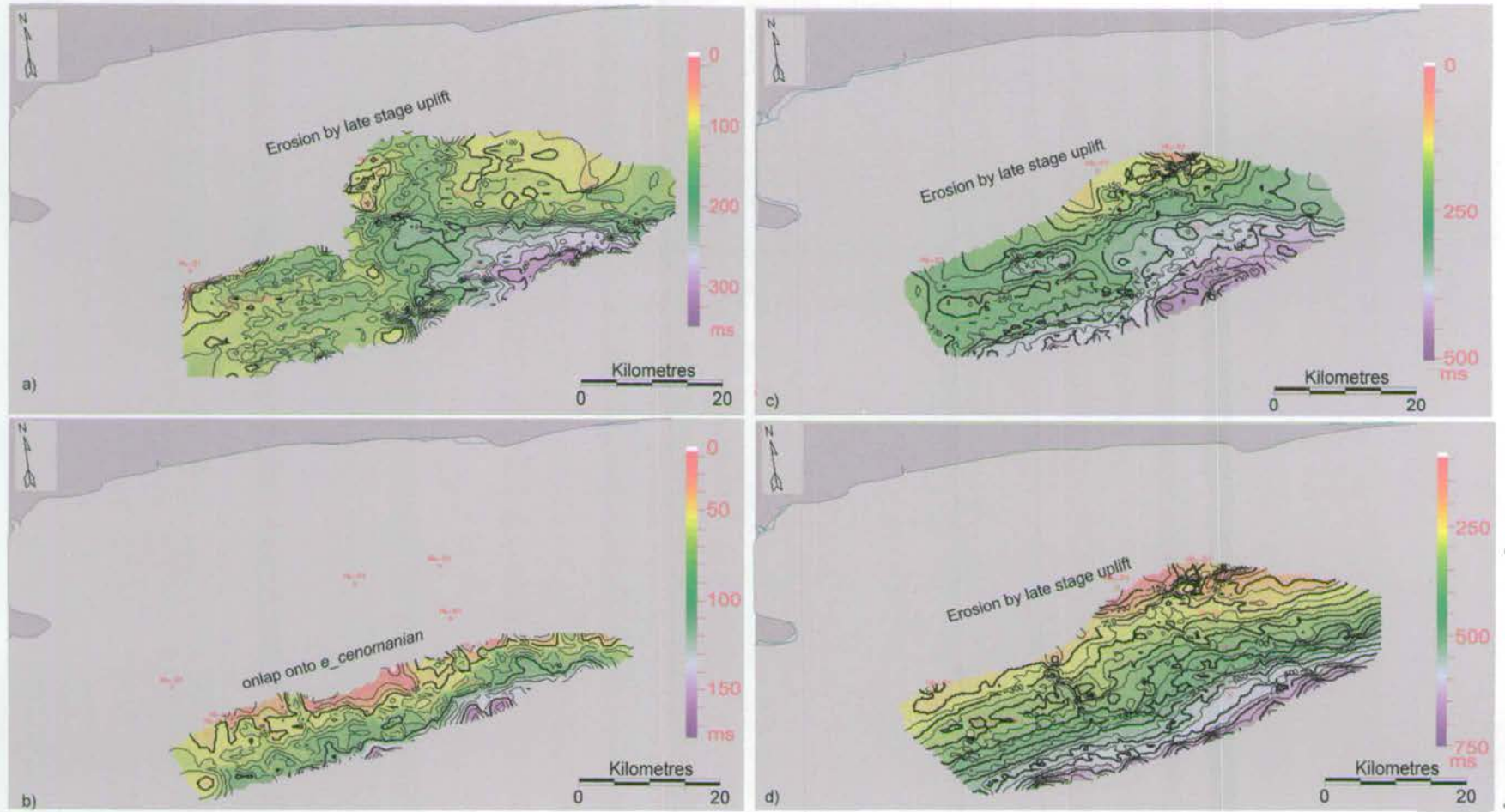


Figure 8.16: Thicknesses of the Post-Rift rift sequences above the *top_canyon/basin-wide_unconformity*. a) Cenomanian (*top_canyon - top_e-cenomanian*), b) Turonian (*top_e-cenomanian - top_turonian*), c) Maastrichtian (*top_e-turonian - top_maastrichtian*), d) Post Maastrichtian (*top_maastrichtian - sea_floor*). There is only limited thickening of the Cenomanian and Turonian sequences compared to the subsequent packages.

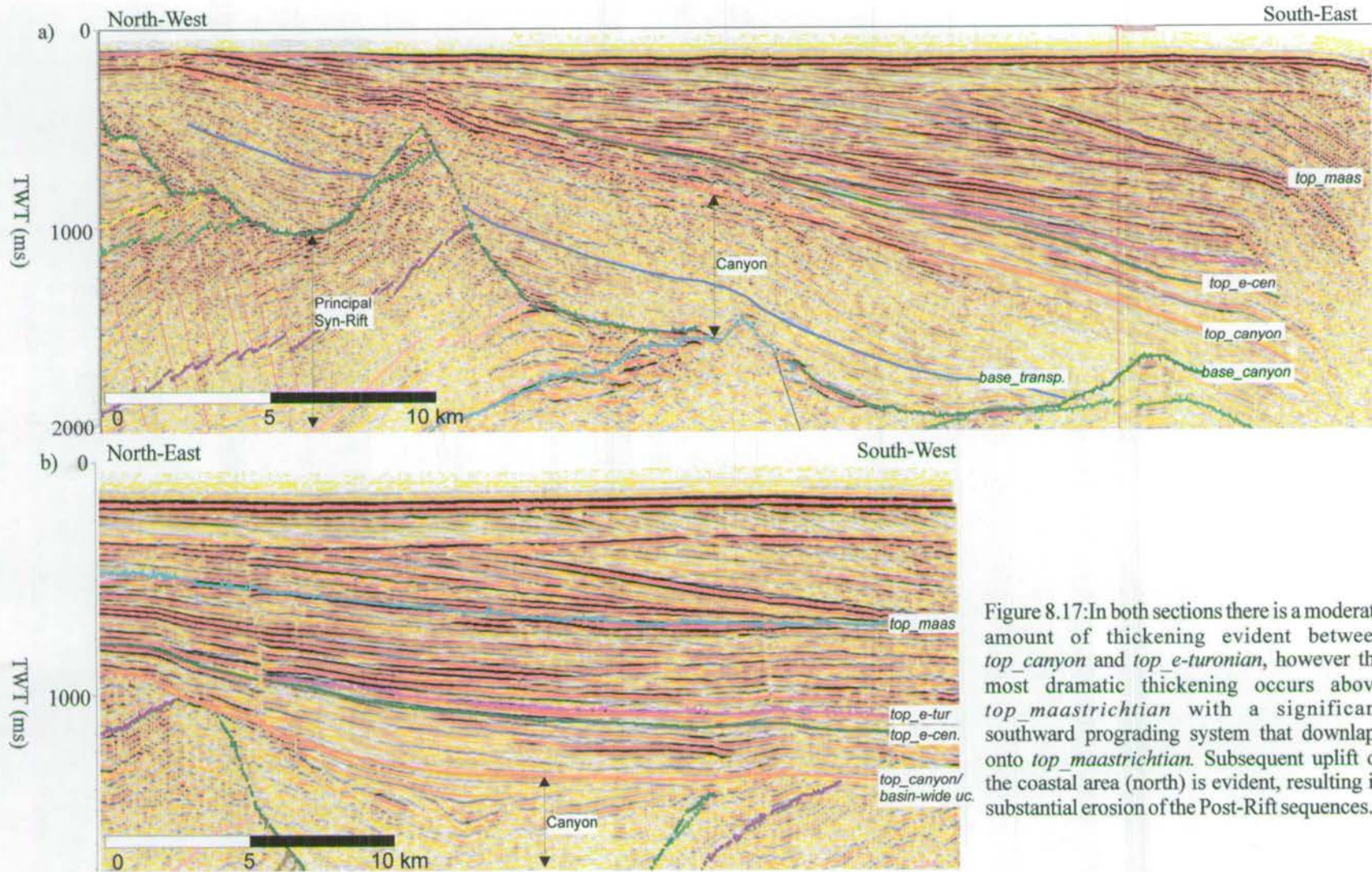


Figure 8.17: In both sections there is a moderate amount of thickening evident between *top_canyon* and *top_e-turonian*, however the most dramatic thickening occurs above *top_maastrichtian* with a significant southward prograding system that downlaps onto *top_maastrichtian*. Subsequent uplift of the coastal area (north) is evident, resulting in substantial erosion of the Post-Rift sequences.

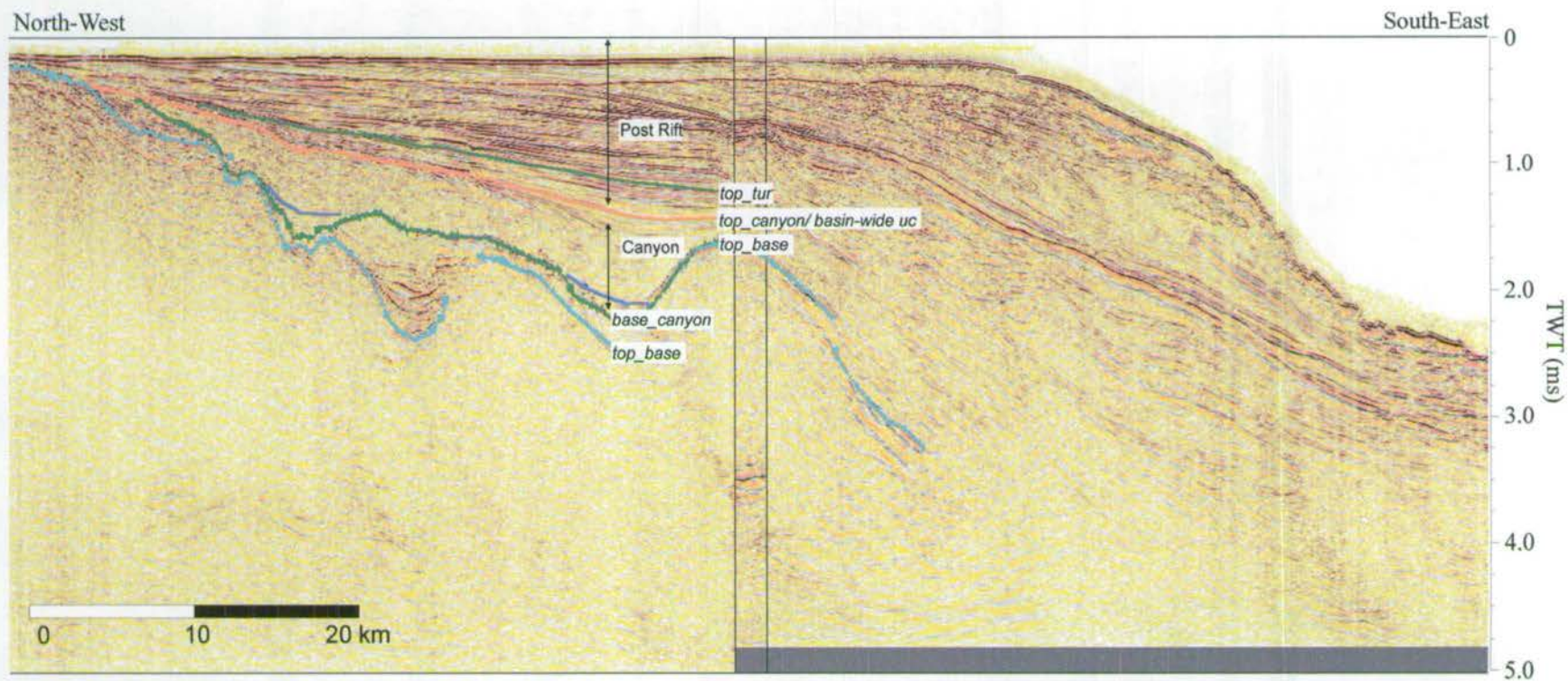


Figure 8.18: Section across the southern margin of the basin that highlights the dramatic increase in water depth towards the Southern Outeniqua Basin (water depth >200m). From this section it is also evident that towards the south the imaging of structures and horizons (including *top_basement*) is very poor. There is also a dramatic thickening of the Post-Rift mega-sequence. Lines (north-south)- Hb 86-018, Hb 89-033, Hb 89-040

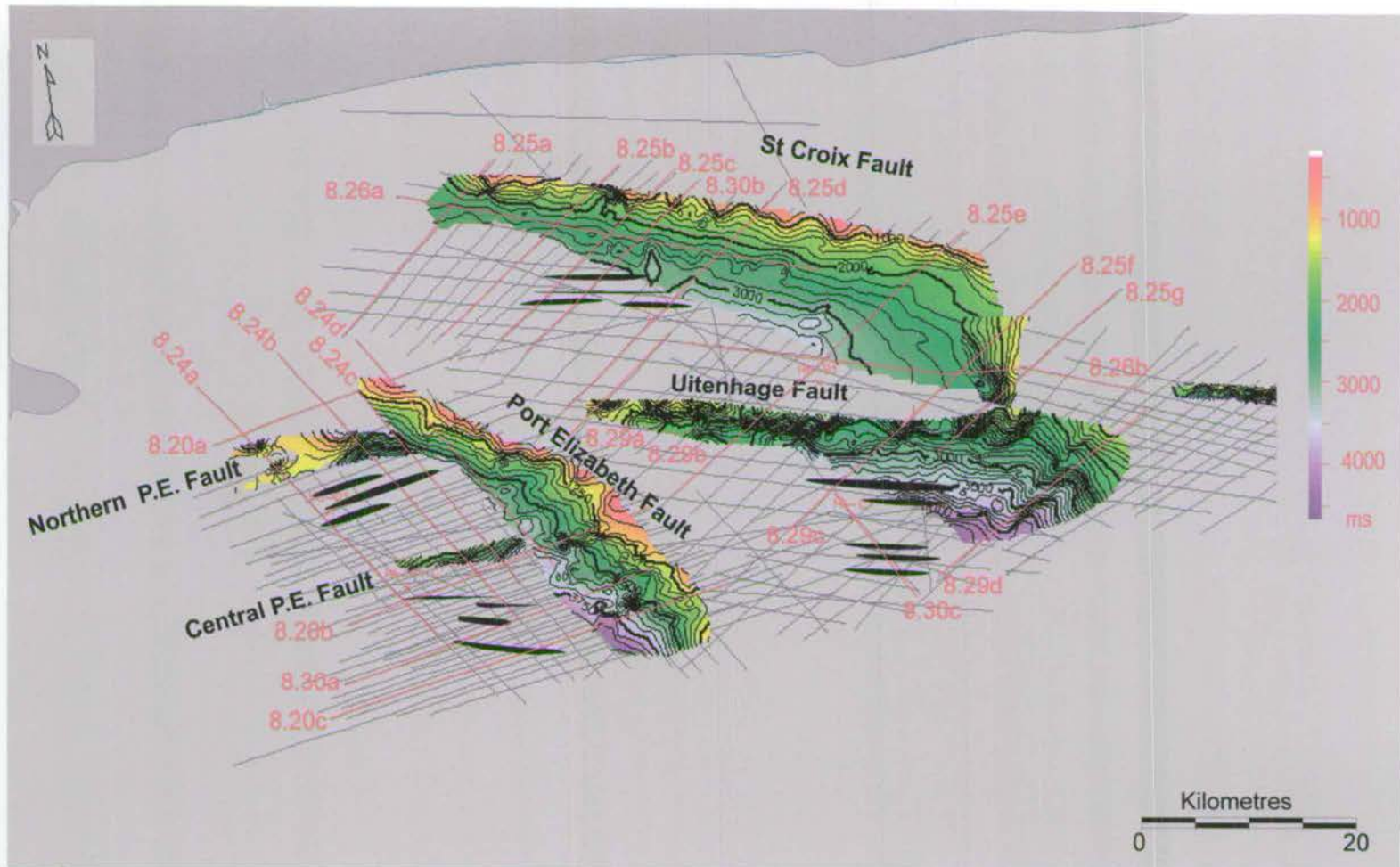


Figure 8.19: TWT plots for the principal fault planes in the Algoa Basin. Black polygons represent intra-basin faults. Red lines and numbers correspond to figures showing sections across the faults, grey lines indicate the seismic array used for the interpretation and shows the areas of low data density.

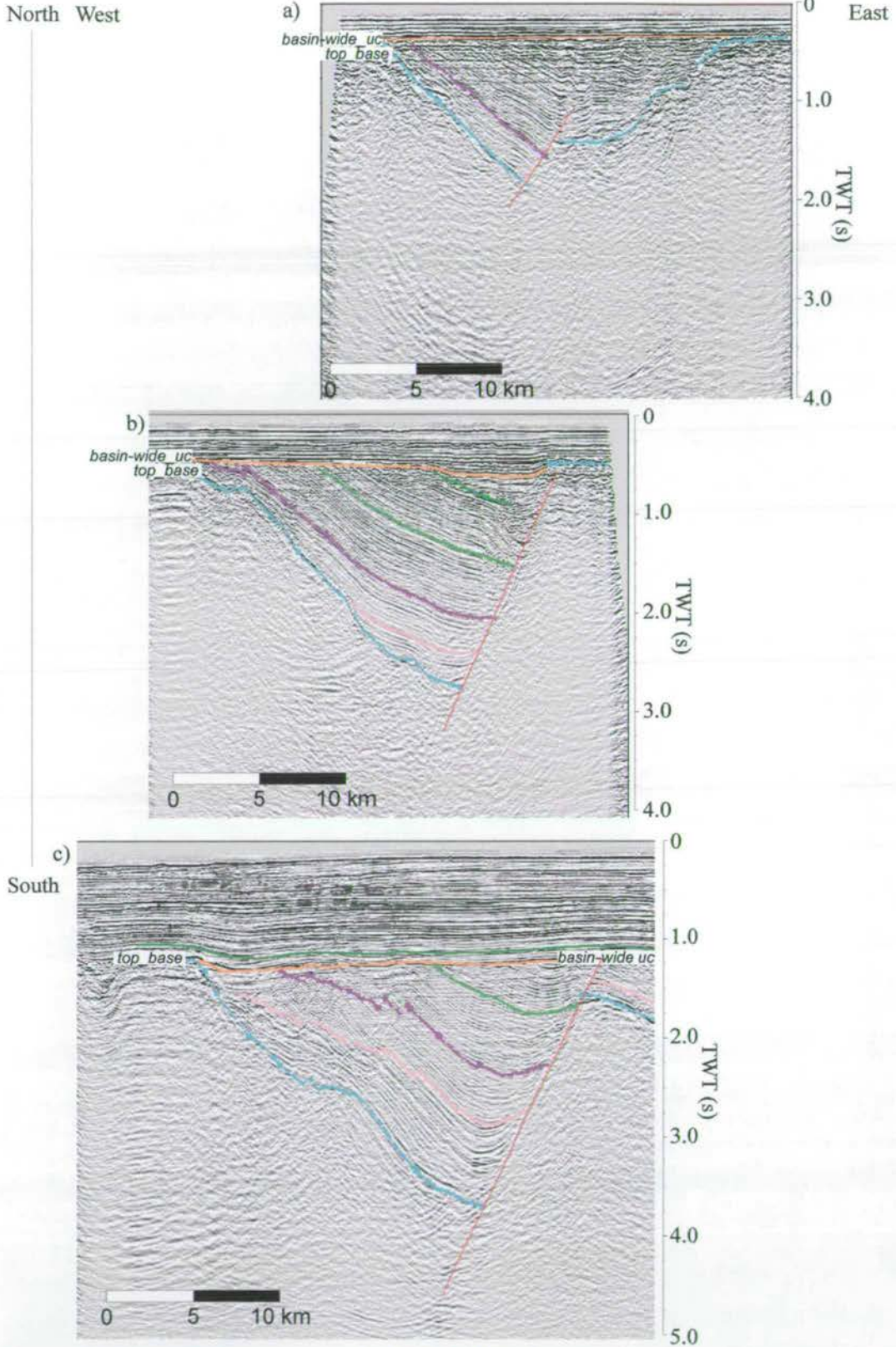
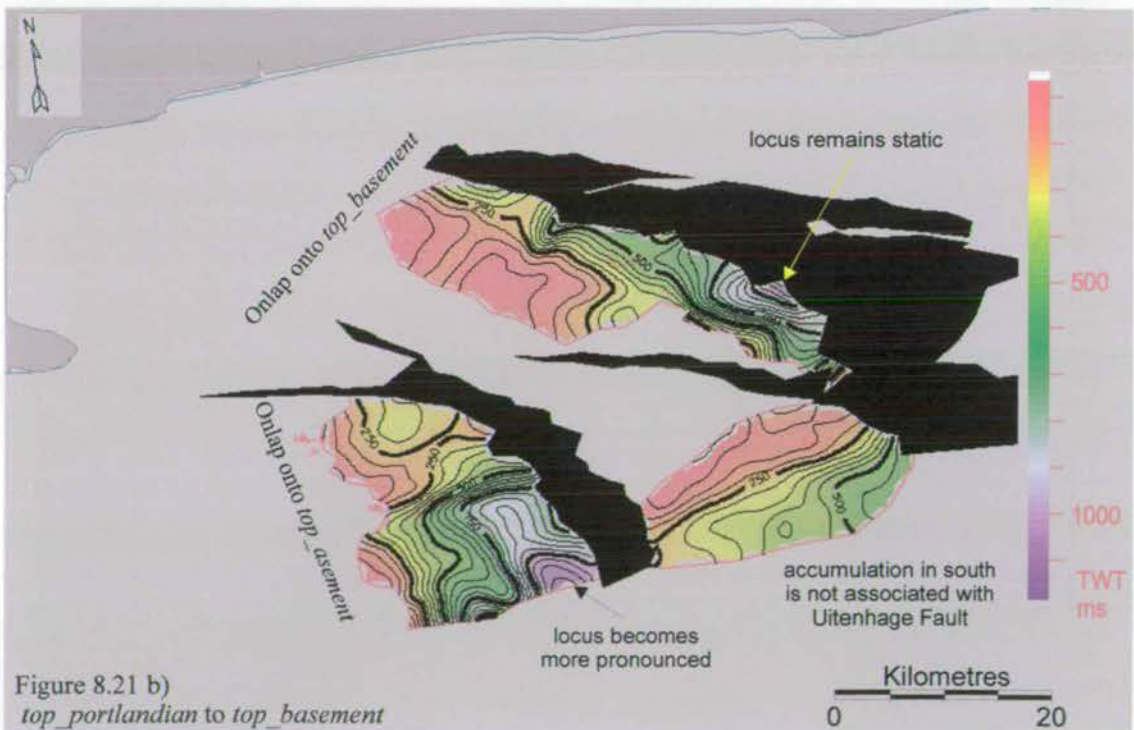
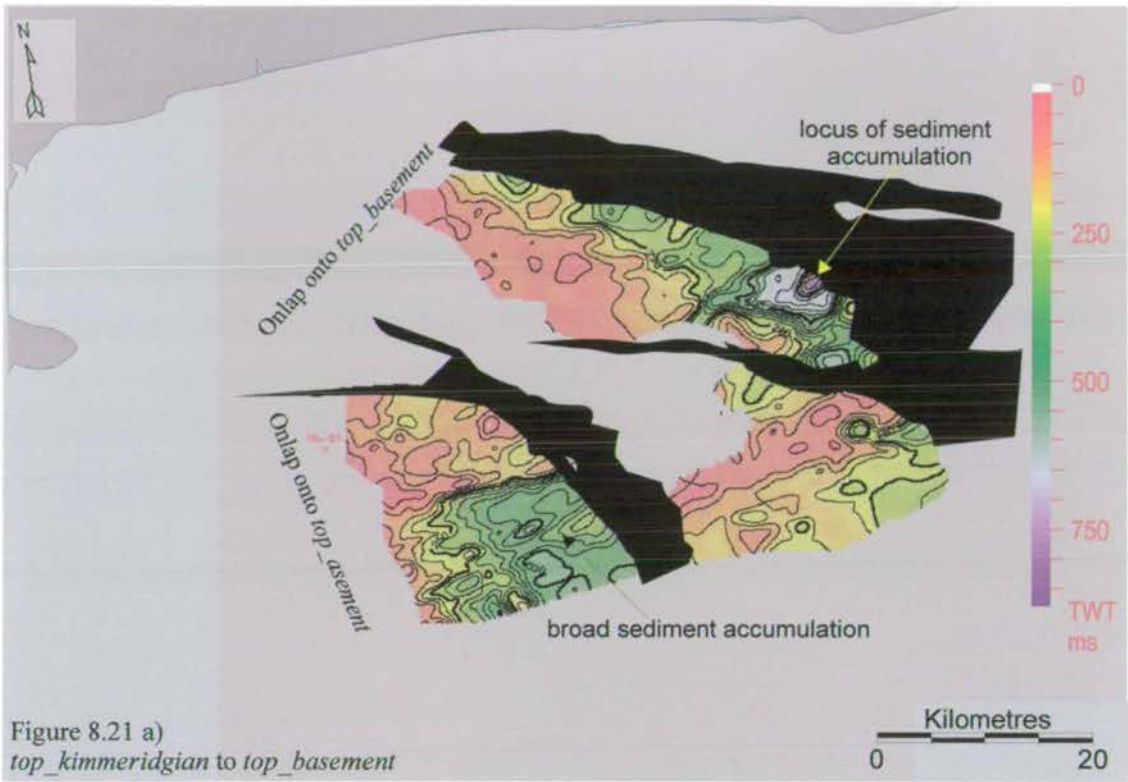


Figure 8.20: West-east sections across the Port Elizabeth Fault from north (a) to south (c). In section (a) the depth to *top base* in the hangingwall is dramatically reduced because of the Northern P.E. Fault (cf. Figure 8.23). Lines: a) 84-002, b) 84-005, c) 84-015.



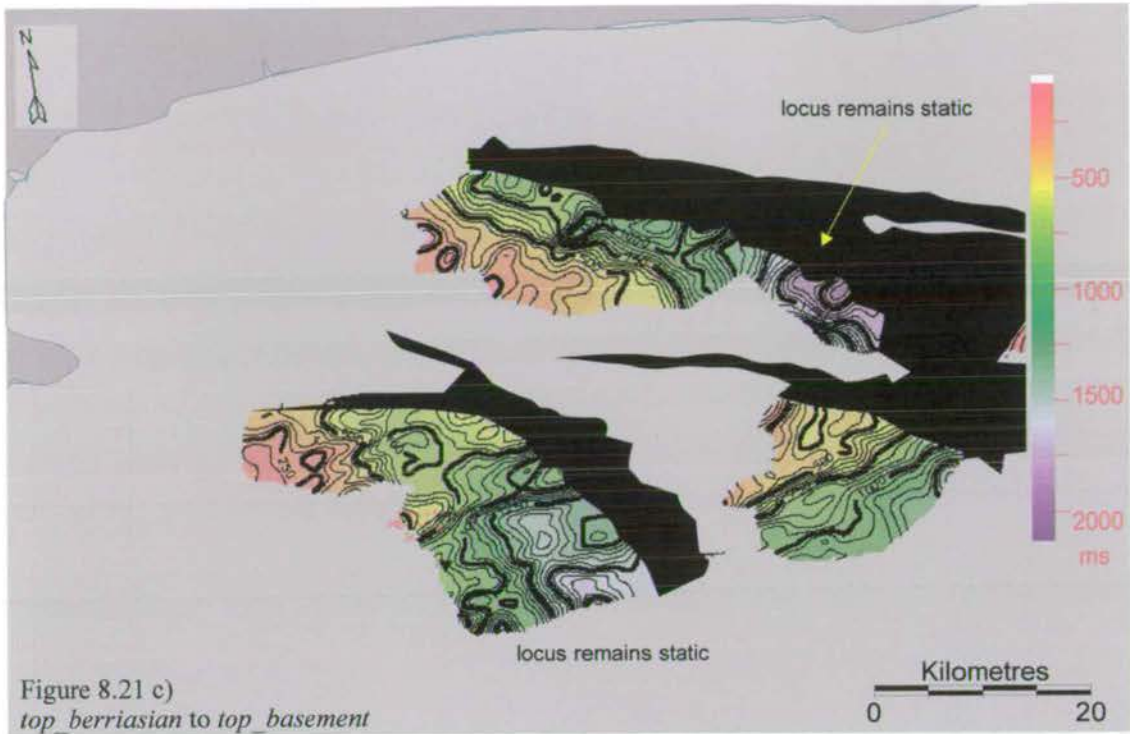


Figure 8.21: Cumulative isochron plots of thickness from *top_basement* to Principal Syn-Rift horizons: a) *top_kimmeridgian*, b) *top_portlandian*, c) *top_berriasian*, and d) *top_e-valanginian*. The calculated isochrons have only been plotted where the complete sequence thickness is present, resulting in the decrease in areal extent from (a) to (d). As the extent of *top_l-valanginian* is very restricted it has not been plotted.

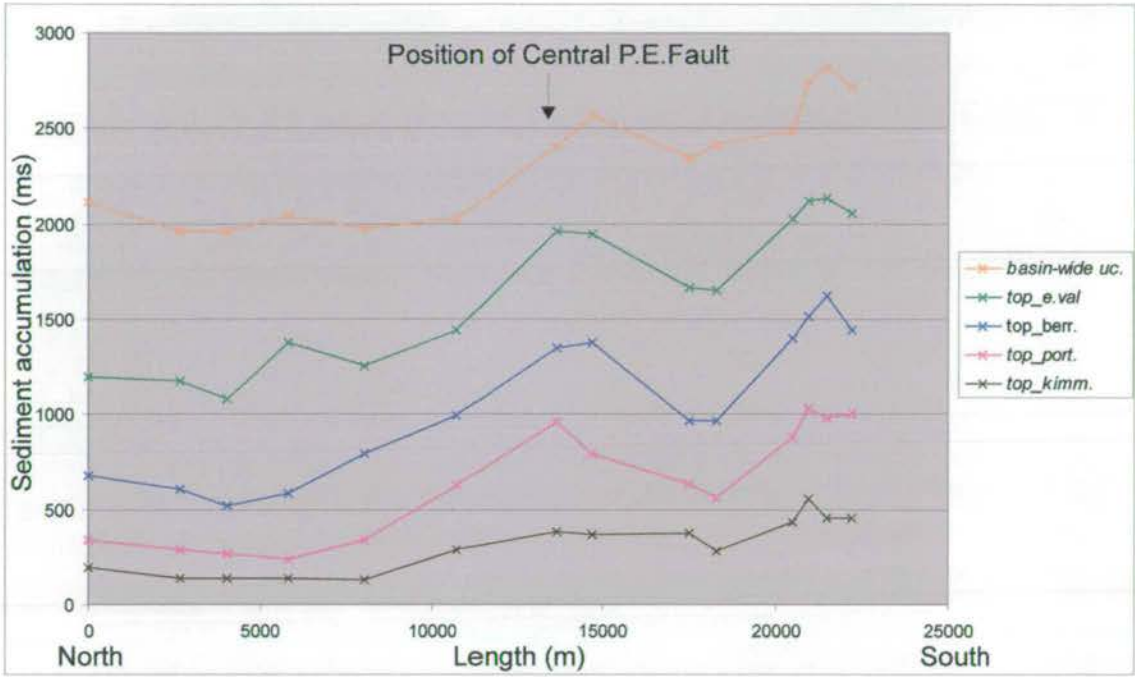


Figure 8.22: Sediment accumulation (TWT) vs. Length plot for the Port Elizabeth Fault. Each line corresponds to the cumulative sediment accumulation from *top_basement* to the relevant horizon and shows that the maximum accumulation occurred towards the southern extent of the data coverage. Length is measured from the most northern seismic section towards the south. The increase in accumulation at 14 km is a result of the Central P.E. Fault.

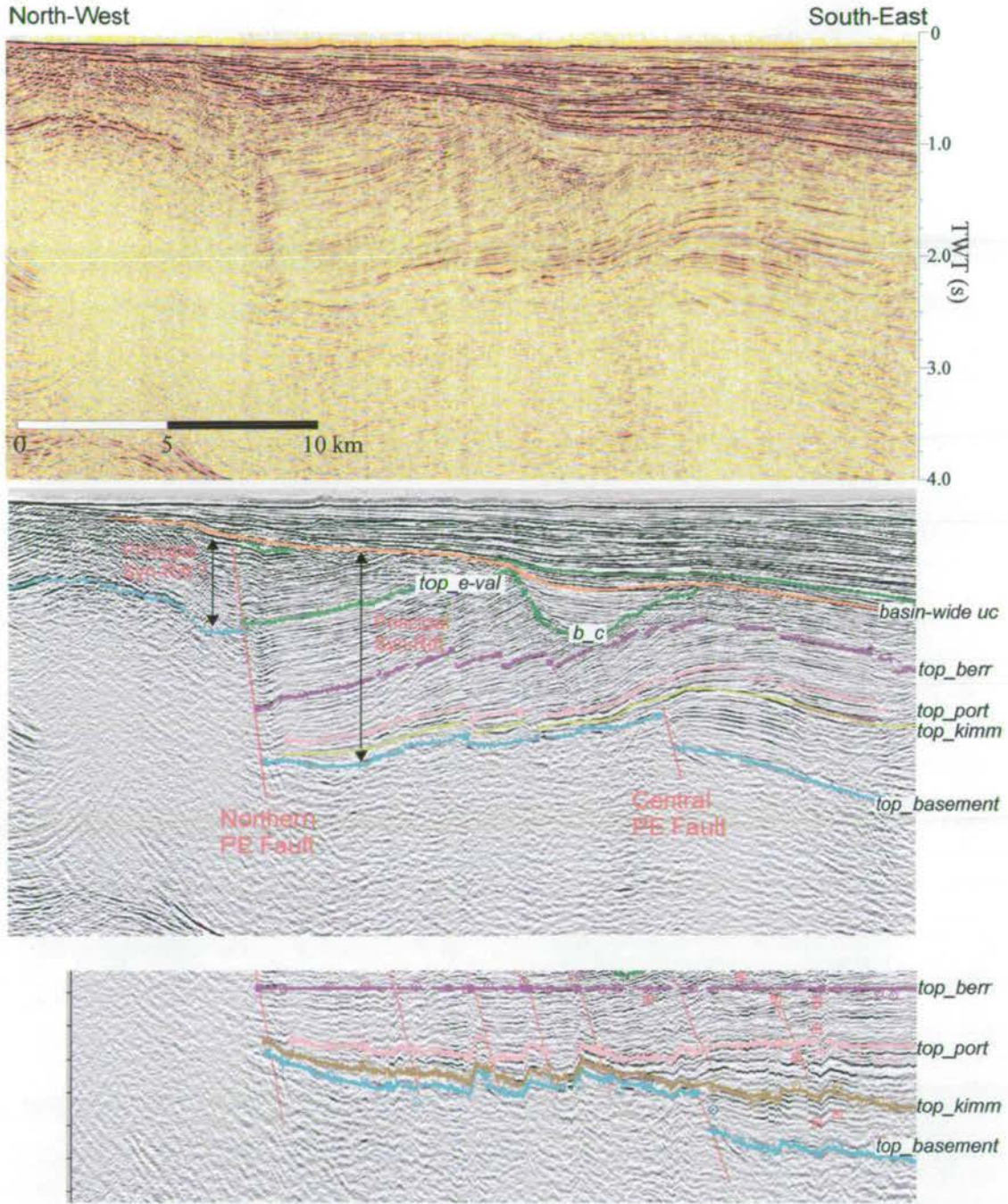


Figure 8.23: North-west to south-east section through the Port Elizabeth Trough. The two east-west trending faults are evident in the (a) uninterpreted and (b) interpreted sections. When the section is flattened to *top_portlandian* (c) there is evidence growth across the Southern Port Elizabeth Fault in the Kimmeridgian. There is no evidence of growth into the Northern Port Elizabeth Fault throughout the Principal Syn-Rift mega-sequence. The seismic character of the sediments on the footwall of the Northern Port Elizabeth Fault are very similar to the Principal Syn-Rift. Line HB 84-019, *b_c* = *base_canyon*.

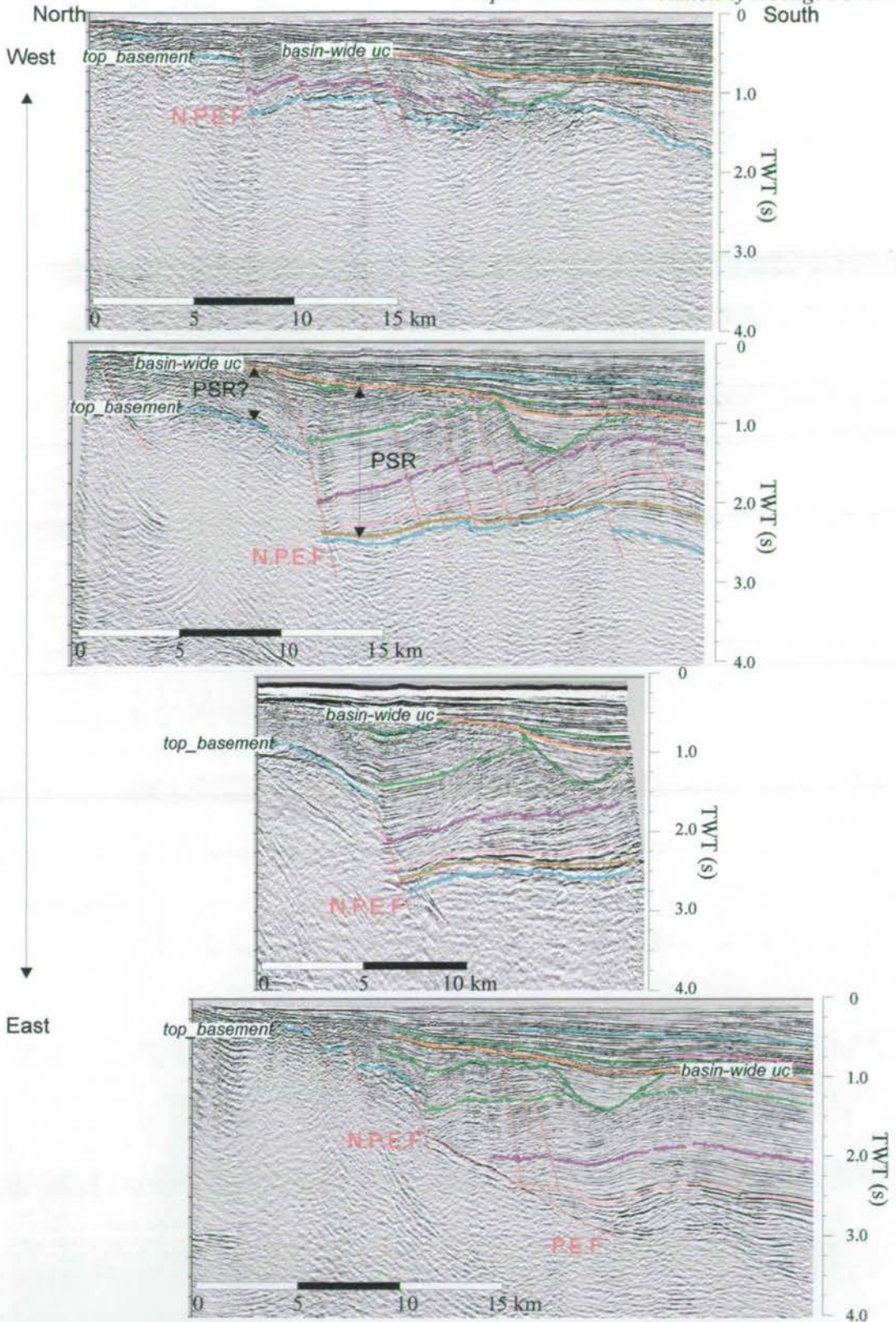


Figure 8.24: North-south sections across the Northern Port Elizabeth. Fault (N.P.E.F.) to show the increase in displacement on the fault towards the centre of the Port Elizabeth Trough. At the eastern extent, the N.P.E. Fault cross-cuts the Port Elizabeth Fault (P.E.F.). The Principal Syn-Rift (PSR) is truncated against the N.P.E.F., although it is inferred that the PSR occurs on its footwall.

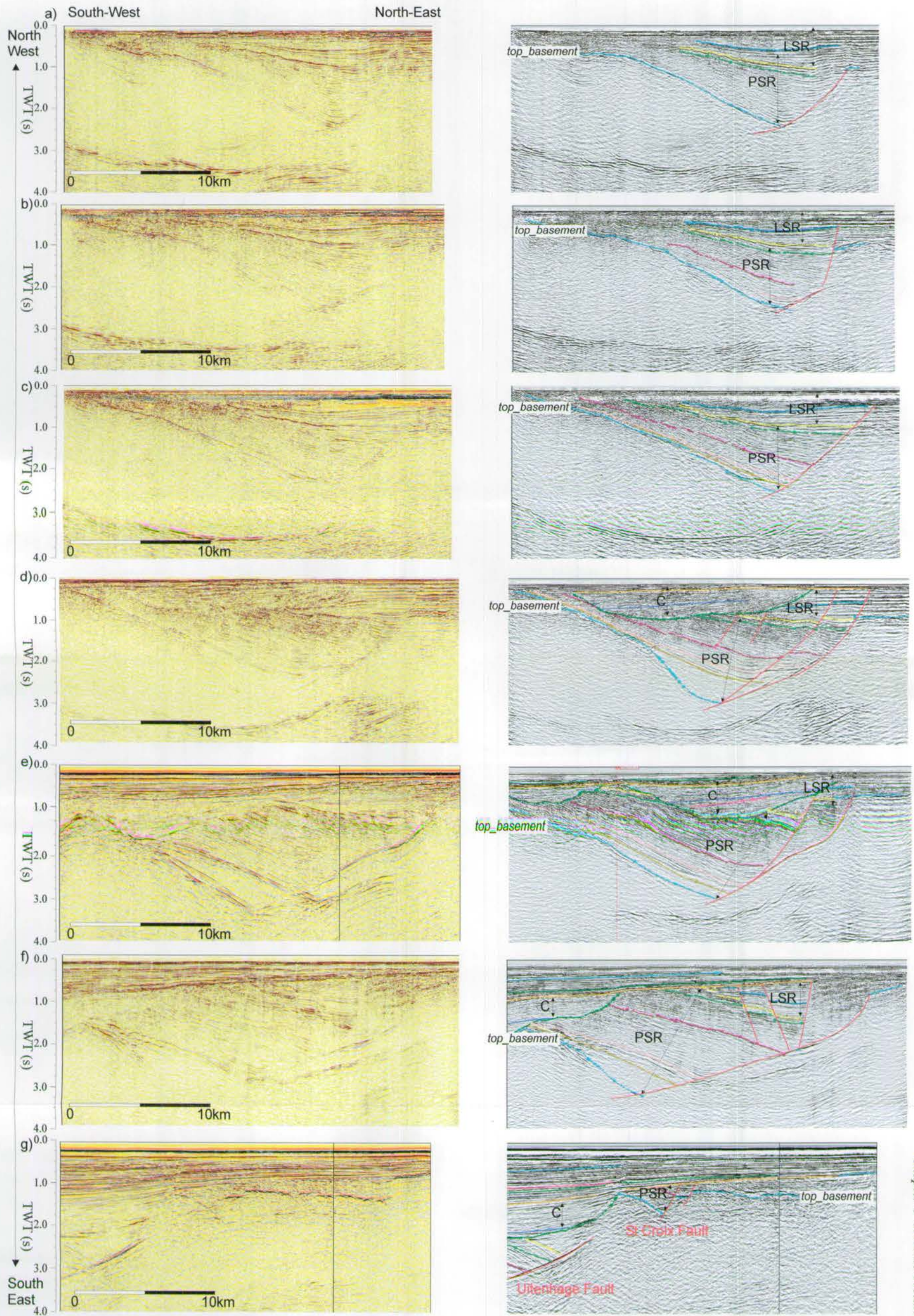


Figure 8.25: Array of seismic sections perpendicular to the St Croix Fault from the north-west (a) to the south-east (g). The geometry of the fault is complex and changes along its trend. There are various Late Syn-Rift Faults that often form short-cut, steeper normal faults that merge with the St Croix Fault at depth. PSR-Principal Post-Rift, LSR - Late Syn-Rift, C- Canyon. Lines: a) Hb86-013, b) Hb86-012, c) Hb86-011, d) Hb86-007, e) Hb86-006, f) Hb86-003, g) Hb83-031.

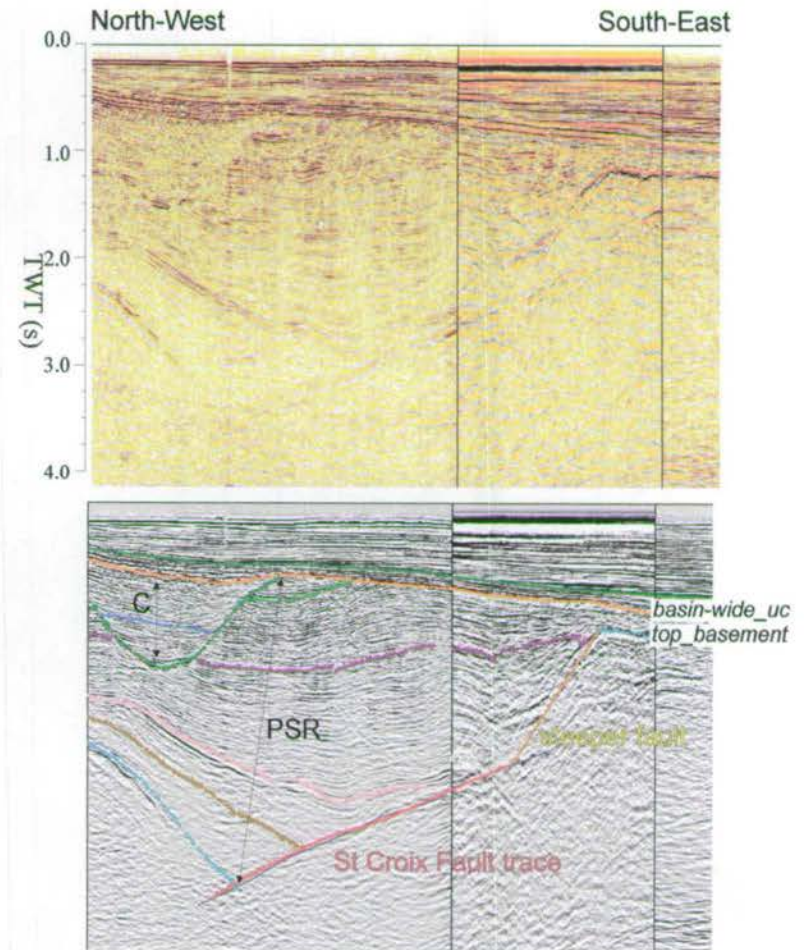
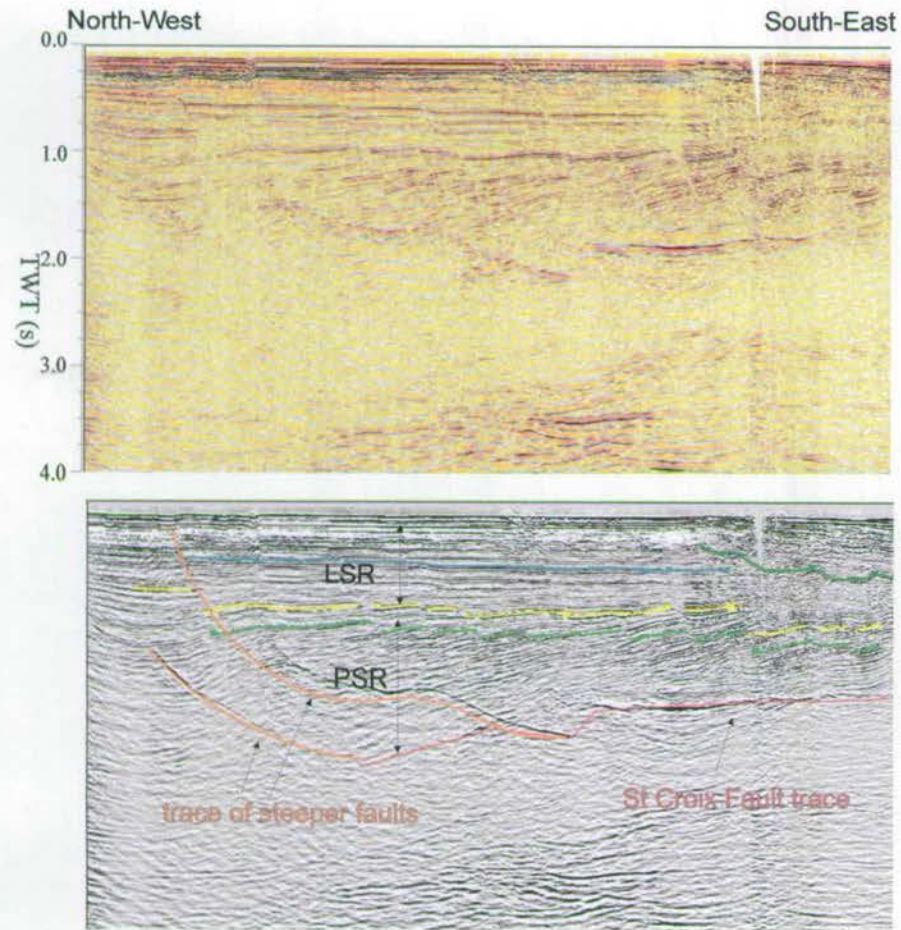


Figure 8.26:- Sections parallel to the St Croix Fault. a) Section at the west of the fault that shows the trace of the St Croix Fault. The two shallower reflectors (orange lines) correspond to the two steeper faults that are illustrated in Figure 8.25b & d. The eastern fault has growth during the Late Syn-Rift. b) The depocentre associated with the St Croix Fault abruptly terminates in the south-east against the low angle trace of the St Croix Fault, and a steeper structure. Lines a) Hb86-025, b) Hb86-021.

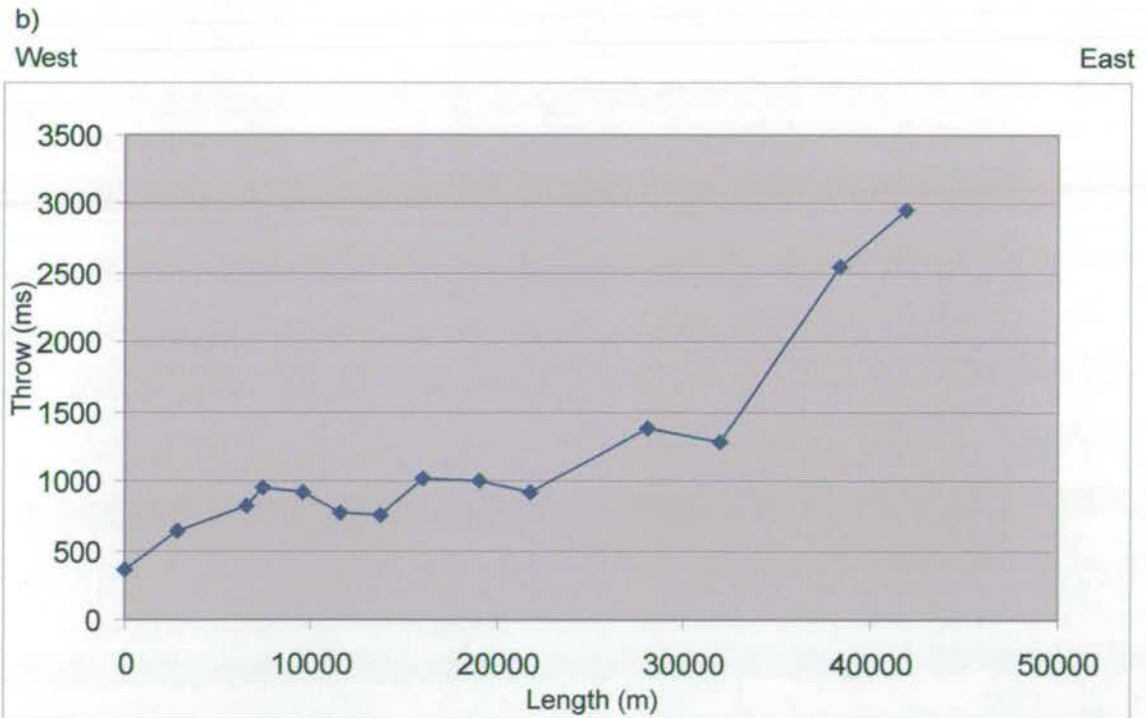
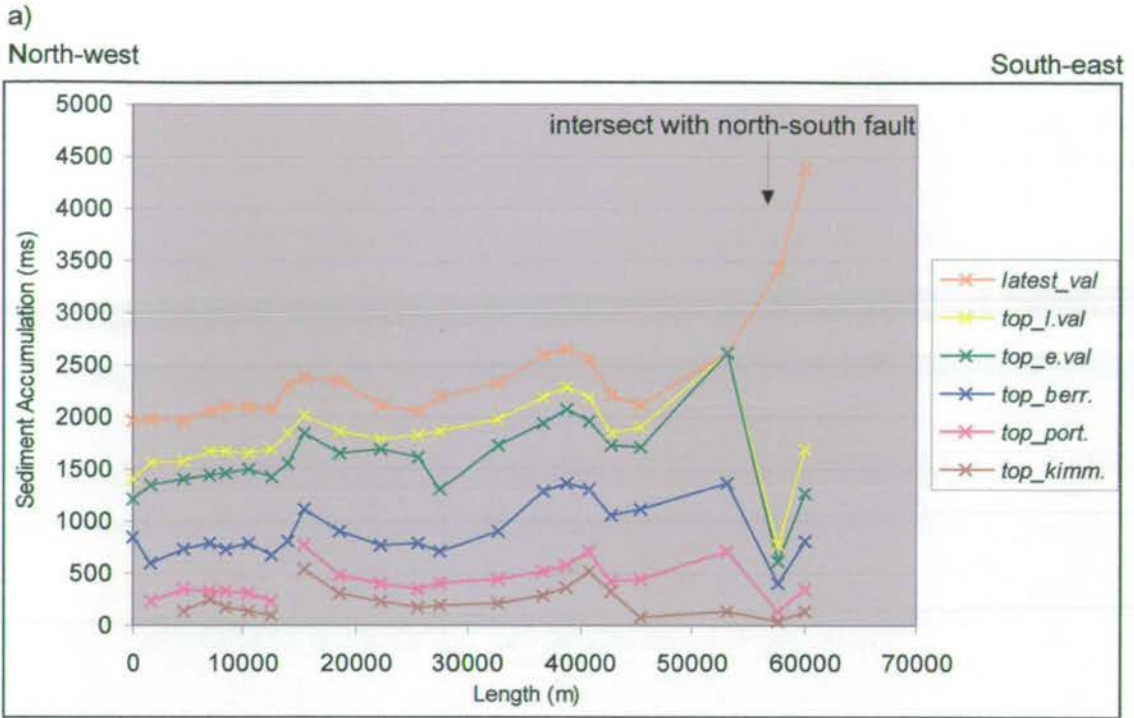


Figure 8.27: a) Sediment accumulation (ms) vs. length plots along St Croix Fault, and (b) throw (calculated from *top_basement* footwall and hangingwall cut-offs) vs. length for the Uitenhage Fault. With the Uitenhage Fault it has been possible to calculate fault throw because basement footwall and hangingwall cut-offs are evident.

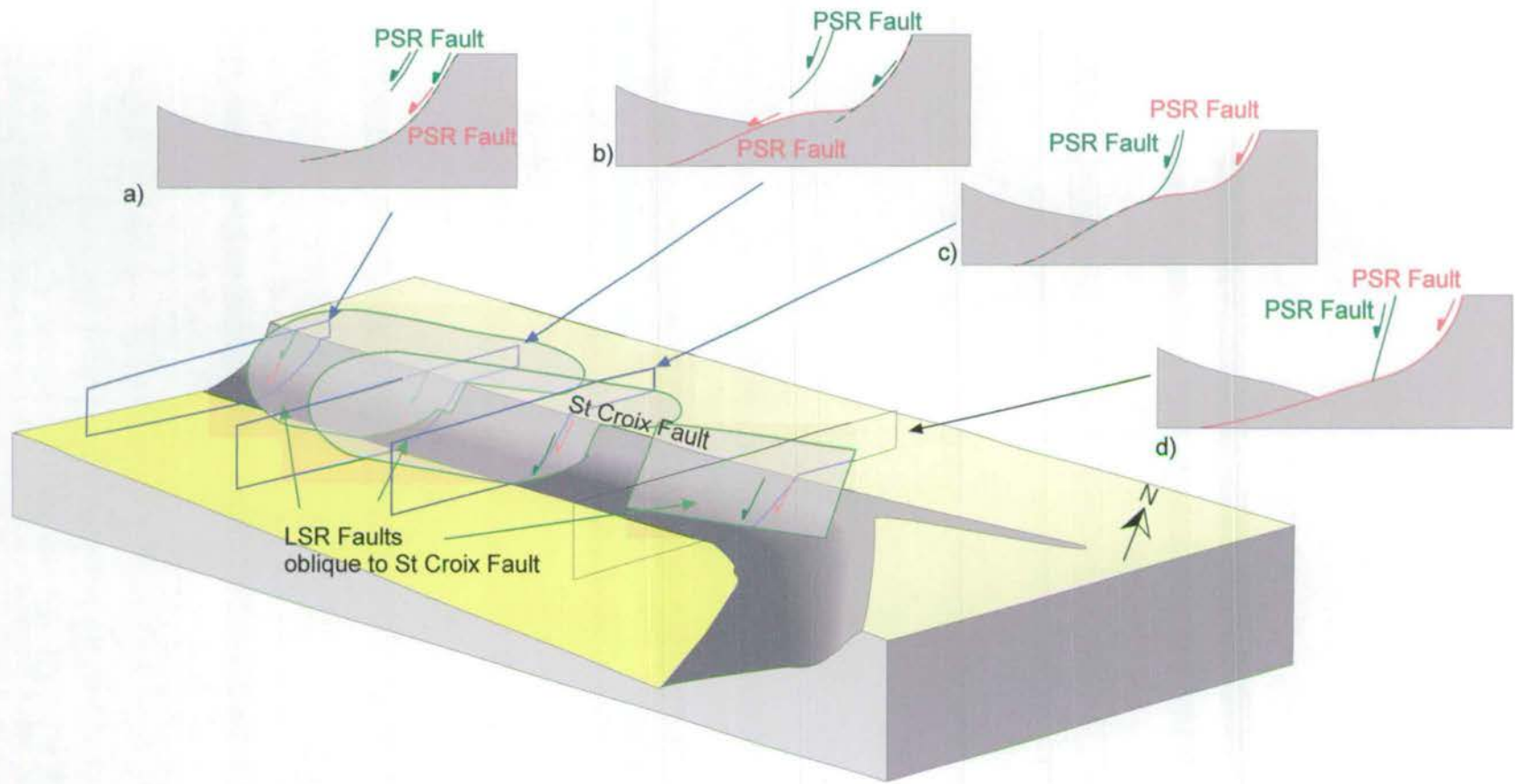


Figure 8.28: 3-D cartoon of the St Croix Fault with sketch sections illustrating various cross-sectional geometries observed in Figure 8.25. In all sections red correspond to Principal Syn-Rift (PSR) faults, green to Late Syn-Rift (LSR) faults and dotted lines to PSR faults reactivated during the LSR. The LSR faults interact with the St Croix Fault in a number of ways: a) complete reactivation of the St Croix Fault; b) reactivation of the steeper section, but cross-cuts the monoclinal geometry of the St Croix Fault; c) steeper LSR fault that intersects with the St Croix Fault; d) LSR fault that terminates at the St Croix Fault. The resultant LSR fault orientations are oblique to the principal St Croix PSR fault.

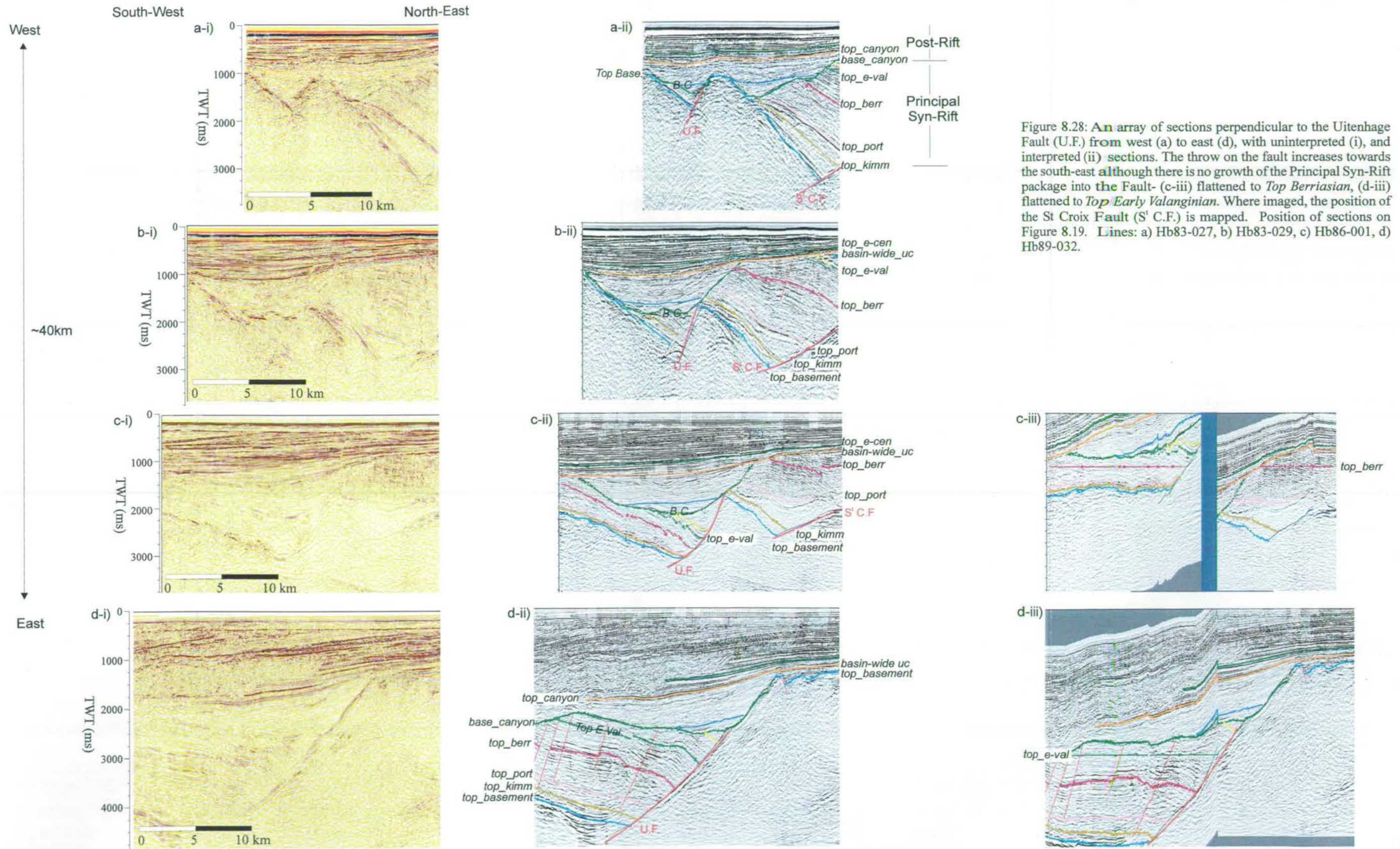


Figure 8.28: An array of sections perpendicular to the Uitenhage Fault (U.F.) from west (a) to east (d), with uninterpreted (i), and interpreted (ii) sections. The throw on the fault increases towards the south-east although there is no growth of the Principal Syn-Rift package into the Fault- (c-iii) flattened to Top Berriasian, (d-iii) flattened to Top Early Valanginian. Where imaged, the position of the St Croix Fault (S' C.F.) is mapped. Position of sections on Figure 8.19. Lines: a) Hb83-027, b) Hb83-029, c) Hb86-001, d) Hb89-032.

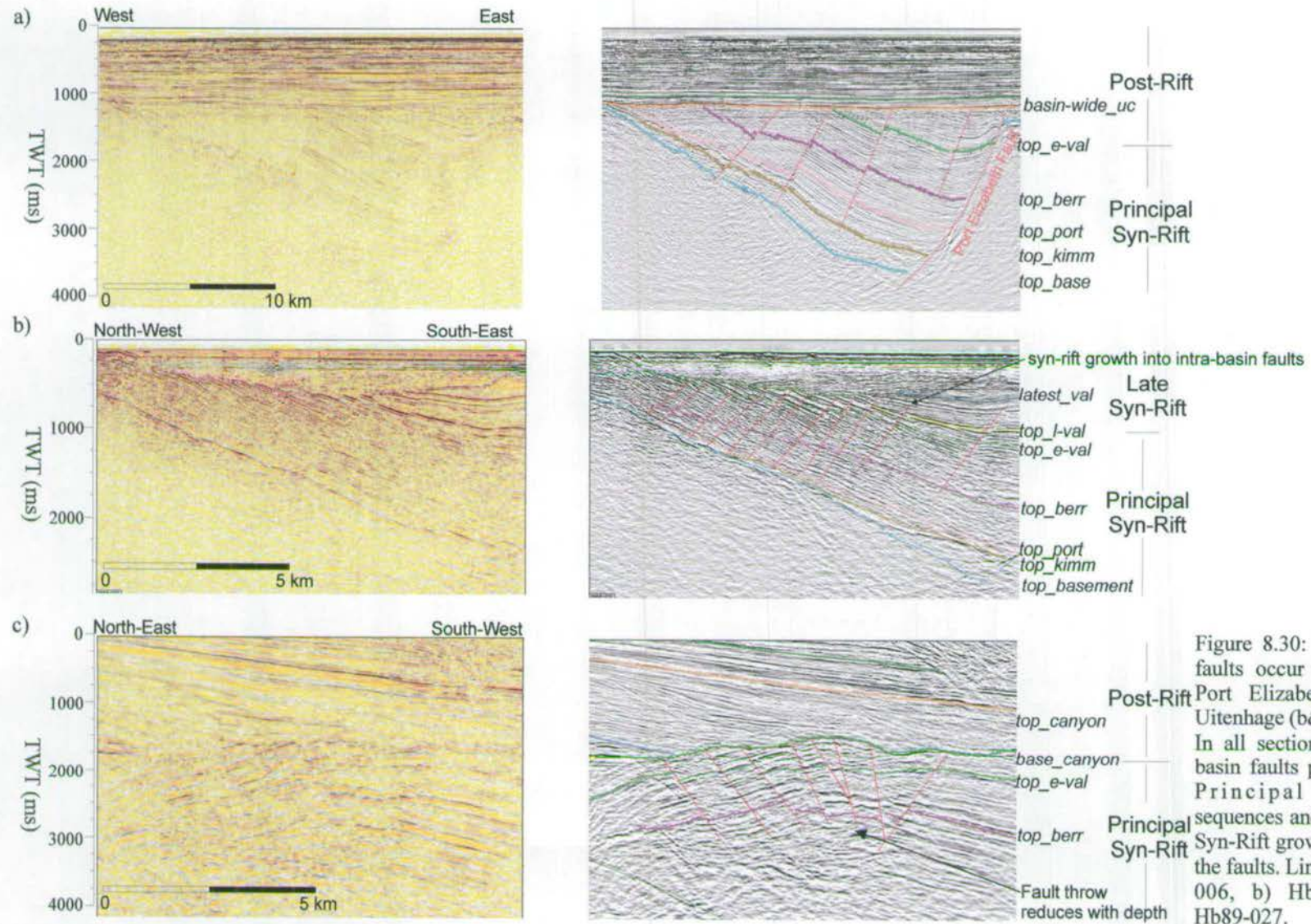


Figure 8.30: Intra-basin faults occur in both the Port Elizabeth (a) and Uitenhage (b&c) Troughs. In all sections the intra-basin faults post-date the Principal Syn-Rift sequences and in (b) Late Syn-Rift growth occurs in the faults. Lines: a) Hb89-006, b) Hb86-010, c) Hb89-027.

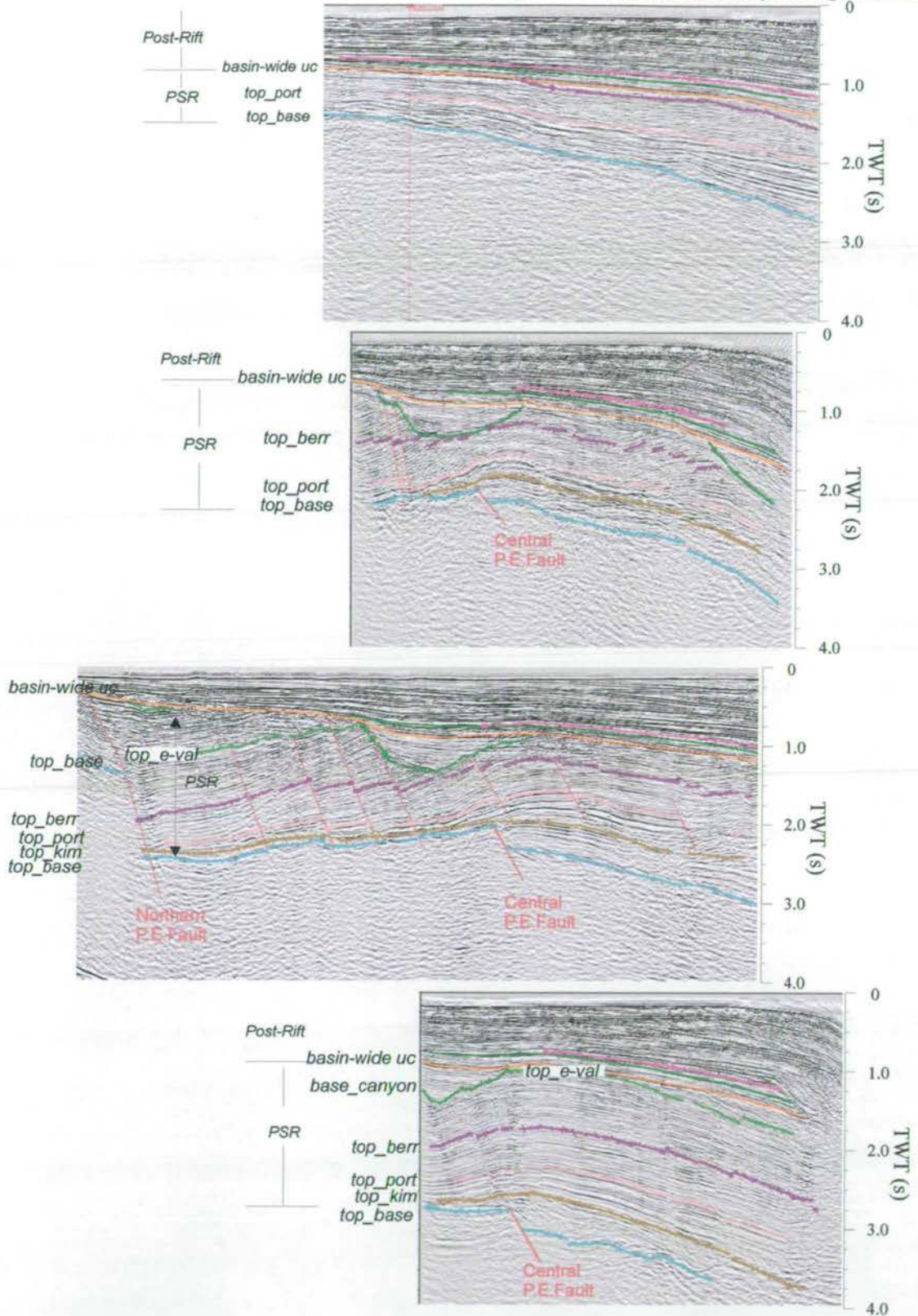


Figure 8.31: North-west to south-east sections across the northern Port Elizabeth Trough showing the increase in both the throw of the Central Port Elizabeth Fault and the amplitude of the Principal Syn-Rift folds.

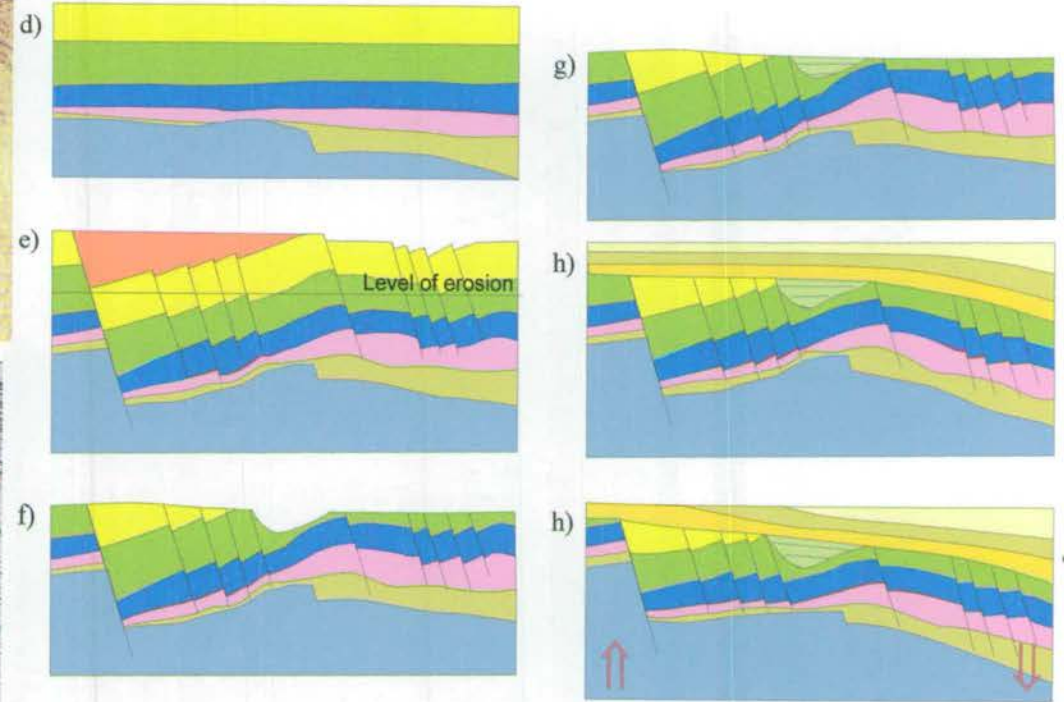
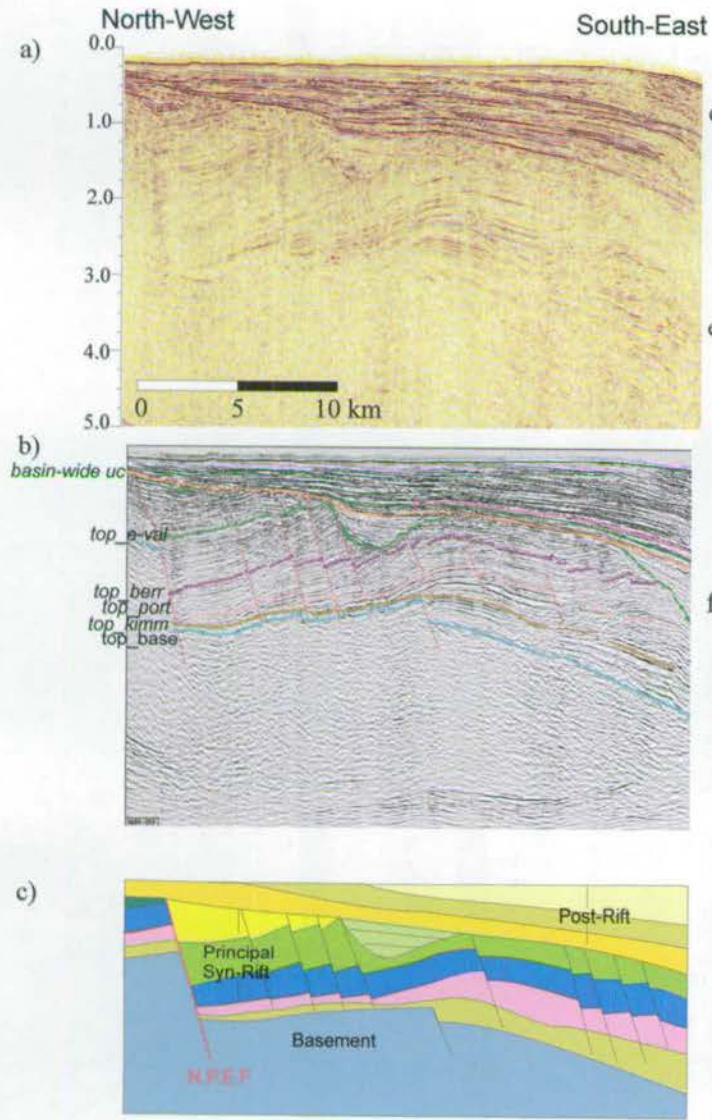


Figure 8.32: North-west to south-east section across the Port Elizabeth Trough. a) uninterpreted and b) interpreted section used to produce model (c) that is restored to: (d) Late Valanginian; (e) Late Hauterivian; (f) Post erosion (pre-Late Aptian); (g) canyon in-fill (Aptian-Albian); (h) Post-Rift deposition on gently subsiding southern margin; (i) significant southward tilting post Maastrichtian and coastal uplift. In this model it is inferred that the northern fault is Hauterivian age and that Principal Syn-Rift sediments are preserved on the fault's footwall. The observed folding of the top_berrisian is a consequence of extension on the Northern Port Elizabeth Fault (N.P.E.F) and subsequent subsidence in the south.

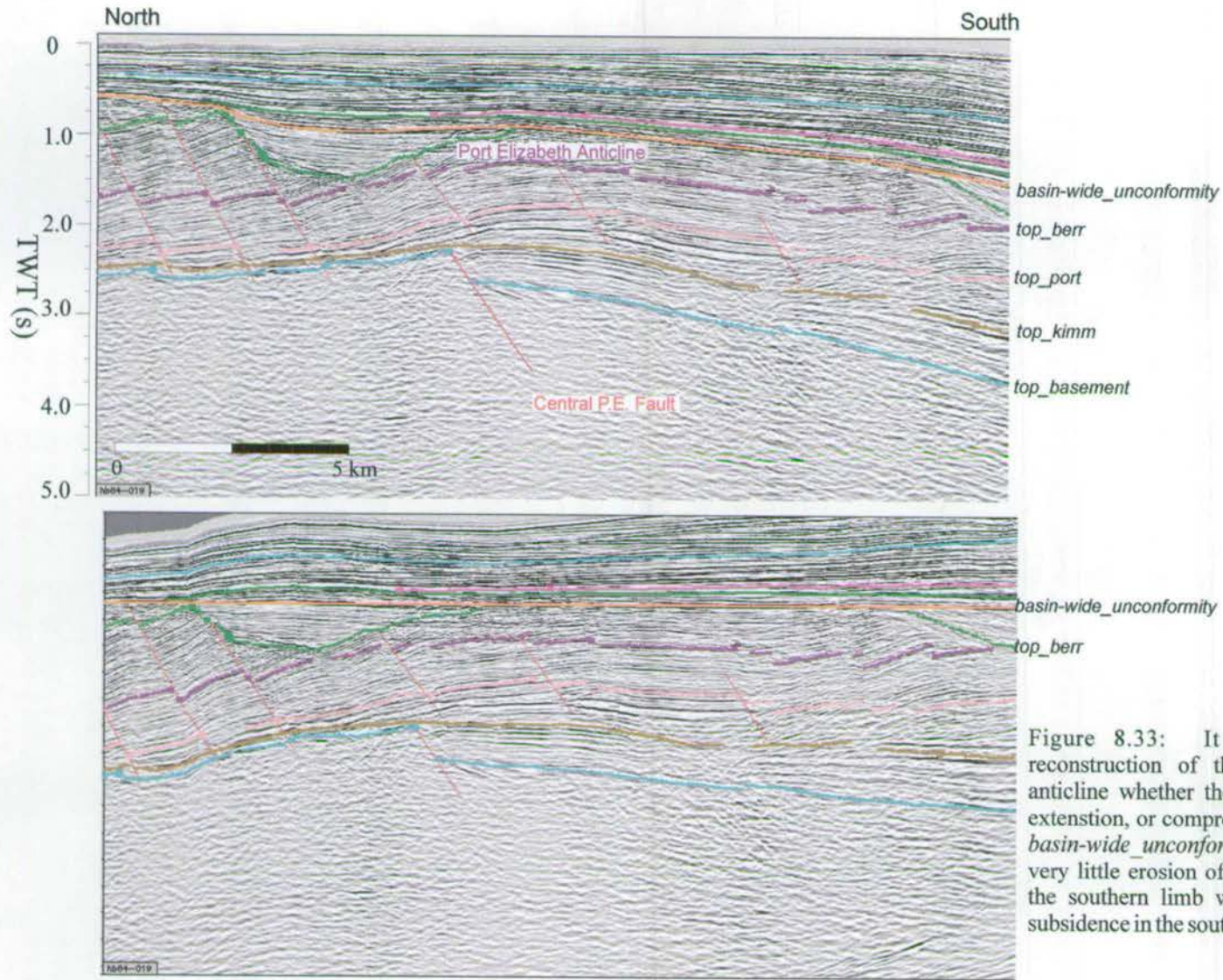
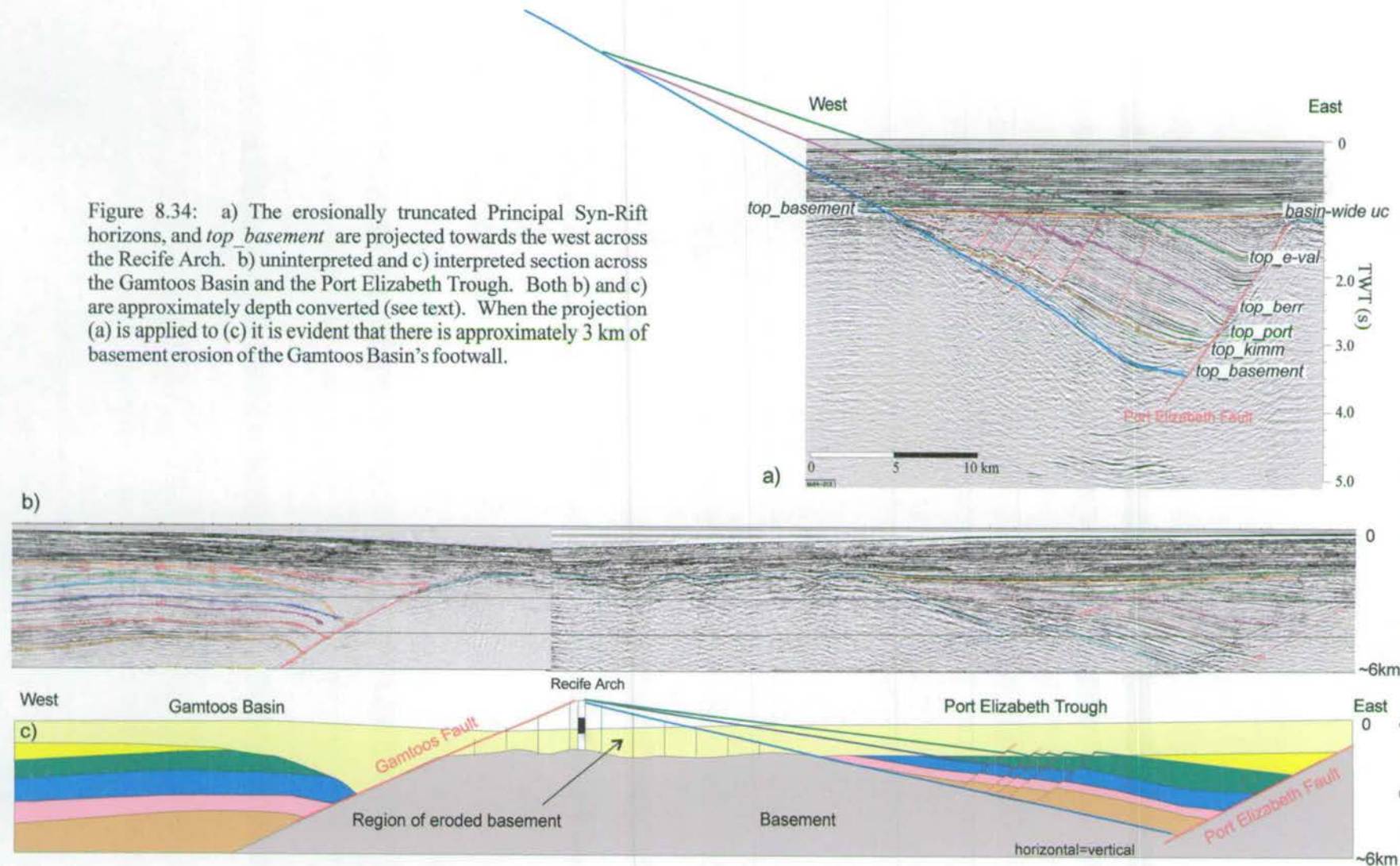
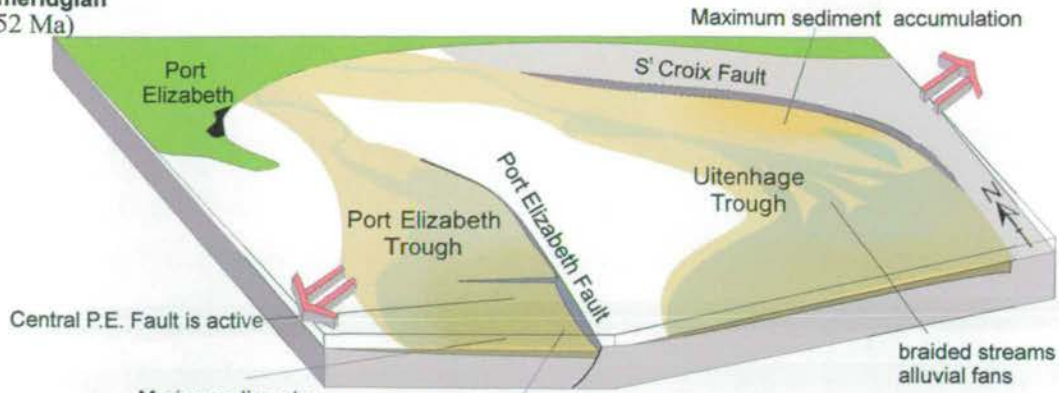


Figure 8.33: It is uncertain from the reconstruction of the Port Elizabeth Trough anticline whether the folding is in response to extension, or compression (see text). When the *basin-wide unconformity* is flattened there is very little erosion of the anticline implying that the southern limb was formed in response to subsidence in the south. Line Hb84-014.

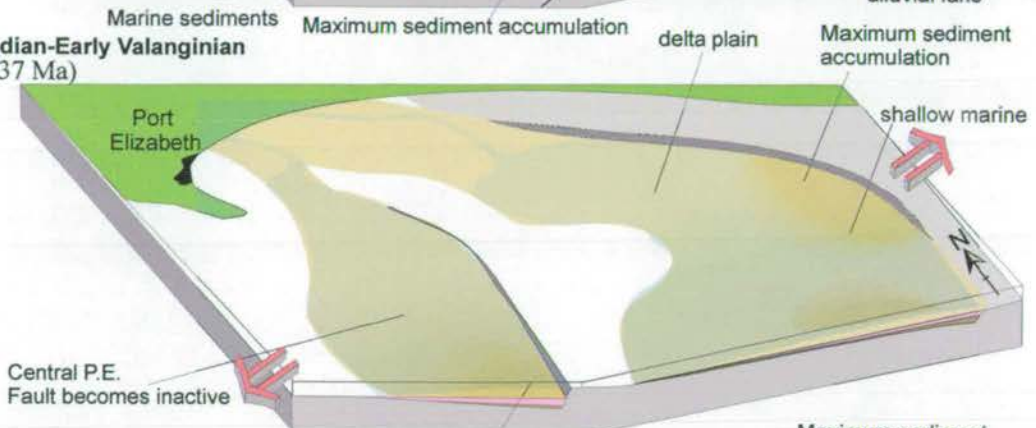
Figure 8.34: a) The erosionally truncated Principal Syn-Rift horizons, and *top_basement* are projected towards the west across the Recife Arch. b) uninterpreted and c) interpreted section across the Gamtoos Basin and the Port Elizabeth Trough. Both b) and c) are approximately depth converted (see text). When the projection (a) is applied to (c) it is evident that there is approximately 3 km of basement erosion of the Gamtoos Basin's footwall.



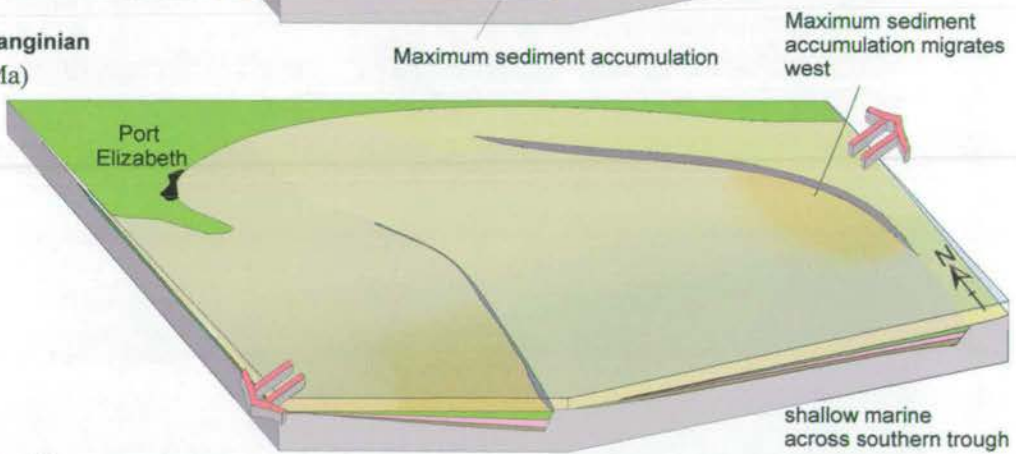
Kimmeridgian
(>152 Ma)



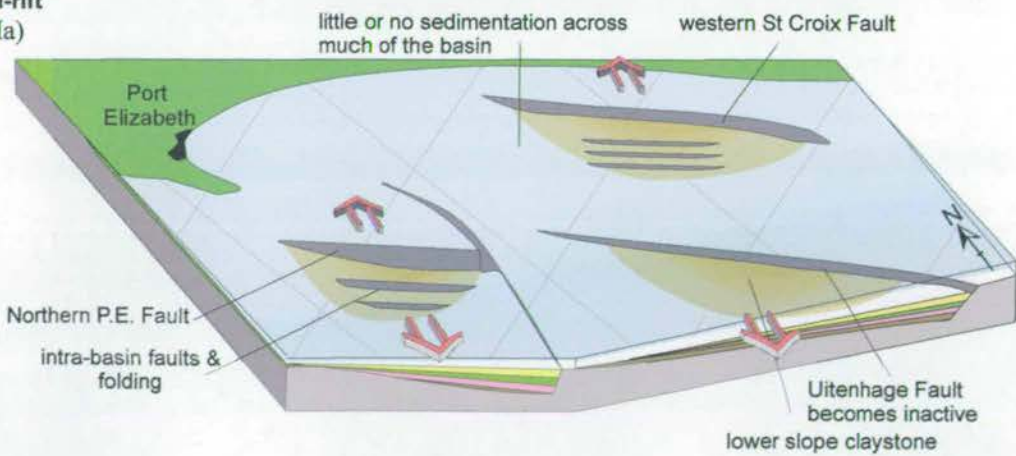
Portlandian-Early Valanginian
(152-137 Ma)



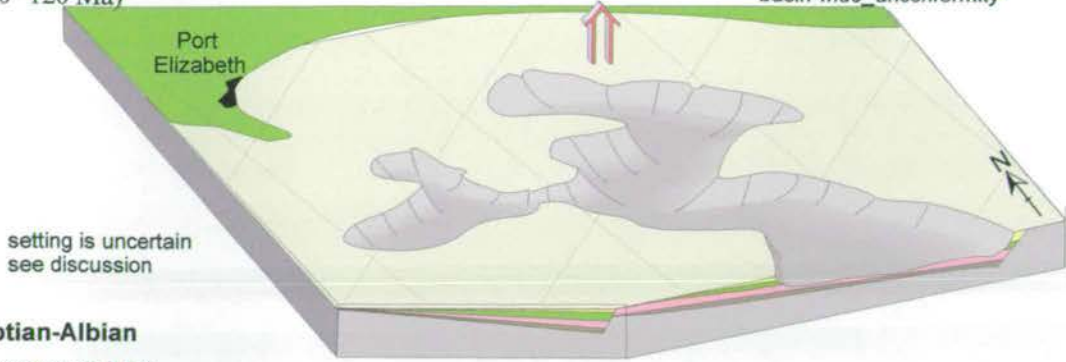
Late Valanginian
(~135 Ma)



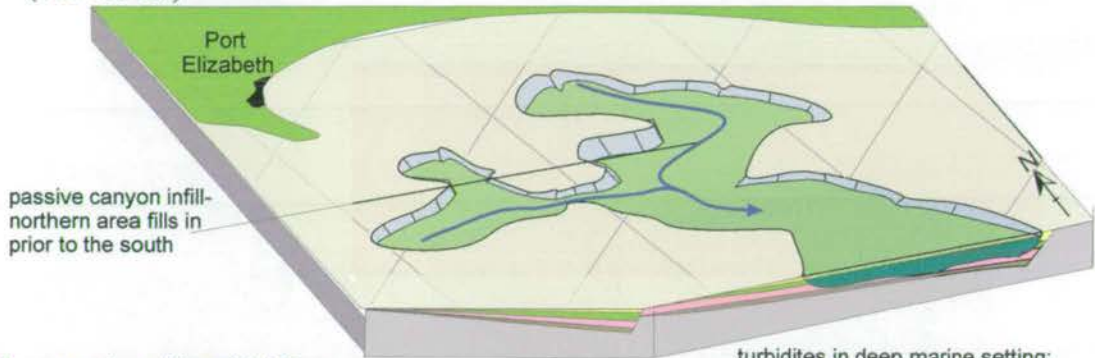
Late Syn-rift
(~133 Ma)



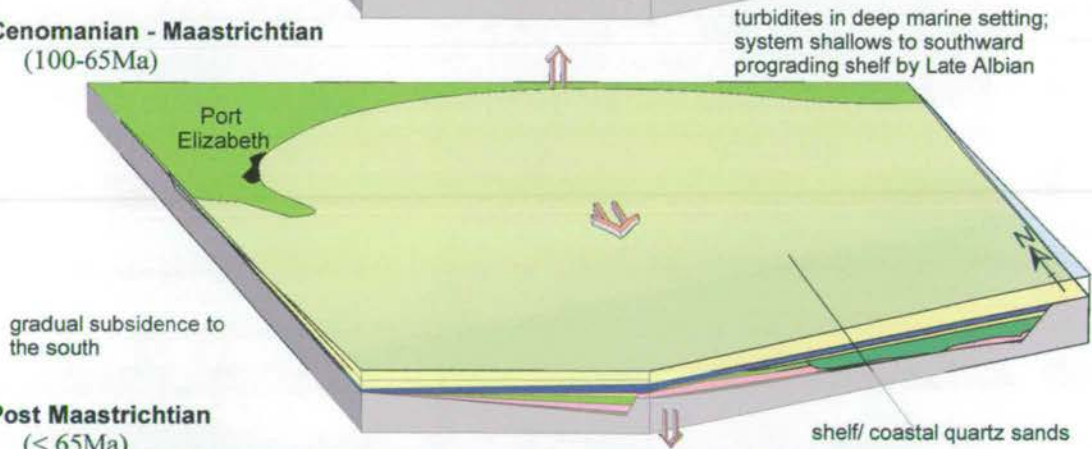
Hauterivian- Aptian
 (130 -120 Ma)



Aptian-Albian
 (120-100 Ma)



Cenomanian - Maastrichtian
 (100-65Ma)



Post Maastrichtian
 (< 65Ma)

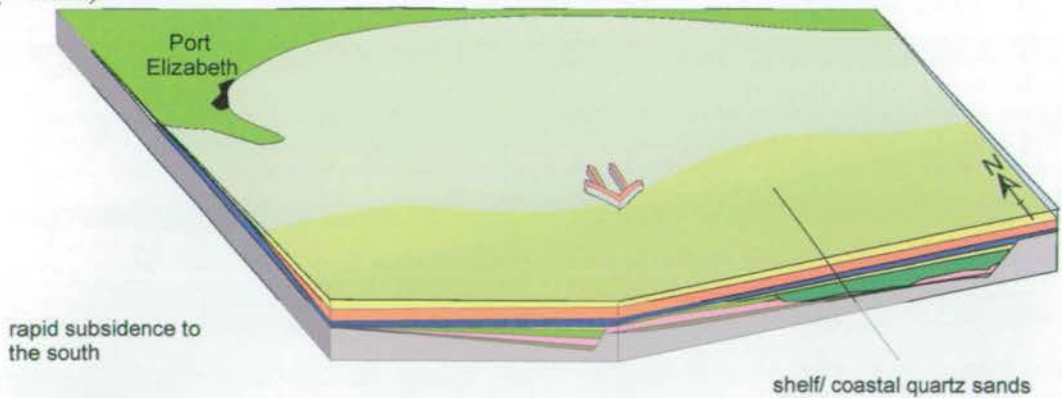


Figure 8.35: Summary of the evolution of the Algoa Basin highlighting the principal tectonic events, relative sea-level, and type of sedimentation. Note that the coast is shown as it is today. Red arrows indicating extension with respect to present orientation, other arrows indicate sediment progradational direction.

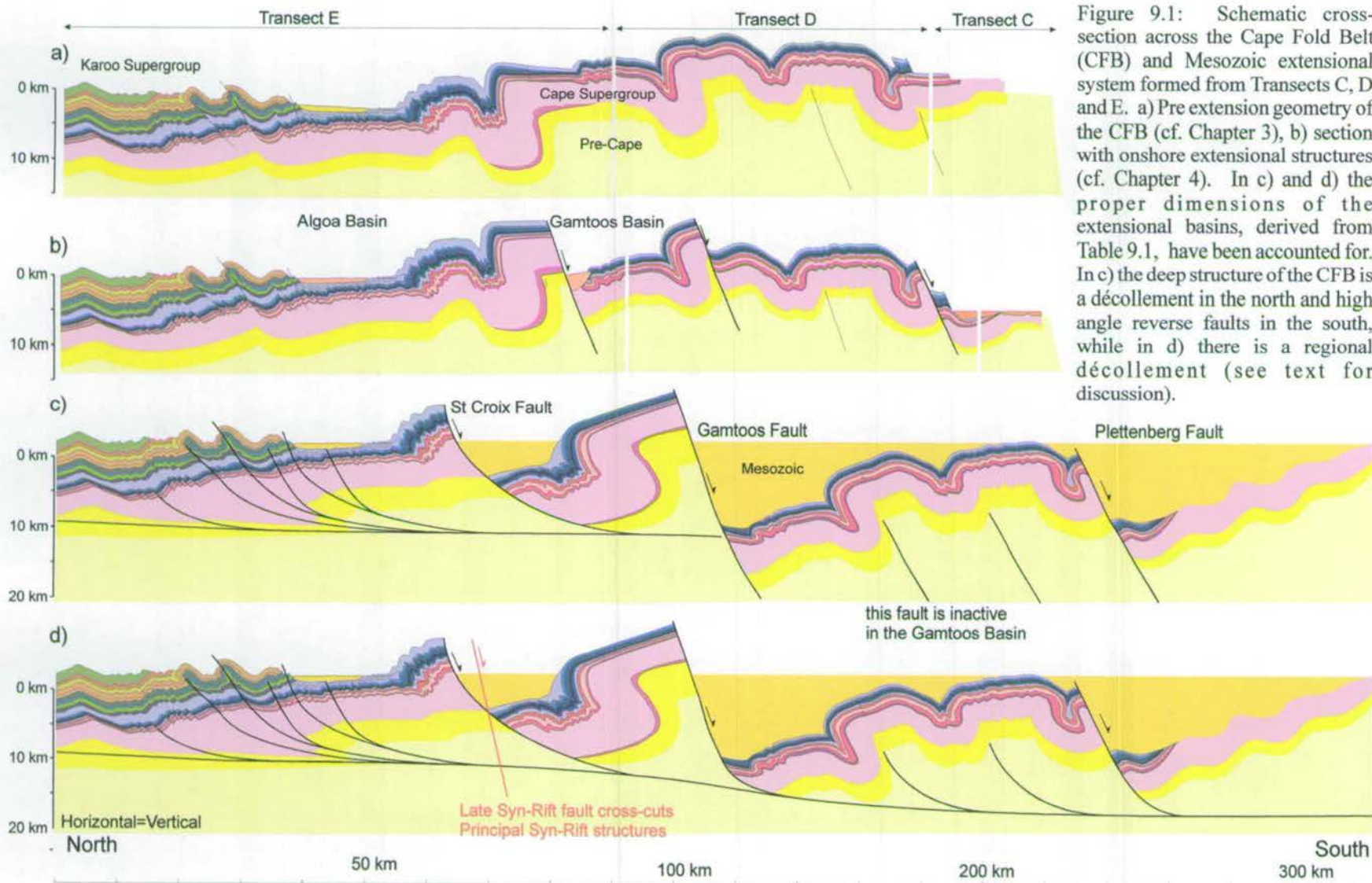
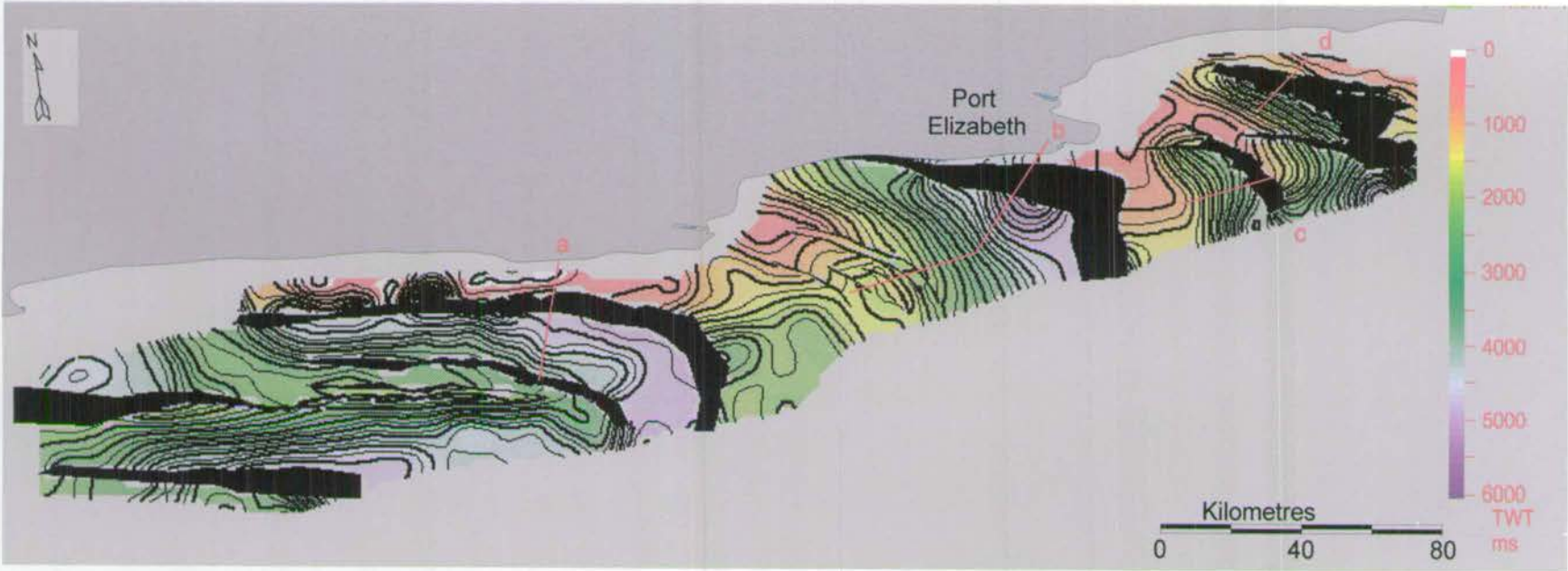
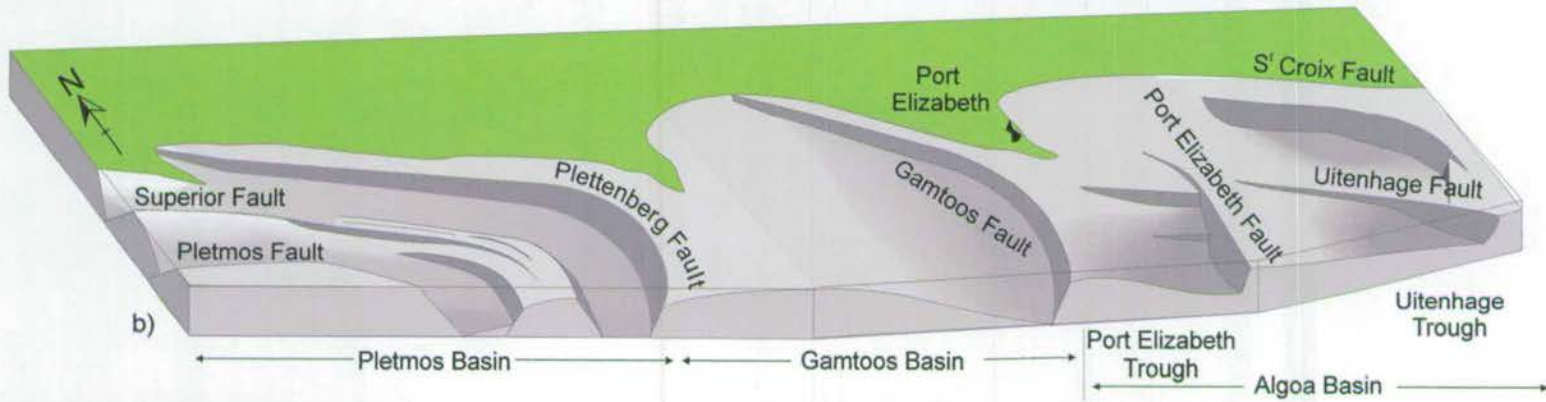


Figure 9.1: Schematic cross-section across the Cape Fold Belt (CFB) and Mesozoic extensional system formed from Transects C, D and E. a) Pre extension geometry of the CFB (cf. Chapter 3), b) section with onshore extensional structures (cf. Chapter 4). In c) and d) the proper dimensions of the extensional basins, derived from Table 9.1, have been accounted for. In c) the deep structure of the CFB is a décollement in the north and high angle reverse faults in the south, while in d) there is a regional décollement (see text for discussion).



a)



b)

Figure 9.2: a) TWT map to *top_basement* horizon across southern South Africa with the principal fault polygons plotted. Red lines and letters correspond to sections in Figure 9.3. b) 3-D cartoon of the architecture of the study area.

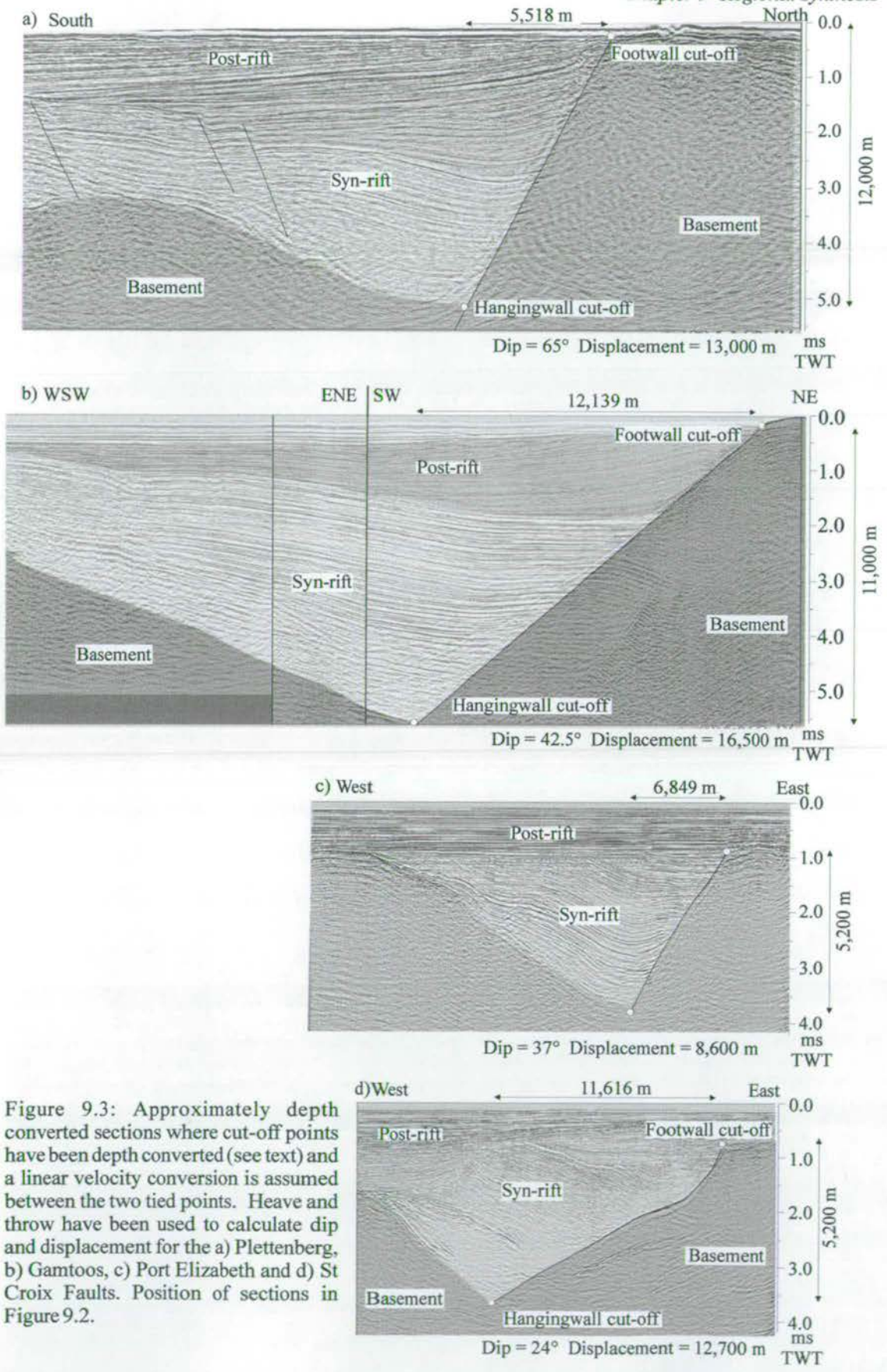


Figure 9.3: Approximately depth converted sections where cut-off points have been depth converted (see text) and a linear velocity conversion is assumed between the two tied points. Heave and throw have been used to calculate dip and displacement for the a) Plettenberg, b) Gamtoos, c) Port Elizabeth and d) St Croix Faults. Position of sections in Figure 9.2.

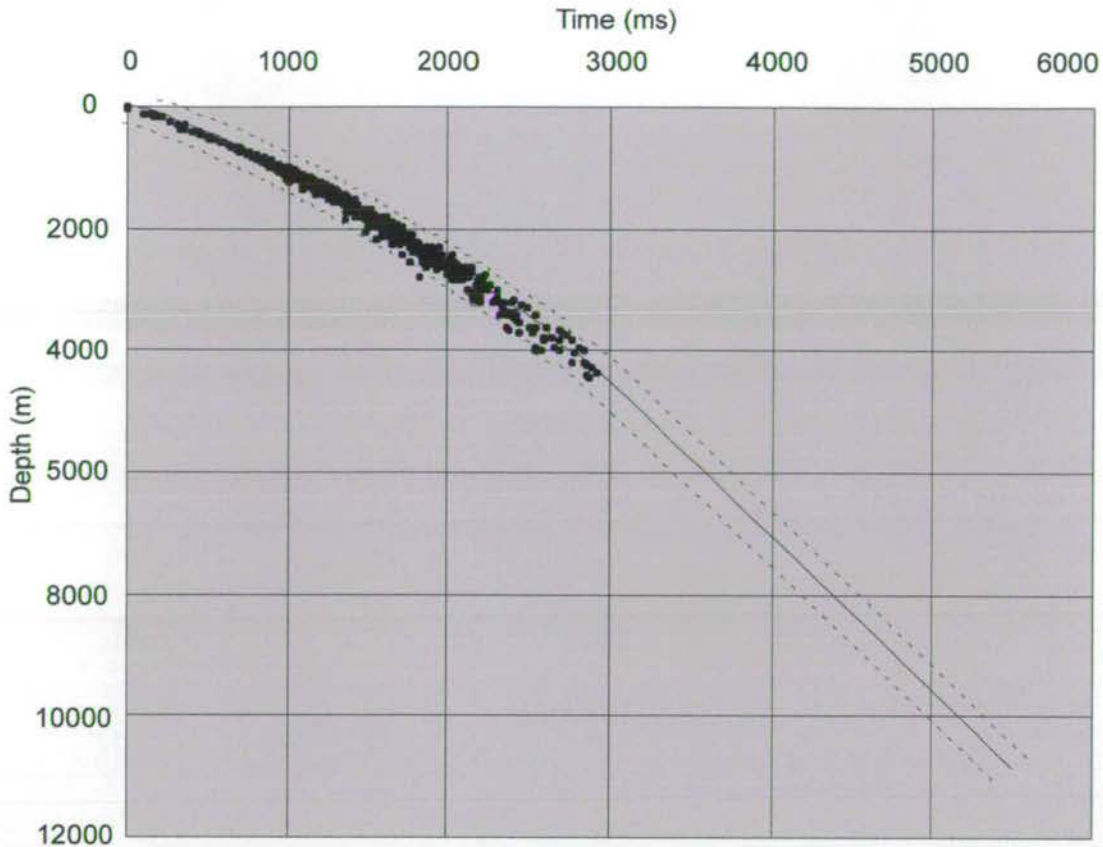


Figure 9.4: Depth-time data compiled from all wells in the three South African basins. The well data only penetrate to ~3000ms (4500m) and have to be extrapolated for depth conversion, see text for discussion.

The best-fit line (calculated using Table Curve 3.0) is

$$\text{TWT(m)} = 22.30 + 0.88z + 1.341 \times 10^{-5}z^2 + 2.2662 \times 10^{-7}z^3 - 1.255 \times 10^{-10}z^4 + 2.420 \times 10^{-14}z^5 - 1.650 \times 10^{-18}z^6$$

$r^2 = 0.99151$. The upper and lower ranges of the data are used as approximate error ranges, and are approximately $\pm 400\text{m}$

Fault	Length (km) ¹	Dip	Throw (m) ⁷	Heave (m)	Displacement (m)	Basin Width (km)	D/L ratio
Plettenberg	158	65°	12,168	5,5518	13,000	19 ³ 36 ⁴	0.08
Gamtoos	96 150 ²	42.5°	11,114	12,139	16,500	63 ⁵	0.17 0.11
Port Elizabeth	38	37°	5,222	6,849	8,600	60 ⁶	0.22
St Croix	52	24°	5,233	11,616	12,700	30	0.24

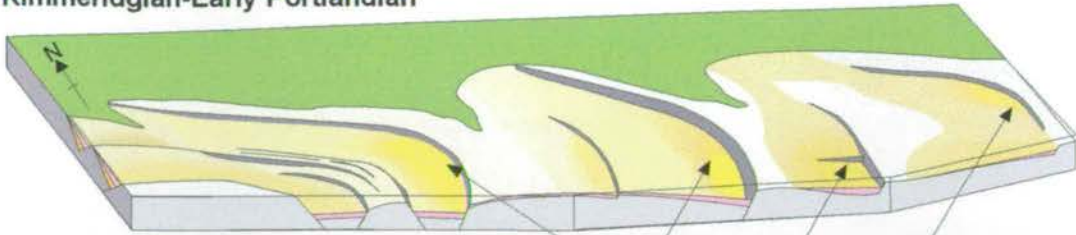
Table 9.1: Compiled data for the dimensions of the extensional systems in South Africa.

Measurements for throw (hence dip and displacement) are lowest estimates, see text for discussion.

Displacement-Length (D/L) ratios are calculated and will be discussed in Chapter 10.

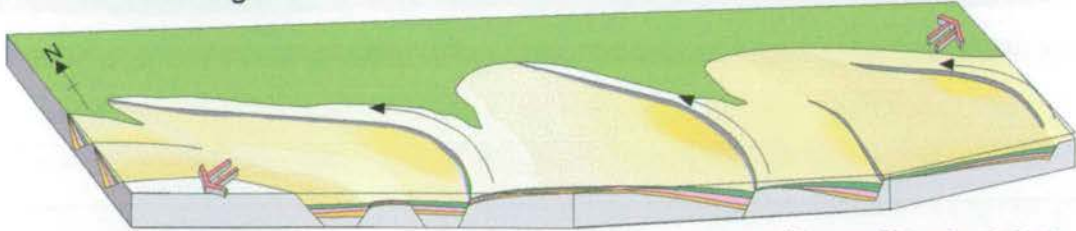
¹-minimum length determined from seismic data only, ²-includes onshore fault portion, ³-taken at west end of the basins ⁴-east end of basin (both ³ & ⁴ measured to the centre of the intra-basin high), ⁵-southern end of fault to western faulted margin, ⁶-fault to Gamtoos Fault to account for reconstruction in Chapter 8, ⁷- the estimated errors derived from the data range in Figure 9.4 is approximately ± 400 m. Other errors are discussed in the text.

Kimmeridgian-Early Portlandian



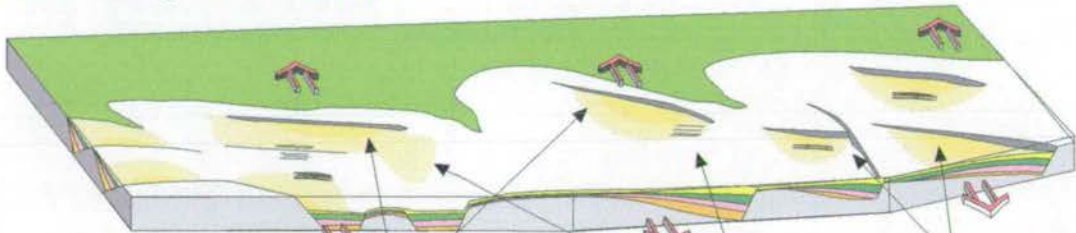
**Principal Syn-Rift
Portlandian-Valanginian**

maximum accumulation into north-south trending faults portions although there is accumulation into east-west portions as well



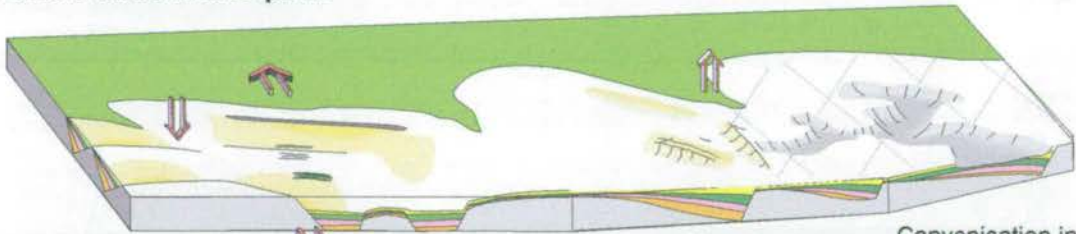
migration of loci of maximum sediment accumulation no evidence of intra-basin faults

**Late Syn-Rift
Latest Valanginian-Hauterivian**



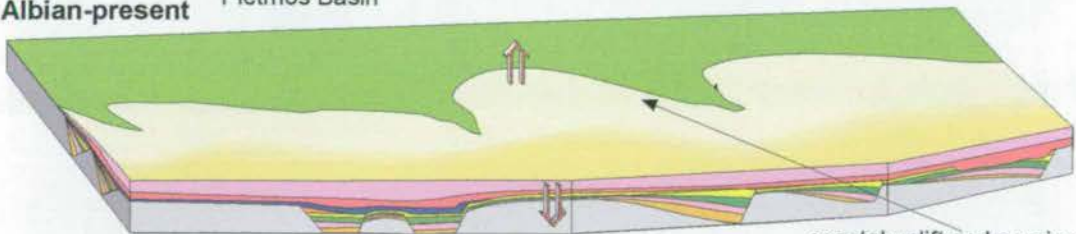
deposition only against east-west trending fault portions deformation of syn-rift pre-existing faults cross-cut

**Eastern uplift
Latest Hauterivian-Aptian**



continued sedimentation in Pletmos Basin uplift and erosion localised compression Canyonisation in the Algoa Basin

**Post-Rift
Albian-present**



regional subsidence in the south coastal uplift and erosion

Figure 9.5: Summary sketches of the evolution of the South African basins. Of particular importance to this study is the temporal variation in fault activity inferred from the migration of maximum sediment accumulation (assumes sedimentation accumulation is a proxy for accommodation space formed through tectonic subsidence, see text).

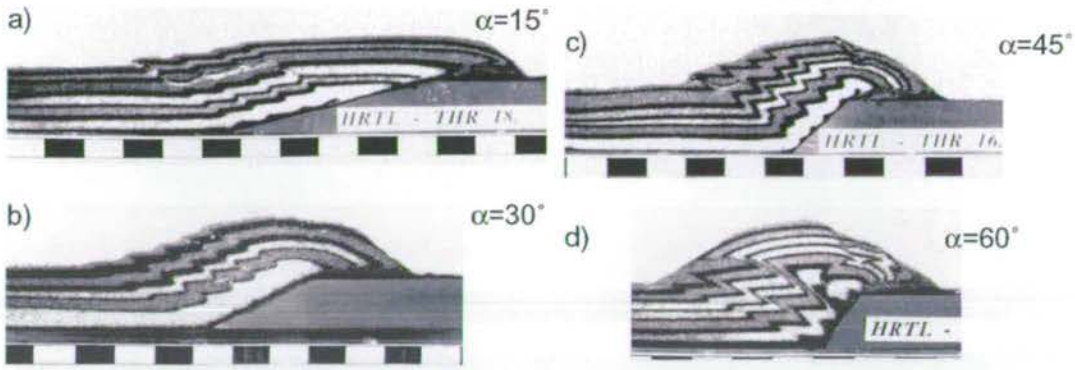


Figure 10.1: Sand-box modeling with a variable ramp angle (α) illustrating that the higher the ramp angle, the shorter the wavelength of the resultant hanging wall deformation (Bonini *et al.*, 2000).

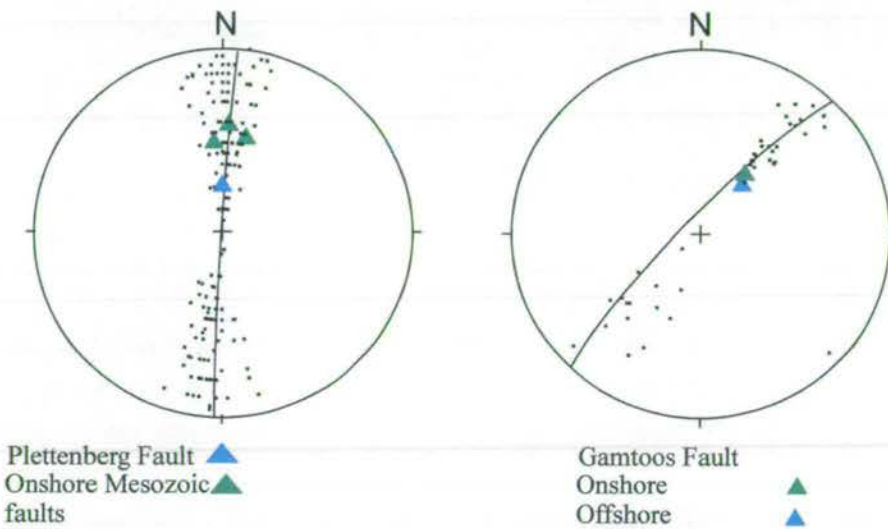


Figure 10.2: Stereonets to show the similarity in trend between basement trend and Mesozoic faults. a) The offshore Plettenberg Fault (Chapter 8), and the Central Cape Mesozoic faults and basement (dots), b) Gamtoos Basin with offshore and onshore fault portions, and basement structures (dots). Onshore data from Chapters 3 & 4. Data have been plotted on lower hemisphere projections, and π -girdles have been plotted.

Method	Result	Reference
Sandbox model	$\alpha > 41^\circ$ full reactivation	Faccenna <i>et al.</i> , 1995
	$32^\circ < \alpha < 41^\circ$ partial reactivation	
	$\alpha < 32^\circ$ no reactivation	
Field observations	$\sim 25^\circ$ no reactivation	Faccenna <i>et al.</i> , 1995
	37° - 40° reactivation	
	low angle thrust cross cut	Powell & Williams, 1989
	Steep reactivation	Ring, 1994

Table 10.1: Summary of negative inversion data from Chapter 2.

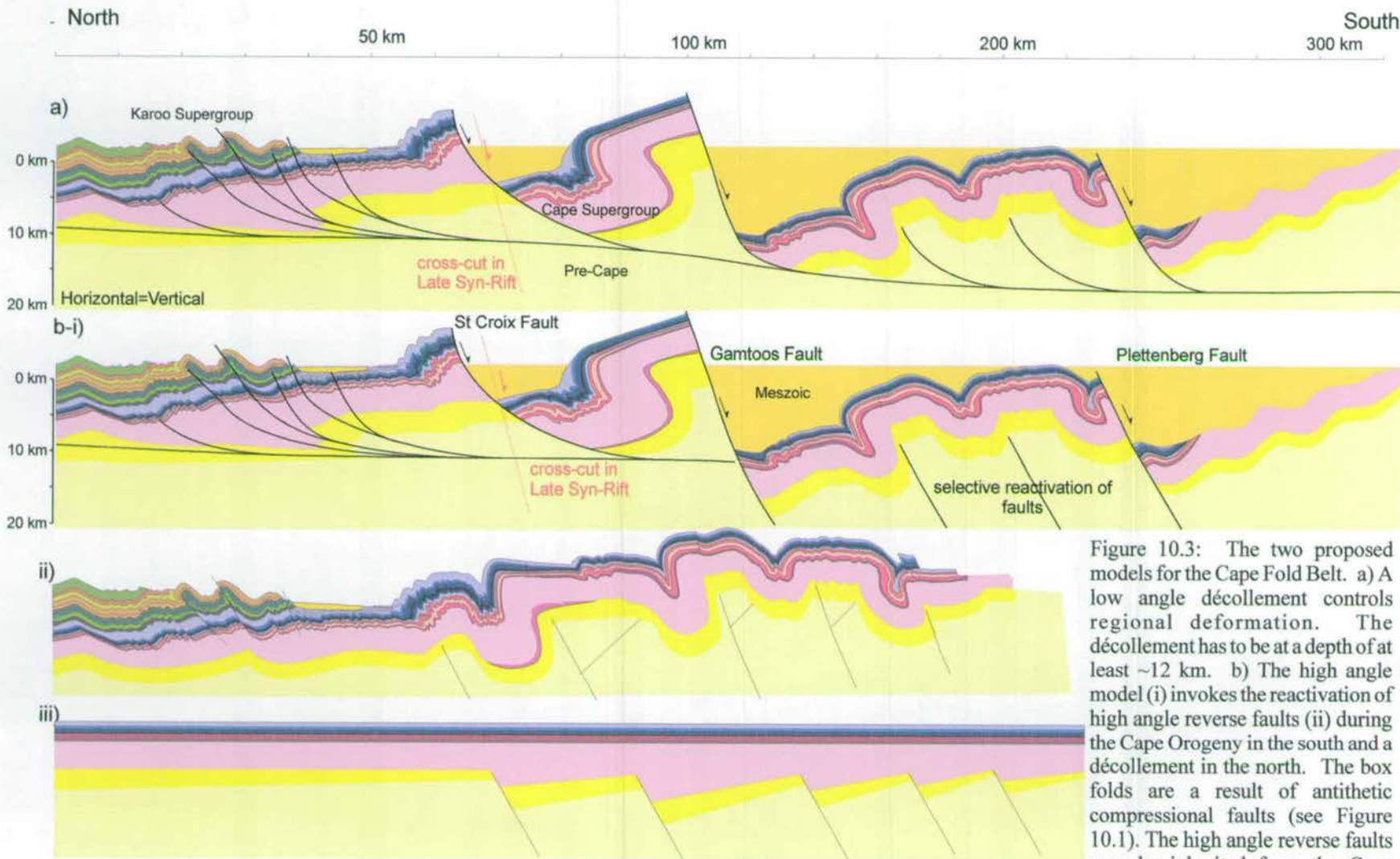


Figure 10.3: The two proposed models for the Cape Fold Belt. a) A low angle décollement controls regional deformation. The décollement has to be at a depth of at least ~12 km. b) The high angle model (i) invokes the reactivation of high angle reverse faults (ii) during the Cape Orogeny in the south and a décollement in the north. The box folds are a result of antithetic compressional faults (see Figure 10.1). The high angle reverse faults may be inherited from the Cape Supergroup passive margin (iii).

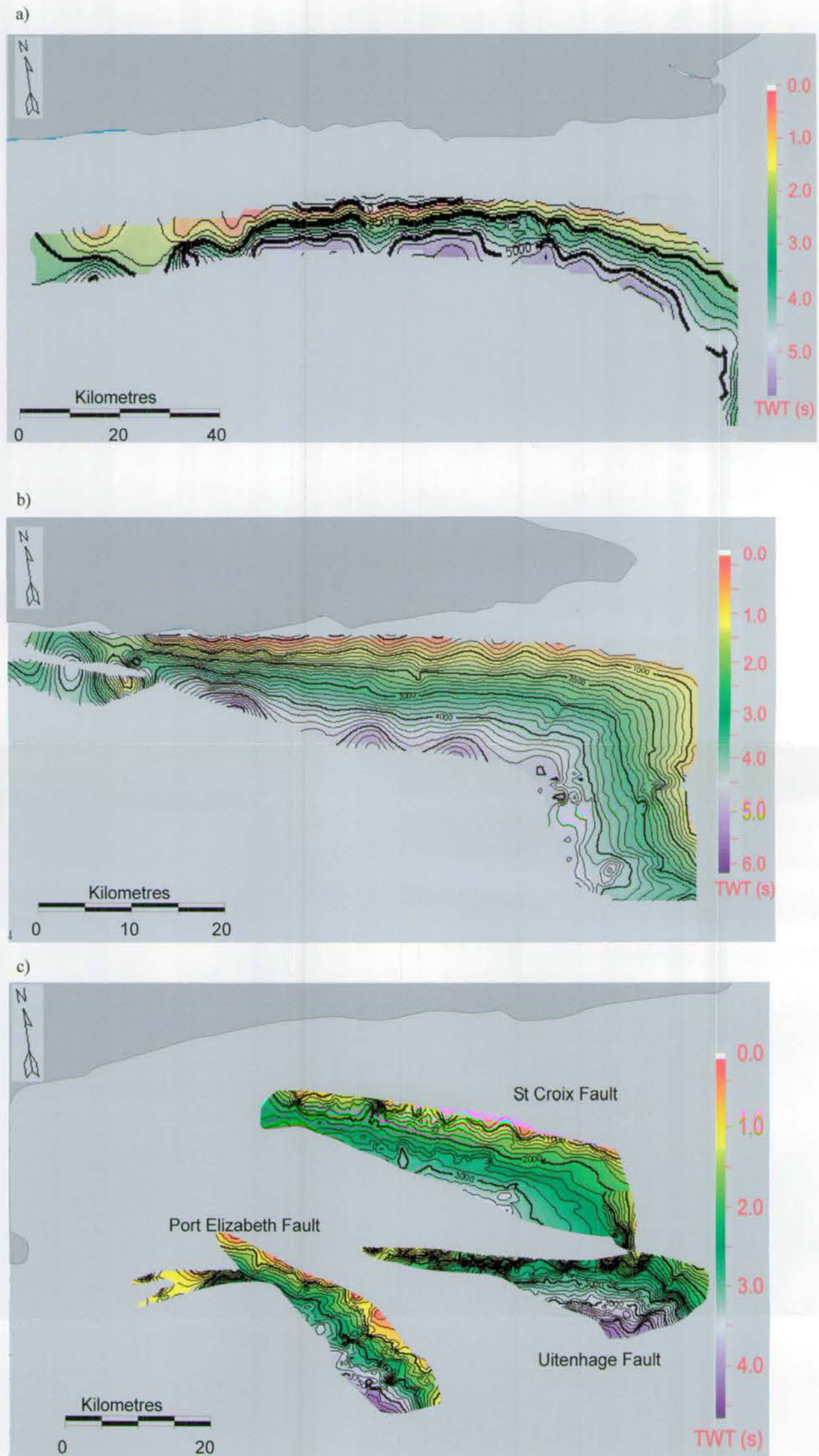


Figure 10.4: TWT plots to the fault planes of the a) Plettenberg Fault, b) Gamtoos Fault, c) Algoa Basin (i- St Croix, ii-Port Elizabeth, iii-Uitenhage Faults). There is no evidence of changes in strike, abandoned faults tips, see text for discussion.

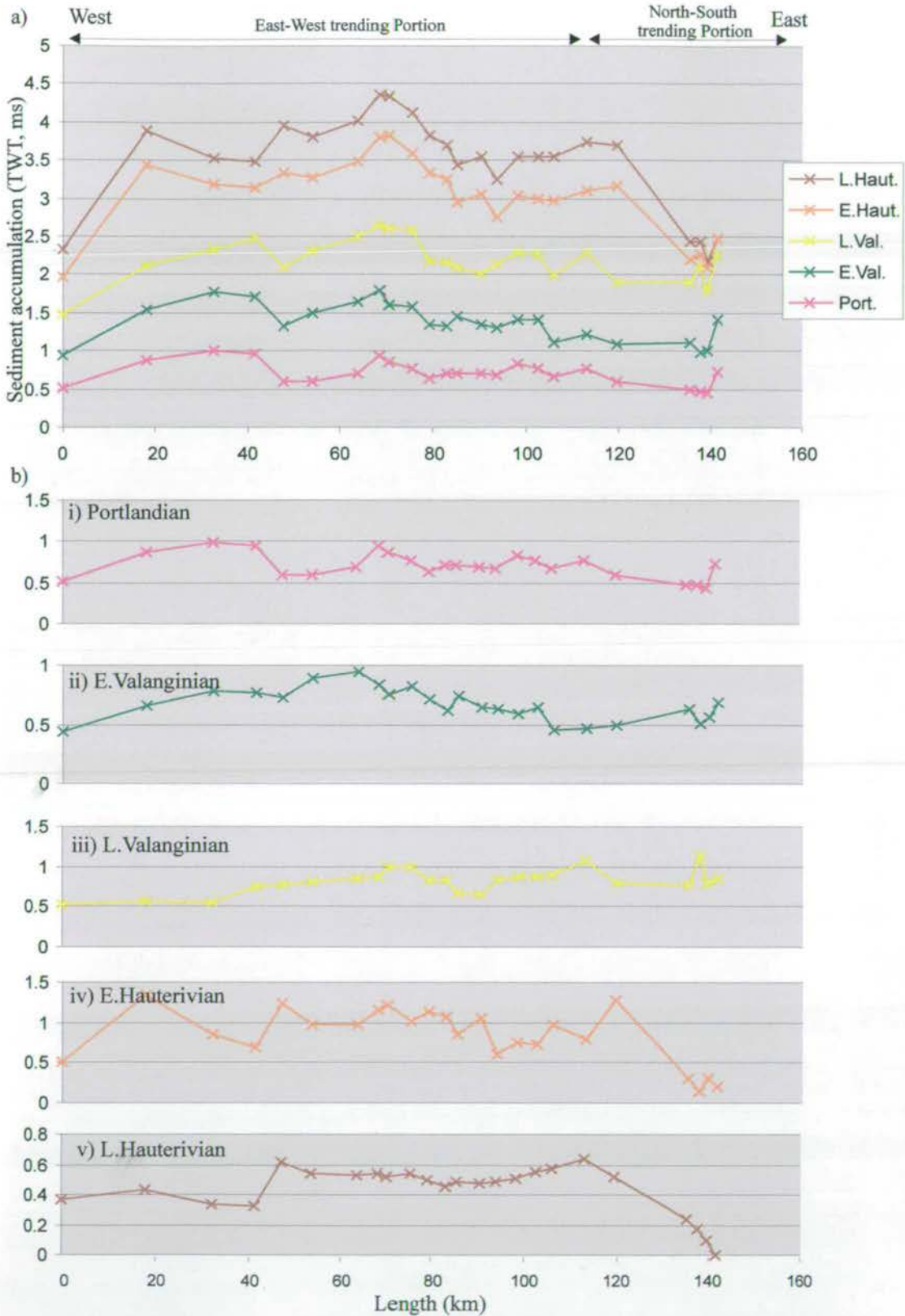


Figure 10.5: Sediment accumulation-length profiles along the Plettenberg Fault. a) Cumulative isochron from *top_basement*. b) Isochron plots for individual syn-rift sequences. See text for discussion.

Figure 10.6a

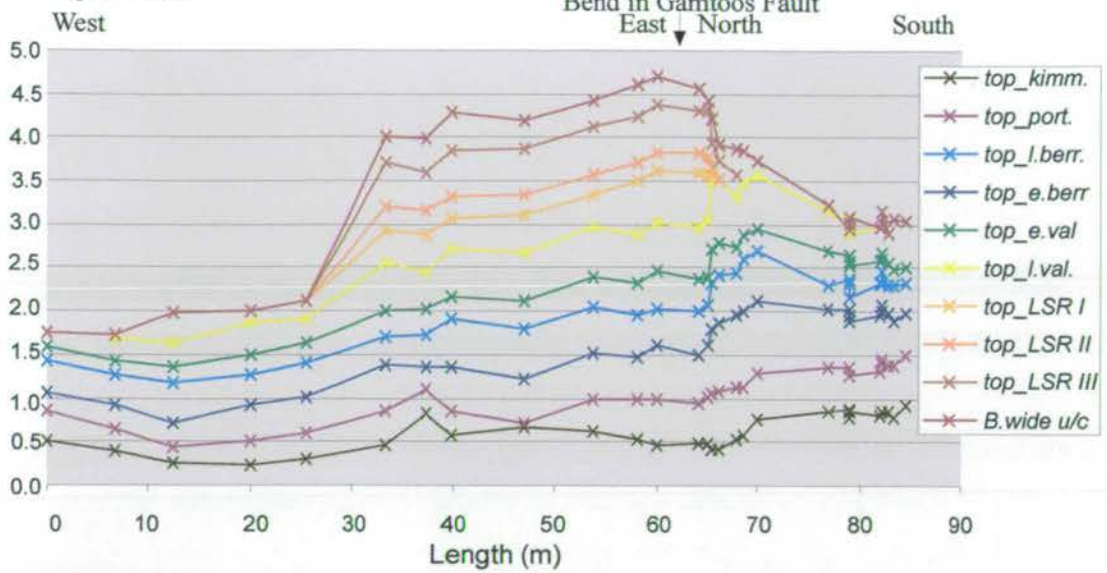
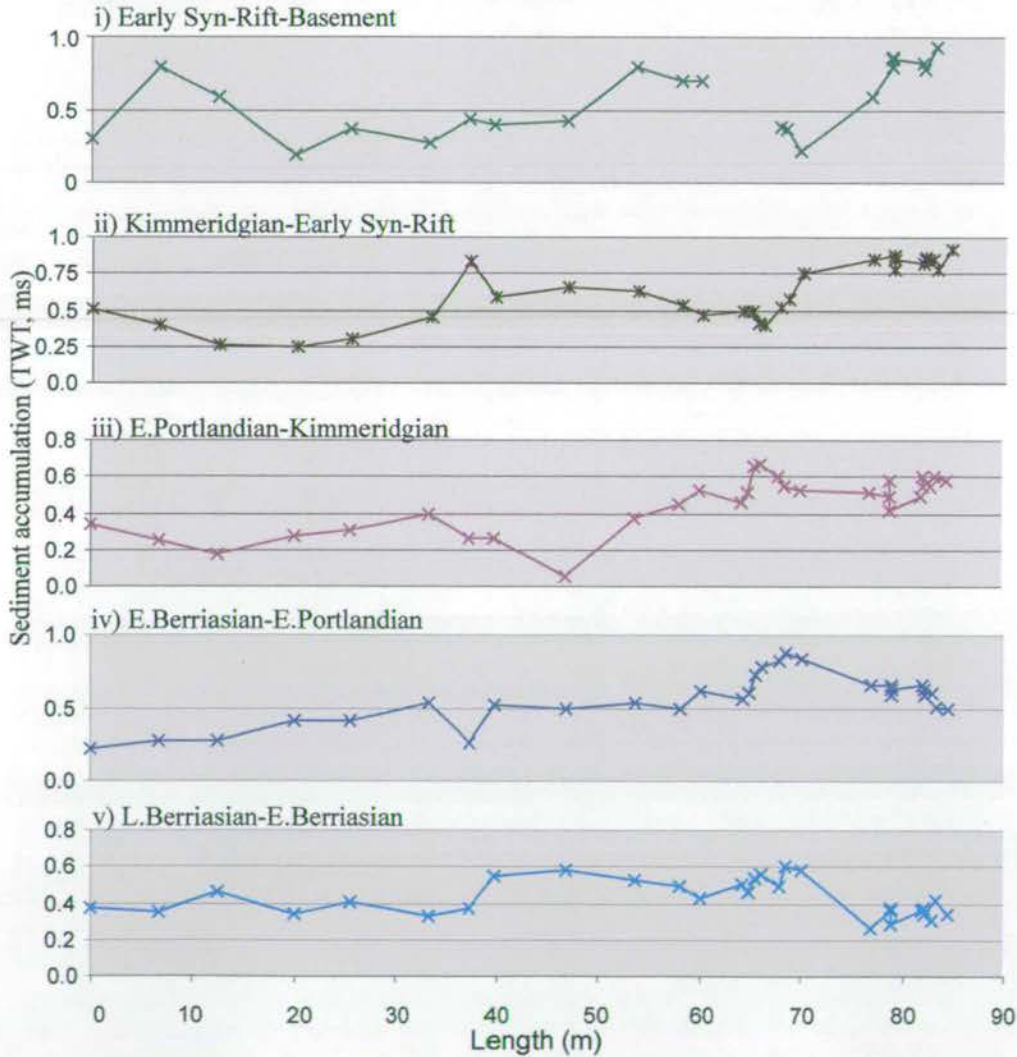


Figure 10.6b



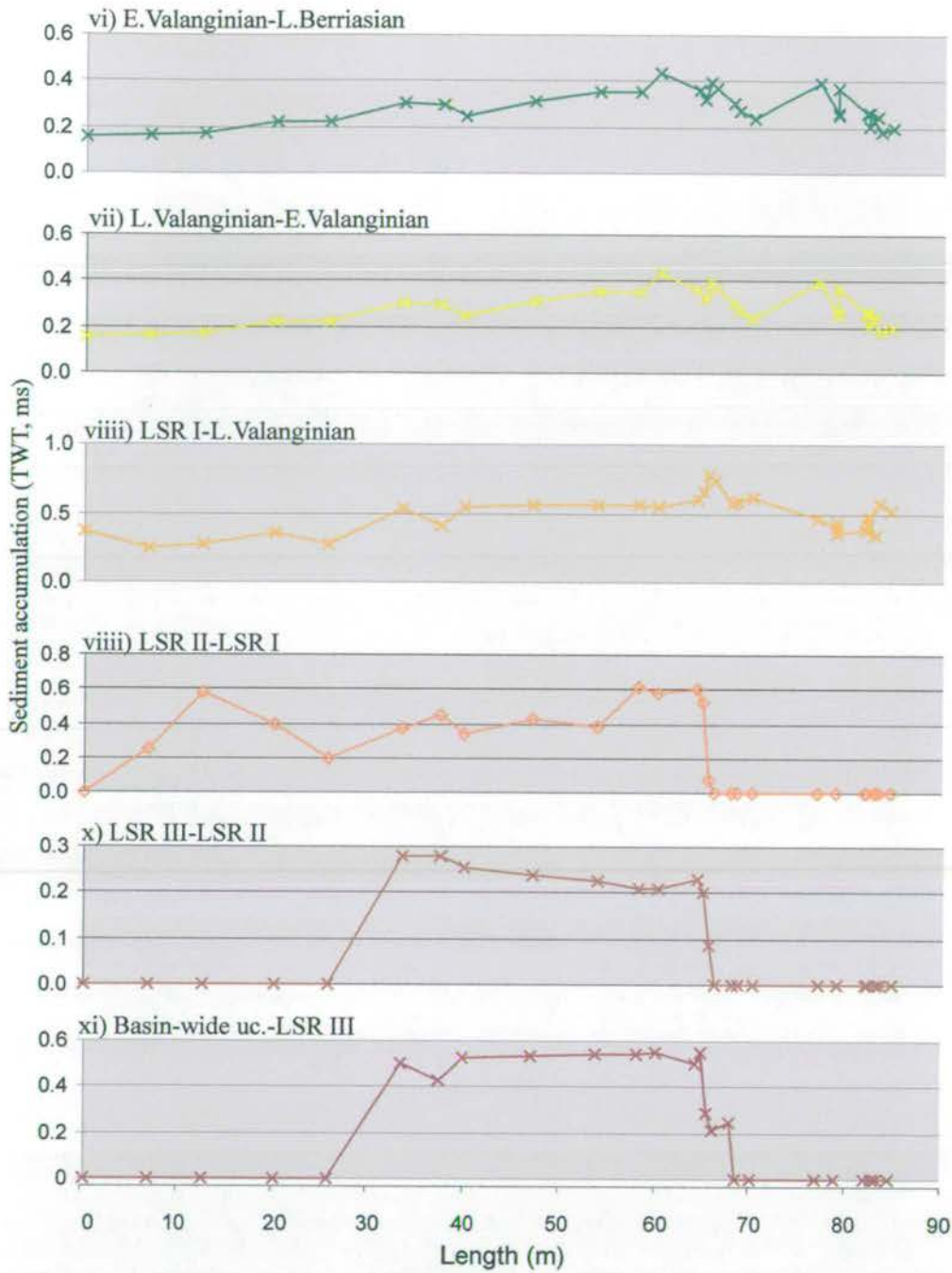


Figure 10.6: Sediment accumulation-length profiles along the Gamtoos Fault. a) Cumulative isochron from . b) Isochron plots of individual syn-rift sequences. Note the significant decrease in active fault length between the Late Valanginian and Latest Valanginian.

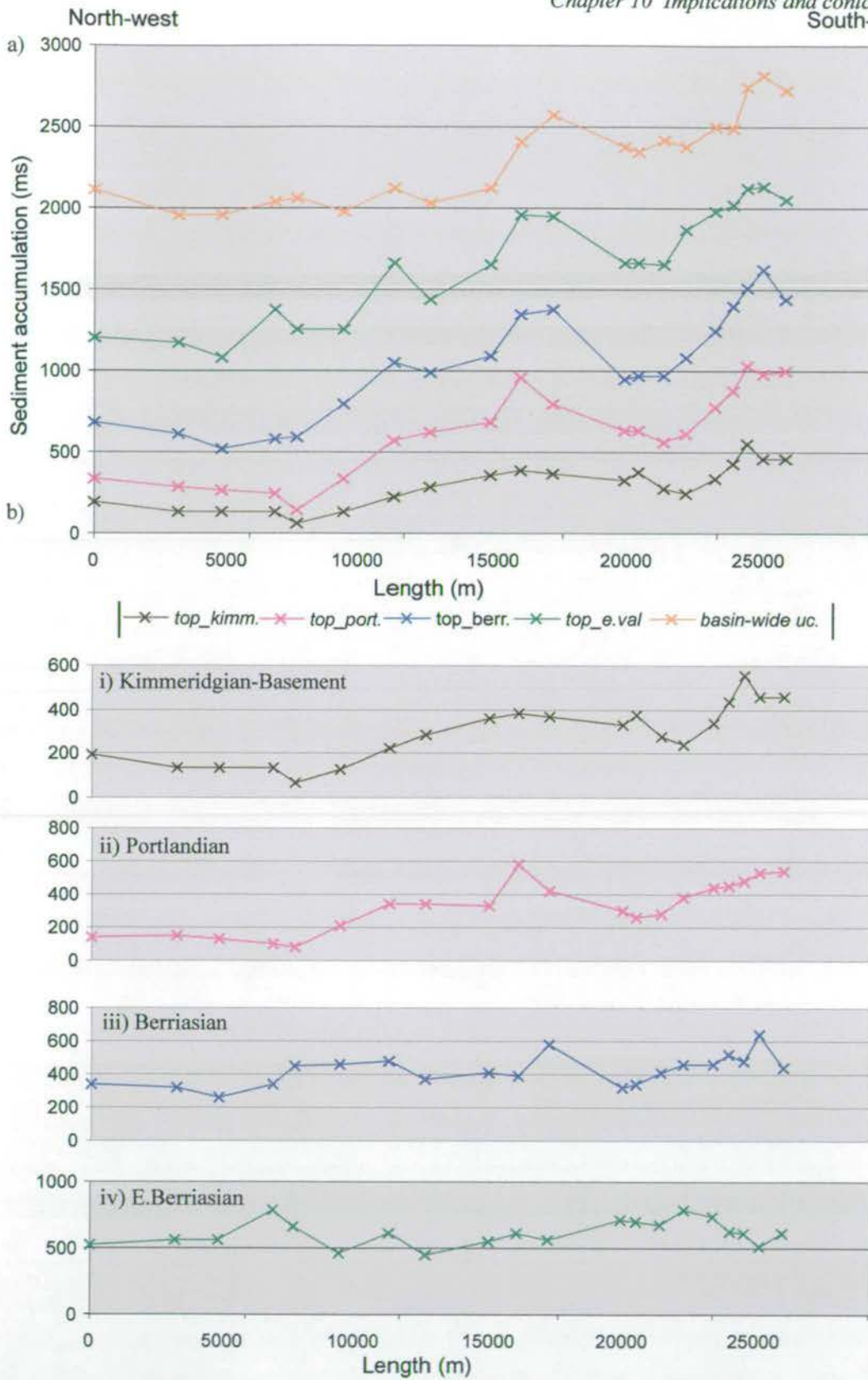


Figure 10.7: Sediment accumulation-length profiles along the Port Elizabeth Fault. a) Cumulative isochron from *top_basement*. b) Isochron plots of individual syn-rift sequences.

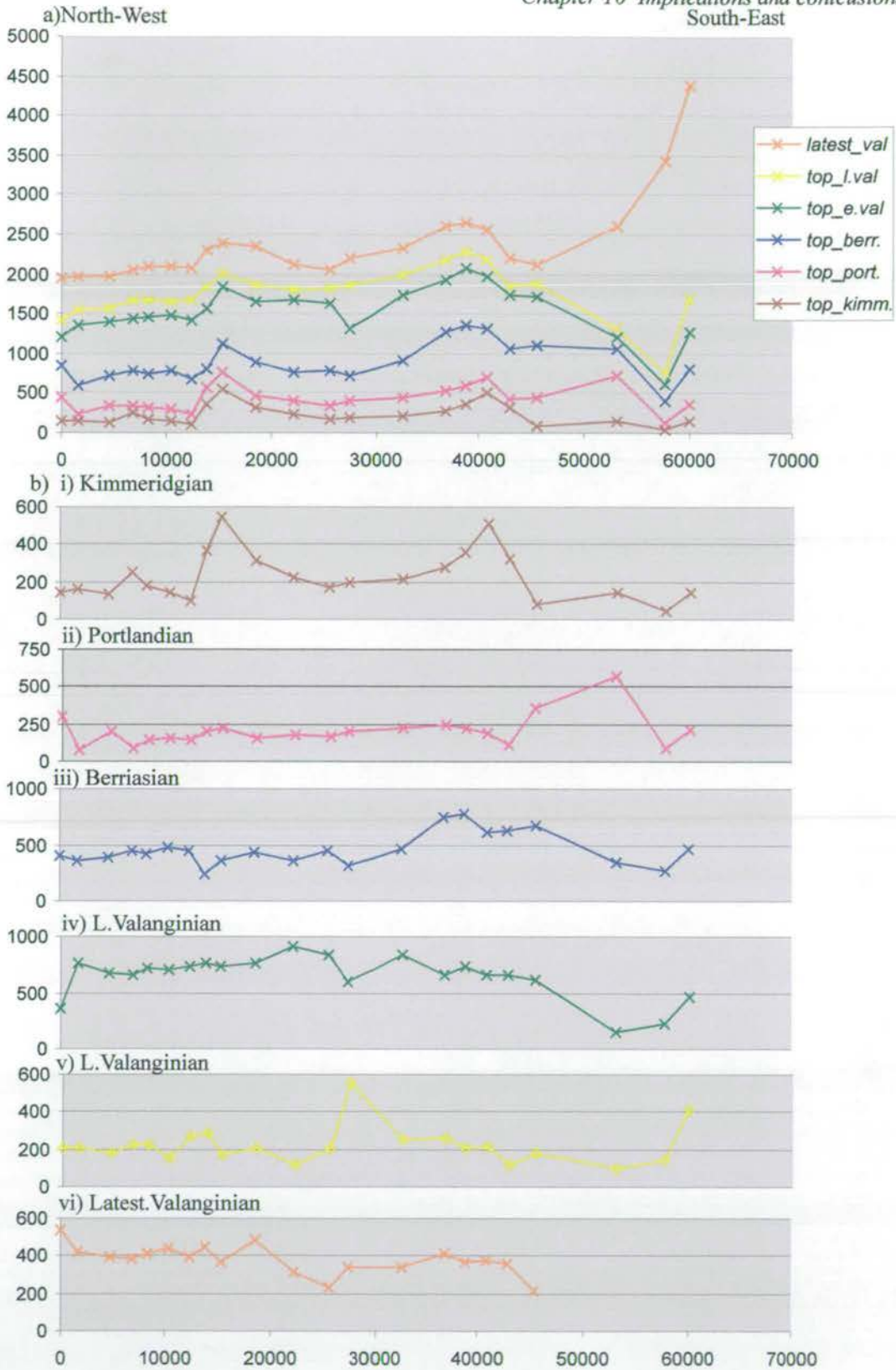


Figure 10.8: Sediment accumulation-length profiles along the St Croix Fault. a) Cumulative isochron from *top_basement*. b) Isochron plots of individual syn-rift sequences.

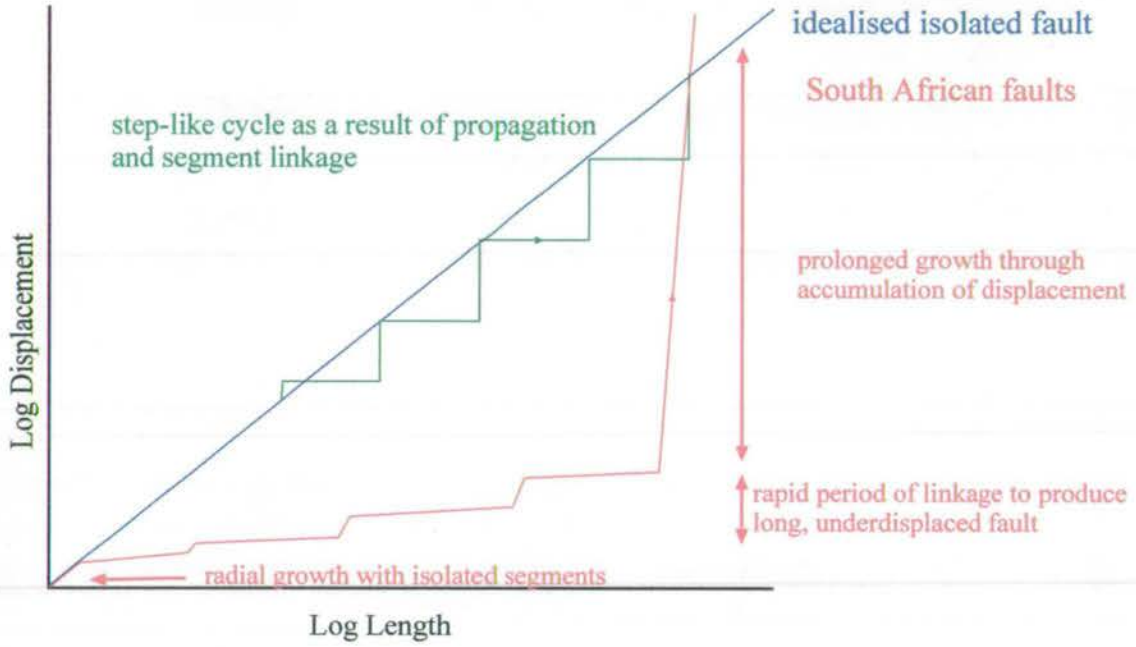


Figure 10.10: Schematic Displacement-Length plot illustrating showing idealised growth by an idealised isolated fault, step-like cycle of linkage, and growth line for the South African faults which have fault lengths established in the very early syn-rift (after Cartwright *et al.*, 1996).

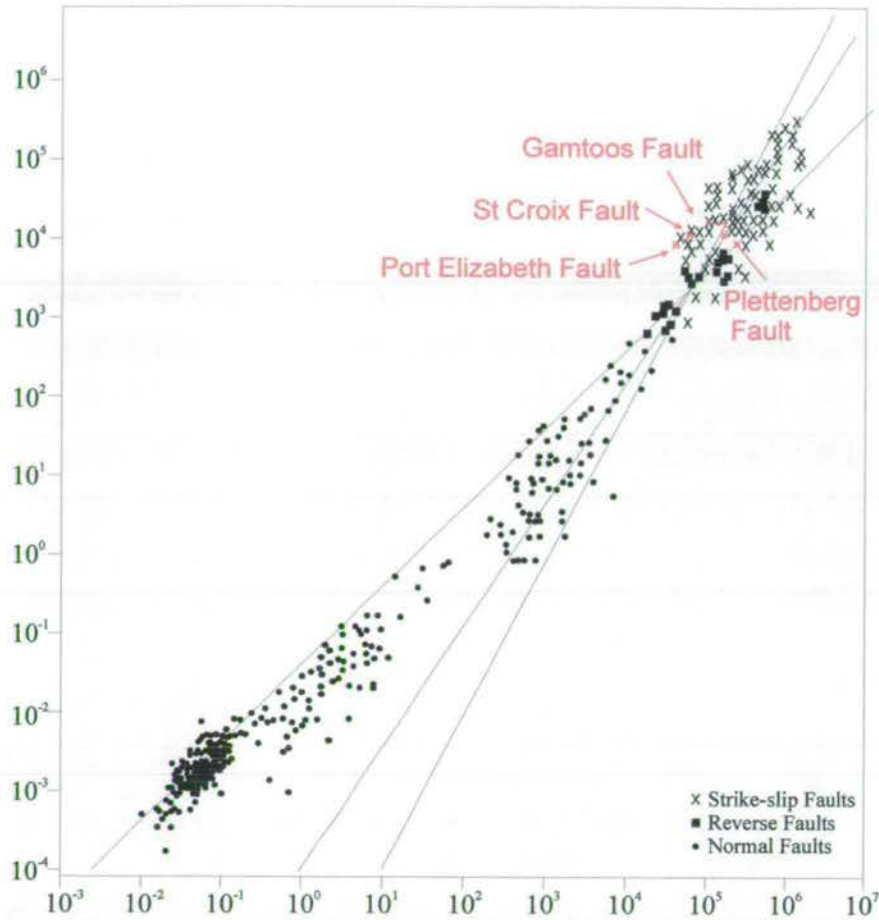


Figure 10.11: Displacement-length plot with global data set for normal, thrust and strike-slip faults plotted (from Schlische *et al.*, 1996). The data for this study have also been plotted and have significantly larger values for both displacement and length compared to other normal faults.

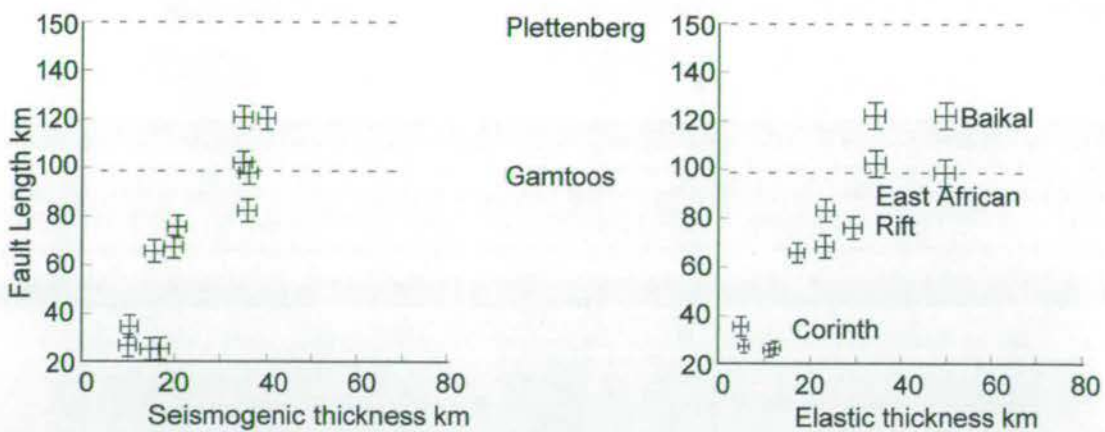


Figure 10.12: Comparison of fault length and a) seismicogenic layer thickness (T_{seis}), and b) effective elastic thickness (T_e). Ebinger *et al.* (1999) infer a linear increase of length with an increase in T_{seis} and T_e . The lengths of the Plettenberg and Gamtoos (offshore only) Faults have been plotted and illustrate that the South African faults are large even compared to Baikal and the East African Rift.

LIST OF APPENDICES – VOLUME 1

APPENDIX A Gamtoos Basin well data

A-i	List of available data	ii
A-ii	Depth-time conversion graphs	ii-iii
A-iii	Depth (ms TWT) converted time top data	iv-v
A-iv	Compilation of available well data for individual wells (Ha-A1, Ha-B2, Ha-F1, Ha-G1, Ha-H1, Ha-I1, Ha-J1, Ha-K1, Ha-N1)	vi-xv

APPENDIX B Pletmos Basin well data

B-i	List of available data	xvi
B-ii	Depth-time conversion graphs	xvi-xix
B-iii	Depth (ms TWT) converted time top data	xx-xxiii

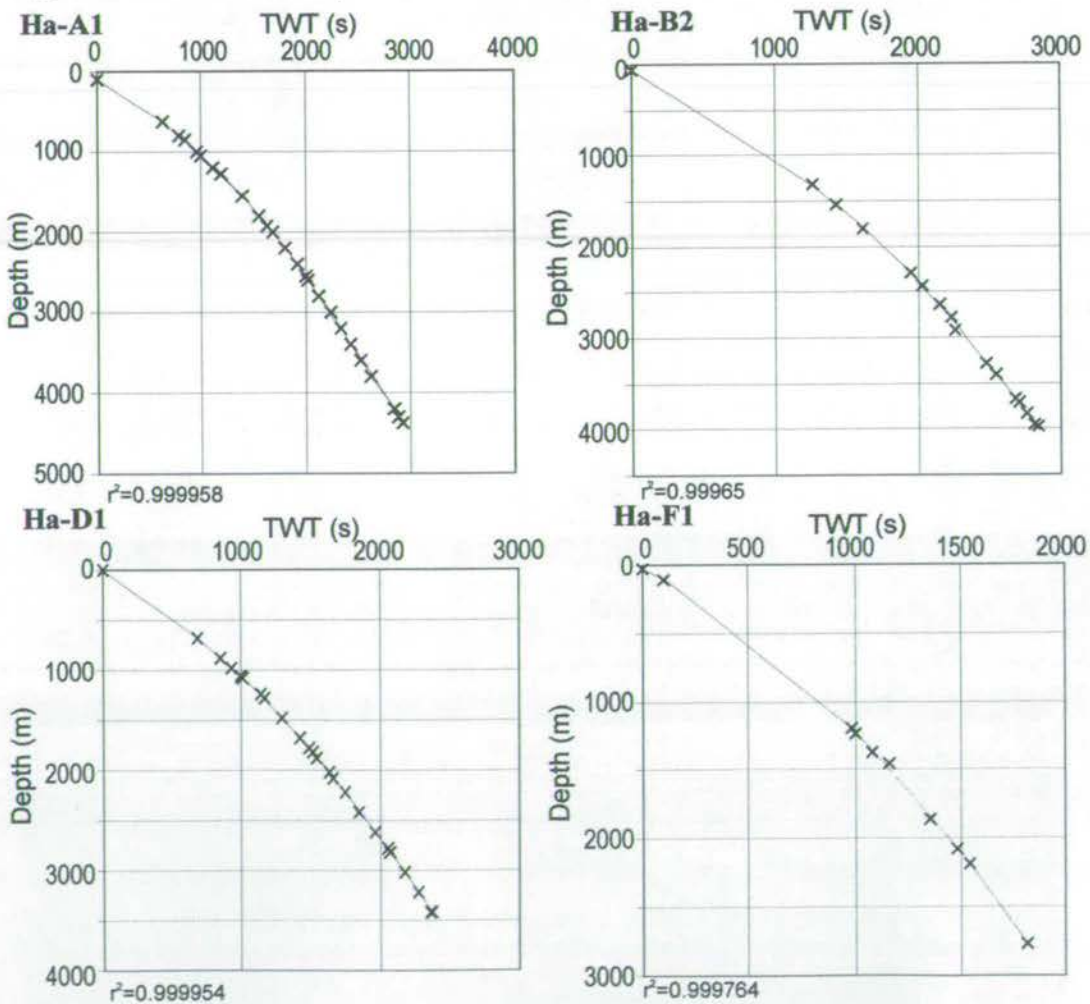
APPENDIX C Algoa Basin well data

C-i	List of available data	xxiv
C-ii	Depth-time conversion graphs	xxiv-xxv
C-iii	Depth (ms TWT) converted time top data	xxvi-xxvii
C-iv	Compilation of available well data for individual wells (Hb-B1, Hb-C1, Hb-D1, Hb-G1, Hb-Hart, Hb-I1, Hb-K1, Hb-P1)	xxviii-xxxv

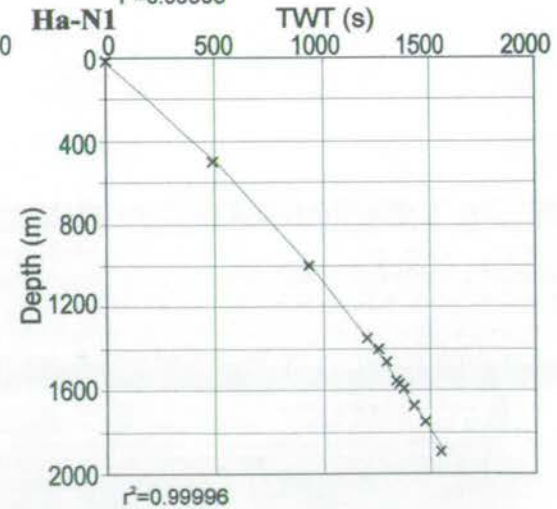
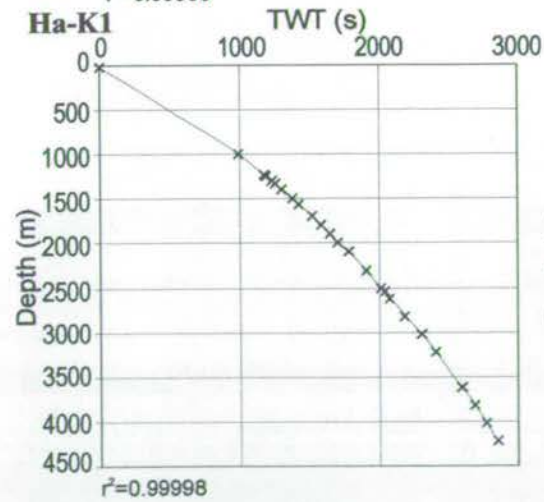
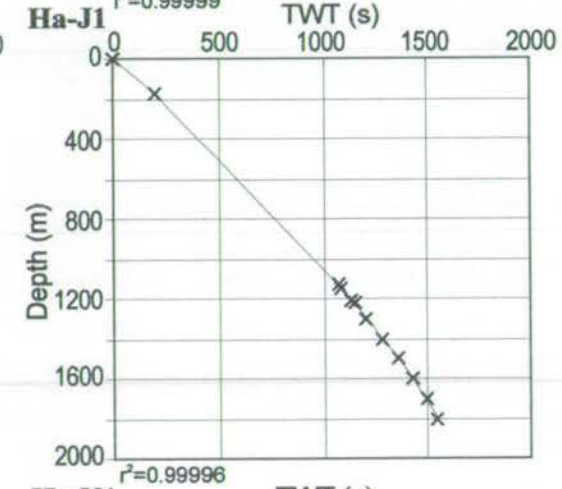
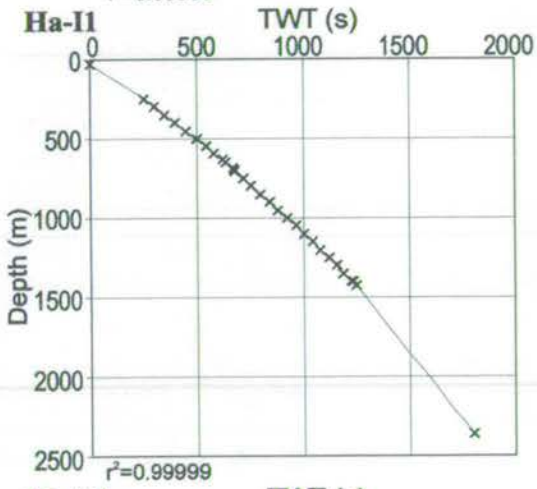
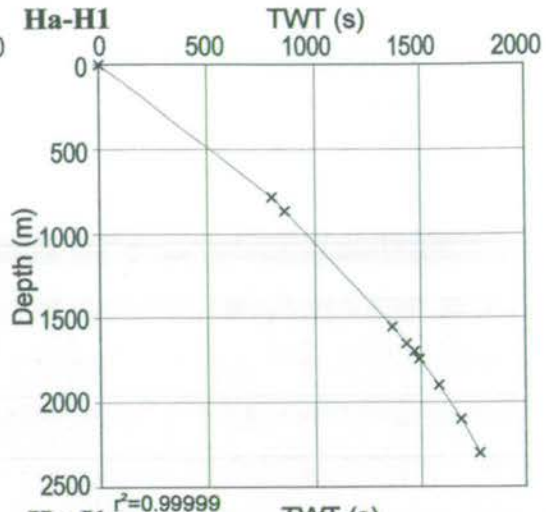
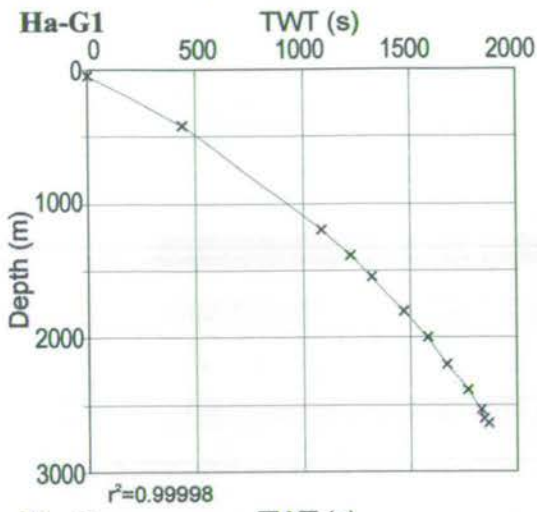
Appendix A-i: Available well data for the Gamtoos Basin

Well Name	Composite	Lithofacies	Palynology	Synthetic	Time top
Ha-A1	Yes	Yes	Yes	Yes	Yes
Ha-B2	Yes	Yes	Yes	Yes	Yes
Ha-D1	Yes	Yes	Yes	Yes	Yes
Ha-F1	Yes	No	Yes	Yes	Yes
Ha-G1	Yes	Yes	Yes	Yes	Yes
Ha-H1	Yes	Yes	Yes	Yes	Yes
Ha-I1	Yes	Yes	Yes	Yes	No
Ha-J1	Yes	Yes	Yes	Yes	Yes
Ha-K1	Yes	Yes	Yes	Yes	Yes
Ha-N1	Yes	No	Yes	Yes	Yes

Appendix A-ii: Time-depth conversion graphs for the Gamtoos Basin



Appendix A-ii (continued)



Appendix A-ii: Depth-time data plotted (with appropriate r^2 values) for each of the wells in the Gamtoos Basin. Regression line were obtained from Table Curve 3.0 plotting programme.

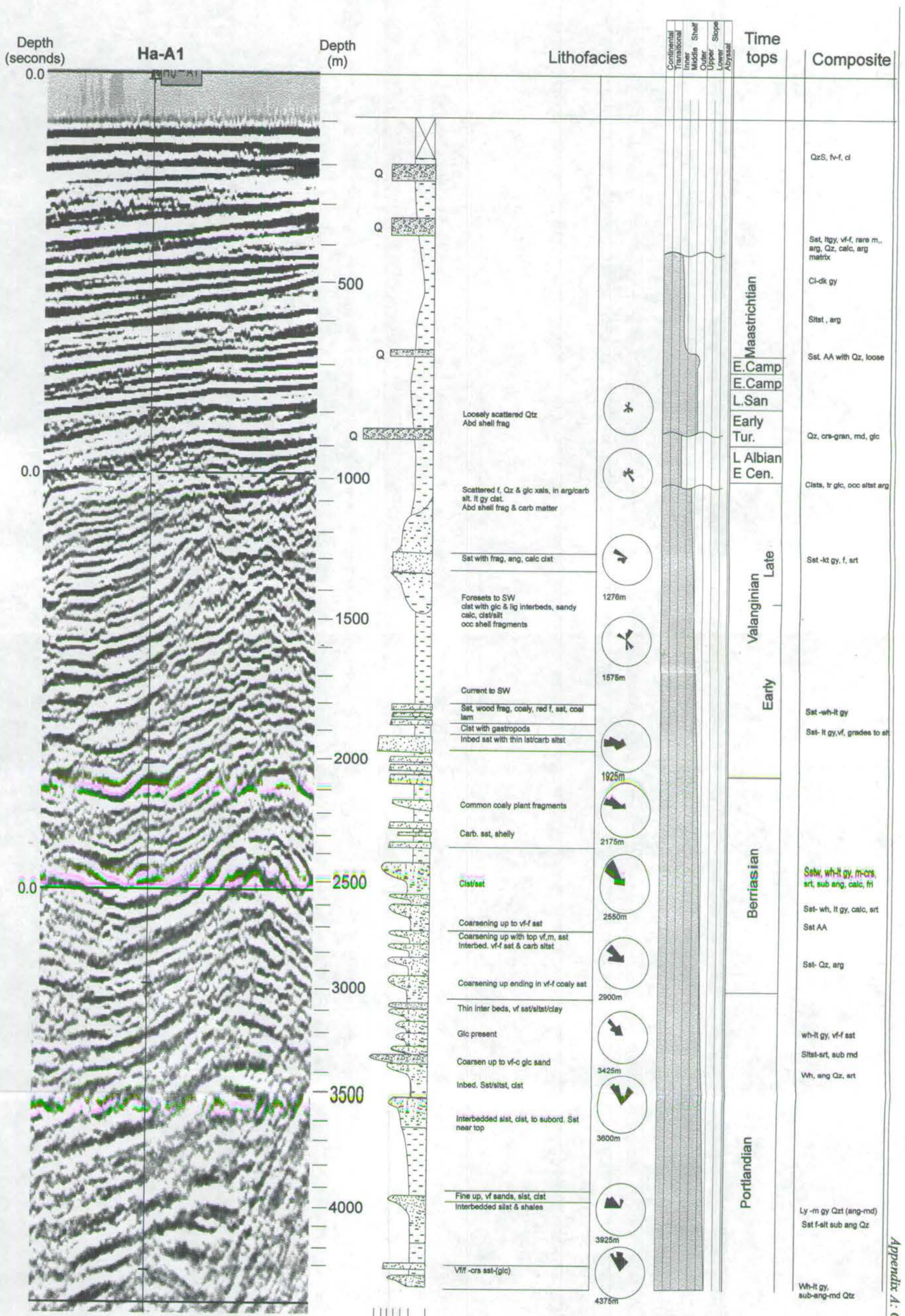
Appendix A-iii: Time-depth converted age-depth data for the Gamtoos Basin

		HA-A1		Ha-B2		HA-D1		HA-F1		Ha-G1
		Z(m)	TWT	Z(m)	TWT	Z(m)	TWT	Z(m)	TWT	Z(m)
Holocene										
Pleistocene	Late									
	Early									
Pliocene										
Miocene	Late									
	Early									
Oligocene	Late									
	Early									
Eocene	Late	185	198	240	239					201
	Mid	360	376	460	461					333
	Early	440	455							
Palaeocene						340	332			370
Maastrichtian		460	475	545	547	380	351			420
Campanian	Late	510	523	690	690	500	482			530
	Early	690	691	760	758					550
Santonian	Late	730	728	820	816					
	Early	790	781	910	901					
Coniacian	Late									
	L. Early									
	E. Early									
Turonian	Late									
	Mid									
	L. Early									600
	E. Early	860	843	980	966					
Cenomanian	Late									
	Early									
Albian	Late	950	920	1100	1074					
	Early	1000	962	1130	1101					810
Aptian	Late									
	L. Early									
	E. Early									
Barremian	Late									
	Early									
Hauterivian	Late					550	560	153	153	
	Early									
Valanginian	Latest					1108	1646	1995	1444	
	Late	1050	1004	1160	1127	1230	1646	2197	1547	
	Early	1438	1306	1550	1445	1665	1577			1100
Berriasian		2068	1726	1890	1689	2899	2232			1435
Portlandian		3010	2229	2828	2241					
Kimmeridgian										
Basement										2542
Bottom of Log		4374	2921	3983	2839	3412	2490	2775	1819	2640

Depth (Z(m)) to top of age horizons (McMillan, 1999) have been converted to time (TWT, ms) using equations obtained from linear regression lines for individual wells (cf. Appendix A-ii).

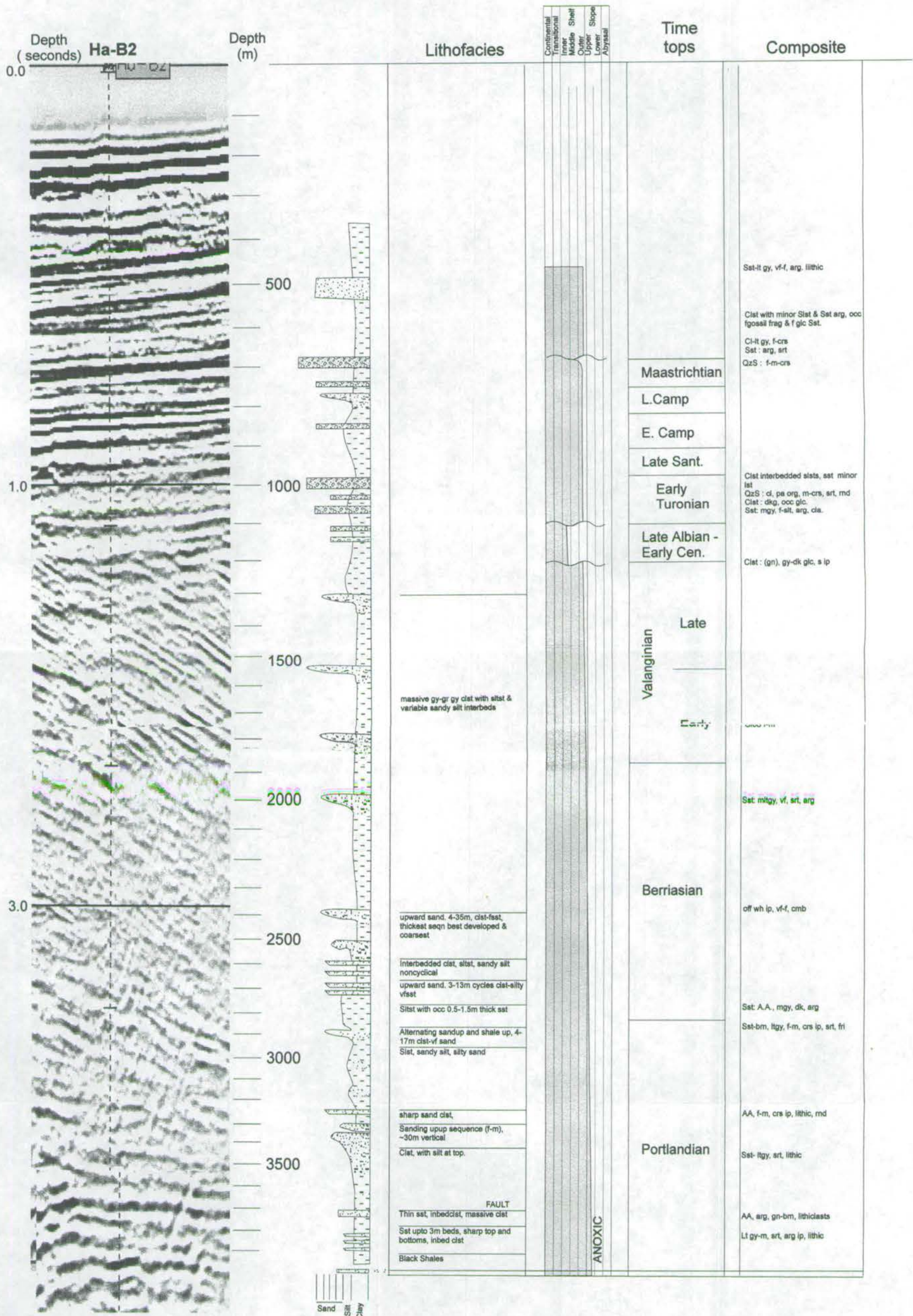
Appendix A-iii (continued)

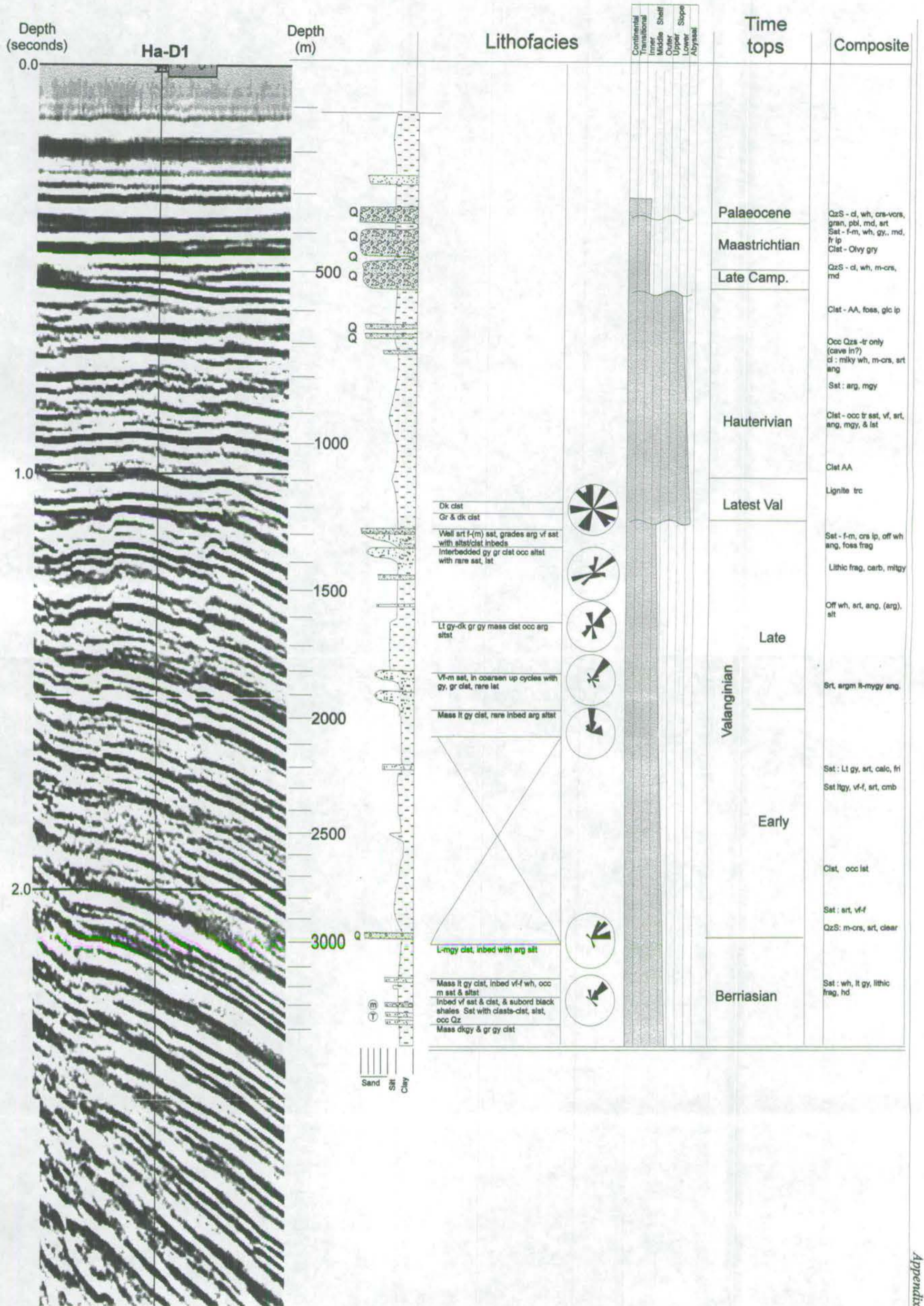
	Ha-G1		Ha-H1		Ha-J1		Ha-K1		Ha-N1
	Z(m)	TWT	Z(m)	TWT	Z(m)	TWT	Z(m)	TWT	Z(m)
Holocene									
Pleistocene									
Pliocene									
Miocene									
Oligocene									
					350	357	370	449	
Eocene	201	227	360	443	450	448	480	557	
	333	363							
Palaeocene	370	400	390	472	510	504	540	613	328
Maastrichtian	420	449	540	606	670	652	680	738	350
Campanian	530	552	640	689	710	690	760	806	460
	550	570			740	718	820	856	490
Santonian							880	905	
Conacian									
Turonian									
	600	615	700	736	810	783	980	985	500
Cenomanian									
			800	814					
Albian			830	837					
	810	793					1200	1156	
Aptian									
Barremian									
					990	946			
Hauterivian									620
					1185	1115			
Valanginian									1510
			860	860	1215	1140			1585
	1100	1016	1030	988	1335	1236	1560	1419	1875
Berriasian	1435	1247	1230	1137	1475	1340	1620	1461	2227
Portlandian			1657	1440			2519	2021	
Kimmeridgian			1996	1643	1673	1475	3797	2674	
Basement	2542	1829	2348	1801	1711	1499			

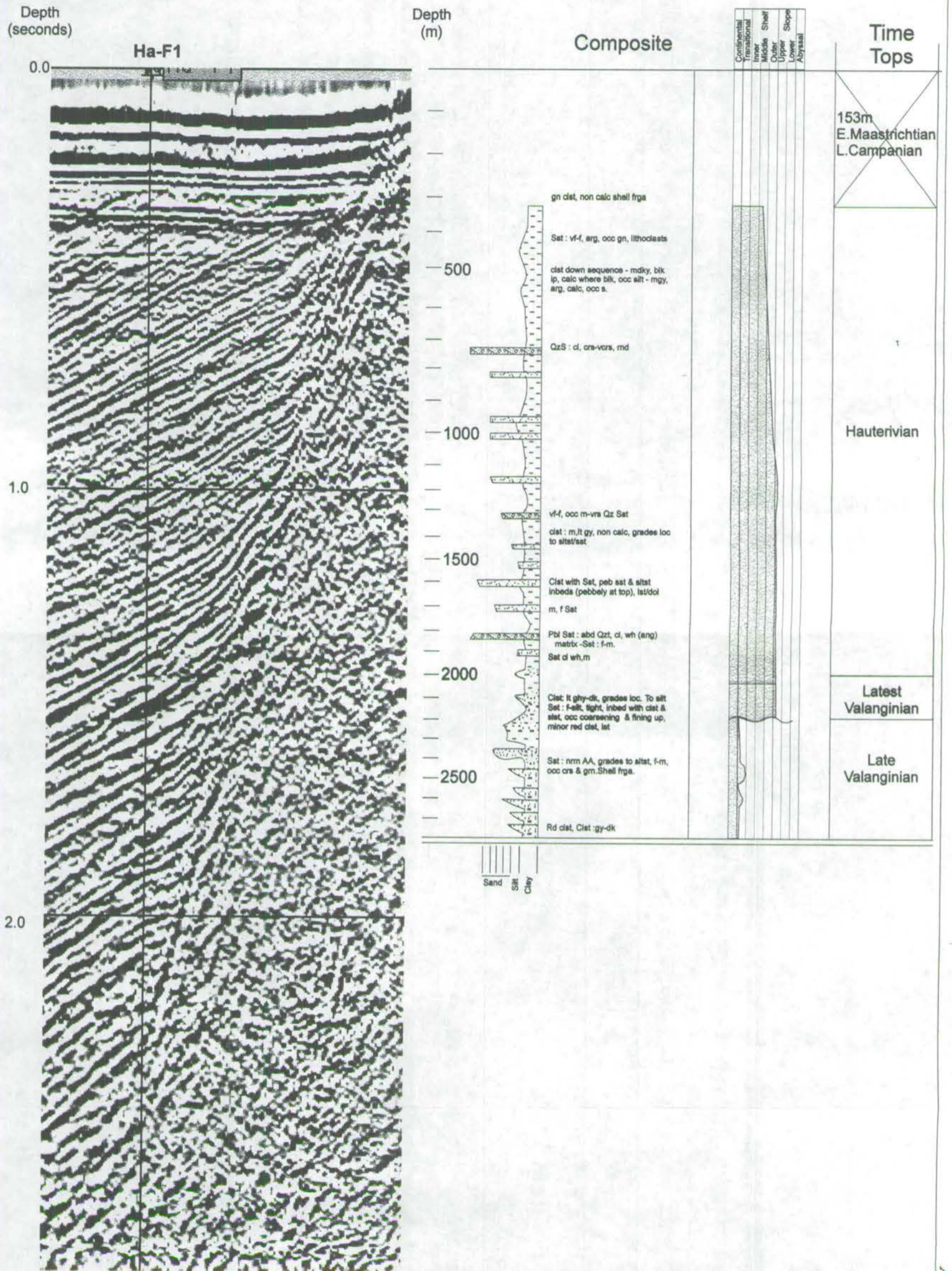


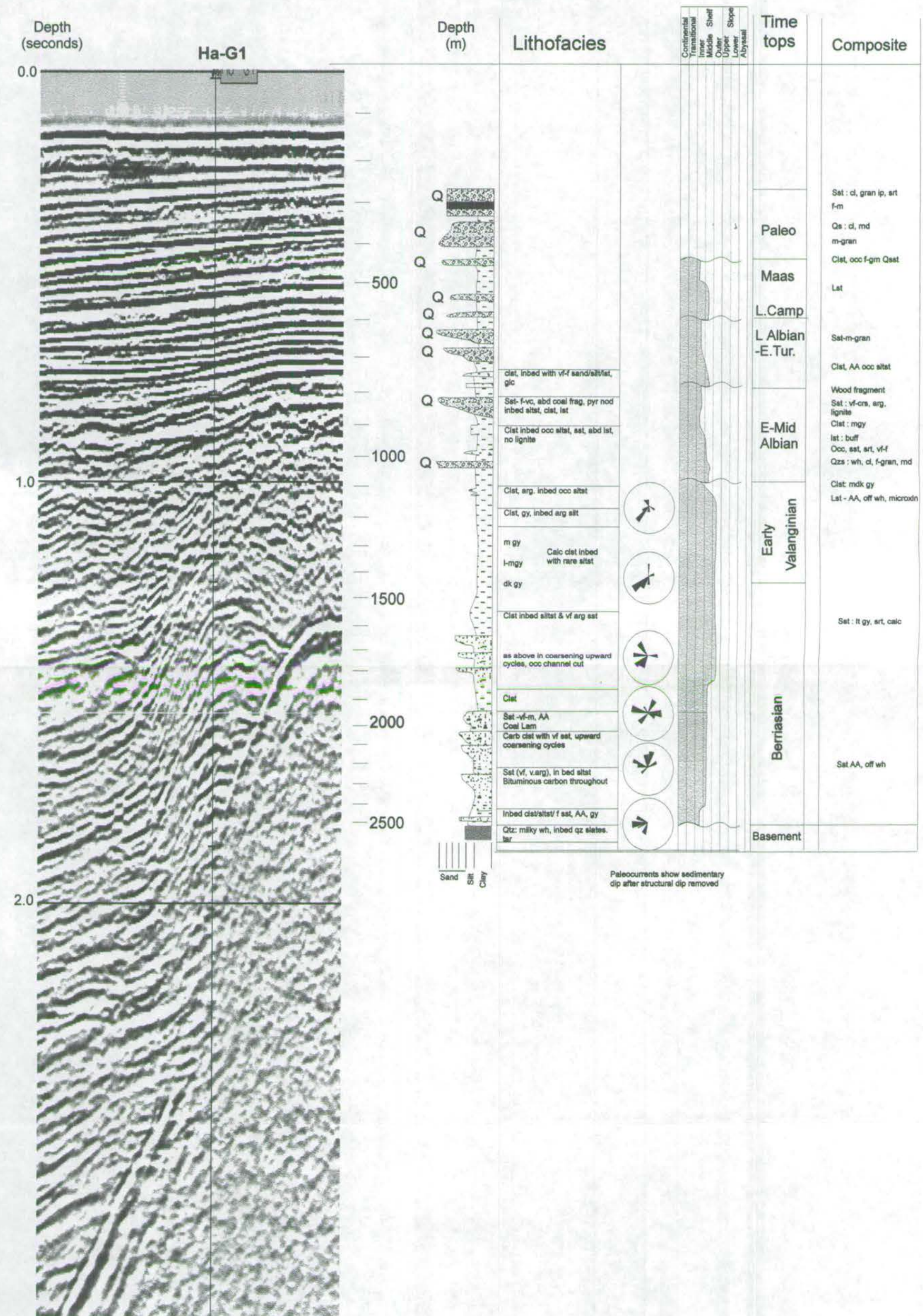
Well Ha-A1 vi

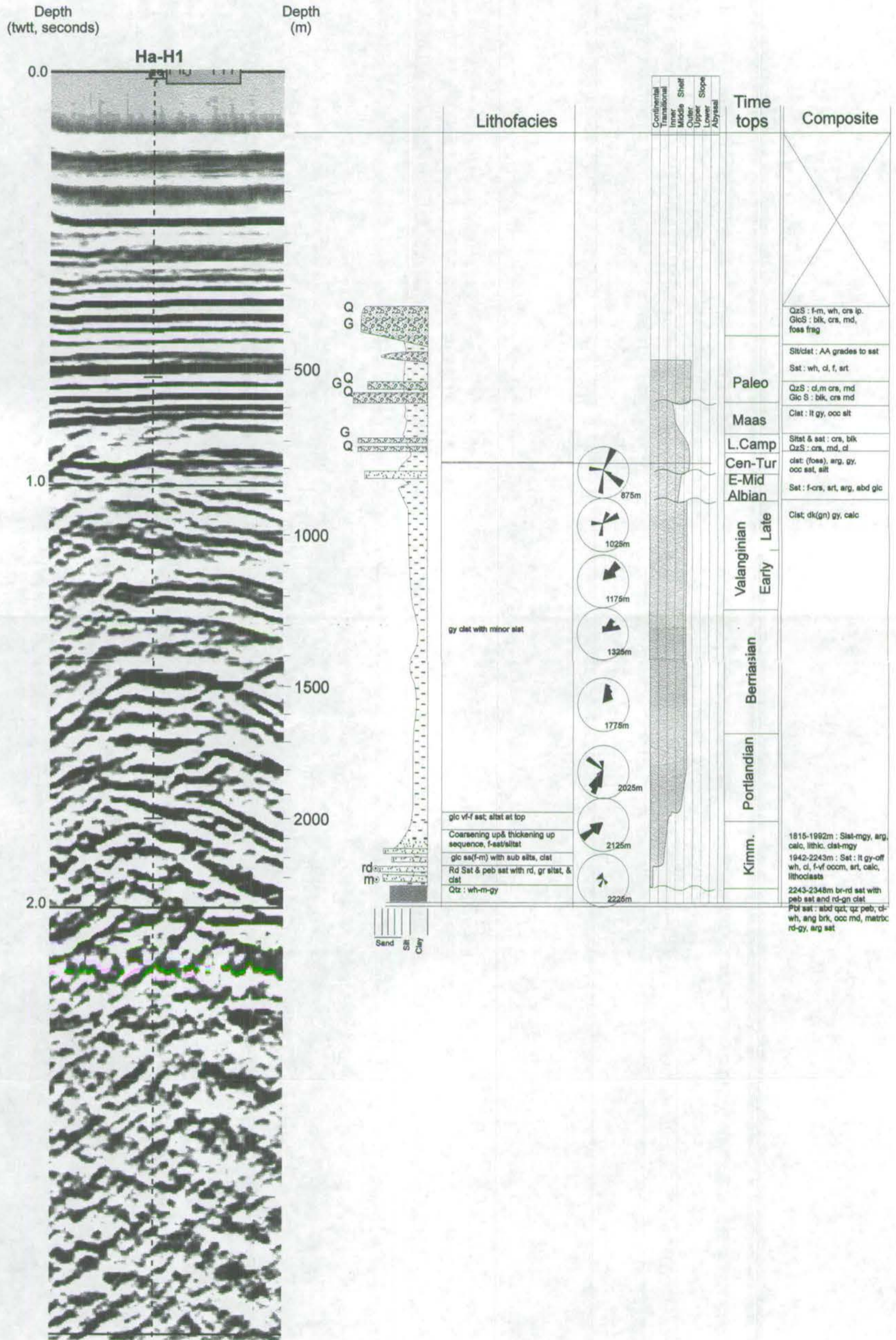
Appendix A: Gamtoos Basin well data

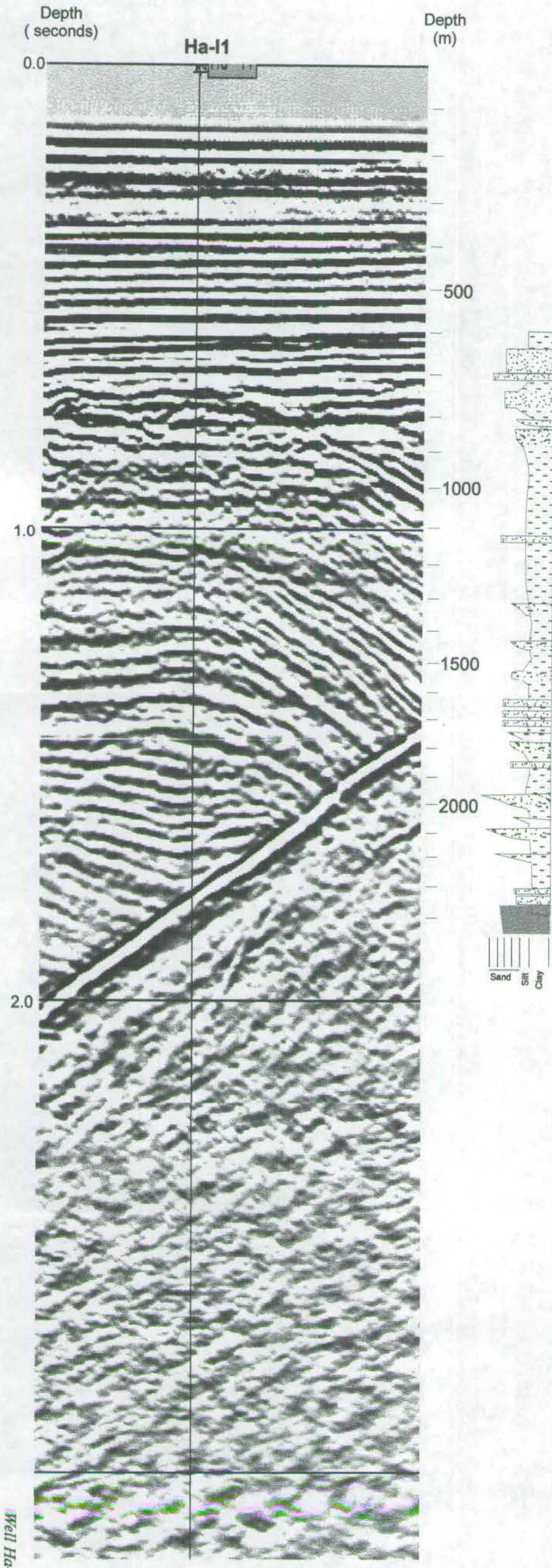






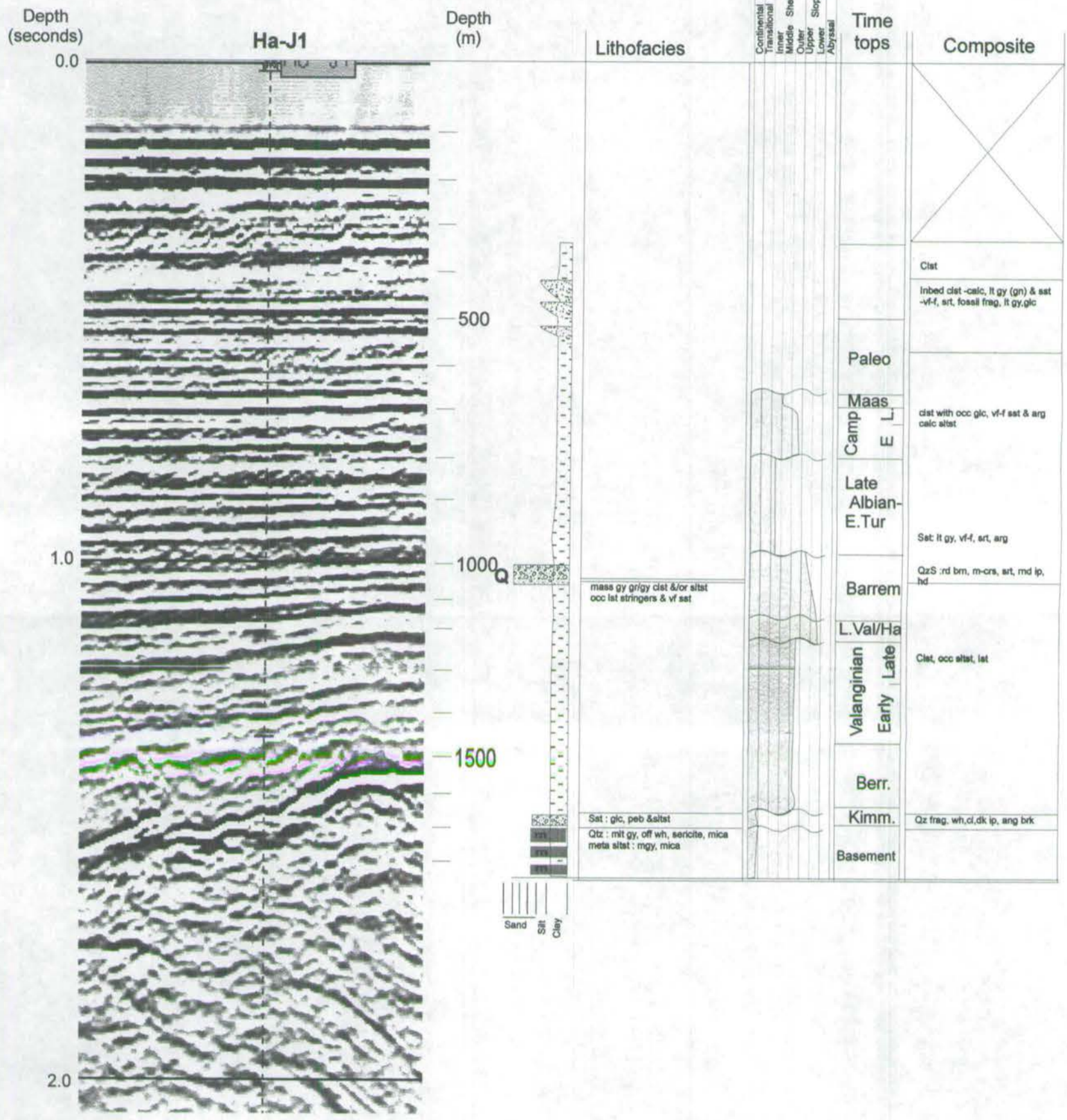


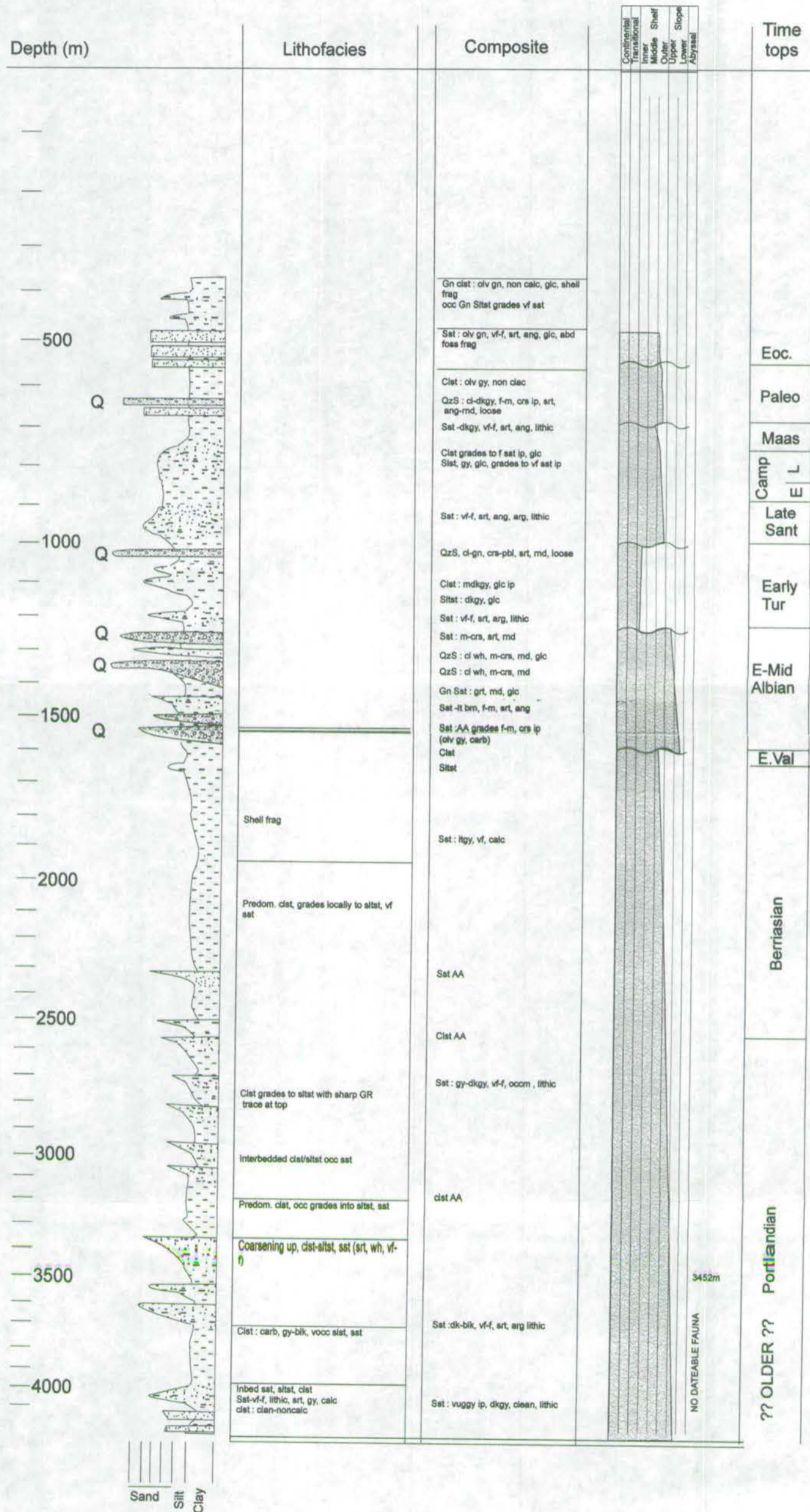




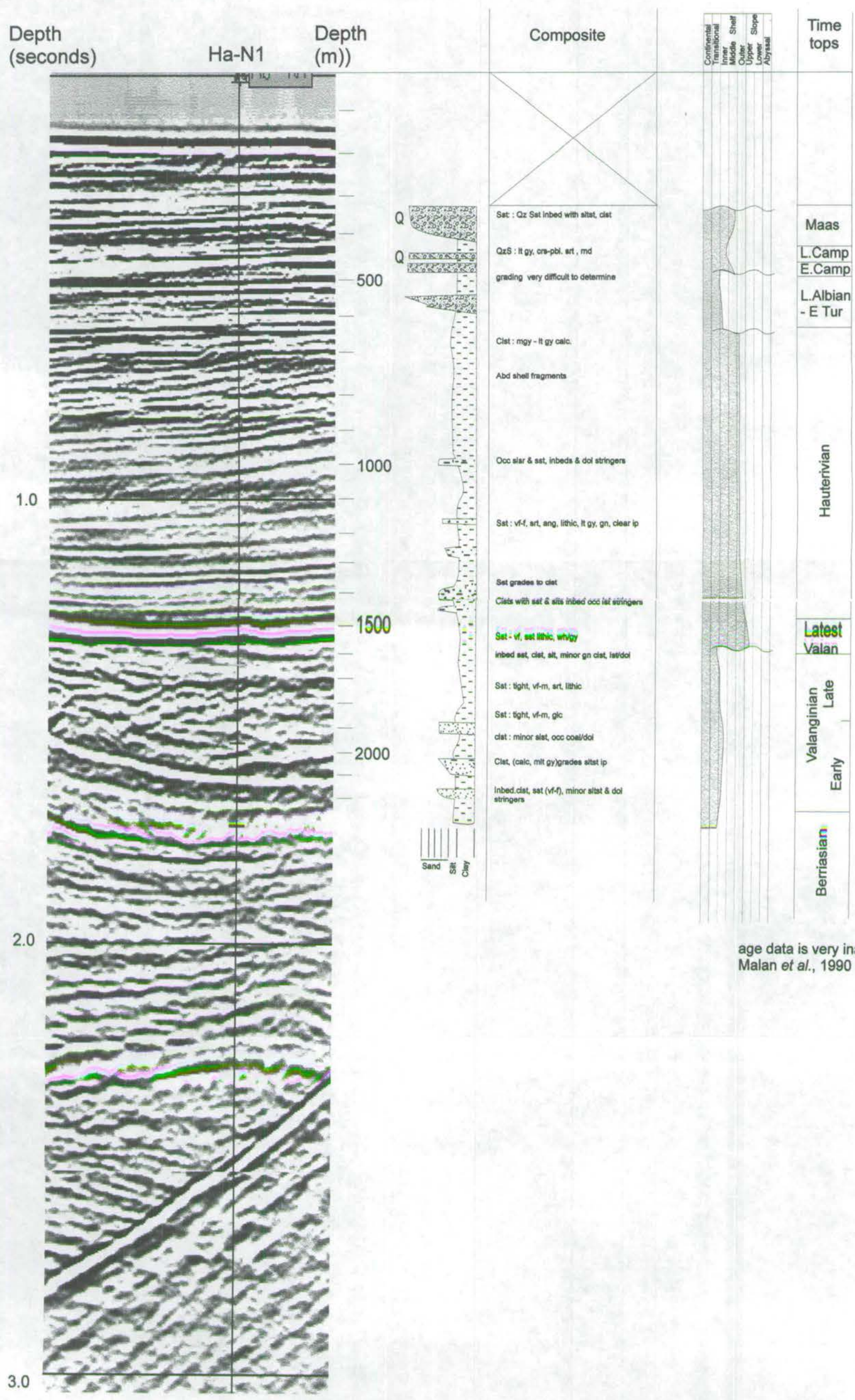
Lithofacies		Composite
Clst	Inner shelf	
QzS :f-m, poly modal transport direction	Coastal above wave base	
Sst : f-crs	Inner shelf	
Sstst / clst	Inter-tidal	
Sst : f-m, srt, mgy coarsens from md gy clst, lignite	Coastal above wave base (sand waves overlying regressive sand bars)	Sst : arg-clean, m dkgy, srt, lithic
clst, calc, (carb), pyr nod. rare lst stringers, occ sand waves	Inner shelf	Sst : mtgy, srt, ang, carb-biky
Stacked thin barrier sands clst (shell) to vf-f, mgy, srt sst Sstst occ Lignite traces	Inner shelf	Sst : vf, srt, biky
	Coastal	Sst : arg ip, lithic, gn, srt, fri
Occ lst at top stacked sand bars, coarsen from clst (non calc) to either sstst, or sst - srt, f, lithic	Coastal	Sst : lt gy, lithic
Clst : mgy, occ m dk gy, non clac, grades to non clac at base	Mid shelf	Sst : vf arg
Qtz : wh, clear, ltgy	Basement, meta shelf seds.	

There is no time top data for this well





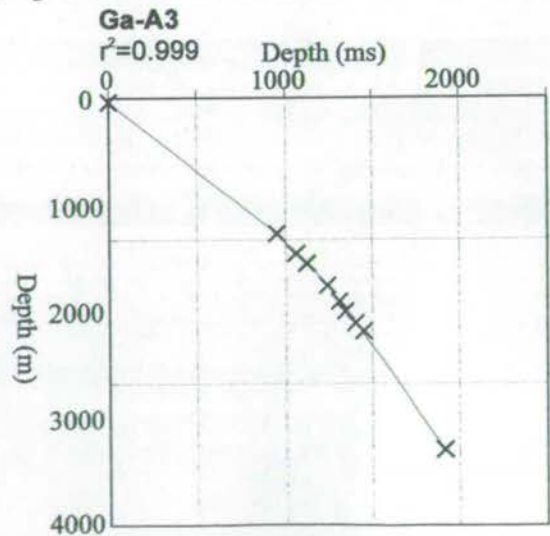
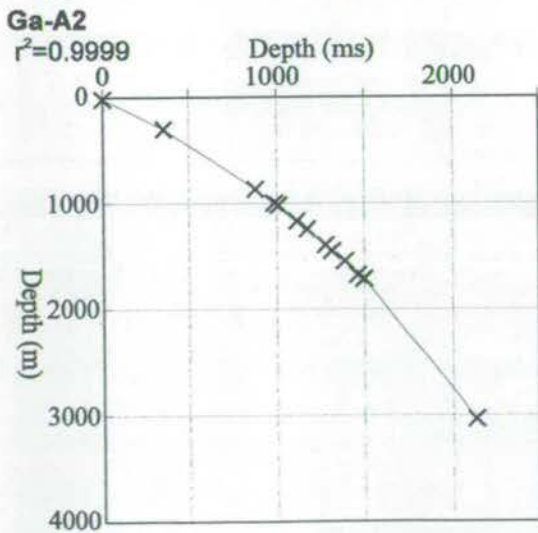
There is no seismic section for this well



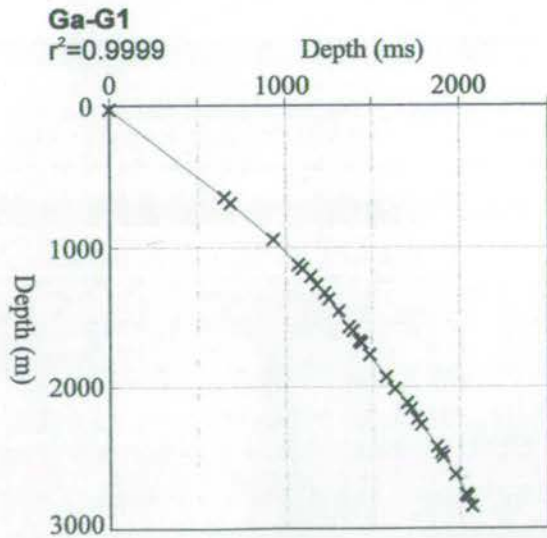
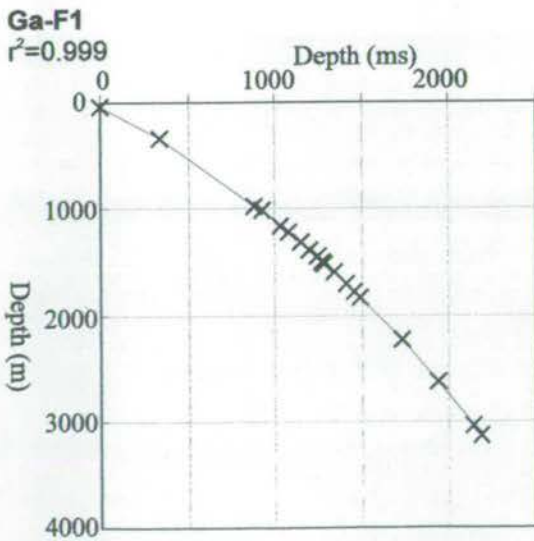
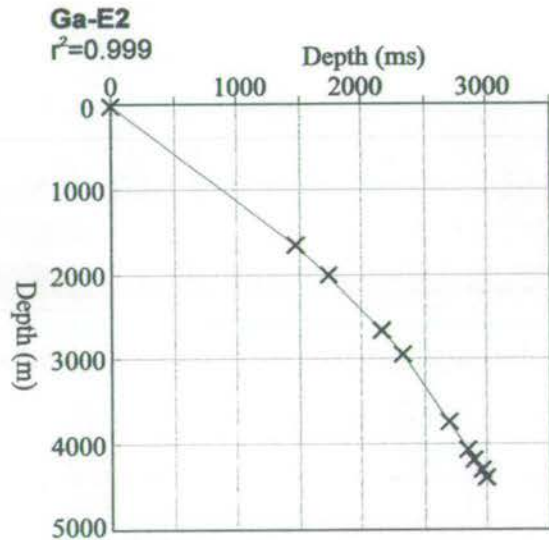
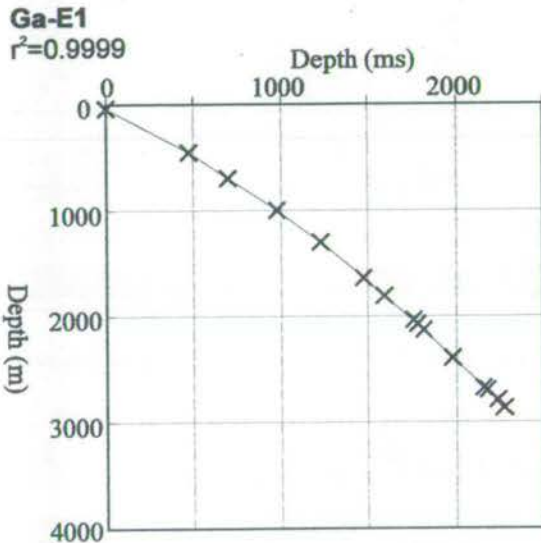
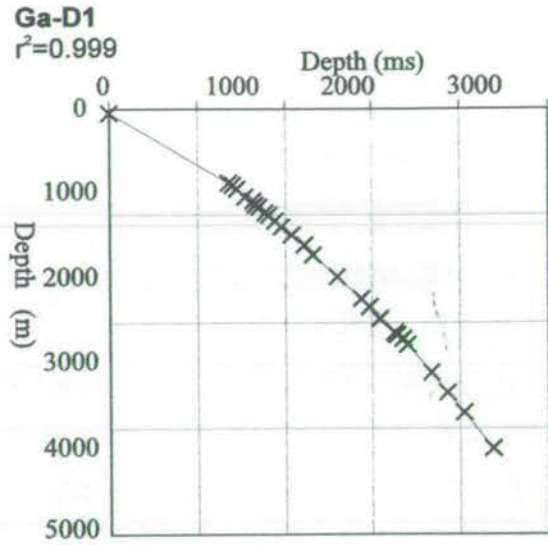
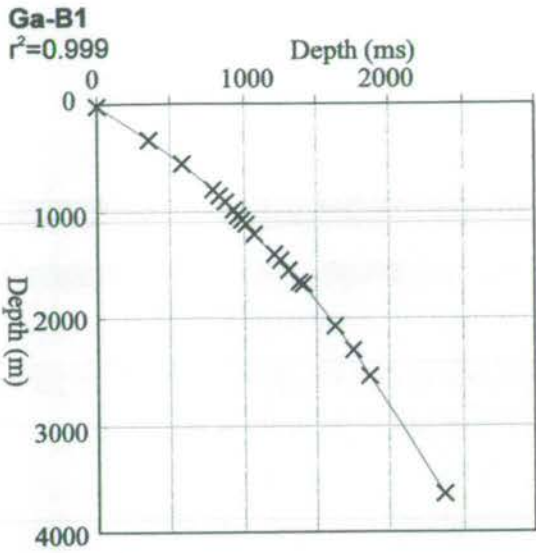
Appendix B-i: Available well data for the Pletmos Basin

Well Name	Composite	Lithofacies	Palynology
Ga-A2	Yes	Yes	Yes
Ga-A3	Yes	Yes	Yes
Ga-B1	Yes	Yes	Yes
Ga-D1	Yes	No	Yes
Ga-E1	Yes	Yes	Yes
Ga-E2	Yes	Yes	Yes
Ga-F1	Yes	Yes	Yes
Ga-G1	Yes	Yes	Yes
Ga-J1	Yes	Yes	Yes
Ga-M1	Yes	No	Yes
Ga-Q1	Yes	Yes	Yes
Ga-S2	Yes	Yes	Yes
Gb-C1	Yes	Yes	Yes
Gb-F1	Yes	No	Yes
Gb-H1	Yes	Yes	Yes
Gb-J1	Yes	Yes	Yes
Gb-K1	Yes	Yes	Yes
Gb-L1	Yes	Yes	Yes
Gb-M1	Yes	Yes	Yes
Gb-Spk1	Yes	No	Yes

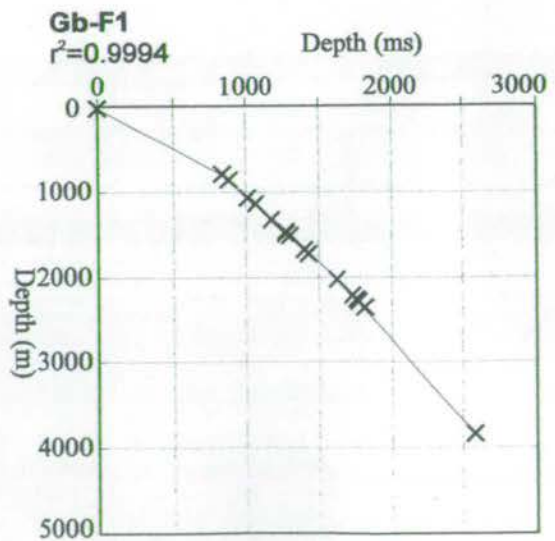
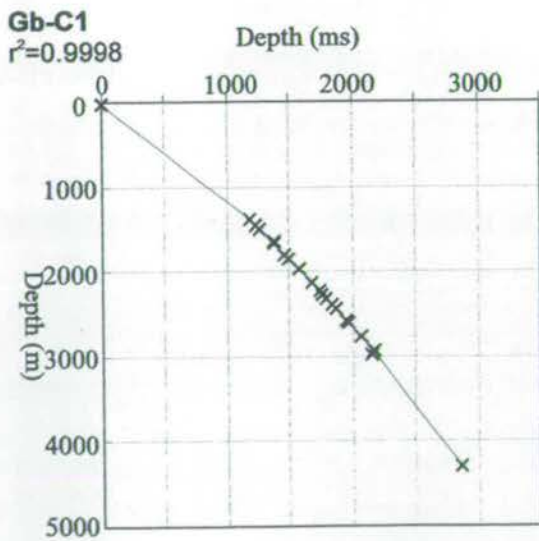
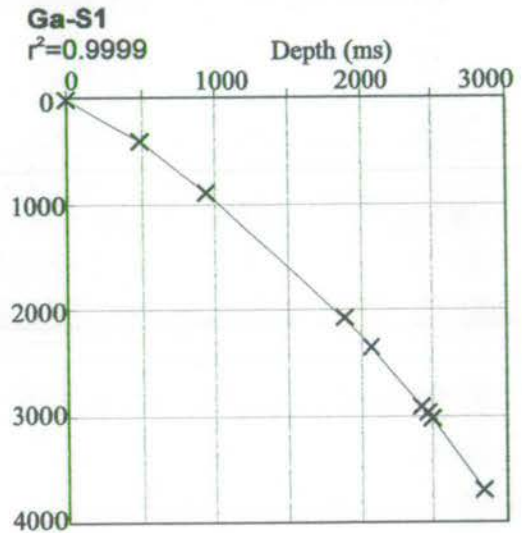
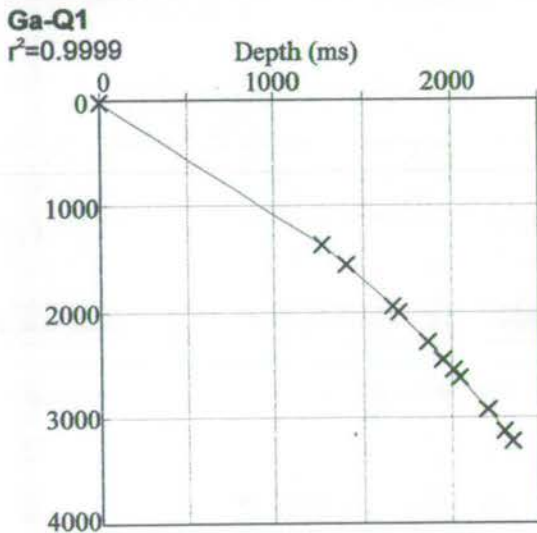
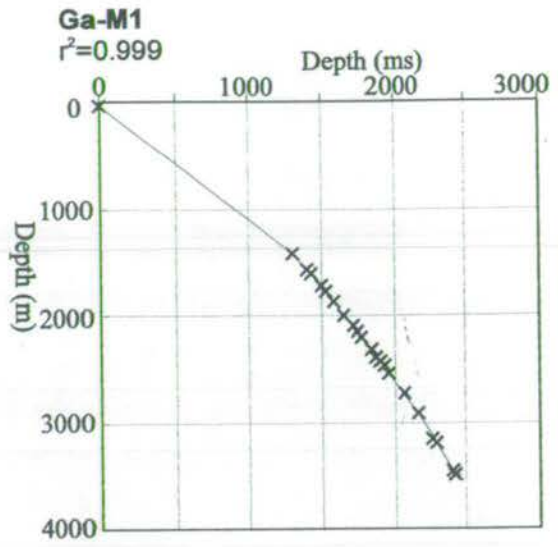
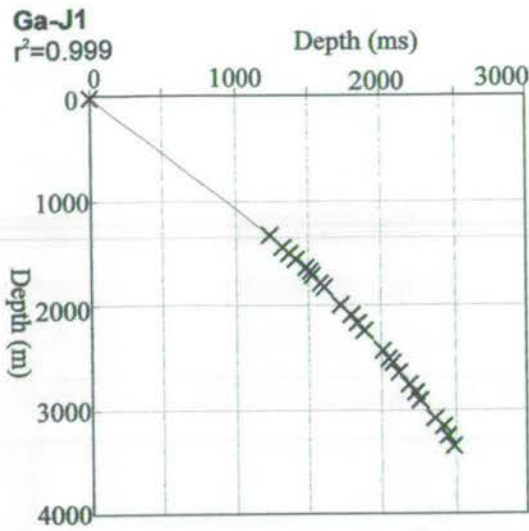
Appendix B-ii: Time-depth conversion graphs for the Pletmos Basin



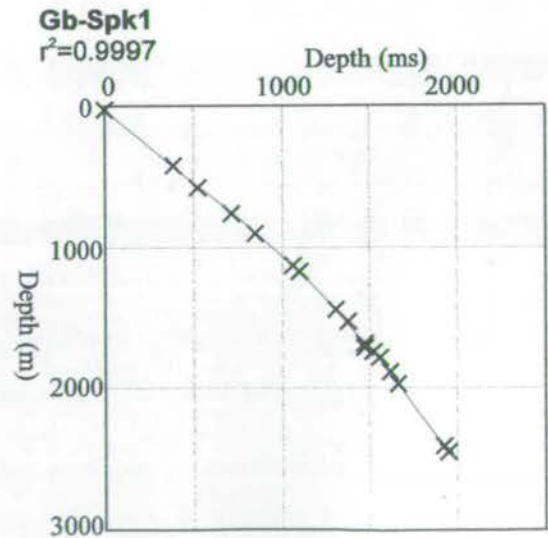
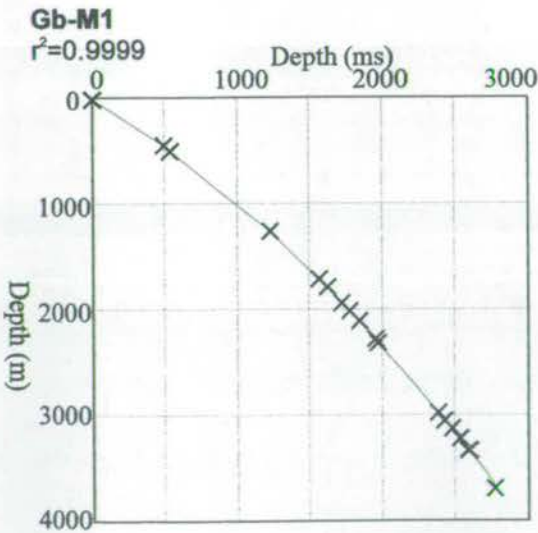
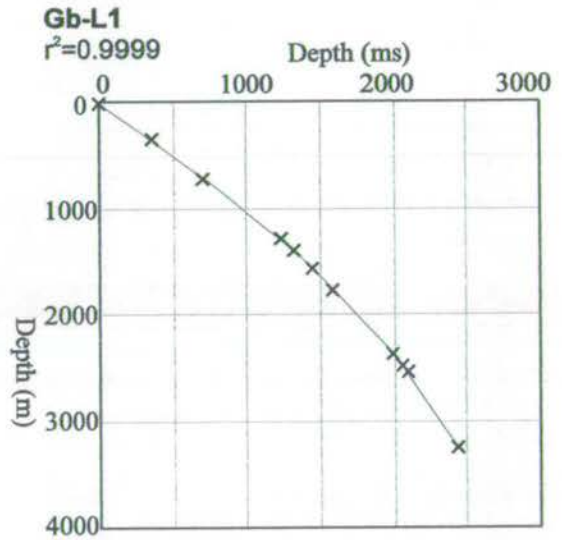
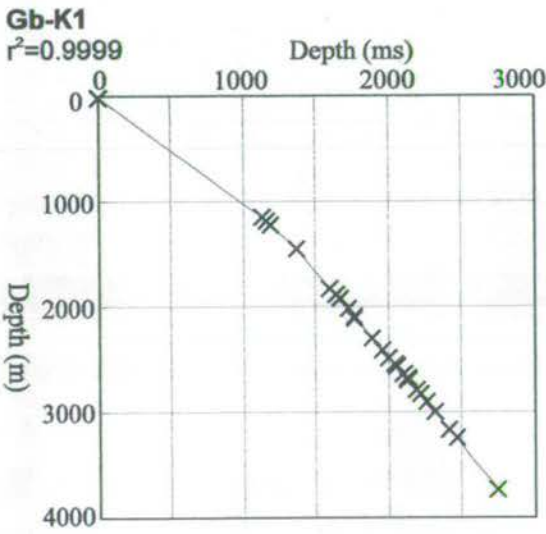
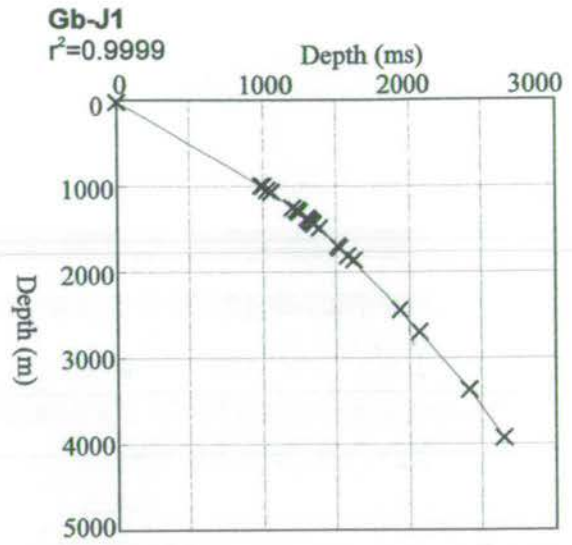
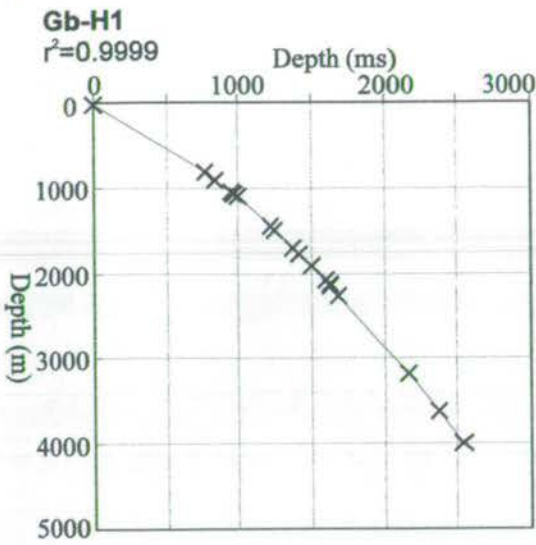
Appendix B-ii (continued)



Appendix B-ii (continued)



Appendix B-ii (continued)



Appendix B-iii: Time-depth converted age-depth data for the Pletmos Basin

Depth (Z(m)) to top of Age Horizons (from McMillan, 1999) have been converted to time (TWT) using equations obtained from linear regression lines for individual wells (cf. Depth-time data plots).

		Ga-A2		Ga-A3		Ga-B1		Ga-D1	
		Z(m)	TWT	Z(m)	TWT	Z(m)	TWT	Z(m)	TWT
Holocene									
Pleistocene	Late								
	Early								
Pliocene									
Miocene	Late								
	Early								
Oligocene	Late								
	Early								
Eocene	Late			317	327				
	Mid	288	340	347	360				
	Early	341	397	390	406				
Palaeocene		366	422	415	432			186	194
Maastrichtian		442	499	494	515	307	328		
Campanian	Late	643	689	683	704	427	452	196	205
	Early	671	713	707	728	442	467	210	220
Santonian	Late								
	Early								
Coniacian	Late	746	780	768	785				
	L.Early	807	832	884	890	506	529	260	274
	E.Early								
Turonian	Late								
	Mid	850	868	940	938				
	L.Early	853	871	945	942	567	586	330	347
	E.Early	990	982	1030	1014			360	377
Cenomanian	Late								
	Early	1137	1096	1170	1124	640	651	430	444
Albian	Late	1243	1175	1183	1133	643	654	440	454
	Mid	1316	1227	1244	1178	680	686	470	481
	Early								
Aptian	Late								
	L.Early								
	E.Early	1402	1288	1329	1239	811	794		
Barremian	Late	1450	1321	1400	1288	1050	968	550	554
	Early							940	867
Hauterivian	Late					1531	1308		
	Early							2168	1664
Valanginian	Latest							2660	1925
	Late	1714	1493	1643	1441	1692	1414	2862	2028
	Early	1944	1631	1814	1540				
Berriasian		2100	1718	1996	1641	2646	1913		
Portlandian		2319	1833	2207	1757	3041	2099		
Kimmeridgian		2358	1852	2251	1782				
Basement		2580	1957	2460	1906				

Appendix B-iii (continued)

		Ga-E1		Ga-E2		Ga-F1		Ga-G1		Ga-J1	
		Z(m)	TWT	Z(m)	TWT	Z(m)	TWT	Z(m)	Z(m)	TWT	Z(m)
Hol.											
Pleist.	L										
	E										
Pli.											
Mio.	L										
	E										
Olig.	L										
	E							198	224		
Eocene	L	451	472	470	458			210	237	351	363
	Mid	480	499	480	467			320	343	430	445
	E	540	554	540	526					500	516
Pal.		600	608	600	583			380	398	560	576
Maas.		690	690	690	668	230	239	470	481	640	653
Camp.	L	980	956	970	920	230	239	660	662	910	902
	E	1040	1010	1020	963			690	691	940	928
Sant.	L									990	971
	E										
Con.	L	1280	1215	1160	1082			780	777	1060	1031
	L.E.	1360	1278	1240	1148			905	892	1260	1195
	E.E.	1545	1414	1395	1273						
Tur.	L										
	Mid	1778	1576	1600	1432					1440	1334
	L.E.	1838	1617	1660				955	937	1490	1372
	E.E.							1025	996		
Cen.	L										
	E	2138	1822	1999	1723			1155	1099	1790	1587
Alb.	L	2168	1841	2085	1782			1185	1122	1830	1615
	Mid	2390	1984	2548	2087			1215	1143	2097	1792
	E										
Apt.	L										
	L.E.	2705	2180	2659	2156					2435	2004
	E.E.							1365	1245	2485	2034
Barr.	L	2727	2194	2760	2217	330	340	1690	1441	2620	2113
	E					1020	924				
Haut.	L										
	E					1455	1244				
Val.	Lst					1675	1388	2474	1900		
	L	2795	2235	2938	2322	1782	1455			3112	2384
	E			4108	2862	2374	1797				
Berr.				4369	2988	2980	2105				
Port.											
Kimm.											
Base.								2775	2042		

Appendix B-iii (continued)

		Ga-M1		Ga-Q1		Gb-C1		Gb-F1	
		TWT	Z(m)	TWT	Z(m)	TWT	Z(m)	TWT	Z(m)
Hol.									
Pleist.	L								
	E								
Pli.									
Mio.	L								
	E								
Olig.	L								
	E								
Eocene	L	350	500	340	353	199	247		
	Mid	380	548	390	403	220	270		
	E	420	614	450	463	290	342		
Pal.		460	680	500	511	350	400	350	437
Maas.		530	798	580	587	440	481	355	442
Camp.	L	740	1171	830	816	550	574	440	523
	E	760	1209	860	843	560	583	480	559
Sant.	L	800	1284			600	615		
	E								
Con.	L	880	1439	930	904				
	L.E.	1030	1746	1100	1049	650	655		
	E.E.								
Tur.	L								
	Mid								
	L.E.	1080	1853	1230	1156	700	694	550	619
	E.E.	1280	2307			720	710	670	718
Cen.	L								
	E	1360	2501	1550	1402	820	786	760	789
Alb.	L	1380	2551	1560	1409	830	793	800	820
	Mid	1400	2601	1710	1514	840	801	820	835
	E								
Apt.	L								
	L.E.								
	E.E.	1560	3018	1950	1669	1030	940	870	872
Barr.	L	1775	3627			1200	1060	1010	973
	E								
Haut.	L								
	E					2448	1874	1935	1568
Val.	Lst								
	L	2728	7022	2022	1713	2829	2095	2289	1774
	E			2487	1973	3768	2595	3039	2184
Berr.				2667	2067				
Port.				2853	2163				
Kimm.				2907	2191				
Base.		3453	10348						

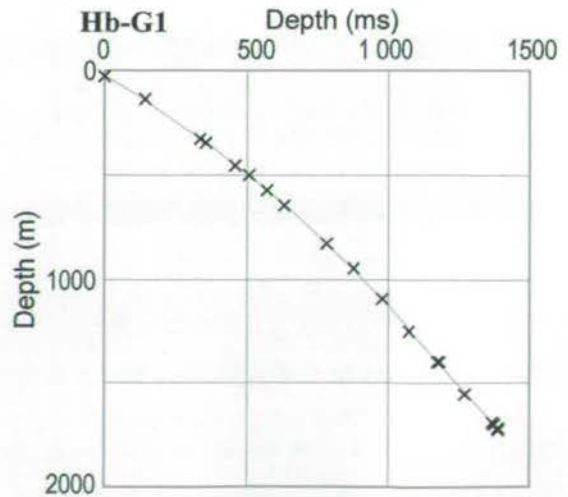
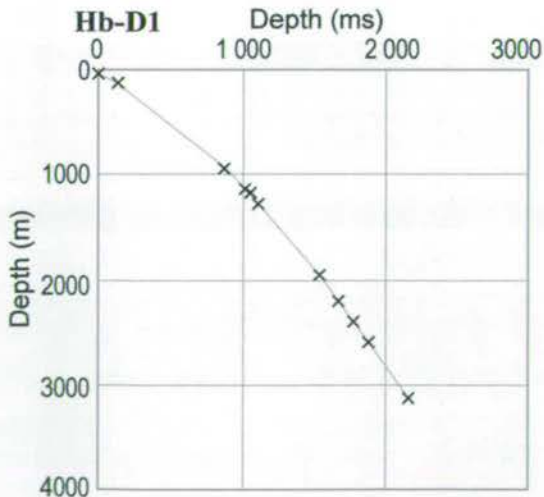
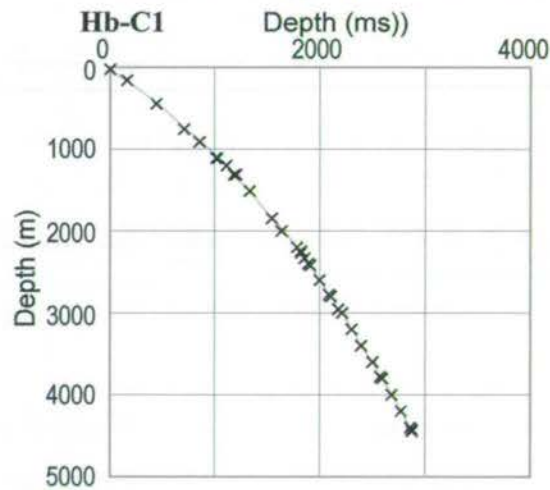
Appendix B-iii (continued)

		Gb-H1		Gb-J1		Gb-K1		Gb-Spr	
		TWT	Z(m)	TWT	Z(m)	Z(m)	TWT	Z(m)	TWT
Hol.									
Pleist.	L								
	E								
Pli.									
Mio.	L								
	E			194	171				
Olig.	L								
	E					175	180		
Eocene	L			348	339	329	352	420	377
	Mid			380	374	400	429	470	428
	E			440	440	410	439	510	468
Pal.		182	167	500	505	500	533	580	539
Maas.		200	186	590	601	650	682	670	628
Camp.	L	280	269	810	824	800	824	880	638
	E			820	834	830	852	910	859
Sant.	L					900	915		
	E								
Con.	L			890	900			990	932
	L.E.			980	982	940	950	1090	1020
	E.E.								
Tur.	L								
	Mid								
	L.E.			1040	1034	990	994	1170	1089
	E.E.			1145	1121	1100	1087	1250	1155
Cen.	L								
	E			1250	1203	1210	1176	1440	1304
Alb.	L			1280	1226	1230	1192	1460	1319
	Mid			1375	1295	1290	1239	1540	1377
	E								
Apt.	L								
	L.E.								
	E.E.	350	339	1505	1384	1440	1350	1680	1476
Barr.	L	510	495	1600	1446	1580	1445	1720	1503
	E					1870	1619		
Haut.	L	4440	2762						
	E					3058	2346		
Val.	Lst	3128	2133						
	L	3621	2363			3247	2464	1780	1544
	E			1867	1609			1800	1557
Berr.				2299	1851			2020	1698
Port.				2707	2071			2340	1891
Kimm.				3208	2326			2375	1911
Base.				3385	2409			2402	1927

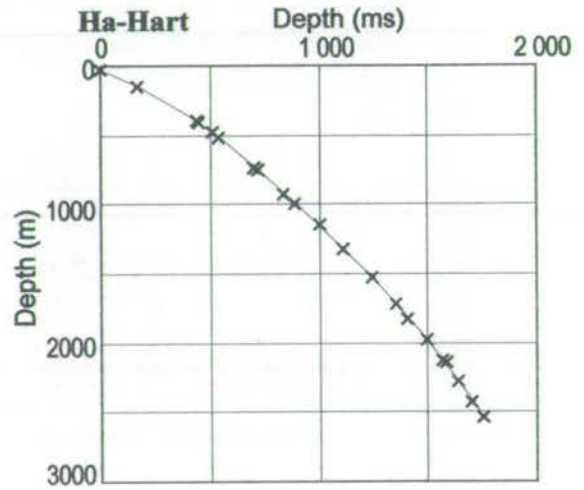
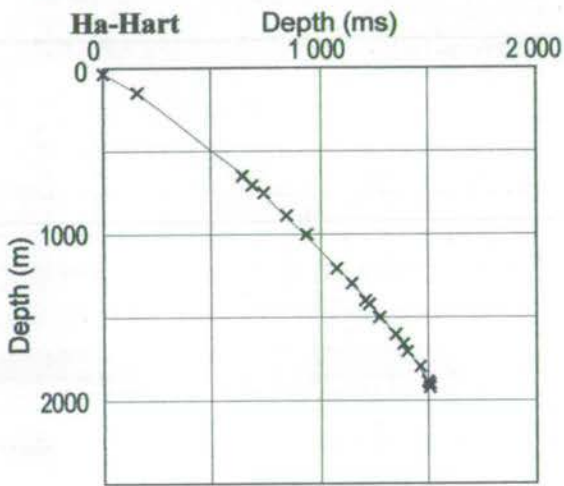
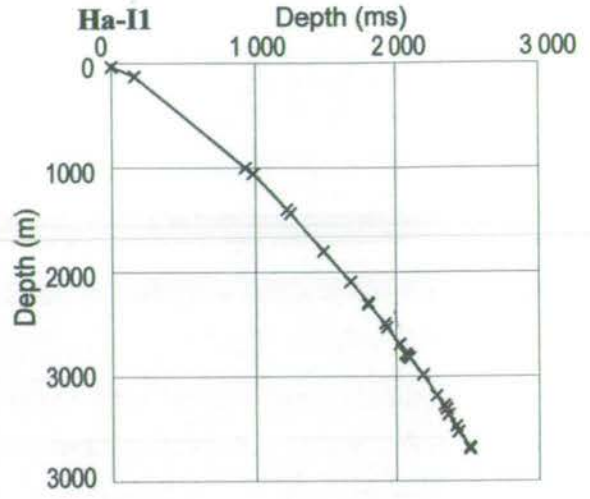
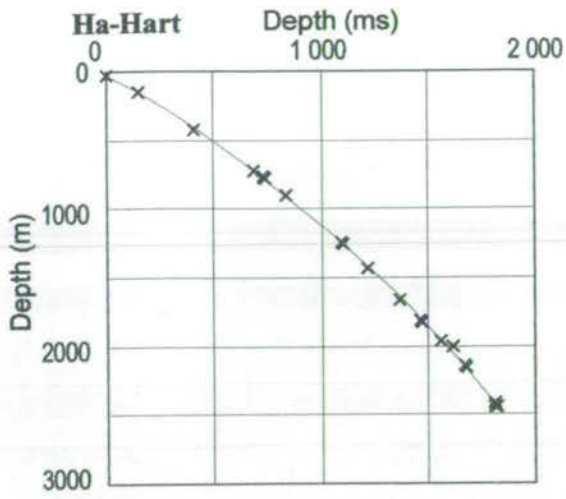
Appendix C-i: Available well data for the Algo Basin

Well Name	Composite	Lithofacies	Palynology	Synthetic	Time top
Hb-B1	Yes	Yes	No	Yes	Yes
Hb-C1	Yes	Yes	No	Yes	Yes
Hb-D1	Yes	No	No	Yes	Yes
Hb-G1	Yes	No	Yes	Yes	Yes
Hb-Hart	Yes	Yes	Yes	Yes	Yes
Hb-I1	Yes	Yes	No	Yes	Yes
Hb-K1	Yes	Yes	No	Yes	Yes
Hb-P1	Yes	Yes	No	Yes	Yes

Appendix C-ii: Time-depth conversion graphs for the Algo Basin



Appendix C-ii (continued)



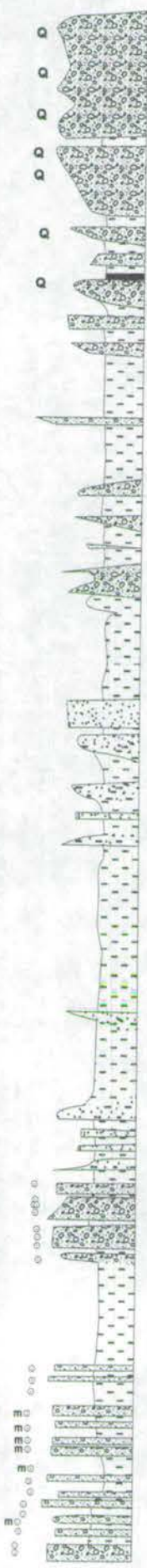
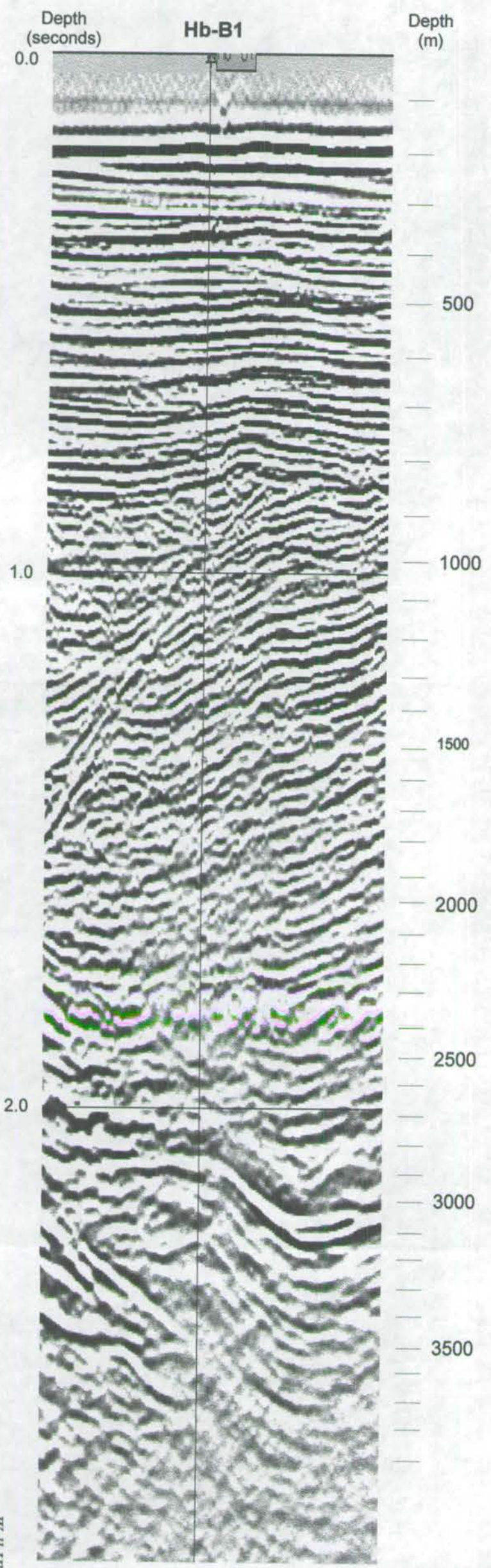
Appendix C-iii: Time-depth converted age-depth data for the Algoa Basin

Depth (Z(m)) to top of Age Horizons (from McMillan, 1999) have been converted to time (TWT) using equations obtained from linear regression lines for individual wells (cf. Depth-time data plots).

		Hb-B1		Hb-C1		Hb-D1		Hb-G1	
		Z(m)	TWT	Z(m)	TWT	Z(m)	TWT	Z(m)	TWT
Holocene				148	136				
Pleistocene	Late								
	Early								
Pliocene				181	173				
Miocene	Late								
	Early			330	330				
Oligocene	Late								
	Early			442	444				
Eocene	Late			570	569				
	Mid			630	625				
	Early								
Palaeocene				650	644			330	344
Maastrichtian				720	708	326	338.4	350	363
Campanian	Late			920	884			450	459
	Early			960	917			480	487
Santonian	Late			1070	1008				
	Early								
Coniacian	Late								
	L. Early			1230	1134				
	E. Early								
Turonian	Late								
	Mid								
	L. Early			1270	1165				
	E. Early								
Cenomanian	Late								
	Early			1380	1247	370	382.5		
Albian	Late			1550	1368				
	Mid			1880	1587	580	579		
	Early					820	779.9		
Aptian	Late								
	L. Early								
	E. Early								
Barremian	Late								
	Early								
Hauterivian	Late								
	Early					1040	946.8		
Valanginian	Latest					1100	989.9		
	Late			2268	1821	1170	1039	540	540
	Early			2618	2013	1320	1141	600	592
Berriasian				2978	2198	1730	1398	1365	1158
Portlandian				4093	2718	3937	2567		
Kimmeridgian									
Basement				4433	2871			1721	1389

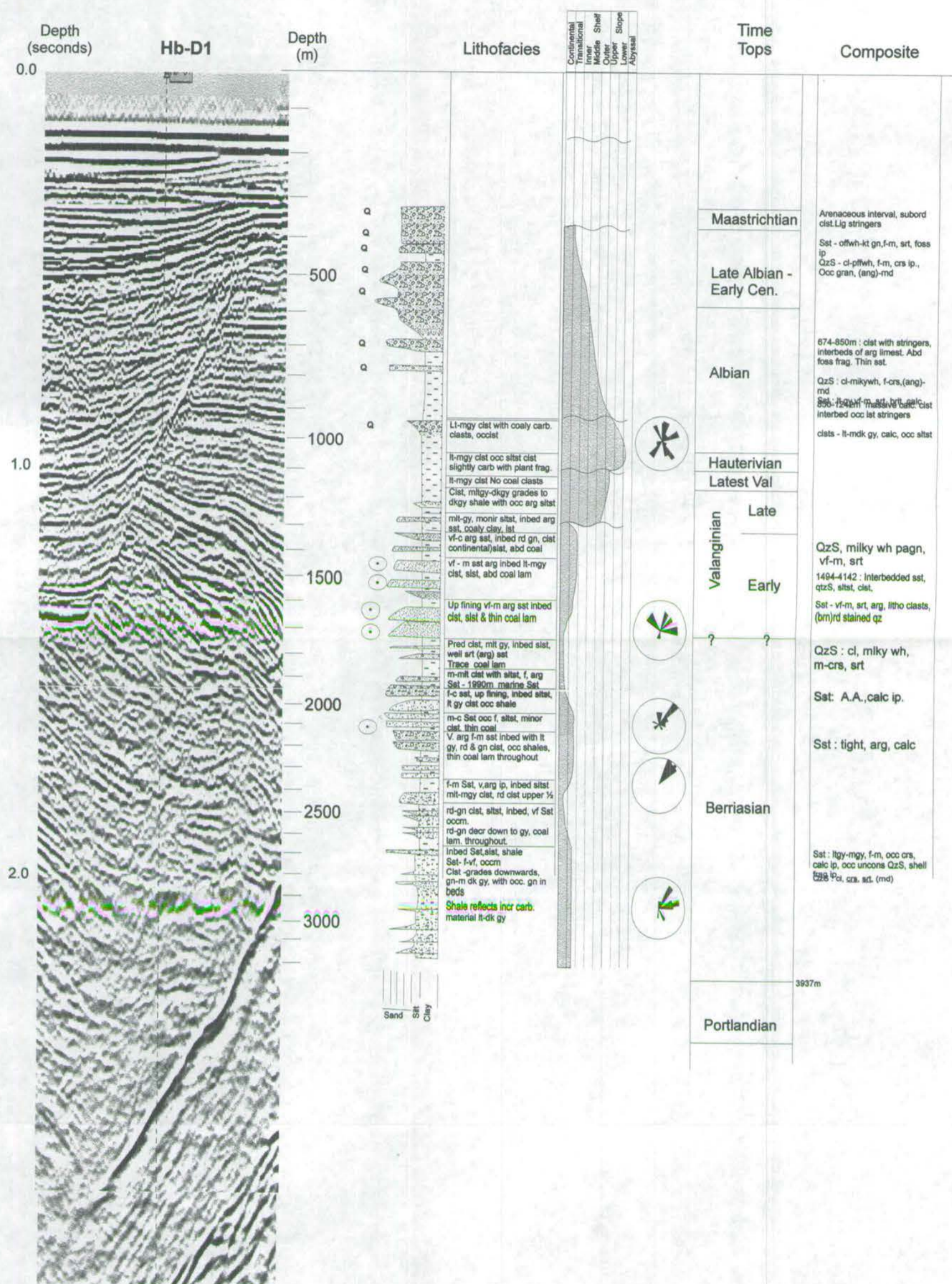
Appendix C-iii (continued)

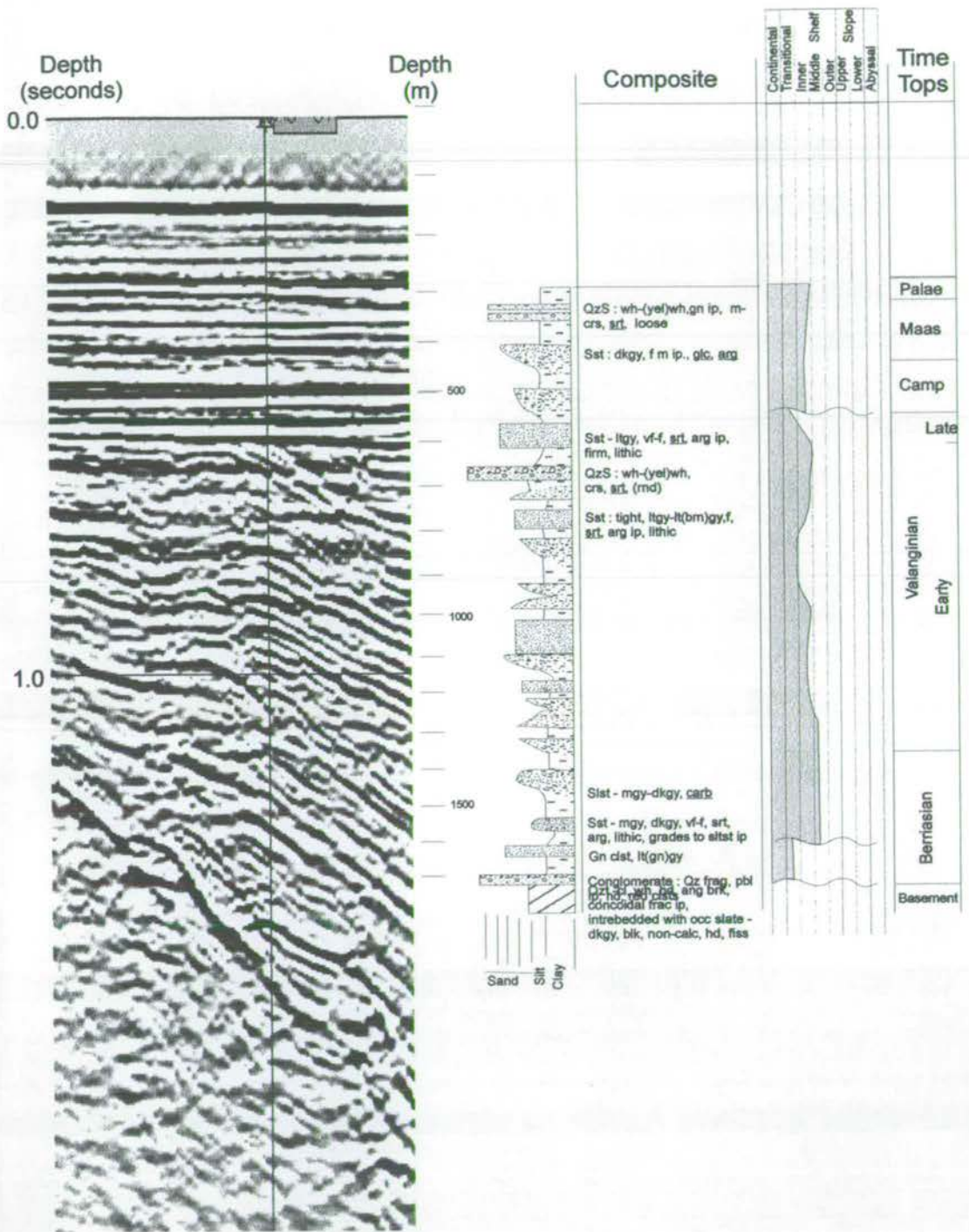
		Hb-Hart		Hb-I1		Hb-K1		Hb-P1	
		Z(m)	TWT	Z(m)	TWT	Z(m)	TWT		
Hol.									
Pleist.	L								
	E								
Pli.									
Mio.	L								
	E								
Olig.	L								
	E					192	206.17		
Eocene	L					336	357.99		
	Mid					338	360		
	E								
Pal.		420	426			390	411.47		
Maas.		440	444.6			470	488.03		
Camp.	L	550	544.3			550	561.8		
	E	570	562			570	579.84		
Sant.	L	600	588.2			600	606.61		
	E								
Con.	L								
	L.E.	660	639.9			660	659.17		
	E.E.								
Tur.	L								
	Mid								
	L.E.	720	690.5	1030	954.4	710	702		
	E.E.								
Cen.	L	760	723.7						
	E	815	768.6	1110	1013	760	743.99		
Alb.	L			1230	1100	815	789.24		
	Mid			1710	1428				
	E			2035	1636				
Apt.	L			2425	1871				
	L.E.								
	E.E.								
Barr.	L								
	E								
Haut.	L			2829	2098			364	405.2
	E								
Val.	Lst							405	442.8
	L			3333	2358			431	465.8
	E	900	836.6						
Berr.		1210	1071			900	857.3		
Port.		1770	1446			1315	1159.4	1350	1127
Kimm.		2140	1663			1655	1372.1	1804	1407
Base.		2417	1811			1877	1495.1	2135	1581

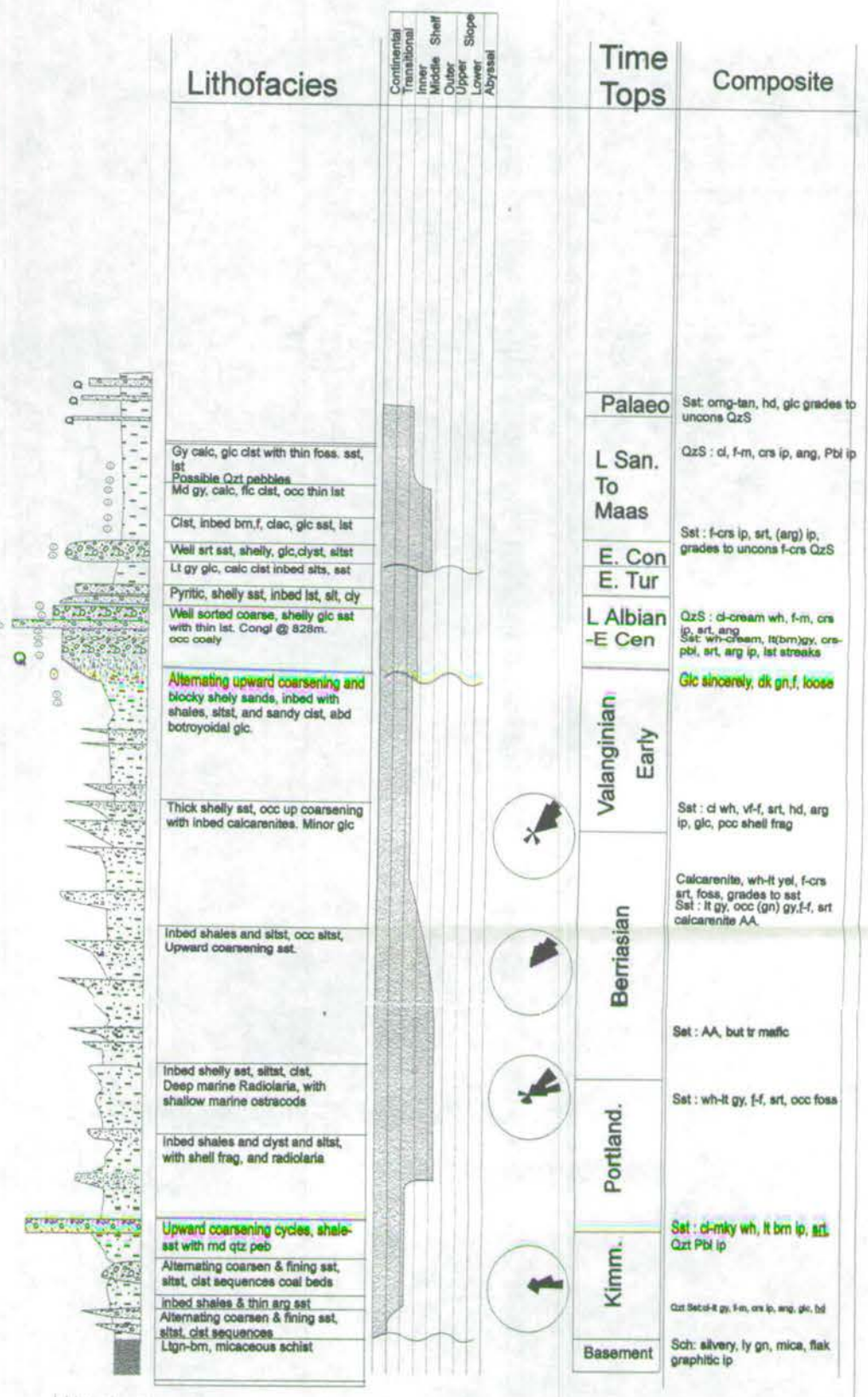
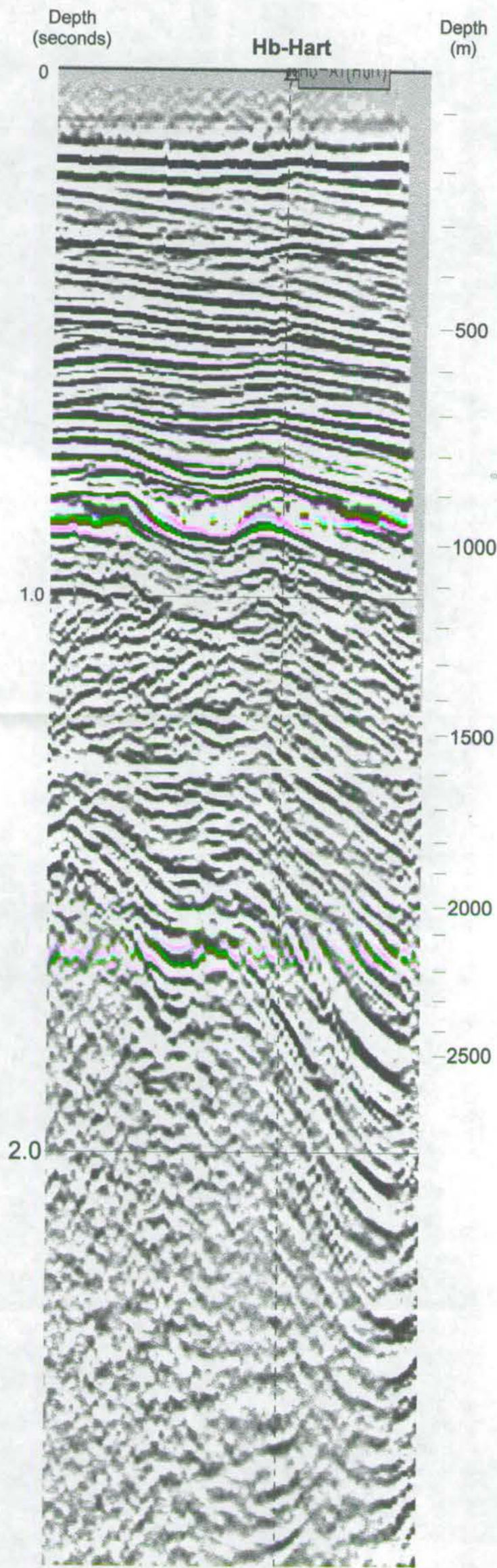


Sand
Silt
Clay

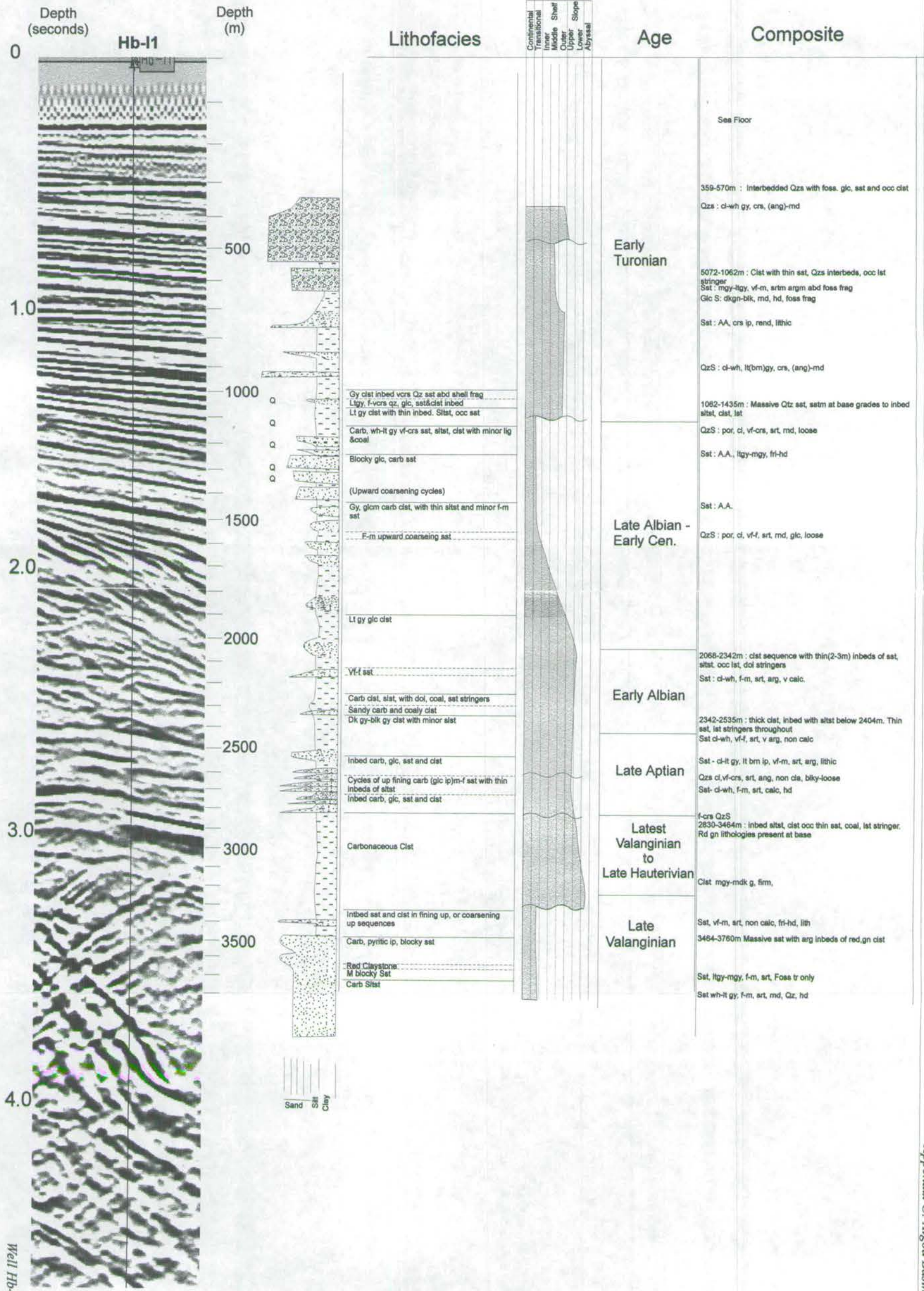
Lithofacies	Continental Shelf						Time tops	Composite
	Transitional	Inner	Middle	Outer	Upper Slope	Lower Slope		
								Sst: cl, f-m, srt, lse, glc, abd foss frag
								GlcS: dkgn-blk, f, srt, md, lse
Blocky, glc and chelly f-crs sst with few cist and minor cist								Sst: (gn)gy, (arg), hd, blk
								QzS: cl-lt-gy, f-m, crs ip, srt, glc, occ foss frag
								Sst: ltgy-cl-yel, f-f, srt, md, lse, glc
Gravel deposits during storm gn, gy sandy, silty cist								Sst: f-m, srt, md, arg, fri-hd, foss frag
m-crs glc sst with lignite gn gy, silty cist with f carb sst						Early Con		Cist: mltgy-dkgy, glc, s, abd qz-m-crs md
crs-pbl glc sst						L Albian		Red cist
gy, (carb), glc cist with minor siltst, sst						-E.Cen		lignite QzS: cl-mod yel, f-crs-pbl, md, Cist: ltgy, sand ip
(carb) rd, gn, arg sst with minor gy cists, and minor organic rich clays						Undated		Sst: cl, f, srt, calc, cmb, blk, glc
rd, cist with minor coal stringers up fining arg sst								SST: cl, f, srt, clean, calc, cmb, glc
Blocky arg sst								QzS: cl-wh, m-crs, srt, md, pyr ip
f-crs, (carb), arg sst with few rd, gn, cists, coal stringers						Berriasian		lignite Sst: lt gy, f, srt, arg, fri, cmb
rd, gn, arg sst with rd, gn, cists								Red and green cist Sst: cl wh, f-f, srt, md, arg, fri, cmb cists: AA
blocky f-crs sst with dk gn lithoclasts								Sst: AA, but arg, non calc dk gy lithoclasts
f-m sst, crs ip, inbed with siltst, cist						<1770		Sst: cl-lt gy, f-m, srt, arg, cmb, dk gn lithoclasts, cmb Lst
lt gy, (carb) cist with minor siltst, sst						Portland		Sst: AA, but crs ip Red cist Cist: AA Sst: mltgy, f-m, srt, arg, cmb, lithic
lt gy, (carb) cist								Sst: lt gy, f-m, srt, cmb, lithic Cist: lt gy, micromic, carb ip Sst: AA Red cist Sst: lt gy, f-f, srt, lithic, cmb
Inbed f-m, crs ip, (carb) sst and cist with a few thincoal stringers						Kimm.		Sst: lt gy, f-f, srt, calc, blk, lithic
Blocky f-crs sst with crs-vcrs qtz frag, minor siltst, cist								Sst: lt gy, f-f, srt, blk, lithic, sl, micromic ip
Carb, gn, cist grading to coal and lignite with subord siliceous, carb f sst								Qtz Frag : cl-wh, hd, ang brk Sst: cl-wh, f-f, srt, clean, abd crs, ang, Qz frag
F-m pbl sst interbedded coal and cist								Gn cist, dkgy-olive Sst: cl-mgy, f-m, srt, clean, arg where mgy, hd
Mors rd pbl sst with thin interbedded rd, gn cist								Qtz frag : crs-crs, cl, hd, conc brk Sst : cl, vf-f, srt, abd Qtz frag, gn lithoclasts ip Cist : AA
								Sst: off wh-cl, f-m, srt, Qtz frag ip Qz Frag: off wh (bm)-f-crs, concoidal frac Red Sst : pale (rd)bm (srt), sl-sl ip, hd, ang brk Red Sst : .od bm-rd, f-m, srt, ang, arg Sst :cl-opaque, wh ip, f-m, occ crs, srt, ang brk Qz frag, off wh, clear, opaque, f-crs, hd, occ concave pbl bound.

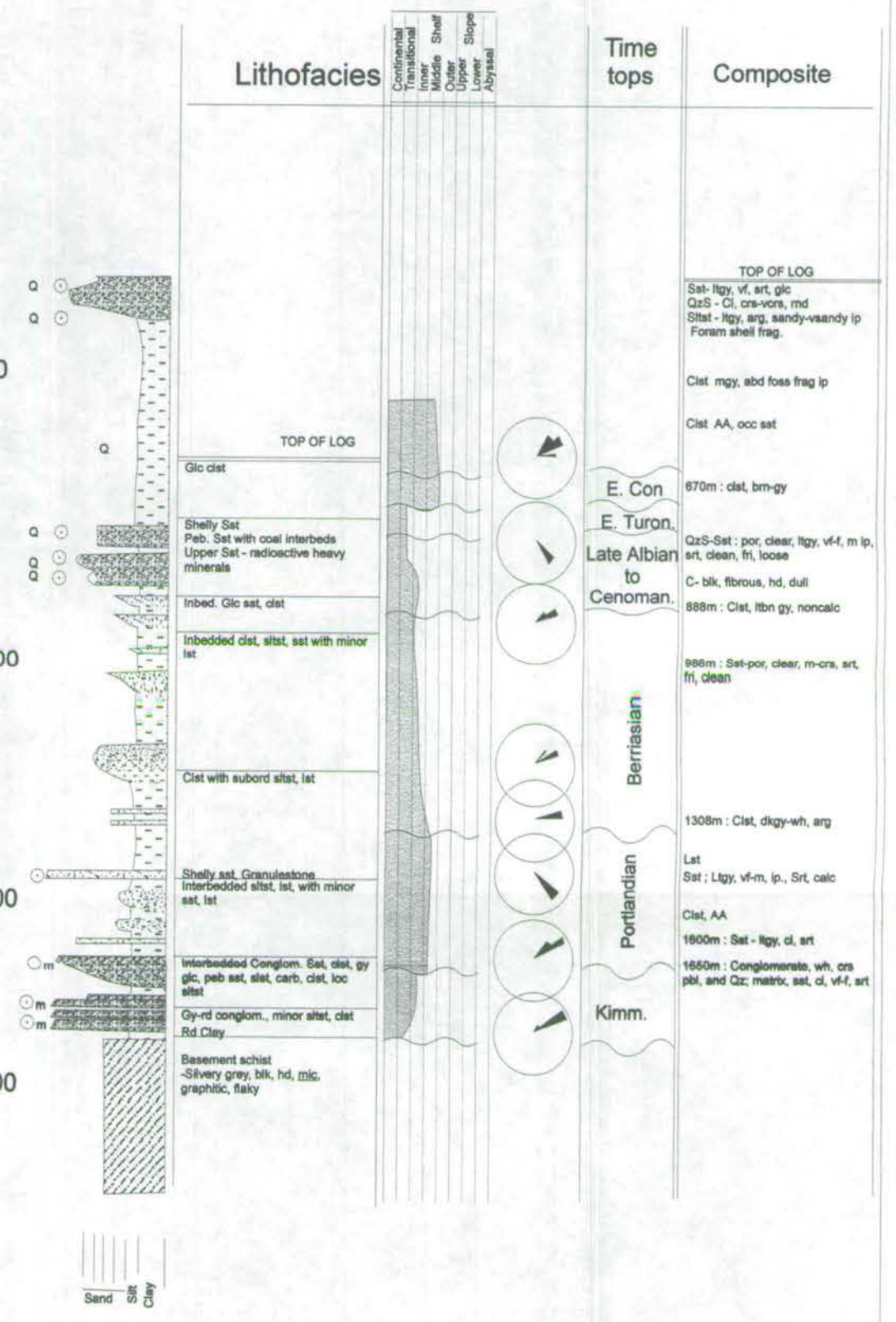
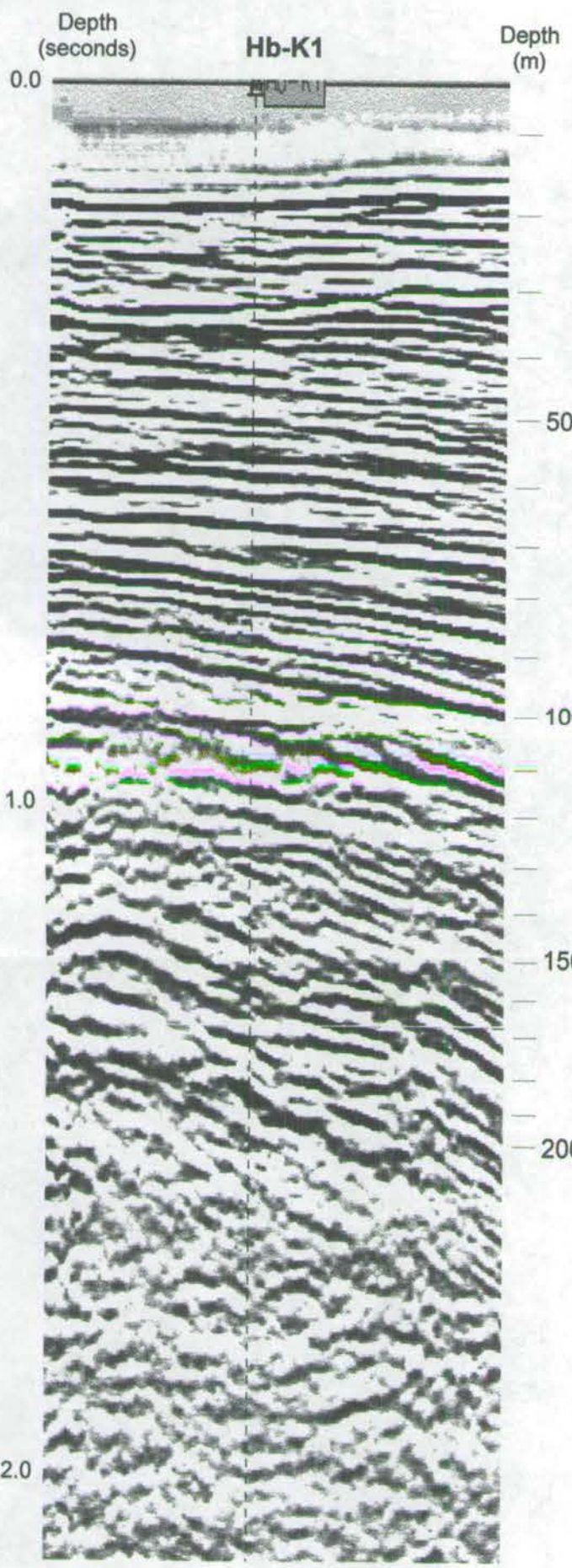


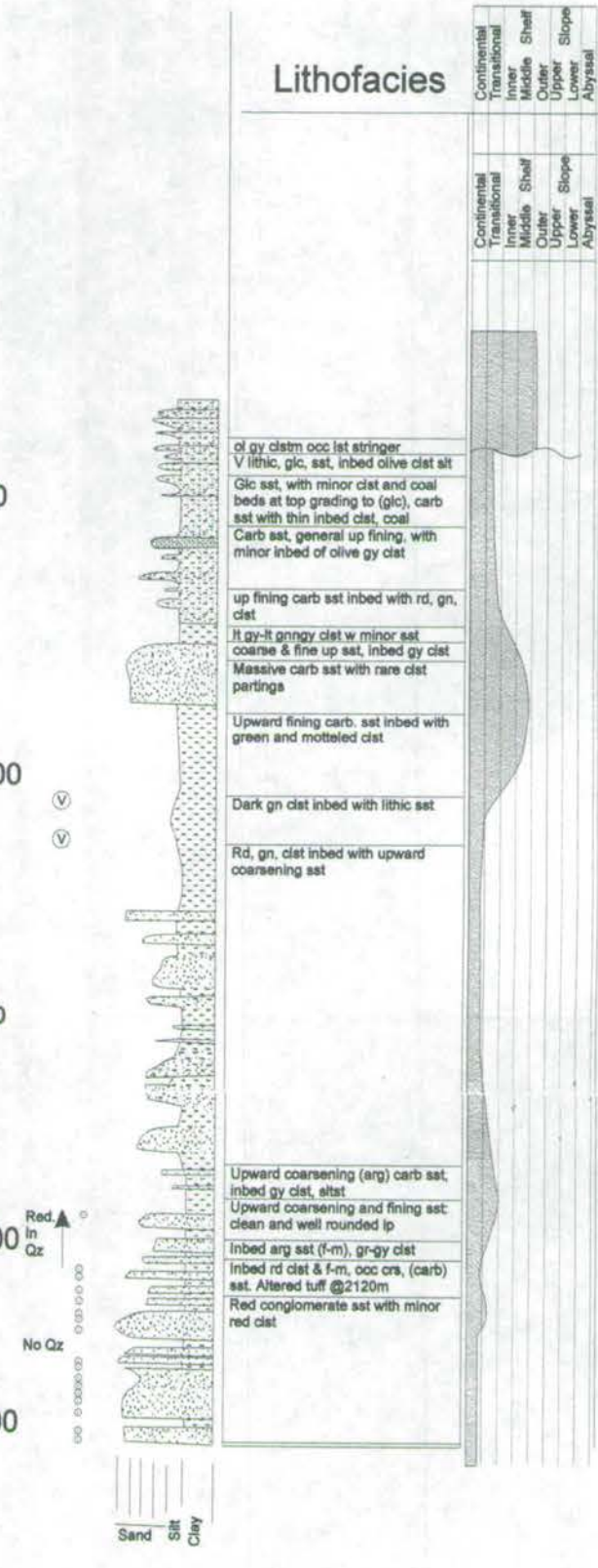
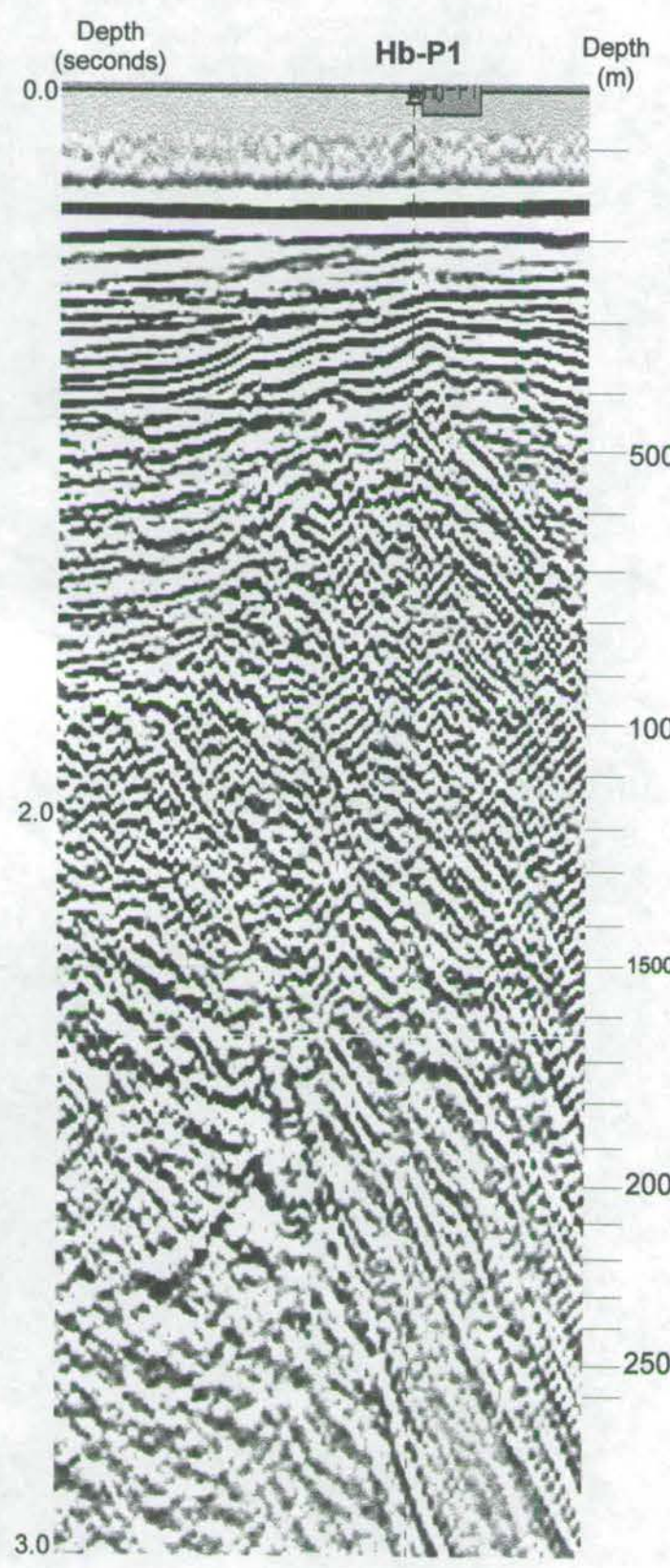




Sand
Silt
Clay







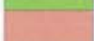






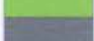
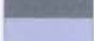


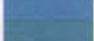







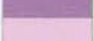








Lithofacies	Time tops	Composite
Continental		
Transitional		
Inner Shelf		
Middle Shelf		
Outer Shelf		
Upper Slope		
Lower Slope		
Abyssal		
	BS -364mHeut	
	Hauterlyvian Latest Val	Clst : lt olv gy, non clac
		Sst : dk gy, f-f, srt, arg
	Late	Sst : wh-lt gy, f-ors, srt, cl, calc, hd bkly, glc ip
	Valanginian	
	Early	Sst : f-m ip, srt, m lt gy, lithic, (arg)
		Sst : f-m,AA, carb
	<1350	Sst : f-m, lty, arg, lithic, non calc
	Berriasian	
		Sst : AA, f-m, ora ip, calc
		Sst : f-m, srt, non calc, lithic
		Rd Clst :AA
		Sst : f-f, lt gy, srt, arg, lithic
		Sst : f-m, wh-dkgy, srt, arg, lithic
	Portland.	Sst : f-m, srt, calc, lithic
		Sst : f-f, lt gy, srt, noncalc
		QzS : cl-wh, ora-ora, srt, unconsol
	Kimm.	Qz Frag, cl-wh, hd, ang brk
		Rd clst : (rd)brm
		Cgl : cl-wh, rd stain ip, ora-ora, phd ip, Qz, Clst matrix: Sst, f-m, arg, clean.
		Sst : AA, (rd)brm ip, ang ip
		Sst : cl-wh, f-m, ora ip, ang, (arg), Qz frag ip

Well Hb-P1 xxxv

Appendix C: Algora Basin well data

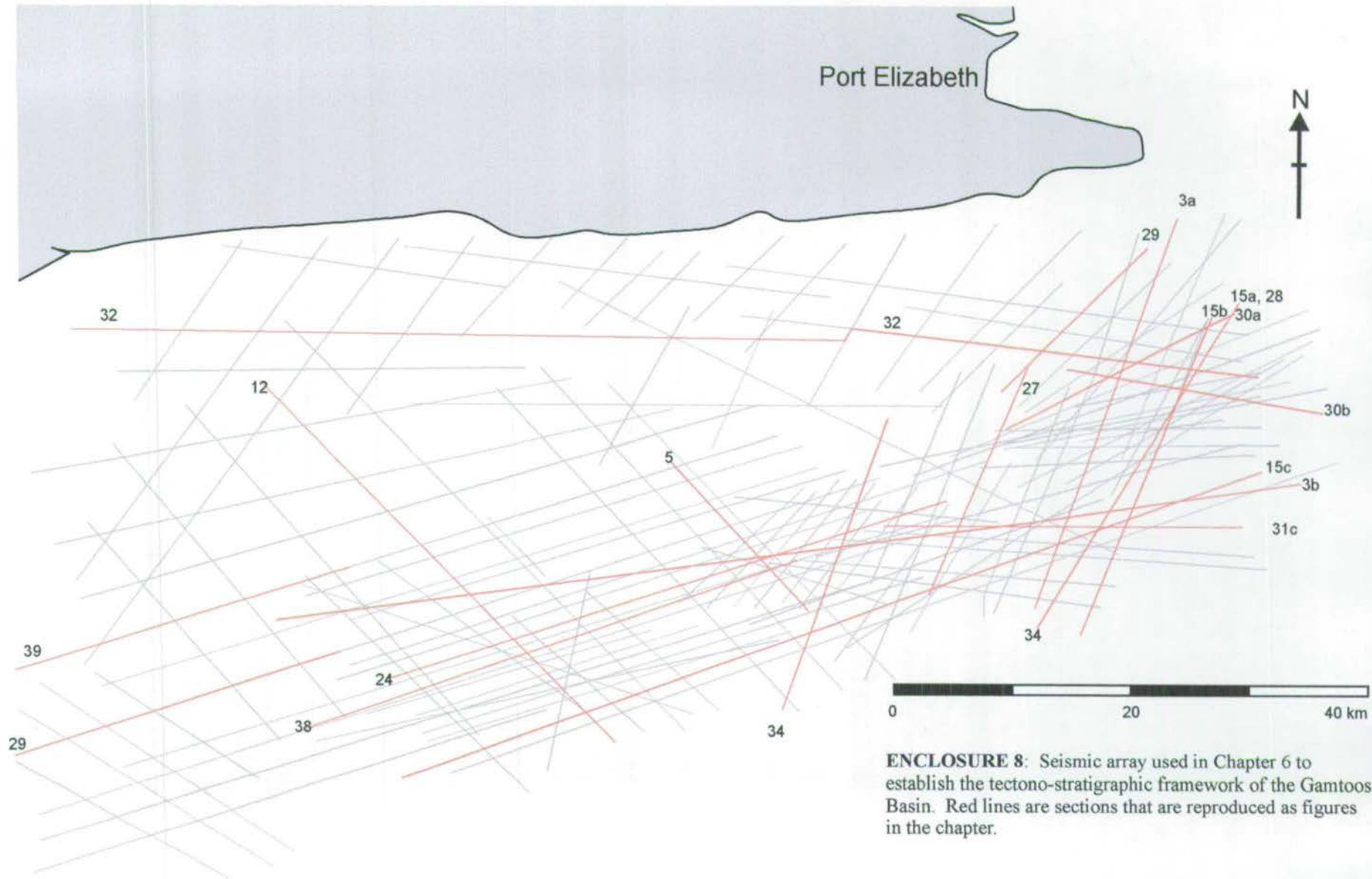
Enclosure 1 Key to transects

		Transect				
		A	B,C,D	E		
	-		Ke	Je, Jm, Js, Jk Jc, K	Mesozoic	
	Pa		Pa	Pk	Permian	Karoo Foreland Basin
	Pwa		Pw	Pw		
	Pf		Pf	Pf		
	Pl		Pr	Pr		
	Pc, Pw, Pp		Pp	Pp		
	C-Pd		Pd	C-Pd	Permian/ Carboniferous	
	Cw, Cf, Ck		Dk	Di	Devonian	Cape Super Group
	Dwi		Dws	Dp/Dr		
	Ds, Dbl, Dwa		Dw	Dw		
	Da, Dk, Dw		Da	Da, Dk		
	Dbo		Db	Db		
	Dt		Dt	Dt		
	Dh		Dh	Dh		
	Dv		Ds	Dv		
	Dga		Dgs	Dga		
	Dg		Dg	Dg		
				Dc (undifferentiated)		
	Dr, Db		Sb	Sdb	Silurian	
	Ss		Sk	Ss		
	Sg		St	Sg		
	Oc		Oc	Oc	Ordovician	
	Op		Op	Op		
	-		-	Os		
	-		N, Ngw, Nv Ng, Nmg		Pre Cambrian	Pre-Cape
	-			Nv		
	-			Nk		
	-			Nw		
	-			Ni		

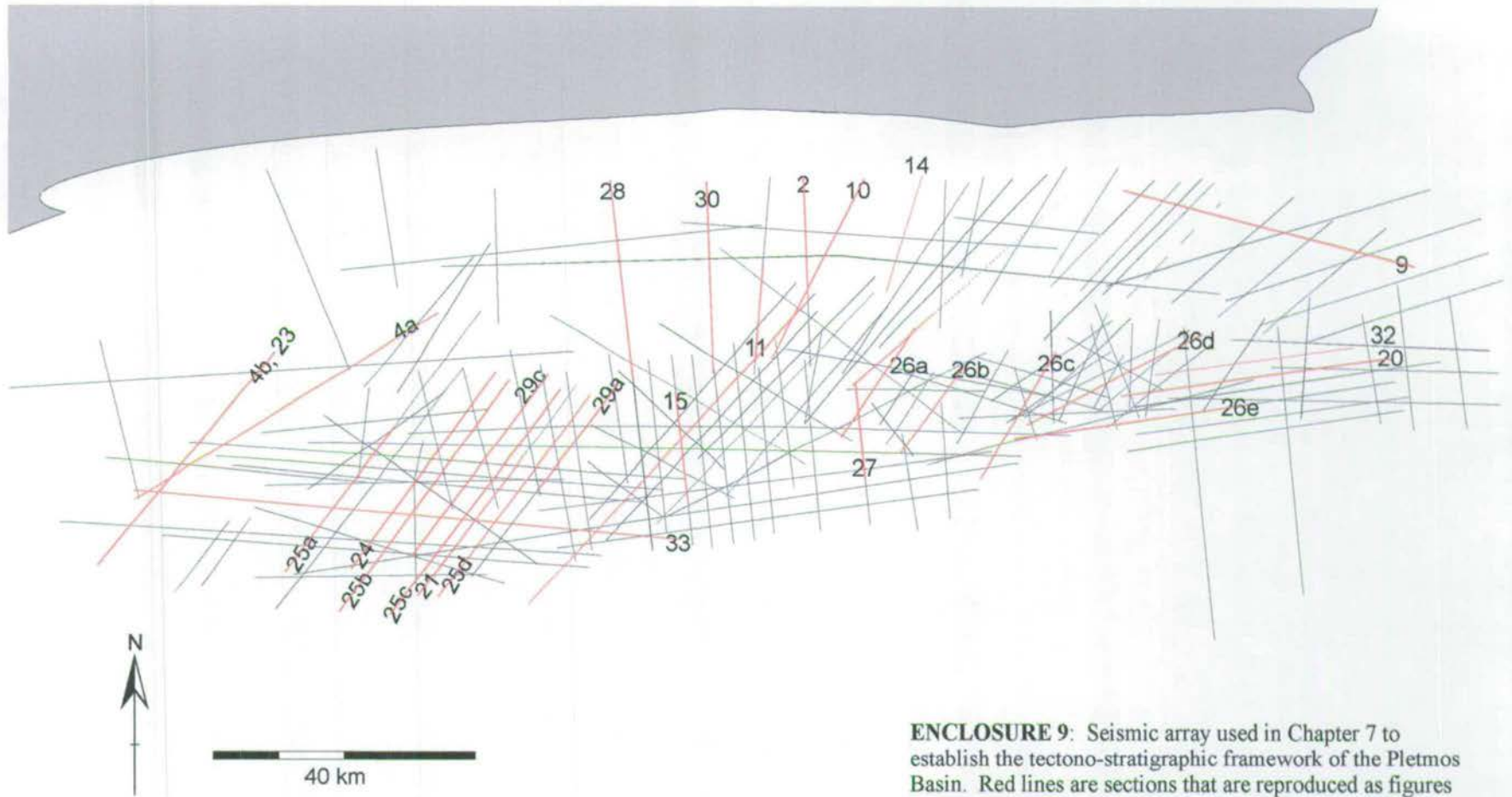
50 Bedding dip from map data (apparent dip calculated where appropriate)

+ Overtured Bedding
 ∨∧ Mapped anticline/syncline
 { Complex folding

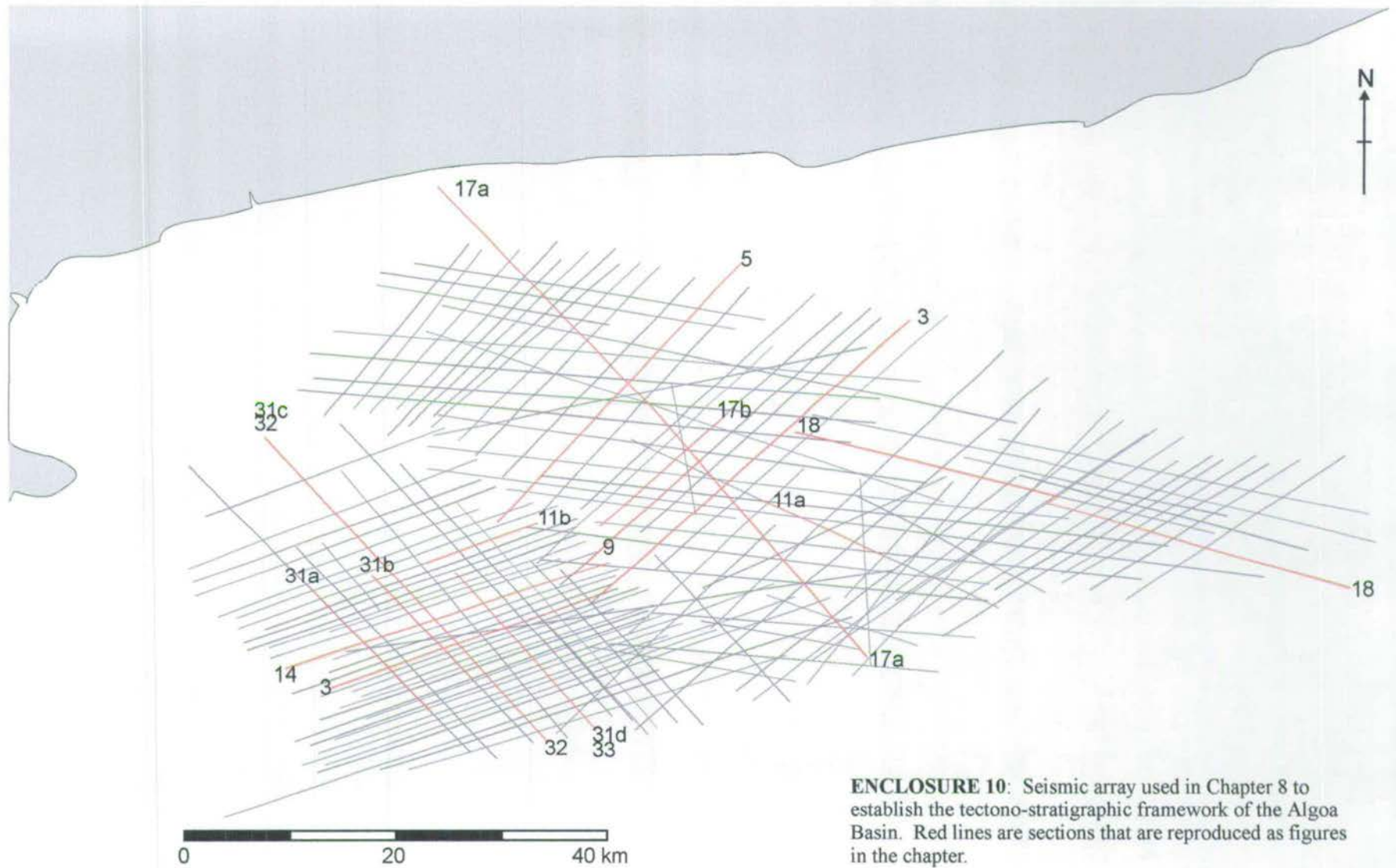
[Cleavage



ENCLOSURE 8: Seismic array used in Chapter 6 to establish the tectono-stratigraphic framework of the Gamtoos Basin. Red lines are sections that are reproduced as figures in the chapter.



ENCLOSURE 9: Seismic array used in Chapter 7 to establish the tectono-stratigraphic framework of the Pletmos Basin. Red lines are sections that are reproduced as figures in the chapter.

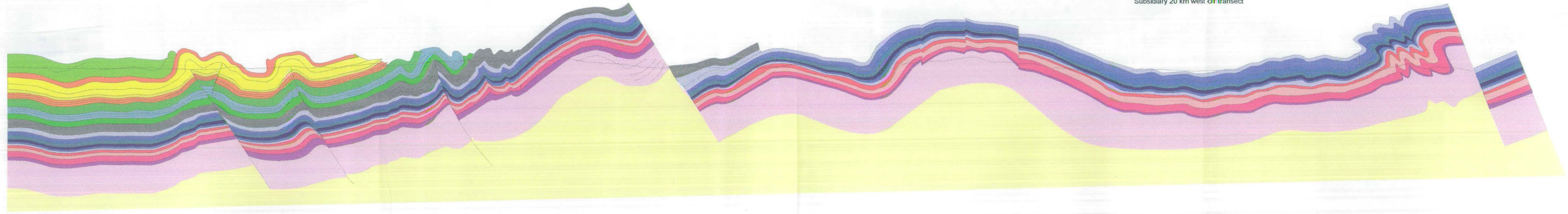
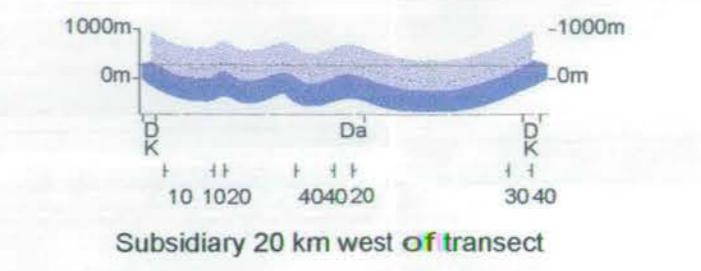
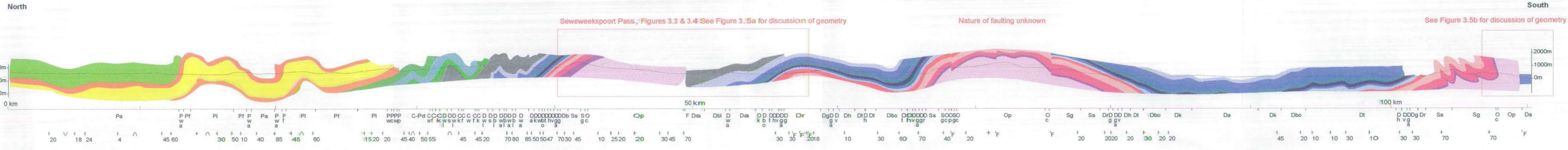


ENCLOSURE 10: Seismic array used in Chapter 8 to establish the tectono-stratigraphic framework of the Algoa Basin. Red lines are sections that are reproduced as figures in the chapter.

The evolution of southern
South Africa: insights into
structural inheritance and
heterogeneous normal fault
growth

Enclosure 2

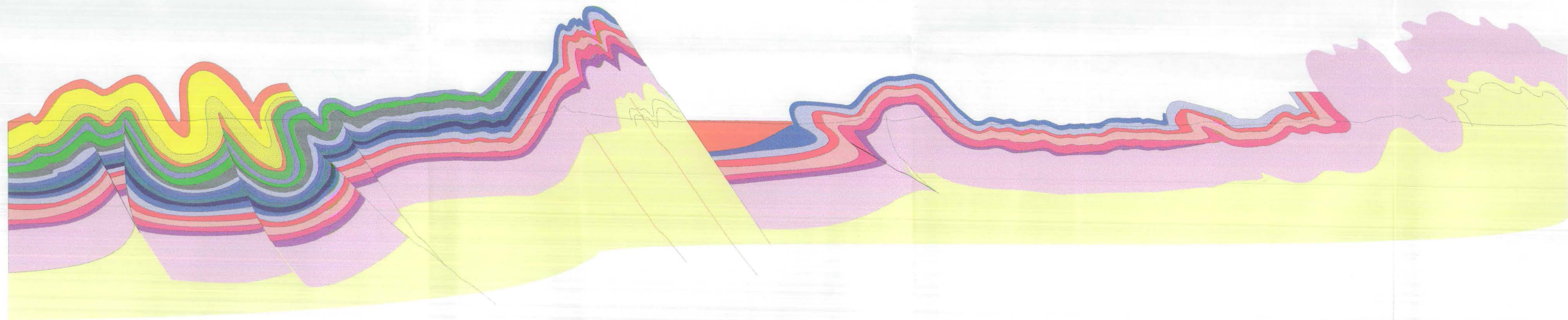
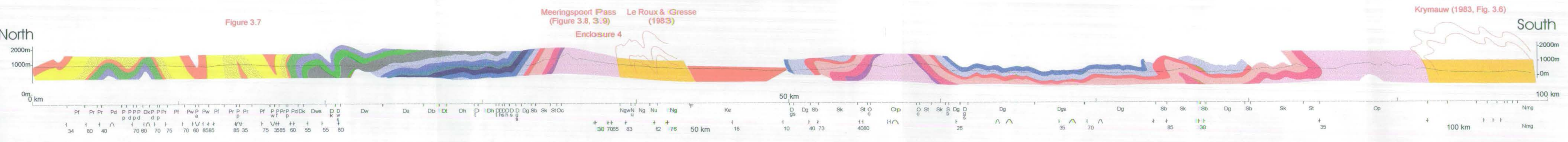
Douglas Alan Paton
February 2002



The evolution of southern
South Africa: insights into
structural inheritance and
heterogeneous normal fault
growth

Enclosure 3

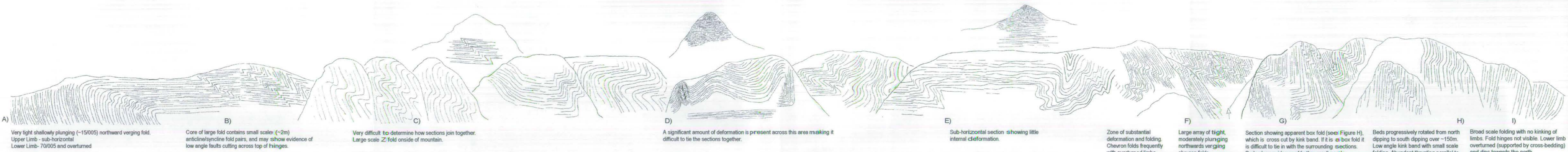
Douglas Alan Paton
February 2002



The evolution of southern
South Africa: insights into
structural inheritance and
heterogeneous normal fault
growth

Enclosure 4

Douglas Alan Paton
February 2002



A) Very tight shallowly plunging (~15/005) northward verging fold. Upper Limb - sub-horizontal Lower Limb- 70/005 and overturned

B) Core of large fold contains small scale (~2m) anticline/syncline fold pairs, and may show evidence of low angle faults cutting across top of hinges.

C) Very difficult to determine how sections join together. Large scale Z fold outside of mountain.

D) A significant amount of deformation is present across this area making it difficult to tie the sections together.

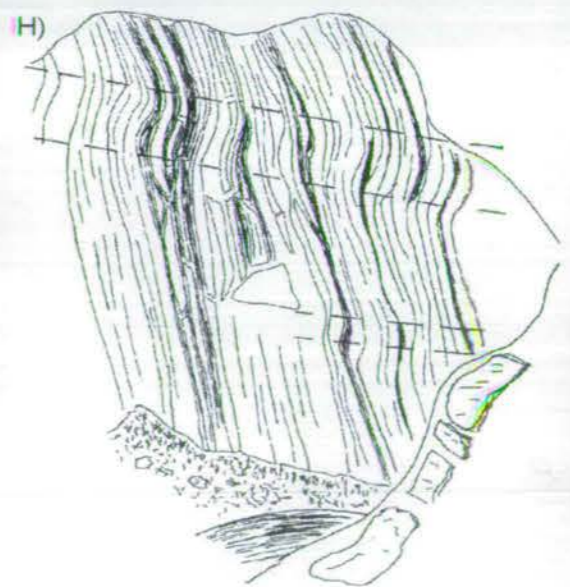
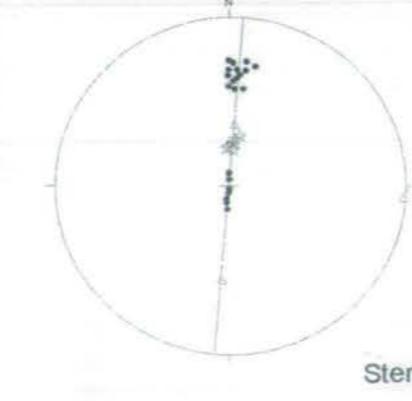
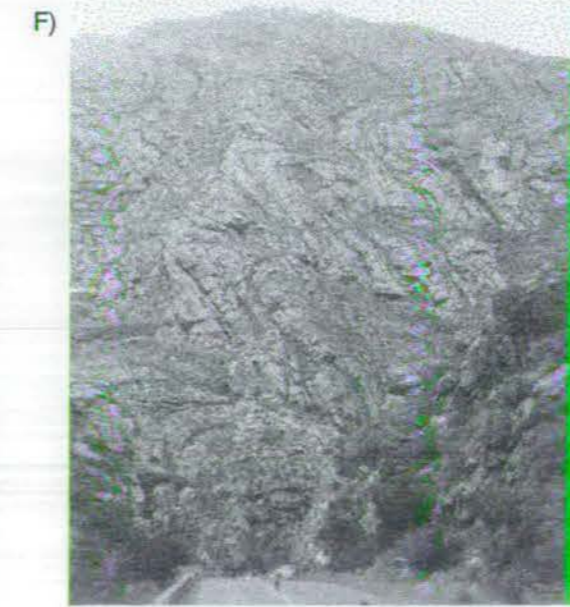
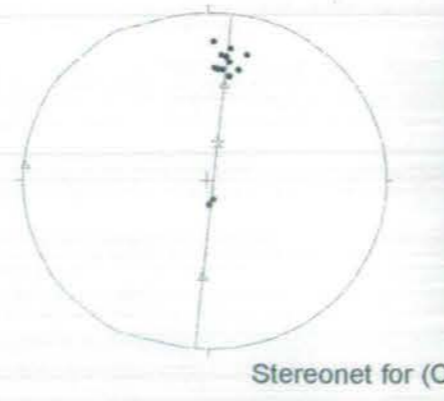
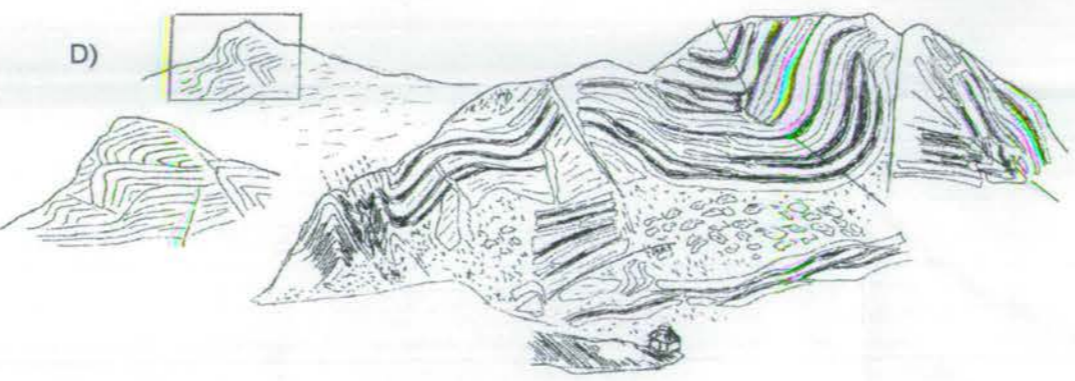
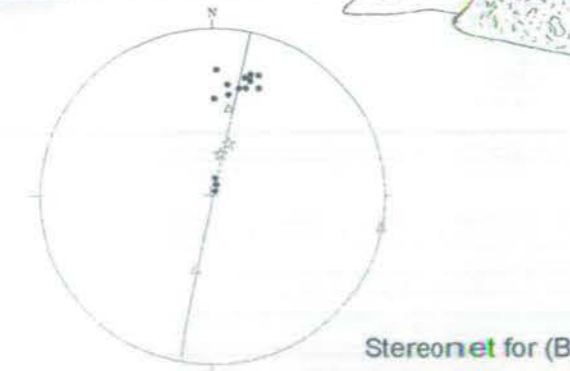
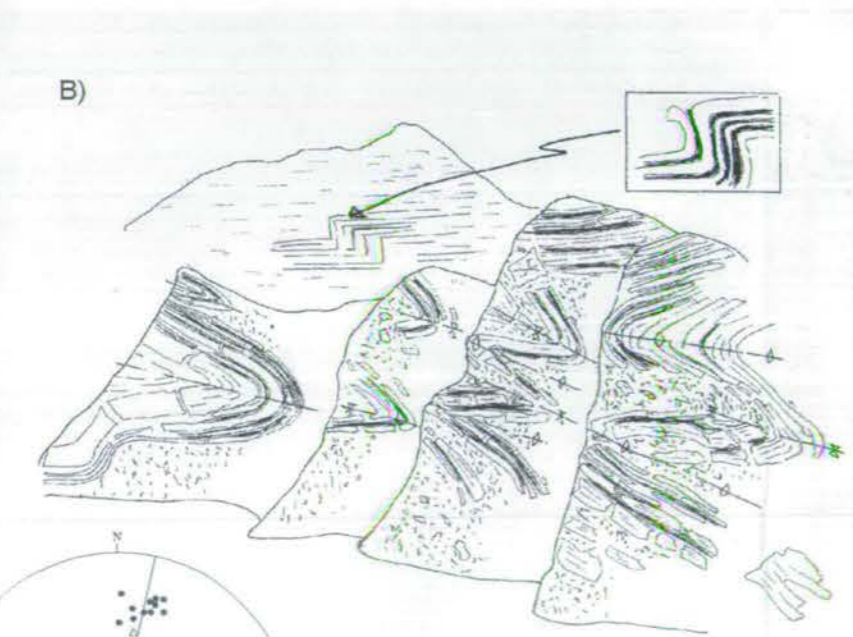
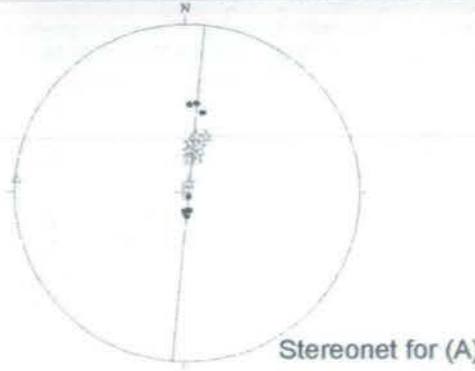
E) Sub-horizontal section showing little internal deformation.

F) Zone of substantial deformation and folding. Chevron folds frequently with overturned limbs.

G) Large array of tight, moderately plunging northwards verging chevron folds.

H) Section showing apparent box fold (see Figure H), which is cross cut by kink band. If it is a box fold it is difficult to tie in with the surrounding sections. Beds show evidence of further small scale deformation.

I) Beds progressively rotated from north dipping to south dipping over ~150m. Low angle kink band with small scale folding. Abundant thrusting parallel to bedding. Broad scale folding with no kinking of limbs. Fold hinges not visible. Lower limb overturned (supported by cross-bedding) and dips towards the north.



Enclosure 5 : Transect through the Merringspoort Pass (see Enclosure 3, Transect B for location). The principal sketch is a traverse through the pass with notes on the important structural features, and sketches and photographs (A-I) highlight specific outcrops. Stereonet data have poles to bedding (circles), fold axes (triangles) and eigenvectors (stars) plotted. Stereonet data are compiled in Figure 3.9.

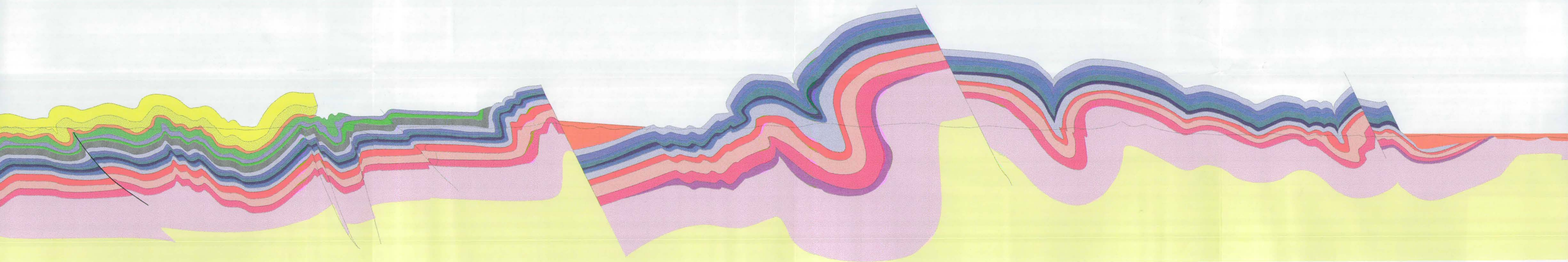
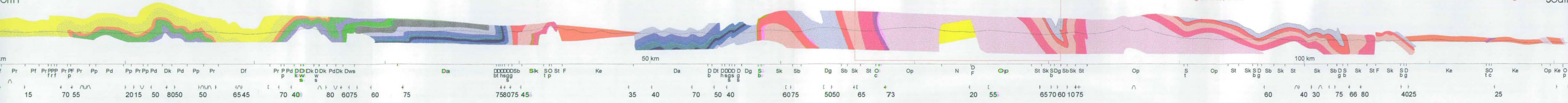
The evolution of southern
South Africa: insights into
structural inheritance and
heterogeneous normal fault
growth

Enclosure 5

Douglas Alan Paton
February 2002

North

South



The evolution of southern
South Africa: insights into
structural inheritance and
heterogeneous normal fault
growth

Enclosure 6

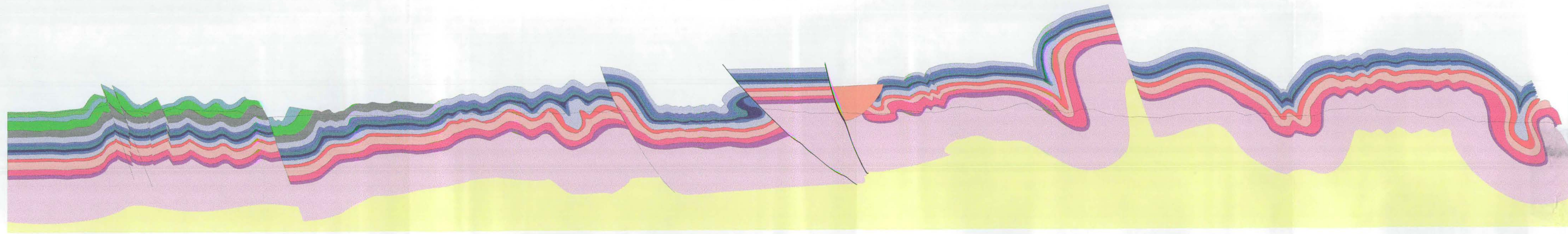
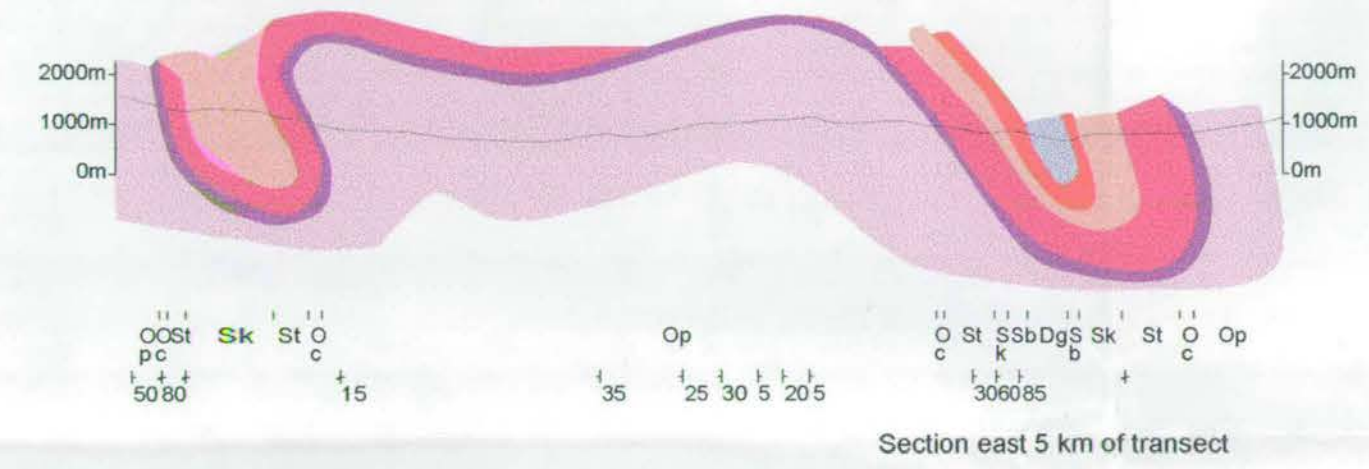
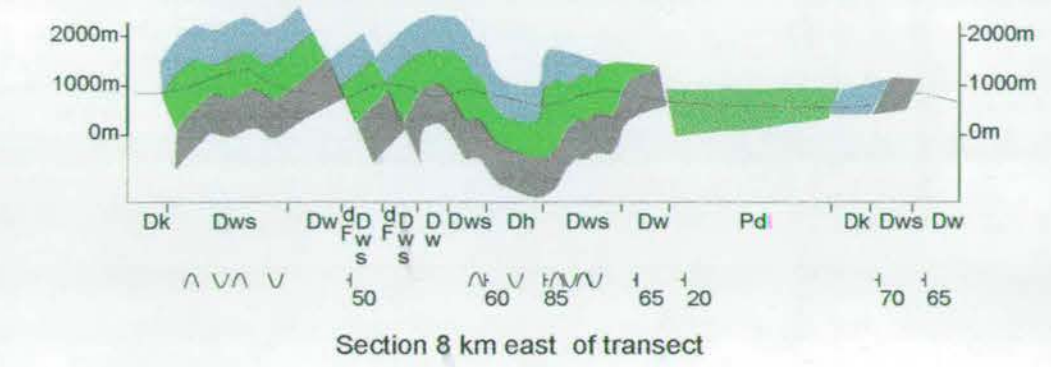
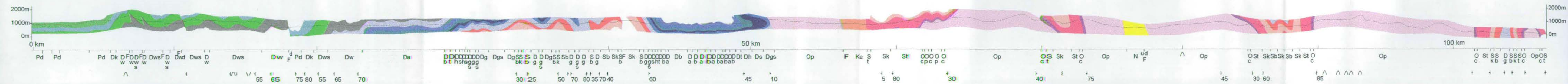
Douglas Alan Paton
February 2002

North

Figure 3.15a

Figure 3.15b

South



The evolution of southern
South Africa: insights into
structural inheritance and
heterogeneous normal fault
growth

Enclosure 7

Douglas Alan Paton
February 2002

